



IJCER

ONLINE PEER REVIEWED JOURNAL

International Journal of Computational
Engineering research

IJCER

Frequency: 12 issues per year

ISSN : 2250-3005



Volume 03, Issue 09

September - 2013

Editorial Board

Editor-In-Chief

Prof. Chetan Sharma

Specialization: Electronics Engineering, India
Qualification: Ph.d, Nanotechnology, IIT Delhi, India

Editorial Committees

DR.Qais Faryadi

Qualification: PhD Computer Science
Affiliation: USIM(Islamic Science University of Malaysia)

Dr. Lingyan Cao

Qualification: Ph.D. Applied Mathematics in Finance
Affiliation: University of Maryland College Park,MD, US

Dr. A.V.L.N.S.H. HARIHARAN

Qualification: Phd Chemistry
Affiliation: GITAM UNIVERSITY, VISAKHAPATNAM, India

DR. MD. MUSTAFIZUR RAHMAN

Qualification: Phd Mechanical and Materials Engineering
Affiliation: University Kebangsaan Malaysia (UKM)

Dr. S. Morteza Bayareh

Qualificatio: Phd Mechanical Engineering, IUT
Affiliation: Islamic Azad University, Lamerd Branch
Daneshjoo Square, Lamerd, Fars, Iran

Dr. Zahéra Mekkioui

Qualification: Phd Electronics
Affiliation: University of Tlemcen, Algeria

Dr. Yilun Shang

Qualification: Postdoctoral Fellow Computer Science
Affiliation: University of Texas at San Antonio, TX 78249

Lugen M.Zake Sheet

Qualification: Phd, Department of Mathematics
Affiliation: University of Mosul, Iraq

Mohamed Abdellatif

Qualification: PhD Intelligence Technology
Affiliation: Graduate School of Natural Science and Technology

Meisam Mahdavi

Qualification: Phd Electrical and Computer Engineering

Affiliation: University of Tehran, North Kargar st. (across the ninth lane), Tehran, Iran

Dr. Ahmed Nabih Zaki Rashed

Qualification: Ph. D Electronic Engineering

Affiliation: Menoufia University, Egypt

Dr. José M. Merigó Lindahl

Qualification: Phd Business Administration

Affiliation: Department of Business Administration, University of Barcelona, Spain

Dr. Mohamed Shokry Nayle

Qualification: Phd, Engineering

Affiliation: faculty of engineering Tanta University Egypt

CONTENTS :

S.No	Title Name	Page No.
Version I		
1.	An Analytical Model Of The Rip Current Flow Dr. Evans F. Osaisai	01-12
2.	A Novel Marker Based Interactive Image Segmentation Method K Vani Sree , A Vanaja	13-18
3.	Design of low power fir filter technique with booth multiplier and delay buffer Gummadi.Lakshmi Pratap ,P.suresh	19-23
4.	Policyholder's Satisfaction of Private Life Insurance Companies With Reference To Tirupur District, Tamilnadu Dr.N.Kathirvel, S.Radhamani	24-28
5.	Agile Methodologies and Its Processes Akanksha, Akansha Rakheja , Latika Kapur , Kanika Ahuja	29-35
6.	Computational Analysis and Design for Precision Forging Of Aluminium AA 6061 Connector Santhosh.N , Vinayaka.N , Dr.Aswatha , Uday.M , Praveena.B.A	36-43
7.	Steady And Unsteady Bubbly Two-Phase Flow (Gas-Liquid Flow) Around A Hydrofoil In Enlarging Rectangular Channel Laith Jaafer Habeeb, Riyadh S. Al-Turaihi	44-62
8.	Cominga Well-Organized Hiding System And Constancy Conservation In Mixture P2P System N. Manjula, R.V. SubbaRayudu , K. Niharika, G.Prathap	63-67

9.	<p>Arima Application as an Alternative Method of Rainfall Forecasts In Watershed Of Hydro Power Plant</p> <p>Sri Mawar Said, Salama Manjang, M.Wihardi Tjaronge, Muh. Arsyad Thaha</p>	68-73
10.	<p>Electrical Energy Consumption Prediction in South–West Sulawesi Electrical Power System</p> <p>Sri Mawar Said, Salama Manjang, M.Wihardi Tjaronge, Muh. Arsyad Thaha</p>	74-78
Version II		
1.	<p>Develop and Design Of the ATM Banking Security System Through Image Processing And GSM Communication</p> <p>R. Jansi Rani, S.Jyothirmayee, M.Sushanth, M.Ravi Prakash</p>	01-05
2.	<p>Design and Implementation of Embedded Media Player Based On ARM9</p> <p>M.Sushanth, K.Somasekhara Rao, M.Ravi Prakash</p>	06-10
3.	<p>Three Dimensional P- Trucks Route Minimum Cost Supply to The Head Quarter From Cities</p> <p>Revathi P, Suresh Babu C, Purusotham S, Sundara Murthy M</p>	11-24
4.	<p>Overview Of Recommender System & A Speedy Approach In Collaborative Filtering Recommendation Algorithms With Mapreduce</p> <p>Prof. Dr. R. Shankar , Prof. Ateshkumar Singh , Ms. Ila Naresh Patil</p>	25-30
5.	<p>Detection and Prevantion of Black Hole Attack over Manet</p> <p>Raghvendra Prasad</p>	31-34

6.	Development of Physical Parameter Extraction Model for Detection and Monitoring Flood Disaster Wawan Setiawan, Wiweka	35-42
7.	Power Line Communications Abdelraheem Mohamed Elkhalfa, Dr. Abdul rasoul J. Alzubaidi	43-53
8.	Mechatronics Design of Ball and Beam System; Education and Research Farhan A. Salem	54-79
9.	Improvement of Pv Systems Power Output Using Sun-Tracking Techniques B. O. Anyaka, D. C. Ahiabuike , M. J. Mbunwe	80-98
10	Prediction of Voltage Instability in Nigeria Interconnected Electric Power System Using V-Q Sensitivity Method Enemuoh F. O., Madueme T. C., Onuegbu J. C., Anazia A. E	99-107
11	Automated Transportation Mechanism and Obstacle Detection Vinita Mathur, Dr. Rajesh Kumar, Mr. Aniruddhu Gautam	108-111
12	Analysis of the Hurst Exponent for M2M Applications Stephen P. Emmons, Farhad Kamangar	112-118
13.	Modelling Mutualism: A Mathematical Model Of Plant Species Interactions In A Harsh Climate E.N. Ekaka , E.O.Chukwuocha , Eziaku Osarolube, E.H. Amadi	119-140

14.	Pedagogical Engineering to Develop Digital Fluency Among Pre-Service Teachers and Educational Leaders Of The 21st-Century Dr Charles Kivunja	141-152
15.	Architectural Design of an Efficient Data Center Sree Bishwjit Chandra Das , Md Kabirul Islam , Syed Akhter Hossain	153-159

An Analytical Model Of The Rip Current Flow

Dr. Evans F. Osaisai

Department of Mathematics, Niger Delta University, PMB 071, Yenagoa, Nigeria
P.O.Box 1693, Yenagoa, Bayelsa State Thu Sep 05 17:31:14 2013

ABSTRACT

In this paper we develop an analytical theory for the interaction between waves and currents induced by breaking waves on time-scales longer than the individual waves. We employed the wave-averaging procedure that is commonly used in the literature. The near-shore zone is often characterized by the presence of breaking waves. Hence we develop equations to be used outside the surf zone, based on small-amplitude wave theory, and another set of equations to be used inside the surf zone, based on an empirical representation of breaking waves. Suitable matching conditions are applied at the boundary between the offshore shoaling zone and the near-shore surf zone. Essentially we derive a model for the interaction between waves and currents. Both sets of equation are obtained by averaging the basic equations over the wave phase. Thus the analytical solution constructed is a free vortex defined in both shoaling and surf zones. The surf zone solution is perturbed by a longshore component of the current. Thus the presence of the rip current cell combined with the longshore modulation in the wave forcing can drive longshore currents along the beach. The outcome, for our set of typical beach profile, is a description of rip currents.

KEYWORDS: Wave-current interactions, surf zone, shoaling zone, matching conditions, wave-averaging, rip currents, radiation stress.

I. INTRODUCTION

The action of shoaling waves, and wave breaking in the surf zone, in generating a wave-generated mean sea-level is well-known and has been extensively studied, see for instance the monographs of Mei (1983) and Svendsen (2006). The simplest model is obtained by averaging the oscillatory wave field over the wave phase to obtain a set of equations describing the evolution of the mean fields in the shoaling zone based on small-amplitude wave theory and then combining these with averaged mass and momentum equations in the surf zone, where empirical formulae are used for the breaking waves. These lead to a prediction of steady set-down in the shoaling zone, and a set-up in the surf zone. This agrees quite well with experiments and observations, see Bowen et al (1968) for instance. However, these models assume that the sea bottom is rigid, and ignore the possible effects of sand transport by the wave currents, and the wave-generated mean currents. Hydrodynamic flow regimes where the mean currents essentially form one or more circulation cells are known as rip currents. These form due to forcing by longshore variability in the incident wave field, or the effect of longshore variability in the bottom topography (Kennedy 2003, 2005, Yu & Slinn 2003, Yu 2006 and others). They are often associated with significant bottom sediment transport, and are dangerous features on many surf beaches (Lascody 1998 & Kennedy 2005).

There is a vast literature on rip current due to wave-current interactions, see the recent works by (Horikawa 1978, Damgaard *et al.* 2002, Ozkan-Haller & Kirby 2003, Yu & Slinn 2003, Yu 2006, Falques, Calvete & Monototo 1998a and Falques *et al.* 1999b, Zhang *et al.* 2004 and others) and the references therein. Our purpose in this paper is to exploit the fully developed but under-utilised wave-current interaction theory in the nearshore. In section 2 we record the usual wave-averaged mean field equations that are commonly used in the literature. In section 3 we introduce a description of the rip current formation and examine the consequences for both shoaling and surf zones. Then in section 4 we employ section 3 to a choice of linear depth profile. We conclude with a discussion in section 5.

II. FORMULATION

2.1 Wave field

In this section we recall the wave-averaged mean flow and wave action equations that are commonly used to describe the near-shore circulation (see Mei 1983 or Svendsen 2006 for instance). We suppose that the

depth and the mean flow are slowly-varying compared to the waves. Then we define a wave-phase averaging operator $\langle f \rangle = \bar{f}$, so that we can express all quantities as a mean field and a wave perturbation, denoted by a “tilde” overbar. For instance,

$$\zeta = \bar{\zeta} + \tilde{\zeta}. \quad (1)$$

where ζ is the free surface elevation above the undisturbed depth $h = h(x)$. Then outside the surf zone, the representation for slowly-varying, small-amplitude waves is, in standard notation,

$$\tilde{\zeta}(x, t) : a \cos \theta. \quad (2)$$

Here $a = a(x, t)$ is the wave amplitude and $\theta = \theta(x, t)$ is the phase, such that the wavenumber k , frequency Ω are given by

$$k = (k, l) = \nabla \theta \quad \Omega = -\theta_t. \quad (3)$$

The local dispersion relation is

$$\Omega = \omega + k \cdot U, \quad \omega^2 = g \kappa \tanh \kappa H \quad (4)$$

$$\text{where } \kappa^2 = k^2 + l^2.$$

Here $U(x, t)$ is the slowly-varying depth-averaged mean current (see below), and $H(x, t) = h(x) + \bar{\zeta}(x, t)$. To leading order, the horizontal and vertical components of the wave velocity field are respectively

$$\tilde{u} : \frac{k}{\kappa} a \Omega \frac{\cosh \kappa(z+h)}{\sinh \kappa H} \cos \theta, \quad \tilde{w} : a \Omega \frac{\sinh \kappa(z+h)}{\sinh \kappa H} \sin \theta. \quad (5)$$

Importantly, note that we have ignored here any reflected wave field, which is assumed to be very weak when the bottom topography is slowly varying.

The basic equations governing the wave field is then the kinematic equation for conservation of waves

$$k_t + \nabla \omega = 0, \quad (6)$$

which is obtained from (3) by cross-differentiation, the local dispersion relation (4), and the wave action equation for the wave amplitude

$$A_t + \nabla \cdot (c_g A) = 0. \quad (7)$$

Here $A = E/\omega$, where $E = g a^2/2$ is the wave energy per unit mass, and $c_g = \nabla_k \cdot \omega = U + c_g k/\kappa$, ($c_g = d\omega/d\kappa$) is the group velocity. Using the dispersion relation (4) in (6) we get

$$k_t + c_g \cdot \nabla k = -\nabla_{e_x} \Omega, \quad (8)$$

$$\Omega_t + c_g \cdot \nabla \Omega = \Omega_{e_t}. \quad (9)$$

Here the subscript “e” denotes the explicit derivative of $\Omega(k, x, t)$ with respect to either x or t , when the wavenumber k is held fixed. In this water case these explicit derivatives arise through the dependence of Ω on the mean height H and the mean current U .

2.2 Mean fields

The equations governing the mean fields are obtained by averaging the depth-integrated Euler equations over the wave phase. Thus the averaged equation for conservation of mass is

$$H_t + \nabla \cdot (HU) = 0. \quad (10)$$

Here $H = h + \bar{\zeta}$ where $h = h(x)$ is the time-independent undisturbed depth. For the velocity field we proceed in a slightly different way, that is we define

$$u = U + u', \quad (11)$$

where we define U so that the mean momentum density is given by

$$M = HU = \langle \int_{-h}^{\zeta} u dz \rangle, \quad (12)$$

But now we need to note that u' does not necessarily have zero mean, and that U and u are not necessarily

the same. Indeed, from (11) and (12) we get that

$$u = U + \langle u' \rangle, \quad \text{and} \quad \langle \int_{-h}^{\zeta} u' dz \rangle = 0.$$

But $u' = u + O(a^2)$, so that $\langle u' \rangle$ is $O(a^2)$ and it follows that, correct to second order in wave amplitude,

$$M = Hu + M_w, \quad \text{where} \quad M_w = -H \langle u' \rangle = \langle \zeta u(x,0,t) \rangle = \frac{E k}{c \kappa}. \quad (13)$$

The term M_w in (13) is called the wave momentum.

Next, averaging the depth-integrated horizontal momentum equation yields (Mei 1983)

$$(HU)_t + \nabla \cdot (HUU) = -\nabla \cdot \langle \int_{-h}^{\zeta} u' u' + pI dz \rangle + \langle p(z = -h) \rangle \nabla h.$$

Next an estimate of the bottom pressure term is made by averaging the vertical momentum equation to get

$$\langle p(z = -h) \rangle = g(\bar{\zeta} + h) = \nabla \cdot \langle \int_{-h}^{\zeta} w u dz \rangle + \langle \int_{-h}^{\zeta} w dz \rangle_t.$$

For slowly-varying small-amplitude waves, the integral terms on the right-hand side may be neglected, and so $\langle p(z = -h) \rangle \approx g(\bar{\zeta} + h)$. Using this in the averaged horizontal momentum equation, and replacing the pressure p with the dynamic pressure $q = p + (z - \bar{\zeta})$ yields

$$HU_t + \nabla \cdot (HUU) = -\nabla \cdot S - gH\nabla \bar{\zeta} \quad (14)$$

$$\text{where} \quad S = \langle \int_{-h}^{\zeta} [uu + qI] dz \rangle = \langle \frac{g}{2} \zeta^2 \rangle I. \quad (15)$$

Here S is the radiation stress tensor. In the absence of any background current, so that U is $O(a^2)$, we may use the linearized expressions (2, 5) to find that

$$S \approx c_g k \frac{E}{\omega} + E \left[\frac{c_g}{c} - \frac{1}{2} \right] I. \quad (16)$$

where the phase speed $c = \omega/\kappa$, correct to second order in the wave amplitude.

2.3 Shoaling zone

These equations hold in the shoaling zone outside the surf zone (defined below). In summary, the equations to be solved are that for the conservation of waves (6) combined with the dispersion relation (4), the wave action equation (7), the averaged equation for conservation of mass (10) and the averaged equation for conservation of horizontal momentum (14), where the radiation stress tensor is given by (16). In this shoaling zone, we assume that wave amplitudes are small, and that there is no background current. Then all mean quantities are $O(a^2)$, and in particular we can systematically replace H with h throughout these equations. Next we shall suppose that $h = h(x)$ depends only on the offshore co-ordinate $x > 0$, where the undisturbed shoreline is at $x = 0$ defined by $h(0) = 0$. Further, in the near-shore region, including all of the surf zone, we shall assume that $h_x > 0$. Then we seek steady solutions of the equation set in which all variables are independent of the time t , and are also independent of the transverse variable y . It then follows from the mean mass equation (10) that HU is constant, and since $H = 0$ at the shoreline, it follows that we can set $U = 0$ everywhere. Then in the dispersion relation (4) $\Omega = \omega$. From the equation for conservation of waves (6) we see that the frequency ω and the transverse wavenumber l are constants, and the offshore wavenumber k is then determined from the dispersion relation (4). As is well-known, it then follows that as $H \rightarrow 0$, $|k| \rightarrow \infty$, that is the waves refract towards the onshore direction, where we assume that the waves are propagating towards the shoreline so that $k < 0$. The wave action equation (7) reduces to Ec_g is constant. Near the shore, we can assume that the shallow water approximation holds and then $c_g \approx -(gh)^{1/2}$, so that

$$a^2 h^{1/2} \approx a_0^2 h_0^{1/2}, \quad (17)$$

where a_0 is the wave amplitude at a location offshore where $h = h_0$. The surf zone $x < x_b, h < h_b = h(x_b)$ can then be defined by the criterion that h_b is that depth where $a/h = A_{cr}$, defining an empirical breaking condition. A suitable value is $A_{cr} = 0.44$, see Mei (1983) or Svendsen (2006).

The last step is to find the wave set-up $\bar{\zeta}$ from the mean momentum equation (14), which here becomes

$$S_x + gH\bar{\zeta}_x = 0, \tag{18}$$

$$\text{where } S = \frac{c_g}{c} E \cos^2 \phi + \left(\frac{c_g}{c} - \frac{1}{2}\right) E.$$

Here ϕ is the angle between the wave direction and the onshore direction, and S is the “ xx ” component of the tensor S . As $h \rightarrow 0$, $\phi \approx 0, c_g \approx c, S \approx 3E/2$, and we recover the well-known result of a wave set-down in the shoaling zone

$$\bar{\zeta} = -\frac{a^2}{4h} = -\frac{a_0^2 h_0^{1/2}}{4h^{3/2}}. \tag{19}$$

Here we have assumed that $\bar{\zeta}$ is zero far offshore. Note that the first expression for $\bar{\zeta}$ does not need the use of the shallow water approximation, as shown by Longuet-Higgins and Stewart (1962).

2.4 Surf zone

In the surf zone $0 < x < x_b, 0 < h < h_b$, we make the usual assumption (see Mei (1983) for instance) that the breaking wave height $2a$ is proportional to the total depth H , so that

$$2a = \gamma H, \text{ or } E = \frac{g\gamma^2 H^2}{8}, \tag{20}$$

Here the constant γ is determined empirically, and a typical value is $\gamma = 0.88$. To determine the mean height $H = h + \bar{\zeta}$, we again use the mean momentum equation (14), but now assume that $S = 3E/2 = \Gamma gH^2/2$ where $\Gamma = 3\gamma^2/8$, so that

$$\Gamma H H_x + H(H - h)_x = 0, \text{ so that } H = H_b + \frac{h - h_b}{(1 + \Gamma)}, \tag{21}$$

where the constant $H_b = h_b + \bar{\zeta}_b$ is determined by requiring continuity of the total mean height at $x = x_b$. Note that using (19)

$$H_b = h_b - a_0^2 h_0^{1/2} / 4h_b^{3/2},$$

and since H_b must be positive, there is a restriction on either the deep-water wave amplitude a_0 or on the breaker depth h_b ,

$$a_0^2 / 4h_0^2 < h_b^{5/2} / h_0^{5/2}. \tag{22}$$

Note that the expression (21) is valid for any depth $h(x)$, although in the literature it is often derived only for a linear depth profile $h = \alpha x$.

We are now in a position to determine the displaced shoreline $x = x_s$, defined by the condition that $H = 0$. That is, if $h_s = h(x_s)$ then $H = (h - h_s) / (1 + \Gamma)$, where

$$h_s = -\Gamma h_b - (1 + \Gamma)\bar{\zeta}_b, \tag{23}$$

Note that to use the expression (23) it may be necessary to extend the definition $h(x)$ into $x < 0$. For instance for a linear beach, $h = \alpha x$, this is straightforward, but for a quadratic beach profile, $h = \beta x^2$, the extension for negative x should be $h = -\beta x^2$ say. Note that from (19),

$$\zeta_b = -\frac{a_0^2 h_0^{1/2}}{4h_b^{3/2}},$$

and, on combining this with the condition (22), it follows that the shoreline recedes (advances), that is $h_s < 0 (> 0)$ when

$$\begin{aligned} \frac{a_0^2}{4h_0^2} &< \frac{\Gamma}{1+\Gamma} \frac{h_b^{5/2}}{h_0^{5/2}}, \\ \text{or} \quad \frac{\Gamma}{1+\Gamma} \frac{h_b^{5/2}}{h_0^{5/2}} &< \frac{a_0^2}{4h_0^2} < h_b^{5/2}/h_0^{5/2}. \end{aligned} \quad (24)$$

Curiously, this anomalous result does not seem to have been noticed previously [5] and [5]. Since there is an expectation that the shoreline should advance (see Dean and Dalrymple (2002) for instance), essentially it states that the present model is only valid for sufficiently small waves far offshore, defined by the first inequality in (24), which slightly refines the constraint (22).

III. A GENERAL DESCRIPTION OF THE RIP CURRENT FORMATION

Here we consider a steady-state model driven by an incident wave field which has an imposed longshore variability. The wave field satisfies equation (7) which in the present steady-state case reduces to

$$\partial\partial x(Ec_g \cos \theta) + \partial\partial y(Ec_g \sin \theta) = 0. \quad (25)$$

Here we again assume that $h = h(x)$ and that consequently the frequency ω and the longshore wavenumber l are constants, while the onshore wavenumber K is then determined from equation (4). We have the wave energy E of the form

$$E = E_0(x) \cos Ky + F_0(x) \sin Ky + G_0(x), \quad (26)$$

where the longshore period $2\pi/K$ is imposed. These equations in the shoaling zone yields

$$(E_0 c_g \cos \theta)_x + K F_0 c_g \sin \theta = 0 \quad (27)$$

$$(F_0 c_g \cos \theta)_x - K E_0 c_g \sin \theta = 0 \quad (28)$$

$$(G_0 c_g \cos \theta)_x = 0. \quad (29)$$

on collecting terms in $\cos Ky$, $\sin Ky$ and the constant term, which form three equations for E_0 , F_0 and G_0 . Equation (29) easily yields that $G_0 c_g \cos \theta = \text{constant}$. In shallow water, we may approximate by putting $c_g \approx gh^{1/2}$ and $\cos \theta \approx 1$, so that then $G_0 \approx \text{constant}/h^{1/2}$. For the remaining equations we can use Snell's law, $\sin \theta/c = \sin \theta_b/c_b = \alpha_b$ (the constant value, here evaluated at the breaker line), and the shallow-water approximation to get that

$$\{(E_0 c)_x\}/c + K^2 \alpha_b^2 E_0 c^2 = 0, \quad (30)$$

while although F_0 satisfies the same equation, once E_0 has been found, then F_0 is given by either (27) or (28). In practice, $Kc \ll 1$ and so approximately we can assume that $(E_0, F_0)c \approx \text{constant}$, the usual shallow-water expressions. Note that here $c \approx \sqrt{gh}$. In the surf zone, the expressions $E_0(x)$, $F_0(x)$, $G_0(x)$ is determined empirically.

Once the expression (26) has been determined, we may then substitute into the expressions (27,28 & 29) to obtain the radiation stress fields. Our aim here then is to describe how steady-state rip currents are forced by this longshore modulation of the incident wave field, especially in the surf zone.

The forced two-dimensional shallow water equations that we use here are characteristic of many nearshore studies (Horikawa 1978, Damgaard *et al.* 2002, Ozkan-Haller & Kirby 2003, Yu & Slinn 2003, Yu 2006, Falques, Calvete & Monototo 1998a and Falques *et al.* 1999b, Zhang *et al.* 2004 and others). Then, omitting the overbars as before, then equations (??) in the present steady-state case reduce to

$$H[U\partial U\partial x + V\partial U\partial y] = -gH\partial\zeta\partial x - [\tau_x], \quad (31)$$

$$H[U\partial V\partial x + V\partial V\partial y] = -g H\partial\zeta\partial y - [\tau_x], \tag{32}$$

where the stress terms are defined;

$$\tau_x = \partial S_{11}\partial x + \partial S_{12}\partial y \quad \text{and} \quad \tau_y = \partial S_{21}\partial x + \partial S_{22}\partial y. \tag{33}$$

Next we observe that equation (10) can be solved using a transport stream function $\psi(x, y)$, that is

$$U = -\frac{1}{H}\partial\psi\partial y \quad \text{and} \quad = \frac{1}{H}\partial\psi\partial x, \tag{34}$$

Next, eliminating the pressure, we get the mean vorticity equation

$$\psi_x \left(\frac{\Omega}{H}\right)_y - \psi_y \left(\frac{\Omega}{H}\right)_x = \left[\frac{\tau_x}{H}\right]_y - \left[\frac{\tau_y}{H}\right]_x \tag{35}$$

where Ω is define as

$$\Omega = V_x - U_y = \left(\frac{\psi_x}{H}\right)_x + \left(\frac{\psi_y}{H}\right)_y. \tag{36}$$

We shall solve this equation (35) in the shoaling zone $x > x_b$ and in the surf zone $x < x_b$, where as before $x = x_b$ is the fixed breaker line. It will turn out that the wave forcing occurs only in the surf zone, but continuity implies that the currents generated in the surf zone must be continued into the shoaling zone.

3.1 Shoaling zone

In $x > x_b$ we shall assume that $H \approx h$ as ζ is $O(a^2)$. Then we shall use the expressions [27 ,28] to evaluate the radiation stress tensor. For simplicity, we shall also use the shallow-water approximation that $c_g \approx c \approx \sqrt{gh}$, and so we get that

$$S_{11} = E(\cos^2\theta + \frac{1}{2}), S_{12} = S_{21} = E \sin\theta \cos\theta, S_{22} = E(\sin^2\theta + \frac{1}{2}) \tag{37}$$

These expressions are in principal known at this stage, and so we can proceed to evaluate the forcing term on the right-hand side of (35). To assist with this we recall Snell's law

$$\sin\theta = \sqrt{h}\sqrt{h_b} \sin\theta_b$$

where h_b and θ_b are the water depth and incidence angle at the breaker-line. Now the energy equation (25) has the approximate form

$$(Ecc\cos\theta)_x + (Ecs\sin\theta)_y = 0,$$

and using Snell's law, this can be written as

$$(E\cos^2\theta)_x + (E\sin\theta\cos\theta)_y + E\frac{c_x}{c} = 0,$$

$$\text{and so} \quad \tau_x = \frac{1}{2}E_x - E\frac{c_x}{c}.$$

We can also deduce from (25) that

$$(E\sin\theta\cos\theta)_x + (E\sin^2\theta)_y = 0,$$

$$\text{and so} \quad \tau_y = \frac{1}{2}E_y.$$

We can now evaluate the right-hand side of (35), and find that its identically zero,

$$\left[\frac{\tau_x}{h}\right]_y - \left[\frac{\tau_y}{h}\right]_x = 0.$$

Thus in the shoaling zone there is no wave forcing in the mean vorticity equation, although of course there will be a mean pressure gradient. However, this does not concern us since here our aim is to find only the flow field. Note that the result that there is no wave forcing in the vorticity equation does *not* need the specific form (26),

and is based solely on the steady-state wave energy equation (25). The specific form (26) is only used in the surf zone.

With no forcing term, the vorticity equation (35) can be solved in the compact form, noting that we again approximate H with h ,

$$\frac{\Omega}{h} = F(\psi). \tag{38}$$

But here $F(\psi) = 0$ from the boundary conditions in the deep water as $x \rightarrow \infty$, where the flow field is zero. Thus our rip current model has zero vorticity in the shoaling zone. It follows that we must solve the equation

$$\Omega = \left(\frac{1}{h}\psi_x\right)_x + \left(\frac{1}{h}\psi_y\right)_y = 0, \tag{39}$$

in $x > x_b$. Since $h = h(x)$ we can seek solutions in the separated form

$$\psi = X(x)Y(y) \tag{40}$$

with the outcome that

$$\left(\frac{X_x}{h}\right)_x - \frac{K^2 X}{h} = 0, \quad Y_{yy} + K^2 Y = 0. \tag{41}$$

We note the separation constant $K^2 = 2\pi/L$ must not be zero, and is in fact chosen to be consistent with the modulation wavenumber of the wave forcing. Without loss of generality, we can choose

$$Y = \sin Ky. \tag{42}$$

For each specific choice of $h(x)$ we must then solve for $X(x)$ in $x > x_b$, with the boundary condition that $X \rightarrow 0$ as $x \rightarrow \infty$. We shall give details in the following subsections. Otherwise we complete the solution by solving the system (35) in the surf zone, and matching the solutions at the breakerline, $x = x_b$, where the streamfunction ψ must be continuous, and in order to have a continuous velocity field we must also have that ψ_x is continuous.

3.2 Surf zone

To make sense of wave forcing, we assume that the expression (26) holds in this region. The functions $E_0(x), F_0(x), G_0(x)$ are then determined empirically. To determine the wave forcing term in the mean vorticity equation (35) we shall assume that $\theta = \theta_b \ll 1$ so that, on using (??) and (37) we get that

$$\tau_x = \frac{3}{2}E_x, \quad \tau_y = \frac{1}{2}E_y.$$

Then (35) now becomes, where we again approximate H with $h(x)$,

$$\partial\psi\partial x\partial\tilde{\Omega}\partial y - \partial\psi\partial y\partial\tilde{\Omega}\partial x = \frac{E_{xy}}{h} + \frac{E_y h_x}{2h^2} = \frac{(h^{1/2}E_y)_x}{h^{3/2}}, \tag{43}$$

where here $\tilde{\Omega} = \Omega/h$ is the potential vorticity. Since the wave forcing is given by (26), that is

$$E = E_0(x)\cos Ky + F_0(x)\sin Ky + G_0(x), \tag{44}$$

we observe that the unmodulated term $G_0(x)$ plays no role here at all, although of course it will contribute to the wave setup. In order to match at $x = x_b$ with the expression (42) for the streamfunction in the shoaling zone, we should try for a solution of (43) of the form

$$\psi = F(x)\sin Ky + G(x), \quad \text{in } x < x_b. \tag{45}$$

The matching conditions for the streamfunction and velocity field at the breakerline $x = x_b$ require that

$$F(x_b) = X(x_b), F_x(x_b) = X_x(x_b), G(x = x_b) = 0, G_x(x_b) = 0.$$

The expression (45) yields

$$\Omega = \tilde{F}\sin Ky + \tilde{G} \tag{46}$$

where \tilde{F} and \tilde{G} are differential operators where they are defined as;

$$\tilde{F} = \left(\frac{F_x}{h}\right)_x - \frac{K^2 F}{h} \tag{47}$$

$$\tilde{G} = Z_x, Z = \frac{G_x}{h} \tag{48}$$

From equation (43) we get a set of three equations that are used to determine the rip-current flow field in the surf zone. These are namely;

$$F_x \frac{\tilde{F}}{h} - F \left(\frac{\tilde{F}}{h}\right)_x = 0, \tag{49}$$

$$\left(G \frac{\tilde{F}}{h} - F \left(\frac{\tilde{G}}{h}\right)_x\right) = \frac{(h^{1/2} F_0)_x}{h^{3/2}}, \tag{50}$$

$$\left(\frac{h^{1/2} E_0}{h^{3/2}}\right)_x = 0. \tag{51}$$

Equation (51) gives $E_0 : 1/h^{1/2}$, which is an unacceptable singularity as $h \rightarrow 0$. Hence we must infer that in the surf zone at least, $E_0 = 0$. The first of the three equations, that is (3.2a) suggests that

$$\frac{\tilde{F}}{h} = CF \text{ where } C \text{ is a constant,} \tag{52}$$

and the second (3.2b) yields that

$$F \left(CG - \left(\frac{\tilde{G}}{h}\right)_x \right) = \frac{(h^{1/2} F_0)_x}{h^{3/2}} \tag{53}$$

The boundary conditions at $x = 0$ where $h = 0$ are that both mass transport fields U, V should vanish, that is from (34) $\psi = constant$ and $\psi_x/h = 0$, which implies that

$$F = F_x = 0, G = constant, \frac{G_x}{h} = 0, \text{ at } x = 0. \tag{54}$$

As above there are also the matching conditions for both F and G separately at the breakerline, that is for F we have that

$$\frac{F_x(x_b)}{F(x_b)} = \frac{X_x(x_b)}{X(x_b)}, \text{ at } x = x_b$$

where we note that here the right-hand side is a known quantity, depending only on K and x_b . Next we see that equation (52) reduces to

$$\left(\frac{F_x}{h}\right)_x - \frac{K^2 F}{h} = ChF \tag{55}$$

Together with the boundary conditions at $x = 0, x = x_b$ this is essentially an eigenvalue problem for $F(x)$ with eigenvalue C . In general it is solved approximately since we shall assume that $Kx_b \ll 1$. Once $F(x)$ is known we can solve (53), together with the appropriate boundary conditions to get $G(x)$ to complete the solution.

Note that the amplitude of $F(x)$ is an arbitrary constant in this solution, and so we can fix it by specifying its value at $x = x_b$ say. Indeed the solution we have constructed is essentially a free vortex defined by $X(x)\sin Ky$ in the shoaling zone $x > x_b$, and $F(x)\sin Ky$ in the surf zone $x < x_b$, perturbed by a longshore component $G(x)$ in the surf zone. Note that in the presence of the wave forcing, both F, G are non-zero, see (53). It is significant that unlike the longshore currents considered in the basic state which depend on an *ad hoc* frictional parametrization, the presence of the rip current cell combined with the longshore modulation in the wave forcing can drive a longshore current.

IV. AN APPLICATION TO LINEAR DEPTH PROFILE

To make sense of the rigorous mathematical derivations and formulations we then suppose that $h = \alpha x$. Then immediately the solutions of equation (41) in the shoaling zone is

$$X(x) = C_1 x K_1(Kx) + C_0 x I_1(Kx).$$

Since I_1 becomes unbounded at $x = \infty$, the boundary condition $X \rightarrow 0$ as $x \rightarrow \infty$ gives $C_0 = 0$, and so we get that

$$X(x) = C_1 x K_1(Kx), x > x_b. \tag{56}$$

The behavior of the Bessel functions depict the rip-current character which decays exponentially away from the breakerline, on the scale K^{-1} . It is interesting to note here that the bottom slope α does not appear in this solution at all. In the surf zone, the boundary condition (54) implies that as $x \rightarrow 0$, $F(x) \approx A_0 x^2$. We shall make the approximation that the shoaling zone has a small cross-shore width, in which case it is easily seen that the right-hand side of (55) is much smaller than the left-hand side, and is $O(x^3)$. Approximating the right-hand side accordingly we get that

$$F_{xx} - \frac{1}{x} F_x - K^2 F = A_0 \lambda x^4, \tag{57}$$

where $\lambda = C\alpha^2$. This is useful, as the solutions of the homogeneous equation on the left-hand side are known, namely $j_a = x I_1(Kx)$ and $j_b = x K_1(Kx)$. By the variation of parameters one gets

$$F(x) = A(x) j_a + B(x) j_b + C_1 j_a + C_2 j_b, \tag{58}$$

noting that $W(j_a, j_b) = -x$, where

$$A(x) = \int_0^x j_b A_0 \lambda x^3 dx, \quad B(x) = -\int_0^x j_a A_0 \lambda x^3 dx. \tag{59}$$

The boundary condition at $x = 0$ shows that $C_2 = 0$, and the normalization of F as $x \rightarrow 0$ implies that $k C_1 = 2A_0$. It remains to apply the boundary condition at $x = x_b$ which then yields λ (that is C). From equations (58), (59) one gets

$$F \approx A_0 x^2 \left(1 + \frac{\lambda x^4}{24}\right).$$

Note that to this order, F is independent of K where λ scales as x_b^{-4} so this small x_b approximation also requires that the constant λ also be very small. Similarly the right-hand side may be approximated by

$$K^2 x_b^2 (\gamma_0 + \ln(Kx_b/2))$$

where γ_0 is Euler's constant. This implies that to leading order

$$\lambda x_b^4 \approx -8. \tag{60}$$

But this is a bit too simple as can be seen from the consequent expression for

$$F \approx A_0 x^2 \left(1 - \frac{x^4}{3x_b^4}\right), \tag{61}$$

so that actually $F_x \approx 0$ at $x = x_b$, which is too simple. The higher-order terms in A and B can be found, and then we get that

$$F = A_0 \left(x^2 - \frac{1}{8} x^4 + \frac{1}{192} x^6 + \lambda \left[\frac{x^6}{24} + \frac{x^8}{128} - \frac{1}{72} K^2 x^8\right]\right).$$

We define $\frac{1}{8} \lambda x_b^4 + 1 = \varepsilon \ll 1$ and keeping the required next order terms we get that

$$\varepsilon = \frac{2}{3} K^2 x_b^2 \left[(\gamma_0 + \ln(Kx_b)) + \frac{1}{12}\right],$$

$$F = A_0 x^2 \left(1 - \frac{1}{8} x^2 - \frac{x^4}{3x_b^4} - \frac{x^6}{16x_b^4} + \frac{K^2 x^6}{9x_b^4} + \left[\frac{2K^2 x^4}{9x_b^2} \right] [\gamma_0 + \ln(Kx_b) + \frac{1}{12}] \right).$$

Figure 1: Plot of $F(x)/A_0$ against x/x_b , where A_0 is arbitrary as given by equation (61). The figure shows that there is only curve at leading order. We note that there is no dependence on the slope α and only a weak dependence on K . We observe that $F(x)$ reaches a maximum value of $F(x)/A_0 \approx 0.7$. Beyond this point

$F(x)$ may probably decrease monotonically.

Next for the y -independent component, we need to solve for $G(x)$ from (53). As above, we approximate $F = A_0 x^2$, and we use the empirical expression $F_0 = \gamma^2 h^2 / 8$. This yields

$$Z_{xx} - \frac{1}{x} Z_x - \alpha^2 x^2 CG = -\frac{5g\alpha^2\gamma^2}{16A_0x} \tag{62}$$

There is a singularity at $x = 0$, which can be analyzed by setting $u = x^2$ so that (62) becomes

$$4Z_{uu} - \lambda Z = -\frac{5g\alpha^3\gamma^2}{16A_0u^{3/2}}, \tag{63}$$

where we have put $\bar{\lambda} = -\lambda > 0$ and the full solution is

$$Z = \frac{5g\alpha^2\gamma^2x_b}{12A_0} \left(\frac{x}{x_b} - \frac{1}{\sin\sqrt{2}} \sin\left[\frac{\sqrt{2}x^2}{x_b^2}\right] \right) \tag{64}$$

Finally the complete the stream function $G(x)$ is found by integrating $G_x = hZ$ subject to the boundary condition that $G = 0$ at $x = x_b$. Thus we get that, for $0 < x < x_b$,

$$G(x) = \frac{5g\alpha^3\gamma^2x_b^3}{12A_0} \left(\frac{x^3}{3x_b^3} + \frac{1}{2\sqrt{2}\sin\sqrt{2}} \cos\left[\frac{\sqrt{2}x^2}{x_b^2}\right] - \frac{1}{3} - \frac{1}{2\sqrt{2}\tan\sqrt{2}} \right). \tag{65}$$

Note in particular that $G(0) \neq 0$ and is the net mean longshore mass transport in the rip current system.

Figure 2: Depicts the plots of normalized $Z(x)$ and $G(x)$ given by equations 64 and 65 where each is normalized by $5g\alpha^2\gamma^2x_b/12A_0$ and $5g\alpha^3\gamma^2/12A_0$ respectively with A_0 arbitrary. Observe that in the figure [2] there is a small region of reversed flow near the breaker line.

The combined expressions (56, 61, 65) complete the solution, where we recall that the constant C is given by (60) (since $\lambda = C\alpha^2$), or their respective higher-order corrections. Note that the amplitude of $F(x)$ at $x = x_b$ is given by

$$F(x_b) = C_1 x_b K_1(Kx_b).$$

On using the approximation $Kx_b \ll 1$, and the approximate expression (61), this reduces to

$$F(x_b) = \frac{2A_0x_b^2}{3} = \frac{C_1}{K}.$$

The rip-current system contains a free parameter A_0 or its equivalent. We choose to define this free parameter to be the value of $F(x_b)$ and normalize the full solution by this value. Thus we get from (40, 42) in $x > x_b$, and (45, 61, 65) in $x < x_b$ that the normalized streamfunction ψ_n is given by

$$\psi_n = \frac{X(x)}{X(x_b)} \sin(Ky), \quad \text{for } x > x_b, \tag{66}$$

$$\psi_n = \frac{F(x)}{F(x_b)} \sin Ky + R \frac{G(x)}{G(0)}, \quad \text{for } 0 < x < x_b. \quad (67)$$

Here $R = G(0)/F(x_b)$ is a free parameter. Thus a larger (smaller) R decreases the circulation of the rip-current system *vis-a-vis* that of the longshore current component. From (61, 65) we find that here

$$R = \frac{5g\alpha^3\gamma^2x_b}{8A_0^2} \left(-\frac{1}{3} - \frac{1}{2\sqrt{2}\tan\sqrt{2}} \right). \quad (68)$$

Note that with all other parameters fixed, a larger (smaller) slope α increases (decreases) R . In order to estimate typical values for R we note that from (61) the longshore velocity field in the “ $\sin(Ky)$ ”-component scales as $V_c = A_0/\alpha$, while the longshore component then scales with RV_c . Taking account of the actual numerical values in the expressions given above, we find that a suitable values are $R \approx -0.1$. Plots of ψ_n are shown in figures 3, ??, 4 for $R = -0.02, -0.1, -0.2, -0.5, -2$ respectively, with $Kx_b = 0.2$ (noting that our present theory requires that Kx_b is small).

Figure 3: Plot of the rip current streamlines for a linear depth profile, given by equation (67) where $F(x)$ and $G(x)$ are equations (61) and (65) respectively for $R = -0.02$ in the left panel and $R = -0.1$ in the right panel

Figure 4: As for figure 3 but $R = -0.5$ in the left panel and $R = -0.2$ in the right panel

From the plots in figures 3, ?? we see that as $|R|$ increases, the core of the rip current circulation moves from the shoaling zone towards the surf zone. The reason for this is that the solution we have constructed is essentially a free vortex defined by $X(x)\sin Ky$ in the shoaling zone $x > x_b$, and $F(x)\sin Ky$ in the surf zone $x < x_b$, perturbed by a longshore component $G(x)$ in the surf zone. Since $R < 0$, this longshore component opposes the vortex flow in the cell $0 < Ky < \pi$ but is in sympathy for $\pi < Ky < 2\pi$. This has the effect of moving the vortex cell further offshore in the sector $\pi < Ky < 2\pi$ relative to the sector $0 < Ky < \pi$. Note that $|R|$ increases as the wave forcing increases, or as the slope α increases, or as the depth αx_b at the breaker line increases.

V. CONCLUSION

We described qualitative solutions for rip currents which are essentially free vortices in both zones. The free vortex in the surf zone is perturbed by a longshore modulation in the wave forcing. Rip current cell combining with the longshore modulation in the wave forcing can drive longshore currents along the beach. Thus the dynamics of the shoaling zone is only dependent on the state-state wave energy equation. The wave forcing in the surf zone sets the wave activities different from those of the shoaling zone. To determine wave forcing in the mean vorticity equation we assume that the wave angle becomes smaller. We also note here that the component of the radiation stress in the y momentum remains unchanged across the entire flow domain. This shows that it is only the x component of the radiation stress that play a leading role in the wave forcing. However, wave forcing encountered in the surf zone has an unmodulated term that *does not play a role* in the vorticity equation but only contribute to wave setup. To ensure continuity of the streamfunctions in the shoaling zone we match the solution at the breakerline by a matching condition with appropriate boundary conditions. Thus the rip currents solution in the surf zone is provided by the terms in the matching condition. The terms in the matching condition has a cross-shore width and a modulated longshore component. The cross-shore width was determined by the application of perturbation method and variation of parameter. It would to interesting to examine the effect of friction on the rip currents.

REFERENCES

- [1] Baldock, T.E, (2006), Long wave generation by the shoaling and breaking of transient wave groups on a beach, *Proceedings of the Royal society*, vol.462, pp 1853-1876.

- [2] Baldock, T.E., O'Hare, T.J. & Huntley, D.A. (2004), Long wave forcing on a barred beach, *Journal of Fluid Mechanics*, vol 503, pp. 321-343.
- [3] Battjes, J. A., (1988), Surf zone dynamics, *Annual Rev. Fluid Mechanics*, vol. 20, pp.257-293.
- [4] Billingham, J & King, A.C., (2000), *Wave Motion- Cambridge Texts in Applied Mathematics*, Cambridge University Press.
- [5] Brocchini, M., Kennedy, A., Soldini, L & Mancinelli, A., (2004) Topographically controlled, breaking-wave-induced macrovortices. Part 1. Widely separated breakwaters, *J. Fluid Mechanics*, vol. 507, pp. 289-307.
- [6] Buhler, O., (2000), On the vorticity transport due to dissipating or breaking waves in shallow-water flow, *Journal of Fluid Mechanics*, vol 407, pp 235-263.
- [7] Buhler, O. & Jacobson, T. E., (2001), Wave-driven currents and vortex dynamics on barred beaches, *Journal of Fluid Mechanics*, vol 449, pp 313-339.
- [8] Damgaard, J., Dodd, N., Hall, L. & Chesher, T., (2002), Morphodynamic modelling of rip channel growth, *Coastal Engineering*, vol.45, pp 199-221.
- [9] Davies, A. M. & Lawrence, J. (1995), Modelling the effect of wave-current interaction on the three-dimensional wind driven circulation of the Eastern Irish Sea, *Journal of Physical Oceanography*, vol. 25, pp. 29-45.
- [10] Falques, A., Calvete, D. & Monoto, A. (1998a), Bed-flow instabilities of coastal currents. In *Physics of Estuaries and Coastal Seas*, pp. 417- 424. A. A. Balkema.
- [11] Falques, A., Montoto, A. & Vila, D. (1999), A note on hydrodynamic instabilities and horizontal circulations in the surf zone, *Journal of Geophysical Research*, vol. 104(C9), pp 20605-20615
- [12] Falques, A., Coco, G & Huntley, D.A (2000), A mechanism for the generation of wave-driven rhythmic patterns in the surf zone, *Journal of Geophysical Research*, vol. 105, No. C10, pp 24701-20615.
- [13] Guza, R. T. & Davis, R. E. (1974), Excitation of edge waves by waves incident on a beach, *Journal of Geophysical Research*, vol. 79, C9, pp. 1285-1291.
- [14] Horikawa, K (1978), *An Introduction to Ocean Engineering*, University of Tokyo Press.
- [15] Kennedy, A.B. (2003), A circulation description of a rip current neck, *Journal of Fluid Mechanics*, vol. 497, pp. 225-234
- [16] Kennedy, A.B. (2005), Fluctuating circulation forced by unsteady multidirectional breaking waves, *Journal of Fluid Mechanics*, vol. 538, pp. 189-198
- [17] Kennedy, A.B., Brocchini, M., Soldini, L., & Gutierrez, E., (2006), Topographically controlled, breaking-wave-induced macrovortices. Part 2. Changing geometries, *J. Fluid Mechanics*, vol. 559, pp. 57-80.
- [18] Lane, E.M & Restrepo, J.M (2007), Shoreface-connected ridges under the action of waves and currents, *Journal of Fluid Mechanics*, vol. 582, pp. 23-52
- [19] Lascody, L. L (1998), East central Florida rip current program, *National Weather Digest*, vol. 22, pp. 25-30.
- [20] List, J.H. (1992), A model for the generation of two dimensional surf beat, *Journal of Geophysical Research*, vol. 97, pp. 5623-5635.
- [21] Longuet-Higgins, M.S. (1970), Longshore currents generated by obliquely incident sea waves, 1, *J. Geophysical Research*, vol. 75, pp 6778-6789.
- [22] Longuet-Higgins, M.S. (1970), Longshore currents generated by obliquely incident sea waves, 2, *J. Geophysical Research*, vol. 75, pp 6790-6801.
- [23] Longuet-Higgins, M.S & Stewart, R.W. (1960), The changes in the form of short gravity waves on long waves and tidal currents, *Journal of Fluid Mechanics*, vol. 8, pp 565-583
- [24] Longuet-Higgins, M.S & Stewart, R.W. (1961), The changes in amplitude of short gravity waves on on steady non-uniform currents, *Journal of Fluid Mechanics*, vol. 10, pp 529-5549
- [25] Longuet-Higgins, M.S & Stewart, R.W. (1962), Radiation stress and mass transport in gravity waves, with application ro surf beats, *Journal of Fluid Mechanics*, vol. 13, pp 481-504
- [26] Longuet-Higgins, M.S & Stewart, R.W. (1964), Radiation stress in water waves: a physical discussion with applications, *Deep-sea Research*, vol. 11, pp. 529-562.
- [27] Longuet-Higgins, M.S. (2005), On wave set-up in shoaling water with a rough sea bed, *Journal of Fluid Mechanics*, vol. 527, pp. 217-234
- [28] Mei, C.C. (1983), *Applied Dynamics of Ocean Surface Waves*, John Wiley and Sons, Inc.
- [29] Osaisai, E. F (2008), *The interaction between waves and currents in the nearshore zone*, PhD thesis, Loughborough University.
- [30] Peregrine, D.H. (1998), Surf zone currents, *Theoretical and Computational Fluid Dynamics*, vol. 10, pp 295-309.
- [31] Rahman, M. (2002), *Mathematical methods with applications*, WITPress, Southampton.
- [32] Restrepo, J. M. (2001), Wave-current interactions in shallow waters and shore-connected ridges, *Continental Shelf Research*, vol. 21, pp. 1331-1360.
- [33] Roger Grimshaw and Evans Osaisai (2012), Modeling the effect of bottom sediment transport on beach profiles and wave set-up, *ocean Modelling*, 59-60 (2012) 24-30
- [34] Shepard, F. P., Emery, K. O. & La Fond, E. C (1941), Rip currents: a process of geological importance, *Translation of American Geophysical Union*, vol. 31, pp. 555-565.
- [35] Tucker, M.J., (1950), Surf beats: sea waves of 1 to 5 min. period, *Proc. R. Soc. London*, vol. 202, pp. 565-573.
- [36] Yu, J. & Mei, C.C. (2000), Formation of sand bars under surface waves, *Journal of Fluid Mechanics*, vol. 416, pp. 315 - 348.
- [37] Yu, J. & Mei, C.C. (2000), Do longshore bars shelter the shore?, *Journal of Fluid Mechanics*, vol. 404, pp. 251 - 268.
- [38] Yu, J. & Slinn, D.N. (2003), Effects of wave-current interaction on rip currents, *Journal of Geophysical Research*, vol 108 (C3), 3088.
- [39] Yu, J. (2006), On the instability leading to rip currents due to wave-current interaction, *Journal of Fluid Mechanics*, vol. 549, pp. 403-428.

A Novel Marker Based Interactive Image Segmentation Method

¹K Vani Sree , ² A Vanaja

¹M.Tech, student , ²Asst.Professor

^{1,2}SRK Institute of Technology
Enikepadu, Vijayawada ,AP ,India

ABSTRACT

An important branch of computer vision is image segmentation. Image segmentation aims at extracting meaningful objects lying in images either by dividing images into contiguous semantic regions, or by extracting one or more specific objects in images such as medical structures. The image segmentation task is in general very difficult to achieve since natural images are diverse, complex and the way we perceive them vary according to individuals. For more than a decade, a promising mathematical framework, based on variational models and partial differential equations, have been investigated to solve the image segmentation problem. The proposed scheme is simple yet powerful and it is image content adaptive. With the similarity based merging rule, a two stage iterative merging algorithm was presented to gradually label each non-marker region as either object or background. We implemented the MSRM algorithm in the MATLAB.

I. INTRODUCTION

This new approach benefits from well-established mathematical theories that allow people to analyze, understand and extend segmentation methods. Moreover, this framework is defined in a continuous setting which makes the proposed models independent with respect to the grid of digital images. In color image segmentation seed selection, region growing and region merging are important stages. It should be noted that there is no single standard approach to perform seed selection, region growing, and region merging for color image segmentation. The appropriate technique is select on the basis of type of image and applications. Ugarriza *et al.* proposed a technique of initial seed selection. This technique uses vector field for edge detection and RGB to L*a*b conversion of image pixels to calculate the threshold by using adaptive threshold generation method. This method uses approximate calculation of threshold. The problem is that approximate calculation does not lead proper conclusion.

II. IMAGE SEGMENTATION

The problems of image segmentation and grouping remain great challenges for computer vision. Since the time of the Gestalt movement in psychology, it has been known that perceptual grouping plays a powerful role in human visual perception. A wide range of computational vision problems could in principle make good use of segmented images, were such segmentations reliably and efficiently computable. For instance intermediate-level vision problems such as stereo and motion estimation require an appropriate region of support for correspondence operations. Spatially non-uniform regions of support can be identified using segmentation techniques. Higher-level problems such as recognition and image indexing can also make use of segmentation results in matching, to address problems such as figure-ground separation and recognition by parts. Our goal is to develop computational approaches to image segmentation that are broadly useful, much in the way that other low-level techniques such as edge detection are used in a wide range of computer vision tasks.

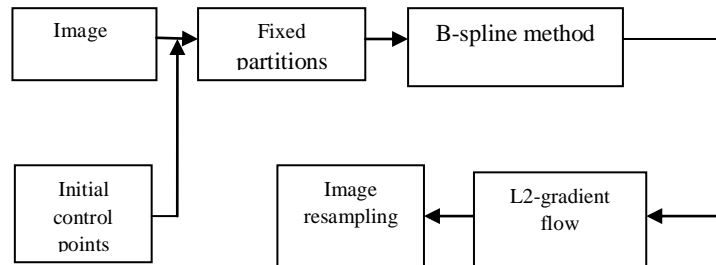
- Thresholding
- Edge finding
- Seed region growing
- Region split and merging

In the analysis of the objects in images it is essential that we can distinguish between the objects of interest and "the rest." This latter group is also referred to as the background. The techniques that are used to find the objects of interest are usually referred to as *segmentation techniques* , segmenting the foreground from background. In this section we will present two of the most common techniques *thresholding* and *edgefinding* and techniques for improving the quality of the segmentation result. It is important to understand that: there is

no universally applicable segmentation technique that will work for all images, and no segmentation technique is perfect.

III. GEOMETRIC FLOW METHOD

The block diagram of geometric flow method as shown below



Geometric flows, as a class of important geometric partial differential equations, have been highlighted in many areas, with Computer Aided Geometric Design is probably the field that benefited most from geometric flow methods. The frequently used geometric flows include mean curvature flow (MCF), weighted MCF, surface diffusion flow and Willmore flow etc. Different flows exhibit different geometric properties that could meet the requirement of various applications. The biharmonic equation, which is linear, has been used for interactive surface design. MCF and its variants, which are second order equations and also the most important and effective flows, have been intensively used for fairing and denoising surface meshes. MCF cannot achieve the G^1 continuity at the boundary, thus for applications demanding high level of smoothness, higher order equations have to be used, e.g. the surface diffusion flow for surface fairing, and the Willmore flow for surface restoration, The construction of geometric flows is not a trivial task. In early days many geometric flows were manually manufactured by combining several geometric entities and differential operators, thus were lack of physical or geometric meaning. This drawback can be overcome by the construction of gradient descent flow. Gradient descent flow method can transform an optimization problem into an initial value (initial-boundary value) problem of an ordinary differential equation and thus is widely used in variational calculus. Constructing gradient descent flow needs to address two main issues, the definition of gradient and suitable choice of inner products. For a generic nonlinear energy functional, the gradient can be defined by G^* ateaux derivative. For the same energy functional, different inner products will generate different geometric flows, some of which have been mentioned above.

IV. MARKER BASED SEGMENTATION

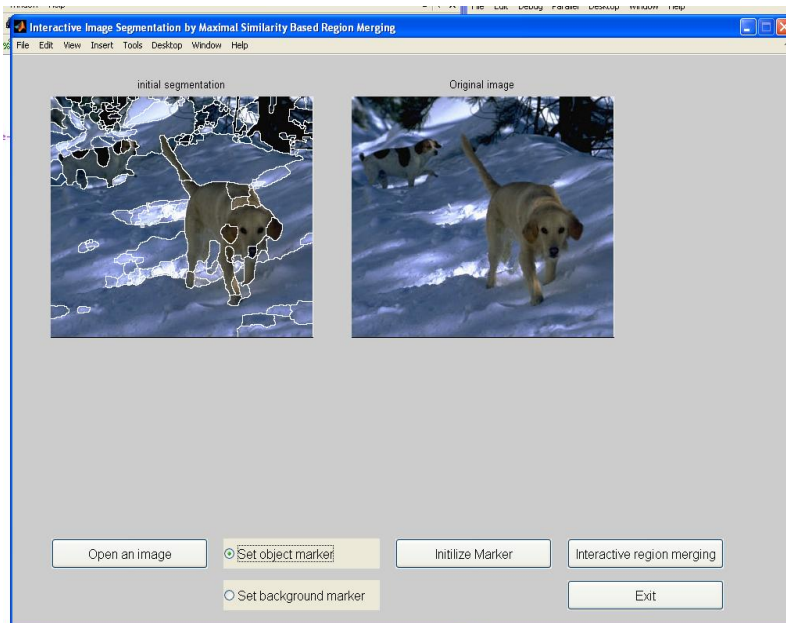
Efficient and effective image segmentation is an important task in computer vision and object recognition. Since fully automatic image segmentation is usually very hard for natural images, interactive schemes with a few simple user inputs are good solutions. This paper presents a new region merging based interactive image segmentation method. The users only need to roughly indicate the location and region of the object and background by using strokes, which are called markers. A novel maximal-similarity based region merging mechanism is proposed to guide the merging process with the help of markers. A region R is merged with its adjacent region Q if Q has the highest similarity with R among all Q 's adjacent regions. The proposed method automatically merges the regions that are initially segmented by mean shift segmentation, and then effectively extracts the object contour by labeling all the non-marker regions as either background or object. The region merging process is adaptive to the image content and it does not need to set the similarity threshold in advance.

Extensive experiments are performed and the results show that the proposed scheme can reliably extract the object contour from the complex background. In marker based segmentation, an initial segmentation is required to partition the image into homogeneous regions for merging. Any existing low level segmentation methods, such as super-pixel [13], meanshift [14,15], watershed [16] and level set [17], can be used for this step. In this paper, we choose to use the mean shift method for initial segmentation because it has less over segmentation and can well preserve the object boundaries. Particularly, we use the mean shift segmentation software—the EDISON System [18]—to obtain the initial segmentation map.

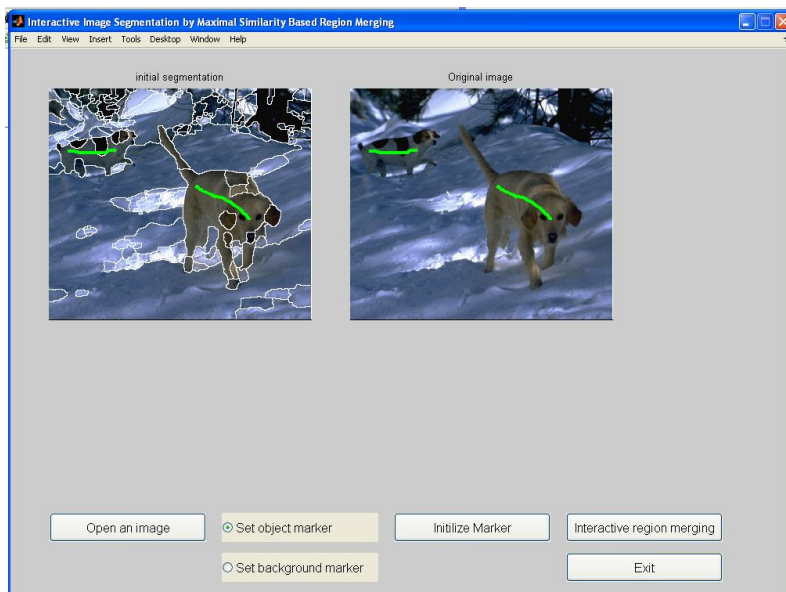
For detailed information about mean shift and the EDISON system, please refer to [19]. In this method, we only focus on the region merging. Several general-purpose algorithms and techniques have been developed for image segmentation. Since there is no general solution to the image segmentation problem, these techniques often have to be combined with domain knowledge in order to effectively solve an image segmentation problem for a problem domain.

V. EXPERIMENTAL RESULTS

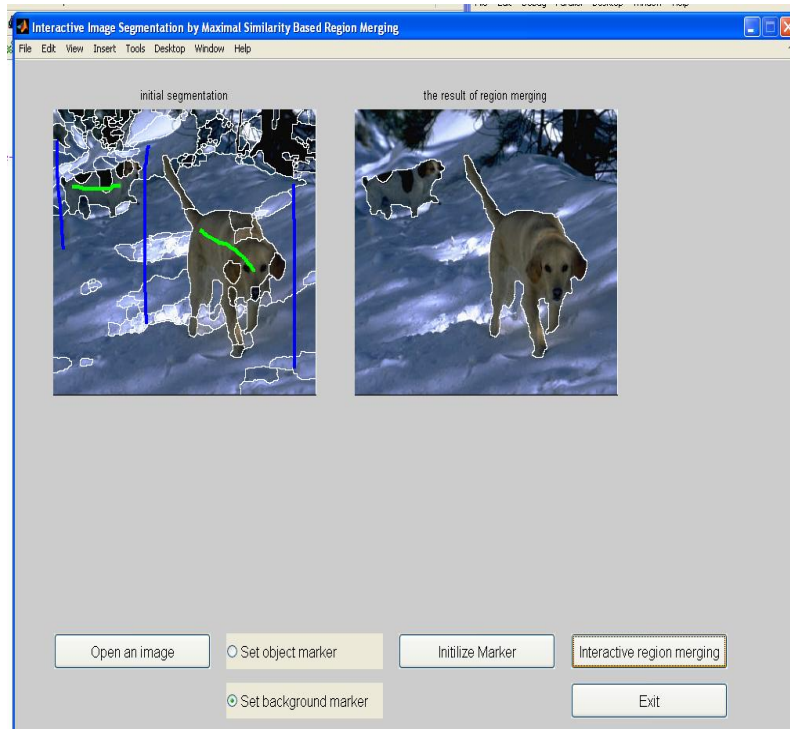
The execution time of the MSRM depends on a couple of factors, including the size of the image, the initial segmentation result, the user input markers and the content of the image. We implement the MSRM algorithm in the MATLAB 7.0 programming environment and run it on a PC with P4 2.6GHz CPU and 1024MB RAM.



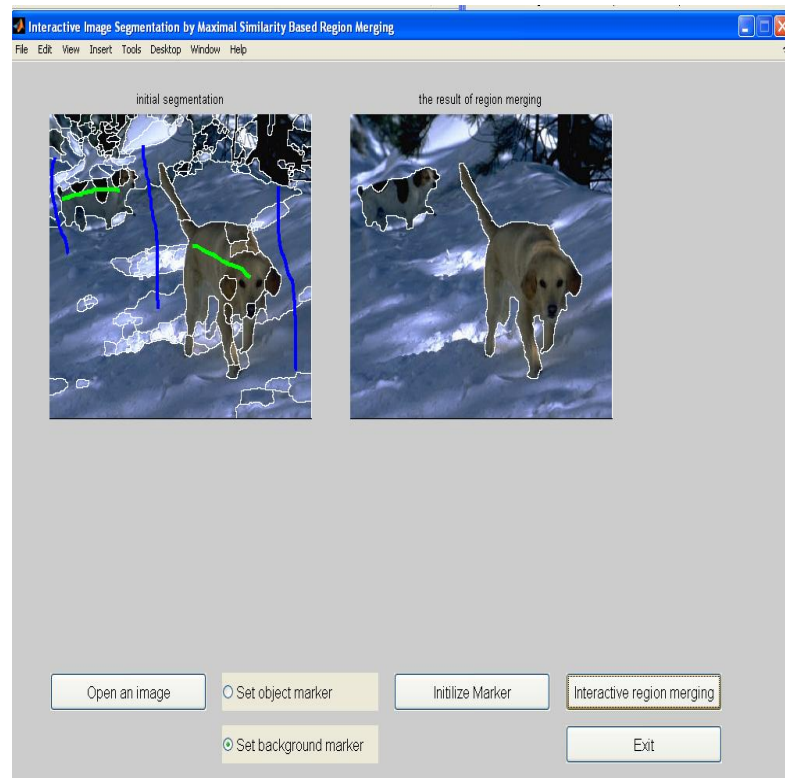
Click the set object marker radio button



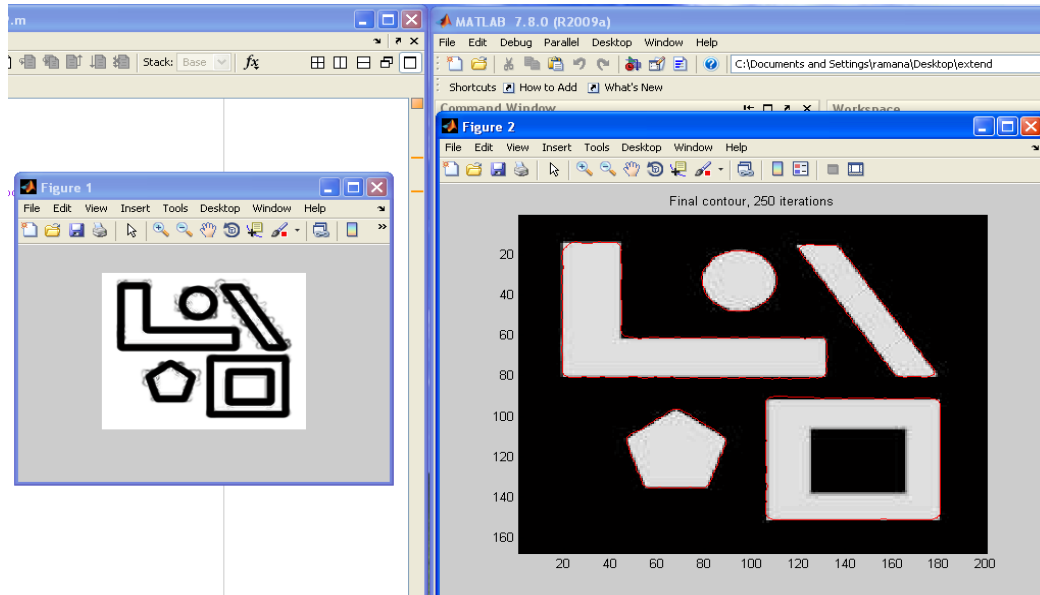
Mark the straight lines on dog objects



Click the set background marker radio button and then straight line(blue line) edges of dog objects and then click interactive region merging



Multiple object extraction: (a) initial mean shift segmentation and interactive information. The two green markers mark two objects. (b) The two extracted objects using the marker based segmentation method.



a) original image b) final segmentation result using geometric flow approach method

VI. CONCLUSION

This paper proposed a novel marker based interactive image segmentation method. The image is initially segmented by mean shift segmentation and the users only need to roughly indicate the main features of the object and background by using some strokes, which are called markers. Since the object regions will have high similarity to the marked object regions and so do the background regions, a novel maximal similarity based region merging mechanism was proposed to extract the object. The proposed scheme is simple yet powerful and it is image content adaptive. With the similarity based merging rule, a two stage iterative merging algorithm was presented to gradually label each non-marker region as either object or background.

REFERENCES

- [1] Chaobing Huang, Quan Liu, "Color image retrieval using edge and edge-spatial features", Chinese Optics Letters 2006, vol.4,no. 8,pp.457-459.
- [2] Luis Ugarriza, Eli saber, "Automatic Image Segmentation by Dynamic Region Growth and Multiresolution Merging" IEEE Transactions On Image Processing ,vol .18no 10):2001
- [3]. J. Fan, David, K. Y. Yau, A. K. Elmagarmid. "Automatic Image Segmentation by Integrating Color-Edge Extraction and Seeded Region Growing". IEEE Transactions On Image Processing, vol.10,no.10:oct2001
- [4]. H.D. Cheng, X.H. Jiang, J. Wang, Color image segmentation based on homogram thresholding and region merging, Pattern Recognition 35 (2002) 373–393.
- [5]. P.K. Saha, J.K. Udupa, Optimum image threshold via class uncertainty and region homogeneity, IEEE Transactions on Pattern Analysis and Machine Intelligence , vol.23, no.7 (2001) 689–706.
- [6]. R. Haralick and L.Shapiro Computer and Robot Vision. New York:Addison-Wesley, 1992, vol. 1, pp. 28–48.
- [7]. T. Cover and J.Thomas, Elements of Information Theory. New York: Wiley, 1991.
- [8]. C. Chou and T. Wu, "Embedding color watermarks in color images," EURASIP J. Appl. Signal Process., vol. 2003, no. 1, pp. 32–40, Oct.2003.
- [9]. Y. J. Zhang, "A survey on evaluation methods for image segmentation," Pattern Recognit. Soc., vol. 29, no. 8, pp. 1335–1346, 1996.
- [10]. R. Adams, L.Bischof, Seeded region growing, IEEE Transactions on Pattern Analysis and Machine Intelligence 16 (6) (1994) 641–647.
- [11]. Schmid, P.: Image segmentation by color clustering, <http://www.schmid-saugeon.ch/publications.html>, 2001
- [12]. Digital Image Processing , R.C. Gonzalez, R.E. Woods, S.L. Eddins.
- [13] Q. Yang, C. Wang, X. Tang, M. Chen, Z. Ye, Progressive cut: an image cutout algorithm that models user intentions, IEEE Multimedia 14 (3) (2007) 56–66.
- [14] M. Sonka, V. Hlavac, R. Boyle, Image Processing, Analysis and Computer Vision, Thomson, 2007.
- [15] B. Sumengen, Variational image segmentation and curve evolution on natural images, Ph.D. Thesis, University of California.
- [16] EDISON software. <http://www.caip.rutgers.edu/riul/research/code.html>.
- [17] Y. Li, J. Sun, C. Tang, H. Shum, Lazy snapping, SIGGRAPH 23 (2004) 303–308.
- [18] Y. Li, J. Sun, H. Shum, Video object cut and paste, SIGGRAPH 24 (2005) 595–600.
- [19] S. Paris, F. Durand, A topological approach to hierarchical segmentation using mean shift, in: Proceedings of the IEEE Conference on Computer Vision and Pattern Recognition, 2007, pp. 1–8.

- [20] A. Levin, A. Rav-Acha, D. Lischinski, Spectral matting, *IEEE Transactions on Pattern Analysis and Machine Intelligence* 30 (10) (2008) 1699–1712.
- [21] R. Carsten, K. Vladimir, B. Andrew, “Grabcut”: interactive foreground extraction using iterated graph cuts, *SIGGRAPH* 23 (2004) 309–314.
- [22] P. Meer, Stochastic image pyramids, *Computer Vision, Graphics, and Image Processing (CVGIP)* 45 (3) (1989) 269–294.
- [23] J.M. Jolion, The adaptive pyramid: a framework for 2D image analysis, *Computer Vision, Graphics, and Image Processing (CVGIP): Image Understanding* 55 (3) (1992) 339–348.
- [24] A. Blake, C. Rother, M. Brown, P. Perez, P. Torr, Interactive image segmentation using an adaptive GMMRF model, in: *Proceedings of the European Conference on Computer Vision*, 2004, pp. 428–441.
- [25] K. Fukunaga, *Introduction to Statistical Pattern Recognition*, second ed., Academic Press, 1990.
- [26] M.J. Swain, D.H. Ballard, Color indexing, *International Journal of Computer Vision* 7 (1) (2002) 11–32.
- [27] D. Comaniciu, V. Ramesh, P. Meer, Kernel-based object tracking, *IEEE Transactions on Pattern Analysis and Machine Intelligence* 25 (5) (2003) 564–577.
- [28] X. Ren, J. Malik, Learning a classification model for segmentation, *ICCV03*, vol. 1, pp. 10–17, Nice, 2003.

Design of low power fir filter technique with booth multiplier and delay buffer

¹Gummadi.Lakshmi Pratap , ²P.suresh

M.Tech student,Professor

*Dept of ECE,Sri Sunflower college og Engg.&Technology
Challapalli, Krishna (D), A.P - 521131*

ABSTRACT

This paper presents the methods to reduce dynamic power consumption of a digital Finite Impulse Response (FIR) filter. These methods include low power serial adder, combinational booth multiplier and low-power delay buffer. The proposed delay buffer uses several new techniques to reduce its power consumption. Since delay buffers are accessed sequentially, it adopts a ring-counter addressing scheme. In the ring counter, double-edge-triggered (DET) flip-flops are utilized to reduce the operating frequency by half and the C-element gated-clock strategy is proposed. A novel gated-clock-driver tree is then applied to further reduce the activity along the clock distribution network. Moreover, the gated-driver-tree idea is also employed in the input and output ports of the memory block to decrease their loading, thus saving even more power. Folding transformation in linear phase architecture and applied to FIR filters to power consumption reduced thus reduce power consumption due to glitching is also reduced. The proposed FIR filters were synthesized implemented using Xilinx ISE Virtex IV FPGA and power is analyzed using Xilinx XPower analyzer.

I. INTRODUCTION

Multipliers are one of the most important arithmetic units in microprocessors and DSPs and also a major source of power dissipation. Reducing the power dissipation of multipliers is key to satisfying the overall power budget of various digital circuits and systems. If multiplication of two 8-bit numbers is performed, then the result is 16-bit. To produce that result array multiplication generates 8 partial products. NOR gates can also be used instead of AND in accordance with the De Morgan's Law:

$$A.B = (A' + B')$$

The proposed work is MAC FIR filter based BOOTH multiplier which reduces the number of partial products by half compared to a traditional implementation. Using the pass logic based implementations; the number of transistors was reduced, resulting in hardware-reduced and consequently power-aware designs. This multiplier has two stages. In the first stage, the partial products are generated by the Booth encoder and the partial product generator (PPG), and are summed by compressors. In the second stage, the two final products are added to form the final product through a final adder [3]. The booth encoder reduces the generation of number of partial products there by reducing power. The objective of the project is to design and implement the FIR filter which consumes less power. To achieve the requirements a low power booth multiplier, adder and delay buffer are used. Along with the low power consumption the proposed technique also increases the speed.

II. BOOTH MULTIPLIER

One of the solutions of realizing high speed multipliers is to enhance parallelism which helps to decrease the number of subsequent calculation stages there by reducing the power consumption.

2.1.Delay Buffer

A serial access memory is needed in temporary storage of signals that are being processed (i.e. delay buffer). Currently, most circuits adopt static random access memory (SRAM) plus some control/addressing logic to implement delay buffers and it is shown in below Figure.

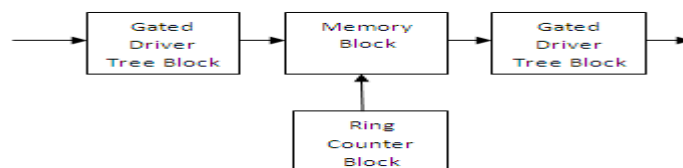


Fig System development

2.2.Implementation

The realization of FIR filters can be accomplished by using the following design procedure

1. Choose filter structure
2. Choose number representation, e.g. signed magnitude, two's compliment
3. Implement software code, or hardware circuit, which will perform actual filtering.
4. Verify the simulation that the resulting design meets given performance specifications.

A simple low pass filter is designed. Any filter specifications can be specified but for the sake of simplicity the following specifications are used in this thesis. Hanning windowing technique is used to generate the finite impulse response of the filter. Filter coefficients are generated by using the Matlab.

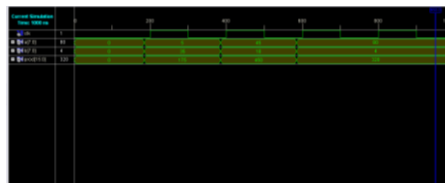
2.3.Simulation results

FIR filter using Array Multiplier

In implementing the FIR filter using Array Multiplier there are various blocks. They are the array multiplier, full adder, 16-bit adder. In this project all the blocks are simulated using Xilinx simulator.

2.4. Multiplier

The below Figure shows the output waveform of an array multiplier with different inputs (i.e., a, b) and outputs (i.e., prod). Here the multiplier (5, 45, 80) and multiplicand (35, 10, 4) both are 8-bit and the final product (175, 450, 320) is 16-bit.



2.5.Full Adder

The full adder consists of three inputs (i.e., a, b, c) and it produces two outputs (i.e., sum, carry) and its corresponding output waveforms are shown in below Figure.

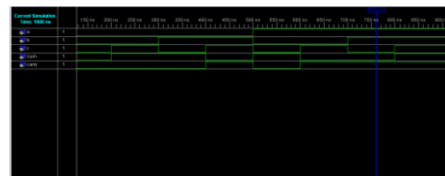


Fig: Output waveform of Full Adder

2.6.16-bit adder

In this project the 16-bit ripple adder is used and it consists of 16 full adders which adds two 16-bit numbers (a, b) and produces two outputs one is sum (here it is y_{out}) of 16-bit and carry (here it is c_{out}) of 1-bit. The corresponding simulated waveforms are shown in below Figure. For example the two 16-bit numbers taken are 33, 43 and its sum is 76 with a carry 0. The ripple adder is shown in below Figure. It consists of the result for the various inputs also.

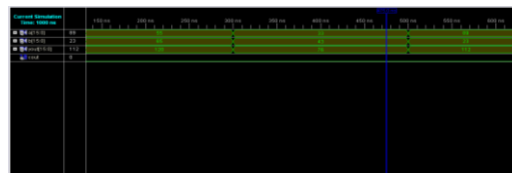


Fig: 16-bit Adder

2.7.FIR filter using Array Multiplier

In the design of FIR filter using array multiplier five inputs are taken (X_1, X_2, X_3, X_4, X_5) and the single output (Y), the output responds to the inputs in synchronous with the clock signal and it is shown in below Figure.

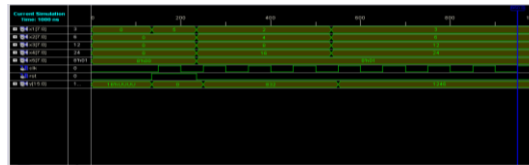


Fig: FIR filter using Array Multiplier

2.8.FIR filter using BOOTH Multiplier

In implementing the FIR filter using Booth Multiplier there are various blocks. The BOOTH multiplier, BOOTH encoder, full adder, 16-bit adder are the various blocks. The outputs of full adder and 16-bit adder are same as the implementation in array multiplier.

2.9.BOOTH Encoder

Booth encoder encodes the given multiplicand depending on the multiplier bits. In this depending on the arg, the input 'a' is encoded and its result 'pprod' is shown in Figure.

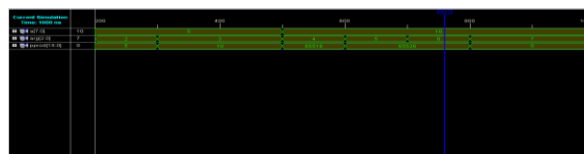


Fig: Output waveform of BOOTH Encoder

2.10.BOOTH Multiplier

It performs multiplication operation depending on the encoded value. Here the inputs are 'a','b' both are 8-bit and it produces result of 16-bit Y_{out} . It also indicates overflow (ovf) if the result exceeds the 16-bit, it is shown in Figure.

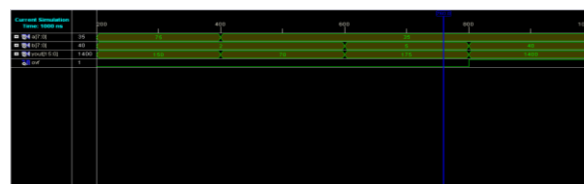


Fig: BOOTH Multiplier

2.11.FIR filter using Booth Multiplier

The filter design contains 5 inputs (X1, X2, X3, X4, X5) according to the specifications. If asynchronous input 'rst' is equal to '1', then the output 'Y' equal to '0'. Otherwise the output responds to the inputs in accordance with the synchronous input 'clk' and is shown in Figure

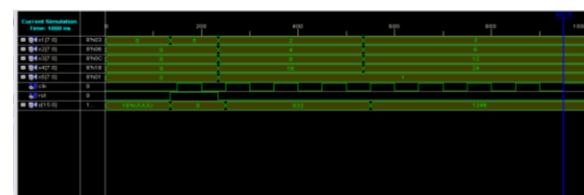


Fig: Output waveform of FIR filter using Booth Multiplier

2.12.Delay Buffer

Delay Buffer consists of the ring counter, gated driver tree, memory block. The ring counter consists of Dual Edge Triggered flip flop, c-element, gated clock.

2.13.C-Element

The output (c_out)of the c-element does not changes when both the inputs (a, b) are not same and it is equal to the input when they are same and it is shown in Figure.

The above figures shows the device utilization summary of both the techniques. FIR filter using booth multiplier utilizes less number of devices when compared with the FIR filter using array multiplier, eg., the number of 4 input LUT's required is 2648 for the present technique where as later one requires 3177 out off 98304 LUT's. Similarly the different devices occupied are also less for FIR filter design using booth multiplier. The maximum frequency of the FIR filter design using booth multiplier is 122.763MHz and it is 120.179MHz for the previous technique. Therefore speed also increases with the new technique. There are so many parameters for comparison but here only 5 are considered. As shown in the figure the no. of LUT's used, the no. of multiplexers used and the no. of occupied slices are less for FIR filter design using booth multiplier so that this technique consumes less power when compared with the FIR filter using array multiplier technique and the maximum frequency is also more the new technique when compared with the other one. With this the minimum delay for each operation is reduced so that speed also increases.

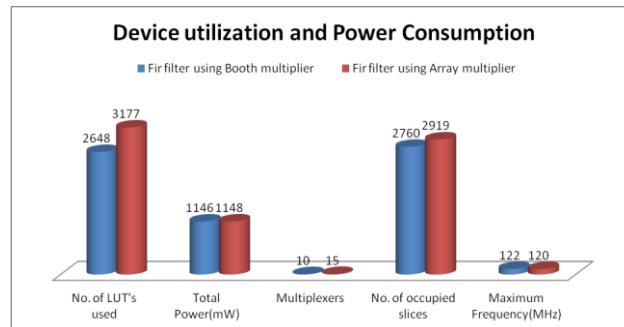


Fig: Performance chart of FIR filter using Booth and Array multiplier for LPF

III. CONCLUSION

In this project, results shows that FIR filter using booth multiplier employs the booth encoder and it generates less number of partial products than the implementation of the FIR filter using the array multiplier. For storing the filter coefficients delay buffer is used to reduce the power. Therefore speed also increases with the new technique. From the results, one can conclude that FIR filter using booth multiplier is the best method and consumes less power.

- [1] Bahram Rashidi, Majid Pourormazd, "Design And Implementation Of Low Power
- [2] Digital FIR Filter Based On Low Power
- [3] Multipliers And Adders On Xilinx FPGA",
- [4] IEEE conference on electronic computer technology (ICECT), Volume 2, 2011.
- [5] Po-Chun Hsieh, Jing-Siang Jhuang, Pei-Yun

REFERENCES

- [1] Tsai, Tzi-Dar Chiueh, "A Low-Power Delay Buffer Using Gated Driver Tree", IEEE
- [2] Transactions On Very Large Scale Integration
- [3] (VLSI) Systems, Vol. 17, No. 9, September 2009
- [4] Thankachan, Shibi, "64 x 64 Bit Multiplier Using Pass Logic" Computer Science Theses, 2006.
- [5] Nam-Phuong D. Nguyen, Hiroyuki Kuwahara, Chris J. Myers, James P. Keener, "The Design of a Genetic Muller C-Element", Async07, March 2006.
- [6] Mirzaei S., Hosangadi A. and Kastner R., "FPGA Implementation of High Speed FIR Filters Using Add and Shift Method", International Conference on Computer Design (ICCD), pp 308-313, 2006
- [7] Jones, D. L., "FIR Filter Structures", Version 1.2: Oct 10, 2004.
- [8] Ronak Bajaj, Saransh Chabra, Sreehari Veeramachaneni, M B Srinivas, "A Novel, Low-Power Array Multiplier Architecture", 2002.
- [9] Yun-Nan Chang, Jhan H. Satyanarayana, and Keshab K. Parhi, "Design And Implementation Of Low Power Digital Serial Multipliers", circuits and systems, 1998.
- [10] Massoud Pedram, Qing Wu, Xunwei Wu, "A New Design for Double Edge Triggered Flip-flops", IEEE, 1998.
- [11] Prokis J. G., Manolakis D. G., "Digital Signal Processing", 4th Edition, PHI publication.
- [12] Vallavraj & Salivhanan, "Digital Signal Processing", TMH publications.
- [13] M. Morris Mano, "Digital design", PTR publications.
- [14] J. Bhasker, "VHDL Primer", 3rd edition, PB publications.

Policyholder's Satisfaction of Private Life Insurance Companies With Reference To Tirupur District, Tamilnadu

Dr.N.Kathirvel* and S.Radhamani**

*Assistant Professor, Department of Commerce, Govt Arts College, Udamalpet

**Ph.D. (P.T), Scholar, Department of Commerce, Karpagam University, Coimbatore

ABSTRACT

The Insurance industry forms an integral part of the Indian financial market, with insurance companies being significant institutional investors. In recent decades, the insurance sectors, like other financial services, have grown in economic importance. The insurance sector, along with other elements of marketing, as well as financial infrastructure, have been touched and influenced by the process of liberalization and globalization in India, every company is trying to implement new creations and innovative product characteristics to attract the entry of private players, the competition is becoming intense. Today numerous public and private insurance companies are providing Life Insurance Services to a large number of clientele and there has been mushroom growth in their numbers and size in India. There is a transition from "sellers market" to "buyers market". The efficiency of insurance sector depends upon how best it can deliver services to its target customers and how far expectations of customers are met. The major objectives of this research are to ascertain the socio-economic profile of sample respondents and identify the determinants of satisfaction of policyholders in private life insurance companies. Methodology of this study is based on the analysis of the data collected from three hundred individual policy holders by using interview schedule method. The interview schedule was kept respondent friendly to make a quality of questionnaire. Interview schedule was the main tool used to collect the pertinent data from the selected sample respondents. Primary data has been collected for this present study. The primary data was collected from three hundred sample respondents from Tirupur district, by adopting simple random sampling method. Through the analysis of the study, it is identified that Marital Status and Number of Policies are found to be associated with policy holder's satisfaction. To conclude this study, is an attempt to measure the various parameters as perspective by the policy holders and to help the insurance company in serving its policy holders in a much better and efficient manner.

KEY WORDS: life Insurance, Policyholder's Satisfaction, mobilization of funds.

I. INTRODUCTION

This section includes introduction to the financial service industry and also establish the need of customer satisfaction in financial services in life insurance service in particular. Companies involved in the insurance industry offer a wide variety of products and supplementary services that consumers in need of insurance coverage could readily infer as being "insurance" related. The financial service industry has not been immune from, or ignored, the quality revolution. Insurance in India has been spurred by product innovation, streamlining of sales and distribution channels along with targeted advertising and marketing campaigns. With increased globalization and presence of a large number of players in the market place, the very definition of customer relationship and satisfaction is in danger of being proved incomplete. Firms use technology as a key tool to enhance the information flow within their various business units, helping their employees better understand the ever changing and increasing needs and wants of their customers. From a company value perspective, fulfilling customer needs are a key source of income to an organization and achieving complete customer satisfaction is the only key for the company to succeed.

II. REVIEW OF LITERATURE

1. Nageswara Rao and Madhavi (2007) in their study "An overview of the Private Insurance Company" divulge that appropriate communication, extended customer service, human approaches, immediate attention to the customers requests and availability of products with less formalities will highly influence the satisfaction level of the customers.

2. Shohit and Sanjay Shukla (2004) analyzed the failure of private insurance players in rural areas. Their study revealed that there are major differences in the objectives and expectations among rural and urban policy holders. They found that in rural area private players have still not achieved much success and have failed to catch the pulse of rural India as compared to public sector players. In urban area consumers belonging to middle income group prefer policies of public sector players and only high income group preferred private sector players. The study also revealed the urban area, services provided at doorstep and efficient customer's services were the two major reasons which helped market penetration by private players.

III. STATEMENT OF THE PROBLEM

Privatization of Insurance eliminated the monopolistic business of Life Insurance Corporation of India. It helps to introduce new range of products which covered wide range of risks. It resulted in better customer services and help improve the variety and price of insurance products. The entry of new player has speed up the spread of life insurance and new generation tech-savvy insurance companies and the expansion of operations of foreign insurance companies, the concept of customer satisfaction has emerged as a principal competitive weapon in insurance also. In fact, customer's expectations rise with the use of latest technology, like on-line services or e- services of insurance company, inspiring them to explore the alternatives available to them. It will increase the insurance penetration and measure of density. Entry of private players will ensure the mobilization of funds that can be utilized for the purpose of infrastructure development. The participation of commercial banks into insurance business helped to mobilization of funds from the rural areas because of the availability of vast branches of the banks. Most important not the least tremendous employment opportunities were created in the field of insurance which is a burning problem of the presence day today issues. There is low penetration in the market and there is great opportunity of more players to participate in this field to increase the life insurance market. The success of the insurance firm will be determined by how effective it has been in meeting the diverse consumer needs and wants by treating each customer as unique and offering products and services to suit his or her needs. Therefore, today, all the firms are engaged in a process of creating a lifetime value and relationship with their customers, a step towards developing knowledge regarding its customer's needs is the most important aspect.

OBJECTIVES OF THE STUDY

1. To ascertain the socio-economic profile of sample respondents.
2. To identify the determinants of satisfaction of private life insurance company policyholders

IV. METHODOLOGY

The validity of any research is based on the systemic method of data collection and analysis. Both primary and secondary data are used for the present study. The primary data was collected from three hundred sample respondents from Tirupur District. Study is conducted for one year i.e. from January 2012 to December 2012. The research conducted shall be of Descriptive and Analytical in nature. The key statistical techniques adopted for the analysis of data are simple percentage and Chi-square test was employed appropriately. Sample respondents are located in Tirupur District.

LIMITATIONS OF THE STUDY

Time is the major constraint in collecting the data from the respondents. The market survey was conducted only in Tirupur District of Tamil Nadu. Hence, utmost care is to be taken while generalizing the result.

ANALYSIS AND INTERPRETATION

Table 1

Demographic Profile of the Respondents

S.No	Factor	Demographics	No of Respondents	percentage
1.	Gender	Male	150	50.00
		Female	150	50.00
2.	Age (in years)	Up to 20	4	1.30
		21 to 40	169	56.30
		Above 40	127	42.30
3.	Educationl Qualification	Illiterate	16	5.30
		SSLC	47	15.70
		Hsc	35	11.70
		Under graduate	79	26.30
		Post graduate	90	30.00
		Professional	33	11.00
4.	Marital status	Married	207	69.00
		Unmarried	93	31.00
5.	Area of Residence	Urban	107	35.70
		Semi-urban	111	37.00
		Rural	82	27.30
6.	Occupation	Daily wage Earners	24	8.00
		Agriculturist	36	12.00
		Employee	112	37.30
		Business	41	13.70
		Professional	24	8.00
		Student	29	9.70
		Housewife	29	11.30
		Housewife	34	11.30
7.	Family income	Up to Rs 15000	13	4.30
		Rs 15000 to Rs 30000	129	43.00
		Above Rs 30000	158	52.70
8.	Status in the Family	Head	96	32.00
		Member	204	68.00
9.	Type of Family	Joint	159	53.00
		Nuclear	141	47.00
10.	No of Family Members	Up to three	128	42.70
		Four and above	172	57.30

Source: Primary Data

The profile of the respondents is shown in the above table. The profile focus on the demographics of respondents. It shows that out of 300 respondents, 50% of the respondents are male and 50% are females. Most of the respondents are married (69%) and in the age group 21-40 year (56.30%). This range shows that married group always feels the importance of insurance policy to complement with their life and families. The highest education level attained by most of the respondents was master degree level (30%), followed by degree level (26.30 %). It shows that majority of respondents were educated with high qualifications. The occupations of respondents were varied. The majority of the respondents are employee (37.30 %). followed by businessman (13.70 %). and Agriculturist are (12. %), Daily wage Earners and Professionals (8%). In term of household income, almost half of the respondents earned more than Rs.30, 000 (per month). Majority of the respondents belong to member`s category.53% of the respondents belong to joint family. Most of the policy holders have more than three family members.

RESEARCH HYPOTHESES

1. **H1** There is no significant relationship between Age and level of satisfaction.
2. **H2** There is no significant relationship between Educational Qualification and Level of Satisfaction.
3. **H3** There is no significant relationship between Marital Status and Level of Satisfaction.
4. **H4** There is no significant relationship between Occupation and level of satisfaction.
5. **H5** There is no significant relationship between Monthly Income and level of satisfaction.
6. **H6** There is no significant relationship between Number of policies and level of satisfaction

DETERMINANTS OF POLICY HOLDER'S SATISFACTION**Table-2**

S.NO	FACTOR	C.V	T.V	D.F	Level of significant	Significant/not significant
1	Age	4.767	9.488	4	5	Rejected
2	Educational qualification	13.937	18.307	10	5	Rejected
3	Marital status	27.623	5.991	2	5	Accepted
4	Occupation	15.669	21.026	12	5	Rejected
5	Monthly income	2.334	9.488	4	5	Rejected
6	Number of policies	11.057	9.488	4	5	Accepted

Source: Primary Data

V. RESULT

Chi- square test reveals that the calculated value of chi- square 4.767 is less than the table value at 5% level ($\chi^2=4.767 < 9.488$) so the null hypothesis is accepted. There is no significant relationship between age and level of satisfaction.

Chi- square test reveals that the calculated value of chi- square 13.937 is less than the table value at 5% level ($\chi^2=13.937 < 18.307$) so the null hypothesis is accepted. There is no significant relationship between Educational Qualification and Level of Satisfaction.

Chi- square test reveals that the calculated value of chi- square 27.623 is greater than the table value at 5% level ($\chi^2=27.623 > 5.991$) so the null hypothesis is rejected. There is significant relationship between Marital Status and Level of Satisfaction.

Chi- square test reveals that the calculated value of chi- square 15.669 is less than the table value at 5% level ($\chi^2=15.669 < 21.026$) so the null hypothesis is accepted. There is no significant relationship between Occupation and Level of Satisfaction.

Chi- square test reveals that the calculated value of chi- square 2.334 is less than the table value at 5% level ($\chi^2=2.334 < 9.488$) so the null hypothesis is accepted. There is no significant relationship between Monthly Income and Level of Satisfaction.

Chi- square test reveals that the calculated value of chi- square 11.057 is greater than the table value at 5% level ($\chi^2=11.057 > 9.488$) so the null hypothesis is rejected. There is significant relationship between Number of Policies and Level of Satisfaction.

FINDINGS OF THE STUDY

1. The satisfaction about life insurance among the respondents is above 40 years is maximum. This shows middle aged people show more interested for taking life insurance than youngsters.
2. According to our study, illiterates are more interested for taking life insurance policies compare to literates.
3. As per our study, 69 % of the respondents are married. This shows married people are more interested in life insurance. From this it is identified that the chi-square indicates that Marital Status is found to be associated with policy holder's satisfaction.
4. The daily wages earners have high level of satisfaction compare to salaried people. And house wives also have low level of satisfaction. There is no significant relationship between Occupation and Level of Satisfaction.
5. 15 % respondents are familiar with the products of life insurance and think insurance is essential for life, but those are in service with monthly income is below Rs 7500 mostly purchased the various life insurance policies.
6. Policyholder who holds two policies have high level of satisfaction and Policyholder who holds one policy has low level of satisfaction. There exists significant relationship between number of policies and satisfaction.

SUGGESTIONS AND RECOMMENDATIONS

1. The unmarried are not interested because of their ignorance and lack of satisfaction. In fact, private life insurance companies have to educate the unmarried about the benefits of taking insurance policies; by and large flexibly private life insurance should change the policies according to their taste, and motivate them effectively.
2. Regarding private life insurance policies despite the fact that already insurance companies introduced policies in the field, those who have only one policy in hand not yet been reached up to the mark. This is the very important thing that should be remembered every now and then to boost up the customer satisfaction in all calibers.
3. The policyholders with monthly income below Rs 7500 are not satisfied because their financial position is very low, life insurance companies have to introduce the low premium amount policies for these middle class populations, and then they can pay the premium amount in time.
4. Life insurance should spread its wings in rural areas; it will enable the rural policy holders to avail insurance at their door step.
5. Life insurance have to introduce special policy for unmarried private insurers will definitely offer benefits to the unmarried policyholders and the society as a whole in terms of cheaper, flexible, innovative and customized products with variety of features.
6. The insurance companies should show genuine concern for the consumers, if they are really serious for their business failing which they will loose the confidence of people.

VI. CONCLUSION

The study observed that, most of the customers are satisfied with the services offered by private Life Insurance Companies. The satisfaction is a strong predictor of the private life insurance, and hence it is recommended that insurance service providers should endeavour to satisfy and delight their customer's satisfaction. When customers are satisfied, they are more likely to recommend the insurance service to their peers, less likely to switch on and more likely to re-patronize services. The company should try to keep their promise to do the work timely, should show sincere interest in customers' problem, and should provide prompt service to satisfy the customer fully. In this competition era private Life insurance Companies have to concentrate on the customers' satisfaction to retain the existing customers and at the same time they have to improve the quality of services day by day to attract new customers. Thus the success of the insurance firm will be determined by the way in which effectively it would have been done to meet the diverse consumer needs and wants by treating each customer as unique and offering products and services to suit their needs. Therefore, today all the firms are engaged in the process of creating a lifetime value and relationship with their customers, a stepping stone towards developing knowledge regarding its customers' needs are the most important aspect.

REFERENCES

- [1] Nageswara Rao and Madhavi (2007) "An overview of the private insurance company" Insurance Theory and practice, PP 104-115.
- [2] Shohit and Sanjay Shukla (2004), "An empirical study and analysis of failure of private insurance players in rural areas Insurance chronicle May 2004 pp 56-62.
- [3] Jagannath and Santhosh Singh Bais "Customer satisfaction in Insurance Sector" usmania Journal of International Business Studies Vol.1 (2)
- [4] Das, N. and Samanta, N. (2005), "Evaluation of customer satisfaction level of different projects", Quality Assurance: Good Practice and Law, Vol. 11, No. 2, pp. 75-84.
- [5] Volume no. 2 (2011), issue no. 8 (august) *issu 0976-2183*
- [6] International Journal of Research in Commerce & Management
- [7] Frank,B.and Enkawa, T. (2009), "Economic influences on perceived value, quality expectations and customer satisfaction", International Journal of Consumer Studies, Vol. 33, No. 1, pp. 72-82.

Agile Methodologies and Its Processes

¹Akanksha²Akansha Rakheja³Latika Kapur⁴Kanika Ahuja

^{1,2,3}Information Tech IT)Dronacharya College of Engineering, Gurgaon

ABSTRACT:

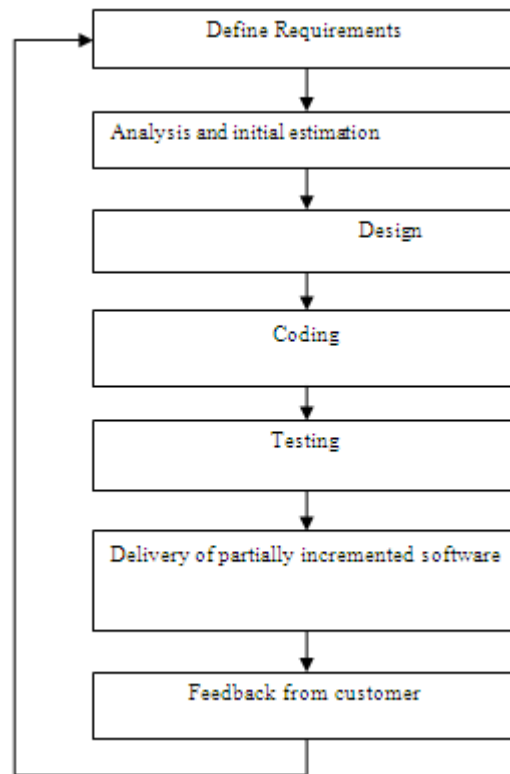
“Agile”-denotes the quality of being agile. This paper deals with the concept of agile methodology. It will include some of the software development process models used. In particular the aim of the agile process is to satisfy the customer through early and continuous delivery of valuable software. This paper compares the agile processes with other software development life cycle models. Advantages and disadvantages of the agile processes are also included in this paper.

Keywords: Extreme Programming (XP), Scrum, Software Development Life Cycle (SDLC)

I. INTRODUCTION

Agile software development (also called “agile”) isn’t a set of tools or a single methodology, but a philosophy put to paper in 2001 with an initial 17 signatories. Agile was a significant departure from the heavyweight document –driven software development methodologies such as waterfall. Plan driven methods are those that begin with the solicitation and documentation of a set of requirements that is as complete as possible. Based on these requirements, one can then formulate a plan of development. Usually, the more complete the requirement the better the plan. Some examples of plan driven methods are various waterfall approaches. An underlying assumption in plan driven processes is that the requirements are relatively static. On the other hand, iterative methods such as spiral-model based approaches described in recently agile approaches count on change and recognize that only constant is changed. With the passage of time, the software industry, software technology and customer expectations were moving very quickly and the customers were becoming increasingly less able to fully state their need up front. As a result, agile methodologies and practises emerged as an explicit attempt to formally embrace higher rates of requirements change. Agile methods are a subset of iterative and evolutionary methods and are based on iterative enhancement and opportunistic development process. In all iterative products, each iteration is a self-contained, mini-project with activities that span requirements analysis, design, implementation, and test. Each iteration leads to an iteration release (which may be only an internal release) that integrates all software across the team and is a growing and evolving subset of the final system. The purpose of having short iterations is so that feedback from iterations N and earlier, and any other new information, can lead to refinement and requirements adaptation for iteration N + 1. The customer adaptively specifies his or her requirements for the next release based on observation of the evolving product, rather than speculation at the start of the project . There is quantitative evidence that frequent deadlines reduce the variance of a software process and, thus, may increase its predictability and efficiency. The pre-determined iteration length serves as a timebox for the team. Scope is chosen for each iteration to fill the iteration length. Rather than increase the iteration length to fit the chosen scope, the scope is reduced to fit the iteration length. A key difference between agile methods and past iterative methods is the length of each iteration. In the past, iterations might have been three or six months long. With agile methods, iteration lengths vary between one to four weeks, and intentionally do not exceed 30 days. Research has shown that shorter iterations have lower complexity and risk, better feedback, and higher productivity and success rates.

Agile process is an iterative approach in which customer satisfaction is at highest priority as the customer has direct involvement in evaluating the software. The agile process follows the software development life cycle which includes requirements gathering, analysis, design, coding, testing and delivers partially implemented software and waits for the customer feedback. In the whole process, customer satisfaction is at highest priority with faster development time. The following figure depicts the software development life cycle of Agile Process.



II. CHARACTERISTICS OF AGILE PROCESS

The core agile delivery principle is that although agile methods differ somewhat in their practices, all of them advocate these core principles--iterative and incremental delivery, collaboration and continuous improvement and here are top reasons to adopt agile methodology.

- Iterative and incremental delivery: Project delivery is divided into small functional releases or increments to manage risk and to get early feedback from customers and end users. These small releases are delivered on a schedule using iterations that typically last between one and four weeks each. Plans, requirements, design, code and tests are created initially and updated incrementally as needed to adapt to project changes.
- Collaboration: All core project team members including an on-site customer are co-located in a shared, open area to facilitate face-to-communication and conduct interactions. Team members self-organize by continuously completing tasks collaboratively without top-down management control.
- Continuous Improvement: Practices that enable delivery process inspection and adaptation are integrated into agile methods. Project Reflections are meetings conducted while the project is underway to facilitate regular reflection on its successes and failures, and any of the tools and techniques applied.
- Modularity: Agile process decomposes the complete system into manageable pieces called modules. Modularity plays a major role in software development processes.
- Convergent: All the risks associated with each increment are convergent in agile process by using iterative and incremental approach.
- Adaptive: Due to the iterative nature of agile process new risks may occurs. The adaptive characteristic of agile process allows adapting the processes to attack the new risks and allows changes in the real time requirements.
- Time Boxing: As agile process is iterative in nature, it requires the time limits on each module with respective cycle.
- Parsimony: In agile processes parsimony is required to mitigate risks and achieve the goals by minimal number of modules.

III. AGILE METHODOLOGIES

This section provides a brief introduction to three agile methodologies. The three were chosen to demonstrate the range of applicability and specification of the agile methodologies. For each methodology we provide an overview of its process.

3.1. Extreme Programming (XP)

Extreme Programming (XP) originators aimed at developing a methodology suitable for “object-oriented projects using teams of a dozen or fewer programmers in one location.” The methodology is based upon five underlying values:

- a. **Communication:** XP has a culture of oral communication and its practices are designed to encourage interaction.
- b. **Simplicity:** Design the simplest product that meets the customer’s needs. An important aspect of the value is to only design and code what is in the current requirements rather than to anticipate and plan for unstated requirements.
- c. **Feedback:** The development team obtains feedback from the customers at the end of each iteration and external release. This feedback drives the next iteration.
- d. **Courage:** The other three values allow the team to have courage in its actions and decision making.
- e. **Respect:** Team members need to care about each other and about the project

XP is the most successful method of developing agile software because of its focus on customer satisfaction. XP requires maximum customer interaction to develop the software. It divides the entire software development life cycle into several number of short development cycles. It welcomes and incorporates changes or requirements from the customers at any phase of the development life cycle.

The Extreme Programming software development process starts with planning, and all iterations consist of four basic phases in its life cycle: designing, coding, testing, and listening. The overriding values that drives the XP life cycle are continual communication with the customer and amongst the team, simplicity by harping on the minimalist solution, frequent feedback through unit and acceptance testing, and the courage to take on problems proactively and integrate testing and changes in the development phase.

A. Planning:

The first phase of Extreme Programming life cycle is planning, where customers or users meet with the development team to create ‘user stories’ or requirements. The development team converts user stories into iterations that cover a small part of the functionality or features required. A combination of iterations provides the customer with the final fully functional product. The programming team prepares the plan, time, and costs of carrying out the iterations, and individual developers sign up for iterations. One planning approach is the critical path method, grouping iterations essential for project progress in a linear fashion, and arranging for completion of other iterations parallel to the critical path.

B. Designing

An iteration of XP programming starts with designing. Thrust on simplicity by expressing a thing only once and not adding functionality in anticipation. It uses systems metaphor or standards on names, class names and methods, and agreeing on uniform styles and formats to ensure compatibility among the work of different team members. It uses Software Class Responsibilities and Collaboration (CRC) Cards that allow for a departure from the traditional procedural mindset and make possible object oriented technology. Such cards allow all members of the project team to contribute ideas, and collate the best ideas into the design. It creates spike solutions or simple programs that explore potential solutions for a specific problem, ignoring all other concerns, to mitigate risk.

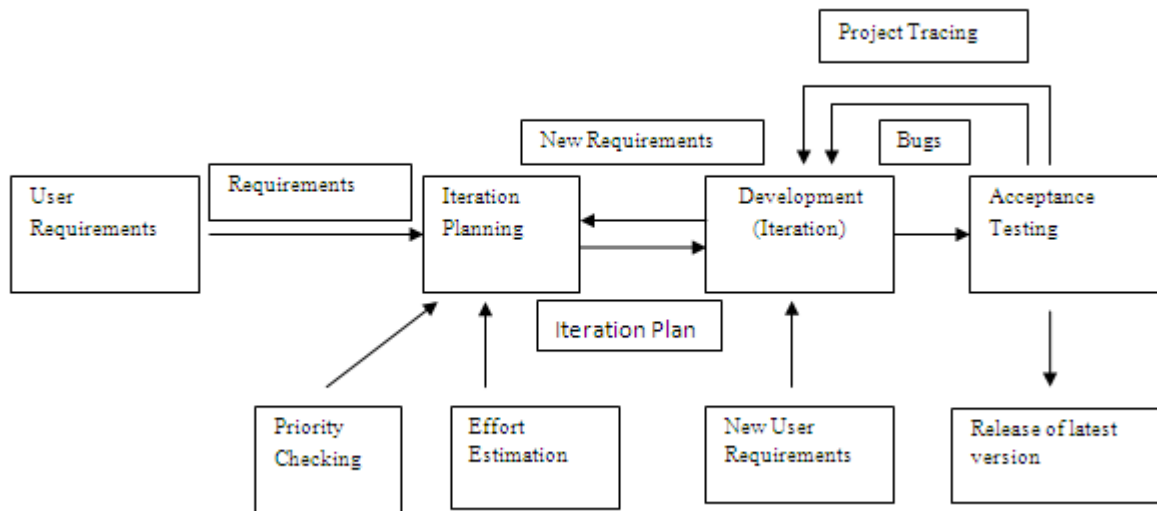
C. Coding

Coding constitutes the most important phase in the Extreme Programming life cycle. XP programming gives priority to the actual coding over all other tasks such as documentation to ensure that the customer receives something substantial in value at the end of the day.

Standards related to coding include:

- Developing the code based on the agreed metaphors and standards, and adopting a policy of collective code ownership.
- Pair programming or developing code by two programmers working together on a single machine, aimed at producing higher quality code at the same or less cost.

- Strict adherence to 40-hour workweeks with no overtime. This ensures the developers work in the peak of their mental and physical faculties.
- Frequent integration of the code to the dedicated repository, with only one pair integrating at a time to prevent conflicts, and optimization at the end.



D. Testing

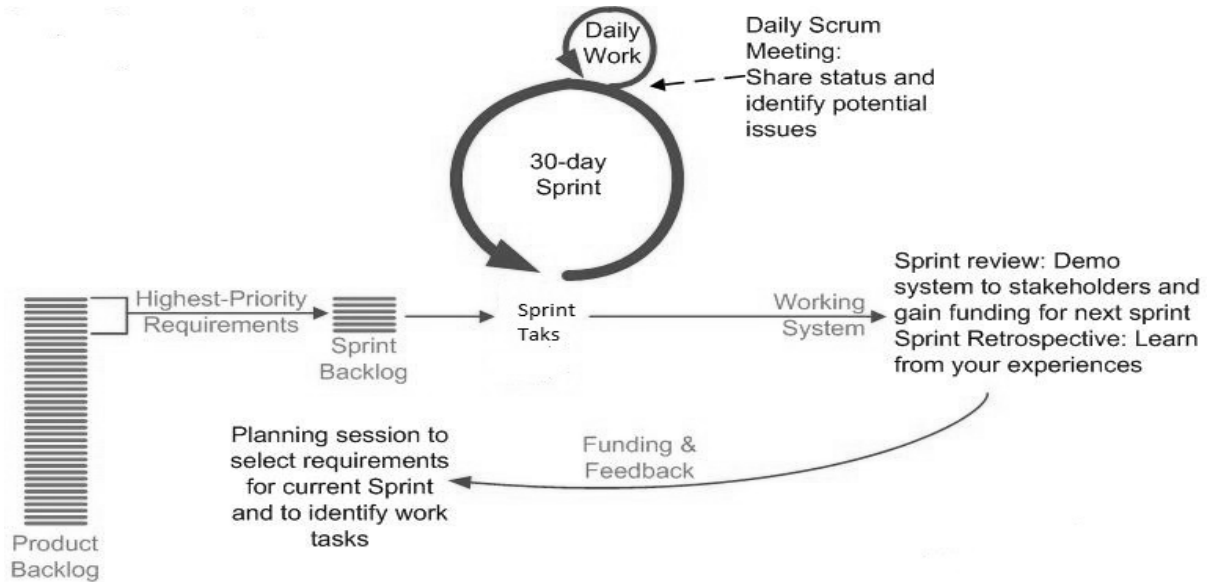
Extreme program integrates testing with the development phase rather than at the end of the development phase. All codes have unit tests to eliminate bugs, and the code passes all such unit tests before release. Another key test is customer acceptance tests, based on the customer specifications. Acceptance test run at the completion of the coding, and the developers provide the customer with the results of the acceptance tests along with demonstrations.

E. Listening

The basis of extreme programming is a continuous mechanism of customer involvement through feedback during the development phase. Apart from the customer, the developer also receives feedback from the project manager. The basis of feedback is the customer acceptance tests. Each feedback of the customer that specifies revised requirement becomes the basis of a new design, and the process of design-coding-tests-listening repeats itself. If the customer remains satisfied with the test results the iteration ends there, and the design for the new iteration starts, which again follows the design-coding-testing-listening cycle.

3.2. SCRUM

Scrum is another popular method of agile development through which productivity becomes very high. It is basically based on incremental software development process. In scrum method the entire development cycle is divided into a series of iteration where each iteration is called as a sprint. Maximum duration of a sprint is 30 days. The main idea of Scrum is that systems development involves several environmental and technical variables (eg. requirements, time frames, technology and resources) that are likely to change during the process. This makes the development process unpredictable and complex, requiring flexibility of the systems development process for it to be able to respond to the changes. As a result of the development process, a system is produced which is useful when delivered.



The method starts with collecting user requirements but it is not expected that all the requirements should come out from the user at the beginning. User can change their mind at any time during development; they can add new features, remove or update some existing features. Next phase is to prioritize the requirements and the list is known as product backlog. A proper planning for sprint should be done i.e. how many sprints are needed to develop the software, duration of the sprint, and what are the requirements from the product backlog should be implemented in each sprint. This particular list is known as sprint backlog. During each sprint one sprint meeting is held every day to take the feedback how much work has been done. After each sprint review is taken to determine whether all the requirements for that particular sprint have already been implemented or not and to decide the requirements should be implemented at the next sprint. After each sprint we get a working increment of the software. A sprint is the basic unit of development in Scrum. The sprint is a "time boxed" effort, i.e. it is restricted to a specific duration. The duration is fixed in advance for each sprint and is normally between one week and one month.

IV. COMPARISON

4.1. Between various process models:

FEATURES	PROCESS MODELS	
	AGILE	WATERFALL
Architecture	Informal and incremental	Well documented and completed before coding
Developer	Shares ownership of code	Responsible for one area
Functionality	Focus on completing stories in short iterations	Focus on completing modules at large milestones
Process	Light process and documentation	Heavy process and documentation
Main roles	Developer	Developer, Architect
Communication	Open door policy	Happens only at beginning or at milestones
Orientation	People oriented	Process oriented
Deliverables	Delivers early partial working solutions	No working solutions is provided until late
Cost of change	Low cost of change	High cost of change
Testing	Fully automated, continuous testing at both functional and unit level	Testing as separate phase at the end of project
Knowledge Required	Product and Domain	Product and Domain
Time Boxing	Available	Not Available

4.2. Between agile methodologies:

CHARACTERISTICS	XP	SCRUM
Development approach	Iterative increments	Iterative increments
Recommended iteration time period	One to six weeks	Two to four weeks
Project team	Smaller team	All sizes
Team communication	Informal daily meetings	Informal daily meetings
Project size	Smaller projects	All types of projects
Customer involvement	Customer involved	Customer involved through the role of Product owner
Project Documentation	Only basic documentation	Only basic documentation
Advantages	Open workspace, customer as a part of team, well defined best practices, feedback	High level of communication and collaboration
Disadvantages	Weak documentation, lack of discipline, customer presence is mandatory	Weak documentation, poor control over projects

V. ADVANTAGES

- Agile methodology has an adaptive team which is able to respond to the changing requirements. Customer satisfaction by rapid, continuous delivery of useful software.
- People and interactions are emphasized rather than process and tools. Customers, developers and testers constantly interact with each other.
- Working software is delivered frequently (weeks rather than months).
- Face to face communication and continuous inputs from customer representative leaves no space for guesswork.
- Continuous attention to technical excellence and good design
- A reduced budget
- Less defects in the final product
- Become responsive by supporting scope adjustments every iteration
- Decrease risk by always having working software

VI. DISADVANTAGES

- In case of some software deliverables, especially the large ones, it is difficult to assess the effort required at the beginning of the software development life cycle.
- There is lack of emphasis on necessary designing and documentation.
- The project can easily get taken off track if the customer representative is not clear what final outcome that they want.
- When change comes so quickly, it is difficult to avoid resistance from stakeholders and complications to end user training.
- Only senior programmers are capable of taking the kind of decisions required during the development process. Hence it has no place for newbie programmers, unless combined with experienced resources.
- Because agile methods are not process-oriented and require quick response to change, a lack of documentation is often a primary characteristic
- Agile is not a silver bullet – Agile can be over-hyped, thus leading to unrealistic expectations

VII. CONCLUSION

In this paper we have discussed the agile development life cycle models, characteristics of agile process, methodologies of agile process, advantages and disadvantages. In the comparative study of agile software development with other software development models we conclude that agile project is much better than other

software development process in terms of productivity, performance, faster time cycles, risk analysis. Agile processes are implemented in important applications such as web based, testing tools, etc.

REFERENCES

- [1] Sheetal Sharma et al. / International Journal on Computer Science and Engineering (IJCSSE) ISSN , Agile Processes and Methodologies: A Conceptual Study.
- [2] [Aoyama 1998] Mikio Aoyama, "Agile Software Process and Its Experience", Proceedings of the 1998 International Conference on Software Engineering,
- [3] [Gilb 1988] Tom Gilb. Principles of Software Engineering Management, Addison Wesley.
- [4] Williams, L., "Agile Software Development Methodologies and Practices ", in *Advances in Computers*, Volume 80,, 2010
- [5] Layman, L., Williams, L., Cunningham, L., *Exploring Extreme Programming in Context: An Industrial Case Study*, Agile Development Conference 2004
- [6] http://en.wikipedia.org/wiki/Agile_software_development

Computational Analysis and Design for Precision Forging Of Aluminium AA 6061 Connector

Santhosh.N^{1*}, Vinayaka.N[#], Dr.Aswatha^{\$}, Uday.M[€], Praveena.B.A[#]

^{*}Assistant Professor, Department of Aeronautical Engineering, NMIT, Bangalore

[#]Assistant Professor, Department of Mechanical Engineering, NMIT, Bangalore

^{\$}Associate Professor, Department of Mechanical Engineering, BIT, Bangalore

[€]Assistant Professor, Department of Mechanical Engineering, SJBIT, Bangalore

ABSTRACT

Development of a new process methodology which satisfies given criteria is a big challenge faced by most of the forging industries. The domain of competition is quite large and hence every firm aims at producing near net shapes thereby eliminating the need for machining and other secondary operations. The present investigation deals with the flow simulation of Aluminium forgings conforming to AA 6061 specification and henceforth studies the mechanical characteristics of the flow simulation results. The Aluminium AA 6061 component considered is precision forged with a hydraulic press in a die having geometrical interlocking. During precision forging it was difficult to achieve the required net shape of the component because of unsymmetrical location of small ribs on cylindrical surface and variation in the cross sections from bottom to top (i.e. unsymmetrical about both X & Y axis). Thus to eradicate the problem encountered, the flow simulation of the precision forging process was carried out and the mechanical characteristics of the flow simulation results obtained were studied.

KEYWORDS: Flow simulation, Precision forging, Mechanical characteristics, Hydraulic press, Billet, Component.

I. INTRODUCTION:

There has been a growing importance for precision forging of various components like Aluminium AA 6061 connector shown in Fig 1, which would otherwise have been produced by die casting processes or other metal forming processes that have many disadvantages compared to precision forging process [1]. Precision forging is a unique technique with a goal to produce a net shape, or at least a near-net shape, in the as-forged condition. The term net describes that no subsequent machining or a minimal of secondary finishing operations on the forged component is required. Thus, a net shape forging or precision forging process aims at minimizing the cost and waste associated with post-forging operations. Therefore, the final product from a precision forging needs little or no final machining. Significant cost savings are achieved from the optimized use of material, resulting in the overall reduction of energy consumption. Precision forging also requires less of a draft, i.e. 1° to 0°. However the downside of this process is its cost; therefore it is only implemented if significant cost reduction can be achieved [2-4]. The main problem for forging process is the high cost and long lead time for the design and production of tooling. For this purpose, CAD, CAM and CAE techniques are used to get faster results in the design and manufacture of tooling by decreasing the trial and error time to produce successful forgings [5]. CAD, CAM and CAE programs also develop satisfactory die design for the required process parameters. 3-D modeling of forging dies is usually made with the aid of CAD software such as Pro/ENGINEER, CATIA, and SOLID WORKS etc. If there are any problems in the simulation of the process then the designer of the forging process can easily change his design parameters in the CAD software packages [6]. The usage of process simulation programs is common for research and development of forging processes. By using this type of programs, forging tool designer can decrease costs by improving achievable tolerances, increasing tool life, predicting and preventing flow defects, part properties [7]. In this context it is proposed to carry out the flow simulation of the entire precision forging process and examine the flow simulation results obtained.

Finite Volume Method is a simulation method in which the grid points are fixed in space and the elements are simply partitions of the space defined by connected grid points. The finite volume mesh is a fixed frame of reference. The material of a billet under analysis moves through the finite-volume mesh; the mass, momentum, and energy of the material are transported from element to element. The finite-volume solver,

therefore, calculates the motion of material through elements of constant volume, and therefore no re-meshing is required [8]. The most common finite volume software's used in forging are MSC Super Forge and Deform 3D to predict the forging variables. Deform 3D is very supportive in optimizing the forging process and defining its parameters. Forging process can be simulated, Problems related with Product and Process design can be observed easily, Various dies can be tried and forging process can be analyzed closely by using Deform 3D. After a number of simulation processes involving different parameters, optimum die set for which the die cavity gets filled completely while maintaining a lower stress can be selected by using Deform 3D [9].

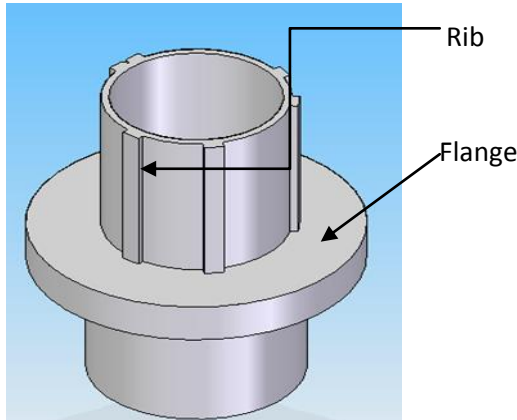


Fig 1 Model of the component

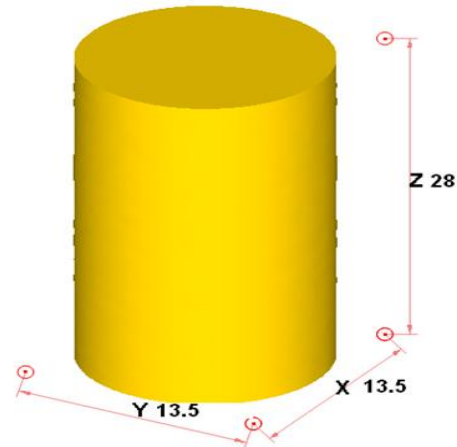


Fig 2 Aluminium AA 6061 billet

II. MATERIAL AND METHODS:

The present investigation examines the intricacies involved in the precision forging of Aluminium AA 6061 billet as shown in Fig 2 into the component as shown in Fig 1. Aluminium alloy 6061 is one of the most extensively used of the 6000 series Aluminium alloys. It is a versatile heat treatable precipitation hardening extruded alloy containing magnesium and silicon as its major alloying elements with medium to high strength capabilities [10].

Element	Weight %
Aluminium (Al)	Min 96.4 to Max 97.9
Silicon (Si)	Min 0.40 to Max 0.8
Copper (Cu)	Min 0.15 to Max 0.40
Magnesium (Mg)	Min 0.8 to Max 1.2
Chromium (Cr)	Min 0.04 to Max 0.35
Manganese (Mn)	Min 0.04 to Max 0.15
Zinc (Zn)	Max 0.25
Titanium (Ti)	Max 0.15
Iron (Fe)	Min 0.15 to Max 0.7
Other elements not more than 0.05% each	0.15 total

Table 1: Composition of Aluminium AA 6061

2.1 Aluminium AA 6061

Aluminum AA 6061 is a silver white alloy that has a strong resistance to corrosion and like gold, is rather malleable. It is a relatively light metal compared to metals such as steel, nickel, brass, and copper with a specific gravity of 2.7. Aluminum AA 6061 is easily machinable and can have a wide variety of surface finishes. It also has good electrical and thermal conductivities and is highly reflective to heat and light, henceforth Aluminium AA 6061 alloy has wide applications ranging from aerospace to marine engineering [11].

2.2 T6 Temper Grade

T6 temper Aluminium AA 6061 has an ultimate tensile strength of at least 42,000 psi (300 MPa) and yield strength of at least 35,000 psi (241 MPa). More typical values are 45,000 psi (310 MPa) and 40,000 psi (275 MPa), respectively. In thicknesses of 0.250 inch (6.35 mm) or less, it has elongation of 8% or more; in thicker sections, it has elongation of 10% [12]. The typical value of thermal conductivity for 6061-T6 at 80°C is around 152 W/m K. A material data sheet defines the fatigue limit under cyclic load as 14,000 psi (100 MPa) for 500,000,000 completely reversed cycles using a standard RR Moore test machine and specimen [13].

2.3 Flow simulation

Flow simulation was carried out using Deform-3D software with the following additional information gathered for the purpose of simulating the whole process using the above mentioned software.

The additional information and parameters that were necessary for simulation were:

1. STP (STEP) and STL format of the model of the component. (I.e. Aluminium connector)
2. STP (STEP) and STL format of the models of the tool and die set as shown in Fig 3 and Fig 4.
3. Type of the press to be used (in the present investigation, we have considered Hydraulic press).
4. Configuration and characteristics of the press used.
5. Constant movement speed of the press.
6. Temperature of the forging operation (in the present investigation, we emphasize on precision forging which is usually done below recrystallization temperature, approximately room temperature i.e. cold forging conditions).

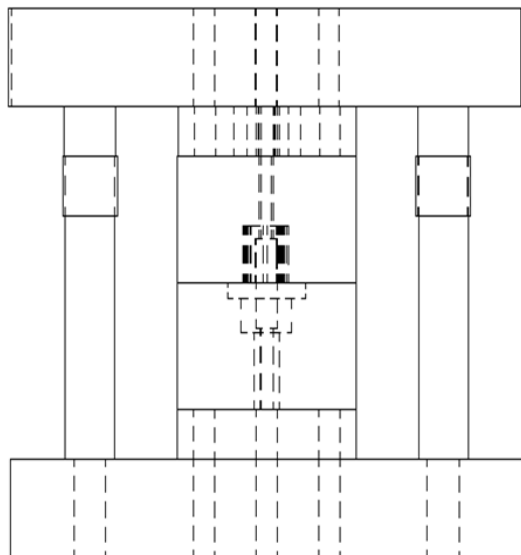


Fig 3 Tool and die set used in the present investigation

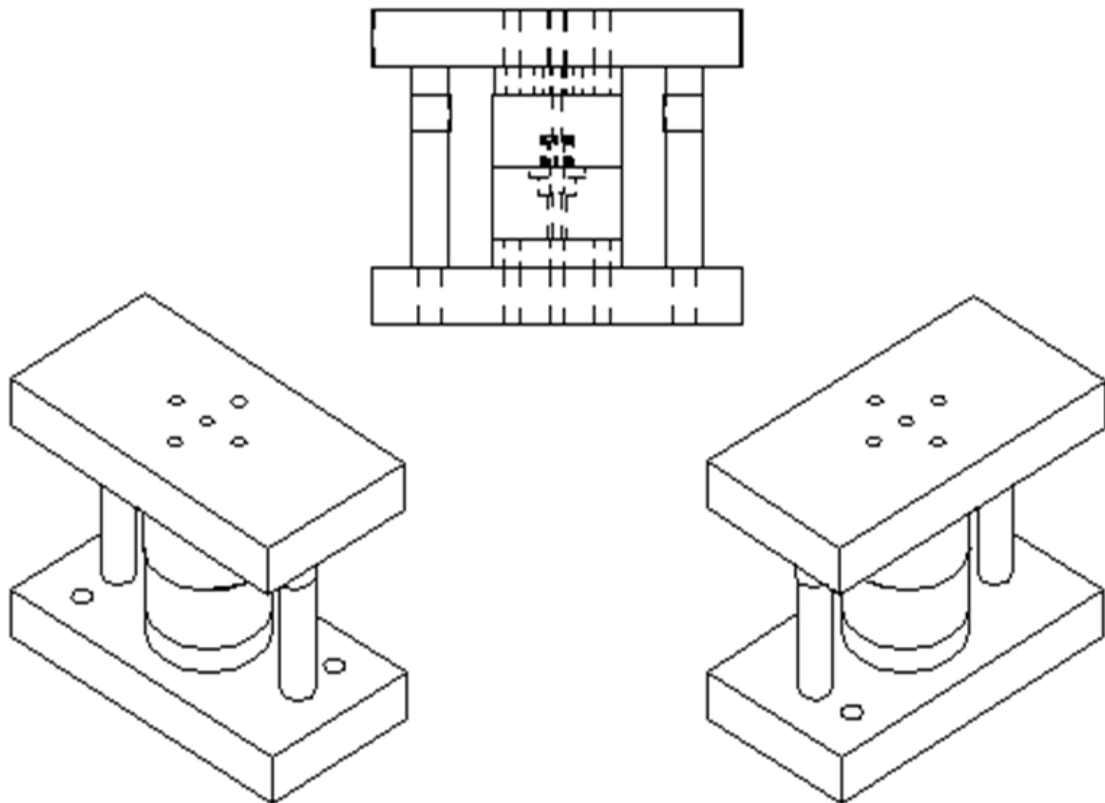


Fig 4 Different views of the tool and die set used in the present investigation

2.4 Procedure

Models of the die set and cylindrical billet were created using SOLID EDGE software package. Contact elements were constructed on all exterior surfaces of the billet, except for the bottom surface and all inner surfaces of the top die. These contact elements were constructed between the die and billet surfaces to prevent the penetration. These elements were modeled by using solid edge software and were converted into STL and STP (STEP) files. Contact elements were on the inside surfaces of the die and utilized the bottom nodes of the die. The die set was modeled with rigid material properties and the billet was modeled with an elasto-plastic material (Aluminium 6061) properties. The front and rear surfaces of die were not explicitly modeled, but were simulated by boundary conditions. Nodes on the front of billet were constrained from moving past the plane of the front portion of upper die, thus representing the front closure. The constraints were incorporated which acts similarly to a contact surface.

The coefficient of friction between the wall-billet interface and the other contact surfaces was kept constant. The planes of symmetry were simulated by using nodal restraints which did not allow the nodes to move across. The volume of the cavity of die had the same volume as that of the billet, the aim being that when the die was completely closed, the billet material would completely fill the die cavity. The top die was pushed downwards over the billet with a constant imposed velocity by hydraulic ram actuated press, while the bottom die was kept stationary. The magnitude of velocity was chosen in such a way that the computer run time of the analysis for this model got drastically reduced. The billet was positioned relative to the die cavity as shown in Fig 5 in such a manner that it allows flow of the billet material within the die cavity in all three directions. This produced a three dimensional flow pattern. The material flow simulation of the billet material carried out in Deform 3D software was studied as it filled the die and the results were obtained. The material model for the billet was that of an isotropic elasto-plastic material (Aluminium 6061) with a bilinear stress-strain curve. This model incorporates isotropic hardening where the cylindrical yield surface expands as the material yields.

The young's modulus, yield stress, and the hardening modulus were specified. The stress calculated by the deform software made use of the following equation (1).

$$\sigma = \sigma_y + E_p \times \epsilon_p \tag{1}$$

Where

σ represents the effective stress,

σ_y represents the yield stress of the material,

ϵ_p represents the plastic strain,

E_p , the plastic modulus is defined as:

$$E_p = E \cdot E_h / (E - E_h)$$

Where E_h is the hardening modulus.

The value of the friction coefficient between the die and billet surface was maintained as a constant, and considered explicitly at locations where a contact surface of the die touched the contact surface of the billet.

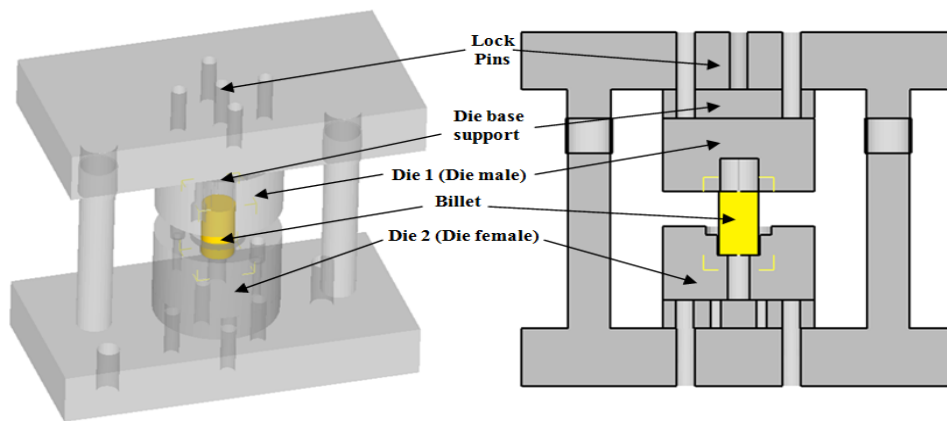


Fig 5 Initial setup of the billet in the die cavity between die halves

III. RESULTS AND DISCUSSION

Flow simulation of the precision forging process carried out has henceforth provided critical results which gives a detailed description of the effective stress, effective strain, principal stress, principal strain, velocity and damage analysis of the component as well as die set used in the process. The effect of stress accumulation, strain distribution, material flow velocity, damage can be clearly visualized and henceforth it can be critically analyzed from the Fig 6, Fig 7, Fig 8, Fig 9, Fig 10 and Fig 11 respectively. The careful observation of the results suggest that the effective stress, effective strain, principal stress, principal strain, velocity and damage are maximum at locations where flange opens out and rib growth begins across the geometrical interlocking between the two halves of die-set and the component surface.

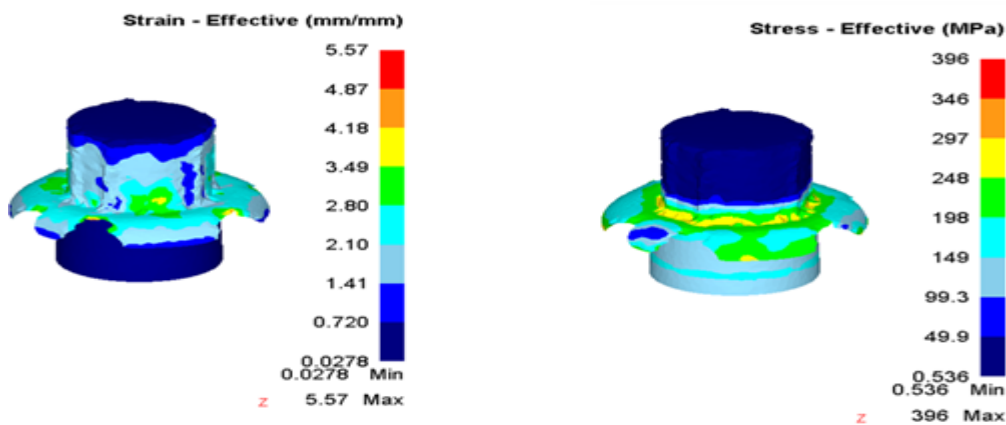


Fig 6 Effective Stress and strain distribution

Fig 6 shows the effective stress and strain distribution along various cross sections of the component, the effective stress varies from a minimum of 0.536 MPa to a maximum of 396 MPa and the effective strain varies from a minimum of 0.0278 to 5.57 mm/mm.

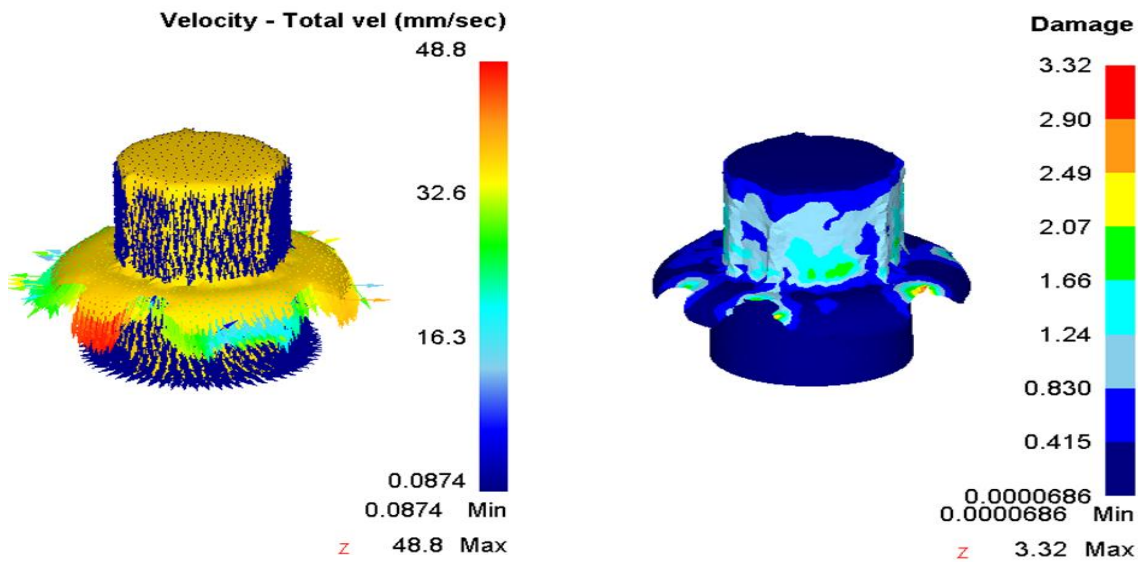


Fig 7 Velocity and Damage analysis

Fig 7 gives a brief outline of the velocity and damage analysis for the component, the velocity of flow of material during plastic deformation of the component varies from a minimum of 0.0874 mm/sec to a maximum of 48.8 mm/sec and the damage caused in the component varies from a minimum of 0.0000686 to a maximum of 3.32.

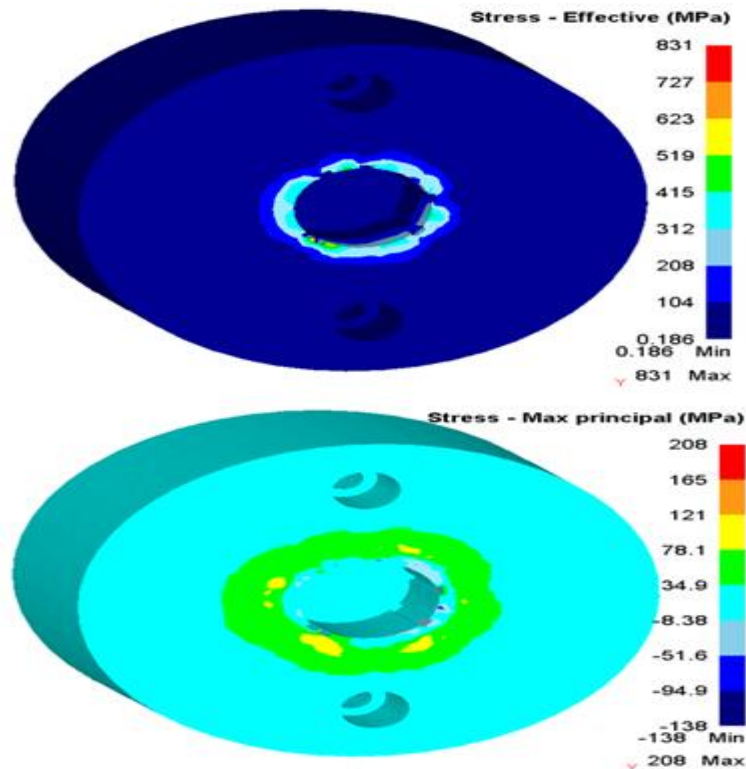


Fig 8 Effective and principal stress variations across the Die-1 cross section

Fig 8 shows the effective and principal stress distribution along various cross sections of Die-1 with a minimum Effective stress value of 0.186 MPa, maximum effective stress value of 831 MPa, and the principal stress value ranging from a minimum of -138 MPa to a maximum of 208 MPa.

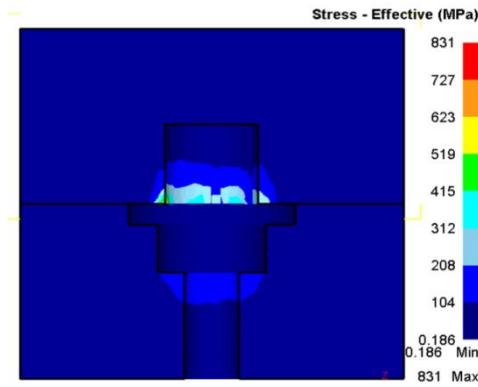


Fig 9 Effective-Stress Analysis of Die assembly in MPa

Fig 9 shows the effective stress distribution along various cross sections of Die assembly with a minimum value of 0.186 MPa and a maximum value of 831 MPa.

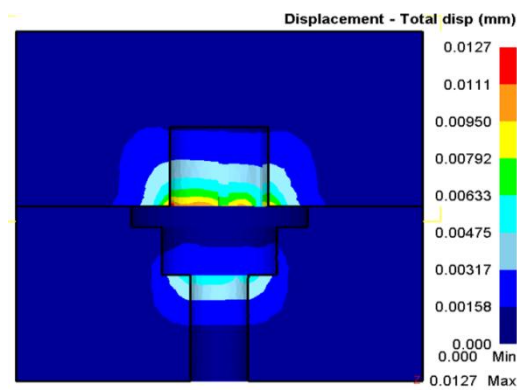


Fig 10 Displacement analysis of die-component setup in mm

Fig 10 shows the displacement analysis for the die-component setup, the displacement for the die-component setup varies from a minimum of 0 mm to a maximum of 0.0127 mm.

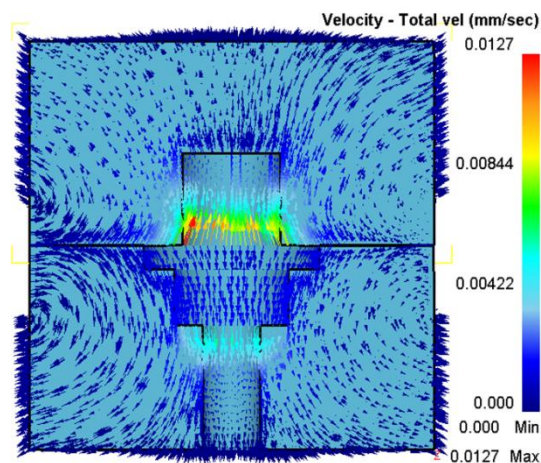


Fig 11 Velocity analysis of die-component setup in mm/sec

Fig 11 shows the velocity analysis for the die-component set-up, the velocity of flow of material during plastic deformation of the component in the die setup varies from a minimum of 0.000 mm/sec to a maximum of 0.0127 mm/sec.

IV. CONCLUSION

- [1] The effective stress on the component decreases as the initial temperature of the billet increases.
- [2] The maximum effective stress occurs during the initial contact of the lower and the upper die with the work piece.
- [3] The maximum effective stress is found to be lesser on the component if open upsetting is carried out on billet before final forging stage.
- [4] The stress concentration is maximum at the contact surface of parting lines of two halves of die set and the flange portion of the component.
- [5] It is observed that presence of small ribs on the outer cylindrical surface restricts the free flow of metal in the small recess of die cavity during forging, which leads to surface cracks, improper and incomplete rib formation.
- [6] The critical evaluation of the results of the investigation carried out suggests that the problems faced in precision forging of the component can be overcome by:
 - Increasing the height of the billet, upsetting the billet and then carrying out the press forging.
 - Providing suitable fillets in the die-set.
 - Ensuring suitable gap between the two die halves when the tool and die setup is pressed.
 - Increasing the dimensions of ribs or eliminating the need for ribs in the component.
- [7] It has also been found that the Aluminium 6061 connector can be press forged (by precision forging) with maximum benefits if the critical conclusions drawn from the analysis are successfully incorporated in the process.

V. REFERENCES

- [1] Santhosh N, "Flow simulation and characterization of Aluminium forgings conforming to AA 6061 Specification", M.E. Thesis, Bangalore University, Bangalore, India 2012.
- [2] Oh, S.I., 1982. "Finite element analysis of metal forming process with arbitrary shaped dies", *Int.J.Mesh.Sci.*, Vol.24.
- [3] Degarmo, E. Paul; Black, J. T.; Kohser, Ronald A. (2003), *Materials and Processes in Manufacturing* (9th ed.), Wiley, ISBN 0-471-65653-4, pp. 398-399.
- [4] O. Jensrud, K. Pedersen, "Cold Forging of High Strength Aluminum Alloys and the Development of New Thermomechanical Processing", *Journal of Materials Processing Technology*, 80–81 (1998). pp. 156–160
- [5] Victor Vazquez, Taylan Altan., "New Concepts in Die Design-Physical and Computer Modelling Applications", *Journal of Materials Processing Technology*, 98 (2000). pp. 212-223.
- [6] J. S. Gunasekera, "CAD/CAM of Dies", *Ellis Horward Series in Mechanical Engineering*, Ohio University, Athens, USA 1989, Ellis Howard Limited.
- [7] Douglas, R., Kuhlmann, D., "Guidelines for precision hot forging with applications". *Journal of Materials Processing Technology*, 98 (2000). pp. 182-188.
- [8] Y.H. Kim, T.K. Ryou, H.J. Choi, B.B. Hwang, "An Analysis of the Forging Processes for 6061 Aluminum-Alloy Wheels", *Journal of Materials Processing Technology*, 123 (2002). pp. 270–276.
- [9] Li, G., W. Wu, P. Chigurupati, J. Fluhrer, and S. Andreoli, "Recent Advancement of Extrusion Simulation in DEFORM-3D," *Latest Advances in Extrusion Technology and Simulation in Europe*, Bologna, Italy, 2007.
- [10] Altan, T., Oh, S.I, 1983. "Metal fundamentals and forming application", ASM International.
- [11] *Materials World*, Vol. 12, No. 3, pp. 37-38, March 2004.
- [12] *ASM Handbook of Heat Treatment*, Vol. 4, ISBN: 978-0-87170-379-8, ASM International, 1991.
- [13] George E. Totten, D. Scott MacKenzie, "Handbook of Aluminum: Physical Metallurgy and Process", Vol. 1, 2003.

Steady And Unsteady Bubbly Two-Phase Flow (Gas-Liquid Flow) Around A Hydrofoil In Enlarging Rectangular Channel

Laith Jaafer Habeeb¹, Riyadh S. Al-Turaihi²

¹Mechanical Engineering Dept., University of Technology, Baghdad(10) – Iraq

²College of Engineering/ Dept. of Mech. Eng., Babylon University, Babil(30) – Iraq

ABSTRACT

Experimental and numerical studies are investigated to study the two-phase flow phenomena around straight hydrofoil for different angle of attacks in a rectangular enlarging channel which has the dimensions (10 × 3 × 70 cm) enlarged from assembly circular tube of the two phases. Experiments are carried out in the channel with air-water flow with different air and water flow rates. These experiments are aimed to visualize the two phase flow phenomena as well as to study the effect of pressure difference through the channel with the existence of the hydrofoil. All sets of the experimental data in this study are obtained by using a pressure transducer and visualized by a video camera for different water discharges (20, 25, 35 and 45 l/min), different air discharges (10, 20, 30 and 40 l/min) and different angle of attack (0, 15 and 30 degree). While the numerical simulation is conducted by using commercial Fluent CFD software to investigate the steady and unsteady turbulent two dimensional flows for different air and water velocities. The results show that when the angle of attack increases at constant air and water discharge or when air discharge increases with constant water discharge and angle of attack or when water discharge increases with constant air discharge and angle of attack, the pressure difference increases at the inlet and the outlet of the rectangular channel.

KEYWORDS: experimental study, Fluent CFD software investigation, two-phase flow phenomena, straight hydrofoil, enlarging channel

I. INTRODUCTION

It is not possible to understand the two-phase flow phenomena without a clear understanding of the flow patterns encountered. It is expected that the flow patterns will influence the two -phase pressure drop, holdup, system stability, exchange rates of moment um, heat and mass during the phase-change heat transfer processes. The ability to accurately predict the type of flow is necessary before relevant calculation techniques can be developed [1]. The flow patterns of gas-liquid two-phase flow could be bubble flow, slug flow, plug flow, stratified flow, wavy flow and disperse flow. There are still many challenges associated with a fundamental understanding of flow patterns in multiphase flow and considerable research is necessary before reliable design tools become available. Gas-liquid flow was extensively used in industrial systems such as power generation units, cooling and heating systems (i.e. heat exchangers and manifolds), safety valves, etc. Thus two-phase flow characteristics through these singularities should be identified in order to be used in designing of the system [2]. In the last decade, the stratified flows are increasingly modeled with computational fluid dynamics (CFD) codes. In CFD, closure models are required that must be validated. The recent improvements of the multiphase flow modeling in the ANSYS code make it now possible to simulate these mechanisms in detail [3]. A comprehensive treatment of all sources of pressure drop within intermittent gas-liquid flows was presented [4]. Pressure loss associated with the viscous dissipation within a slug was calculated, and the presence of dispersed bubbles in a slug was accounted for, without recourse to the widely used assumption of homogenous flow. Experiments were conducted to measure pressure gradient within two air-water pipes of 32 and 50 mm internal diameter at 0 and +10° inclination to the horizontal. The results show that existing intermittent flow models predict pressure gradients considerably lower than were observed. The model predicted pressure gradients in good agreement with all the measurements and this was achieved without introducing any additional reliance on empirical information. The scope of a numerical-experimental collaborative research program, whose main objective was to understand the mechanisms of instabilities in partial cavitating flow, was carried out [5]. Experiments were conducted in the configuration of a rectangular foil located in a cavitation tunnel. Partial cavitation was investigated by multipoint

wall-pressure measurements together with lift and drag measurements and numerical videos. The algorithm of resolution was derived from the SIMPLE approach, modified to take into account the high compressibility of the medium. Three-dimensional unsteady cavitating flow around a NACA0015 hydrofoil fixed between the sidewalls was simulated [6] and the mechanism of U-shaped cloud cavity formation was clarified. A local homogeneous model was used for the modeling of the vapor– liquid two-phase medium. The compressible two-phase Navier–Stokes equations as the governing equations were solved. The cell-centered finite volume method was employed to discretize the governing equations. Assuming turbulent flow, the turbulent eddy viscosity coefficient was computed. As a result, even in the case of cavitating flow without sidewalls, the shed cloud cavities have slightly 3D structure, which was not so much large as extending across the whole spanwise direction. On the other hand, in the case of cavitating flow with sidewalls, the end of sheet cavities bows in the spanwise direction because of the development of boundary layer near both sidewalls. After that, due to the occurring of the reentrant jet towards the mid-span region, the sheet cavities breaks off from mid-span region near the leading edge of the hydrofoil, and became the vortical cloud cavities, which have the large-scale U-shaped structure. The two-dimensional simulation for an air-water bubbly flow around a hydrofoil was studied [7]. The vortex method, proposed by the authors for gas-liquid two-phase free turbulent flow in a prior paper, was applied for the simulation. The liquid vorticity field was discretized by vortex elements, and the behavior of vortex element and the bubble motion were simultaneously computed. The effect of bubble motion on the liquid flow was taken into account through the change in the strength of vortex element. The bubbly flow around a hydrofoil of NACA4412 with a chord length 100 mm was simulated. The Reynolds number is 2.5×10^5 , the bubble diameter was 1 mm, and the volumetric flow ratio of bubble to whole fluid was 0.048. It was confirmed that the simulated distributions of air volume fraction and pressure agreed well with the trend of the measurement and that the effect of angle of attack on the flow was favorably analyzed. These results demonstrate that the vortex method was applicable to the bubbly flow analysis around a hydrofoil. Particle image velocimetry was used to examine the flow behind a two-dimensional heaving hydrofoil of NACA 0012 cross section [8]. The deflection angle of the wake, which was related to the average lift and drag on the hydrofoil, was found to lie between 13 and 18. An examination of the swirl strength of the vortices generated by the hydrofoil motion reveals that the strongest vortices, which were created at the higher Strouhal numbers, dissipated most rapidly.

The two-phase pressure drop in a hydrofoil-based micro pin fin heat sink has been investigated using R-123 as the working fluid [9]. Two-phase frictional multipliers have been obtained over mass fluxes from 976 to 2349 kg/m²s and liquid and gas superficial velocities from 0.38 to 1.89 m/s and from 0.19 to 24 m/s, respectively. It has been found that the two-phase frictional multiplier was strongly dependent on flow pattern. The theoretical prediction using Martinelli parameter based on the laminar fluid and laminar gas flow represented the experimental data fairly well for the spray-annular flow. For the bubbly and wavy-intermittent flow, however, large deviations from the experimental data were recorded. The Martinelli parameter was successfully used to determine the flow patterns, which were bubbly, wavy-intermittent, and spray-annular flow in that study. Cavitating flows, which can occur in a variety of practical cases, can be modeled with a wide range of methods. One strategy consists of using the RANS (Reynolds Averaged Navier Stokes) equations and an additional transport equation for the liquid volume fraction, where mass transfer rate due to cavitation is modeled by a mass transfer model. Three widespread mass transfer models for the prediction of sheet cavitation around a hydrofoil were compared [10]. These models share the common feature of employing empirical coefficients, to tune the models of condensation and evaporation processes, which can influence the accuracy and stability of the numerical predictions. In order to compare the different mass transfer models fairly and congruently, the empirical coefficients of the different models were first well-tuned using an optimization strategy. The resulting well-tuned mass transfer models are then compared considering the flow around the NACA66 (MOD) and NACA009 hydrofoils. The numerical predictions based on the three different tuned mass transfer models were very close to each other and in agreement with the experimental data. Moreover, the optimization strategy seemed to be stable and accurate, and could be extended to additional mass transfer models and further flow problems.

From the previous review it is denoted that the recent researches for the turbulent two phase bubbly flow in enlarging channel and existence of a hydrofoil with different angle of attack are very limited. So, our concern in this investigation is to study the effects of wide range of air/water discharge in the steady and unsteady cases on the flow behavior with the enlargement from the circular tube of the water phases which contains the air phase tube, to the rectangular channel with the existence of a hydrofoil. The channel allows in particular the study of air-water bubbly/wavy flow under atmospheric pressure. Parallel to the experiments,

CFD-Fluent simulations were carried out. The behavior of bubbly/wavy generation and propagation was qualitatively reproduced by the simulation.

II. THE PHYSICAL MODEL AND EXPERIMENTAL APPARATUS

Fig.1 shows a schematic and photograph of the experimental Apparatus and measurements system. The rig is consists of, as shown in Fig. 2:

- 1- Main water tank of capacity (1 m^3).
- 2- Water pump with specification quantity ($0.08 \text{ m}^3/\text{min}$) and head (8 m).
- 3- Valves and piping system (1.25 in)
- 4- Adjustable volume flow rate of range ($10\text{-}80 \text{ l/min}$) is used to control the liquid (water) volume flow rates that enter test section.
- 5- Air compressor and it has a specification capacity of (0.5 m^3) and maximum pressure of (16 bars).
- 6- Rotameter was used to control the gas (air) volume flow rates that enter the test section. It has a volume flow rate range of ($6\text{-}50 \text{ l/min}$).
- 7- Valves and piping system (0.5 in) and gages.
- 8- Pressure transducer sensors which are used to record the pressure field with a range of (0-1 bar) and these pressure transducer sensors are located in honeycombs at the entrance and at the end of the test section. The pressure sensors with a distance of (80 cm) between each other are measuring with an accuracy of (0.1%).
- 9- The hydrofoil used is made of stainless steel and its dimensions are (3 cm) for the height and all other dimensions is given in figures (3-a & b). The hydrofoil is coated with a very thin layer of gray paint and its center located at (11.5 cm) from the entrance of the test section.
- 10- The test section is consisting of rectangular channel and a hydrofoil. The rectangular cross sectional area is ($10 \text{ cm} \times 3 \text{ cm}$) and has length of (70 cm) which is used to show the behavior of the two phase flow around the hydrofoil and to measure the pressure difference and records this behavior. The hydrofoil is mounted and fixed by screw and nut on a blind panel on the bottom of the rectangular channel. The three large Perspex windows of the channel (two lateral sides with lighting and the top side) allowing optical access through the test section. Two enlargement connecting parts are made of steel and manufactured with smooth slope. The first one is used to connect the test section with the outside water pipe in the entrance side while the second one is used to connect the test section with the outside mixture pipe in the exit side. The inside air pipe, in the entrance side, is holed and contained inside the water pipe by a steel flange.
- 11- Interface system consists of two parts which are the data logger and the transformer which contains in a plastic box. The data logger has a three connections two of them are connected to the outside of the box (one connected to the sensors and the other connected to the personal computer), the third connection is connected to the transformer, which is work to receive the signals as a voltage from the sensors and transmit it into the transformer and then re-received these signals after converting it to ampere signals in the transformer.
- 12- The interface system which is connected with a personal computer so that the measured pressure across the test section is displayed directly on the computer screen by using a suitable program.
- 13- A Sony digital video camera recorder of DCR-SR68E model of capacity 80 GB with lens of Carl Zeiss Vario-Tessar of 60 x optical, 2000 x digital is used to visualize the flow structure. The visualized data are analyzed by using a AVS video convertor software version 8.1. A typical sequence snapshots recorded by the camera using a recording rate of 30 f/s.

The flows of both gas and liquid are regulated respectively by the combination of valves and by-passages before they are measured by gas phase flow meter and liquid phase flow meter. The gas phase and the liquid phase are mixed in the enlargement connection part before they enter the test section. When the two-phase mixture flows out of the test section, the liquid phase and the gas phase are separated in liquid storage tank. Experiments were carried out to show the effect of different operation conditions on pressure difference across the test section and to visualize the flow around the hydrofoil. These conditions are water discharges, air discharges and angles of attack. The selected experimental values for water discharges are (20, 25, 35 and 45 l/min), for air discharges are (10, 20, 30 and 40 l/min) and for angles of attack are (0° , 15° , 30°).

The experimental procedures are:

- 1- Fix the hydrofoil at the channel bottom side at the first value of angle of attack (0°).
- 2- Turn on the water pump at the first value (20 l/min).
- 3- Turn on the air compressor at the first value (10 l/min).
- 4- Record the pressure drop through the test section and photograph the motion of the two-phase flow by the digital camera.

- 5- Repeat steps (2 to 5) after changing the water discharge.
 - 6- Repeat step (5) after changing the air discharge.
 - 7- Repeat the above steps after changing the hydrofoil angle of attack.
- These give sixteen (16) experimental cases for volume fraction (Air/Water ratios) for each angle of attack.

III. Numerical Modeling

In this study, the computational fluid dynamics (CFD) software have been applied for the numerical simulation for adiabatic gas-liquid flow characteristics through a horizontal channel contain a hydrofoil (different angle of attack every time) with smooth expansion from the liquid pipe in steady and unsteady cases for 2D. In order to compare numerical results with experimental ones, air-water couple has been selected as the representative of the gas-liquid two-phase flow. Construction of the numerical domain and the analysis are performed via GAMBIT and FLUENT (ANSYS 13.0) CFD codes, respectively. Two-phase flow variables such as void fraction and flow velocity for liquid (water) and gas (air) at the inlet condition, and the geometrical values of the system (i.e. channel length, width and height, pipes and inlet enlargement connecting part dimensions, and hydrofoil angle of attack) used in the analysis are selected as the same variables as the experimental part. Atmospheric conditions are valid for the experimental facility. Total test rig length in the experiments, thus in the numerical domain, is (100 cm) including (70 cm) for the test section containing the obstacle, and (30 cm) for the inlet enlargement part. Water pipe diameter is (3.175 cm) and air pipe diameter is (1.27 cm) as shown in Fig. 4. The 2D physical model is established using a model of flow focusing channel in CFD. The enlargement connecting part length consists of: (0.05 m) circular pipe, (0.15 m) diverge-link to change the shape from circular to rectangular and (0.1 m) rectangular duct. Air and water are selected to be working fluids and their fluid properties are in Table 1.

Table 1 Property parameters of the gas and liquid in CFD.

Fluid	Density (kg/m ³)	Viscosity (kg/m.s)	Surface Tension
Water	998.2	10.03×10^{-04}	0.072
Air	1.225	1.7894×10^{-05}	---

The model geometry structure was meshed by the preprocessor software of GAMBIT with the Quad/Pave grids. After meshing, the model contained (2D) 23009 grid nodes for 0° angle of attack (23154 for 15° and 23218 for 30°), 22433 cells for 0° angle of attack (22578 for 15° and 22642 for 30°) and 44290 faces for 0° angle of attack (44290 for 15° and 44708 for 30°) -as demonstrated in Fig. 4 for 15° angle of attack- before importing into the processor Fluent for calculation. This refinement grid provided a precise solution to capture the complex flow field around the hydrofoil and mixing region in the enlargement connecting part. The boundary conditions are the velocity inlet to the air and water feeding (Table 2) and the pressure outlet to the model outlet. In Fluent, the Mixture Multiphase model was adopted to simulate the flow. The mixture model is a simplified Eulerian approach for modeling *n*-phase flows [11]. Because the flow rates of the air and water in the channel are high, the turbulent model (*k-ε* Standard Wall Function) has been selected for calculation. The other options in Fluent are selected: SIMPLE (Semi-Implicit Method for Pressure-Linked Equations) scheme for the pressure-velocity coupling, PRESTO (pressure staggering option) scheme for the pressure interpolation, Green-Gauss Cell Based option for gradients, First-order Up-wind Differencing scheme for the momentum equation, the schiller-naumann scheme for the drag coefficient, manninen-et-al for the slip velocity and other selections are described in Table 3. The time step (for unsteady case), maximum number of iteration and relaxation factors have been selected with proper values to enable convergence for solution which is about to (0.001) for all parameters.

Table 2 Air-water flow cases.

Case number	Air/water discharges (l/min)	Air/water velocities (m/sec)	Case number	Air/water discharge (l/min)	Air/water velocities (m/sec)
1	10/20	1.32/0.50	5	20/20	2.63/0.50
2	10/25	1.32/0.63	6	20/25	2.63/0.63
3	10/35	1.32/0.87	7	20/35	2.63/0.87
4	10/45	1.32/1.12	8	20/45	2.63/1.12
Case number	Air/water discharge (l/min)	Air/water velocities (m/sec)	Case number	Air/water discharge (l/min)	Air/water velocities

					(m/sec)
9	30/20	3.95/0.50	13	40/20	5.26/0.50
10	30/25	3.95/0.63	14	40/25	5.26/0.63
11	30/35	3.95/0.87	15	40/35	5.26/0.87
12	30/45	3.95/1.12	16	40/45	5.26/1.12

Table 3 Other mixture model selections for Fluent.

Solver type	$k-\varepsilon$ Model	Solution Methods
Pressure-Based	Cmu=0.09, C1-Epsilon=1.44, C2-Epsilon=1.92	Volume Fraction and Turbulent Kinetic Energy (First-order Up-wind)
Starting Solution Controls (Under-Relaxation Factors)		
Pressure=0.3, Momentum=0.7, Turbulent Kinetic Energy & Turbulent Dissipation Rate=0.8		
Specification Method for turbulence		
Turbulent Intensity (=3%) and Hydraulic Diameter = (0.0127 m, 0.0191 m and 0.1 m) for inlet air, inlet water and mixture outlet respectively		
Solution Initialization		
Turbulent Kinetic Energy (m^2/s^2)=0.0003375, Turbulent Dissipation Rate (m^2/s^3)= 0.0007620108 and air-bubble Volume Fraction=0		

The hydrodynamics of two-phase flow can be described by the equations for the conservation of mass and momentum, together with an additional advection equation to determine the gas-liquid interface. The two-phase flow is assumed to be incompressible since the pressure drop along the axis orientation is small. For the incompressible working fluids, the governing equations of the Mixture Multiphase Model are as following [11]-[12]:

- The continuity equation for the mixture is:

$$\frac{\partial}{\partial t}(\rho_m) + \nabla \cdot (\rho_m \vec{v}_m) = 0 \quad (1)$$

Where \vec{v}_m is the mass-averaged velocity:

$$\vec{v}_m = \frac{\sum_{k=1}^n \alpha_k \rho_k \vec{v}_k}{\rho_m} \quad (2)$$

and ρ_m is the mixture density:

$$\rho_m = \sum_{k=1}^n \alpha_k \rho_k \quad (3)$$

α_k is the volume fraction of phase k .

- The momentum equation for the mixture can be obtained by summing the individual momentum equations for all phases. It can be expressed as:

$$\frac{\partial}{\partial t}(\rho_m \vec{v}_m) + \nabla \cdot (\rho_m \vec{v}_m \vec{v}_m) = -\nabla p + \nabla \cdot [\mu_m (\nabla \vec{v}_m + \nabla \vec{v}_m^T)] + \rho_m \vec{g} + \vec{F} + \nabla \cdot (\sum_{k=1}^n \alpha_k \rho_k \vec{v}_{dr,k} \vec{v}) \quad (4)$$

where n is the number of phases, \vec{F} is a body force and μ_m is the viscosity of the mixture:

$$\mu_m = \sum_{k=1}^n \alpha_k \mu_k \quad (5)$$

$\vec{v}_{dr,k}$ is the drift velocity for secondary phase k :

$$\vec{v}_{dr,k} = \vec{v}_k - \vec{v}_m \quad (6)$$

From the continuity equation for secondary phase p , the volume fraction equation for secondary phase p can be obtained:

$$\frac{\partial}{\partial t} (\alpha_p \rho_p) + \nabla \cdot (\alpha_p \rho_p \vec{v}_m) = -\nabla \cdot (\alpha_p \rho_p \vec{v}_{dr,p}) + \sum_{q=1}^n (\dot{m}_{qp} - \dot{m}_{pq}) \quad (7)$$

The relative velocity (also referred to as the slip velocity) is defined as the velocity of a secondary phase (p) relative to the velocity of the primary phase (q):

$$\vec{v}_{pq} = \vec{v}_p - \vec{v}_q \quad (8)$$

The mass fraction for any phase (k) is defined as:

$$c_k = \frac{\alpha_k \rho_k}{\rho_m} \quad (9)$$

The drift velocity and the relative velocity (\vec{v}_{qp}) are connected by the following expression:

$$\vec{v}_{dr,p} = \vec{v}_{pq} - \sum_{k=1}^n c_k \vec{v}_{qk} \quad (10)$$

ANSYS FLUENT's mixture model makes use of an algebraic slip formulation. The basic assumption of the algebraic slip mixture model is that to prescribe an algebraic relation for the relative velocity, a local equilibrium between the phases should be reached over a short spatial length scale. The form of the relative velocity is given by:

$$\vec{v}_{pq} = \frac{\tau_p (\rho_p - \rho_m)}{f_{drag} \rho_p} \vec{a} \quad (11)$$

where τ_p is the particle relaxation time:

$$\tau_p = \frac{\rho_p d_p^2}{18 \mu_q} \quad (12)$$

d is the diameter of the particles (or droplets or bubbles) of secondary phase p , \vec{a} is the secondary-phase particle's acceleration. The default drag function f_{drag} :

$$f_{drag} = \begin{cases} 1 + 0.15 Re^{0.687} & Re \leq 1000 \\ 0.0183 Re & Re > 1000 \end{cases} \quad (13)$$

and the acceleration \vec{a} is of the form:

$$\vec{a} = \vec{g} - (\vec{v}_m \cdot \nabla) \vec{v}_m - \frac{\partial \vec{v}_m}{\partial t} \quad (14)$$

The simplest algebraic slip formulation is the so-called drift flux model, in which the acceleration of the particle is given by gravity and/or a centrifugal force and the particulate relaxation time is modified to take into account the presence of other particles.

In turbulent flows the relative velocity should contain a diffusion term due to the dispersion appearing in the momentum equation for the dispersed phase. ANSYS FLUENT adds this dispersion to the relative velocity:

$$\vec{v}_{pq} = \frac{(\rho_p - \rho_m) d_p^2}{18 \mu_q f_{drag} \rho_p} \vec{a} - \frac{\eta_t}{\sigma_t} \left(\frac{\nabla \alpha_p}{\alpha_p} - \frac{\nabla \alpha_q}{\alpha_q} \right) \quad (15)$$

where σ_t is a Prandtl/Schmidt number set to 0.75 and η_t is the turbulent diffusivity. This diffusivity is calculated from the continuous-dispersed fluctuating velocity correlation, such that:

$$\eta_t = C_\mu \frac{k^2}{\varepsilon} \left(\frac{\gamma_y}{1 + \gamma_y} \right) \left(1 + C_\beta \frac{\varepsilon^2}{\gamma_y} \right)^{-1/2} \quad (16)$$

$$\frac{\varepsilon}{\gamma_y} = \frac{|\vec{v}_{pq}|}{\sqrt{2/3} k} \quad (17)$$

Where $C_\beta = 1.8 - 1.35 \cos^2 \theta$, $\cos \theta = \frac{\vec{v}_{pq} \cdot \vec{v}_p}{|\vec{v}_{pq}| |\vec{v}_p|}$ and γ_y is the time ratio between the time scale of the energetic turbulent eddies affected by the crossing-trajectories effect and the particle relaxation time. If the slip velocity is not solved, the mixture model is reduced to a homogeneous multiphase model. In FLUENT application, boundary conditions like "velocity inlet" is taken as the inlet condition for water and air while "interior" and "outflow" are employed as the water-air mixture. Air is injected to the water via an air pipe in the experiments, therefore, the gas flow through the air pipe and the mixture occurred outlet of it are modeled in 3D. According to the simulation, air with known mass flow rate flows through air pipe and then disperses into the water at the exit of the pipe. At air flow rates (thus volumetric void fraction), phase inlet velocity and void fraction profiles obtained at the air and water pipes outlet are extracted from the experimental calculations in order to be introduced as the inlet condition for the flow analysis regarding the numerical 2D domain. In the present study bubble diameter is equal to (1 cm). Assuming the bubbles are in spherical shape and neglecting the coalescence between them along the channel.

IV. EXPERIMENTAL RESULTS

The experimental results are represent the gas-liquid flow through channel with the existence of the hydrofoil for different water discharges (20, 25, 35 and 45 l/min), different air discharge (10, 20, 30 and 40 l/min) and different angle of attack (0° , 15° and 30°) as photographs and pressure graphs. Below are some of these cases.

4.1. Effect of Air and Water Discharges

Figs (5 and 6) show photographs for the two phase flow behavior around the hydrofoil of water discharge ($Q_w=20$ and 25 l/min) respectively and air discharges ($Q_a =$ (a)10, (b)20, (c)30 and (d)40 l/min) for the three angles of attack (0° , 15° and 30°) from top to bottom. It shows that the number (amount) of bubble is few and has small size at low water discharge. These photographs describe the flow behavior and it appears that it is near to slug region when the discharge is low. This is due to the low velocity of water at low water discharge. Also when increase the air discharge the size and number of bubbles increases and the bubble cavities develops to cloud cavitations especially at high air discharge. This is due to the high velocity of water at high water discharge which leads to more turbulence in the flow and the flow becomes bubbly as shown. It is clear that the flow becomes unstable and unsymmetrical around the hydrofoil and the number and size of bubble becomes higher compared with the low velocities cases. It appears that the vortices behind and beside the hydrofoil becomes more strong compared with the low discharge cases. When the two phases increases, more unsteady behavior is noticed and the flow oscillates between bubble and disperse regions. Also, when water discharge increases with increase air discharge, flow becomes unsteady, vortices developed around the hydrofoil surface and most bubbles transformed to cloudy flow, then a disperse region and strong vortex shedding is observed. This is due to the important effect of the hydrofoil existence in the rectangular channel which effect on pressure difference across the inlet and outlet of the channel. The experimental data shows that the average number of bubbles generally increases with increasing mixture velocities. Independently of the inlet velocities, the highest number of bubbles is found in the mixing region. Moreover, higher gas velocities have a higher number of bubbles in the mixing region.

4.2. Effect of Angle of Attack

Figures (7, 8, 9, 10, 11 and 12) show photographs for the two phase flow behavior around the hydrofoil of water discharges ($Q_w=35$ and 45 l/min) respectively and air discharges ($Q_a=$ (a)10, (b)20, (c)30 and (d)40 l/min) from top to bottom for different values of angles of attack for the straight hydrofoil (0° , 15° and 30°). These figures show that the number and size of bubbles increases and cavities become larger when the angle of attack increases at constant air and water discharge and the flow becomes unstable behind and beside the straight hydrofoil. Also the increase in the angle of attack leads to the vortex generation, the flow becomes unsteady and asymmetric around and behind the straight hydrofoil and most bubbles cavity develop to cloud cavities.

4.3. Pressure Difference

Figures (13 and 14) represent the mean pressure difference with air discharge for different values of water discharge for the three angles of attack. When air or water discharge increases, the mean pressure difference increases. This is due to the increase of air or water discharge resulting in velocity increases. Also, the mean pressure difference has a significant influence on two-phase flow behavior. Therefore, it is expected that the flow instability will also depend upon the pressure difference. Moreover when the air discharge increases, the pressure fluctuation increases. This is due to the high inertia force in the two phase flow. At these angles of attack, the increase in air and water discharges resulting in pressure difference increasing. This is due to the transition from laminar to turbulent boundary layer, therefore the pressure difference increases.

4.4. Time Evolution of Pressure

Figure 15 represents the effect of time evolution of pressure for different angle of attack, air and water discharges obtained by experiments. The pressure sensor at the inlet and outlet of the test section are record pressures that fluctuating as a function of time due to two-phase flow effect. At the same air and water discharge the increase in the angle of attack increasing the pressures fluctuation. Also, at the same angle of attack the increase in the air and water discharge increasing the pressures fluctuation.

V. NUMERICAL RESULTS

The numerical results are represented as colored contours for the same air-water discharges cases in the experimental part. As mentioned above, the 2D inlet (line) air or water velocities are calculated from the 3D experimental inlet (surface) area for the air or water discharge. These give thirty-two (32) numerical cases for volume fraction (Air/Water ratios) at each angle of attack including steady and unsteady states. In the present calculations the air-water mixture of any finite bubbles existing in each control volume is approximated to those

of infinite number of infinitesimal bubbles. Thus, the local mixture condition in the air–water two-phase medium is specified in each computational cell having the same void fraction. Below are some of these cases.

5.1. Steady State

Fig.s (16-a, b, c and d) depict volume fraction (water) contours for selected cases (case1, 2, 6 and 10) respectively for angle of attack (0°). While Fig.s (17-a, b, c and d) depict volume fraction contours for other selected cases (case3, 11, 12 and 16) respectively for angle of attack (15°). Also, Fig.s (18-a, b, c and d) depict volume fraction (water) contours for selected cases (case4, 7, 9 and 13) respectively for angle of attack (30°). The differences between the experimental snapshots and numerical figures are due to two reasons; the first is the differences in the overall flow rates of air and water for the same inlet velocities from the inlet regions (small lines in 2D numerical cases and big square and annulus areas in 3D experimental cases), and the second reason is that the snapshots are taken roughly from the experimental movies for each case and may be for another snapshot from the same case movie, the differences will be less. From these figures it is appear that a slug to disperse/bubbly regions flow pattern is achieved. The flow rates of air and water have a large range and it show the increase in water phase and with the decrease of the gas flow rate, the volume fraction of the gas decreased and the volume fraction of the water increased simultaneously. According to these figures, stratified water-air mixture enters the singularity section and begins to decelerate due to the smoothly enlarging cross-section and it show how the volume fraction affected the flow behavior. A uniform dispersed two-phase flow, in which the dispersed phase (either air bubbles) moves with their carrier fluid (water), approaches to the hydrofoil. Due to strong changes of both magnitude and direction of local velocities of the fluid flow (i.e. local fluid velocity gradients) and density difference between the dispersed phase and the fluid, the local phase distribution pattern changes markedly around the hydrofoil. Strong air flows are induced and a strong vortex is created as a result of the entered air and small vortices are also produced. A recirculation zone in the wake, a flow separation at the edge of the hydrofoil and a wavy motion are noticed. It is appear that maximum turbulent viscosity and high turbulence regions depends on the volume fraction ratio. Also, when air velocity increases, separation area is detected after the hydrofoil.

5.2. Unsteady State

Fig.s (19-a, b, c and d) represent volume fraction (water) contours development for selected unsteady case5 for angle of attack (0°). Fig.s (20-a, b, c, and d) represent volume fraction (water) contours development for unsteady case14 for angle of attack (15°). Fig.s (21-a, b, c and d) represent volume fraction (water) contours development for unsteady case8 for angle of attack (30°). Also, fig.s (22-a, b, c and d) represent volume fraction (water) contours development for unsteady case15 for angle of attack (30°). It show how the volume fraction develops with time. As can be seen, the cavitating flow behind the foil is achieved in two regions. The increase in the angle of attack leads to a cavity flow and the flow becomes unsteady behind the straight hydrofoil and most bubbles cavity develops to cloud cavities.

VI. CONCLUSIONS

The partial cavitating flow and resulting cloud cavitation around a two-dimensional hydrofoil was investigated in this study both numerically and experimentally. The computations were performed in the configuration of the 2D hydrofoil section. This study consists of a theoretical part of a more general nature and an experimental part highlighting bubbly flows around a hydrofoil in horizontal channel. The numerical results were more closely investigated to explain the different behaviors obtained at the three angles of attack. Concluding remarks are summarized below:

- 1- Three different flow patterns are detected in flow visualization study, which are bubbly, wavy-intermittent, and spray flow patterns.
- 2- In the wavy-intermittent flow pattern, a thick liquid layer is present around the hydrofoil surface, and the air phase core and liquid layer are separated by a wavy interface.
- 3- When air discharge increases, high turbulence is appear which generate more bubbles and waves.
- 4- The pressure sensor at the inlet and outlet of the test section are record pressures that fluctuating as a function of time due to two-phase effect. Also, when air or water discharge increases, the mean pressure difference increases.
- 5- Due to strong changes of both magnitude and direction of local velocities of the fluid flow and density difference between the dispersed phase and the fluid, the local phase distribution pattern changes markedly around the hydrofoil.
- 6- It should be noted that the prediction on the bubble size does not correctly describe the size observed in experiments. This is due to the difference in the numerical definition of vapor bubble and visual bubble boundary.

- 7- In a water slug, bubbles move slower than the liquid. The average velocity of the bubbles is slightly slower than the slug tail velocity. This means that the dispersed bubbles in the liquid slug will be caught up by the arriving elongated bubble.
- 8- Realistic bubble trajectories, with a number of bubble trajectories entering the wake of a hydrofoil, are only obtained if the effect of liquid velocity fluctuations (or turbulence in the liquid) is simulated and some kind of sliding phenomenon for colliding bubbles is taken into account.
- 9- The effect of the existence of a hydrofoil is clear in dividing the two-phase flow, generate vortices and finally enhance mixing and the smooth obstacle (hydrofoil) generates less bubble and turbulence.

In this study, diameter of the bubbles is considered constant and coalescence between the bubbles is neglected. However, bubbles in the actual flow break down and unite as the flow develops along the channel and this gives a varying diameter distribution which causes lift and drag forces to be calculated locally. Therefore, a simulation considering the effects of differing bubble diameter and interfacial forces is suggested for better modeling of the flow investigated.

REFERENCES

- [1] Brennen and Christopher Earls, "Flow Pattern, Pressure Drop and Void Fraction of Two-Phase Gas-Liquid flow In an Inclined Narrow Annular Channel", *Experimental Thermal and Fluid Science* (30), 345–354, 2006.
- [2] Brennen and Christopher Earls, "Fundamentals of Multiphase Flow", Cambridge University Press. ISBN 13 978-0-521-84804-6, 2005.
- [3] Thomas HÖHNE, "Experiments and Numerical Simulations of Horizontal Two Phase Flow Regimes", Seventh International Conference on CFD in the Minerals and Process Industries, CSIRO, Melbourne, Australia, December 2009.
- [4] E. Krepper, P. Ruyer, M. Beyer, D. Lucas, H.-M. Prasser and N. Seiler "CFD Simulation of Polydispersed Bubbly Two-Phase Flow around an Obstacle", *Science and Technology of Nuclear Installations* 239, 2372–2381, 2009.
- [5] Jean-Baptiste Leroux, Olivier Coutier-Delgosha and Jacques André Astolfi, "A Joint Experimental and Numerical Study of Mechanisms Associated to Instability of Partial Cavitation on Two-Dimensional Hydrofoil", *PHYSICS OF FLUIDS*, American Institute of Physics, 17, 052101, 2005.
- [6] Yoshinori Saito, Rieko Takami, Ichiro Nakamori and Toshiaki Ikohagi, "Numerical Analysis of Unsteady Behavior of Cloud Cavitation around a NACA0015 Foil", *Comput Mech* (2007) 40:85–96, Springer-Verlag.
- [7] Tomomi Uchiyama and Tomohiro Degawa, "Vortex Simulation of the Bubbly Flow around a Hydrofoil", *International Journal of Rotating Machinery*, Hindawi Publishing Corporation, Volume 2007.
- [8] K. D. von Ellenrieder and S. Pothos, "PIV Measurements of the Asymmetric Wake of a Two Dimensional Heaving Hydrofoil", *Exp Fluids* (2008) 44:733–745, Springer-Verlag.
- [9] Ali Koşar, "Two-Phase Pressure Drop across a Hydrofoil-Based Micro Pin Device Using R-123", *Experimental Thermal and Fluid Science* 32 (2008) 1213–1221, Scencedirect, Elsevier.
- [10] Mitja Morgut, Enrico Nobile and Ignacijo Biluš, "Comparison of Mass Transfer Models for the Numerical Prediction of Sheet Cavitation around a Hydrofoil", *International Journal of Multiphase Flow* 37 (2011) 620–626, Scencedirect, Elsevier.
- [11] Introductory FLUENT Notes, FLUENT v6.3, Fluent User Services Center, December 2006.
- [12] ANSYS 13.0 Help, FLUENT Theory Guide, Mixture Multiphase Model.
- [13] Esam M. Abed and Riyadh S. Al-Turaihi, "Experimental Study of Two-Phase Flow around Hydrofoil in Open Channel", *Journal for Mechanical and Materials Engineering*, Iraq, 2012, accepted and submitted for publication.
- [14] Riyadh S. Al-Turaihi, "Experimental Investigation of Two-Phase Flow (Gas –Liquid) around a Straight Hydrofoil in Rectangular Channel", *Journal of Babylon University*, Iraq, 2012, accepted and submitted for publication.

Nomenclature

c_k	Mass fraction (-)	
d	Diameter of the particles	(m)
F	Body force	(N)
f_{drag}	Drag function	(-)
g	Gravity acceleration	(m/s ²)
\dot{m}	Mass flow rate	(kg/m ³ .s)
n	Number of phases	(-)
Q	Discharge	(l/min)
t	Time	(sec)

Greek Symbols

α_k	Volume fraction of phase k	(-)
\vec{a}	Secondary-phase particle's acceleration	(m/s ²)
	Turbulent diffusivity	(N/m ² .s)
ρ_m	Mixture density	(kg/m ³)

- τ_p Prandtl/Schmidt number (-)
- τ_p Particle relaxation time (sec)
- v_m Mass-averaged velocity (-)
- $\vec{v}_{dr,k}$ Drift velocity for secondary phase k (velocity of an algebraic slip component relative to the mixture) (-)
- μ_m Viscosity of the mixture (N/m².s)

Subscripts

- a Air
- k,p Secondary phase
- m Mixture
- w Water

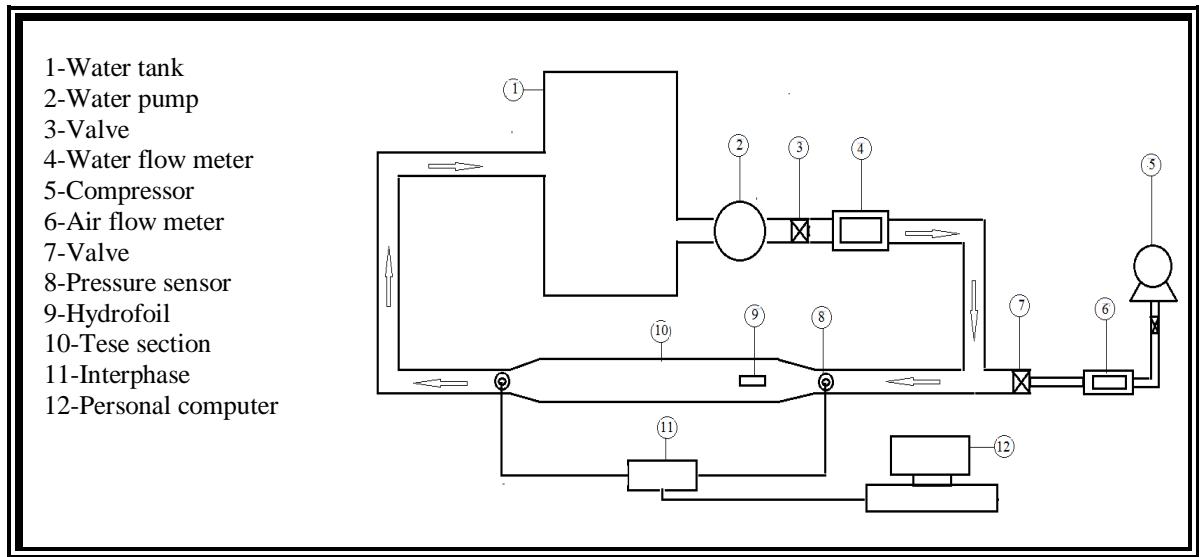


Figure 1. The experimental rig and measurements system [13]-[14].



Figure 2. (a) Water system, (b) Air flow meter, (c) Enlargement connecting part, flange, piping system and pressure transducer sensor [13]-[14].

Symbol	Dimension in(mm)	Symbol	Dimension in(mm)
A	50	D	20
B	26	E	10
C	20	F	5

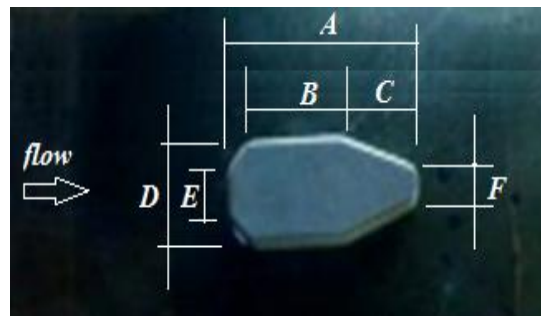


Figure 3. The straight hydrofoil dimensions (mm) [14].

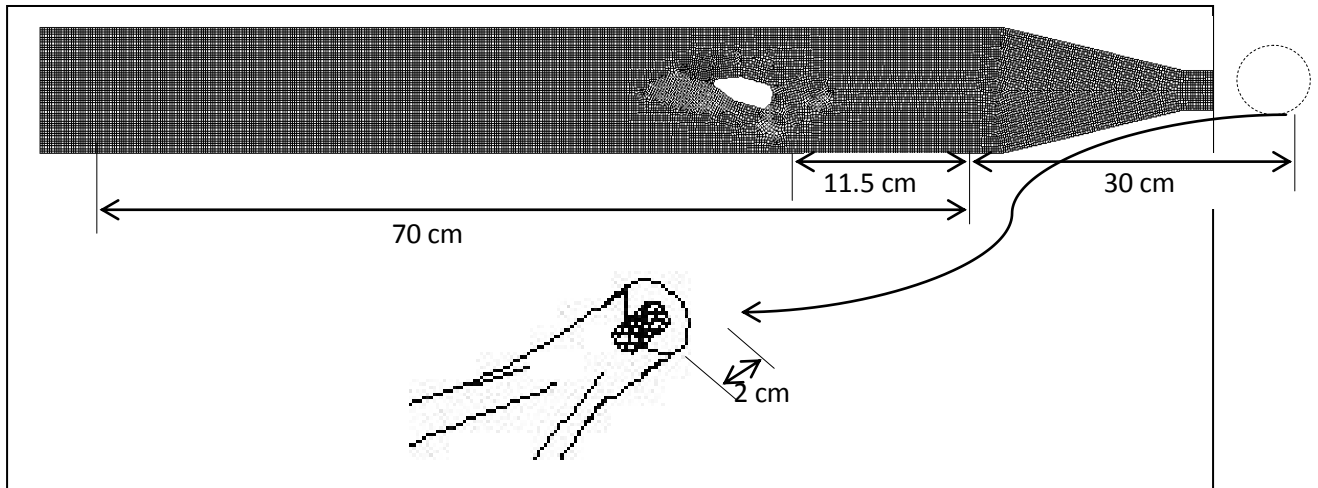


Figure 4. 2D model geometry structure mesh.

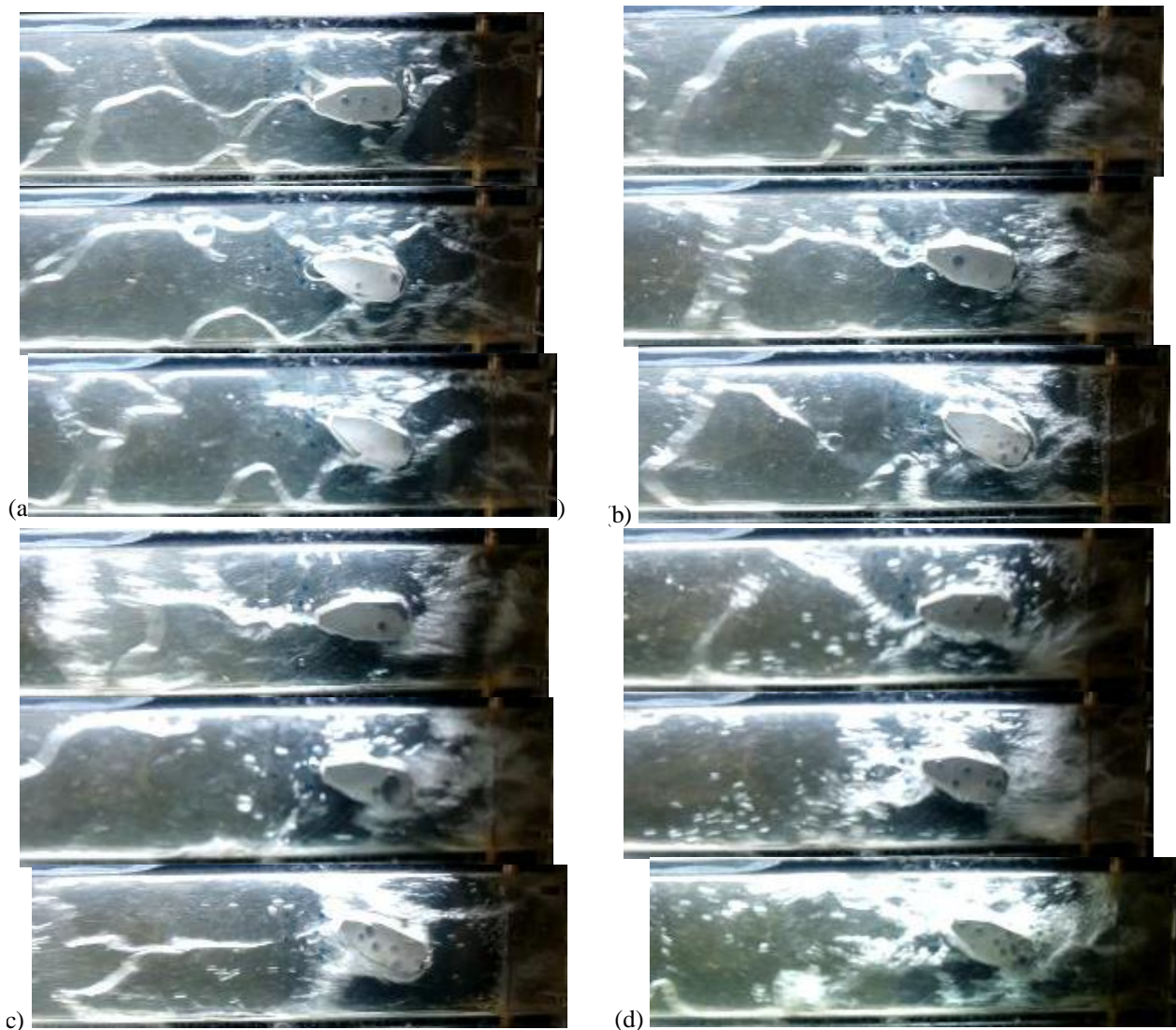


Figure 5. Photographs for the two phase flow behavior at $Q_w=20$ l/min, $Q_a=10, 20, 30, 40$ l/min and angle of attack= 0, 15, 30 degree respectively.

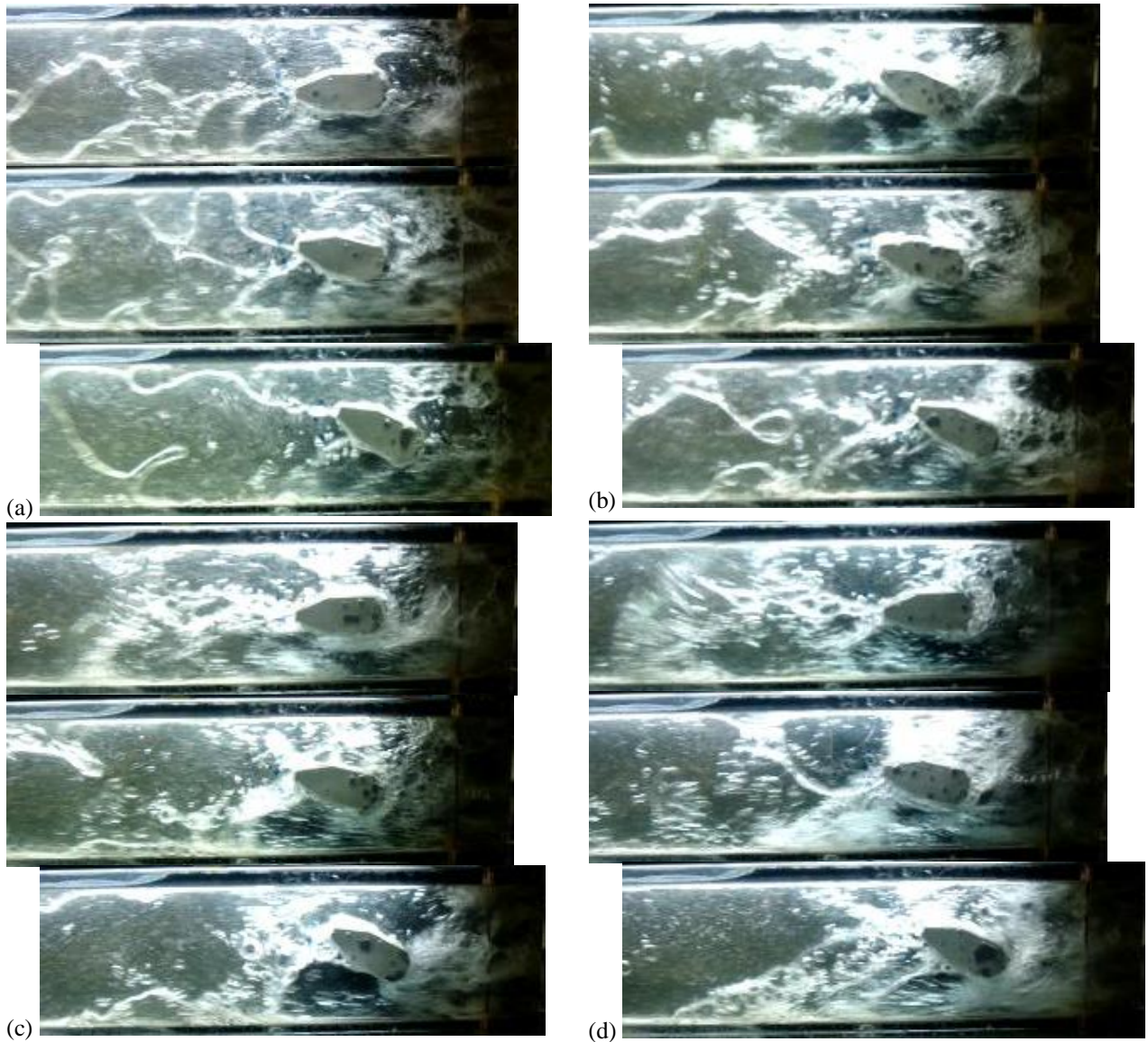


Figure 6. Photographs for the two phase flow behavior at $Q_w=25$ l/min, $Q_a=10, 20, 30, 40$ l/min and angle of attack= 0, 15, 30 degree respectively.

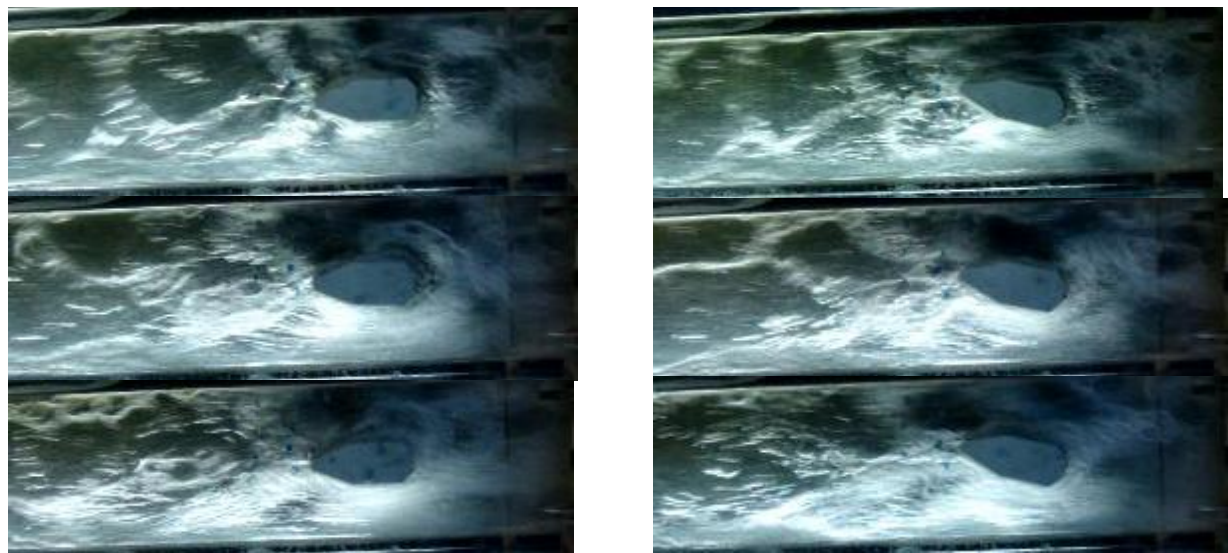
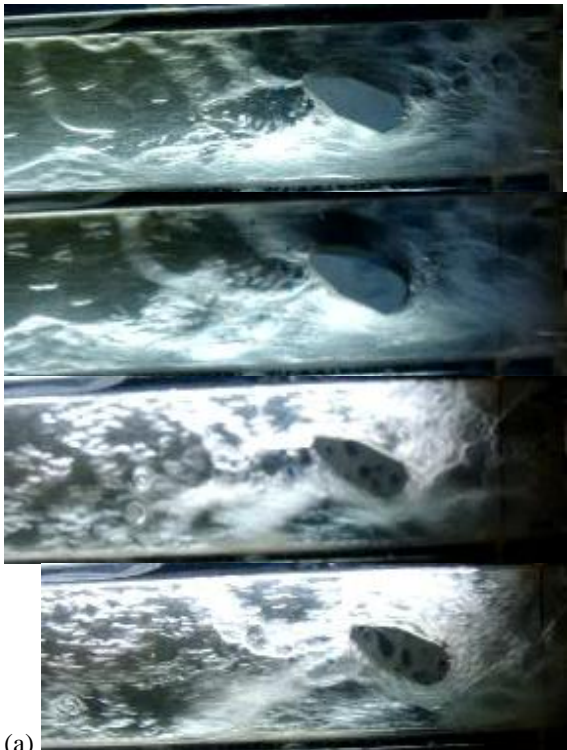




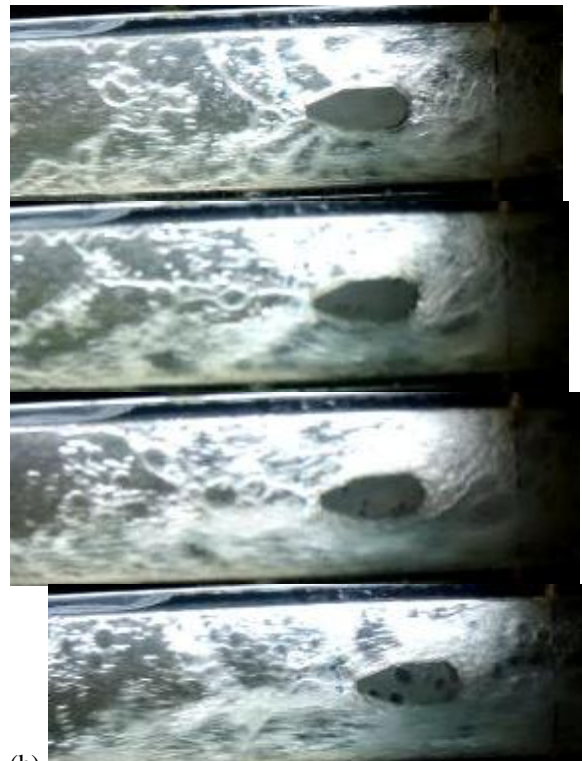
Figure 7. Photographs for the two phase flow behavior at $Q_w=35$ l/min, angle of attack= 0 degree and $Q_a=10, 20, 30, 40$ l/min respectively.



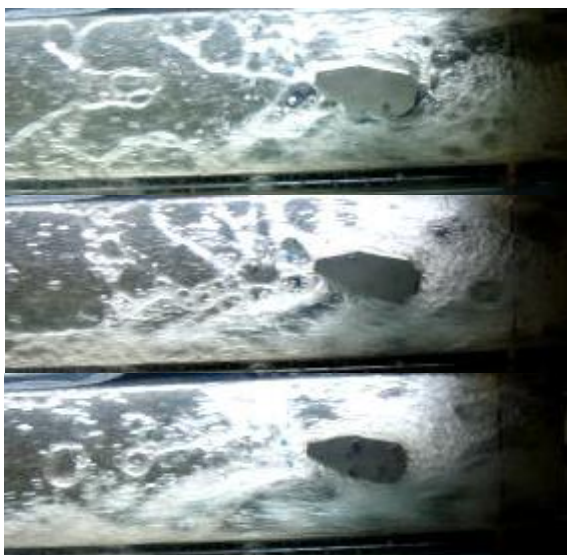
Figure 8. Photographs for the two phase flow behavior at $Q_w=35$ l/min, angle of attack= 15 degree and $Q_a=10, 20, 30, 40$ l/min respectively.



(a) Figure 9. Photographs for the two phase flow behavior at $Q_w=35$ l/min, angle of attack= 30 degree and $Q_a=10, 20, 30, 40$ l/min respectively.



(b) Figure 10. Photographs for the two phase flow behavior at $Q_w=45$ l/min, angle of attack= 0 degree and $Q_a=10, 20, 30, 40$ l/min respectively.





(c) Figure 11. Photographs for the two phase flow behavior at $Q_w=45$ l/min, angle of attack= 15 degree and $Q_a=10, 20, 30, 40$ l/min respectively.



(d) Figure 12. Photographs for the two phase flow behavior at $Q_w=45$ l/min, angle of attack= 30 degree and $Q_a=10, 20, 30, 40$ l/min respectively.

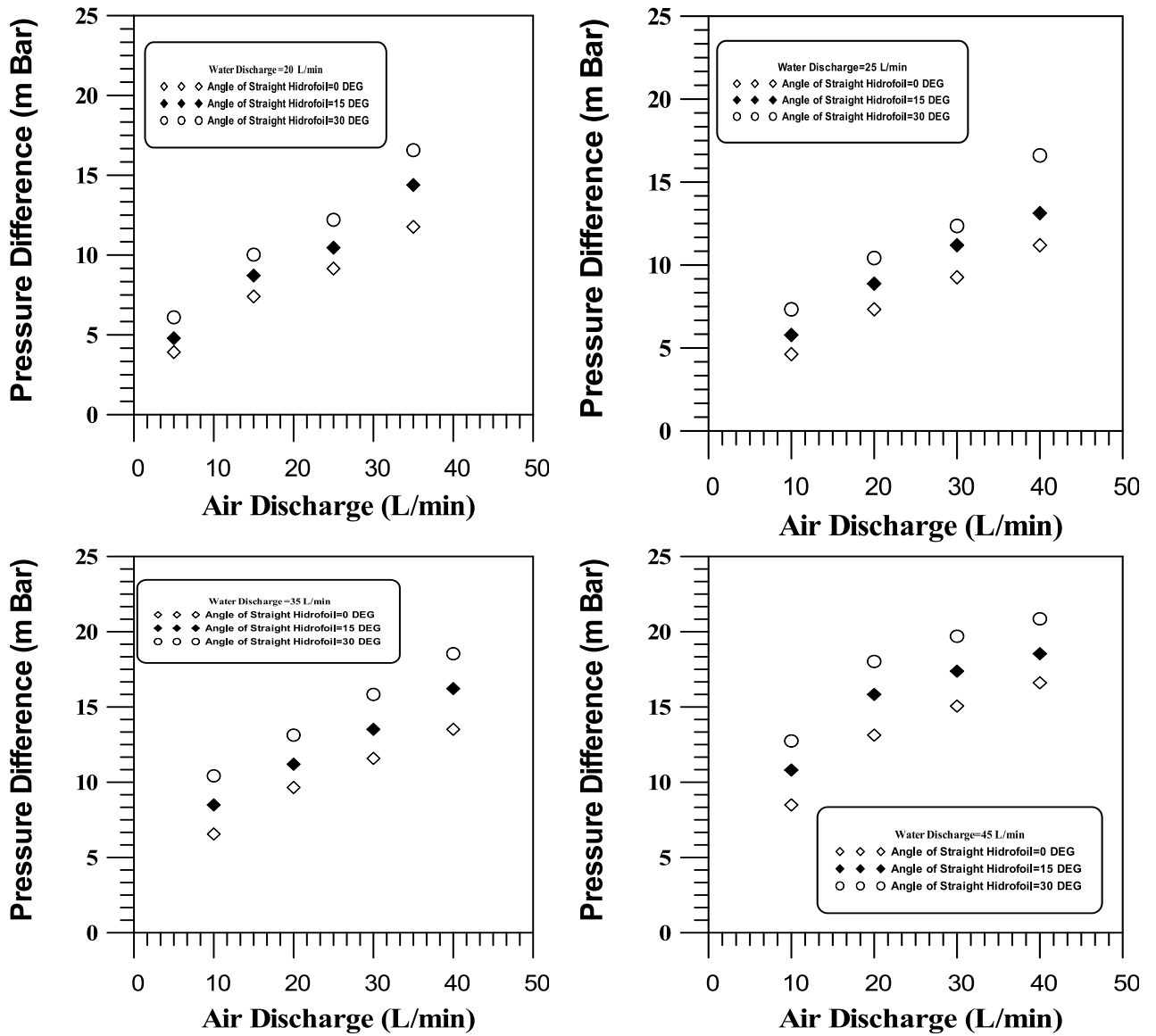


Figure 13. Mean pressure difference with air discharge for different values angle of attack.

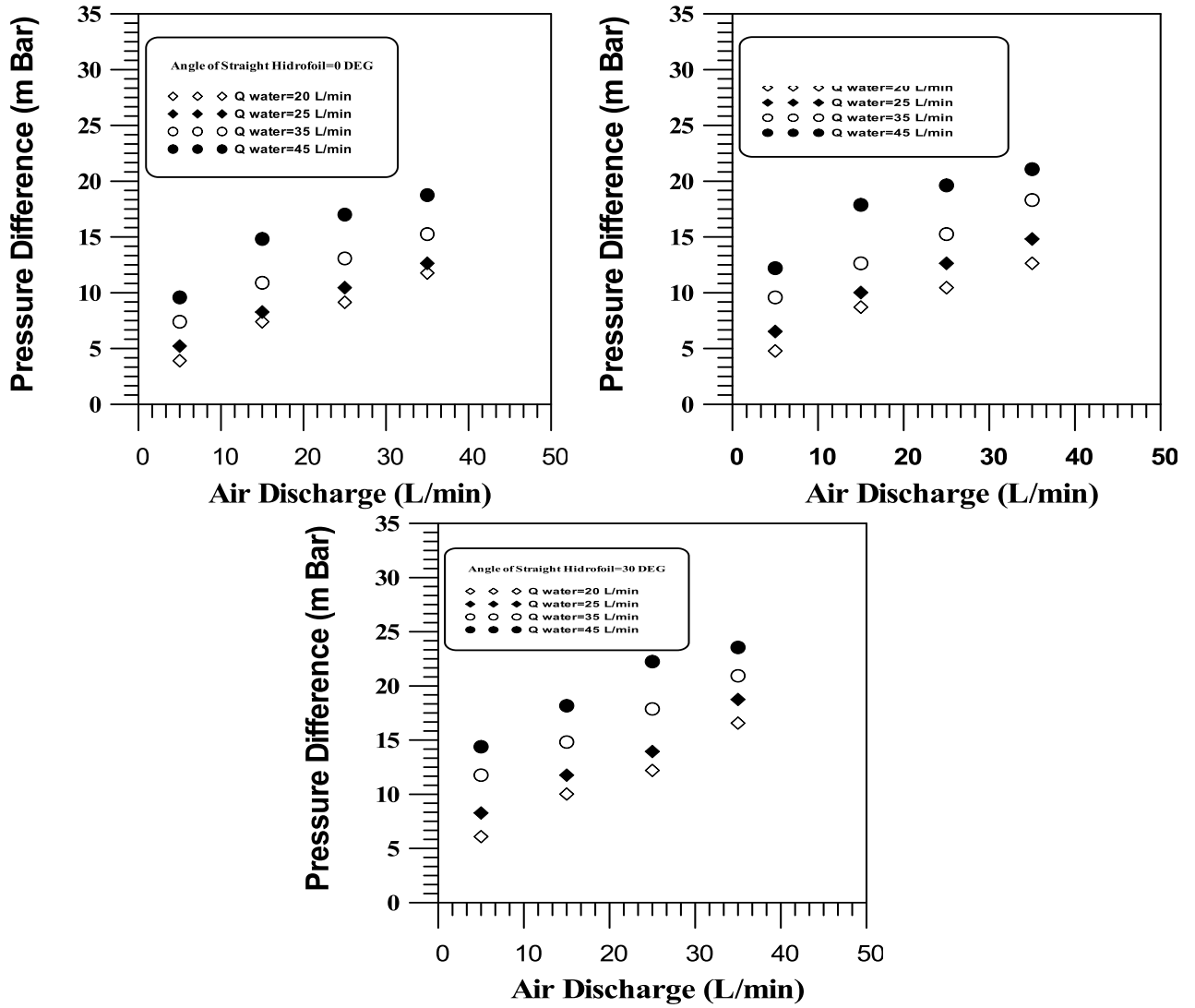
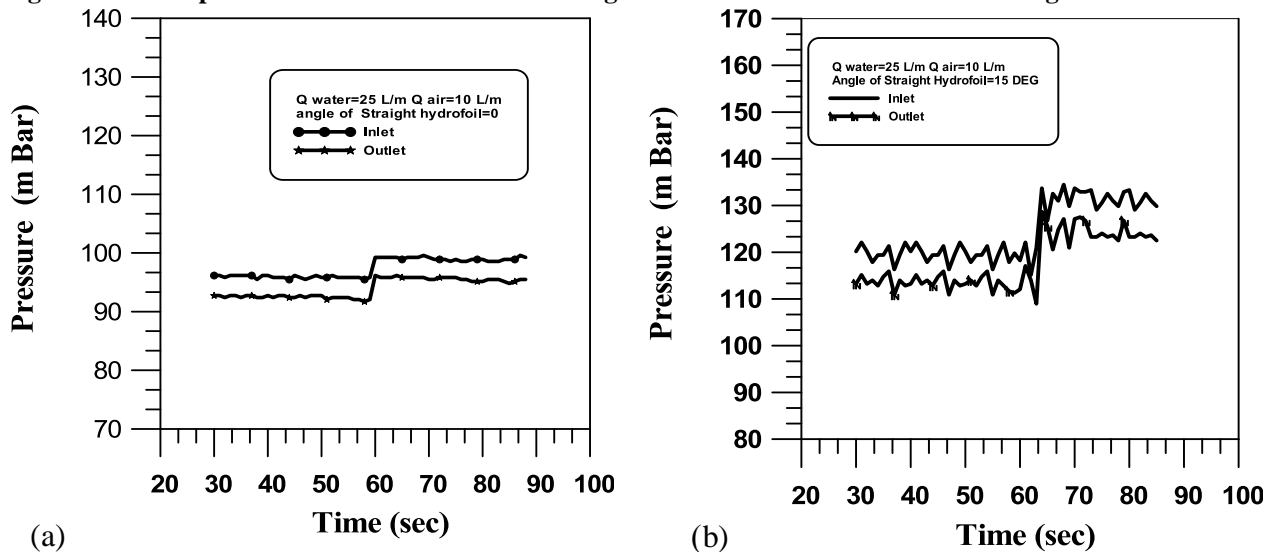


Figure 14. Mean pressure difference with air discharge for different values of water discharge.



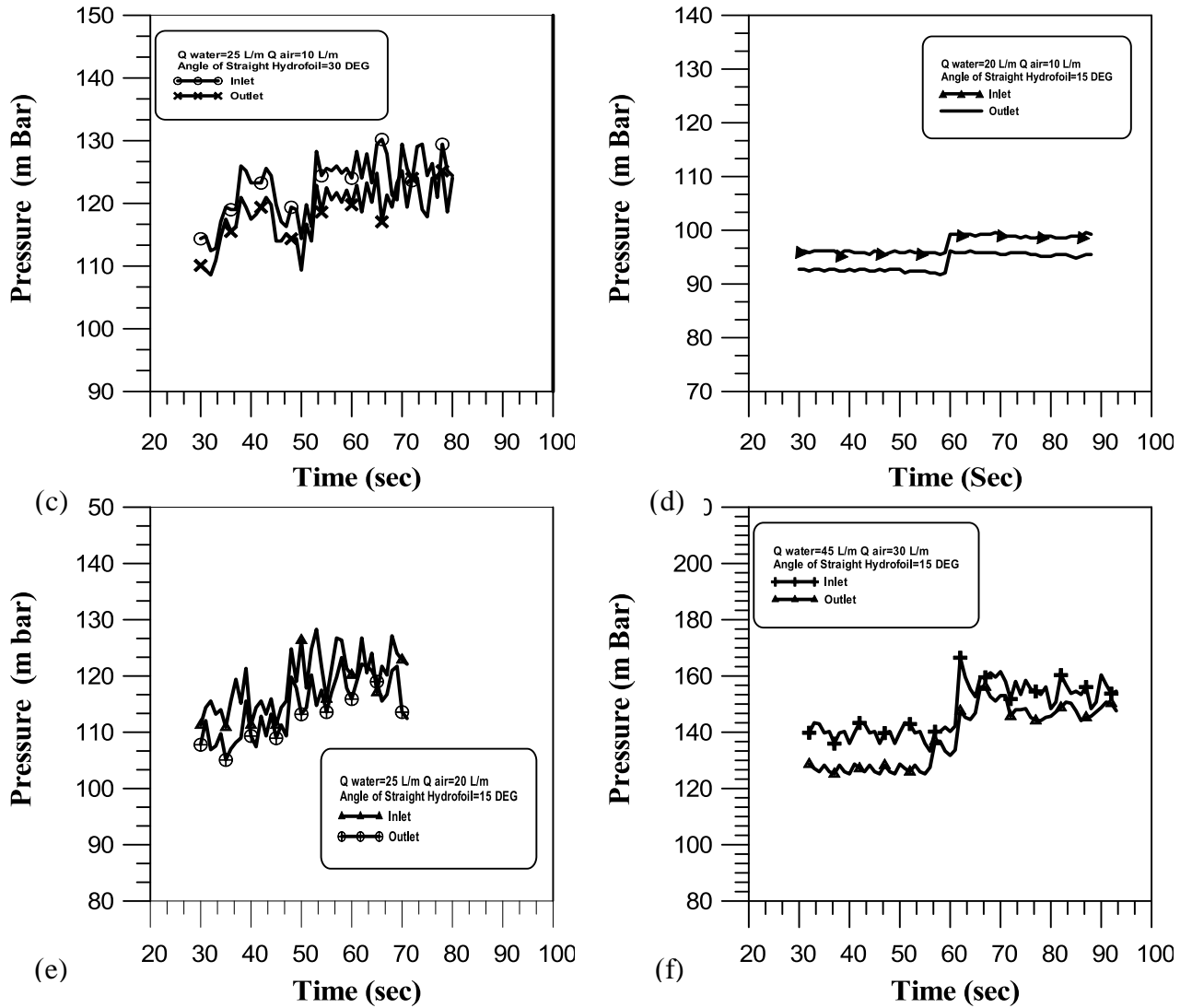


Figure 15. Effect of time evolution of pressure for different angle of attack, air and water discharges.

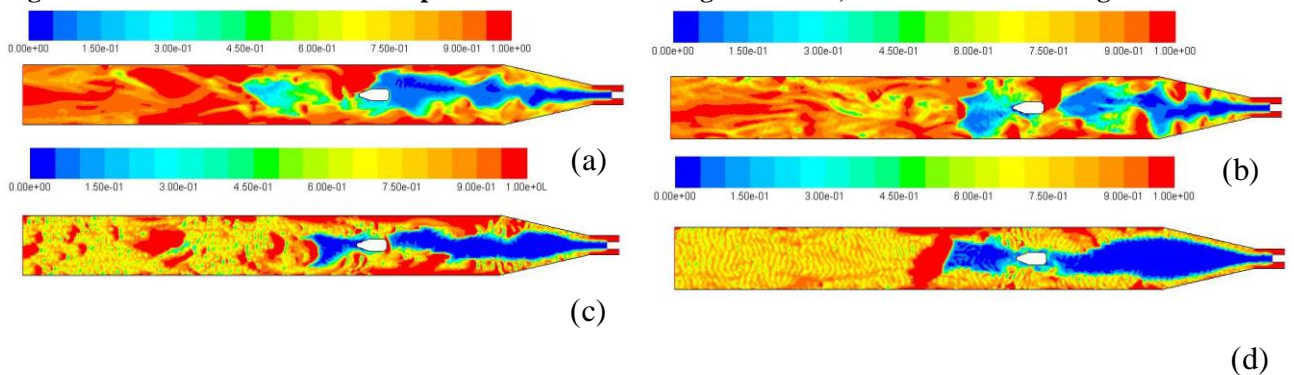


Figure 16. Volume fraction (water) contours for cases (1, 2, 6 and 10) respectively.

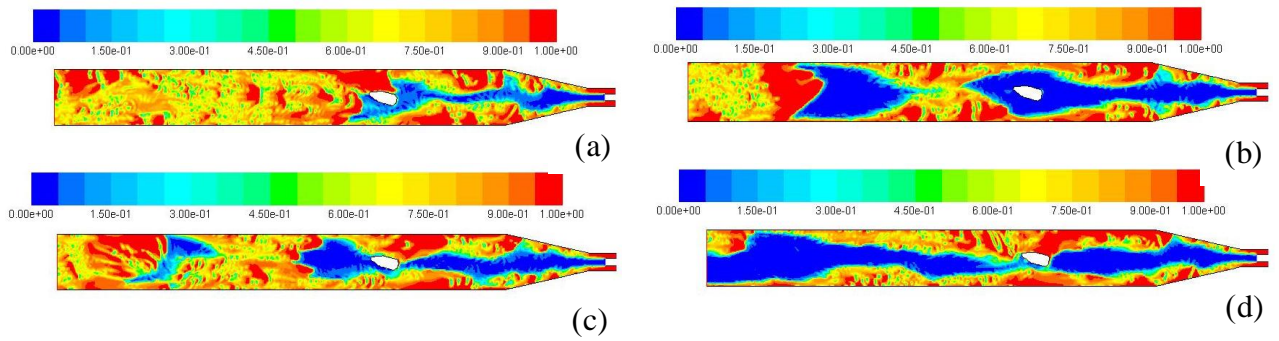


Figure 17. Volume fraction (water) contours for cases (3, 11, 12 and 16) respectively.

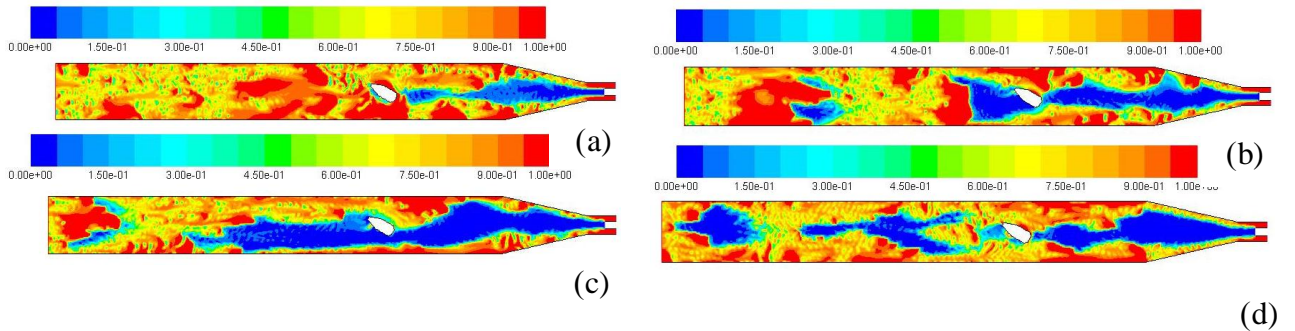


Figure 18. Volume fraction (water) contours for cases (4, 7, 9 and 13) respectively.

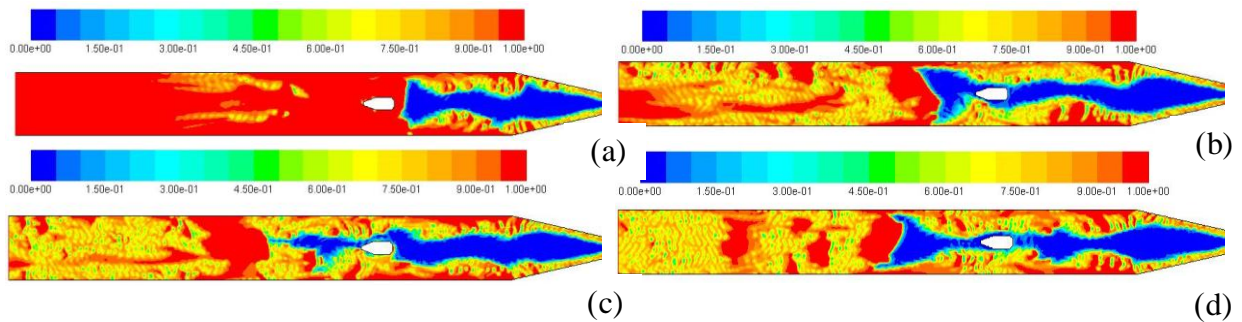


Figure 19. Volume fraction (water) contours development for unsteady case 5.

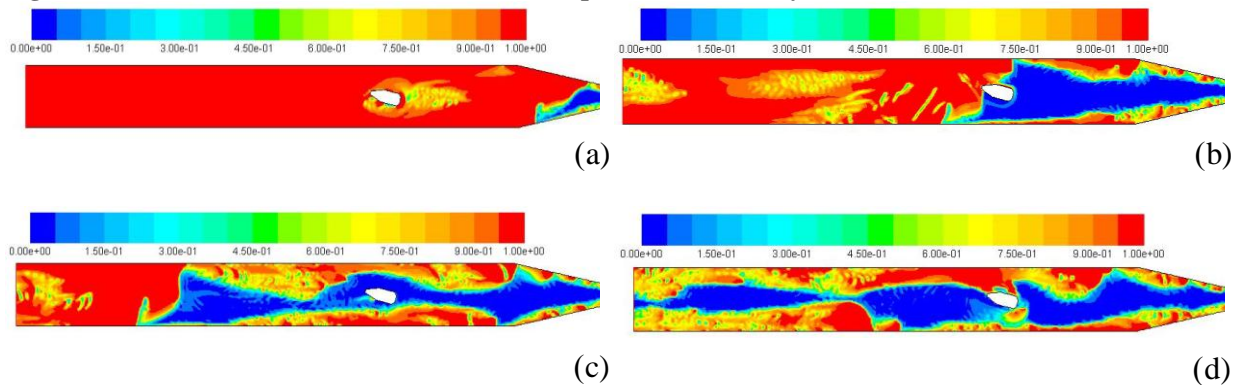


Figure 20. Volume fraction (water) contours development for unsteady case 14.

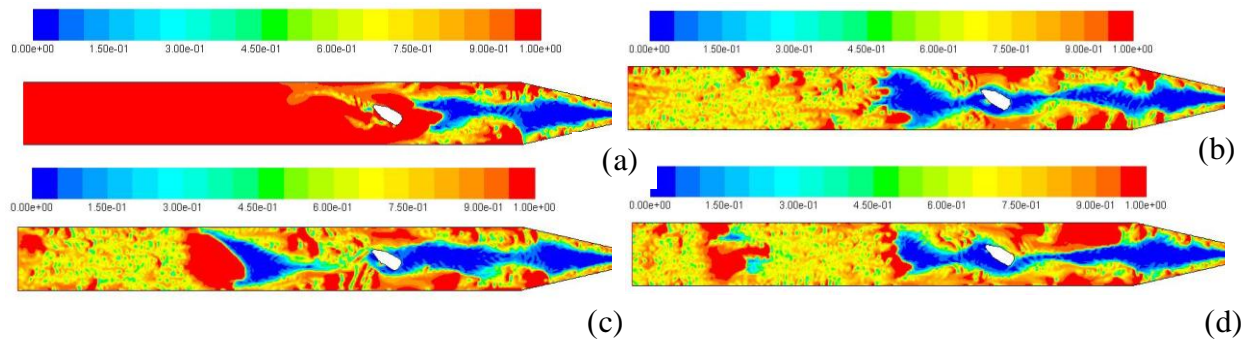


Figure 21. Volume fraction (water) contours development for unsteady case8.

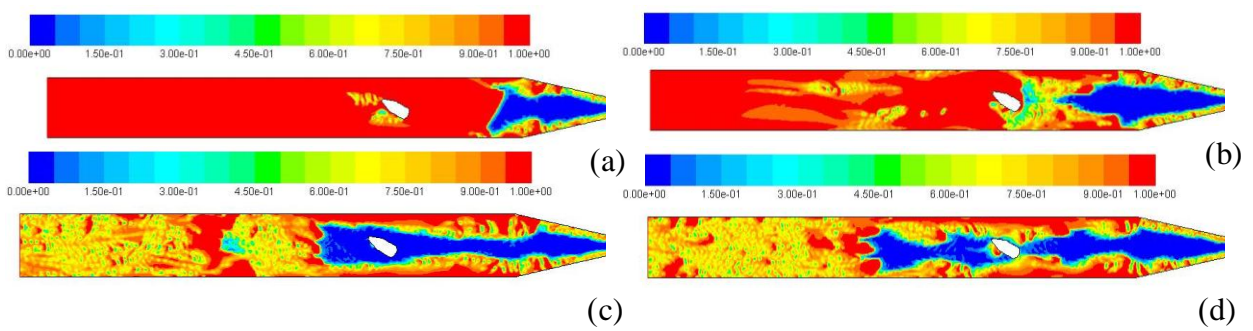


Figure 22. Volume fraction (water) contours development for unsteady case15.

Cominga Well-Organized Hiding System And Constancy Conservation In Mixture P2P System

N. Manjula¹, R.V. SubbaRayudu², K. Niharika³, G.Prathap⁴

^{1, 3, 4} M.Tech students, ² Assistant Professor Global College of Engineering & Technology, Kadapa.

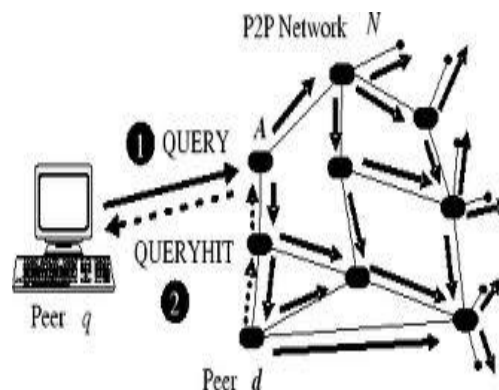
ABSTRACT

Peer-to-peer overlay networks are widely used in distributed systems. P2P is a popular technology used for file sharing. File replication and Consistency maintenance are the techniques used in P2P for high system performance. The objective of this work is to design a hybrid peer-to-peer system for distributed data sharing which combines the advantages of both types of peer-to-peer networks and minimizes their disadvantages. However, in peer-to-peer networks, Information Retrieval (IR) performance is determined by both technology and user behavior, and little attention has been paid in the literature to improving IR performance through incentives to change user behavior. The proposed hybrid peer-to-peer system is composed of two parts: the first part is a structured core network the second part is multiple unstructured peer-to-peer networks each of which is attached to a node in the core network. Our caching scheme can deliver lower query delay, better load balance and higher cache hit ratios.

KEY WORDS: hybrid, peer-to-peer systems, consistency maintenance.

I. INTRODUCTION:

Peer-to-peer overlay networks are widely used in distributed systems. Based on whether a regular topology is maintained among peers, peer-to-peer networks can be divided into two categories: structured peer-to-peer networks in which peers are connected by a regular topology, and unstructured peer-to-peer networks in which the topology is arbitrary. Structured peer-to-peer networks usually can provide efficient and accurate services but need to spend a lot of effort in maintaining the regular topology. On the other hand, unstructured peer-to-peer networks are extremely resilient to the frequent peer joining and leaving but this is usually achieved at the expense of efficiency. Our simulation results demonstrate that the hybrid peer-to-peer system can utilize both the efficiency of structured peer-to-peer network and the flexibility of the unstructured peer-to-peer network and achieve a good balance between the two types of networks. In peer-to-peer file sharing systems, file replication and consistency maintenance are widely used techniques for high system performance.



Hybrid peer-to-peer architectures use special nodes to provide directory services for regions of the network ("regional directory services"). Hybrid peer-to-peer architectures are a potentially powerful model for developing large-scale networks of complex digital libraries, but peer-to-peer networks have so far tended to use very simple methods of resource selection and document retrieval. In this paper, we study the application of content-based resource selection and document retrieval to hybrid peer-to-peer networks.

Recently, a number of technologies in peer-to-peer (P2P) networking have been developed. This pure P2P personal and social networking paradigm, however, has its own limitations. For example, P2P networks without any infrastructure support offer no connectivity guaranties. In this paper, we propose a hybrid peer-to-peer system for distributed data sharing which combines the structured and unstructured peer-to-peer networks.

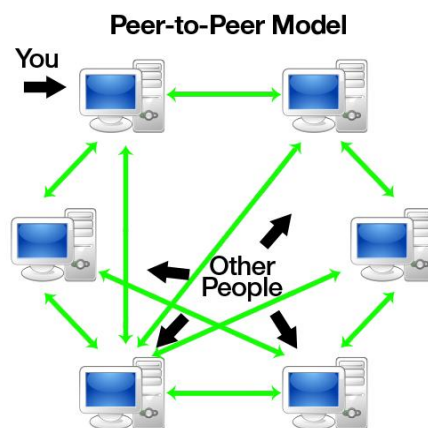
RELATED WORK:Peer-to-peer networking is the utilization of the relatively powerful computers (personal computers) that exist at the edge of the Internet for more than just client-based computing tasks. They do not aim to integrate P2P systems with general Internet services. Furthermore, infrastructure-nodes are not perceived and used by the users as personal devices. Some existing file-sharing P2P systems assume that the shared data are static or read-only, so that no update mechanism is needed. Peer-to-peer networking has the following advantages over client/server networking:

- Content and resources can be shared from both the center and the edge of the network. In client/server networking, content and resources are typically shared from only the center of the network.
- A network of peers is easily scaled and more reliable than a single server. A single server is subject to a single point of failure or can be a bottleneck in times of high network utilization.
- A network of peers can share its processor, consolidating computing resources for distributed computing tasks, rather than relying on a single computer, such as a supercomputer.
- Shared resources of peer computers can be directly accessed. Rather than sharing a file stored on a central server, a peer can share the file directly from its local storage.
- Peer-to-peer networking solves the following problems:
- Allows the processing resources of edge computers to be utilized for distributed computing tasks.
- Allows local resources to be shared directly, without the need for intermediate servers.
- Allows efficient multipoint communication without having to rely on IP multicast infrastructure.

Peer-to-Peer Networking Scenarios

Peer-to-peer networking enables or enhances the following scenarios:

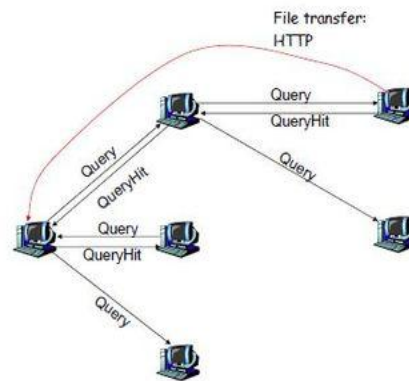
- Real-time communications (RTC)
- Collaboration
- Content distribution
- Distributed processing
- Improved Internet technologies



GNUTELLA: This is a large peer-to-peer network. It was the first decentralized peer-to-peer network of its kind, leading to other, later networks adopting the model. It celebrated a decade of existence on March 14, 2010 and has a user base in the millions for peer-to-peer file sharing. The gnutella network is a fully distributed alternative to such semi-centralized systems as FastTrack and the original Napster. The Gnutella network is a fully decentralized, peer-to-peer application layer network that facilitates file sharing; and is built around an open protocol developed to enable host discovery, distributed search, and file transfer. It consists of the collection of Internet connected hosts on which Gnutella protocol enabled applications are running. The Gnutella protocol makes possible all host-to-host communication through the use of messages.

GUID	Type	TTL	Hops	Payload Size
16 bytes	1 byte	1 byte	1 byte	4 bytes
23 bytes				

Message Format



The gnutella search and retrieval protocol

Peer-to-peer file sharing: Peer-to-peer file sharing is the distribution and sharing of digital documents and computer files using the technology of peer-to-peer (P2P) networking. P2P file sharing allows users to access media files such as books, music, movies, and games using a specialized P2P software program that searches for other connected computers on a P2P network and locates the desired content. The nodes (peers) of such networks are end-user computer systems that are interconnected via the Internet. Peer-to-peer file sharing technology has evolved through several design stages from the early networks like Napster, which popularized the technology, to the later models like the Bit Torrent protocol. Several factors contributed to the widespread adoption and facilitation of peer-to-peer file sharing. These included increasing Internet bandwidth, the widespread digitization of physical media, and the increasing capabilities of residential personal computers. Users were able to transfer either one or more files from one computer to another across the Internet through various file transfer systems and other file-sharing networks.

II. CONSISTENCY ALGORITHM:

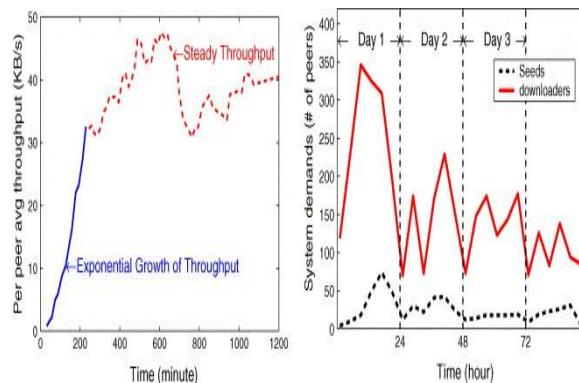
In the distributed data sharing, the consistency of the data needs to be focused because there are two different networks are built on single. Maintaining consistency between frequently updated or even infrequently updated files and their replicas is a fundamental reliability requirement for a P2P system. P2P systems are characterized by dynamism, in which node join and leave continuously and rapidly. Moreover, replica nodes are dynamically and continuously created and deleted. For consistency maintenance, we introduce an algorithm for hybrid network, which is known as Adaptive File Consistency Algorithm (AFCA). File consistency maintenance in P2P systems is a technique for maintaining consistency between files and their replicas. Most previous consistency maintenance methods depend on either message spreading or structure-based pushing. The following is algorithm for maintaining consistency in distributed peer-to-peer networks.


```
//Algorithm for file consistency maintenance
1. If a query is requested for a file then
2. include an update request within query of the file
3. else send the update request
4. if the acceptance reply is given from the owner of
   the file
   //check the conditions
5. If the file is a valid one then
   TTR = TTRold + α. // α is a constant
6. If the file is a stale one then
7. TTR = TTRold / β. // β is a constant. we need to
   update replica of a file.
8. if Time to refresh rate(TTR) is greater then
   maximum or less then minimum TTR then
9. TTR = max(TTRmin, min(TTRmax, TTR))
10. if time to refresh rate is less than or equal to query
    then TTRpoll = Tquery
11. else
12. TTRpoll = TTR
    when TTR > Tquery, that is, the file is queried at a
    higher rate than change rate, then the file should be
    updated timely based on TTR. As a result, TTRpoll should be
    calculated based on the following formula [1]
```

$$TTR_{poll} = \begin{cases} T_{query} & TTR \leq T_{query}, \\ TTR & TTR > T_{query}. \end{cases}$$

III. PERFORMANCE EVALUATION OF P2P NETWORKS:

In this paper we have studied and carried out performance evaluation of Peer-to-Peer (P2P) networking in context of satellite image processing. The application scenarios identified are sharing of satellite image data, P2P enabled now casting and forecasting and sharing of distributed computing resources using P2P. Performance evaluation of peer-to-peer search techniques has been based on simple performance metrics, such as message hop counts and total network traffic, mostly disregarding their inherent concurrent nature, where contention may arise. This paper is concerned with the effect of contention in complex P2P network search, focusing on techniques for multidimensional range search.



IV. CONCLUSION AND FUTURE WORK:

In this, we propose new system which combines both the structured peer-to-peer network and the unstructured peer-to-peer networks to form a two-tier hierarchy to provide efficient and flexible distributed data sharing service. The proposed hybrid architecture enables the creation of a wide range of MaIS that can be easily customized. The efficiency can be further increased when considering link heterogeneity and topology awareness. Compared to unstructured peer-to-peer networks, the hybrid system has much lower data lookup

failure ratio. We have now finished our analysis of security in P2P networks. As a conclusion we can re-express the fact that only pure P2P stand a chance against attacks, any kind of shortcuts taken in the implementation can be turned around in order to attack the P2P application in a more dangerous manner. This application should not solely worry about authenticating users (binding public keys to physical identities) but also how much trust can be given to a public key. If such an application existed, it could be used by P2P applications as a very efficient protection against malicious attacks.

REFERENCES:

- [1] Min Yang, Yuanyuan Yang., "An Efficient Hybrid Peer-to-Peer System for Distributed Data Sharing "IEEE transaction on Computers, Vol.59, no.9, September 2010.
- [2] Haiying (Helen) Shen, "IRM: Integrated File Replication and Consistency Maintenance in P2P Systems", IEEE trans on parallel and distributed systems, vol. 21, no. 1, Jan 2010.
- [3] Yuh-JzerJoung, Zhang-WenLin, "On the self-organization of a hybrid peer-to-peer system", ELSEVIER, Journal of Network and Computer Appln 33 (2010).
- [4] Z. Li, G. Xie, Z. Li, "Efficient and scalable consistency maintenance for heterogeneous peer-to-peer systems", TPDS (2008).
- [5] B.T. Loo, R. Huebsch, I. Stoica, and J.M. Hellerstein, "The Case for a Hybrid p2p Search Infrastructure," Proc. Workshop Peer-to-Peer Systems (IPTPS '04), pp. 141-150, Feb. 2004.
- [6] V. Gopalakrishnan, B. Silaghi, B. Bhattacharjee, P. Keleher, "Adaptive replication in peer-to-peer systems", in: Proc. of ICDCS, 2004.
- [7] P2P traffic is booming, "BitTorrent The Dominant Protocol". <http://torrentfreak.com/p2p-traffic-still-booming-071128>.
- [8] P. Linga, I. Gupta, and K. Birman. Kache: "Peer-to-peer web caching using kelips". In submission, June 2004.

Arima Application as an Alternative Method of Rainfall Forecasts In Watershed Of Hydro Power Plant

Sri Mawar Said¹, Salama Manjang², M.Wihardi Tjaronge³, Muh. Arsyad Thaha³
*S3 students Civil Engineering¹, Electrical Engineering Lecture², Civil Engineering Lecturer³
Hasanuddin University, Makassar-Indonesia*

ABSTRACT

Water resources of a hydro power plant generally is influenced by rainfall in the watershed. Rainfall prediction is done by using monthly rainfall data at each station. Water resources are usually derived from some streams that flow into the hydropower reservoirs. The research was conducted by predicting rainfall at three locations. These locations are considered to have a very large impact on water resources of the plant. The method used is the time series.

KEYWORDS: water resources, hydropower, time series.

I. INTRODUCTION

Hydro power plans is a plant that uses water as the potential energy of a turbine to drive a generator. Hydro power plant in Indonesia generally uses the reservoir to accommodate the flow of water from a river. The amount of water that can be accommodated in the reservoir depends on the intensity of rainfall in the watershed at the catchment area of a hydroelectric plant. The problems that occurred in Indonesia is a lots of the hydro power plant do not operate optimally after operated more than 15 years^[1,2,3,4]. It is because water resources in the power plant is degraded by time, therefore we need to conduct a study research about the sustainability of water resources by making predictions of the rainfall will occurrence in the watershed hydropower. The study was conducted in the watershed Mamasa. This watershed supplies the resource of Bakaru hydro power plans (hydropower Bakaru). Location of the plant's reservoir is geograp-hically located between 3⁰30'00"-2⁰51'00"LS and 119⁰15'00"-119⁰45'00" BT.

II. REVIEW OF LITERATURE

1.1 Rainfall

The amount of rainfall affects the flow of water in hydro power plans reservoirs in Bakaru. Rainfall data obtained from the Meteorological Agency, Climatology and Geophysics Maros. Data used is collected from the Mamasa station, Sumororang station, and the Lembang Station. The amount of the average monthly rainfall can be seen in Table 1, the annual rainfall in the reservoir in 2012 Mamasa of 1465 mm, 4087 mm of Sumarorang station, and 3331 mm at Lembang Station. Assuming all three recording station can represent the flow of water into the reservoir hydropower before it is deducted by the sediment carried by the flow of surface water is equal to 8883 mm.

Table1. Average Rainfall at Each Station

Month	Average rainfall per year at each station (mm)					
	Mamasa (I)		Sumarorong (II)		Lembang (III)	
	1990	2012	1990	2012	1995	2012
January	94	250	155	316	286	261
February	270	44	481	275	514	458
March	61	77	210	344	310	376
April	254	246	373	346	354	313
May	93	99	307	241	375	211
June	135	135	201	227	192	231
July	70	44	256	227	209	175
August	77	22	100	210	8	19
September	117	116	185	299	135	62
October	46	218	233	211	32	220
November	30	223	225	504	319	478
December	95	63	380	362	308	527
Average rainfall per year (mm)	112	128	259	297	254	278

1.2 Time series

Time series is a series of observations of an event, occurrence, phenomenon or variables are taken from time to time. The data is recorded accurately in the time sequence and then compiled as statistics, data recording is generally done on a daily, monthly, or yearly. Analysis of time series with methods Arima Box-Jenkin has been done by BagusRahmat W, ie by doing "Rainfall Forecasting in Ngawi district" and Wahyudi Lewis published "Electrical Load Forecasting in PT. PLN APJ South Surabaya. Time series analysis is a quantitative analysis, which is used to determine the pattern of historic data. The distinctive feature of this analysis is a series of observation in one variable is viewed as a realization of a random variable with distribution, which is considered to be a function of the probability with random variance Z_1, \dots, Z_n , for example $f_{1, \dots, n}(Z_1, \dots, Z_n)$; subscript 1, ..., n the density function pointed to the fact that in general the parameters or even the density function that depends on the particular point of time is concerned, this model is called stochastic models. As a simple example of a stochastic process is considered a random walk, where in each successive changes taken independently from a probability distribution with mean zero. Then the variable Z following the forecast made at time t for k steps ahead is seen as the expectation value of Z_{t+k} with the condition known observation ago to Z_n .

$$Z_t - Z_{t-1} = a_t$$

Where a_t is a random variable with mean zero and independently drawn each period, thus making each successive step is undertaken Z is random.

Pattern of time series data is the data pattern observed on a vulnerable time. Exploration of the data to determine how the behavior of the data throughout the observation period. Time series data are assumed to be divided into three data patterns are: trend, seasonal variations and stationary.

1.2.1 Time series analysis

Analysis of time series such as Autoregressive (AR), Moving Average (MA), Autoregressive Moving Average (ARMA) and Autoregressive Integrated Moving Average (ARIMA).

1) Autoregressive models (AR)

Autoregressive model is a model that illustrates that the dependent variable is affected by the dependent variable itself in the periods and previous times. In general autoregressive models (AR) has the following form.

$$Y_t = \theta_0 + \theta_1 Y_{t-1} + \theta_2 Y_{t-2} + \dots + \theta_p Y_{t-p} - e_t$$

where:

Y_t = stationary time series

θ_0 = constant

Y_{t-1}, \dots, Y_{t-p} = value past linked

$\theta_1, \dots, \theta_p$ = coefficients or parameters of autoregressive models

e_t = residual at time t

The above model is referred to as autoregressive models (regression myself) because the model is similar to the regression equation in general, it's just that being an independent variable instead of the different variables with the dependent variable but the previous value (lag) of the dependent variable (Y_t) itself.

Number of past values used by the model, determining the level of the model. If only used one lag dependent, then the model is called the model autoregressive level one (firstorder autoregressive) or AR (1) and when used as the dependent lag, then the model is called autoregressive level p (p-th order autoregressive) or AR (p).

2) Moving Average Models(MA)

In general, the model has the form of a moving average as follows:

$$Y_t = \phi_0 + \phi_1 e_{t-1} - \phi_2 e_{t-2} - \dots - \theta_n e_{t-q}$$

where:

Y_t = stationary time series

ϕ_0 = constant

ϕ_1, \dots, ϕ_p = coefficient model of moving average which indicates the weight. Coefficient can have a negative or positive value, depending on the results of estimation.

e_{t-q} = residual past used by the model as q, determines the level of the model.

Difference moving average models with autoregressive models lies in the independent variable. When the independent variables in the model is the autoregressive previous value (lag) of the dependent variable (Y_t) itself, then the moving average models as the independent variable is the residual value in the previous period.

3) Autoregressive moving average models(ARMA)

Often the characteristics of Y can not be explained by the AR or MA alone, but must be explained by both. Model that includes both of these processes is called ARMA models. The general form of this model are:

$$Y_t = \gamma_0 + \delta_1 Y_{t-1} + \delta_2 Y_{t-2} + \dots + \delta_n Y_{t-p} - \lambda_1 e_{t-1} - \lambda_2 e_{t-2} - \lambda_n e_{t-q}$$

where:

Y_t = stationary time series

γ_0 = constant

δ and λ = coefficient models

e_t = residuals ago

4) ARIMA Models

Arima model is a model developed intensively by George Box and Jenkins Gwilyen so that their name is often synonymous with Arima processes applied to the analysis and forecasting of time series data. Arima is actually a technique to find the most suitable pattern from a group of data (curve fitting), Arima thus fully utilizing the data of the past and present to make accurate short-term forecasting.

Arimahas very good accuracy for short-term forecasting, while for long-term forecasting it is unfavorable. Will usually tend to flat / constant (flat) for a sufficiently long period.

III. RESEARCH METHODS

3.1 Types and sources of data

Rainfall data were used from 1990 to 2012, the data is derived from measurements of Mamasa station, stations and station SumarorangLembang. These stations are under the coordination of the Meteorology, Climatology and Geophysics Agency (BadanMeteorologi, Klimatologi, danGeofisika-BMKG) Maros. Rainfall data at each station are shown in Figures 1, 2 and 3 below.

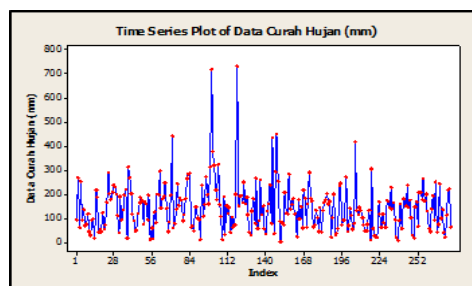


Figure 1. Rainfall Data of Mamasa Station year1990 to 2012

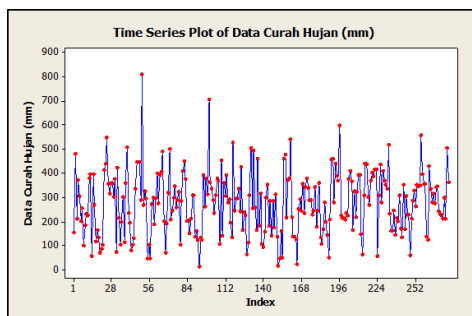


Figure2. Rainfall Data of Sumarorong Station year 2009 to 2012

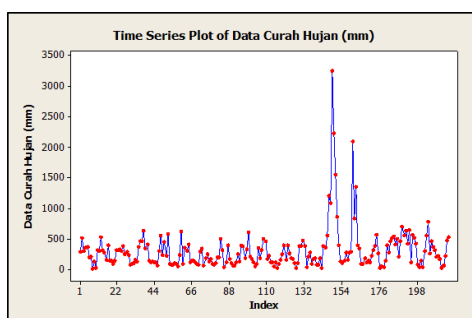


Figure3. Rainfall Data of Lembang Station year 2009 to 2012

From data above it show the static trend each figure. The next step is to check the stationary model.

3.2 Data Analysis

Data analysis using monthly rainfall data from 1990 to 2012. The method used to predict the rainfall is the method of Arima. Flow forecast rainfall data shown in the figure 4. Processing data using Minitab software.

3.2.1 Selection of Model

Model selection is done by comparing the value of SS (sum square) and MSE (mean Square Error) of each model is obtained after differentiation. Description of each rainfall data at each station are described as follows:

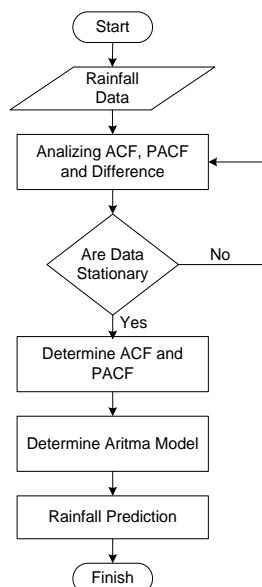


Figure 4. Flow chart prediction with ARIMA models

IV. RESULTS

Arima model results from each station are shown in Table 2.

Table 2. Rainfall Arima models

No.	Month	ARIMA Models at Station		
		I	II	III
1	January	(4,0,3)	(4,0,1)	(3,0,3)
2	February	(4,0,5)	(3,0,2)	(4,0,4)
3	March	(5,0,4)	(3,0,1)	(4,0,4)
4	April	(4,0,4)	(3,0,2)	(3,0,3)
5	May	(5,0,4)	(3,0,2)	(3,0,2)
6	June	(5,0,4)	(4,0,1)	(4,0,3)
7	July	(4,0,4)	(4,0,1)	(4,0,3)
8	August	(5,0,4)	(3,0,2)	(2,0,2)
9	September	(4,0,3)	(4,0,1)	(2,0,2)
10	October	(5,0,4)	(3,0,2)	(2,0,2)
11	November	(4,0,4)	(4,0,1)	(3,0,2)
12	December	(4,0,4)	(4,0,1)	(4,0,4)

Prediction of rainfall at each station is done by using the above model of Arima. Results predicted rainfall at each station in the form of curves shown.

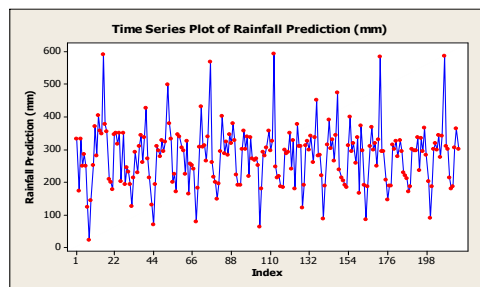


Figure 5. Results predicted rainfall in 2013 and 2030 Mamasa station

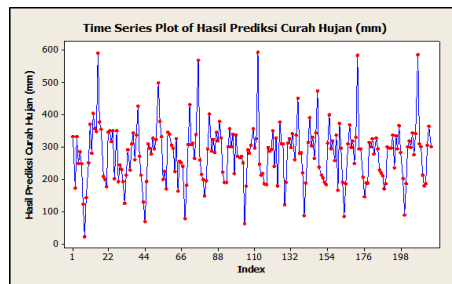


Figure 6. Results predicted rainfall in 2013 and 2030 Sumarorong station

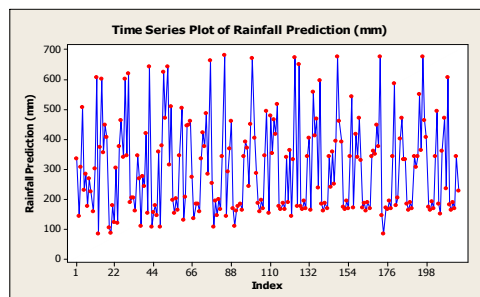


Figure 7. Results predicted rainfall in 2013 and 2030 Lembang station

Results predicted rainfall on average per year in each station can be seen on table 3.

Table 3. Average rainfall prediction at each station

Year	Prediction of average rainfall per year at station (mm)			
	I	II	III	Amount
2013	163	234	294	692
2014	125	336	265	726
2015	136	244	342	722
2016	152	261	241	653
2017	134	311	375	820
.
.
2029	146	270	361	777
2030	159	308	273	740

V. CONCLUSIONS

Of rainfall prediction results obtained by the average rainfall per year is:

- 1) Station Mamasa rainfall lowest annual average occurred in 2018 and 2025 is 119 mm and the highest occurred in 2013 is 163 mm.
- 2) Sumarorong station rainfall lowest annual average occurred in 2013 is 234 mm and the highest happened in 2014 that is 336 mm.
- 3) Lembang station rainfall lowest annual average occurred in 2016 is 241 mm and 2017 the highest is 375 mm.
- 4) Water resources hydroelectric power derived watersheds, can be predict the highest of rainfall predicted results of the three rainfall stations that gather in 2017 is about to 820 mm and in the other is between the value of 690 mm up to 780 mm.

REFERENCE

[1] Pemerintah RI, "Government Regulation Nomer 7 year 2004, About The Water Resources - *Undang-undang Republik Indonesia Nomor 7 tahun 2004, Tentang Sumber Daya Air*",

[2] www.bpkp.go.id/uu/filedownload/2/39/213.bpkp accessed on February 7th2013.

[3] Dyah Ari Wulandari, "Sediment Handling in Mrica Reservoir-*Penanganan Sedimentasi Waduk Mrica*", Marine Technic Annual Journal volume 13, No.4-Desember 2007, ISSN 0854-4549 Akreditasi No. 23a/DIKTI/KEP/2004, accessed on March 20th 2013

[4] Hari Krisetyana, "Level of Efficiency Flushing Sediment Deposition in PLTA PB. Sudirman Reservoir – *Tingkat Efisiensi pengelontoran endapan sedimentasi pada waduk PLTA PB. Sudirman*", Master Degree in Civil Engineering Diponegoro University, Semarang, year 2008, <http://eprints.undip.ac.id/>, accessed on February 7th2013.

[5] Abdul wahid, "Sediment Rate Progress Model in Bakaru Reservoir Caused by Sub DAS Mamasa Eroton - *Model Perkembangan Laju Sedimentasi di waduk Bakaru Akibat Erosi yang Terjadi di Hulu Sub DAS Mamasa*", Smartek Journal, volume 7. N0. Pebruari 2009: 1-12, <http://jurnal.untad.ac.id/jurnal/index.php/SMARTEK/article/view/576>, accessed on February 7th 2013.

[6] Bagoes Rahmat W, "Rainfall prediction in Ngawi District Using Arima Box-Jenkins Method - *Peramalan Curah Hujan di kabupaten Ngawi menggunakan Metode Arima Box-Jenkins*"

[7] <http://digilib.its.ac.id/public/TTS-paper-23642-1309030041-Presentation.pdf>, accessed on June 10th2013

[8] Wahyudi Sugianto, "Electrical Load Forcasting using Arima Box-Jenkins in PT. PLN APJ South Surabaya - *Peramalan Beban Listrik di PT. PLN APJ Surabaya Selatan Menggunakan Metode Arima Box-Jenkins*", <http://digilib.its.ac.id/public/TTS-paper-23632-1309030065-Presentation.pdf>, accessed on June 10th2013

[9] Umi Rosyidahdkk, "Arima Model for Train Passenger Prediction at IX Jember District Operation - *Pemodelan Arima dalam Peramalan Penumpang Kereta Api pada Daerah Operasi IX Jember*". <http://www.scribd.com/doc/110734128/>, accessed on June 21th 2013.

Electrical Energy Consumption Prediction in South–West Sulawesi Electrical Power System

Sri Mawar Said¹, Salama Manjang², M. Wihardi Tjaronge³, Muh. Arsyad Thaha³
S3 Civil Engineering Students¹, Electrical Engineering Lecture², Civil Engineering Lecturer³
Universitas Hasanuddin Makassar-Indonesia

ABSTRACT

Prediction of electrical energy consumption in an electrical power system is needed to determine the electrical energy need every time. This prediction is required in order to scheduling operation of existing power plants and preparing for new power plant to meet the energy needs of each month or year. This study was conducted to predict the electrical energy need to 2030. Validation of prediction results are evaluated by RMSE values for 2011 and 2012. The method used is the Adaptive Splines Threshold Autoregression (ASTAR). Results showed that predictions for the year 2011 is 0.031 and the RMSE values for 2012 predictions RMSE value is 0.322

KEYWORDS: Energy consumption prediction, Adaptive Splines threshold Autoregression, RMSE

I. INTRODUCTION

ELECTRICITY IS A form of energy that is needed in human life. The Growth of electrical energy consumption per capita, shows rising standards of human life. Prediction is needed in order to predict electrical energy need every time (every month or every year), in recognition of this prediction can be known when the plant required the addition of new power plant in the current electrical system. Method used to predict electrical energy consumption is very diverse, including using software LEAP (Long-range Energy Alternatives Planning System) has been carried out by Ahmad Agus Setiawan et al⁽¹⁾. Prediction using Fuzzy Logic Applications and Neural Network, using the electric energy consumption data per hour, this is done by Yadi Mulyadi et al⁽²⁾. Researcher try to apply the ASTAR method to predict electrical energy needs. It has chosen because this method has been applied for forecasting ENSO index by Sutino and Boer (2004). In their study, it was found that the prediction result using ASTAR method has good accuracy⁽³⁾. Sutino and Boer (2004) stated that the ASTAR is a method of non-linear timeseries analysis algorithm which is based on multiple adaptive regression splines or commonly known as Multiple Adaptive Regression Splines (MARS). Problems that occurred in the electrical power system in South and West Sulawesi is the electrical energy consumption is greater than the available generation capacity, resulting in blackouts during peak loads. Therefore we need to conduct a research about electrical energy consumption prediction, in order to estimate demand for electrical energy per month or per year. Research conducted in South -West Sulawesi Electrical Power System by retrieve data monthly number of customers, connected power capacity, population and energy consumption.

II. REVIEW OF LITERATURE

2.1. Energy Consumption

Consumption of electric energy in the electrical power system in South Sulawesi and West Sulawesi has increased every year, it is because the system which supply the province of South Sulawesi and West Sulawesi are experiencing economic growth (GRDP growth rate) is about 8.2% for South Sulawesi Province and West Sulawesi 6.3%⁽⁴⁾.

Electrical power system in South Sulawesi and West Sulawesi has an increasing rate of customers (consumers) about 3.81 percent, the increasing rate of connected power (MVA) of 2.92 percent and the rate of energy consumption (GWh) about 2.43 percent⁽⁵⁾. Considering the development of energy consumption on the electrical system, it is necessary to estimate (predict) the electrical energy consumption for year to year. Prediction aims to estimate the consumption of electrical energy consumption in order to meet the needs of electrical energy in electrical power system in South Sulawesi and West Sulawesi continually.

2.2. Time Series

The energy consumption prediction data used are periodic data collected per month. Data analysis describes the relationship between the dependent variable with the independent variable. The approach used to estimate the energy consumption of electricity is the simple non-linear regression method namely adaptive threshold splines Autoregression (ASTAR).

1) Multivariate Adaptive Regression Splines (MARS)

MARS method is developed by Friedman in 1991. This method can analyze large data (50 ≤ N ≤ 10,000). Spline regression modeling is implemented by forming a set of base functions that can be reached-spline order to estimate the coefficients N-q* and basis functions using a least-squares.

Estimator of MARS models can be written as follows:

$$f(x) = a_0 + \sum_{m=1}^M a_m \prod_{k=1}^{K_m} [S_{k,m}(x_{v(k,m)} - l_{k,m})]$$

with:

a₀ = function stem base

a_m = coefficient of the function to the base-m

M = maximum base function

K_m = the number of interactions

x_{v(k,m)} = independent variable

l_{k,m} = knots value of the independent variable x_{v(k,m)}

v = number of independent variables

2) Adaptive Splines Threshold Autoregression (ASTAR)

Adaptive Threshold Autoregression Splines is a method of nonlinear time series that uses MARS algorithm method with the explanatory variables lagged value of time series data. ASTAR model is the development of MARS with variable response and Z_t as Z_{t-j} as a predictor variable, so that ASTAR models can be written as follows:

$$f(x) = a_0 + \sum_{m=1}^M a_m \prod_{k=1}^{K_m} [S_{k,m}(Z_{(t-j),(k,m)} - l_{k,m})]$$

III. RESEARCH MODEL

3.1 Data Type and Source

The data used to predict the energy consumption is the number of customers, the connected power and the residents from 2004 to 2011, data is obtained from PT. PLN Region South-West Sulawesi. Research data are shown in Table 1 below.

Tabel 1 Research Data

No	Month	Number of customers		Connected power (VA)		Number of residents		Energy Consumption (GWh)	
		2004	2011	2004	2011	2004	2011	2004	2011
1	January	1,331,026	1,602,542	1,334,708	1,907,816	8,214,491	8,862,459	172,046	309,183
2	February	1,333,609	1,606,862	1,339,874	1,916,813	8,221,884	8,870,435	174,850	311,229
3	March	1,335,081	1,613,189	1,345,552	1,932,522	8,229,284	8,878,419	176,281	312,248
4	April	1,336,063	1,629,777	1,347,281	1,961,211	8,237,513	8,885,521	179,676	313,604
5	May	1,337,145	1,643,947	1,350,299	1,989,022	8,245,751	8,892,630	181,857	315,401
6	June	1,337,857	1,654,284	1,352,696	2,016,896	8,253,996	8,899,744	183,576	317,205
7	July	1,338,372	1,667,978	1,358,114	2,064,416	8,261,425	8,907,754	185,543	319,149
8	August	1,339,251	1,680,634	1,361,667	2,099,644	8,268,860	8,915,771	186,012	321,011
9	September	1,340,170	1,690,831	1,363,671	2,120,941	8,276,302	8,923,795	189,652	322,840
10	October	1,340,713	1,697,865	1,369,321	2,136,480	8,283,751	8,931,826	191,449	324,099
11	November	1,341,767	1,708,044	1,372,910	2,205,860	8,291,206	8,939,865	192,604	325,782
12	December	1,347,356	1,749,034	1,379,632	2,209,371	8,298,668	8,947,911	193,839	327,610

Method used to predict the energy consumption is the ASTAR Method. Flow chart of energy consumption prediction is shown in Figure 4. All data are processed using Matlab software.

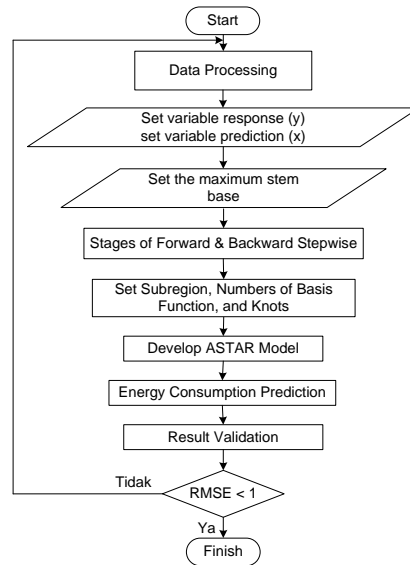


Figure 1. Flow chart of Energy Consumption Prediction using ASTAR Model

Proses to predict the energy consumption has several step :

a. Data Processing

The data as the input variables are: number of customer, connected power, and number of residents. Output data is the variable energy consumption. The data was processed with the normalization process

b. Determining Variable

Predictor variables or independent variable (x) is used as the input variables and the response variable or dependent variable (y) is the output variable.

c. ASTAR Modelling

ASTAR model building stages as follows:

- Specifies the maximum base functions
- Stages of forward and backward stepwise

d. Develop ASTAR model

e. Electrical energy consumption prediction

Electrical energy consumption predictions for 2011 and 2012

f. Result Validation

Electrical energy consumption prediction results for 2011 and 2012 using validated RMSE values are:

$$RMSE = \frac{\sqrt{\frac{1}{N} \sum_{t=h}^N (y_t - \hat{y}_t)^2}}{y_{\max} - y_{\min}}$$

3.2 Data Analysis

Electrical energy consumption prediction using three input variables are number of customers, connected power, and number of residents. Output variables are the energy consumption. The initial process is to normalize the data into the interval [0 1]. The output of this process will be used as input data in the prediction process with the ASTAR method. The final stage of this method is denormalization, to return the signal shape of the prediction to the data input.

3.3 Model Selection

Simulation models for the prediction made in 2009, 2010, 2011 and 2012. From the results of these predictions can be selected the best model to be used to determine predictions of energy consumption in the next year. Model selection is done by comparing the RSME of each model, as shown in Table 2.

Table 2. Response Model Y to X

No	Model	Response variabel Y to X	RMSE Value
1	Prediction 2009	Number of residents (X_3) and number of customers	0.09365
2	Prediction 2010	Number of residents (X_3)	0.06439
3	Prediction 2011	Number of residents (X_3)	0.03131
4	Prediction 2012	Number of residents (X_3)	0.32215

Selected model is the model prediction in 2011, the energy consumption equation model are:

$$BF_1 = \max(0, X_3 - 0.435)$$

$$BF_2 = \max(0.435 - X_3)$$

$$Y = 0.509 + 1.24 BF_1 - 1.17 BF_2$$

IV. RESULT

Selected model to predict energy consumption in 2011 is the model prediction. Comparison between predicted results 2012 and real energy consumption 2012 can be seen in Table 3 and Figure 2.

Table 3. Energy Consumption Comparison

Month	Energy Consumption (GWh) 2011	
	Real data	Prediction
January	309.183	309.857
February	311.229	311.536
March	312.248	313.216
April	313.604	314.711
May	315.401	316.207
June	317.205	317.704
July	319.149	319.390
August	321.011	321.078
September	322.840	322.766
October	324.099	324.457
November	325.782	326.149
December	327.610	327.842

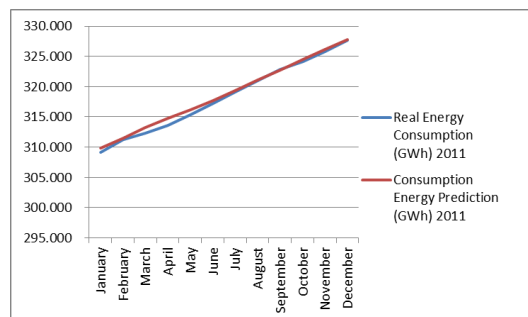
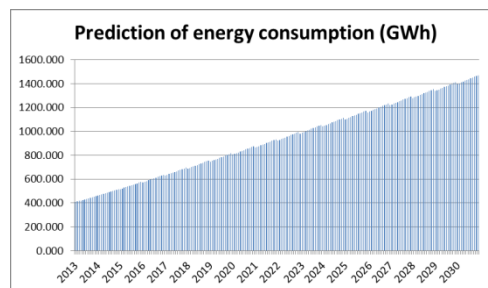


Figure 2. Energy Consumption Curve (GWh) 2011

From the results predicted in 2012 can be seen from a relatively small difference between the energy consumption of the results of the prediction and the real data, it can be concluded that the energy consumption equation model can be used to predict the energy consumption next year. Energy consumption prediction results can be seen in Table 4 and Figure 3.

Table 4. Energy Consumption Prediction Result

No	Month	Consumption Energy Prediction (GWh)			
		2013	2015	2020	2025
1	January	407.474	515.565	804.717	1099.951
2	February	411.889	521.011	811.019	1106.556
3	March	416.303	526.456	817.320	1113.160
4	April	420.718	531.901	823.621	1119.764
5	May	425.132	537.346	829.922	1126.369
6	June	429.547	542.791	836.223	1132.973
7	July	433.961	548.236	842.524	1139.578
8	August	438.376	553.681	848.826	1146.182
9	September	442.790	559.126	855.127	1152.786
10	October	447.205	564.571	861.428	1159.391
11	November	451.619	570.016	867.729	1165.995
12	December	456.034	575.461	874.030	1172.599



CONCLUSION

Based on the research can be concluded that:

- 1) Accuracy validation of predictions for the year 2011 and in 2012 is 0.031 and 0.322. Based on the RMSE values, it can be said that in general, the model predictions ASTAR well enough to predict electrical energy consumption.
- 2) The results of the prediction of energy consumption from 2013 to 2030 tend to occur in a linear manner.

REFERENCE

- [1] Ahmad Agus Setiawan, et al "Early studies Electrical Energy Needs and Potential Utilization of Renewable Energy sources in the district of Sleman, Yogyakarta - *Studi Awal Kebutuhan Energi Listrik dan Potensi Pemanfaatan sumber Energi Terbarukan di kabupaten Sleman, daerah Istimewa Jogjakarta*", http://akhisuhono.files.wordpress.com/2010/04/bss7_aas_shn.pdf, accessed on July 7th, 2013
- [2] Yadi Mulyadi, et al "Application of Fuzzy Logic and Neural Networks As Alternative methods of short-term electricity load prediction - *Aplikasi Logika Fuzzy dan Jaringan Syaraf Tiruan Sebagai metode Alternatif prediksi beban Listrik jangka Pendek*", http://file.upi.edu/direktori/fptk/jur_pend.teknik_elektro, accessed on July 7th 2013
- [3] Sutikno, et al. 2010. "Rainfall Forecasting using Autoregressive Integrated Moving Average, Neural Network, dan Adaptive Splines Threshold Autoregression Method in Juanda Station Surabaya - *Prakiraan Cuaca dengan Metode Autoregressive Integrated Moving Average, Neural Network, dan Adaptive Splines Threshold Autoregression di Stasiun Juanda Surabaya*" Statistics of Institute Technology Sepuluh Nopember (ITS) Surabaya. http://jurnal.lapan.go.id/index.php/jurnal_sains accessed on March 2nd, 2013.
- [4] Badan Pusat Statistik Indonesia, "Key Indicators of Social Development - Economic Indonesia - *Perkembangan Beberapa Indikator Utama Sosial - Ekonomi Indonesia*", http://www.bps.go.id/booklet/Booklet_Mei_2012.pdf, accessed on July 18th, 2013.
- [5] PT. PLN, "PLN Statistik 2011", <http://www.pln.co.id>, accessed on June 29th, 2012.

Develop and Design Of the ATM Banking Security System Through Image Processing And GSM Communication

R. Jansi Rani¹, S.Jyothirmayee², M.Sushanth³, M.Ravi Prakash⁴

¹M.Tech (Embedded systems), Geethanjali collage of Engineering and Technology AP

²M.Tech Associate Professor, Geethanjali collage of Engineering and Technology AP

³M.Tech (Embedded systems), Geethanjali collage of Engineering and Technology AP

⁴M.Tech, Research scholar (Electronic Communication), JNTU Hyderabad AP.

ABSTRACT:

ATM - originally designed for WAN communications, but quickly adapted for LANs as well, ends this historical separation and forms a universal platform for data communication, In both ATM LAN AND ATM WAN networks the data transport is achieved via connection-oriented communication paths, which are set up though high-speed switching systems. These ATM switches perform the cell routing from the input ports of the switch to the destination port in real time and in parallel for the ports. ATM can handle all of today's data services (telephone, data, video-broadcast and interactive) in an efficient way ATMs have become very popular with the general public for their availability and general user friendliness. ATMs are now found in many locations having a regular or high volume of consumer traffic. For example, ATMs are typically found in restaurants, supermarkets, Convenience stores, malls, schools, gas stations, hotels, work locations, banking centers, airports, entertainment establishments, transportation facilities and a myriad of other locations. ATMs are typically available to consumers on a continuous basis such that consumers have the ability to carryout their ATM financial transactions and/or banking functions at any time of the day and on any day of the week..

KEYWORDS: ATM, LAN, LPC2148 , MATLAB, MMS , PCA algorithm , Voice Announcer, WAN

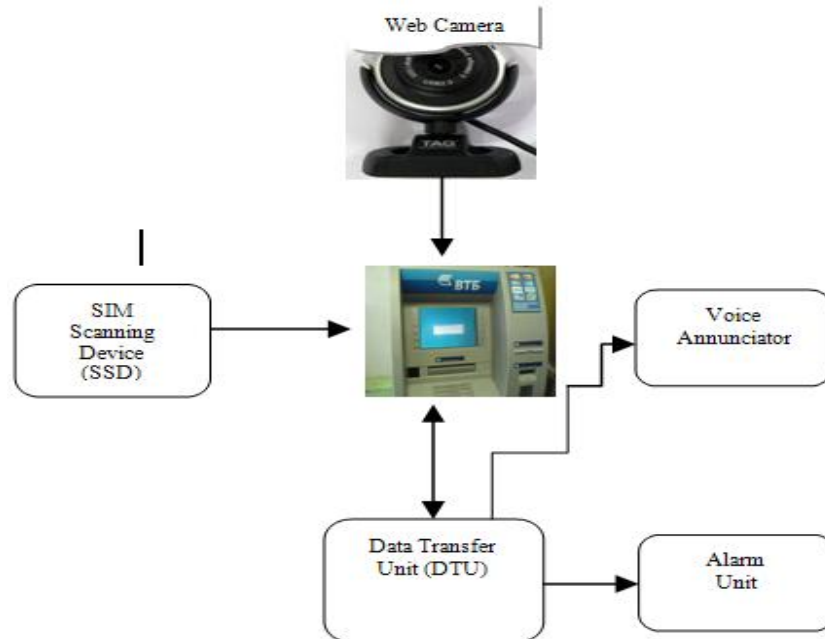
I. INTRODUCTION

3G Technology have to be created the new generation ATM machine which can be operator without the ATM card. By using this system ATM machine is going to operate by using our SIM in the mobile phone. When we insert our SIM in the reader unit of the ATM machine it transfers the mobile to the server. In server we can collect the related information of the mobile number (i.e.) the users account details, their photo etc. the camera presented near the ATM machine will capture the users image and compare it with the user image in the server using MATLAB. Only when the image matches it asks the pin number and further processing starts. Otherwise it will send the sms to owner mobile and it asks do you want continue or not If he will reply YES means it move for the further transaction if reply is NO means it give indication to the particular ATM . So by using this system need of ATM card is completely eliminated we can operate the ATM machine by using our SIM itself. By using this system malfunctions can be avoided. Our transaction will be much secured. One more application can also be added in this system for helping the blind people. In the existing system all the transactions are done through keyboard only. It may be difficult for blind people so we can also add voice enunciator to indicate each and very process to the blind people. It that enables a visually and/or hearing impaired individual to conveniently and easily carry out financial transactions or banking functions

II. SCALABILITY AND MODULARITY

ATM networks can be implemented on any one of number of transfer media. until now the network standards have been strictly defined right down to the physical level (Ethernet, FDDI, and so on).for ATM networks this is not the case .there is thus no explicit specification as to which physical medium ATM cells

should be transferred over, or at what speed in addition, ATM based networks can be to accommodate new users without the bandwidth available to existing users being restricted as a result. It is simply a matter of adding more connection modules to the ATM switch serving the users. so that ATM can be used is the transmission mechanism in practically all areas of data communications .this makes ATM equally suitable for local and wide area traffic.



“Figure 1 Block diagram of 3G ATM”

III. DESIGN IMPLEMENTATION

The Design implementation is of two types

A) Connection-Less Authentication System and B) MMS-Based Authentication System

3.1 Connection-Less Authentication System

A onetime password (OTP) is generated without connecting the client to the server. The mobile phone will act as a token and use certain factors unique to it among other factors to generate a one-time password locally. The server will have all the required factors including the ones unique to each mobile phone in order to generate the same password at the server side and compare it to the password submitted by the client. The client may submit the password online or through a device such as an ATM machine. A program will be installed on the client’s mobile phone to generate the OTP.

3.2 MMS-Based Authentication System

In case the first method fails to work, the password is rejected, or the client and server are out of sync, the mobile phone can request the one time password directly from the server without the need to generate the OTP locally on the mobile phone. In order for the server to verify the identity of the user, the mobile phone sends to the server, via an MMS message, information unique to the user. The server checks the MMS content and if correct, returns a randomly generated OTP to the mobile phone. The user will then have a given amount of time to use the OTP before it expires. Note that this method will require both the client and server to pay for the telecommunication charges of sending the MMS message.

IV. STATISTICS

The entire subject of statistics is based around the idea that you have this big set of data, and you want to analyze that set in terms of the relationships between the individual points in that data set. I am going to look at a few of the measures you can do on a set of data, and what they tell you about the data itself.

V. CHOOSING COMPONENTS AND FORMING A FEATURE VECTOR

In general, once eigenvectors are found from the covariance matrix, the next step is to order them by eigenvalue, highest to lowest. This gives you the components in order of significance. Now, if you like, you can decide to *ignore* the components of lesser significance. You do lose some information, but if the eigenvalues are

small, you don't lose much. If you leave out some components, the final data set will have less dimensions than the original. To be precise, if you originally have n dimensions in your data, and so you calculate n eigenvectors and eigenvalues, and then you choose only the first k eigenvectors, then the final data set has only k dimensions. What needs to be done now is you need to form a *feature vector*, which is just a fancy name for a matrix of vectors. This is constructed by taking the eigenvectors that you want to keep from the list of eigenvectors, and forming a matrix with these eigenvectors in the columns.

VI. PCA FOR IMAGE COMPRESSION

Using PCA for image compression also known as the Hotelling, or Karhunen and Loeve (KL), transform. If we have 20 images, each with 256×256 pixels, we can form 20 vectors, each with 65,536 dimensions. Each vector consists of all the intensity values from the *same* pixel from each picture. This is different from the previous example because before we had a vector for *image*, and each item in that vector was a different pixel, whereas now we have a vector for each *pixel*, and each item in the vector is from a different image. Now we perform the PCA on this set of data. We will get 65,536 eigenvectors because each vector is 65,536-dimensional. To compress the data, we can then choose to transform the data only using, say 15 of the eigenvectors. This gives us a final data set with only 15 dimensions, which has saved us 99.77% of the space. However, when the original data is reproduced, the images have lost some of the information. This compression technique is said to be *lossy* because the decompressed image is not exactly the same as the original, generally worse.

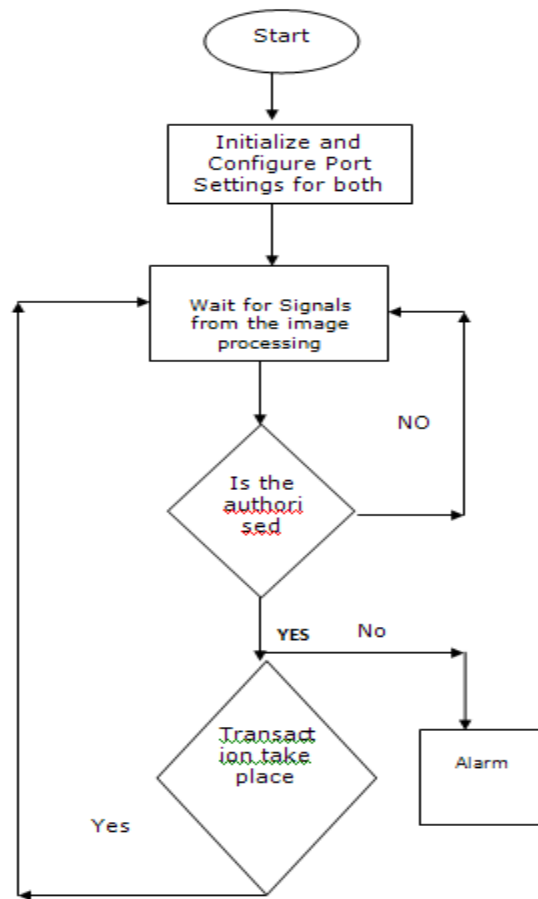
VII. IMAGE RECOGNITION

Image recognition is composed of two parts: classification and validation. The classification can be done somewhat easily by statistics of dimensions and pattern features of each type of image. On the other hand, validation is very difficult because we cannot obtain counterfeits that might appear in future, while we can collect plenty of genuine images. Moreover, statistics for a two-class (genuine and counterfeit banknotes) problem has less power because counterfeits could not actually be collected. Our approach is therefore to carefully select observation points at which a physical feature has a small deviation amongst genuine banknotes and looks difficult to imitate.

VIII. WIRELESS COMMUNICATION

A GSM modem can be an external modem device, such as the Wave com FASTRACK Modem. Insert a GSM SIM card into this modem, and connect the modem to an available serial port on your computer. A GSM modem can be a PC Card installed in a notebook computer, such as the Nokia Card Phone. A GSM modem could also be a standard GSM mobile phone with the appropriate cable and software driver to connect to a serial port on your computer. Phones such as the Nokia 7110 with a DLR-3 cable, or various Ericsson phones, are often used for this purpose. A dedicated GSM modem (external or PC Card) is usually preferable to a GSM mobile phone. This is because of some compatibility issues that can exist with mobile phones. For example, if you wish to be able to receive inbound MMS messages with your gateway, and you are using a mobile phone as your modem, you must utilize a mobile phone that does not support WAP push or MMS. This is because the mobile phone automatically processes these messages, without forwarding them via the modem interface. Similarly some mobile phones will not allow you to correctly receive SMS text messages longer than 160 bytes (known as "concatenated SMS" or "long SMS"). This is because these long messages are actually sent as separate SMS messages, and the phone attempts to reassemble the message before forwarding via the modem interface. (We've observed this latter problem utilizing the Ericsson R380, while it does not appear to be a problem with many other Ericsson models.) When you install your GSM modem, or connect your GSM mobile phone to the computer, be sure to install the appropriate Windows modem driver from the device manufacturer. To simplify configuration, the Now SMS/MMS Gateway will communicate with the device via this driver. An additional benefit of utilizing this driver is that you can use Windows diagnostics to ensure that the modem is communicating properly with the computer. The Now SMS/MMS gateway can simultaneously support multiple modems, provided that your computer hardware has the available communications port resources.

DEVELOPMENT CHART



“Figure 2. Flow Chart”

IX. STANDARD DEVIATION

To understand standard deviation, we need a data set. Statisticians are usually concerned with taking a *sample* of a *population*. To use election polls as an example, the population is all the people in the country, whereas a sample is a subset of the population that the statisticians measure. The great thing about statistics is that by only measuring (in this case by doing a phone survey or similar) a sample of the population, you can work out what is most likely to be the measurement if you used the entire population. In this statistics section, I am going to assume that our data sets are samples of some bigger population. There is a reference later in this section pointing to more information about samples and populations.



“Figure 3. GSM smart modem”

X. CONCLUSION

All the functions of the ATM, the authors are now concentrating on developing the intention recognition mobile based processing and alert module. This paper presents a novel architecture that can be used as a means of interaction between mobile phone, ATM machine and a Banking application for the purpose of withdrawing cash. The proposed design; the secure M-cash withdrawal allows the use of mobile phones as a tool of interaction and provide flexibility through a robust identity management architecture. The first part of the architecture is the process of being implemented and all the process involved has been analyzed and justified where possible.

REFERENCES

- [1] P. J. Phillips, A. Martin, C. L. Wilson and M. Przybocki, “An Introduction to Evaluating Biometric Systems,” *IEEE Computer*, Vol.33, No.2, Feb. 2000, pp. 56-63.
- [2] S. Pankanti, R.M. Bolle and A. Jain, “Biometrics: The Future of Identification,” *IEEE Computer*, Vol.33 No.2, Feb. 2000, pp. 46-49.
- [3] M. Ejiri, T. Uno, M. Mese and S. Ikeda, “A Process for Detecting Defects in Complicated Patterns,” *Computer Graphics and Image Processing*, Vol.2, No.3-4, 1973, pp. 326-339.
- [4] S. Kashioka, M. Ejiri and Y. Sakamoto, “A Transistor Wire-Bonding System Utilizing Multiple Local Pattern Matching Techniques,” *IEEE Trans. on SMC*, Vol.SMC-6, No.8, Oct. 1977, pp. 562-570.
- [5] H. Yoda, Y. Ohuchi, Y. Taniguchi and M. Ejiri, “An Automatic Wafer Inspection System Using Pipelined Image Processing Techniques,” *IEEE Trans. on PAMI*, Vol. PAMI-10, No.10, 1988, pp.4-16

Design and Implementation of Embedded Media Player Based On ARM9

M.Sushanth¹, K.Somasekhara Rao², M.Ravi Prakash³

M.Tech (Embedded systems), Geethanjali collage of Engineering and Technology AP

M.Tech Professor Geethanjali collage of Engineering and Technology AP

M.Tech, PhD Electronic Communication, JNTU Hyderabad AP

ABSTRACT:

In this paper of Embedded Media Player we have selected Samsung S3C2440A as microprocessor from the family of Samsung ARM9. And we have been using 64MByte Nand Flash kwon to be K9F1208 an external memory and a Nor Flash of 2MByte SST39VF1601 to play the Video and audio files and to display the picture frames effectively and smoothly. The memory external interface is been updated with micro SDcard and USB which is meant to be an expandable memory. We have installed the optimized Linux operating system in the processor and transplanted the SDL_FFMPEG library into S3C2440 after the cross compilation. Of this whole system come together in playing the audio/video and picture formats files smoothly and effectively.

KEYWORDS: ARM9, Linux, Nand Flash, Nor flash, SDcard, SDL, SDL_FFMPEG, SST39VF1601

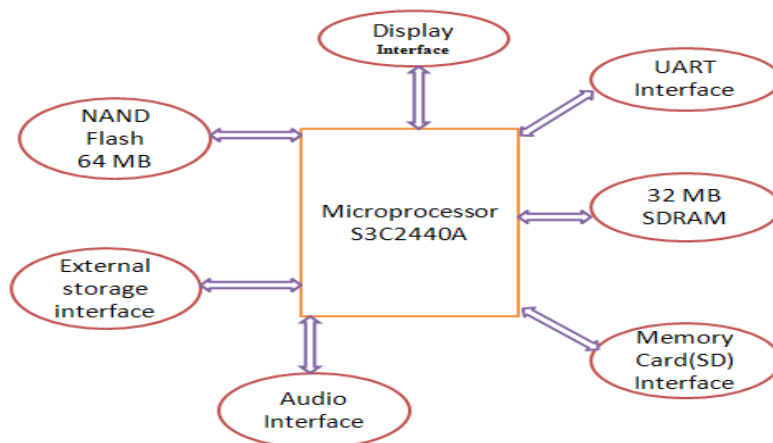
I. INTRODUCTION

Embedded media player is one of the popularly used electronic products for the entertainment purpose. People especially need them when they are in travel, outings and tourism. Because of the popularity the manufacturers make their market targets and produce a large number of products year by year which increases the market rate. In the market competition the manufacturer with best quality and effective cost will gain profits in the market. Because of this we have been using S3C2440 as microprocessor with an extended memory interfacing of USB and SDcard. The external interfacing are done with LCD, UART, EATHERNET, audio ports. In the software optimized Linux operating system is imaged on to the S3C2440. The SDL library which is been included in the OS uses SDL_FFMPEG library to encode and decode the audio/ video or picture frames.

II. SYSTEM HARDWARE DESIGN

We have been using 32-bit RISC processor, 64Mbytes Nand flash, 32Mbytes SDRAM externally S3C2440 as core processor. The main reason in using the S3C2440 core processor is famous in its low power consumptions and working in high frequencies. Where the frequency can be maximum up to 400MHZ. OF all those price comparatively low, which means it is cost effective. The LCD which is of 3.5 inches ensures the better picture quality with multiple touch and TFT (Thin Film Transistor) technologies respectively for the better touch and picture qualities. Since the video files would be big in size the extended USB and SDcard are interfaced to use the externally memory effectively.

The System hardware structure is shown below in the Figure 1. From the above figure 1 we notice that operating system uses NandFlash for the data storage for Boot Loader and other software applications placed in it. SDcard and USB acts as expanded external memory to store the files which are needed. When the system works SDRAM is used as dynamic memory for the whole system. Audio information or data is played through the audio interface. To display and to choose the menu options we use Touch screen LCD. One of the provisions observed is the UART port acts as the bridge to the developers and the system for the designing and developing purpose after which it can be dropped or removed as per the convenience.



“Figure 1. System Hardware Design”

III. SYSTEM SOFTWARE DESIGN

Linux is derived from the UNIX-based operating system which was originally developed from INTEL-compatible PC's OS

3.1. Customization of Operating System

These days Linux is available for wide range of PAD's (Personal Digital Assistance) ranging from wrists watches to mainframes. Linux is known as “modern operating system” for its silent features such as Multitasking, Multiuser, Multi platform, Multithreading, crash proof, virtual memory, memory protection etc...For which it is been developed by a large number of international community of users and developers as an open-source software. These developers believe it is an alternative for the mostly used Windows and Solaris operating systems and few applications such as MS Office, Internet Explorer, Outlook and other application software. Before the optimization the Linux operation system is huge it use in such a portable electronic devices. Since that we need don't need the full functioning of the huge operating system. For which it have been optimized and scaled to a portable devices friendly. In the optimization of Linux the few of the functions removed such as power management, network, wireless communication, hard disk etc...The command ARCH for arm and CROSS_COMPILE for arm-linux has to be entered in the root directory to remove and configures the menu configurations of Linux kernel.

3.2. Software Interface Design of Media Player

Simple Direct Media Layer (SDL) is the basic cross-platform used for the multimedia library which provides a unified programming interface and also used for the software development which intern provides convenient for the code transplanted. SDL is written basic C language which provides functions to the user through library and also provides programming language interface in large number. One of the most important features of SDL is it is an open source, through which the user can get the source code from the SDL's homepage itself which can be used freely by using the licensed second version of GNU LGPL. SDL is very simple to use, it contains eight subsystems such as event handler, timer, video, sound etc...To initialize the system the user need to call the function `SDL_Init()`, he can also initialize the system by setting the parameters of `SDL_Init()` by which he can choose the audio interfacing by calling the function `SDL_Init(SDL_INIT_AUDIO)` in this paper we need multiple software subsystems which can call functions to initialize with the `SDL_Init(SDL_INIT_AUDIO|SDL_INIT_VIDEO|SDL_INIT_TIMER)` together. For the particular and specific equipment SDL provides that particular function to accesses information through that equipment such as `SDL_VideoInfo` to access the video information through display equipment and we can call the function `SDL_SetVideoMode` which Set up a video mode with the specified width, height and bits-per-pixel. Similarly we have functions such as `SDL_ListModes` which returns a pointer to an array of available screen dimensions for the given format and video flags. For audio files functions like `SDL_OpenAudio()` to access to the sound information through sound equipment similarly functions like `SDL_CloseAudio` -- Shuts down audio processing and closes the audio device, `SDL_BuildAudioCVT` -- Initializes a `SDL_AudioCVT` structure for conversion, `SDL_PauseAudio` -- Pauses and play the audio callback processing for necessary corrections and configuring the files provided with the hardware equipment. In designing this media player its takes lot of time for the research in the video subsystem. As per video is concern we concentrate on the unity

video buffer to be shown, any thing operated on the display screen it corresponds to the video buffer. The video buffer can be selected as physical memory or a physical video graphic device memory at the time of video initialization. Here in this paper we selected the video graphic device memory which is known as physical memory and used as a buffer. So that we call functions like `SDL_SetVideoMode` -- Set up a video mode with the specified width, height and bits-per-pixel, and we select `SDL_SWSURFACE` for the parameter flag and we use `SDL_ListModes` which Returns a pointer to an array of available screen dimensions for the given format and video flags. The software interface I broken down into small pieces implemented on the paper and the drawing software with decorative things such as window types, buttons, display pattern and other display parameters on the screen. SDL acts as a stick pad and allows sticking all the display elements on it to me pasted in the display for the better view of the display screen. We cannot use the source code provided in the SDL website directly into the hardware system. Before using the source code we need to compile the using the cross compiler `arm-linux-gcc`. Then source code can be copied to the PC's Linux operating system to the following directory `/root/work/SDL/` and get on to the newly created directory to compile with the following command line up.

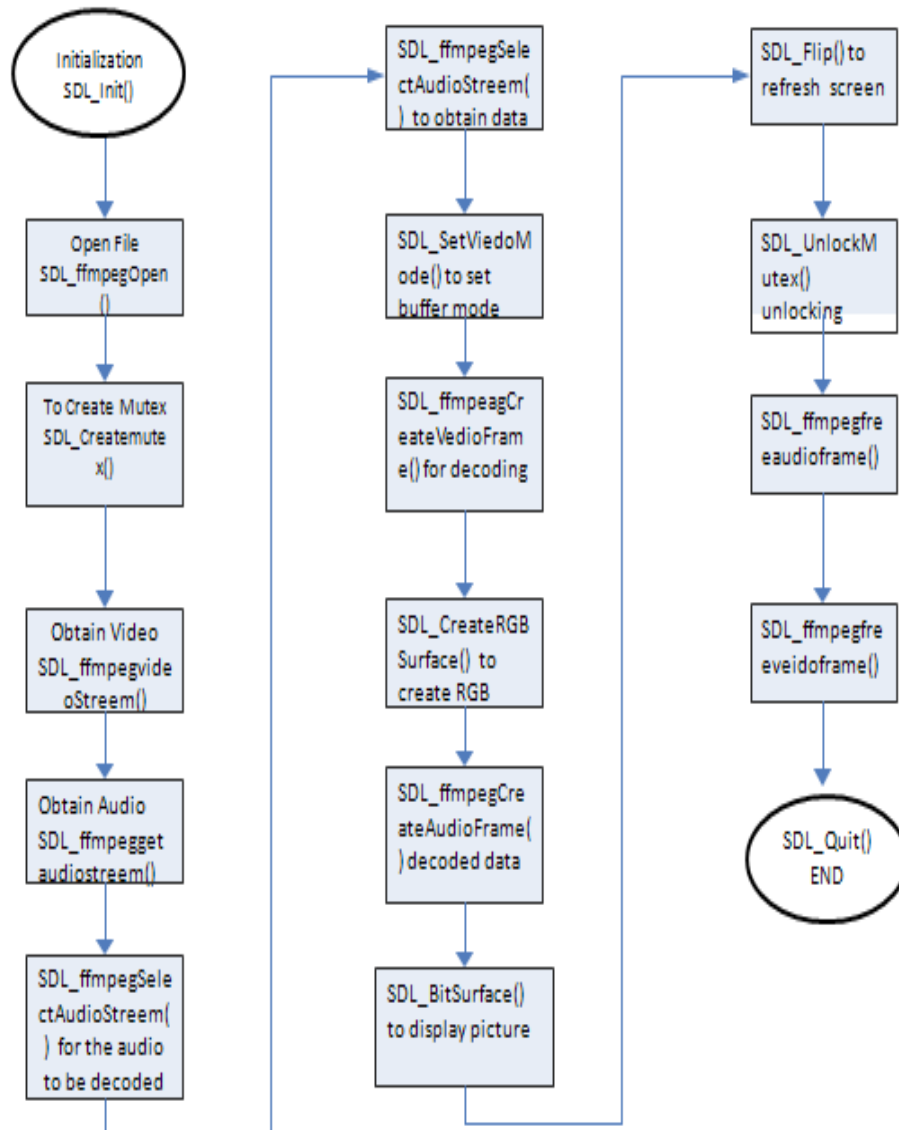
3.3.Commands

```
./configure
--disable-video-gtopia --disable-video-dummy
--disable-video-fbcon --disable-video-dga --disable-esd
--disable-alsa --disable-cdrom --disable-video-x11
--disable-nasm --target=arm-linux --host=arm-linux
--enable-video-fbcon
```

are the functions used to compile the source code. After the compilation is done it can be copied to the hardware system.

3.4.Core Design of Media Player

Encoding and decoding of the video or audio files and to synchronies the audio stream and video stream between them is the core of the media player. The SDL is contained with the powerful library kwon as FFmpeg which provides perfect and complete solution for the audio and video files. Since the FFmpeg library is difficult to understand a simple modified version developed for the beginner's kwon as `SDL_FFmpeg`, this version library is called `libavcodec`. `SDL_FFmpeg` is packed with some multiple functions for the interfacing purpose. Such that users need not know the typical FFmpeg commands rather uses `SDL_FFmpeg` functions to operate. `SDL_ffmpegFile*` `SDL_ffmpegOpen(const char* filename)` is used to open the video files, which is also call with the command `SDL_ffmpegAddVideoFrame()` to add an video frame for the `SDL_ffmpegFrame` directory. At the time of video streaming we have to call the functions `SDL_ffmpegVideoDuration()` and `SDL_ffmpegAudioDuration()` to synchronize the two streams. To set the speed of the media player we need to cal the function `SDL_ffmpegGetFrameRate()` if we want to record the current playing video on the screen `SDL_ffmpegGetPosition` is to be called and to seek the position of the video which is playing `SDL_ffmpegSeek()` is to be realized.



“Figure 3. Media Player Flow Chart”

3.5.Functions and their Effects

```

--SDL_ffmpegInit () */Initializes the SDL_ffmpeg library/*
-- SDL_ffmpegFree (SDL_ffmpegFile *file) */Use this to free an SDL_ffmpegFile/*
--SDL_ffmpegFreeAudioFrame(SDL_ffmpegAudioFrame*frame)*/Use this to free an SDL_ffmpegAudioFrame/*
--SDL_ffmpegFreeVideoFrame (SDL_ffmpegVideoFrame *frame) */Use this to free an
SDL_ffmpegVideoFrame/*
--SDL_ffmpegOpen (const char *filename) */Use this to open the multimedia file of your choice/*
--SDL_ffmpegCreate (const char *filename) */Use this to create the multimedia file of your choice/*
--SDL_ffmpegAddVideoFrame (SDL_ffmpegFile *file, SDL_ffmpegVideoFrame *frame) */Use this
to add a SDL_ffmpegVideoFrame to file/*
--SDL_ffmpegAddAudioFrame (SDL_ffmpegFile *file, SDL_ffmpegAudioFrame *frame) */Use this to add a
SDL_ffmpegAudioFrame to file/*
--SDL_ffmpegCreateAudioFrame (SDL_ffmpegFile *file, uint32_t bytes) */Use this to create a
SDL_ffmpegAudioFrame/*
--SDL_ffmpegCreateVideoFrame (const SDL_ffmpegFile *file, const uint32_t format, SDL_Surface *screen)
*/Use this to create a SDL_ffmpegVideoFrame/*
  
```

```

--SDL_ffmpegGetVideoFrame (SDL_ffmpegFile *file, SDL_ffmpegVideoFrame *frame) */Use this to get new
video data from file/* SDL_ffmpegStream *
--SDL_ffmpegGetAudioStream (SDL_ffmpegFile *file, uint32_t audioID) */Get the desired audio stream from
file/* SDL_ffmpegStream *
--SDL_ffmpegGetVideoStream (SDL_ffmpegFile *file, uint32_t videoID) */Get the desired video stream from
file/*

```

The above are the few functions used to access the video/audio file that need to be accessed



“Figure 4. A Designed Media Player with Hardware”

IV. CONCLUSION

After the software and the audio/video and picture files are observed with their effective synchronization between audio and video. The practical implemented media player is shown in the figure 4. The practical implementation emphasizes the advantages for being low power consumption, less memory footprint, cost reliable, simple structure, compressed size for the comfortable portability with simple structure, stable with the audio video synchronization for the effective and quality output of the media files when executed. By all these seasons make the product with the effective development in the fierce in the market and to improve the sales with simple structure and implementation design.

REFERENCES

- [1] Wenhao Wang, Mingyu Gao, Hangzhou, Zhejiang “Design Of Embedded Media Player Based on S3C2440 and SDL_FFMPEG”
- [2] SAMSUNG, “S3C2440A 32-BIT CMOS MICROCONTROLLER USER'S MANUAL Revision 1”.2004 Samsung Electronics.
- [3] www.friendlyarm.com
- [4] Sam Lantinga: <http://sdl.org>
- [5] SDL's home page: <http://www.libsdl.org/index.php>.
- [6] SDL_FFMPEG's home page: http://www.arjanhouben.nl/SDL_ffmpeg
- [7] www.dranger.com
- [8] <http://en.wikipedia.org/wiki/Video>
- [9] <http://en.wikipedia.org/wiki/mp>
- [10] <http://en.wikipedia.org/wiki/codecs>

Three Dimensional P- Trucks Route Minimum Cost Supply to The Head Quarter From Cities

Revathi P¹, Suresh Babu C², Purusotham S³, Sundara Murthy M⁴

Research Scholar, Dept. of Mathematics, S. V. University, Tirupati, Andhra Pradesh, India.

Academic Consultant, Dept. of Mathematics, S. V. University, Tirupati, Andhra Pradesh, India.

Asst. Professor, Statistics and OR Division, VIT University, Vellore, Tamil Nadu, India

4. Professor, Dept. of Mathematics, S. V. University, Tirupati, Andhra Pradesh, India.

ABSTRACT:

Many Combinatorial programming problems are NP-hard (Non Linear Polynomial), and we consider one of them called P-path minimum cost connectivity to head quarter{1} from the cities. Let there be n cities and the cost matrix $D(i, j, k)$ is given from i^{th} city to j^{th} city using k^{th} facility. There can be an individual factor which influences the distances/cost and that factor is represented as a facility k . We consider $m < n$ cities are in cluster and to connect all the cities in subgroup (cluster) from others by using same facility k . From different cities to Head Quarter city in P-path the supply of load will be according to the requirement. The problem is to find minimum cost to connect all the cities to head quarter (say 1) through p-paths with the requirements of the load and subject to the above considerations. For this problem we developed a Pattern Recognition Technique based Lexi Search Algorithm.

KEYWORDS: Lexi Search Algorithm, Pattern Recognition Technique, Partial word, Pattern, Mathematical formation, load

I. INTRODUCTION:

In recent years the development of networks in the area of telecommunication and computer has gained much importance. One of the main goals in the design process is to reach total connectivity at minimum cost/distance. The total connections are in some paths (say P). Similar problems arise in the planning of road maps, integrated circuits. The technical restriction that the number of connections at a node is bounded is modelled by introducing constraints that bound the node degrees. Garey at al [2] proved that the resulting degree-constrained minimum. In this paper we studied a variation of Minimum spanning models. For this we developed a Lexi- algorithm based "Pattern Recognition Technique" to solve this problem.

Some of the researchers studied variations in the Minimum Spanning Tree (MST) problems. They are Pop, P.C [6], Karger [3] found a linear time randomized algorithm based on a combination of Boruvka's algorithm and the reverse-delete algorithm. The problem can be solved deterministically in linear by Chazelle [1]. Its running time is $O(m, \alpha(m,n))$ where function α grows extremely slowly. Thus Chazelle's algorithm takes very close to linear time. Seth Pette [4, 5] have found a probably optimal deterministic comparison-based minimum spanning tree algorithm. The general network design, given a directed graph $G(N,A)$ where $N = \{1, 2, \dots, n\}$ denotes the set of nodes and the set of arcs, each arc $(i, j) \in A$, various algorithms are available in the literature to find the Shortest Path between one or any pair of nodes. For example Dijkstra's algorithm solves the single-pair, single-source, problem if edge weights may be negative. Floyd-Warshall algorithm solves all pair's shortest paths. Perturbation theory finds (at worst the locally shortest path). The path finding is applicable to many kinds of networks, such as roads, utilities, water, electricity telecommunications and computer networks alike, the total number of algorithms that have been developed over the years is immense. A selected cross-section of approaches towards path finding and the related fields of research, such as transportation, GIS, network analysis, operation research, graph theory, artificial intelligence and robotics, to mention just a few examples where path finding theories all are employed. Even though the different research literature tends to group the types of shortest paths problems slightly different, one can discern, in general, between paths that are calculated as one-to-one, one-to-some, one-to-all, all-to-one and all-to-all shortest paths.

Sobhan Babu [8] studied a variation of spanning models using pattern recognition technique [9]. Let there be N cities to be connected to the headquarter city $\{1\}$. There is an individual factor which influences the distances/cost and that factor is represented as a facility K . If the city j_1 and j_2 different cities are connected from city i_1 then k_1 and k_2 should be same. Suresh Babu [10] studied another variation of spanning models, which is reverse case of [8]. The problem is to find optimal solution for all the cities connected to head quarter $\{1\}$ with minimum cost by using k facility.

II. LEXICOGRAPHIC SEARCH USING PATTERN RECOGNITION TECHNIQUE:

Lexicographic Search Approach is a systematized Branch and Bound approach, developed by Pandit in the context of solving of loading problem in 1962. In principle, it is essentially similar to the Branch and Bound method as adopted by Little et.al-1963. This approach has been found to be productive in many of the Combinatorial Programming Problems. Its significance mentioning that. Branch and Bound can be viewed as a particular case of Lexicographic Search approach [Pandit-1965]. The name Lexicographic Search itself suggests that, the search for an optimal solution is done in a systematic manner, just as one searches for the meaning of a word in a dictionary and it is derived from Lexicography the science of effective storage and retrieval of information. This approach is based on the following grounds [Pandit -1963].

- (i) It is possible to list all the solutions or related configurations in a structural hierarchy which also reflects a hierarchical ordering of the corresponding values of these configurations.
- (ii) Effective bounds can be set to the values of the objective function, when structural combinatorial restraints are placed on the allowable configurations.

The basic principle is described as follows [Rajbhongshi-1982]. Consider set of symbols. $A = (1, 2, 3, \dots, n)$ and the different possible sequences of length k of these symbols. Thus $(\alpha_1, \alpha_2, \dots, \alpha_k)$ is a k -word, formed from the alphabetic order on the elements of A . We will be able to define a unique ordered list of words of length not exceeding m , where m is finite. Words of length $k \leq m$ are called incomplete words standing for the set or block of the $(m - k)$. Words of length k Searching for an optimum word is a problem of finding the word of minimum value (in the case of a minimizing problem). In the Lexi search defined by the solution of the problem. The search efficiency of a Lexi Search algorithm is based in this approach depends on the choice of an appropriate Alphabet-Table, where two conflicting characteristics of the search list have to be taken into account; one is the difficulty in setting bounds to the values of the partial words (that defines partial solutions representing subsets of solutions). The other difficulty is checking the feasibility of a partial word. Thus we get two situations in the choice of the alphabet-table [Sundara Murthy-1979]. By this method, in this problem we get Computation of lower bound is easy, while the feasibility checking is difficult. When the process of feasibility checking of a partial word becomes difficult and the lower bound computation is easy, a modified Lexi- Search i.e. Lexi- Search with recognising the Pattern of the Solution known as Pattern Recognition Technique which was the main efficiency of the algorithm, first the bounds are calculated and then the partial word, for which the value is less than the initial trial value are checked for the feasibility. The Pattern-recognition technique can be described as follows.

“A unique pattern is associated with each solution of a problem. Partial pattern defines a partial solution. An alphabet-table is defined with the help of which the words, representing the pattern are listed in a Lexicographic order. During the search for an optimal word, when a partial word is considered, first bounds are calculated and then the partial words for which the value is less than the trail value are checked for the feasibility”

Using Pattern Recognition technique reduces the dimensions requirement of the problem. For this problem find an optimal solution X which is a three dimensional array, the problem can be reduced to a linear form of finding an optimal word of length n . This reduction in the dimension for some problems reduces the computational word in getting an optimal solution [Sundara Murthy – 1979, Vidyulata – 1992, Ramana and Uma shankar -1995]. The present paper uses the Lexicographic Search in general and makes use of the Pattern Recognition present paper uses the Lexicographic Search in general and makes use the Pattern Recognition approach.

III. PROBLEM DESCRIPTION:

In this paper we study the problem called “Three dimensional P- Trucks route minimum cost supply to the Head Quarter {1} from cities”. The objective is to find the minimum total cost to supply required capacities through P trucks in P paths from each city to head quarter city {1}. Each path requirement is not greater than ‘α’ units of capacity. The total capacity is ‘Pα’ units. Let there be N= {1, 2, 3, 4.....n} cities whose costs $N \times N \times K$ are given. In this chapter we consider Pattern Recognition Technique based Lexi-Search Approach for minimum spanning network connectivity problem (msncp). There is a restriction that M is subset of N cities must have same facility. An exact algorithm is proposed for this minimum spanning network connectivity problem (msncp). The algorithm solves the problem by identify the key patterns which optimize the objective of the cost/distance.

Let N be the set of n stations defined as $N=\{1,2,3,4,\dots,n\}$ and the set of q facilities in $K = \{1,2, \dots, q\}$. Let D (i, j, k) be the cost from ith city to jth city using kth facility where i, j ∈ N and k ∈ K. Let there are set of m cities in $M= \{1, 2, 3... m\}$ such that M be the cluster and M is subset of N. We want to connect all the (n-1) cities to head quarter city by P-paths. Each city connected to head quarter city {1} either directly or indirectly. The P- trucks starts at different cities in P paths and has to reach to head quarter city {1}. The total capacity in P- trucks (Pα) is greater than or equal to the availability of the cities. In each city there is availability of some material (TL(i)). The objective of the problem is to find minimum cost to connect all the n-1 cities having availability capacity of load at each city supply to head quarter city {1}. For this we developed an algorithm called as Lexi-Search algorithm using pattern recognition Technique and it is illustrated with a suitable numerical example for three paths.

IV. MATHEMATICAL FORMULATION:

$$\text{Minimize } Z(X) = \sum_{i=1}^n \sum_{j=1}^n \sum_{k=1}^q D(i, j, k), X(i, j, k) \dots \dots \dots (1)$$

Subject to constraints.

$$\sum_{i=1}^n \sum_{j=1}^n \sum_{k=1}^q X(i, j, k) = n - 1 \dots \dots \dots (2)$$

$$\sum_{s=1}^P X(1, n_{s1}) = P \dots \dots \dots (3)$$

$1, \alpha_{11}, \alpha_{12}, \dots, \alpha_{1n1}$ be the cities in the first path to the Head Quarter city,

$1, \alpha_{i1}, \alpha_{i2}, \dots, \alpha_{ini}$ (i=1,2,...P) be the cities in the ith path with n_{i+1} cities. (cities taken in reverse order)

$$\sum_{s=1}^{n_i-1} X(\alpha_{is}, \alpha_{is+1}) = n_i - 1 \dots \dots \dots (4)$$

$$\sum_{s=1}^{n_i} TL(\alpha_{is}) \leq \alpha \dots \dots \dots (5)$$

Let $i_1, i_2 \in M$,

$$\text{If } X(i_1, j_1, k_1) = X(i_2, j_2, k_2) = 1. \text{ Then } k_1 = k_2 \dots \dots \dots (6)$$

$$X(i, j, k) = 0 \text{ or } 1 \dots \dots \dots (7)$$

Equation (1) represents the objective of them problem i.e. to find minimum total distance from the cities to head quarter city. Equation (2) represents total number of connections in the network. The equation (3) represents the total number of paths from cities to head quarters (say p). Equation (4) represents the total number of cities connected in each path in reverse order. Equation (5) represents load/ capacity in each path. Equation (6) represent that the total cities in M using same facility. Equation (7) describes that if a city ‘i’ is connected to city ‘j’ using facility ‘k’ then $X(i,j,k) = 1$. Otherwise it will be equal to ‘0’.

V. NUMERICAL FORMULATION:

The concept and algorithm developed will be illustrated by a numerical example for which total number of cities $N = \{1, 2, 3, 4, 5, 6, 7, 8, 9\}$. In each path the capacity of load (say α) has to supply from cities to Head Quarter city. The number of paths is 3. Among them the cities 2,4&7 are taken as separate cluster say

$M = \{2, 4, 7\}$. All the cities in M have connected to other cities should be used same facility. Then the distance matrices $D(i, j, k)$ are as follows.

TABLE-1

	∞	∞	∞	∞	∞	∞	∞	∞	∞
	01	∞	21	-	25	-	09	28	31
	19	05	∞	11	03	18	27	-	01
	31	28	-	∞	16	-	11	26	32
D(i,j,1)	17	28	15	06	∞	30	14	24	20
	23	13	-	-	22	∞	-	04	33
	29	10	12	20	02	-	∞	32	16
	21	27	25	08	-	23	09	∞	-
	18	-	03	-	26	-	17	3	∞

TABLE-2

	∞	∞	∞	∞	∞	∞	∞	∞	∞
	26	∞	11	-	-	09	29	14	10
	07	15	∞	02	-	-	24	01	-
	25	07	01	∞	-	15	13	22	29
D(i,j,2)	03	22	-	19	∞	-	28	10	19
	17	13	-	02	30	∞	-	32	12
	14	04	-	20	16	-	∞	27	31
	01	-	03	08	33	18	-	∞	23
	24	05	21	-	12	-	-	06	∞

In the above table (1&2) the value distances $d(i, i, k)$, where $(i=1,2,...n)$ as ‘∞’ and $d(i,j,k)$, where $(j=1,2,...n)$ as ‘-’ indicates the disconnectivity between cities. Here the entire $D(i,j,k)$ are taken as positive integers and in this numerical example we are given 9 cities. Suppose $D(2, 6, 2)=09$ means the distance of the connecting the city 2 to 6 by using facility 2 is 09. For our convenience the total cities in cluster M identified by the array B as follows in Table-3.

Table-3

cites	1	2	3	4	5	6	7	8	9
Cluster	0	1	0	1	0	0	1	0	0

In the above numerical example given in Table-3, $B(i) = 1$ means that the city i belongs to cluster M , Otherwise $B(i) = 0$. Suppose $B(2) = 1$, city 2 is cluster M .

Table-4

LOAD

	1	2	3	4	5	6	7	8	9
Q	-	30	30	40	50	70	60	40	40

From the above table-4, $Q(i) = \beta$ means Load requirement of city j is β . suppose $Q(2) = 30$ means that the requirement of load at city 2 is 30. Here $Q(1) = ‘-’$ means that the city 1 act as head quarter has no load. Each path has capacity of load to supply from cities in that path to Head Quarters is $\alpha = LD = 150$ units. The total number of paths (P) is 3.

VI. CONCEPT AND DEFINITIONS:

6.1 Definition of a pattern: An indicator three-dimensional array X which is associated the an assignment is called a “pattern”. A pattern is said to be feasible if X is solution.

$$V(X) = \sum_{i \in N} \sum_{j \in N} \sum_{k \in K} D(i, j, k) X(i, j, k)$$

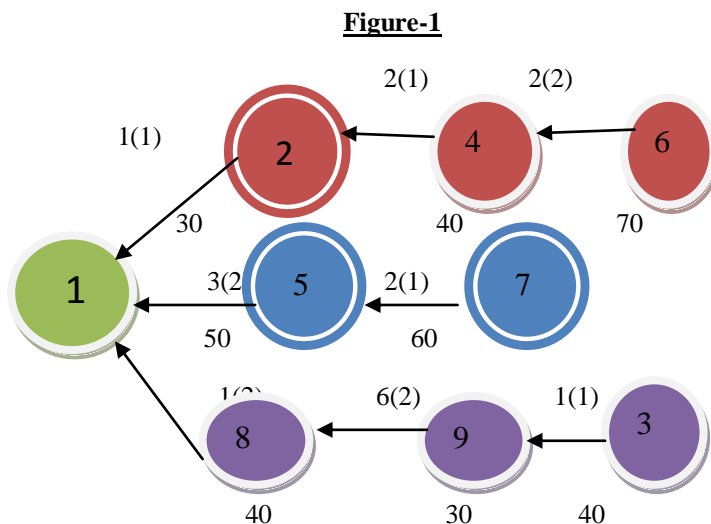
The pattern represented is a feasible pattern. The value $V(X)$ gives the total time represented by it. In the algorithm, which is developed in the sequel a search is made for a feasible pattern with the least value, each pattern of the solution X is represented by the set of ordered triples $X(i, j, k)=1$, which understanding that the other $X(i, j, k)$ ‘s are zeros.

6.2 Feasible Solution: Consider the ordered pairs $\{ (2,1,1), (3,9,2), (4,2,1), (5,1,2), (6,4,2), (7,5,1), (8,1,2), (9,8,2) \}$ represents the pattern given in the tables 5 & 6, which is a feasible solution.

<p>Table-5</p> $X(i, j, 1) = \begin{pmatrix} 0 & 0 & 0 & 0 & 0 & 0 & 0 & 0 & 0 & 0 \\ 1 & 0 & 0 & 0 & 0 & 0 & 0 & 0 & 0 & 0 \\ 0 & 0 & 0 & 0 & 0 & 0 & 0 & 0 & 0 & 1 \\ 0 & 1 & 0 & 0 & 0 & 0 & 0 & 0 & 0 & 0 \\ 0 & 0 & 0 & 0 & 0 & 0 & 0 & 0 & 0 & 0 \\ 0 & 0 & 0 & 0 & 0 & 0 & 0 & 0 & 0 & 0 \\ 0 & 0 & 0 & 0 & 1 & 0 & 0 & 0 & 0 & 0 \\ 0 & 0 & 0 & 0 & 0 & 0 & 0 & 0 & 0 & 0 \\ 0 & 0 & 0 & 0 & 0 & 0 & 0 & 0 & 0 & 0 \end{pmatrix}$	<p>Table-6</p> $X(i, j, 2) = \begin{pmatrix} 0 & 0 & 0 & 0 & 0 & 0 & 0 & 0 & 0 & 0 \\ 0 & 0 & 0 & 0 & 0 & 0 & 0 & 0 & 0 & 0 \\ 0 & 0 & 0 & 0 & 0 & 0 & 0 & 0 & 0 & 0 \\ 0 & 0 & 0 & 0 & 0 & 0 & 0 & 0 & 0 & 0 \\ 1 & 0 & 0 & 0 & 0 & 0 & 0 & 0 & 0 & 0 \\ 0 & 0 & 0 & 1 & 0 & 0 & 0 & 0 & 0 & 0 \\ 0 & 0 & 0 & 0 & 0 & 0 & 0 & 0 & 0 & 0 \\ 1 & 0 & 0 & 0 & 0 & 0 & 0 & 0 & 0 & 0 \\ 0 & 0 & 0 & 0 & 0 & 0 & 0 & 1 & 0 & 0 \end{pmatrix}$
-------------------------------------------------------------------------------------------------------------------------------------------------------------------------------------------------------------------------------------------------------------------------------------------------------------------------------------------------------------------------------------------------------------------------------------------	-------------------------------------------------------------------------------------------------------------------------------------------------------------------------------------------------------------------------------------------------------------------------------------------------------------------------------------------------------------------------------------------------------------------------------------------

The above solution $X(2, 1, 1) = 1$, represents that city 2 is connected to city 1 using facility 1. In similar way $X(5,1,2)$ represents city 5 is connected to city 1 by facility 2 and all the cities are connected directly or indirectly to head quarter 1. So the above solution gives a feasible solution shown in the figure-1.

In following figure-1, the values in circles indicates name of the cities. Also values at each arc in parenthesis and before parenthesis represent the facility and distance between the respective two nodes. The value below the circles represents the availability of load (capacity) to that particular city.



The above figure-1 represents a feasible solution. In first path the city 4 is connected by the city 6 using facility 2, city 2 is connected by city 4 using facility 1, city 1 is connected by city 2 using facility 1. In second path, the city 5 is connected by city 7 using facility 1, city 1 is connected by city 5 using facility 2. In third path city 9 is connected by city 3 using facility 1, city 8 is connected by city 9 using facility 2, city 1 is connected by city 8 using facility 1. Hence the solution of the above pattern X is as follows

$$Z = D\{(2,1,1), (3,9,1), (4,2,1), (5,1,2), (6,4,2), (7,5,1), (8,1,2), (9,8,2)\}$$

$$= 1+1+2+3+2+2+1+6 = 18.$$

6.3 Definition of Pattern:

An indicator three-dimensional array which is associated with connection is called a 'pattern'. A Pattern is said to be feasible if X is a solution.

$$V(X) = \sum_{i \in N} \sum_{j \in N} \sum_{k \in K} D(i, j, k) X(i, j, k)$$

The value $V(x)$ is gives the total cost of the tour for the solution represented by X. The pattern represented in the tables-5&6 is a feasible pattern. The value $V(X)$ gives the total distance of the network for the solution represented by X. Thus X is the feasible pattern gives the total distance represented by it. In the algorithm, which is developed in the sequel, a search is made for a feasible pattern with the least value. Each pattern of the solution X is represented by the set of ordered triple (i, j, k) for which $X(i, j, k)=1$, with understanding that the other $X(i,j,k)$ are zeros. The ordered triple set $\{(2,1,1),(3,9,1),(4,2,1),(5,1,2),(6,4,2),(7,5,1),(8,1,2),(9,8,2)\}$ represents the pattern given in table – 4&5, which is feasible solution.

6.4: ALPHABET TABLE:

There are $n \times n \times k$ ordered triples in the three-dimensional array X. For convenience these are arranged in ascending order of their corresponding cost and are indexed from 1 to M (Sundara murthy-1979). Let $SN = \{1, 2, 3 \dots\}$ be the set of indices. Let D be the corresponding array of cost/Distance. If $a, b \in SN$ and $a \leq b$ then $D(a) \leq D(b)$. Also let the array R, C, K be the array of row, column and facility indices of the ordered triple represented by SN and CD be the array of cumulative sum of the elements of D. For convenience same notation D and K are used for the cost array and facility array in the alphabet table. The array S, D, CD, R, C, and K for the numerical example is given in the table-7. If $p \in SN$ then $(R(p), C(p), K(p))$ is the ordered triple and $D(a) = T(R(a), C(a), K(a))$ is the value of the ordered triple and $CD(a) = \sum_{i=1}^a D(i)$

TABLE-7

SN	D	CD	R	C	K
1	01	01	2	1	1
2	01	02	3	9	1
3	01	03	3	8	2
4	01	04	4	3	2
5	01	05	8	1	2
6	02	07	4	2	1
7	02	09	7	5	1
8	02	11	3	4	2
9	02	13	6	4	2
10	03	16	3	5	1
11	03	19	9	3	1
12	03	22	5	1	2
13	03	25	8	3	2
14	04	29	6	8	1
15	04	33	7	2	2
16	05	38	3	2	1
17	05	43	9	2	2
18	06	49	5	4	1
19	06	55	9	8	2
20	07	62	3	1	2
21	07	69	4	2	2
22	08	77	8	4	1
23	08	85	8	4	2
24	09	94	2	7	1
25	09	103	8	7	1
26	09	112	2	6	2
27	10	122	7	2	1
28	10	132	2	9	2
29	10	142	5	8	2
30	11	153	3	4	1
31	11	164	4	7	1
32	11	175	2	3	2
33	12	187	7	3	1
34	12	199	6	9	2
35	12	211	9	5	2
36	13	224	6	1	2
37	13	237	4	6	2
38	13	250	6	2	2
39	14	264	5	7	1

40	14	278	2	8	2
41	14	292	7	1	2
42	15	307	5	3	1
43	15	322	3	2	2
44	15	337	4	6	2
45	16	353	4	5	1
46	16	369	7	9	1
47	16	385	7	5	2
48	17	402	5	1	1
49	17	419	9	7	1
50	17	436	6	1	2
51	18	454	3	6	1
52	18	472	9	1	1
53	18	490	8	6	2
54	19	509	3	1	1
55	19	528	5	4	2
56	19	547	5	9	2
57	20	567	5	9	1
58	20	587	7	4	1
59	20	607	7	4	2
60	21	628	2	3	1
61	21	649	8	1	1
62	21	670	9	3	2
63	22	692	6	5	1
64	22	714	4	8	2
65	22	736	5	2	2
66	23	759	6	1	1
67	23	782	8	6	1
68	23	805	8	9	2
69	24	829	5	8	1
70	24	853	3	7	2
71	24	877	9	1	2
72	25	902	2	5	1
73	25	927	8	3	1
74	25	952	4	1	2
75	26	978	4	8	1
76	26	1004	9	5	1
77	26	1030	2	1	2
78	27	1057	3	7	1
79	27	1084	8	2	1
80	27	1111	7	8	2
81	28	1139	2	8	1
82	28	1167	5	2	1
83	28	1195	5	7	2
84	29	1224	7	1	1
85	29	1233	2	7	2
86	29	1262	4	9	2
87	30	1292	5	6	1
88	30	1322	9	8	1
89	30	1352	6	5	2
90	31	1383	2	9	1
91	31	1414	4	1	1
92	31	1445	7	9	1
93	32	1477	4	9	1
94	32	1509	7	8	1
95	32	1541	6	8	2
96	33	1607	6	9	1
97	33	1607	8	6	2

Let us consider $92 \in SN$. It represents the ordered triple $(R(92), C(92), K(92)) = (7, 9, 1)$.

Then $D(92) = 31$ and $CD(92) = 1445$.

6.5 Definition of the Alphabet –Table and the Word: Let $SN = (1, 2, \dots)$ be the set of indices. CD be an array of cumulative sums of elements in D . Let arrays R, C and K be respectively, the row, column and facility indices of the ordered triples. Let $L_k = \{a_1, a_2, \dots, a_k\}$, $a_i \in SN$ be an ordered sequence of k indices from SN . The pattern represented by the ordered triples whose indices are given by L_k is independent of the order of a_i in the sequence. Hence for uniqueness the indices are arranged in the increasing order such that $a_i \leq a_{i+1}$, $i=1, 2, \dots, k-1$. The set SN is defined as the “Alphabet-Table” with alphabet order as $(1, 2, \dots)$ and the ordered sequence L_k is defined as a “word” of length k . A word L_k is called a “sensible word”. If $a_i \leq a_{i+1}$, for $i=1, 2, \dots, k-1$ and if this condition is not met it is called a “insensible word”. A word L_k is said to be feasible if the corresponding pattern X is feasible and same is with the case of infeasible and partial feasible pattern. A Partial word L_k is said to be feasible if the block of words represented by L_k has at least one feasible word or, equivalently the partial pattern represented by L_k should not have any inconsistency. Any of the letters in SN can occupy the first place in the partial word L_k . Our interest is only in set of words of length at most $n-1$, since the words of length greater than $n-1$ are necessarily infeasible, as any feasible pattern can have only $n-1$ unit entries in it. If $k < n$, L_k is called a partial word and if $k = n$, it is a full length word or simply a word. A partial word L_k represents, a block of words with L_k as a leader i.e. as its first k letter. The condition for feasibility of a word requires the existence of at least a word and the feasibility of the word defines the position of the Leader.

6.6: Value of the Word: Let the value of the (partial) word defined as L_k . $V(L_k)$ is defined recursively as $V(L_k) = V(L_{k-1}) + V(a_k)$ with $V(L_0) = 0$, where $D(a_i)$ is the distance array arranged such that $D(a_i) \leq D(a_{i+1})$. $V(L_k)$ and $V(X)$ the values of the pattern X will be the same. Since X is the (partial) pattern represented by $L_k = (a_1, a_2, \dots, a_k)$ (Sundara Murthy-1979).

Consider a partial word $L_4 = (1, 2, 5, 6)$
Then $V(L_4) = 1+1+1+2=5$

6.7: Lower Bound of A partial Word $LB(L_k)$: A lower bound $LB(L_k)$ for the values of the block of words represented by $L_k = (a_1, a_2, \dots, a_k)$ can be defines as

$$LB(L_k) = V(L_k) + \sum_{j=1}^{n-k} D(a_{k+j}) = V(L_k) + DC(a_k + n - 1 - k) - DC(a_k)$$

Consider the partial word $L_4 = (1, 2, 5, 6)$

$$\text{Then } V(L_4) = 1+1+1+2=5$$

$$\begin{aligned} LB(L_k) &= V(L_k) + DC(a_4 + n - 1 - k) - DC(a_k) \\ &= 5 + DC(6 + 8 - 4) - DC(6) = 5 + DC(10) - DC(6) = 5 + 16 - 7 = 14. \end{aligned}$$

This is obtained by concatenating the first $(n-k)$ letters of SN to the partial word.

6.8: Feasibility criterion of partial word:

An algorithm was developed, in order to check the feasibility of a partial word $L_{k+1} = (a_1, a_2, \dots, a_k, a_{k+1})$ given that L_k is a feasible word. We will introduce some more notations which will be useful in the sequel.

- IR be an array where $IR(i) = 1$, $i \in N$ indicates that the i^{th} city is connected to some city j . Otherwise $IR(i) = 0$
- IC be an array where $IC(j) = 1$, $j \in N$ indicates that the i^{th} city is connected from some city i . Otherwise $IC(j) = 0$
- M be an array, where $M(i) = N_i$, indicates that the i^{th} city is belongs to N_i cluster, otherwise $M(i) = 0$.
- SW be an array where $SW(i) = j$ indicates that the i^{th} city is connected to some city j , Otherwise $SW(i) = 0$
- LW be an array where $L[i] = \alpha_i$, $i \in N$ is the letter in the i^{th} position of a word.

The values of the arrays IR, IK, SW and LW are as follows

$$IR(R(a_i)) = 1, i = 1, 2, \dots, k \text{ and } IR(j) = 0 \text{ for other elements of } j.$$

$$IC(C(a_i)) = 1, i = 1, 2, \dots, k \text{ and } IC(j) = 0 \text{ for other elements of } j.$$

$$SW(R(a_i)) = C(a_i), i = 1, 2, \dots, k \text{ and } SW(j) = 0 \text{ for other elements of } j.$$

$$LW(i) = N_i, i = 1, 2, \dots, k, \text{ and } LW(j) = 0 \text{ for other elements of } j.$$

The recursive algorithm for checking the feasibility of a partial word L_k is given as follows. For this algorithm we have $TR = R(a_{k+1})$, $TC = C(a_{k+1})$ and $TK = K(a_{k+1})$. We start with the partial word $L_1 = (a_1) = (1)$. A partial word L_k is constructed as $L_k = L_{k-1} * (\alpha_k)$. Where * indicates chain formulation. We will calculate the values of $V(L_k)$ and $LB(L_k)$ simultaneously. Then two situations arises one for branching and other for continuing the search.

1. $LB(L_k) < VT$. Then we check whether L_k is feasible or not. If it is feasible we proceed to consider a partial word of under $(k+1)$. Which represents a sub-block of the block of words represented by L_k . If L_k is not feasible then consider the next partial word p by taking another letter which succeeds a_k in the position. If all the words of order p are exhausted then we consider the next partial word of order $(k-1)$.

2. $LB(L_k) \geq VT$. In this case we reject the partial word L_k . We reject the block of word with L_k as leader as not having optimum feasible solution and also reject all partial words of order k that succeeds L_k .

❖ For example consider a sensible partial word $L_4 = (1, 2, 5, 6)$ which is feasible. The array IR, IC, L, SW takes the values represented in table - 8 given below.

TABLE-8

	1	2	3	4	5	6	7	8	9
L	1	2	5	6					
IR	1	1	1	1	1			1	1
IC	2	1	1				1	1	
SW		1	9	2				1	1

The recursive algorithm for checking the feasibility of a partial word L_p is given as follows. In the algorithm first we equate $IX = 0$, at the end if $IX = 1$ then the partial word is feasible, otherwise it is infeasible. For this algorithm we have $TR=R(a_i)$, $TC=C(a_i)$.

VII. ALGORITHMS:

ALGORITHM 1: (Algorithm for feasibility checking)

STEP 0:	IX=0	GO TO 1
STEP1:	IS (TC=HC)	IF YES GOTO 2 IF NO GOTO 3
STEP 2:	IS (PA ≤ P)	IF YES GOTO 4 IF NO GOTO 16
STEP 3:	IS (IC [TC] =1)	IF YES GOTO 16 IF NO GOTO 4
STEP 4:	IS (IR [TR] =1)	IF YES GO TO 16 IF NO GOTO 5
STEP 5:	Z=P-PA RP=N-1-I IS RP ≥ Z	IF YES GO TO 6 IF NO GO TO 16
STEP 6:	W=TR	GOTO 7
STEP 7:	IS (SW [TR] = =0)	IF YES GOTO 15 IF NO GOTO 8
STEP 8:	W=SW [W]	GOTO 9
STEP 9:	IS (W= TC))	IF YES GOTO 16 IF NO GOTO 7

STEP10:	IS (b [TR] = =1)	IF YES GO TO 11 IF NO GOTO 15
STEP11:	IS NM = 0	IF YES GO TO 12 IF NO GOTO 13
STEP 12:	A = b [TR] F [A] = TK	GO TO 14
STEP 13:	IS F (A) = TK	IF YES GOTO 14 IF NO GOTO 16
STEP 14:	NM = NM +1	GOTO 15
STEP 15:	IX=1	
STEP 16:	STOP	

$L_k = L_{k-1} *$ Where * indicates chain formulation. We will calculate the values of V (L_p) and LB (L_p) simultaneously. Then two situations arises one for branching and other for continuing the search.

1. $LB (L_p) < VT$. Then we check whether L_p is feasible or not. If it is feasible we processed to consider a partial word of under (P+1). Which represents a sub-block of the block of Words represented by L_p
2. $LB (L_p) \geq VT$. In this case we reject the partial word L_p . We reject the block of word with L_p as leader as not having optimum feasible solution and also reject all partial words of order p that succeeds L_p .

ALGORITHM 2: (Lexi -Search Algorithm)

STEP 1: (Initialization)

The arrays SN, D, CD, R, C and K, the values of n, M, LD,P,MAX are made available, IR,IC,SW, L, V, LB are initialized to zero. The values I=1, J=0, PA =0, ST (TL) = 0, VT= ∞ .

STEP 2:	J=J+1 ST (TL) = 0 IS (J>MAX)	IF YES GOTO 15 IF NO GOTO 3
STEP3:	L (I) =J TR= R (J) TC= C (J) TK= T (J)	GOTO 4
STEP4:	V (I) =V (I-1) +D (J) LB (I) =V (I) +CD ((J+N-1-I)-CD (J))	GOTO 5
STEP5:	IS (LB (I)>=VT)	IF YES GOTO 11 IF NO GOTO 6
STEP 6:	(CHECK FEASIBILITY BY USING ALGORITHM 1) IS IX =0	IF YES GO TO 2 IF NO GO TO 7
STEP 7:	IS (I= n-1)	IF YES GOTO 8 IF NO GOTO 12
STEP 8:	ST (TL) =ST (TL) + Q (TR)	GO TO 9
STEP 9:	IS ST (TL) < LD	IF YES GOTO 10 IF NO GO TO 2
STEP 10:	W = SW (TR)	GOTO 11
STEP11:	IS (SW [TR] = =0)	IF YES GOTO 14 IF NO GOTO 8
STEP12:	L [I] =J IR [TR] =1 SW [TR] =TC IS (TC= HC)	IF YES {PA=PA+1}, GOTO 13 IF NO {IC [TC] =1}, GOTO 13
STEP 13:	I=I+1	GOTO2
STEP 14:	VT=V [I] L [I] =J	GOTO 15
STEP 15:	I=I-1	GOTO 16

STEP 16: J=L [I]
 TR=R [J]
 TC=C [J]
 IR [TR] =0
 SW [TR] =0
 L [I+1] =0
 IS (TC= HC) IF YES {PA = PA -1, GOTO 17}
 IF NO {IC [TC] =0, GOTO 17}

STEP 17: ST (TL) =ST (TL) - Q (TR) GO TO 18

STEP 18: W = SW (TR) GOTO 19

STEP19: IS (SW [TR] = =0) IF YES GOTO 20
 IF NO GOTO 17

STEP 20: IS (b [TR] = 1) IF YES GOTO 21
 IF NO GOTO 2

STEP 21: NM=NM-1 GOTO 22

STEP 22: IS (I= 1) IF YES GOTO 23
 IF NO GOTO 15

STEP 23: STOP

$L_k = L_{k-1} *$ Where * indicates chain formulation. We will calculate the values of $V(L_p)$ and $LB(L_p)$ simultaneously. Then two situations arises one for branching and other for continuing the search.

1. $LB(L_k) < VT$. Then we check whether L_k is feasible or not. If it is feasible we processed to consider a partial word of under $(k+1)$. Which represents a sub-block of the block of Words represented by L_p
2. $LB(L_k) \geq VT$. In this case we reject the partial word L_k . We reject the block of word with L_k as leader as not having optimum feasible solution and also reject all partial words of order p that succeeds L_k .

VIII. SEARCH TABLE:

The working detail of getting an optimal word using the above algorithm for the illustrative numerical example is given in the following table-9. The columns named (1), (2),(3).....gives the letters in the first, second, third and so on places respectively. The columns R, C,K gives the row, column, facility and load indicates by 'TL'. The last column gives the remarks regarding the acceptability of the partial word. In the following table 'A' indicates ACCEPT and 'R' indicates REJECT.

TABLE- 9

SL.NO	1	2	3	4	5	6	7	8	V	LB	R	C	K	Q	REMARKS
1	1								1	11	2	1	1	30	A
2		2							2	11	3	9	1	70	A
3			3						3	11	3	8	2		R
4			4						3	12	4	3	2		R
5			5						3	14	8	1	2	40	A
6				6					5	14	4	2	1	70	A
7					7				7	14	7	5	1	110	A
8						8			9	14	3	4	2		R
9						9			9	15	6	4	2	110	A
10							10		12	15	3	5	1		R
11							11		12	15	9	3	1		R
12							12		12	15	5	1	2	50	A
13								13	15	15	8	3	2		R
14								14	16	16	6	8	1		R
15								15	16	16	7	2	2		R
16								16	17	17	3	2	1		R
17								17	17	17	9	2	2		R
18								18	18	18	5	4	1		R
19								19	18	18VT	9	8	2		A
20							13		12	16	8	3	2		R
21							14		13	17	6	8	1		R

22						15			13	18	7	2	2		R _i =VT
23						10			10	16	9	3	1		R
24						11			10	16	9	3	1		R
25						12			10	17	5	1	2	50	A
26							13		13	17	8	3	2		R
27							14		14	18	6	8	1		R _i =VT
28							13		10	18	8	3	2		R _i =VT
29					8				07	15	3	4	2		R
30					9				07	16	6	4	2	110	A
31						10			10	16	3	5	1		R
32						11			10	16	9	3	1		R
33						12			10	17	5	1	2		A
34							13		13	17	8	3	2		R
35							14		14	18	6	8	1		R _i =VT
36							13		10	18	8	3	2		R _i =VT
37					10				08	17	3	5	1		R
38					11				08	18	9	3	1		R _i =VT
39				7					05	15	7	5	1	110	A
40					8				07	15	3	4	2		R
41					9				07	16	6	4	2	110	A
42						10			10	16	3	5	1		R
43						11			10	16	9	3	1		R
44						12			10	17	5	1	2	50	A
45							13		13	17	8	3	2		R
46							14		14	18	6	8	1		R _i =VT
47							13		10	18	8	3	2		R _i =VT
48					10				08	17	3	5	1		R
49					11				08	18	9	3	1		R _i =VT
50				08					05	16	3	4	2		R
51				09					05	17	6	4	2	110	A
52					10				08	17	3	5	1		R
53					11				08	18	9	3	1		R _i =VT
54				10					06	19	3	5	1		R _i >VT
55			6						04	16	4	2	1	70	A
56				7					06	16	7	5	1	110	A
57					8				08	16	3	4	2		R
58					9				08	17	6	4	2	110	A
59						10			11	17	3	5	1		R
60						11			11	17	9	3	1		R
61						12			11	18	5	1	2		R _i =VT
62					10				09	18	3	5	1		R _i =VT
63				8					06	17	3	4	2		R
64				9					06	18	6	4	2		R _i =VT
65			7						04	17	7	5	1	110	A
66				8					06	17	3	4	2		R
67				9					06	18	6	4	2		R _i =VT
68			8						04	18	3	4	2		R _i =VT
69		3							02	12	3	8	2	70	A
70			4						03	12	4	3	2		R
71			5						03	14	8	1	2	40	A
72				6					05	14	4	2	1	70	A
73					7				07	14	7	5	1	110	A
74						8			09	14	3	4	2		R
75						9			09	15	6	4	2	110	A
76							10		12	15	3	5	1		R
77								11	12	15	9	3	1	70	A
78								12	15	15VT	5	1	2	50	A
79								12	12	15	5	1	2		R _i =VT
80						10			10	16	3	5	1		R _i >VT
81					8				07	15	3	4	2		R _i =VT
82				7					05	15	7	5	1		R _i =VT

83			6						04	16	4	2	1		R,>VT
84		4							02	14	4	3	2		R
85		5							02	16	8	1	2		R,>VT
86	2								01	12	3	9	1	70	A
87		3							02	12	3	8	2		R
88		4							02	14	4	3	2		R
89		5							02	16	8	1	2		R,>VT
90	3								01	14	3	8	2	70	A
91		4							02	14	4	3	2		R
92		5							02	16	8	1	2		R,>VT
93	4								01	16	4	3	2		R,>VT

At the end of the search the current value of VT is 15 and it is the value of the optimal feasible word $L_8 = (1, 3, 5, 6, 7, 9, 11, 12)$. It is given in the 78th row of the search table. The arrays IR, IC, SW, SWI and LW take the values represented in the table-10 given below. Hence the pattern gives the optimal feasible word.

TABLE-10

	1	2	3	4	5	6	7	8	9
L	1	3	5	6	7	9	11	12	
IR		1	1	1	1	1	1	1	1
IC	3	1	1	1	1			1	
SW		1	8	2	1	4	5	1	3

From the above arrays optimal feasible word $L_8 = (1, 3, 5, 6, 7, 9, 11, 12)$ and the respective ordered triplets $\{(2,1,1),(3,8,2),(4,2,1),(5,1,2),(6,4,2),(7,5,1),(8,1,2),(9,3,1)\}$ represents the pattern given in the table-11 & 12.

Table-11

$$X(i, j, 1) = \begin{pmatrix} 000000000 \\ 100000000 \\ 000000000 \\ 010000000 \\ 000000000 \\ 000000000 \\ 000010000 \\ 000000000 \\ 001000000 \end{pmatrix}$$

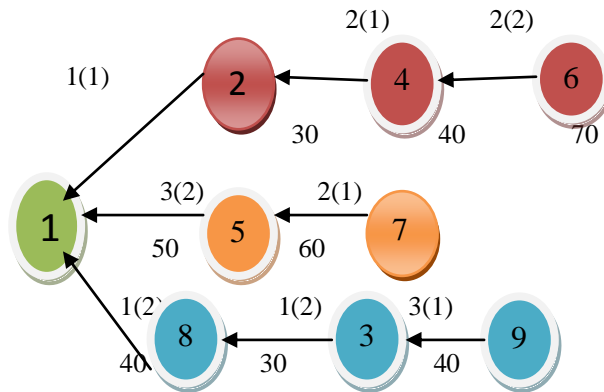
Table-12

$$X(i, j, 2) = \begin{pmatrix} 000000000 \\ 000000000 \\ 000000010 \\ 000000000 \\ 100000000 \\ 000100000 \\ 000000000 \\ 100000000 \\ 000000000 \end{pmatrix}$$

The paths represented by the above pattern is $\{(2,1,1),(3,8,2),(4,2,1),(5,1,2),(6,4,2),(7,5,1),(8,1,2),(9,3,1)\}$. The cities $\{2,4,7\}$ used the same facility 1. The diagrammatic representation of this solution can also see in figure-2.

In following figure-2, the values in circles indicates name of the cities. Also values at each arc in parenthesis and before parenthesis represent the facility and distance between the respective two nodes. The value below the circles represents the availability of load (capacity) to that particular city.

Figure-2



The above figure-2 represents an **optimum feasible** solution. In first path the city 4 is connected by the city 6 using facility 2, city 2 is connected by city 4 using facility 1, city 1 is connected by city 2 using facility 1. In second path, the city 5 is connected by city 7 using facility 1, city 1 is connected by city 5 using facility 2. In third path city 3 is connected by city 9 using facility 1, city 8 is connected by city 3 using facility 2, city 1 is connected by city 8 using facility 2. Hence the solution of the above pattern X is as follows

$$Z = D\{(2,1,1),(3,8,2),(4,2,1),(5,1,2),(6,4,2),(7,5,1),(8,1,2),(9,3,1)\}$$

$$= 1+1+2+3+2+2+1+3 = 15$$

IX. CONCLUSION:

In this paper, we developed an **Alphabet Table** and **Lexi-search Algorithm** by using pattern recognition technique for solving this model. The model is formulated as a Zero-One programming problem. By using a suitable numerical example to understand the concepts and steps involved in the algorithm to find an **optimum solution** with the given constraints. Based on this experience we can say that this **algorithm** is applicable for higher dimensions also and more over it is very efficient. For this paper References given below.

REFERENCES:

- [1]. A Minimum Spanning Tree Algorithm with Inverse-Ackermann Type Complexity, B. Chazelle, Journal ACM 47 (2000), 1028-1047. Prelim. Version in FOCS 1997.
- [2]. Garey, Michael R.; Johnson, David S. (1979), Computers and Intractability: A Guide to the Theory of NP-Completeness, W. H. Freeman, ISBN 0-7167-1045-5.
- [3]. Karger, David R.; Klein, Philip N.; Tarjan, Robert E. (1995), "A randomized linear-time algorithm to find minimum spanning trees", *Journal of the Association for Computing Machinery* 42 (2): 321–328, doi:10.1145/201019.201022, MR 1409738
- [4]. Pettie, Seth; Ramachandran, Vijaya (2002), "A randomized time-work optimal parallel algorithm for finding a minimum spanning forest", *SIAM Journal on Computing* 31 (6): 1879–1895, doi: 10.1137/S0097539700371065, MR 1954882.
- [5]. Pettie, Seth; Ramachandran, Vijaya (2002), "Minimizing randomness in minimum spanning tree, parallel connectivity, and set maxima algorithms", *Proc. 13th ACM-SIAM Symposium on Discrete Algorithms (SODA '02)*, San Francisco, California, pp. 713–722.
- [6]. Pop, P.C. "New models of the Generalized Minimum Spanning Tree Problem", *Journal of Mathematical Modeling and Algorithms*, Volume 3, issue 2, 2004, 153-166.
- [7]. Reeves, C.R., "Modern Meta heuristics Techniques for Combinatorial Problems", Blackwell, Oxford, 1993.
- [8]. Sobhan Babu, K., Chandra Kala, K., Purusotham, S. and Sundara Murthy, M. "A New Approach for Variant Multi Assignment Problem", *International Journal on Computer Science and Engineering*, Vol.02, No.5, 2010, 1633-1640.
- [9]. Sundara Murthy, M. "Combinatorial Programming: A Pattern Recognition Approach," A Ph.D. Thesis, REC, Warangal. 1979.
- [10]. Suresh Babu C, Sobhan Babu K and Sundara Murthy M, 2011, published a paper entitled "Variant Minimum Spanning Network Connectivity Problem" by the International Journal of Engineering Science and Technology for publication. Volume 3, No. 1, Jan-Feb 2012

Overview Of Recommender System & A Speedy Approach In Collaborative Filtering Recommendation Algorithms With Mapreduce

¹Prof. Dr. R. Shankar , ² Prof. Ateshkumar Singh , ³Ms. Ila Naresh Patil

¹IES College of Technology, ²M Tech. CSE * M Tech. CSE*

¹Bhopal, MP, India IES College of Technology, ² IES College of Technology,

¹Bhopal, MP, India ²,Bhopal, MP, India

ABSTRACT

Recommender systems suggest people items or services of their interest and proved to be an important solution to information overload problem. The big problem of collaborative filtering is its. In order to solve scalability problem, we can implement the Collaborative Filtering algorithm on the cloud computing platform using Hadoop's MapReduce. The work given here is focusing on the algorithm of recommendation mechanism for mobile commerce using combination of MapReduce and user based CF algorithm to overcome scalability. MapReduce is a programming model for expressing distributed computations on massive amounts of data and an execution framework for large-scale data processing on clusters of commodity servers. It was built on well-known principles in parallel and distributed processing.

KEYWORDS: *recommender system, collaborative filtering, speedup, partitioning, cloud-computing, hadoop, Map-Reduce.*

I. INTRODUCTION

Recommender systems provide an important response to the information overload problem as it presents users more practical and personalized information services. Three types of recommender systems: content-based recommender systems, collaborative recommender systems and trust based recommender system. Recommendation systems generate a ranked list of items on which a user might be interested. It is useful to approximate the degree to which specific user will like a specific product. The Recommender systems are useful in predicting the helpfulness of controversial reviews [1]. Recommender systems are a powerful new technology & help users to find items they want to buy from a business. Recommender systems are rapidly becoming a crucial tool in E-commerce on the Web.

In this paper we propose a new method that is implementing the user-based Collaborative Filtering algorithm on distributed implementation model, MapReduce model, on Hadoop platform to solve sparse data problem. The MapReduce model is inspired by the Lisp programming language map and reduces operations. Typically, the Map/Reduce framework and the Hadoop Distributed File System (HDFS Architecture) are running on the same set of nodes. This configuration allows the framework to effectively schedule tasks on the nodes where data is already present, resulting in very high aggregate bandwidth across the cluster.

The Map/Reduce framework consists of a single master JobTracker and one slave TaskTracker per cluster-node. The master is responsible for scheduling the jobs' component tasks on the slaves, monitoring them and re-executing the failed tasks. The slaves execute the tasks as directed by the master. This paper is organized as follows. Section 2 explains related work in commonly used recommendation strategies. Section 3 explains MapReduce model on Hadoop platform. Section 4 includes the experimental analysis & Section 5 concludes the paper.

II. RELATED WORK

2.1. Classification of Recommender Systems

2.2. Ontology-based Recommender System

In [2], the peer-to-peer network (P2P network) is based on decentralized architecture has the progress of ontology-based recommender system. This is basically works with dynamically changing large scale environment. In [3] a ontology-based multilayered semantic social network, is introduced. This model works on a set of users having similar interest and the correlation at different semantic levels.

2.3. Collaborative Tagging-based Recommender System

In [4], the collaborative tagging-based recommender allows users particularly consumers to freely connect tags or keywords to data contents. In [5] & [6] a generic model of collaborative tagging to recognize the dynamics behind it. The tag-based system suggests the use of high quality tags, by which spam and noise can be avoided.

2.4. Recommendation Methodologies

Basically there are three methods as content based, collaborative and trust based [7].

2.5. Content based Strategy

In [8], the Content Based (CB) method provides suggestions based on items similar to those that user has previously purchased or reviewed. It provides the recommendations based on the contents of documents & each user's preferences.

2.6. Collaborative Filtering Strategy

Collaborative filtering (CF) provides personalized recommendations based on the knowledge of similar users in the system. CF is focused on the principle that the finest recommendations for an individual are given by people who have similar interest. Collaborative filtering identifies users with choice similar to the target user and then built predictions based on the score of the neighbors. The job in collaborative filtering is to guess the usefulness of product to a particular user which is based on a database of user votes. The CF algorithms predicts ranking of a target item for target user with the help of ranking of the similar users that are known to item under consideration[9]. There are six collaborative filtering algorithms are evaluated. These algorithms accepts values for a interaction matrix A of order $M \times N = a_{ij}$ where M represents number of consumers ($C_1, C_2, C_3, \dots, C_M$) and N represents number of products or services ($P_1, P_2, P_3, \dots, P_N$). The value of a_{ij} varies based on transaction. The value of a_{ij} can be either 0 or 1. When $a_{ij} = 1$, means transaction between C_i & P_j (C_i has brought P_j). when $a_{ij} = 0$, means absence of transaction between C_i & P_j . The outcome of the algorithm is a list of probable ranked product for each consumer.

The user-based CF algorithm

This algorithm generates a list of recommendation of user interest in three steps. In first step, it searches N users in database which are similar to active user by creating customer similarity matrix $W_C = (W_{C_{st}})$. The high value of $W_{C_{st}}$ indicates the consumers X & Y have similar liking as they have already brought many similar products. In second step, it calculates union of the items purchased by these users & link a respective weight with every item based on its significance in the set. Finally, in the third step, generates the list of recommended items & which have not already been brought by the active user. The resulting matrix will have element at C^{th} row & P^{th} column combine S the scores of the similarities between consumer C and other consumers who have purchased the product.

2.7. The item-based CF algorithm

This algorithm is based on the similar principal of user-based. The item-based algorithm determines product similarities instead of consumer similarity. It generates a product similarity matrix, $W_P = (W_{P_{st}})$ which is based on the column vectors of A . A high $W_{P_{st}}$ shows that products X and Y are similar as many consumers have brought both of them. A W_P will give the products' probable scores for each consumer. Resulting matrix will be containing the element at the C^{th} row and P^{th} column combines the scores of the similarities between product P and other products that consumer C has purchased. This algorithm provides higher efficiency and comparable or better recommendation quality than the user-based algorithm for many data sets [10].

2.8. The dimensionality-reduction algorithm

This algorithm compresses original interaction matrix & produce recommendations which are based on compressed, less-sparse matrix to simplify the scarcity problem. It applies standard singular-vector

decomposition (SVD is a technique of matrix factorization) to decompose the interaction matrix A into $U \cdot Z \cdot V^T$ where U and V are two orthogonal matrices of size $M \times R$ and $N \times R$ respectively, and R is the rank of matrix A . Z is diagonal matrix of size $R \times R$ which has all singular values at its diagonal values. SVD can be used in recommender systems & has two features. SVD can be used to construct a low-dimensional image of customer-product space & calculates region in reduced space[11].

2.9.The generative-model algorithm

This algorithm approximates appropriate possibility & conditional probability. Based on estimated probability it creates score of product p for consumer c [12]. The approach is a statistical technique called as probabilistic Latent Semantic Analysis which was initially extended in the context of information retrieval. The method accomplishes competitive recommendation and calculation accuracies, is highly scalable, and extremely flexible.

2.10.The spreading-activation algorithm

This algorithm focuses on scarcity problem by discovering transitive associations between consumers & products by using bipartite consumer-product transitive-graph. The algorithm uses the graph to find out transitive connections [13]. It focuses on high quality recommendations when sufficient data is not available. The spreading activation algorithm consists of a series of nodes both user and item nodes. These nodes are then connected by edges where each weighted edge represents the ratings the item has received from the users. The higher the weight of the edge the higher the rating that item has received. The item nodes then send back “pulses” to the active user and their neighbors thus spreading the activation to the other nodes in the neighborhood of the active user.

2.11.The link-analysis algorithm

In this consumer-product graph, the global graph structure is used to help collaborative filtering under sparse data [14]. In this graph first set of nodes consists of products, services & information items for probable utilization. The second set consists of consumers or users. The feedback and transaction are represented as links connecting nodes between these two sets. This graph is referred as consumer-product graph. The link analysis algorithms such as HITS (Hypertext Induced Topic Selection) & PageRank are used for identifying essential web pages in a Web graph. The algorithm focuses on the extract helpful link structure details from the consumer-product graph & make more effective recommendation with sparse data.

2.12.Trust-Based Strategy

In Trust Based Recommendation systems, trust network is used in which users are joined by trust scores which indicate how much faith they have in each other. The user’s trust network is constructed for generating predictions [15] & [16]. It has three steps. In first step, considers direct trust. The direct has two methods: explicitly or implicitly. The second step is propagation of trust. It is possible to propagate the trust i.e. create new relations among users. The third step is predicting ratings. From the trust network, we can predict what ratings the particular user would give for items.

2.13.MapReduce Collaborative Filtering Model

The conventional Collaborative Filtering consumes intensive computing time & computer resources especially when the dataset is very high. Here the MapReduce model is a distributed implementation model which is proposed by Google com. We introduce the MapReduce model and describe its working mechanism on Hadoop platform. The MapReduce model abstracts the calculation process into two core phases:

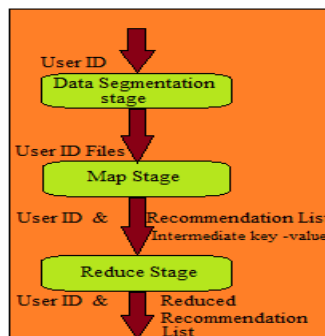


Figure1. Collaborative Filtering Using MapReduce

A. Data segmentation stage

In this phase[17], we separate the user ID into different files, in these files, each row store a user ID. These files as the input files of map phase, the data partitioning should satisfy 2 principles as follows: In the total running time, the proportion of computing time, the bigger the better. That means the most proportion of run time should be spent in the computation process, rather than frequently initialize the mapper. The same end of the tasks running time. That is the end of each mapper task time should be at the same time.

B. Map stage : Map stage : It is the function written by user which takes a set of input key/value pairs, and produces a set of output key/value pairs. In the Map, written by the user, takes a set of input key/value pairs, and produces a set of output key/value pairs. At this stage, the Hadoop platform estimate the algorithm’s memory and others resources consumption, specified each DataNode the number of mapper it can be initialized. The Hadoop platform determines whether initialize a mapper to deal with the user ID files. If there have enough resources to initialize a mapper, the Hadoop platform initializes a new mapper. The mapper’s setup function build the ratings-matrix between the users and the items at first, the mapper read the user ID file by line number, take the line number as the input key and this line corresponding user ID as the value. The next step is to calculate the similarity between this user and other users. The final step is to identify the user’s nearest neighbors (by similarity values), and in accordance with the predict rating on items. We sort the predict ratings and store them in recommendation list. The user ID and its corresponding recommend-list as the intermediate key/value, output them to the reduce phase. Mapping creates a new output list by applying a function to individual elements of an input list[18].

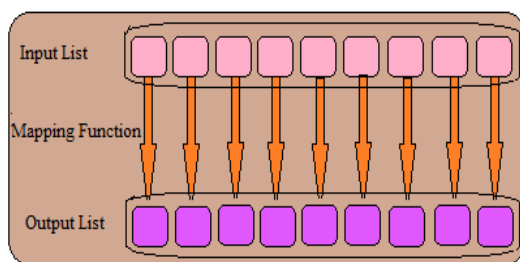


Figure2. Mapping

C. Reduce stage

It is also user defined function, accepts an intermediate key I and a set of values for that key. It merges together these values to form a possibly smaller set of values. Typically, none output value or only one is produced per Reduce invocation. In the reduce phase, the reducer collects the users ID and its corresponding recommend list, sort them according to user ID, and then output them to the HDFS in which the reducers are generated by hadoop platform. The computation takes a set of input key/value pairs, and produces a set of output key/value pairs. The user of the MapReduce library expresses the computation as two functions: map and reduce. Map, written by the user, takes an input pair and produces a set of intermediate key/value pairs[19]. The MapReduce library groups together all intermediate values associated with the same intermediate key I and passes them to the reduce function. The reduce function, also written by the user, accepts an intermediate key I and a set of values for that key. It merges these values together to form a possibly smaller set of values. Typically just zero or one output value is produced per reduce invocation. The intermediate values are supplied to the user’s reduce function via an inter-mediator. This allows us to handle lists of values that are too large to fit in memory.

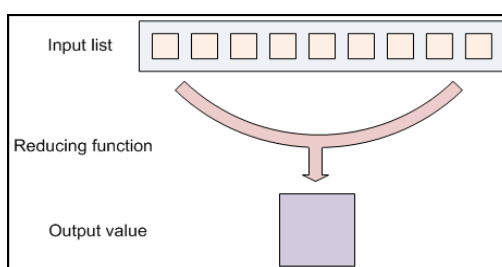


Figure3. Reducing

3.1 MapReduce framework for CF

Here, we present the implementation of the Collaborative-Filtering algorithm within the MapReduce framework. In [20], when we make recommendation, we would store the user ID which need to calculate in some txt files, then these files as the input of the Map function. The MapReduce framework initializes some mapper to deal with these user ID files. Our algorithm could be divided into the following stages, as shown in Figure 4:

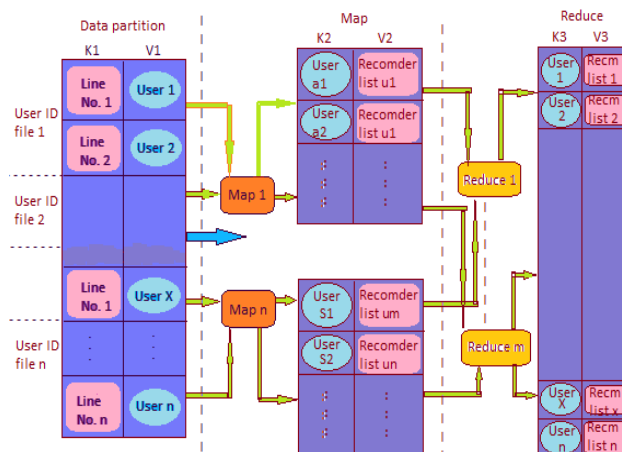


Figure 4. Collaborative Filtering with MapReduce

3.2. Experimental Analysis

We have implemented our experiments for CF algorithm on Java platform. As explained earlier in section 3, the Hadoop computer-cluster created on five computers. Here, we refer one of the computers as MainNode & remaining four as DataSetNodes. Each computer is having 4 GB RAM & Intel(R)core(TM) i5 CPU with 2.5GHz speed & Operating System Ubuntu 10.10. also the software used for the experiments are Hadoop MapReduce framework, Java JDK 1.6, the Mobile device (Android 3.0 & above), wireless Router are additional hardware we have used. The dataset is created by Netflix data set. The list of different movies is maintained in the dataset and more than 10,000 users. The users will define different ratings for each movie, not necessary the same rating. The role of our CF algorithm is to compare the runtime between standalone & Hadoop platform, so that we don't focus on accuracy. We take 3 copies of sub-datasets with 100 users, 200 users, 500 users & 1000 users. The DataSetNode is also divided into 2 nodes, 3 nodes, 5 nodes.

For the comparative analysis of standalone & Hadoop platform, we have considered average time t_{avg} as the Hadoop platform at current DataSetNode and the data set running time. Here the speedup is an important criteria to measure the efficiency of our algorithm. The speedup is given by,

$$\text{Speedup} = t_{avg} / t_{sd1}$$

In our CF algorithm the recommendation is based on the division of each user theoretically, if we consider N nodes the speedup should be N. in other words, ideally the speedup should be linearly related to the number of DataSetNode. In the figure 5 we have shown the analytical result in graph which implies, increase in number of DataSetNodes, the speedup increases linearly. Also from the graph we can observe for 100 users, 200 users, the speedup is not linearly increase, this is because the data set is too small, thus the Hadoop platform is unable to demonstrate its efficiency.

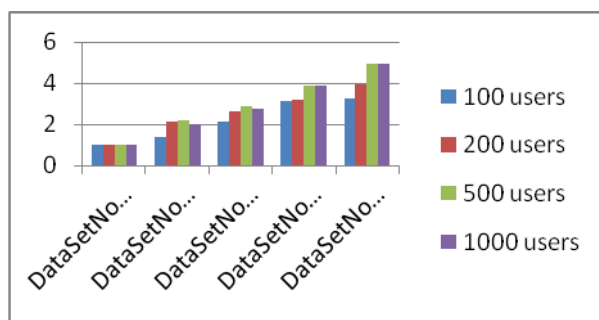


Figure 5. Speedup of CF of MapReduce

CONCLUSION

MapReduce can be used to parallelize Collaborative Filtering. We propose to apply this concept to Recommender System for the Web & Mobile Commerce as well.

REFERENCES :

- [1] Patricia Victor and Chris Cornelis , Martine De Cock and Ankur M. Teredesai Trust- and Distrust-Based Recommendations for Controversial Reviews 15411672/11/\$26.00 © 2011 IEEE INTELLIGENT SYSTEMS
- [2] V. Diaz-Aviles, "Semantic peer-to-peer recommender systems," M.S.thesis, Comput.-Based New Media Group, Inst. Comput. Sci., Albert Ludwigs Univ. Freiburg, Freiburg, Germany, 2005.
- [3] I. Cantador and P. Castells, "Multilayered semantic social network modeling by ontology-based user profiles clustering: Application to collaborative filtering," in Proc. Manag. Knowl. World Netw., 2006, pp. 334–349.
- [4] S. Golder and B. Huberman, "The structure of collaborative tagging systems" in Proc. CoRR, 2005, pp.1–8.
- [5] Z. Xu, Y. Fu, J. Mao, and D. Su, "Towards the semantic Web: Collaborative tag suggestions," in Proc. CollaborativeWeb Tagging Workshop WWW, Edinburgh, U.K., 2006
- [6] Shang Ming-Sheng, Zhang Zi-ke. Diffusion-Based Recommendation in Collaborative Tagging Systems. Chin. Phys. Lett.,2009,26(11): 118903
- [7] Shang Ming-Sheng, Jin Ci-Hang, Zhou Tao, Zhang Yi-Cheng. Collaborative filtering based on multi-channel diffusion.Physica A: Statistical Mechanics and its Applications. 2009,388(23):4867-4871. M. D. Dikaiakos, D. Katsaros, G. Pallas, A.
- [8] J.S. Breese, D. Heckerman, and C. Kadie, "Empirical Analysis of Predictive Algorithms for Collaborative Filtering," Proc.14th Conf. Uncertainty in Artificial Intelligence (UAI 98), Morgan Kaufmann, 1998, pp. 43– 52.
- [9] M. Deshpande and G. Karypis, "Item-Based Top-N
- [10] Recommendation Algorithms," ACM Trans. Information Systems, vol.22, no.1, 2004, pp. 143–177.
- [11] B. Sarwar et al., "Application of Dimensionality Reduction in Recommender Systems: A Case Study," Proc. WebKDD Workshop at the ACM SIGKDD, 2000; <http://glaros.dtc.umn.edu/gkhome/node/122>
- [12] T. Hofmann, "Latent Semantic Models for Collaborative Filtering," ACM Trans. Information Systems, vol. 22, no. 1,2004,pp.89–115.
- [13] Z. Huang, H. Chen, and D. Zeng, "Applying Associative Retrieval Techniques to Alleviate the Sparsity Problem in Collaborative Filtering," ACM Trans. Information Systems, vol. 22, no. 1, 2004, pp. 116–142
- [14] Z. Huang, D. Zeng, and H. Chen, "A Link Analysis Approach to Recommendation under Sparse Data," Proc. 2004 Americas Conf. Information Systems, 2004
- [15] Kleinberg, J. Authoritative sources in a hyperlinked environment. in Proceedings of the ACM-SIAM Symposium on Discrete Algorithms (1998).
- [16] Leonardo Zanette, Claudia L.R. Motta, Flávia Maria Santoro, Marcos Elia "A Trust-based Recommender System for Collaborative Networks" 2009 IEEE.
- [17] [Zhili Wu, Xueli Yu and Jingyu "An Improved Trust Metric for Trust-aware Recommender Systems" 2009 IEEE.
- [18] Vrba Z., Halvorsen P., Griwodz C., Beskow P. Kahn Process Networks are a Flexible Alternative to MapReduce", High Performance Computing and Communications, 2009. HPCC '09. 11th IEEE International Conference on ,25-27 June 2009.
- [19] Dean J, Ghemawat S. Distributed programming with Mapreduce. In: Oram A, Wilson G, eds. Beautiful Code. Sebastopol: OReilly Media, Inc., 2007. 371 384.
- [20] Dean J, Ghemawat S. MapReduce: Simplified data processing on large clusters. Communications of the ACM, 2005,51(1):107 113.
- [21] Ranger C, Raghuraman R, Penmetsa A, Bradski G,Kozyrakis C. Evaluating MapReduce for Multi-core and Multiprocessor Systems. High Performance Computer Architecture, 2007. HPCA 2007. IEEE 13th International Symposium on,10-14 Feb. 2007.

Detection and Prevention of Black Hole Attack over Manet

Raghvendra Prasad

Fourth Semester M.Tech, LNCT Indore

ABSTRACT

The black hole attack is one of the well-known security threats in wireless mobile ad hoc networks. The intruders utilize the loophole to carry out their malicious behaviors because the route discovery process is necessary and inevitable. Many researchers have conducted different detection techniques to propose different types of detection schemes. In this paper, we survey the existing solutions and discuss the state-of-the-art routing methods. We not only classify these proposals into single black hole attack and collaborative black hole attack but also analyze the categories of these solutions and provide a comparison table. We expect to furnish more researchers with a detailed work in anticipation.

KEYWORDS: mobile ad hoc networks, routing protocols, single black hole attack, collaborative black hole attack

I. INTRODUCTION

A mobile ad hoc network (MANET) is a collection of wireless mobile nodes which have the ability to communicate with each other without having fixed network infrastructure or any central base station. Since mobile nodes are not controlled by any other controlling entity, they have unrestricted mobility and connectivity to others. Routing and network management are done cooperatively by each other nodes. Due to limited transmission power, multi hop architecture is needed for one node to communicate with another through network. In this multi hop architecture, each node works as a host and as well as a router that forwards packets for other nodes that may not be within a direct communication range. Each node participates in an ad hoc route discovery protocol which finds out multi hop routes through the mobile network between any two nodes. These infrastructure-less mobile nodes in ad hoc networks dynamically create routes among themselves to form own wireless network on the fly. Thus, mobile ad hoc networks provide an extremely flexible communication method for any place where geographical or terrestrial constraints are present and need network system without any fixed architecture, such as battlefields, and some disaster management situations. Recent research on MANET shows that the MANET has larger security issues than conventional networks [1,2]. Any security solutions for static networks would not be suitable for MANET. Zhou et al. [1] and Lundberg [3] discussed several types of attacks that can easily be performed against a MANET. In the black hole attack, malicious nodes provide false routing information to the source node whose packets they want to intercept. In denial of service attacks, malicious node floods the targeted node so that the network or the node no longer operates correctly. In route table overflow attacks, an attacker tries to create lots of routes to non existence nodes and overflows the routing tables. In impersonation attacks, malicious node may impersonate another node while sending the control packets to create an anomaly update in routing table. In this paper, we will focus on the black hole and cooperative black hole attacks. The main contributions of this work are threefold. First, we implement the simulation of the solutions proposed for the cooperative black hole attacks. Second, we also add some changes to the algorithm to improve the accuracy in preventing black hole attacks. For example, previously the algorithm does not check current intermediate node for black hole if the next hop is not reliable. This proposed algorithm does not give any details about the implementation of the algorithm. In this paper we completely describe the implementation details which we address the several issues which are not considered in [9]. Finally, we compare the performance of the modified solution with other existing solutions in terms of throughput, end-to-end delay,

II. RELATED WORKS

The routing protocols proposed for MANETs can be classified into four broad categories [4]: Flat routing, Hierarchical routing, GPS routing, and Power based routing. Flat routing is the most widely used category. These flat routing protocols can be further classified into two main sub groups [6]: table driven and on-demand routing protocols. The table driven routing protocol is a proactive scheme in which each node maintains consistent and up to date routing information to every other node in the network. Every routing change in the network should be propagated through the network in order to maintain consistent routing information. In the on-demand routing (reactive routing), any node creates route only when it needs to send some data to the destination. The source node initiates route discovery process when necessary. There are three main routing protocols proposed for MANETs [4]: Ad hoc on demand Distance Vector (AODV) [5] routing, Dynamic Source Routing [DSR] [6], and Destination Sequence Distance Vector routing (DSDV) [7]. AODV and DSR belong to on-demand routing protocols and DSDV is a table-driven routing protocol. In this paper, we focus on AODV. However, the proposed solution is also applicable to other on-demand protocols, such as DSR. The AODV protocol is vulnerable to the well-known black hole attack. A black hole is a node that always responds positively with a RREP message to every RREQ, even though it International Journal of Software Engineering and Its Applications Vol. 2, No. 3, July, 2008 41 does not really have a valid route to the destination node. Since a black hole node does not have to check its routing table, it is the first to respond to the RREQ in most cases. Then the source routes data through the black hole node, which will drop all the data packets it received rather than forwarding them to the destination. In this way the malicious node can easily misroute lot of network traffic to itself and could cause an attack to the network with very little effort on it. These black hole nodes may work as a group. That means more than one black hole nodes work cooperatively to mislead other nodes.

This type of attack is called cooperative black hole attack. Researchers have proposed solutions to identify and eliminate black hole nodes . Deng et al. proposed a solution for individual black holes. But they have not considered the cooperative black hole attacks. According to their solution, information about the next hop to destination should be included in the RREP packet when any intermediate node replies for RREQ. Then the source node sends a further request (FREQ) to next hop of replied node and asks about the replied node and route to the destination. By using this method we can identify trustworthiness of the replied node only if the next hop is trusted. However, this solution can not prevent cooperative black hole attacks on MANETs. For example, if the next hop also cooperates with the replied node, the reply for the FREQ will be simply “yes” for both questions. Then the source will trust on next hop and send data through the replied node which is a black hole node. Ramaswamy et al. proposed a solution to defending against the cooperative black hole attacks. no simulations or performance evaluations have been done. Ramaswamy et al. studied multiple black hole attacks on mobile ad hoc networks. However, they only considered multiple black holes, in which there is no collaboration between these black hole nodes. In this paper, we evaluate the performance of the proposed scheme in defending against the collaborative black hole attack. Yin et al. proposed a solution to defending against black hole attacks in wireless sensor networks. The scenario that they considered in sensor networks is quite different than MANETs. They consider the static sensor network with manually deployed cluster heads. They did not consider the mobility of nodes. Also they have one sink node and all sensors send all the data to the sink. Each node needs to find out the route only to the sink. Since this scenario is not compatible with MANET, we are not going to discuss it further. In this paper we simulate the algorithm proposed with several changes to improve the accuracy of preventing cooperative black hole attacks and to improve the efficiency of the process. We also simulate AODV

Blackhole attack: In this attack a malicious node may advertise a good path to a destination during routing process. The intention of the node may be to hinder the path finding process or interpret the packet being sent to destination. Alternatively black-hole scenario may be defined as the one in which the channel properties tend to be asymmetric i.e. the signal strength in both direction may not be same. In this case a node which receives the data packet but does not forward it is termed as black hole. In either case the normal operation of the MANET is disrupted.

Wormhole attack: In this attack , an attacker receives packets at one location and tunnels them at another location where these packets are resent into the network. In the absence of proper security mechanisms, most of the existing routing protocols may fail to find the valid routes.

Byzantine attack: Here compromised intermediate nodes carries out attack such as loops, routing packets on non optimal paths and selectively dropping packets.

Information disclosure: A compromised network node may leak the important or confidential information such as network topology, geographical information of nodes and optimal routes to the nodes etc.

Resource consumption attack: An attacker node acting as intermediate node may initiate unnecessary request for routes, frequent generation of beacon packets or forwarding stale routes to nodes. This result in over consumption of nodes limited resources and keeps the node unnecessary occupied.

In this paper we analyze the impact of the presence of the black-hole nodes on the MANET performance. We have found that as the percentage of black hole nodes increases, the network performance degrades.

AD-HOC ROUTING PROTOCOLS AND BLACK HOLE ATTACK : An ad-hoc routing protocol[8] is a convention, or standard, that controls how nodes decide which way to route packets between computing devices in a mobile ad hoc network. Being one of the category of ad-hoc routing protocols, on-demand protocols such as AODV [4] (Ad-hoc On demand Distance Vector) and DSR (Dynamic Source Routing) establish routes between nodes only when they are required to route data packets. AODV is one of the most common ad-hoc routing protocols used for mobile ad-hoc networks. As its name indicates AODV is an on-demand routing protocol that discovers a route only when there is a demand from mobile nodes in the network. In an ad-hoc network that uses AODV[4][6] as a routing protocol, a mobile node that wishes to communicate with other node first broadcasts an RREQ (Route Request) message to find a fresh route to a desired destination node. This process is called route discovery Every neighboring node that receives RREQ broadcast first saves the path the RREQ was transmitted along to its routing table. It subsequently checks its routing table to see if it has a fresh enough route to the destination node provided in the RREQ message. The freshness of a route is indicated by a destination sequence number that is attached to it. If a node finds a fresh enough route, it unicast an RREP (Route Reply) message back along the saved path to the source node or it re-broadcasts the RREQ message otherwise. Route discovery is a vulnerability of on-demand ad-hoc routing protocols, especially AODV, which an adversary can exploit to perform a black hole attack on mobile ad-hoc networks. A malicious node in the network receiving an RREQ message replies to source nodes by sending a fake RREP message that contains desirable parameters to be chosen for packet delivery to destination nodes. After promising (by sending a fake RREP to confirm it has a path to a destination node) to source nodes that it will forward data, a malicious node starts to drop all the network traffic it receives from source nodes. This deliberate dropping of packets by a malicious node is what we call a black hole attack.

III. CONCLUSION

In this paper, we studied the problem of cooperative black hole attacks in MANET routing. Due to the inherent design disadvantages of routing protocol in MANETs, many researchers have conducted diverse techniques to propose different types of prevention mechanisms for black hole problem. The proposals are presented in a chronological order and divided into single black hole and collaborative black hole attack. According to this work, we observe that both of proactive routing and reactive routing have specialized skills. The proactive detection method has the better packet delivery ratio and correct detection probability, but suffered from the higher routing overhead due to the periodically broadcast packets. The reactive detection method eliminates the routing overhead problem from the event-driven way, but suffered from some packet loss in the beginning of routing procedure. Therefore, we recommend that a hybrid detection method which combined the advantages of proactive routing with reactive routing is the tendency to future research direction. However, we also discover that the attacker's misbehavior action is the key factor. The attackers are able to avoid the detection mechanism, no matter what kinds of routing detection used. Accordingly, some key encryption methods or hash-based methods are exploited to solve this problem. The black hole problem is still an active research area. This paper will benefit more researchers to realize the current status rapidly.

REFERENCES

- [1] C. E. Perkins and P. Bhagwat, "Highly Dynamic Destination-Sequenced Distance-Vector Routing (DSDV) for Mobile Computers," Computer Communications Review, pp. 234-244, October 1994.
- [2] Hongmei Deng, Wei Li, and Dharma P. Agrawal, "Routing Security in Wireless Ad Hoc Network," IEEE Communications Magazine, vol. 40, no. 10, October 2002.
- [3] Sanjay Ramaswamy, Huirong Fu, Manohar Sreekantharadhya, John Dixon, and Kendall Nygard, "Prevention of Cooperative Black Hole Attack in Wireless Ad Hoc Networks", 2003 International Conference on Wireless Networks (ICWN'03), Las Vegas, Nevada, USA
- [4] Jian Yin, Sanjay Madria, "A Hierarchical Secure Routing Protocol against Black Hole", IEEE SUTC 2006 Taiwan, 5-7 June 2006.
- [5] Xiaoyan Hong, Kaixin Xu, and Mario Gerla, "Scalable Routing Protocols for Mobile Ad hoc Networks," IEEE Network Vol. 16(4) pp11-21, July/August 2002.
- [6] Elizabeth M. Royer and Chai-Keong Toh, "A Review of Current routing Protocols for Ad Hoc Mobile Wireless Networks," IEEE Personal Communications, pp 46-55, April 1999.

- [7] Sanjay Ramaswamy, Huirong Fu, and Kendall E. Nygard, "Simulation Study of Multiple Black Holes Attack on Mobile Ad Hoc Networks," International Conference on Wireless Networks (ICWN' 05), Las Vegas, Nevada, Jun. 2005.
- [8] H Yang, H Y. Luo, F Ye, S W. Lu, and L Zhang, —Security in mobile ad hoc networks: Challenges and solutionsl (2004). IEEE Wireless Communications. 11 (1), pp. 38-47.
- [9] Hao Yang,Haiyun Luo, Fan Ye, Songwu Lu, Lixia Zhang,"Security in mobile ad hoc networks: challenges and solutions",Wireless Communications, IEEE Feb 2004.
- [10] Hongmei Deng, Wei Li, D.P.Agrawal,"Routing security in wireless ad hoc networks",Communications Magazine, IEEE Oct 2002.
- [11] B.Kannhavong, H.Nakayama, Y.Nemoto, N.Kato, A.Jamalipour,"A survey of routing attacks in mobile ad hoc networks",Wireless Communications, IEEE October 2007.

Development of Physical Parameter Extraction Model for Detection and Monitoring Flood Disaster

Wawan Setiawan¹ and Wiweka²

¹Computer Science, Indonesia University of Education

²Application Remote Sensing Center, Indonesia National Institute Aeronautics and Space

ABSTRACT:

Natural hazards, including floods can be seen from the characteristics of the danger, which is of magnitude (magnitude, intensity) and frequency. Remote sensing data can be used to support flood mitigation efforts. This study aims to develop a model of the physical parameter extraction from remote sensing data is for the detection and monitoring of floods. Research study conducted on the detection and monitoring of inundated areas using optical imagery, particularly Landsat and MODIS. Floodwaters identification method is done by comparing the values of reflectance and indices on suspected areas affected by floods in the period before the flood, during the flood, and after the flood. Parameter value is used reflectance reflectance in bands 1 to 7. While the parameter values used index is NDVI, EVI, NDWI, MNDWI, LSWI and DVEL. Based on the results of the analysis seen that all variables except LSWI can be used to detect the floodwaters. The study concluded that the MODIS optical images can be used to identify a pool of water caused by floods.

KEYWORDS: Flood. Optical Image. Reflectance Parameters. Parameter Index Value

I. INTRODUCTION

Flooding is a natural phenomenon that can be caused by natural factors, human factors, or a combination of both. According to Richard (1955), flooding can be interpreted in two senses, namely: 1) the overflow of river water caused by the river flow exceeds the capacity of the river in the state of high rainfall, and 2) a puddle on the flat low-lying areas that normally do not flooded. Sudaryoko (1987) defines a flood as a condition in an area where there is an increase in the amount of water that can not be accommodated in the water channels or shelters so that the water overflowed and flooded areas outside of the channel, the river valley, the water nor shelter. According Sutopo (1999), causes flooding can be divided into flooding problems caused by natural events and conditions and flooding problems caused by the activity of the population. Conditions and natural events such as heavy rainfall, a large amount of surface runoff, river water melimpasnya; damming estuaries and tidal rivers from the sea. Factors influence the activity of the population flood events, such as the growth of cultivated areas in floodplains, wetlands hoarding / situ or reclamation, narrowing the river channel as a result of settlements along the river border, and control settlements along the river banks are not implemented properly. Natural hazards, including floods can be seen from the characteristics of the danger, which is of magnitude (magnitude, intensity) and frequency (Ayala, 2002).

Magnitude of flood hazards can be known from the extensive inundation, depth or water level, water flow rate, material is washed away, water density or thickness of silt, long inundation, peak flow, and total flow volume. While the frequency of flooding can be measured from the number of flood events in an area within a certain time unit (Ayala, 2002). Flood disasters often cause harm either physically, economically, and socially and culturally. Demands on the development of information technology often raises issues that were raised, namely how the flood affected area distribution can be determined with more fast, precise, and accurate. Additionally, Which areas affected by the floods. It is closely tied to the condition of land cover and infrastructure affected by floodwaters. Remote sensing data are expected to be used to support flood mitigation efforts. One of them is to provide fast and accurate information about the areas affected by the floods. This study aims to develop a model of the physical parameter extraction from remote sensing data is for the detection and monitoring of floods. The study will be conducted this research focuses on the study of literature on methods of detection and monitoring of inundated areas using optical imagery, particularly Landsat and MODIS.

II. PREVIOUS STUDIES

Floodwaters can be identified from remote sensing image based on the spectral appearance of objects that exist in a puddle of water is. Wang et al. (2002) have developed an efficient method for mapping flood inundation broad multitemporal using Landsat imagery and Digital Elevation Model (DEM). The research took place in North Carolina USA. The method developed is based on differences in spectral appearance of objects by non-water water on the Landsat series before and during flood events. It also said the DEM data is helpful in identifying flood. Wang et al. (2002) also stated that the method can be applied to a wide scope of areas with flat topography. Furthermore, Wang (2004) have also conducted research using Landsat imagery recording date the day after the flood event to determine the maximum extent of inundation on floodplains in coastal areas in the same region (North Carolina USA). The resulting map accuracy rate in the range of 82.5 to 99.3%. Ho et al. (2010) tried to flood hazard mapping using ASTER imagery, Landsat and DEM SRTM (Shuttle Radar Topography Mission). The method used to separate the area flooded and non-flooded is MNDWI (Modified Normalized Difference Water Index). Area of research taking place in the area in the alluvial plains Watershed Vu Gia - Thu Bon System, Central Vietnam. This study reveals the close relationship between water-saturated region, altitude, and flooding conditions in the area with water levels below 4 meters (classed as flood basins and plains deltaik) that were flooded in the long term. The results showed that the method can be used to separate MNDWI moist soil to predict flooding. Sakamoto et al. (2009) has developed the use of MODIS imagery to evaluate the agro-ecological interpretation of rice farming systems in flood-prone areas in the Mekong Delta of Vietnam. The parameters used was EVI (Enhanced Vegetation Index), LSWI (Land Surface Water Index), and DVEL (Value Difference between EVI and LSWI). EVI parameters, DVEL LSWI and has also been successfully used by Yan et al. (2010) to detect changes in spatial-temporal tidal flooding in the wetlands (wetland) around the mouth of the river. Moreover, Islam et al. (2009) also uses parameters NDVI, NDWI, and LSWI EVI from MODIS imagery to map flood inundation in Bangladesh and concluded that the MODIS imagery is very useful to clarify the spatial-temporal distribution of flood inundation in Bangladesh.

III. PHYSICAL PARAMETERS EXTRACTION MODEL

Based on a literature review of the methods of identification floodwaters can be done by comparing the reflectance values and indices on suspected areas affected by floods in the period before the flood, during the flood, and after the flood. Parameter value is used reflectance reflectance in bands 1 to 7. While the parameter values used index is NDVI, EVI, NDWI, MNDWI, LSWI and DVEL. Equation to calculate NDVI, EVI, NDWI, LSWI, and DVEL as table 1.

Table 1. The Parameter Values Used Index

$NDVI = \frac{\rho_{NIR} - \rho_{RED}}{\rho_{NIR} + \rho_{RED}}$	Huete et al. (2002)
$EVI = 2.5 * \frac{\rho_{NIR} - \rho_{RED}}{\rho_{NIR} + 6 * \rho_{RED} - 7.5 * \rho_{BLUE} + 1}$	Huete et al. (2002)
$NDWI = \frac{\rho_{RED} - \rho_{SWIR}}{\rho_{RED} + \rho_{SWIR}}$	McFeeters (1996)
$MNDWI = \frac{\rho_{GREEN} - \rho_{MIR}}{\rho_{GREEN} + \rho_{MIR}}$	Xu (2006)
$LSWI = \frac{\rho_{NIR} - \rho_{SWIR}}{\rho_{NIR} + \rho_{SWIR}}$	Xiao et al. (2006)
$DVEL = EVI - LSWI$	Sakamoto et al. (2009)

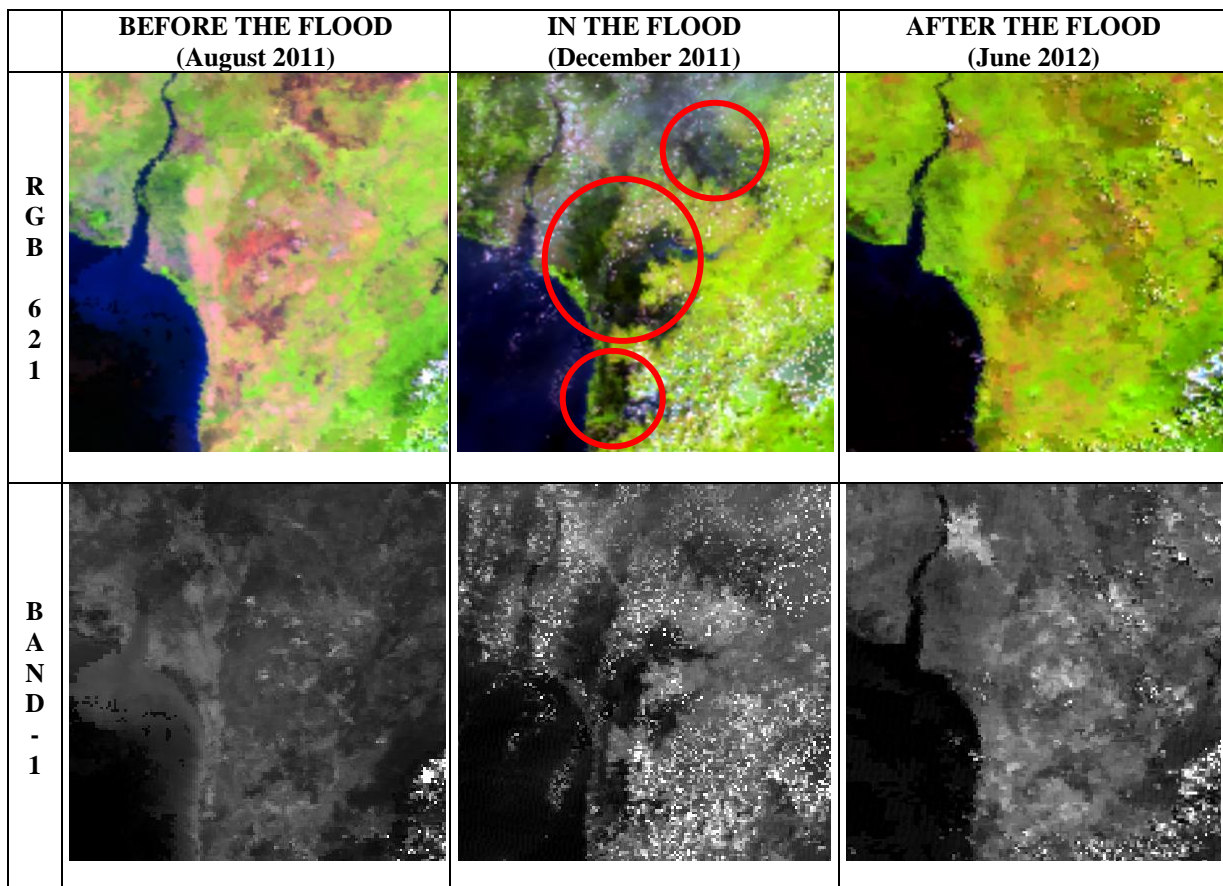
Where ρ_{NIR} is near infrared reflectance (841-875 nm, MODIS band 2), ρ_{RED} red reflectance (621-670 nm, MODIS band 1), ρ_{BLUE} blue reflectance (459-479 nm, MODIS band 3), ρ_{GREEN} green reflectance (545 - 565 nm, MODIS band 4), ρ_{SWIR} short infrared reflectance (1628-1652 nm, MODIS band 6) (see Table 2).

Table 2. Characteristic spectral and spatial resolution of MODIS reflectance channels 1-7

Channel	Central Wavelength (nm)	Bandwidth (nm)	Spatial resolution (m)
1	645	620 - 670	250 m
2	858.5	841 - 876	250 m
3	469	459 - 479	500 m
4	555	545 - 565	500 m
5	1240	1230 - 1250	500 m
6	1640	1628 - 1652	500 m
7	2130	2105-2155	500 m

IV. RESULTS AND DISCUSSION

The data used in the application of the model is the preferred data remote sensing image acquired by Space agency, which especially optical Landsat and MODIS imagery. Location chosen for the study is the application of the model flood inundation areas in Banjar Regency South Kalimantan Province of Indonesia. At the end of 2011 (December 2011), the flood-affected areas, where floods inundated 90 villages in the region are home to about 68.264 inhabitants (BNPB, 2012).



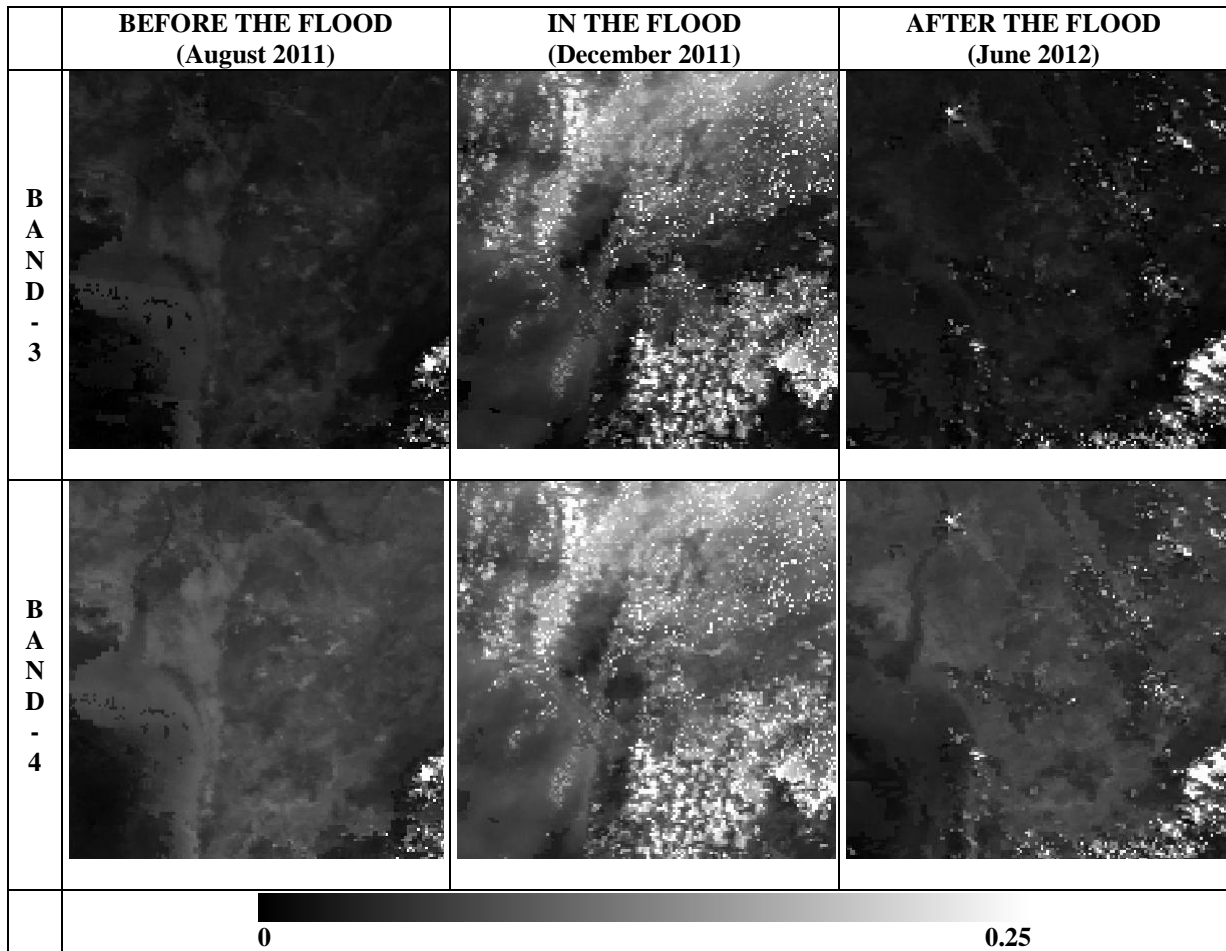
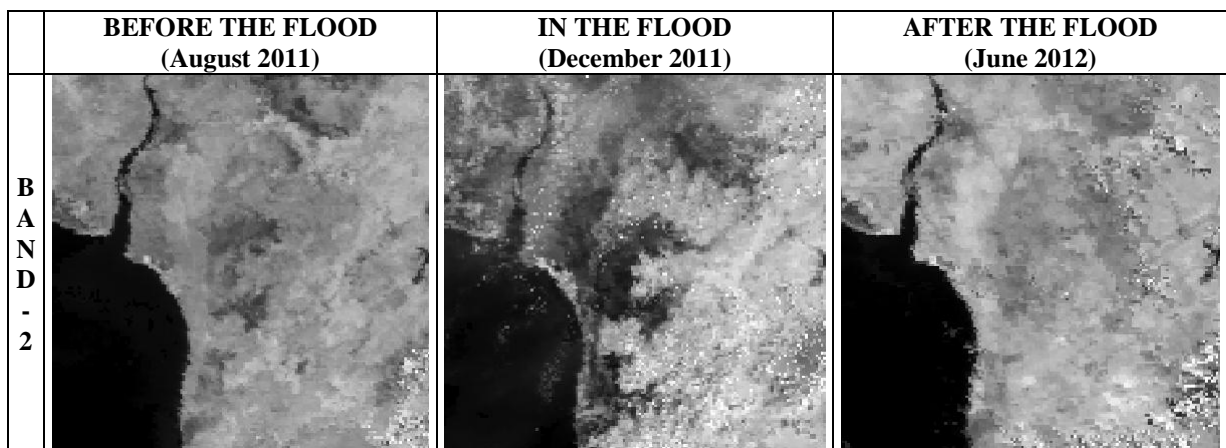


Figure 1. Floodwaters appearance on MODIS visible channel (1, 3 and 4). Red circles are the locations of floodwaters



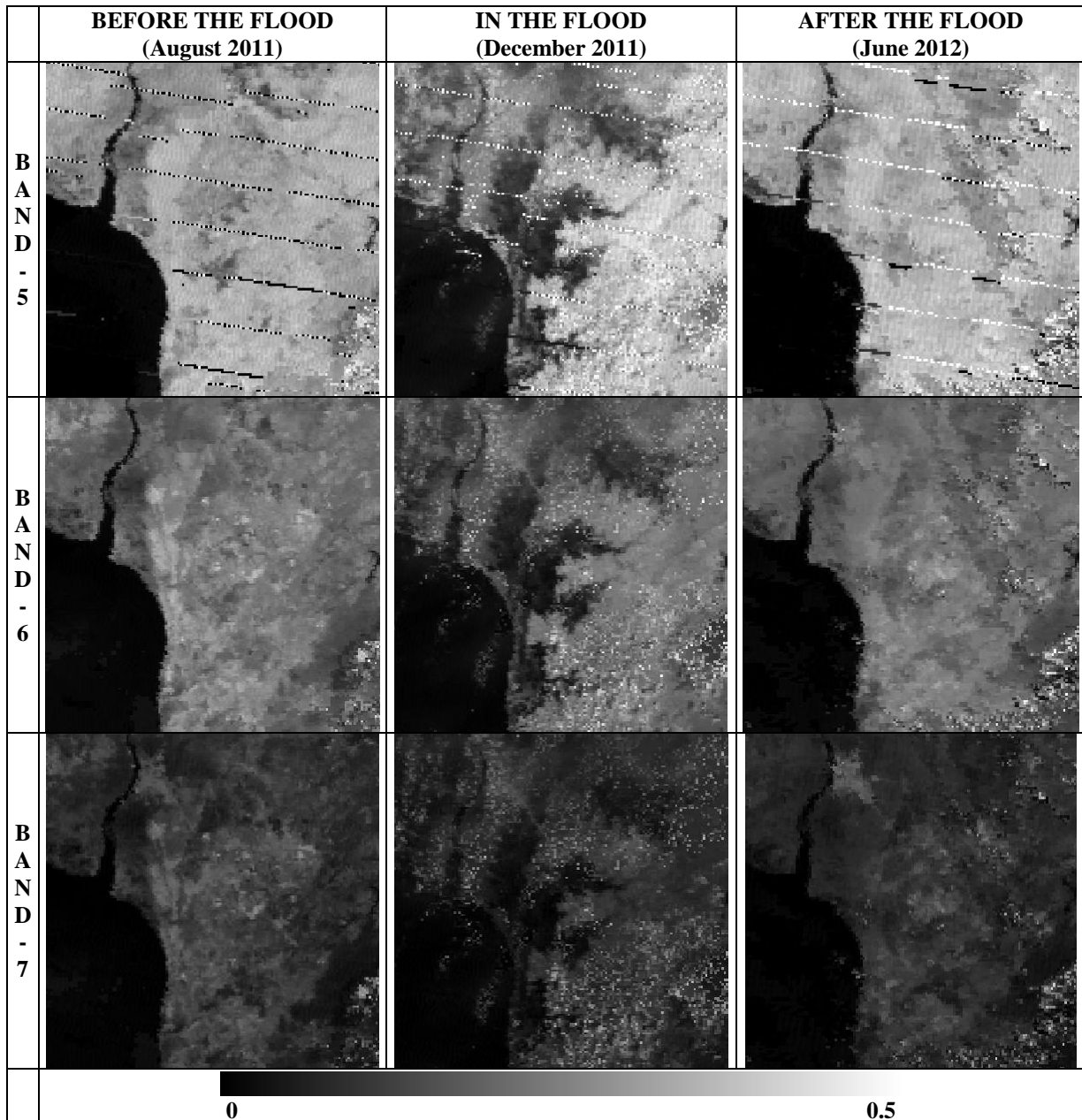
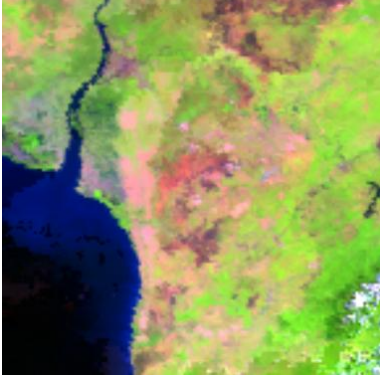
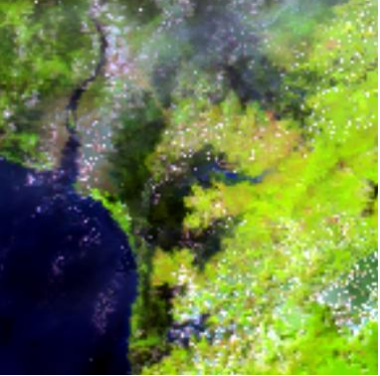
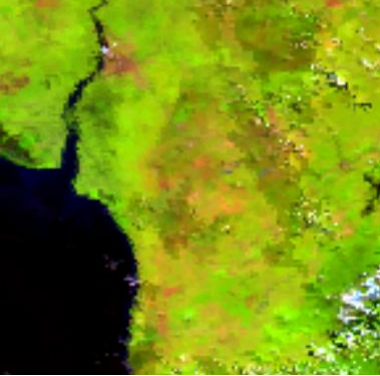
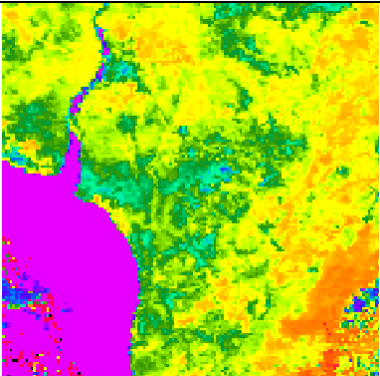
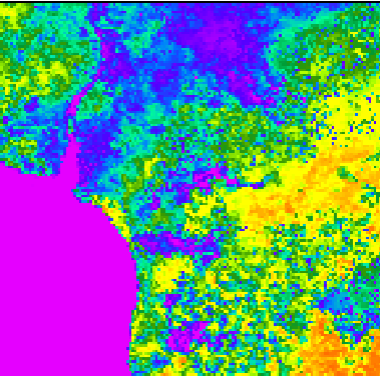
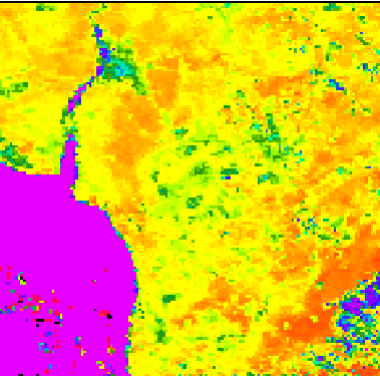
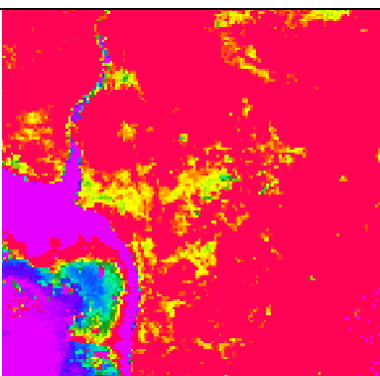
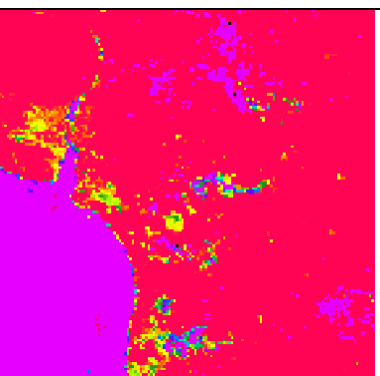
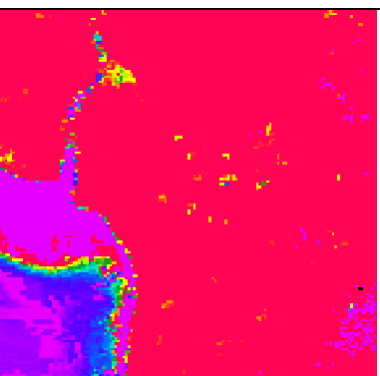
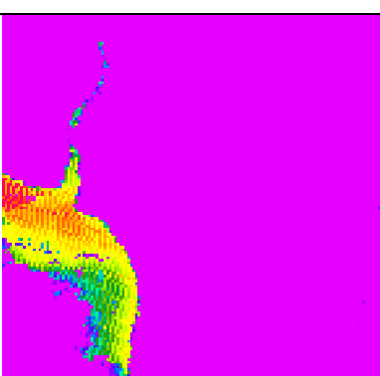
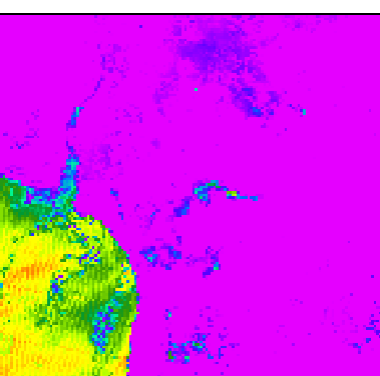



Figure 2. Floodwaters appearance on MODIS infrared channels (2, 5, 6 and 7)

Figure 1 and 2 show 621 RGB MODIS imagery and MODIS reflectance per band (1-7) in the period before the disaster, during disaster (floods) and after a disaster. Floodwaters location indicated by the red circle. The data used is the 8 daily composite MODIS reflectance (MOD09). Data pre-disaster period selected in 2011 on 217 Julian Date (5 to 12 August 2011), the period during selected events in 2011 on 361 Julian Date (27 to 31 December 2011), and the period after the events selected in 2012 on 177 Julian Date (2 June to 2 July 2012). Based on these data it can be seen that the reflectance MODIS band 2 (NIR), 5 and 6 (SWIR) provide better results in detecting floodwaters as compared to other bands, especially the channel appears (visible).

	BEFORE THE FLOOD (August 2011)	IN THE FLOOD (December 2011)	AFTER THE FLOOD (June 2012)
R G B 6 2 1			
N D V I			
E V I			
N D W I			

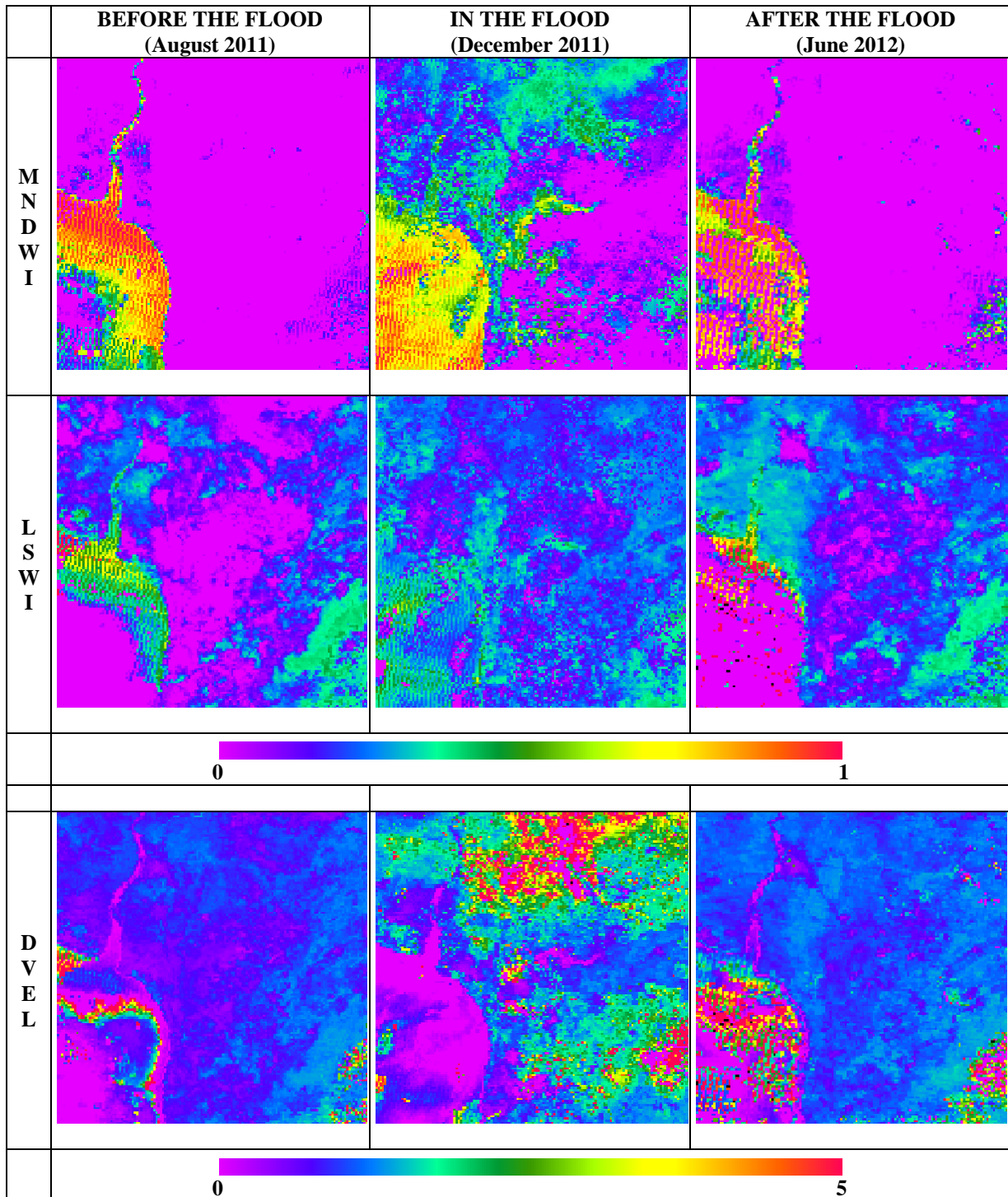


Figure 3. Floodwaters appearance on MODIS NDVI, EVI, NDWI, MNDWI, LSWI, and DVEL

While Figure 3 shows the MODIS RGB image 621 and the calculation of the value of the index (NDVI, EVI, NDWI, MNDWI, LSWI, and DVEL) are expected to be used for the identification of flood inundation. Based on the results of the analysis can be seen that all variables except LSWI can be used to detect the floodwaters.

V. CONCLUSIONS AND RECOMMENDATIONS

The study concluded that the MODIS optical images can be used to identify a pool of water caused by floods. Physical parameters that can be extracted for identification of the floodwaters is reflectance value channel 2, 5 and 6 and the index values are calculated from the reflectance values, such as NDVI, EVI, NDWI,

MNDWI, and DVEL. Based on the results of this study should be followed up with a more focused research, namely by applying models based on physical parameters of MODIS imagery for identification of flood inundation, particularly for rapid mapping purposes (rapid mapping) flood affected areas.

REFERENCES

- [1]. Ayala, I.A., 2002. Geomorphology, natural hazards, vulnerability and prevention of natural disaster in developing countries. *Geomorphology*, 47,107-124.
- [2]. McFeeters, S. K., 1996. The use of the Normalized Difference Water Index (NDWI) in the delineation of open water features. *International Journal of Remote Sensing*, 17(7), 1425-1432.
- [3]. Huete, A., K. Didan, T. Miura, E.P. Rodriguez, X. Gao, & L.G. Ferreira, 2002. Overview of the radiometric and biophysical performance of the MODIS vegetation indices. *Remote Sensing of Environment*, 83, 195–213.
- [4]. Ho, L.T.K., Umitsu, M., & Yamaguchi, Y., 2010. Flood hazard mapping by satellite images and SRTM DEM in the Vu Gia-Thu Bon Alluvial Plain, Central Vitenam. *International Archive of the Photogrammetry, Remote Sensing and Spatial Information Science*, 38(8), 275-280.
- [5]. Islam, A.K., Bala, S.K., & Haque, A., 2009. *Flood inundation map of Bangladesh using MODIS surface reflectance*. 2th International Conference on Water & Flood Management (ICWFM-2009).
- [6]. Richard, B.D., 1955. *Flood Estimation and Control*, Ed-3. Chapman & Hall Ltd., London.
- [7]. Sakamoto, T., Cao, P.V., Nguyen, N.V., Kotera, A., & Yokozawa, M., 2009. *Agro-ecological interpretation of rice cropping systems in flood-prone areas using MODIS imagery*. *Photogrammetric Engineering & Remote Sensing*, 75(4), 413–424.
- [8]. Sudaryoko, Y., 1987. *Pedoman Penanggulangan Banjir*. Badan Penerbit Pekerjaan Umum, Jakarta.
- [9]. Wang, Y., Colby, J.D., & Mulcahy, K.A., 2002. An efficient method for mapping flood extent in a coastal floodplain using Landsat TM and DEM data. *International Journal of Remote sensing*, 23(18), 3681-3696.
- [10]. Yan, Y.E., Ouyang, Z.T., Guo, H.Q., Jin, S.S., & Zhao, B., 2010. *Detecting the spatiotemporal changes of tidal flood in the estuarine wetland by using MODIS time series data*. *Journal of Hydrology*, 384, 156–163.
- [11]. Xu, H., 2006. Modification of normalised difference water index (NDWI) to enhance open water features in remotely sensed imagery. *International Journal of Remote sensing*, 27(14), 3025-3033.

Power Line Communications

Abdelraheem Mohamed Elkhalfa , Dr. Abdul rasoul J. Alzubaidi

¹ Sudan Academy of Sciences (SAS); Council of Engineering Researches & Industrial Technologies,

² Electronic Dept- Engineering College –Sudan University for science and Technology

ABSTRACT:

This paper is about power-line communication over the low-voltage grid, which has interested several researchers and utilities during the last decade, trying to achieve higher bit-rates and more reliable communication over the power lines. The main advantage with power –line communication is the use of an existing infrastructure. Wires exist to every household connected to the power – line network. This paper starts with a general introduction to power-line communication.

Then an existing application, communicating on a low voltage grid is investigated in order to obtain some knowledge of how the power line acts as a communication channel. I did experiment to verify that result. The power line communication channel can in general be modeled as a system with frequency dependent signal-to-noise ratio varying with time over the communication bandwidth. Finally we describe the basic parts of the system that eventually could be used for information transfer over the power line communication channel.

KEYWORDS: PLC, Transmissions, Modem, Modulations, Ethernet, Power, adapter, Socket, frequency, grid, Customers, electrical, computer, Internet.

I. INTRODUCTION

In the last decade there was a large growth in small communication networks in the home & in the office places. Several computers & their peripherals interconnected together resulting the network to expand globally to the state of Internet. A number of networking technologies are invented which purely concentrates on home networks. But users are limited due to its nature of high cost. Some are over engineered or difficult to install in pre-existing buildings. This paper is based on one such communication medium, which has a very high potential growth. I.e. the power line, which gives rise to power line carrier communication, refers to the concept of transmitting information using the main power line as a communications channel. Our project mainly aims at applicability of power line carrier communication techniques towards home networking. Communication over the power line will have the following advantages:-

- The modem electric grids are well maintained & far superior to any of the wired communication networks.
 - No. of electrical consumers are higher than telephone, cable or other wired communication customers. This will give a high potential market for the investors.
 - The analog spread spectrum waves have much greater bandwidths or carrying capacity than the digital switched systems.
 - Move your computers and appliances where you want.
 - Utilizes existing power source for all your communications needs.
 - Secure data –encryption.
 - No more wires just plug in.
 - Share your Internet connections.
- Also the communications over the power line will have the following limitations:-
- Electro-Magnetic Radiations Issues.
 - Addressing Issues.
 - Security.
 - Noise Interference.
 - Regulatory and Standardizations Issues

II. PROJECT AIM

Power line carrier techniques would appear to be an economical and user –friendly method of installing a home network adapter in any building. This project explores such claim, investigating the challenges of using the power line for communication and to identify the possible methods to overcome these challenges. We expect to send a data from one computer to another computer through the existing domestic power line (Low Voltage).

2.1. Applications of power line network adapters

- High-definition (HD) and standard-definition (SD) video distribution.
- Broadband Internet sharing.
- Internet protocol Television (IPTV) and voice over Internet protocol (VoIP).
- Home Automation
- Automatic Meter reading
- Process Control
- Heating and Ventilation Control
- Air conditioning Control
- Lighting Control
- Status Monitoring and Control
- Low Speed data communication Networks
- Intelligent Buildings
- Fire and Security Alarm System
- Signs and Information Displays
- Power distribution Managements

III. POWER LINE CARRIER CHALLENGES

Power lines and their associated networks are not designed for communication use. They are hostile environments that make the accurate propagation of communication signals difficult. Two of the biggest problem faced in using power lines for communications is excessive noise levels and cable attenuation. Noise levels are often excessive, and cable attenuation at the frequencies of interest is often very large. The most common causes of excessive noise in a domestic situation are the various household devices and office equipment connected to the network. Noise and disturbances on the power network include over voltages, under voltages frequency variations and so on. However, the most harmful noise for PLC applications is that superimposed on a power line. Switching devices such as light dimmers, induction motors in many common appliances and high-frequency noise caused by computer monitors and televisions often causes such superimposed noise. For a power line carrier communications system to perform reliably it must be able to avoid, or cope with, the different types of noise encountered on its communications channel. These different types of noise exist at different frequencies, and occur at unpredictable times. Thus, it is not sufficient to design a system that simply avoids using certain parts of the available bandwidth. Rather, a technique called frequency hopping can be used to overcome this problem. When a frequency –hopping communications system encounters noise at a certain bandwidth, it skips to a different bandwidth moving away from the original interference. From the above definition the following points are represented a challenging technical problem in power line networks.

- Electrical wires were never designed for high speed transmission.
- Uncontrolled and (almost unpredictable) environment.
- Impedance mismatch causes strong multipath effect.
- Unknown, non –flat and non-stationary channel frequency response.
- Electrical devices connected to the network generate non- Gaussian, non- -white, non-stationary noise.
- Risk of EMC problems because of unshielded wires.

IV. AVAILABLE BANDWIDTH & REGULATORY STANDARDS

Bandwidth available for power line communication is not limited by the physical capabilities of the line. Rather, regulatory authorities limit the available bandwidth for power line communication in order to prevent radio interference, other device interference and other such contentions. It is to be noted that bandwidth is proportional to the bit rate, thus a large bandwidth is needed in order to communicate with high bit rates. Various standards exist that provide regulations on the operating specifications of PLC systems. In our project we use devices complies with part 15 of the Federal Communication Commission (FCC) Interference Statement rules. Operation is subject to the following two conditions:

- This device may not cause harmful interference.
- This device must accept any interference received, including interference that may cause undesired operation. Which is the European standard viz. CENELEC? The standard only allows frequencies between 3 kHz and 148.5 kHz. This puts a hard restriction on power –line communications and might not be enough to support high bit rate applications, such as real-time video, depending on the performance needed.

V. MAC ENCAPSULATION

Unlike IEEE 802.11 frames, on which the protocol layers of the Wi-Fi technologies are based, the PLC frames can be considered as MAC encapsulations. Fig. 6.1 illustrates the MAC encapsulation of Home Plug 1.0 PLC frames. From the point of view of the data link layer, the MAC Ethernet frames are de-encapsulated from the physical frames for their presentation to the Ethernet interface of the PLC devices.

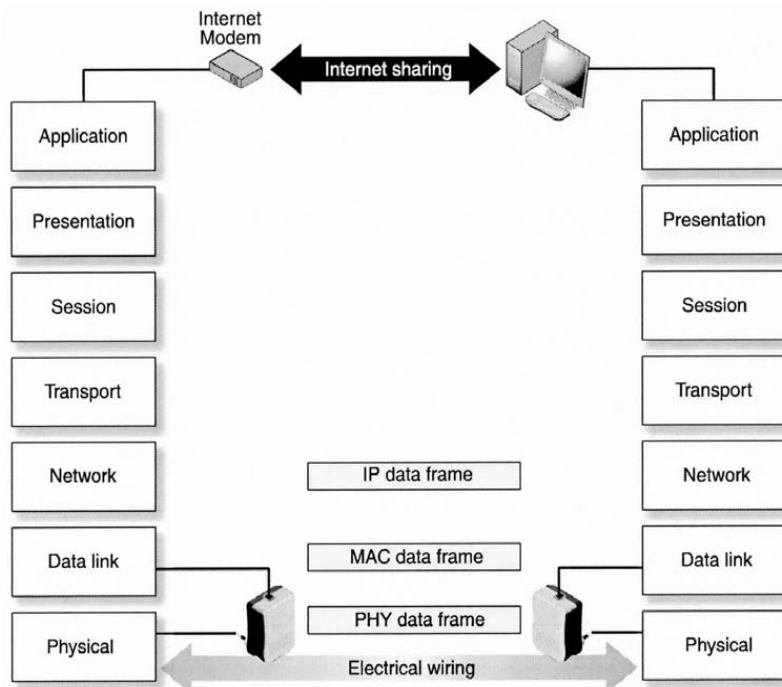


Fig. 6.1: PLC technologies and the OSI model.

VI. PRACTICAL ISSUES

In designing the power line communication system we were to address even some the salient features. Modulation technique, transmission methods and so on were selected to give suitable performance in communication environment which we were expected to use.

4.1. Modulation Methods

The fundamental digital modulation techniques are based on keying. Phase –shift keying (PSK), a finite number of phase are used. In this form of modulation phase of the carrier wave is varied by a binary input stream. As the binary input signal changes from logic 0 to logic 1, and vice –versa, the PSK output shifts between two angles that are 180 degrees out of phase while keeping the frequency a constant. Frequency- shift keying (FSK), a finite number of frequencies is used. In this form of modulation carrier wave frequency is varied by a binary input stream. As the binary input signal changes from logic 0 to logic 1 and vice- versa, the FSK output shifts between two frequencies. Amplitude shift keying (ASK), a finite number of amplitudes is used. Quadrature amplitude modulation (QAM), a finite number of at least two phases, and at least two amplitudes are used. Due to the nature of high attenuation prevailing in the power line frequency shift keying and phase shift keying will give simpler results over others although both of them are robust. In order to decide the method of modulation to be used in power line communication it is important to keep in mind the hostile environment in which it operates.

It is difficult to say which method to use, whether FSK or PSK. Phase delay in the PLC channel is expected and unpredictable in the case of PSK technique. The reliable performance of FSK with the any reasonable amount of phase delay makes it modulation scheme of choice for PLC techniques. The difference between FM (frequency modulation) and PM (Phase modulation) is that the bandwidth is independent of signal bandwidth in FM, while it is strongly dependent on signal bandwidth in PM. Orthogonal Frequency Division Multiplexing Frequency division Multiplexing (FDM) is the technology that transmits multiple signals simultaneously over a single transmission path, such as a cable or wireless system. Each signal travels within its own unique frequency range (carrier), which is modulated by the data (text, voice, video, etc.). Orthogonal FDM's (OFDM) spread spectrum technique distributes the data over a large number of carriers that are spaced a part at precise frequencies. This spacing provides the “orthogonally” in this technique, which prevents the demodulators from seeing frequencies other than their own. Basic approach of OFDM is illustrated in the bellow fig. 7.1.

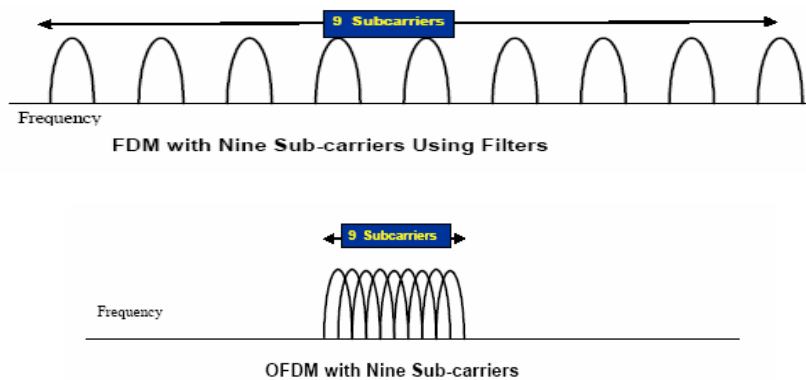


Fig. 7.1: Difference between band-width requirements in

FDM vs. OFDM.

OFDM is similar to FDM but much more spectrally efficient by spacing the sub-channels much closed together (until they are actually overlapping). This is done by finding frequencies that are orthogonal, which means that they are perpendicular in mathematical senses allowing the spectrum of each sub-channel to overlap another without interfering.

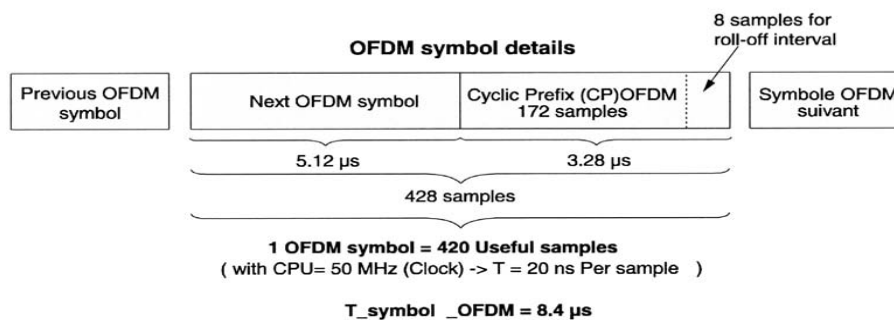


Fig. 7.2: OFDM symbol details.

The Coupling Network

A coupling circuit is used to connect the communication system to power line. The purpose of the coupling circuit is two- fold. Firstly, it prevents the damaging 50 Hz signal, used for power distribution, to enter the equipment. Secondly, it certifies that the major part of the received/transmission signal is within the frequency band used for communication.

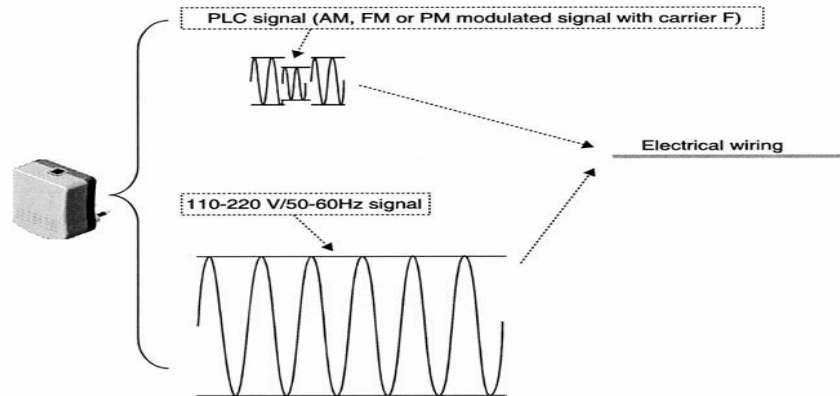


Fig. 8.1: Sum of the modulated PLC signal and the power signal (for example, 110 -220V/50-60 Hz).

These increase the dynamic range of the receiver and makes sure the transmitter introduces no interfering signals on the channel. Thus ultimate coupler network design becomes a compromise between the different characteristics for receive and transmit direction, plus impedance.

Different ways exist in order to couple a communication device in to an electrical power line. Two main categories can be described as below.

Differential mode coupling: In this case the line or active wire is used as one terminal, and the neutral wire as the second terminal. In cases where a neutral line is not present (high voltage network), the ground line acts as the second terminal.

Common mode coupling: In this case the line (active) wire and neutral wires are used together forming one terminal and the ground wire serves as the second terminal. One might think this coupling mode is impossible, due to the connection of neutral and ground wires at the transformer.

In practice, the inductance between points of coupling and the short-circuit point is large enough to allow signal transmission. However, problems exist in using common mode coupling in the presence of earth leakage protection devices, and certain countries do not allow common mode coupling because of perceived dangers to customers.

Considering the physical implementation of the coupling two can be identified.

Capacitive coupling: A capacitor is used to couple the communication signal on to the power line.

Inductive coupling: An inductor is used to couple the communication signal on to the power network. Inductive coupling provides a physical separation between power network and communications network, making it safer to install.

In the electrical field, coupling can be defined as how two electrical circuits connect together in order to generate an electron flow between these two circuits. This electron flow is conveyed by an electric and a magnetic field created between the two electrical circuits due to their inductive and capacitive nature.

Inductive coupling is much more efficient than capacitive coupling. It uses the electromagnetic induction method between two electrical wiring and a coil wound around this wiring. An inductive coupler reduces the attenuation by 10 to 15 dB for some frequencies in comparison with a capacitive coupler. The attenuation between the outlet and the switch box varies from 10 to 30 dB It is maximum between 15 MHz to 20 MHz. In the field of PLC networks, the injectors are devices used to connect a PLC device to the electrical network via an inductive coupling directly a round electrical wirings, for example, at the level of the electrical switchboard of a building.

Fig.8.2 illustrates the principle of a PLC signal injector consisting of the two following elements.

1. A magnetic coil wound around the natural cable of electrical network. As we know the neutral cable is the most interesting cable for the injection of the PLC signal over an electrical network, since it is distributed over all the electrical equipment.
2. A cable TV modem connected by a cable (for example, a coaxial cable) to the magnetic coil.

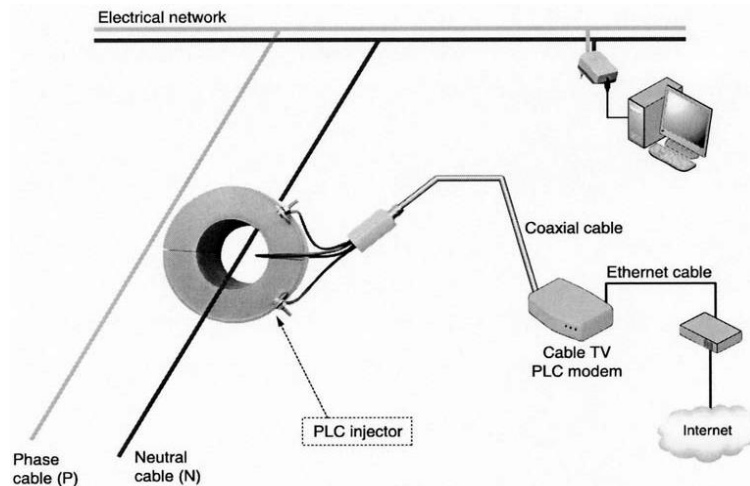


Fig. 8.2: PLC signal injection by inductive coupling with coil over a single phase network.

Choice of injection cable

It is preferable to inject the signal over the neutral cable for a single –phase network and on one of the phase for a three –phase network. Better performance is achieved by injecting the signal over a single cable than over several cables at the same time. This method for connecting PLC devices requires access to the electrical wirings of 110 to 220/50 to 60 Hz network, unlike capacitive coupling, which is restricted to the connection of a device to an outlet. Therefore, it is important to knowledge of the electrical hazards close to the cables and components of the electrical network. Our project is focused with using two power line adapters, connected with two computers in peer-to-peer mode.

Master –Slave mode : Fig. 9.1a illustrates the architecture of an LV (Low Voltage) PLC network for electrical distribution in the master- slave mode. We find the master device at the ML/LV (medium voltage to low voltage) transformer level. This device checks the good working order of the PLC network and more particularly the existing network links with the slave devices located between the electrical meters of houses.

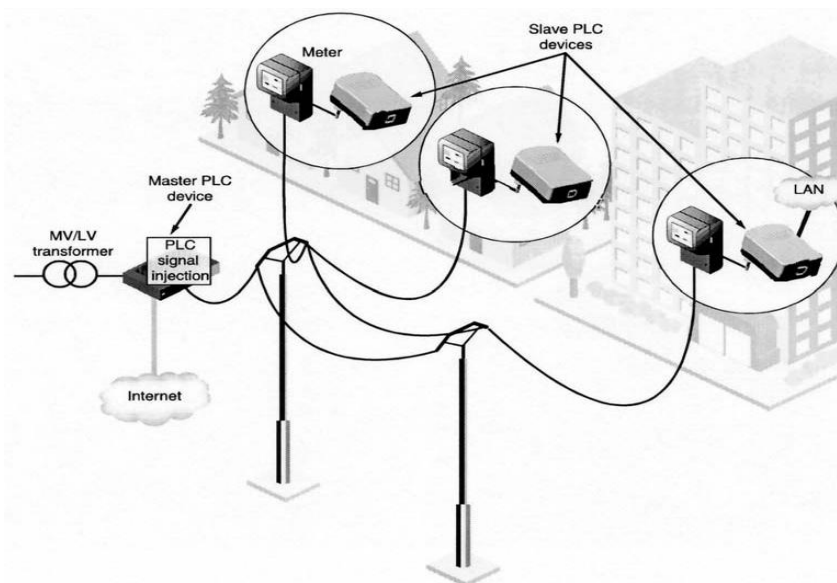


Fig. 9.1a: Simplified architecture of the master-slave mode

Some PLC devices are used for remote telephone interfaces over the PLC network. Some companies for example, develop devices with RJ-11 interfaces to carry voice analog communications over the electrical network. In the master –slave mode, a master device is at a high hierarchical level (it manages and controls the network), and the slave devices are at a lower hierarchical level (their function is limited to communications with the master device). In peer-to-peer mode, all the devices have the same hierarchical level and exchange data with all the other PLC devices of the network. Therefore, the network consists of N to N links. As illustrated in figure (9.1b), the peer-to-peer mode is ideal for local area networks since the LAN architecture must enable any terminal (typically PC) to exchange data with any other LAN terminal. Homeplug 1.0 and Turbo use this mode.

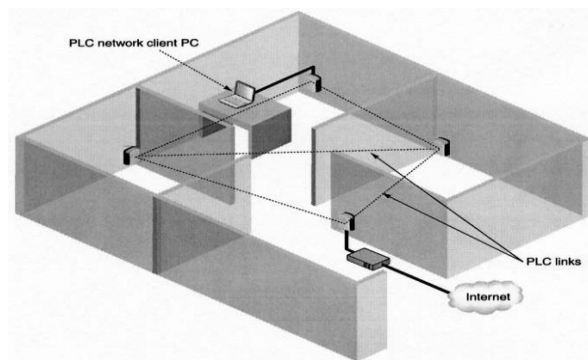


Fig. 9.1b: Architecture of a PLC network in peer-to-peer mode

PLC Modems

As PLC technology intrinsically uses the electrical network, the PLC devices, irrespective of their nature, connect to the outlets or directly inject the signal into the electrical wirings. This allows a PLC device to connect directly to the electrical wirings. Although the PLC technology does not use the modulation-demodulation process implemented in the modems, we talk about a PLC modem to designate the device to which the terminals that want to take part in the PLC network are connected. The PLC modem, which is the most widespread device in the PLC networks, is also the easiest to use, since it appears as a standard electrical appliance fitted with a male receptacle to be connected into an outlet and a USB or Ethernet interface to be connected to the terminal. When viewed from the outside, a PLC modem therefore has the two following interfaces:

- Male receptacle.
- RJ-45 Ethernet or USB network interface.

The modem generally has three indicators (LED) that indicate the presence of the 110 to 220V/50 to 60 Hz, PLC signal on the electrical interface and that of the Ethernet network on the RJ-45 interface to the user (see Figure (9.2a)).

Some devices have up to five indicator lights so that the user can check that the device is in good working order.



Fig. 9.2a: Outside of a HomePlug Power PLC modem

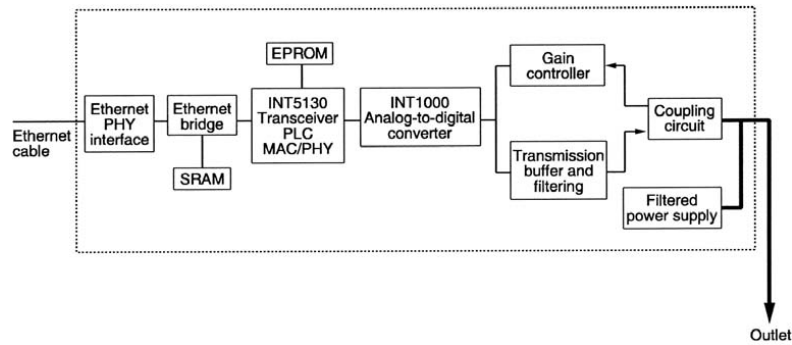


Fig. 9.2b: Hardware architecture of a PLC modem

The manufacturers have developed two types of PLC modems: “desktop” modems, which appear as packages to be placed on a table or on a pedestal, with a cord to connect to outlets; and “wallmount” modems, which appear as integrated packages directly connected into outlets. Most PLC modems are wallmount modems since they are easy to use. Figure (9.2c) illustrates examples of wallmount (left) and desktop (right) modem

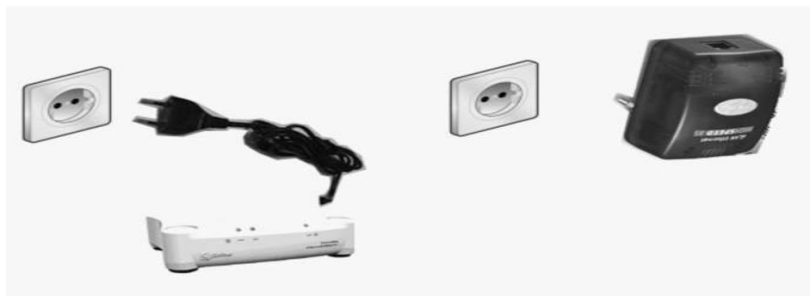


Fig. 9.2c: Wallmount and desktop PLC modems

PLC Ethernet Modems

The generalization of network interface cards in computers, network terminals, and electronic devices, even in household appliances, simplifies the building of networks by using the Ethernet board’s RJ-45 connectors. This type of modem has become the most widely used PLC device. As well as being simple to use and configure, its price continues to fall. Figure (9.2.1) illustrates an Ethernet PLC modem of the companies Ethernet High Speed 85 type. The Ethernet network interface card of PLC modems was the first of the 10 baseT type (10 Mbit/s) for HomePlug 1.0 modems providing a maximum useful throughput at the MAC layer level of 8.2 Mbit/s, then of the 100baseT type (100 Mbit/s) for HomePlug Turbo and AV modems.



Fig: 9.2.1 Ethernet PLC modem

The increased performance of HomePlug PLC devices will probably lead the manufacturers to use 1,000baseT (1,000 Mbit/s) boards so that the throughput is not limited over the Ethernet interface. It would not be surprising to come across optical fiber PLC devices.

Practical Implantation

Figure (9.3) gives the block diagram of PLC system which we design on our project.

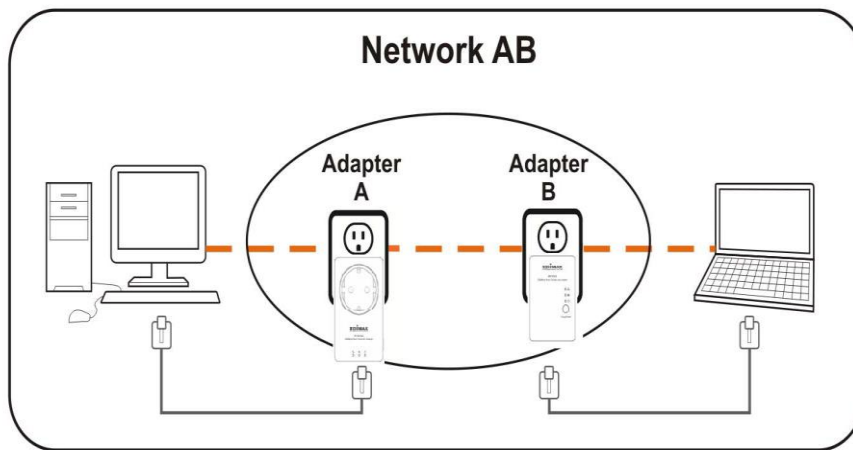


Fig. 9.3: Schematic diagram of PLC system

This design included the two computers connected in peer-to-peer mode, two power line adapters with Ethernet cables, and Transmission range up to 300 meters. The design requirement, computer with Ethernet port, running Windows XP/vista/7, Linux, MAC OSX and any other operating system. Any connected devices must feature a network port, and utility software supports windows XP/vista/7.

Connection set up : Connect a power line adapter to your computer ‘A’ (router) via Ethernet cable, and then plug it into a power socket.

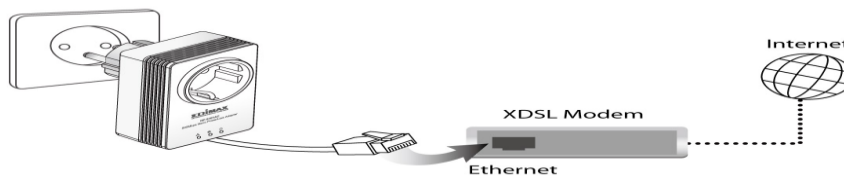


Fig. 9.3.1a: Illustrated the connection for computer “A” (Router)

- Connect another power line adapter to your computer, and then plug it into a power socket.

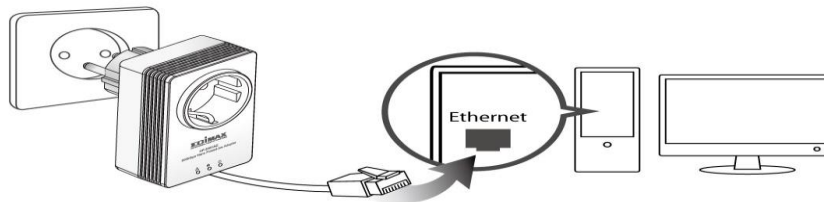
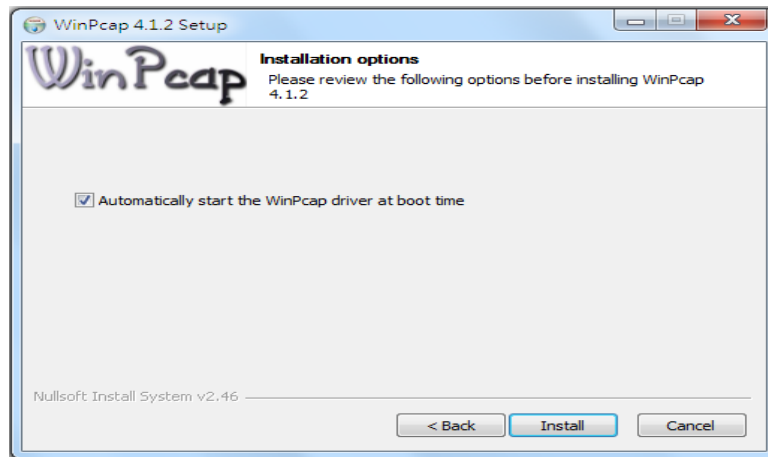


Fig. 9.3.1b: Illustrate the connection to the other computer

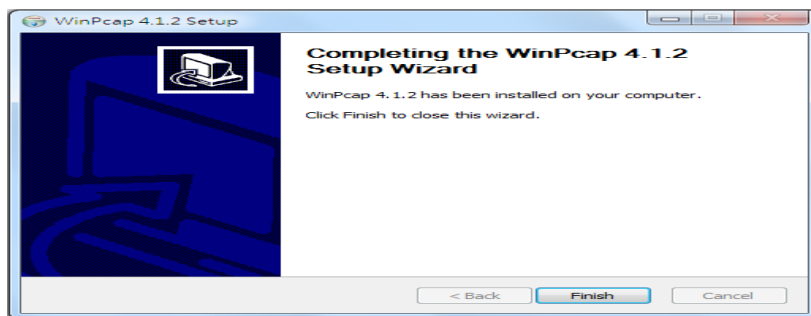
We can also connect the adapter to a printer, set top box, gaming console, TV or other device with a network port, to add the device into the power line network.

- We monitor that on PLC and LAN LEDs light up on both PLC adapters.
- The computer “B” and the router (Computer “A”) will be connected to the power line network automatically.
- Then click “Setup Utility”.

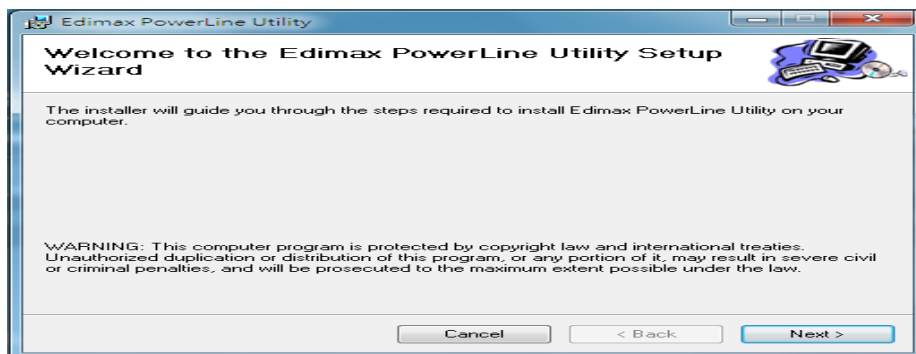
The wizard will guide you through the entire win Pcap installation.



- Then click install.



- Winpcap 4.1.2 has been installed on your computer. Click finish to close the wizard.



- After click finish the above dialog will appears .We go through this procedure until we reached the end of installation.
After the installation finished connect the computer “A” with Internet after reply from the other computer.
Proxing the Internet on the computer “B”.

Testing Operation of the PLC Network

Once the various PLC devices of the network are configured, it is recommended that you check the good operation of the domestic installation network links by performing a test with the PLC configuration tool. To test the good operation of the PLC network, it can also be useful to run “Ping” commands from the PC connected to the PLC network at adapter (A), to the LAB Top computer connected to that network at adapter (B),

As illustrated in Figure bellow.

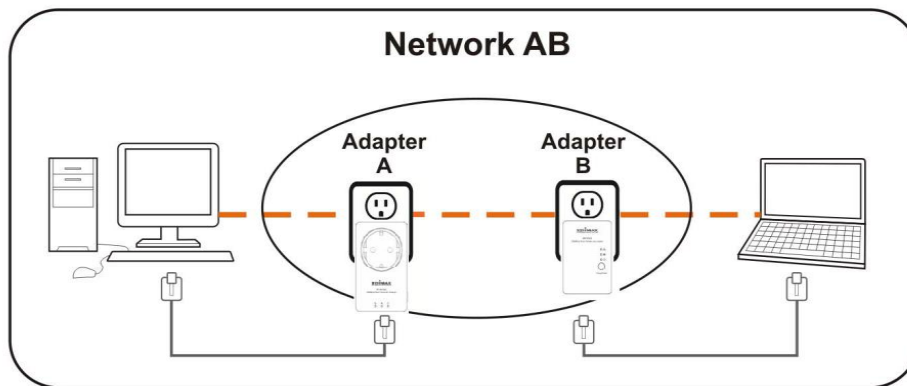


Fig. 9.4: Schematic diagram of PLC system

For this purpose, all the PCs or terminals must be in the same addressing plane (for example, for an IP network of the 192.168.10.1 for computer @ adapter A and the other devices in IP =192.168.10.100, 101,102 and so forth). @ Adapter B or others.

To start the “Ping” command, just proceed as follows:

- Click on “Start” then on “Execute.”
- Enter cmd. A DOS window opens.
- Enter the following command:

```
C:\>ping 192.168.10.1
```

Pinging 192.168.10.1 with 32 bytes of data:

```
Reply of 192.168.10.1: bytes=32 time=3 ms TTL=64
```

```
Reply of 192.168.10.1: bytes=32 time=2 ms TTL=64
```

```
Reply of 192.168.10.1: bytes=32 time=2 ms TTL=64
```

```
Reply of 192.168.10.1: bytes=32 time=2 ms TTL=64
```

If replies are sent back with this command, this means that the network links are configured and ready to be used by this application.

VII. CONCLUSION

This project has been a successful one with all project aims and goals are met. Addressing the individual project goals, a number of conclusions can be made. After detailed studies, we have gained an in-depth knowledge of the issues faced with power line carrier communications with three phases.

So, today’s point of view the first challenge is to reduce the cost. So, in future we definitely proved that power line communication is the most efficient, powerful & cheapest media of communication.

- We have addressed possible methods to overcome these issues, mainly noise and attenuation caused in the power line.
- We introduced the possible uses of PLC techniques.
- The PLC system we designed is a primary stage of a home networking system in which we tried to send a data from one computer to another which is installed in the same building.
- A successful power line carrier communication link could be created by the addition of frequency hopping, variable gain stage and error correction techniques.

REFERENCES

- [1] Xavier Carcelle.- Power Line Communications in Practice
- [2] Klaus Dostert. Prentice Hall. 2001. Powerline Communications”
- [3] Hrasnica, Haidine, and Lehnert. Wiley. 2004, “Broadband Powerline Communications Network Design.”
- [4] Gotz, Rapp, and Dosert, University of Karlsruhe. IEEE Communications Magazine. April 2004. Power Line Channel Characteristics and Their Effect on Communication System Design.”
- [5] Jerry Ramie. Conformity. October 2005. Review of FCC Report & Order 04-245 on Broadband Over Power Lines (BPL).”
- [7] www.powerlineworld.com



Mechatronics Design of Ball and Beam System; Education and Research

Farhan A. Salem^{1,2}

¹Department of Mechanical Engineering, Faculty of Engineering, Mechatronics prog, , Taif University, 888, Taif, Saudi Arabia.,

²Alpha Center for Engineering Studies and Technology Researches, Amman, Jordan.

ABSTRACT:

The key element in Mechatronics design is the concurrent synergetic integration, modeling, simulation, analysis and optimization of multidisciplinary knowledge through the design process from the very start of the design process. Mechatronics engineer is expected to design engineering systems with synergy and integration toward constrains like higher performance, speed, precision, efficiency, lower costs and functionality. This paper proposes the conception and development of ball and beam system based on Mechatronics design approach. A complete overall system and subsystems selection, modeling, simulation, analysis, and integration are presented. The proposed Mechatronics design and models were created and verified using MATLAB /Simulink software and are intended for research purposes, as well as, application in educational process.

KEYWORDS: Mechatronics, Mechatronics design approach, Ball and beam, modeling/simulation.

I. INTRODUCTION

Mechatronics is defined as synergistic integration of mechanical engineering, electric engineering, electronic systems, information technology, intelligent control system, computer hardware and software to manage complexity, uncertainty, and communication in design and manufacture of products and processes, a working definition can be; the synergistic integration of sensors, actuators, signal conditioning, power electronics, decision, control algorithms, computer hardware and software to manage complexity, uncertainty, and communication in engineered systems. The key element in Mechatronics design is the concurrent synergetic integration (instead of sequential), analysis and optimization of these areas through the design process resulting in products with more synergy [1] and a balance between modeling/analysis and experimentation /hardware implementation. Based on this, Mechatronics engineer is expected to design engineering systems with synergy and integration toward constrains like higher performance, speed, precision, efficiency, lower costs and functionality. Reference to [1-2], Mechatronics system design process can be divided into systematic, simple and clear design steps including; Problem statement; Conceptual design and functional specifications; Parallel (concurrent) design and integration of system and all subsystems as whole and concurrently including; selection, design and synergetic integration of mechanical, electronics, software, control unit, control algorithm and interface sub-systems; Modeling and simulation; Prototyping, Testing and Optimization; and finally Manufacturing, and commercialization, these steps will be followed and explained in this paper, were this paper proposes the conception and development of ball and beam system based on Mechatronics design approach. A complete overall system's and subsystem's components' selection, design, integration, as well as, modeling, simulation and analysis are to be presented. The significance of the ball and beam system is due to it's complexity, and at the same time it's simplicity, where it is a double integrator system that is open-loop unstable and simply, it is a position control system, presents a challenging design and control problem, it is often used by many control theorists and engineers as a bench mark problem for testing and analyzing the results of many different theoretical control schemes and new controller and observer methods.

II. PRE-STUDY PROCESS-PROBLEM STATEMENT

The ball and beam system is motion control system consisting of three main parts; control system, a servo or electric motor , free rolling back and forth, Ball on top of long V-grooved Beam whose inclination can be adjusted by manipulating the angular position of the servo. Ball and beam system is often used as a bench mark problem for many different control schemes and presents a challenging design and control problem, due to fact that it is double integrator (two poles at the origin) system that is open-loop unstable, in such system even at optimal beam position conditions the ball will swing on Beam, up to roll off the end of the beam. *Target user;*

Researchers and Educators. *User's requirements*; it is required to develop a ball and beam system; linear, one-dimensional single-variable experimental unit, that can be used for testing, analysis, education, and demonstration the effect of various control strategies, mainly SISO systems, precise, cost-efficient, with simple, easy to understand and use interface allowing the users to manipulate a machine, gathering and outputting data, space saving, and with attractive design. System parameters, requirements and analysis, are listed in Table 1.

III. CONCEPTUAL DESIGN

The purpose of design is to propose the conception and development of ball and beam system based on Mechatronics design approach, it is required to propose a design of a ball and beam system that fits user's (Researchers, Educators , students) needs and requirements, with overall function (intended) to help users to test , visualize and analyze the selected and designed control strategy to continually measure and stabilize the rolling ball position a long a given beam by adjusting the rotating angle of a beam by tilting it frontwards, backwards, leftwards, or rightwards, all this accomplished by manipulating the angular position of a selected servo. System's functional structure block diagram is shown in Figure 1. Morphological table, analysis and evaluating the best solution are shown in Table 2. Block diagram representations, preliminary structures including mechanical, electronic and system dynamics are shown in Figure 2 and Figure 3
Table 1 requirements analysis

Requirements		Value/ Unit	Requirements type			
			Fixed Req.	Soft Req.	Quantitative Req.	Qualitative Req.
Control system	Compact, cost effective.	-	Fixed			Qual.
Control algorithm	Simple, quick, precise, efficient, easy to program	-		Soft		
Beam	V-grooved,	40 cm	Fixed		Quan.	
	Mass , m	1.5 kg				
	Beam length, m	40 cm				
Ball	Radius	0.015 m	Fixed			
	Mass, M	0.111 kg				
Actuators	One actuator, for adjusting the beam rotating angle, available, inexpensive, simple to interface, and control.	12-24 v	-	Soft		Qual.
Sensors	Position sensor, simple to interface, available, inexpensive		-	Soft		Qual.
Transmission	Gears, belt, chain	0.03 m		Soft		
	Output gear radius					
	Overall gear ratio	n				
Overall System dimensions	Height:	40 Cm	Fixed	-		Qual.
	Width	30 Cm				
	Length	50 Cm				
User Interface	Simple and easy to use and understand					Qual.
Machine aesthetics design	Compact, attractive fits user requirements.			Soft	Quan	

Function	Solution 1	Solution 2	Solution 3	Solution4
Control system	Microcontroller	Microcomputer	Analogue	
Control algorithm: <i>Position control</i>	PID	PD : deadbeat, prefilter	Fuzzy	
Ball : steel	Rigid	hollow		
Beam: aluminium	Two parallel thin bars	V-grooved	U-grooved	
Actua tor	DC motor	Stepper motor		
Position Sensor	Potentiometer	Encoder	Ultrasonic	Linear resistive wire
Transmission	Belt	Chains	Flexible cable	Gears and shaft
Interface	Touch screen	Keypad	Switches	
Support	Slides	Linkage-joint	Wheels	
Power	Electric			
Operator	Standing	Seating at front	Seating at rear	Remote control

Table 2 Morphological table, analysis and evaluating the best solution selection

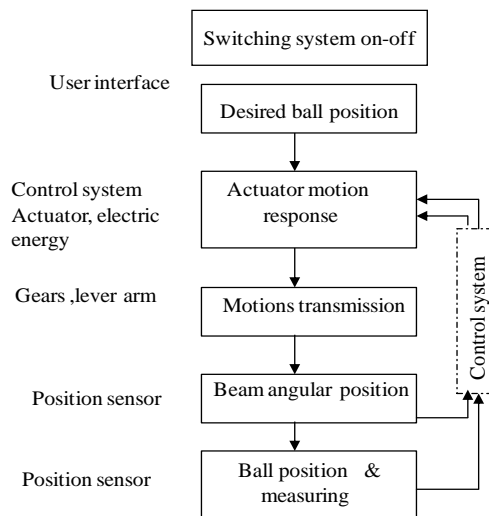


Figure 1 Functional Structure block diagram

IV. PARALLEL (CONCURRENT) SELECTION, DESIGN AND INTEGRATION OF SUB-SYSTEMS AND OVERALL SYSTEM.

Mechatronics design is the synergistic selection, evaluation and integration of the system and all its components as a whole and concurrently including sensors, actuators, signal conditioning, power electronics, decision, control algorithm, computer hardware and software. All the design disciplines work in parallel and collaboratively throughout the design and development process to produce an overall optimal design. The ball and beam system is to be divided into realizable hardware and software subsystems including; Mechanical subsystem; sensor subsystem ; actuator subsystem ; power supplies, controller and Control algorithm, drive, and conditioning circuits), the optimal selection, modeling, simulation, integration, optimization and the exchange of information between different modules are to be designed concurrently.

4.1 The optimal mechanical design:

The mechanical design is the skeleton of Mechatronics systems, there are several arrangements of constructing ball and beam system, three system's arrangements are shown in Figure 2. In Figure 2 (a), one end of the beam is coupled to electric motor through lever arm and gears, the other end is fixed, and supported with vertical beam. In Figure 2(c) one end of the beam is coupled to electric motor through lever arm and gears, the other end is free to move up and down, the beam is supported with vertical bar at its center. In Figure 2(d) the

beam at its center, is mounted on the output shaft of an electric motor. System CAD model is shown in Figure 2(e). The whole system layout is shown in Figure 2(a), and the mechanical system parts, materials and optimal dimensions are listed in Table 3. Preliminary block diagram and layout representations of proposed system and main components are shown in Figure 2(f),

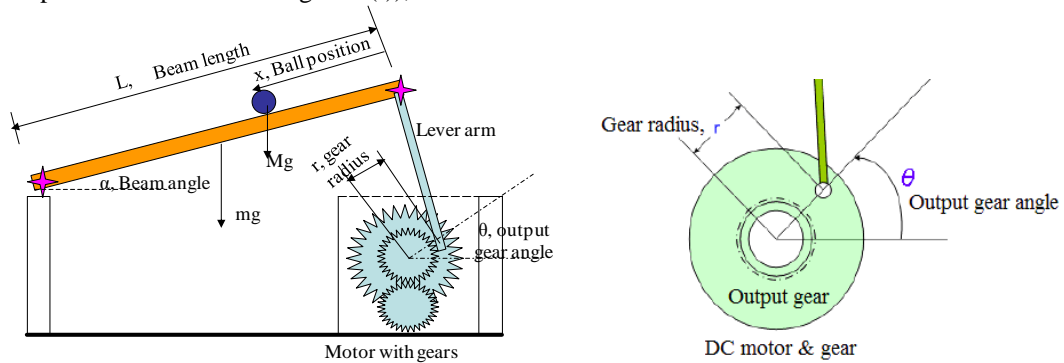


Figure 2(a) One end of the beam is coupled to electric motor through lever arm and gears, the other end is fixed.

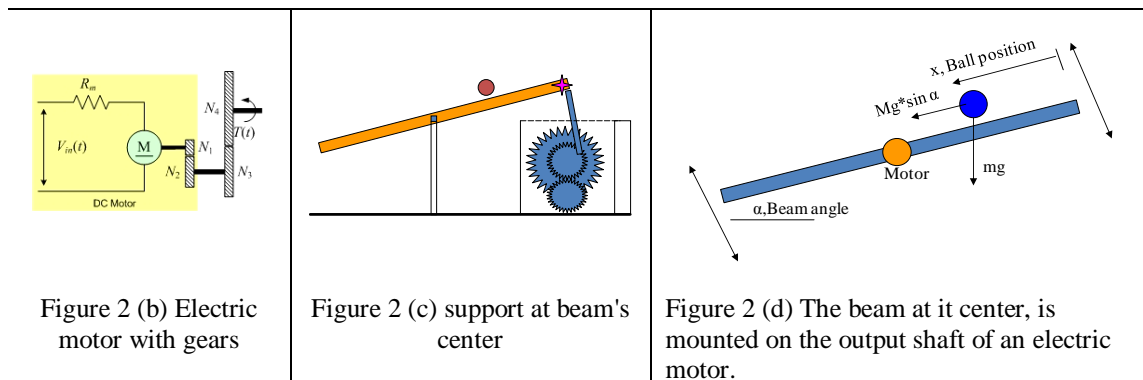


Figure 2 (b) Electric motor with gears

Figure 2 (c) support at beam's center

Figure 2 (d) The beam at its center, is mounted on the output shaft of an electric motor.

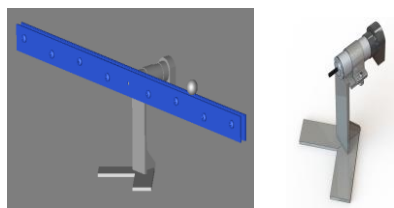


Figure 2 (e) 3-D CAD model

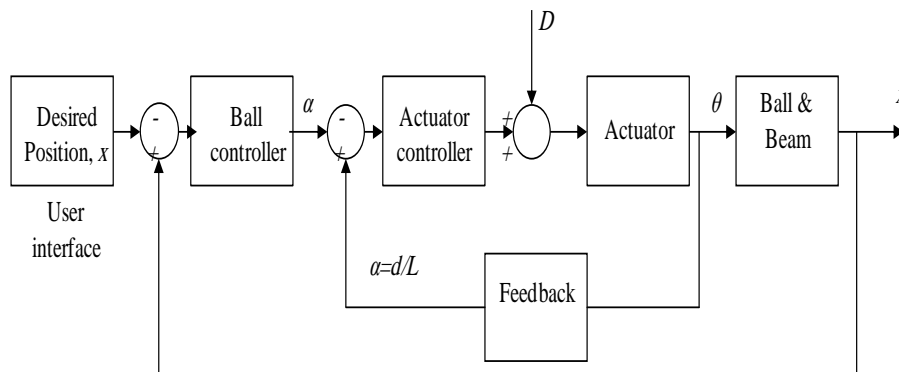


Figure 2 (f) system block diagram

Table 3 mechanical system parts, type of joints materials and dimensions

	Value:	Unit
System dimensions	Height	40 Cm
	Width	30 Cm
	Length	50 Cm
Beam	Shape & material	V-grooved ,steel
	Beam mass, m	1.5 kg
	Beam length, L	40 cm
Ball	Shape & material	Steel
	Radius	0.015 m
	Mass, M	0.111 kg
Transmission	Outer gear radius	0.03 m
	Overall gear ratio	n
Joints	Revolute joint	-
Support	Steel bar	-
Type of joints	Revolute joints	3J
Base, Frame		

4.2. Controller and control algorithm selection

Due to fact that Ball and beam system is double integrator (two poles at the origin) system, the behavior of moving Ball on a beam is behavior of open loop unstable system, in order to stabilize the double integrator and open-loop unstable ball and beam system, a special control system is to be designed. The control of unstable systems is critically important to many of most difficult control problems and must be studied in laboratory, the problem is that real unstable systems are usually dangerous and can not brought in laboratory, such unstable systems include; the control model in the rocket or aircraft toppling control system during vertical take-off, it is the control where a feedback system is used to prevent rocket or aircraft to topple out of balance during launch by forces and moments that could perturb the vertical motion, the angle of thruster jets or diverters must be continually controlled to prevent the rocket tumbling or aircraft tipping [2-4]. The ball and beam system was developed to resolve this paradox, it is simple, safe mechanism and yet it has the important dynamic features of unstable system [2],.

Control algorithm selection is the most critical decision in the Mechatronics design process, there are number of alternative control algorithm strategies that can be applied to the ball and beam system, including but not limited to ; PD control, lead compensator, Fuzzy control, Robust control, Linear quadratic Gaussian, Linear quadratic regulator. The control system task, in ball and beam system, is to continually measure and stabilize the rolling ball position a long the beam by adjusting the rotating angle of a beam (tilting it frontwards or backwards) by manipulating the angular position of the servo, in such a way that the actual position of the ball reaches desired position, this is difficult control task, because even at optimal beam position conditions the ball will swing on Beam with acceleration proportional to tilt angle, this behavior is behavior of open loop unstable system, where the system output (ball position on beam) increases without limits for fixed input (beam angle) and is a challenging design and control problem. In [5] W. Yu and F. Ortiz studied complete nonlinear model of beam and ball system and stability analysis of PD control. In [6] a designed and implemented both conventional pole-placement and neural network methods for beam and ball system are introduced. In [7] the robust nonlinear servomechanism theory was applied to design a tracking controller for beam and ball system. In [8] switching control for beam and ball system is studied. In [9] fuzzy logic controller and real time implementation of beam and ball balancing system is studied. In this paper will be introduce PD controller with deadbeat response, PID, and Lead integral compensator.

Controller selection :A vast variety of controllers (physical controller) are available in the market, embedded Microcontroller is optimal selection, since it is inexpensive single chip computer, easy to embed into larger electronic circuit designs, also, because of their versatility, Microcontrollers add a lot of power, control, and options at little cost; capable of storing and running programs, programmed to perform a wide range of control tasks. Optimal microcontroller is PICmicro Microcontroller, supplied with 5VDC.

4.3 Actuator (electric machine) selection and integration

Actuator converts an information signal from the microcontroller control unit, into energy acting on the basic system. Mechatronics systems often use electric motors to drive their work loads, the electric actuator most suitable to be used for ball and beam is DC motor, due to simple principle of working, quick instantaneous and accurate torque generation, available, inexpensive, reversible, and ease designing and implementing controller to achieve optimal instantaneous, precise motion control performance. PMDC motor turns electrical energy into mechanical energy and produces the torque required to move (rotate) the beam to the desired position, θ_L ,

Actuator placement and integration: to physically integrate Mechatronics system components, and to give the overall system safe, compact and attractive design, the selected DC motor and gears, are embedded within mechanical design and to be located on adjacent (right side, a whole system base) cuboide housing, with slots for digital user interface and input/output ports(see Figure 3).

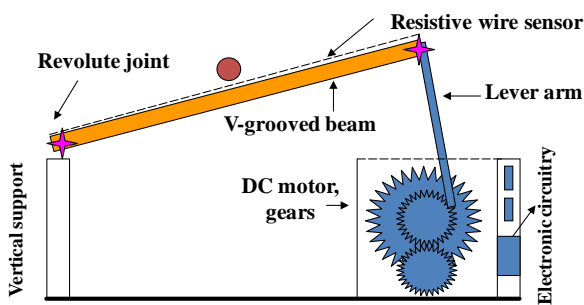


Figure 3(a)

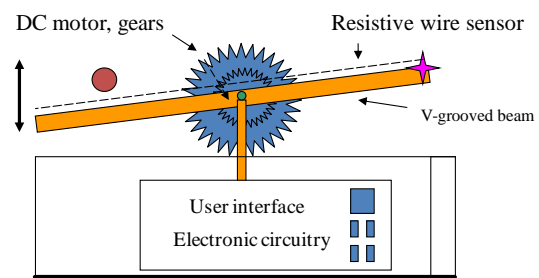


Figure 3(b)

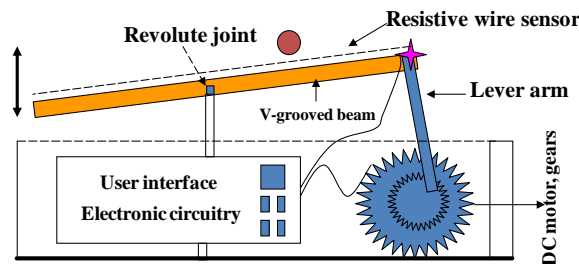


Figure 3(c)

Figure 3(a)(b)(c) Three arrangements of overall system design, components and integration

4.4 Sensor selection

Sensor converts a state variable of the basic system, into an information signal to the control unit. To calculate the error between the actual and desired positions, we need to convert the actual position, into voltage, V , and then compare this voltage with the input voltage; the difference between both is the error signal in volts. Ball and beam system, provides two outputs measurements and correspondingly two sensors, one to measure ball *translational* position, x a long the beam and other to measure motor shaft angular position θ , correspondingly, the optimal control system design requires two control loops designs, inner for motor angle control, to make motor follow the input angle and other outer loop to control the ball position on the beam, to make ball position follow the reference input position. The two angular quantities the beam angle, α and DC motor output position angle, θ are not the same, but are correlated in simple relationship, relating these two quantities result in that only one sensor can be used to measure the position. The position of the ball on the beam can be measured using a special sensor, e.g. linear Potentiometer, infrared, and a linear resistive wire, the optimal selection is linear resistive wire, to used as a position sensor and the conductive ball moving along it acting as a voltage divider (see Figure 3).

4.5 Output signal, Conditioning and Interfacing selection, design and integration

A most suitable and simple to implement drives for PMDC motor are H-bridge and IC circuit e.g.L93D. The H-bridge circuit is supplied with 12VDC and the four bits outputs of microcontroller to drive the desired conditions of electric Motor. By H-bridge four NPN Power transistors are used as switch to control the direction of current flows to the Motor, and correspondingly control the angular position of beam, selected microcontroller type is supported with ADC pins, to convert the analog input of sensor readings to digital value, fed to microcontroller. A common carrier (see Figure 3-4) for electronics, data outputting and control circuitry to be located inside the cuboid housing, that will include slots for user interface and input/output ports

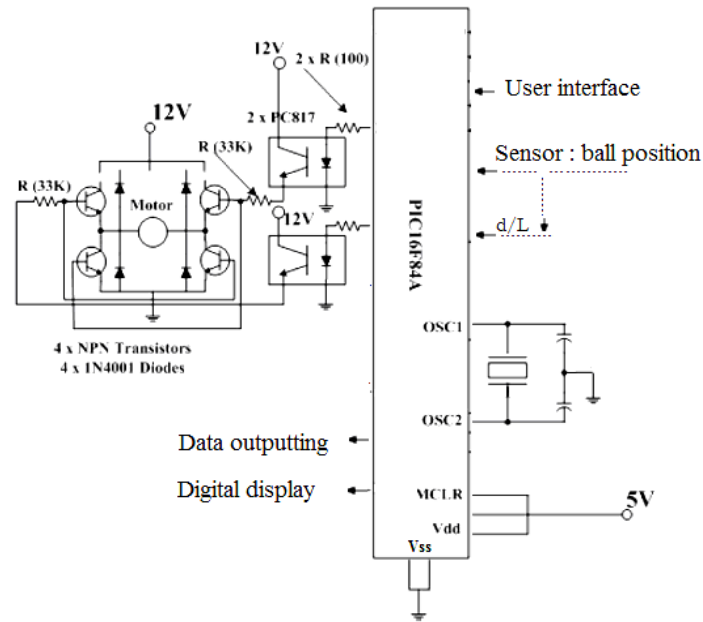


Figure 4 Microcontroller based control Circuitry and interfacing diagram

V. Modeling, simulation, analysis and evaluation

The key essential characteristics of a Mechatronics engineer are a balance between modeling/analysis skills and experimentation/hardware implementation skills. Modeling, simulation, analysis and evaluation processes in Mechatronics design consists of two levels, sub-systems models and whole system model with various sub-system models interacting similar to real situation, all engineering subsystems should be included in whole system model. Based on the specification of requirements and design, the subsystems models and the whole system model, are to be tested and analyzed, specifications to test and check whether the given design specifications are satisfied, If the specification are not satisfied,, modifications can be made, if the specifications are satisfied the model can be Optimized. The derivation of complete and accurate ball and beam system's dynamics is quite complicated, in this paper, different system designs and dynamic models will be introduced, simplified and more actual models and corresponding control system strategies selection and design. Ball and beam dynamics are shown in Figure 5.

5.1 Modeling of basic physical sub-system model with no control involved; Ball and beam balancer System Modeling

5.1.1 Ball and beam system's dynamics, basic mathematical model derivation: *sliding* ball.

In this paper, different approaches for deriving the mathematical model of ball and beam will be introduced. Based on [1] and on system arrangement shown in Figure 2(a), dynamics are shown in Figure 5. In the absence of friction or other disturbances and assuming the ball is *sliding*, the dynamics of the ball and beam system can be obtained as follows; The ball moves along the beam with acceleration, the forces that accelerate the ball as it rolls comes from the component of gravity that acts parallel to the beam. The equation of motion for the Ball is given by the following equation:

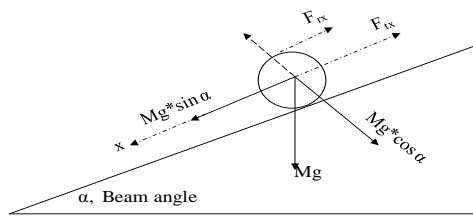


Figure 5 (a) Ball dynamics

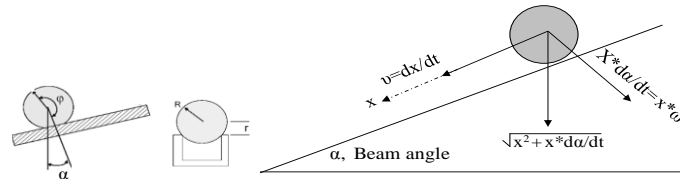


Figure 5 (b) Ball dynamics

$$\Sigma F = M * a \Leftrightarrow \Sigma F = M * g * \sin(\alpha)$$

Substituting and manipulating, gives:

$$M * \frac{d^2 x}{dt^2} = M * g * \sin(\alpha) \Leftrightarrow \frac{d^2 x}{dt^2} = g * \sin(\alpha)$$

This model can be linearized, where for small angles, $\sin(\alpha) \approx \alpha$, the model becomes:

$$\frac{d^2 x}{dt^2} = g * \alpha \tag{1}$$

This is the basic mathematical model of the ball and beam system, this simple mathematical model shows that, *the acceleration* of the ball is proportional to *the beam angle* α and to *gravity* g . Where: x : the ball position on the beam, M : the ball mass. to write an approximated *overall transfer function* of the ball and beam system, that relates *the input voltage and measured output acceleration*, we need to replace the beam angle α , by control voltage, V_{in} , and replace the ball position x , by the position sensor output y , and finally Combine the actuator and sensor constants with the gravity constant, we have a single constant b , Substituting, performing Laplace transform and rearranging, we have the transfer function that relates *the input voltage and measured output acceleration*

$$\frac{d^2 y}{dt^2} = b * V_{in} \Leftrightarrow Y(s) s^2 = b * V_{in}(s) \tag{2}$$

$$\frac{Y(s)}{V_{in}(s)} = \frac{b}{s^2} \Leftrightarrow \frac{Y(s)}{V_{in}(s)} = \frac{g}{s^2}$$

Where: b : the actuator and sensor with the gravity constants. The state space representation of this approach is given by:

$$\begin{bmatrix} \dot{x}_1 \\ \dot{x}_2 \end{bmatrix} = \begin{bmatrix} 0 & 1 \\ 0 & 0 \end{bmatrix} \begin{bmatrix} x_1 \\ x_2 \end{bmatrix} + \begin{bmatrix} 0 \\ b \end{bmatrix} u$$

$$y = [1 \quad 0] \begin{bmatrix} x_1 \\ x_2 \end{bmatrix}$$

The linear model given above is good approximation of true system dynamics, all what we need is to measure the constant parameter, b , it can be obtained by measured the time taken for the ball to accelerate from one end of the beam to the other at fixed angle of the beam, the laws of motion can be then used to integrate Eq.(1) and calculate constant b . The real ball and beam system has additional dynamic components due to the motor, plus non-linear and noise components that influence its control behavior,(coulomb friction, dead zone saturation in the motor input amplifier)[4].

5.1.2 Ball and beam system's dynamics, second approach: rolling ball without slipping.

Based on system arrangement shown in Figure 2(a), Ball dynamics shown in Figure 5(b), and in the absence of friction or other disturbances and assuming the ball is *rolling* without slipping, the dynamics of the ball and beam system can be obtained as follows;

There are two forces influencing the motion of the *rolling* ball, these forces are: F_{tx} : the force due to translational motion and F_{rx} : the force due to ball rotation. The equation of motion for the Ball is given by:

$$\Sigma F = M * a = M * g * \sin(\alpha)$$

Substituting forces influencing the motion of the *rolling* ball, gives:

$$\Sigma F = F_{tx} + F_{rx} = M * g * \sin(\alpha) \tag{3}$$

Now, to find forces influencing the motion of the *rolling* ball, and substituting in Eq.(3). Force F_{tx} due to translational motion is given by:

$$F_{rx} = m\ddot{x} \tag{4}$$

The force due to ball rotation, F_{rx} is found as follows: The torque produced by the ball's rotational motion is equal to the radius of the ball, R , multiplied by the rotational force, and is given by

$$T_r = F_{rx} R$$

Also, the torque is equal to the ball's moment of inertia, J , multiplied by its angular acceleration, $d\omega_b/dt$, which then can be written as its moment of inertia multiplied by the double-derivative of its translational motion (x_b) divided by its radius, this is as shown next:

$$T_r = F_{rx} R = J \frac{d\omega_b}{dt}$$

$$T_r = F_{rx} R = J \frac{d\omega_b}{dt} = J \frac{d(v_b / R)}{dt} = J \frac{d^2(x_b / R)}{dt^2} = \frac{J}{R} \ddot{x}$$

$$F_{rx} = (J * a) / R^2$$

Substituting, the moment of inertia, J , for the ball and given by ($J=(2/5)MR^2$), we have:

$$F_{rx} = (2 / 5) M \frac{d^2 x}{dt^2} \tag{5}$$

Substituting Eq.(5) and Eq. (4), in Eq.(3) we have the basic mathematical model of ball and beam system that relates the *ball displacement* and *angular position* of the motor shaft, and given as:

$$\Sigma F = F_{ix} + F_{rx} = M * g * \sin(\alpha)$$

$$M * g * \sin(\alpha) = \left(\frac{2}{5}\right) M \frac{d^2 x}{dt^2} + M \frac{d^2 x}{dt^2}$$

Manipulating and rearranging, gives:

$$M * g * \sin(\alpha) = d^2 x / dt^2 [(2/5) M + M]$$

$$g * \sin(\alpha) = d^2 x / dt^2 [(7/5)]$$

$$(5/7) * g * \sin(\alpha) = d^2 x / dt^2$$

This model can be linearized, since for small values of angle α , $\sin(\alpha) = \alpha$, this approximation is good for angle values $-\pi/4 < \alpha < \pi/4$, sine of the angle is approximately the angle itself. Taking Laplace transform and rearranging *input* displacement, $X(s)$, over output angular position, $\alpha(s)$, of the motor shaft gives :

$$(5/7) g \alpha (s) = X(s) s^2$$

$$\frac{X (s)}{\alpha (s)} = \frac{(5 / 7) g}{s^2} \tag{6}$$

The state space representation of for this approach is given by:

$$\begin{bmatrix} \dot{x}_1 \\ \dot{x}_2 \end{bmatrix} = \begin{bmatrix} 0 & 1 \\ 0 & 0 \end{bmatrix} \begin{bmatrix} x_1 \\ x_2 \end{bmatrix} + \begin{bmatrix} 0 \\ 5 / 7 \end{bmatrix} u$$

$$y = [1 \quad 0] \begin{bmatrix} x_1 \\ x_2 \end{bmatrix}$$

The transfer function can be derived based on system arrangement shown in Figure 2(b), as follows; the beam angle controls acceleration, not position, from gravity the equation of motion for the Ball is given by:

$$\Sigma F = M * a = M * g * \sin(\alpha)$$

Assuming the ball is *rolling* without slipping, we have $r * \omega = dx/dt$, The moment of inertia of the solid ball is given by: ($J=(2/5)MR^2$). Given centripetal acceleration with rotation of the rod as $a_{centripetal} = x\alpha^2$, altogether we have:

$$\frac{d^2 x}{dt^2} - x \frac{d^2 \alpha}{dt^2} = -g \sin \alpha - \frac{2}{5} \frac{d^2 x}{dt^2}$$

By linearization, taking Laplace transform, rearranging for transfer function, gives:

$$\frac{X (s)}{\alpha (s)} = \frac{(5 / 7) g}{s^2} \tag{7}$$

5.1.3 The Lagrangian approach to the Ball and Beam system's dynamics:

In the absence of friction or other disturbances, the dynamics of the ball and beam system can be obtained by Lagrangian method based on the energy balance of the system, The Lagrangian method is utilized to derive the equation of motions for the ball and beam system in the most model based research works on the ball and beam system [6][11-13]. In order to derive the Euler-Lagrange equation, the first step is to define the kinetic and potential energy for the ball and beam. The kinetic energy of the system is given by:

$$T = T_1 + T_2 \tag{8}$$

Where T_1 and T_2 are kinetic energies of the beam and the ball, these kinetic energies include radial and circular motions. The rotational kinetic energy of the beam is given by:

$$T_1 = 0.5 J_1 a^2$$

Where: J_1 , is the moment of inertia of the beam and a is the angle velocity of the frame. The ball has kinetic energy, given by:

$$T_2 = 0.5(M x^2) * a^2 + 0.5 M v^2 + 0.5 J_b \omega^2$$

Substituting $v = R\omega$ and $J_b = (2/5) * M * R^2$, the rotational kinetic energy of the ball is given by: $0.5((2/5) * M * R^2)$, substituting, the kinetic energy of the system in Eq.(8) will give:

$$T = 0.5 ((J + M x^2) * a^2 + (7 / 5) M x^2)$$

The potential energy of the system is exhibited by the rolling ball alone, and given by:

$$P = M * g * x * \sin \alpha + 0.5 m * g * L * \sin \alpha$$

$$P = (M * g * x + 0.5 * m * g * L) \sin \alpha$$

Where m : the mass of the beam, M : the mass of the ball, L : the beam length. We can now write the Lagrangian, where the difference between kinetic and potential energy is called the Lagrange function, which is defined by (L) equation and given by:

$$L = T - P$$

Where : T is the kinetic energy and P is the potential energy in the system.

$$L = [0.5 ((J + M x^2) * a^2 + (7 / 5) M v^2)] - [(M * g * x + 0.5 * m * g * L) \sin \alpha]$$

The dynamics equation representing the variation effect of system variable is given by:

$$\frac{d}{dt} \left(\frac{\partial L}{\partial \dot{q}} \right) - \frac{\partial L}{\partial q} = Q \tag{9}$$

$$0 = \left(\frac{J}{R^2} + M \right) \frac{d^2 x}{dt^2} + M g * \sin \alpha - m * x * \alpha^2 \tag{10}$$

Where θ : the motor output position angle. α : the beam angle. x : ball coordinate position, m : beam mass . As shown in Figure 2 (a) and Figure 7, It should be considered, that *the beam angle, α , and DC motor output shaft angle, θ , are not the same*, but there is also relationship between these two angles that can be seen from Figure 6, this relation can be approximated as linear, where the distance traveled by the beam at radius equals to L , is equal to distance traveled by gear at radius, r , that is:

$$r \theta = L \alpha \Leftrightarrow \alpha = \frac{r}{L} \theta \quad \text{for } r \ll L \tag{11}$$

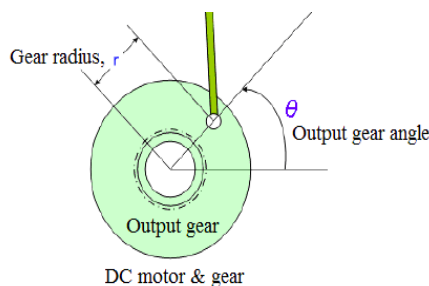


Figure 2 (a)

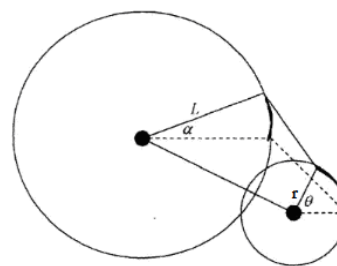


Figure 7 the beam angle, α , and DC motor output position angle, θ

Ball and beam system's dynamics in terms of ball radius R , and r : based on system arrangement shown in Figure 2 (a), dynamics shown in Figure 5, and in the absence of friction or other disturbances, we have:

$$x = r \phi \Leftrightarrow \omega = \dot{\phi} + \dot{\theta} = \frac{\dot{x}}{r} + \dot{\theta} \Leftrightarrow v = \sqrt{\dot{x}^2 + (x \dot{\theta})^2}$$

$$U = \frac{1}{2} m v^2 + \frac{1}{2} I_b \omega^2 + \frac{1}{2} I_a \dot{\theta}^2$$

Writing and substituting the Lagrangian equation, gives:

$$L = \frac{1}{2} \left\{ m [\dot{x}^2 + (x \dot{\theta})^2] + I_b \left[\frac{\dot{x}}{r} + \dot{\theta} \right]^2 + I_a \dot{\theta}^2 \right\}$$

$$\frac{d}{dt} \left(\frac{d}{dx} L \right) - \frac{d}{dx} L = m g \sin \theta$$

$$\left(m + \frac{I_b}{r^2} \right) \ddot{x} + \left(\frac{I_b}{r^2} \right) \ddot{\theta} - m x \dot{\theta}^2 = m g \sin \theta$$

$$\left(m + \frac{I_b}{r^2} \right) \ddot{x} = m g \theta$$

Taking Laplace transform, Substituting $I_b = (2/5)MR^2$, and manipulating for transfer function gives:

$$G(s) = \frac{X(s)}{\Theta(s)} = \frac{mg}{m + \frac{I_b}{r^2}} \frac{1}{s^2} = \frac{mg}{m + \frac{2mR^2}{5r^2}} \frac{1}{s^2} = \frac{g}{1 + \frac{2}{5} \left(\frac{R}{r} \right)^2} \frac{1}{s^2}$$

The transfer function in terms of input gear angle, θ , to output ball position, X , also can be written as follows: Linearization of Eq.(10) about the beam angle, $\alpha=0$, gives

$$0 = \left(\frac{J}{R^2} + M \right) \frac{d^2 x}{dt^2} + M g \sin \alpha - m x \alpha^2$$

$$\left(\frac{J}{R^2} + M \right) \frac{d^2 x}{dt^2} = -M g \alpha$$

Linearization of this equation, substituting Eq.(11) taking Laplace transforms, and manipulating for transfer function gives:

$$\left(\frac{J}{R^2} + M \right) \frac{d^2 x}{dt^2} = -M g \alpha \Leftrightarrow \frac{X(s)}{\Theta(s)} = \frac{M g}{L \left(\frac{J}{R^2} + M \right)} \frac{1}{s^2}$$

The state space representation of this model is given below, here it is important to notice in these models, that by combining the ball radius R , and r constants with the gravity constant, g , we have a single constant b , this will give the basic transfer function model previously obtained, this is shown in below comparison of different approaches for model derivations:

$$\begin{aligned} \begin{bmatrix} \dot{x}_1 \\ \dot{x}_2 \end{bmatrix} &= \begin{bmatrix} 0 & 1 \\ 0 & 0 \end{bmatrix} \begin{bmatrix} x_1 \\ x_2 \end{bmatrix} + \begin{bmatrix} 0 \\ \frac{mgd}{L \left(\frac{J}{R^2} + m \right)} \end{bmatrix} \theta \Leftrightarrow \begin{bmatrix} \dot{x}_1 \\ \dot{x}_2 \end{bmatrix} = \begin{bmatrix} 0 & 1 \\ 0 & 0 \end{bmatrix} \begin{bmatrix} x_1 \\ x_2 \end{bmatrix} + \begin{bmatrix} 0 \\ b \end{bmatrix} u \Leftrightarrow \begin{bmatrix} \dot{x}_1 \\ \dot{x}_2 \end{bmatrix} = \begin{bmatrix} 0 & 1 \\ 0 & 0 \end{bmatrix} \begin{bmatrix} x_1 \\ x_2 \end{bmatrix} + \begin{bmatrix} 0 \\ g \end{bmatrix} u \\ y &= \begin{bmatrix} 1 & 0 \end{bmatrix} \begin{bmatrix} x_1 \\ x_2 \end{bmatrix} & y &= \begin{bmatrix} 1 & 0 \end{bmatrix} \begin{bmatrix} x_1 \\ x_2 \end{bmatrix} & y &= \begin{bmatrix} 1 & 0 \end{bmatrix} \begin{bmatrix} x_1 \\ x_2 \end{bmatrix} \\ \frac{X(s)}{\theta(s)} &= \frac{M g d}{L \left(\frac{J}{R^2} + M \right)} \frac{1}{s^2} \Leftrightarrow \frac{X(s)}{\theta(s)} = \frac{b}{s^2} \quad \text{and} \quad \frac{X(s)}{\Theta(s)} = \frac{g}{1 + \frac{2}{5} \left(\frac{R}{r} \right)^2} \frac{1}{s^2} \Leftrightarrow \frac{X(s)}{\theta(s)} = \frac{b}{s^2} \end{aligned}$$

The transfer function between the ball position and rotor angle can be obtained based on basic transfer function

$$\frac{Y(s)}{V_{in}(s)} = \frac{b}{s^2} = \frac{g}{s^2} \quad \text{and on relation given by Eq.(11), and given by}$$

$$\frac{Y(s)}{V_{in}(s)} = \frac{r g}{L s^2} = \frac{r g}{L} \frac{1}{s^2}$$

5.2 MATLAB/Simulink representation, simulation and analysis

The loop system Simulink models for the simplified models is shown in Figure 8. The Simulink model of mathematical model given by Eq.(6) is the same as Simulink model shown in Figure 8, but the constant b , now is more accurately defined and is given by $(5/7)*g$, the Simulink model of open loop ball and beam system is shown in Figure 8(c), The system response using MATLAB, can be found using the following codes

```
>> g=9.8; num=[5*g/7]; den=[1 0 0]; G_open=tf(num,den); printsys(num,den); step(num,den); [A,B,C,D]=tf2ss(num,den); figure, step(A,B,C,D)
```

Now, Based on [14], the nonlinear Lagrangian equation of motion is directly modeled, where Eq.(10) gives $d(x)/dt$ as a function of the state and input variables, x , $d(x)/dt$, α , and $d(\alpha)/dt$. The reference made use of the nonlinear function block to express this function; the function takes the input vector $u=[x \ dx/dt \ \alpha \ da/dt]$ and returns d^2x/dt^2 , where each component is referred to as $u[1]$, $u[2]$, etc, and correspondingly, $u[1]=x$, $u[2]=d(x)/dt$, $u[3]=\alpha$, and $u[4]=d(\alpha)/dt$, the function is given by:

$$\frac{d^2 x}{dt^2} = (-1 / (J / R^2 + M)) (M g \sin \alpha - M x \frac{d^2 \alpha}{dt^2})$$

And can be written in MATLAB as:

$$(-1/(J/(R^2)+m))*(m*g*\sin(u[3])-m*u[1]*(u[4])^2)$$

This model is shown in Figure 9 (a), first it is required, to define ball mass m , Ball radius, R , beam length, L , gear radius, r , and ball's moment of inertia J , (e.g. $m=0.111$; $R=0.015$; $g=-9.8$; $L=0.6$; $d=0.03$; $J=9.99e-6$). Running all Simulink models for derived system's models, when subjected to random input, will result in the same position, speed and acceleration response curves shown in Figure 10(a). In Figure 10(b) is shown ball position and acceleration open loop response when subjected to step input.

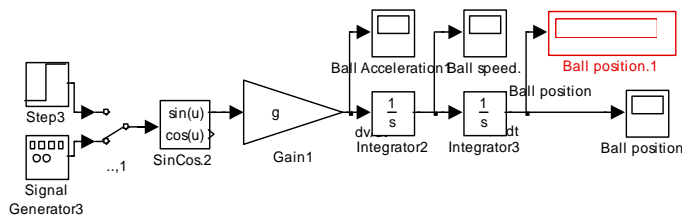


Figure 8(a) Simulink model of simplified representation

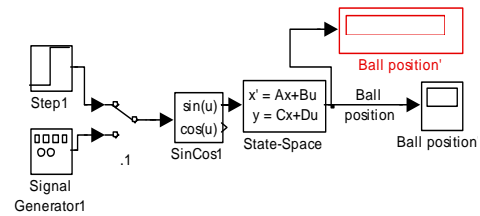


Figure 8(b) Simulink model of state space representation

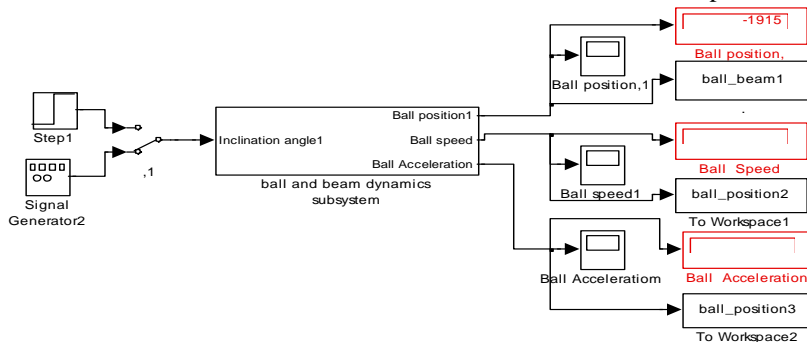


Figure 8(c) Simulink mode of open loop ball and beam sub-system

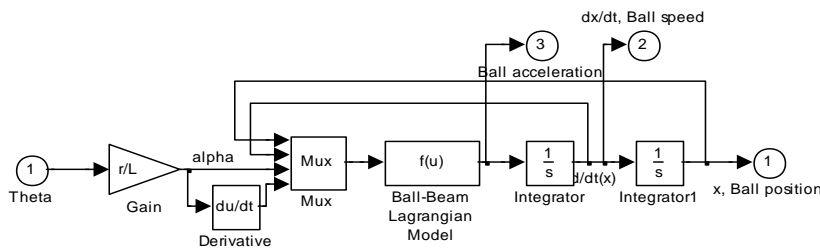


Fig. 9 (a) The nonlinear Lagrangian equation of ball and beam open loop motion sub-system model

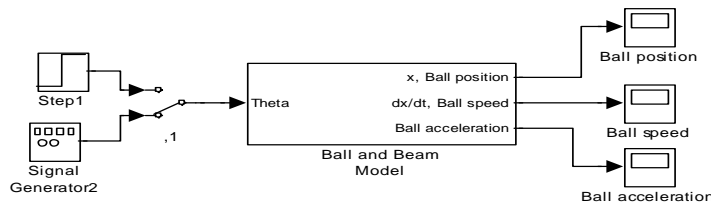
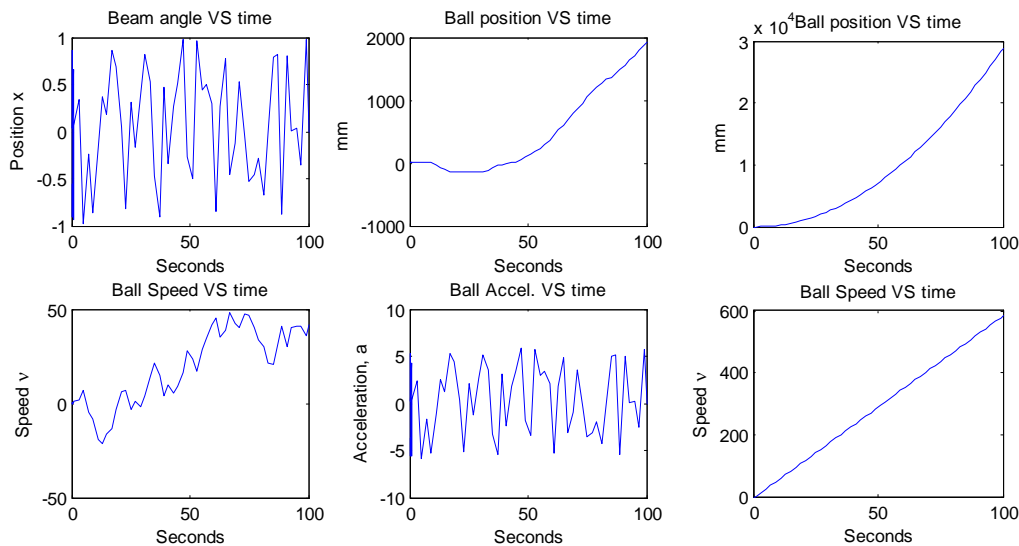


Figure 9 (b) The ball and beam sub-system open loop model and subsystem.



(a) Response for randomly changing input (b) Response for step input
Figure 10 open loop, ball position/time, speed/time and acceleration/time response curves

The next MATLAB code can be used to define system's parameters in MATLAB and return transfer function and open loop step response

clc, clear all

```
M=input('Enter mass of the ball, M = ');
m=input('Enter mass of the beam, m = ');
R=input('Enter radius of the ball, R = ');
d=input('Enter lever arm offset , d = ');
L=input('Enter length of the beam , L = ');
J=input('Enter ball"s moment of inertia , J= ');
g= -9.8; % gravitational acceleration
s = tf([1 0],1); G_open1 = -(M*(g)*d)/(L*((J/R^2)+ M)*s^2); step(G_open1)
% another simplified way of obtaining the transfer function
K = (M*(g*d)/(L*(J/R^2+M))); num = [-K]; den = [1 0 0]; G_open2 =tf(num,den); step(G_open2); [A,B,C,D]=
tf2ss(num,den); step(A,B,C,D);
% Obtaining closed loop transfer function with unity feedback , no gain
G_close=feedback(G_open1,1); axis([1,100,0,2]);
title ('step response of closed loop system with H(s)=1 ')
```

5.3 Modeling of actuator sub-system dynamics

The DC motor is an example of electromechanical systems with electrical and mechanical components, a simplified equivalent representation of DC motor's two components with gears attached are shown in Figure 2(c) up . DC motor turns electrical energy into mechanical energy and produces the torque required to move the beam to the desired angular position, θ_L , [15]. In [16] a detailed derivation of DC motor electric and mechanical parts dynamics are introduced. Based on the Newton's law combined with the Kirchoff's law, the mathematical model in the form of differential equations describing dynamics characteristics of the armature controlled PMDC motor can be derived, and correspondingly DC motor transfer function open loop transfer function without any load attached relating the input voltage, $V_{in}(s)$, to the motor shaft output angle, $\theta_m(s)$, to be given by:

$$G_{angle}(s) = \frac{\theta(s)}{V_{in}(s)} = \frac{K_t / n}{s \left[(L_a s + R_a)(J_m s + b_m) + K_t K_b \right]} \tag{12}$$

$$V_{in}(s) = \frac{K_t / n}{\left\{ \left[L_a J_m s^3 + (R_a J_m + b_m L_a) s^2 + (R_a b_m + K_t K_b) s \right] \right\}}$$

The PMDC motor open loop transfer function relating the input voltage, $V_{in}(s)$, to the angular velocity, $\omega(s)$, given by:

$$G_{speed}(s) = \frac{\omega(s)}{V_{in}(s)} = \frac{K_t / n}{\left\{ \left[(L_a J_m s^2 + (R_a J_m + b_m L_a) s + (R_a b_m + K_t K_b) \right] \right\}} \tag{13}$$

Modeling nonlinearities: Coulomb friction is a non-linear element in which forces tend to appose the motion of bodies in contact in mechanical systems, it acts as disturbance torque feedback for the mechanical system, Coulomb friction is considered to be a constant retarding force but is discontinuous over zero crossings, that is, when a DC motor reverses direction it must come to a stop at which point Coulomb friction drops to zero and then opposes the reversed direction. In effect Coulomb friction is constant when rotational velocity is not zero. Based on differential equations describing mechanical characteristics of DC motor; the sum of the torques must equal zero, we have:

$$\sum T = J * \alpha = J * d^2 \theta / dt^2$$

Coulomb friction and dead zone friction, where ($T_{load} = 0$), we have:

$$K_t * i_a = T_a + T_\omega + T_{load} + T_f$$

Where: i_a armature current, K_t : torque constant, T_f : Coulomb friction torque, taking Laplace transform:

$$K_t * I(s) - J_m * s^2 \theta(s) - b_m * s \theta(s) - T_f = 0$$

At steady state conditions, $d/dt = 0$, gives:

$$K_t * i_a = - b * \omega - T_f$$

5.4 Simplification of open loop PMDC motor system transfer functions models.

Referring to [16] and based on the fact that, the PMDC motor response is dominated by the *slow* mechanical time constant, where the electric time constant is much faster (e.g. ten times) than the mechanical time constant, this can motivate us to assume that the armature inductance, L_a is low compared to the armature resistance, R_a . neglecting motor inductance, ($L_a = 0$), will result in the following simplified first order form of PMDC motor transfer function in terms input voltage, $V_{in}(s)$ and output speed, $\omega_m(s)$ given by:

$$G_{speed}(s) = \frac{\omega(s)}{V_{in}(s)} = \frac{K_t}{\{(R_a J_m)s + (R_a b_m) + K_t K_b\}}$$

Rearranging this first order equation into standard first order transfer function form yields:

$$G_{speed}(s) = \frac{\omega(s)}{V_{in}(s)} = \frac{K_b K_t}{(R_a b + K_t K_b)} / \left[\left(\frac{R_a J}{(R_a b + K_t K_b)} \right) s + 1 \right] = \frac{K_B}{\tau s + 1} \tag{14}$$

A simplified first order form of PMDC motor transfer function in terms of output angle can also be obtained by substituting ($L_a = 0$), and given by:

$$\frac{\theta(s)}{V_{in}(s)} = \frac{K_t / n}{\{[L_a J_m s^3 + (R_a J_m + b_m L_a) s^2 + (R_a b_m + K_t K_b) s]\}} \Rightarrow \frac{K_t}{[R_a J_m s^2 + (R_a b_m + K_t K_b) s]} = \frac{\frac{K_t}{R_a J_m}}{s \left[s + \frac{1}{J_m} \left(b_m + \frac{K_t K_b}{R_a} \right) \right]} = \frac{K}{s(s+a)} \tag{15}$$

by substituting, ($L_a = 0$), motor equation can be simplified to first and second order system relating input voltage and output angle, as well as equation relating input voltage and output speed, to be given by:

$$G_{angle}(s) = \frac{\theta(s)}{V_{in}(s)} = \frac{K_t}{s(R_a J_m s + K_t K_b)}, \quad G_{speed}(s) = \frac{\omega(s)}{V_{in}(s)} = \frac{K_t}{(R_a J_m s + K_t K_b)}$$

The transfer function relating input voltage and output angle can be more simplified to have the next form:

$$G_{angle}(s) = \frac{\theta(s)}{V_{in}(s)} = \frac{1}{s \left[\left(\frac{s J_m R_a}{n * K_b} \right) + n * K_t \right]}$$

The geometry of the mechanical part determines the moment of inertia, the total equivalent inertia, J_{equiv} and total equivalent damping, b_{equiv} at the armature of the motor with gears attaches, are given by Eq.(16), The inertias of the gears, sensor, beam and ball have to be included in the calculations of total equivalent inertia and damping, for simplicity are given by Eq.(17):

$$b_{equiv} = b_m + b_{Load} \left(\frac{N_1}{N_2} \right)^2 \Leftrightarrow J_{equiv} = J_m + J_{Load} \left(\frac{N_1}{N_2} \right)^2 \tag{16}$$

$$J_{load} = J_{beam} + J_{ball} \Leftrightarrow J_{load} = (m l^2) / 12 + (2 * M * R^2) / 5 \tag{17}$$

5.4.1 DC motor sub-system simulation and analysis.

The derived mathematical models of DC motor, simplified and more actual, can be represented in Simulink, as shown in Fig 11, with applied input voltage and output angular position, angular speed, current and torque; where in Figure 11 (a) is shown Simulink model of more accurate DC motor mathematical model

and the corresponding function block window is shown in 11(b). The Simulink model of simplified mathematical model of DC motor is shown Fig 11(c) and the corresponding function block window is shown in Figure 11 (d). These models can be used to analyze and evaluate DC motor sub-system performance, as well as, designed control system. Defining in MATLAB DC motor parameters used, and running the Simulink model will return angular position,/time, angular speed/time, current/time and torque/time response curves shown in Figure 11 (e). The following code can be used to plot response curves:

```
load Motor ,load Motor1,load Motor2,load Motor3,subplot(2,2,1),plot( motor_angle ), xlabel(' Seconds'),ylabel(' Position \theta'),title(' Shaft angular position VS time '), grid,subplot(2,2,2),plot( motor_speed ), xlabel(' Seconds'),ylabel(' Speed \omega '),title(' Shaft angular Speed VS time '), grid, subplot(2,2,3),plot( motor_torque ), xlabel(' Seconds'),ylabel(' Torque N.m'), title(' Torque VS time '), grid, subplot(2,2,4),plot( motor_current ), xlabel(' Seconds'),ylabel(' Current Amp'),title(' Current VS time '), grid,
```

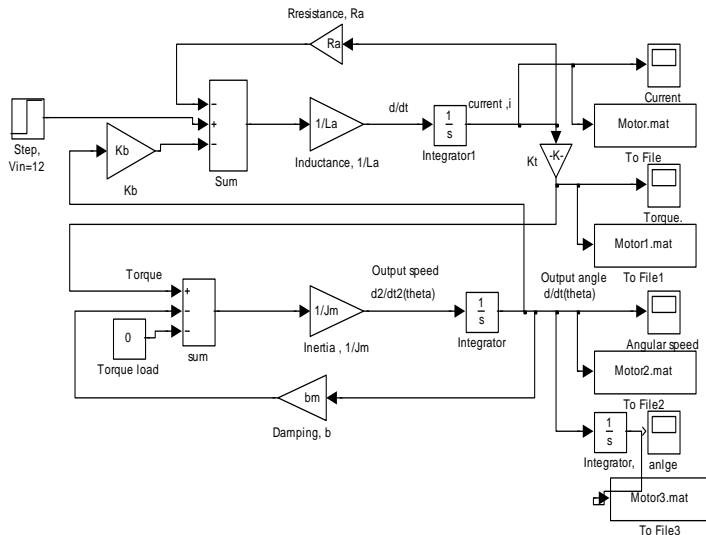


Figure 11 (a) DC motor simulink model

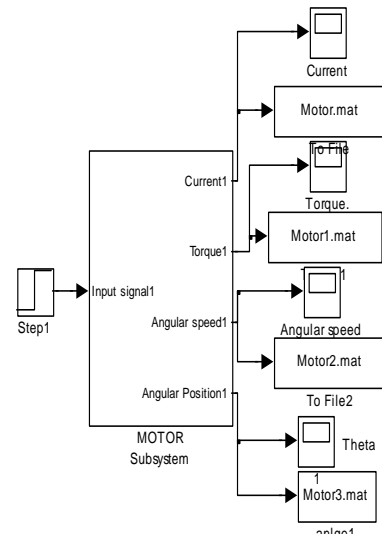


Figure 11 (b) function block model

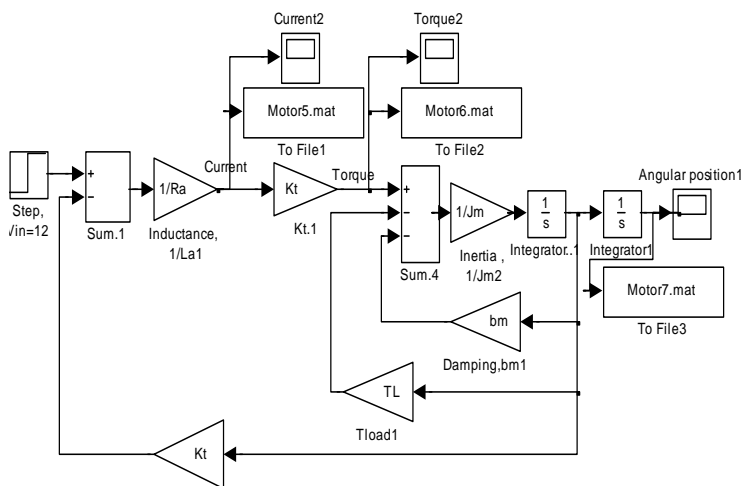


Figure 11 (c) Simplified DC motor Simulink model

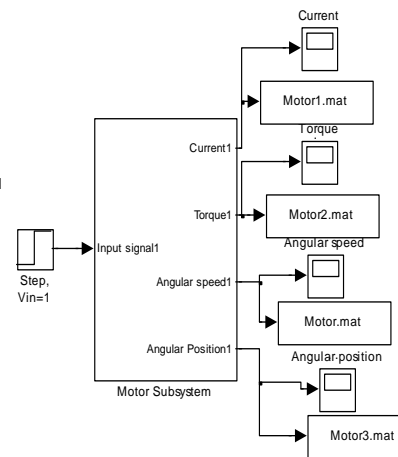


Figure 11 (d) function block model

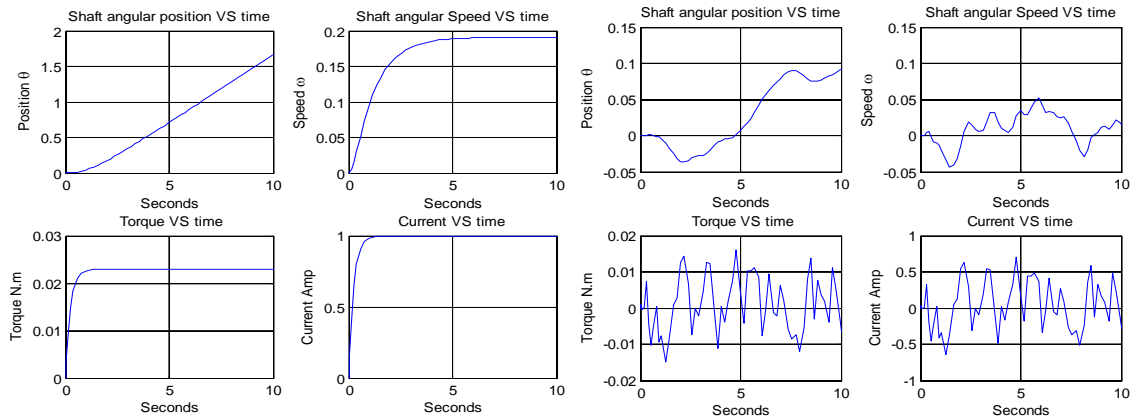


Figure 11 (e) DC motor position,/time, angular speed/time, current/time and torque/time , both for step and random response curves

5.4.2 Overall Ball and beam open loop system simulation and analysis

As shown in Figure 12(a), building overall Ball and beam open loop system Simulink model, can be accomplished by connecting ,in series, both open loop transfer functions of DC motor and ball and beam sub-systems, given by Eqs.(18) .all three proposed DC motor Simulink models, can be merged in one function block model shown in Figure 12(b), that can be connected to ball and beam subsystem model, and any DC motor model can be activated by using Simulink manual switches, based on all this, the open loop Simulink model of ball and beam system will have the form shown in Figure 12(c). Depending on required accuracy, selected control system type, algorithm and design requirement, the input signal can be connected to any of three DC motor models. This proposed open loop ball and beam model gives designer readings (numerical and graphical) about both sub-systems' dynamics, ball and beam as well as, DC motor subsystems. By defining in MATLAB, both DC motor and ball and system parameters, and running the Simulink model will return the following response curves of DC motor : angular position,/time, angular speed/time, current/time and torque/time response curves, and the following response curves of ball system: ball position,/time, ball speed/time, ball acceleration/time responses, applying random input signal (to mimic ball position and corresponding shaft angle response) will result in all these response curves are shown in Figure 12(d)

$$G_{open}(s) = \frac{K_t / n}{(L_a s + R_a)(J_{equiv} s^2 + b_{equiv} s) + (L_a s + R_a)(T) + K_b K_t} \Leftrightarrow G(s) = \frac{X(s)}{\Theta(s)} = \frac{g}{1 + \frac{2}{5} \left(\frac{R}{r}\right)^2 s^2} \quad (18)$$

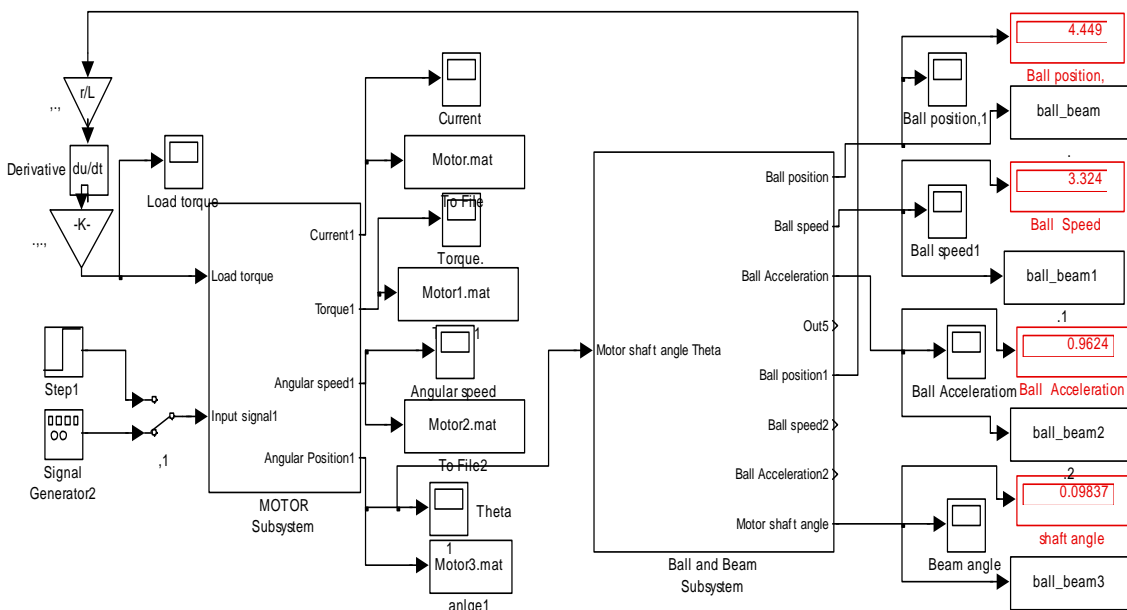


Figure 12(a) Open loop simulink model of ball and beam system.

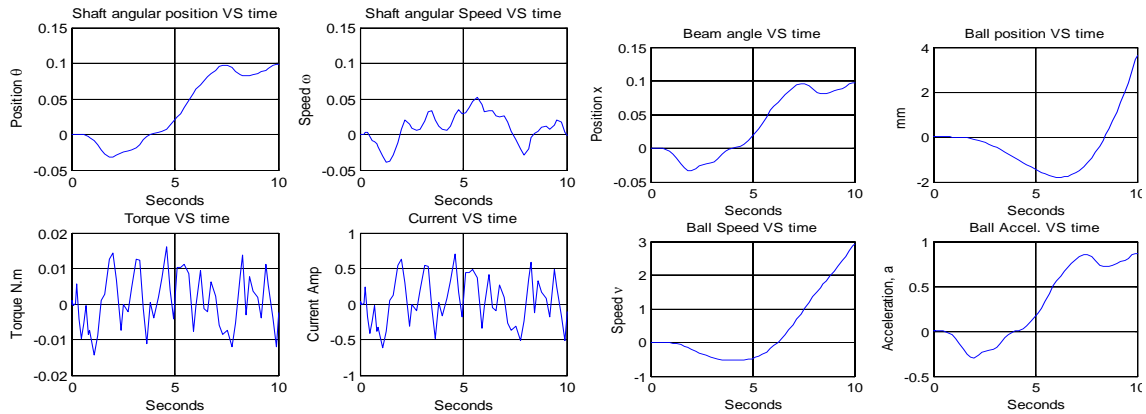


Figure 12 (d) angular position,/time, angular speed/time, current/time and torque/time response curves of used DC motor and ball position,/time, ball position,/time, ball speed/time, ball acceleration/time responses, both for random input.

5.5 Control system selection, modeling, design, and simulation

Due to fact that it is double integrator (two poles at the origin) system and is open-loop unstable, in order to stabilize the system a special control system is to be designed. Ball and beam system, provides two outputs measurements and correspondingly two sensors one to measure ball *translational* position, x , and other to measure motor shaft angular position, θ . Correspondingly, the control system design requires two control loops design, inner for motor angle control, to make motor follow the input angle and other outer loop to control the ball position on the beam, to make ball position follow the reference input position. These controllers can be designed as one or separately, mainly if the motor system is required to be faster than the beam controller.

5.5.1 Proportional Derivative, PD- controller:

The transfer function of PD-controller is given by Eq.(19), Rearranging, we have the form given by Eq.(20):

$$G_{PD}(s) = K_p + K_D s \tag{19}$$

$$G_{PD}(s) = K_p + K_D s = K_D [s + (K_p / K_D)] = K_D (s + Z_{PD}) \tag{20}$$

The PD-controller is equivalent to the addition of a *simple zero* at $Z_{PD} = K_p / K_D$. The addition of zeros has the effect of improving the transient response

Systems design with prefilter: Prefilter is defined as a transfer function $G_p(s)$ that filters the input signal $R(s)$ prior to calculating the error signal. Adding a control system to plant, will result in the addition of poles and/or zeros, that will effect the response, mainly the added zero, will significantly inversely effect the response and should be cancelled by prefilter, therefore the required prefilter transfer function to cancel the zero is given by (21).

$$G_{Prefilter}(s) = Z_o / (s + Z_o) \tag{21}$$

5.5.2 Inner Motor PD controller loop with deadbeat response

Often, the goal for a control system is to achieve a fast response to a step command with minimal overshoot. Deadbeat response means the response that proceeds rapidly to the desired level and holds at that level with minimal overshoot. The characteristics of deadbeat response include; Zero steady state error, Fast response, (short rise time and settling time) , percent overshoot greater or equal to 0.1% and less or equal 2 % and minimal undershoot, less than $\pm 2\%$ error band. In controller design for deadbeat response approach, the controller's coefficients,(controller gains, poles and zeros), depend on the physical parameters of the system. To determine the optimal coefficients, that yield the optimal deadbeat response, the system's overall equivalent closed-loop transfer function, $T(s)$ is compared with standard, of corresponding order, and normalized transfer function, (particularly the characteristic equations are compared) .These coefficients were selected to achieve deadbeat response and minimize settling time T_s and rise time, T_R to 100% of the desired command. The desired Standard second order closed-loop transfer function for achieving desired deadbeat response specifications is given by Eq.(22):

$$T(s) = \frac{\omega_n^2}{s^2 + \alpha \omega_n s + \omega_n^2} \tag{22}$$

Based on [18], the following derivation and design for PD controller with desired deadbeat response specifications in terms of desired output angular position. Considering that system dynamics and disturbance torques depends on application shape and dimensions (robot arm, conveyer etc), the mechanical DC motor part, will have the form:

$$K_t * i_a = T_a + T_\omega + T_{load} + T_f$$

The coulomb friction can be found at steady state, to be: ($K_t * i_a - b * \omega = T_f$). In the following calculation the disturbance torque, T, is all torques including coulomb friction, and given by: $T = T_{load} + T_f$. Applying PD controller with deadbeat response design for output desired output angular position, the open-loop transfer function of the PMDC, is given by:

$$G_{open}(s) = \frac{K_t / n}{(L_a s + R_a)(J_m s^2 + b_m s) + (L_a s + R_a)(T) + K_b K_t}$$

Manipulating for forward and closed loop transfer functions, including disturbance torques, sensor and gear ratio, gives:

$$G_{open}(s) = \frac{K_t}{(L_a s + R_a)(J_m s^2 + b_m s) + (L_a s + R_a)(T) + K_b K_t} = \frac{n K_{pot} K_t}{L_a J_m s^3 + (R_a J_m + b_m L_a) s^2 + (R_a b_m + L_a T) s + (R_a T + K_b K_t)}$$

$$G_{open}(s) = \frac{n K_{pot} K_t}{T J_m s^3 + (T_a R_a + T) s^2 + (R_a T + K_b K_t) T} = \frac{n K_{pot} K_t K_D s + n K_{pot} K_t K_P}{L_a J_m s^3 + (R_a J_m + b_m L_a) s^2 + (R_a b_m + L_a T) s + (R_a T + K_b K_t)}$$

$$G_{closed}(s) = \frac{n K_{pot} K_t K_D s + n K_{pot} K_t K_P}{L_a J_m s^3 + (R_a J_m + b_m L_a) s^2 + (R_a b_m + L_a T + n K_{pot} K_t K_D) s + R_a T + K_b K_t + n K_{pot} K_t K_P}$$

$$G_{closed}(s) = \frac{L_a J_m}{s^3 + \frac{(R_a J_m + b_m L_a)}{L_a J_m} s^2 + \frac{(R_a b_m + L_a T + n K_{pot} K_t K_D)}{L_a J_m} s + \frac{(R_a T + K_b K_t + n K_{pot} K_t K_P)}{L_a J_m}}$$

Comparing with standard normalized third order system and manipulating, for K_D and K_P , given by Eq.(22)

$$\text{by: } T(s) = \frac{\omega_n^3}{s^3 + \alpha \omega_n s^2 + \beta \omega_n^2 s + \omega_n^3} \Leftrightarrow \beta \omega_n^2 = \frac{(R_a b_m + L_a T + n K_{pot} K_t K_D)}{L_a J_m} \Leftrightarrow K_D = \frac{\beta \omega_n^2 L_a J_m - (R_a b_m + L_a T)}{n K_{pot} K_t}$$

$$\omega_n^3 = \frac{(R_a T + K_b K_t + n K_{pot} K_t K_P)}{L_a J_m} \Leftrightarrow K_P = \frac{\omega_n^3 L_a J_m - (R_a T + K_b K_t)}{n K_{pot} K_t}$$

For design consideration, and based on required design accuracy we can use the simplified second order model, assuming $L_a = 0$, and manipulating for closed loop with PD controller, gives:

$$G_{angle}(s) = \frac{\theta(s)}{V_{in}(s)} = \frac{K_t}{\left\{ \left[L_a J_m s^3 + (R_a J_m + b_m L_a) s^2 + (R_a b_m + K_t K_b) s \right] \right\}} \Leftrightarrow G_{angle}(s) = \frac{\frac{K_t}{R_a J_a}}{s \left[s + \frac{1}{J_m} \left(b_m + \frac{K_t K_b}{R_a} \right) \right]}$$

$$G_{angle}(s) = \frac{\theta(s)}{V_{in}(s)} = \frac{n K_t}{s \left[(R_a J_m) s^2 + (R_a b_m + K_t K_b) \right]} \Leftrightarrow G_{forward}(s) = \frac{\theta(s)}{V_{in}(s)} = \frac{K_t K_P + K_t K_D s}{s \left[(R_a J_m) s + (R_a b_m + K_t K_b) \right]}$$

$$G_{closed}(s) = \frac{\theta(s)}{V_{in}(s)} = \frac{n K_t K_P + n K_t K_D s}{s \left[(R_a J_{equiv}) s + (R_a b_{equiv} + K_t K_b + n K_{pot} K_t K_D) \right] + n K_{pot} K_t K_P}$$

Comparing with standard normalized second order system and manipulating, for K_D and K_P , gives :

$$G_{closed}(s) = \frac{\frac{n K_t K_P + n K_t K_D s}{(R_a J_{equiv})}}{s^2 + \left(\frac{R_a b_{equiv} + K_t K_b + n K_{pot} K_t K_D}{R_a J_{equiv}} \right) s + \frac{n K_{pot} K_t K_P}{(R_a J_{equiv})}} = \frac{\omega_n^2}{s^2 + \alpha \omega_n s + \omega_n^2}$$

$$\alpha \omega_n = \frac{R_a b_{equiv} + K_t K_b + n K_{pot} K_t K_D}{R_a J_{equiv}} \Leftrightarrow K_D = \frac{\alpha \omega_n R_a J_{equiv} - (R_a b_{equiv} + K_t K_b)}{n K_{pot} K_t}$$

$$\omega_n^2 = \frac{nK_{pot}K_tK_p}{(R_aJ_{equiv})} \Leftrightarrow K_p = \frac{R_aJ_{equiv}\omega_n^2}{nK_{pot}K_t}$$

$$Z_{PD} = \frac{K_p}{K_D}$$

Referring to [18] The controller gains K_p and K_D depend on the physical parameters of the actuator drives, to determine gains that yield optimal deadbeat response, the overall closed loop transfer function $T(s)$ is compared with standard second order transfer function given by (22), and knowing that parameters α and ω_n are known coefficients of system with deadbeat response given by [13], $\alpha = 1.82$ and $\omega_n T_n = 4.82$, $T_n = 2$ and gives the following: $\omega_n T_n = 4.82$, $\omega_n = 4.82/2 = 2.41$. In [18] to simplify and accelerate Mechatronics design process, a new MATLAB built-in function with specific purpose, which is design and verification for desired deadbeat response specification, particularly for desired settling time. The presented built-in function is named `deadbeat(a)`, the input argument `a`, can have the value of 1 or 2. The input argument 2 for controlling electric motor system output angular displacement with PD-controller design for deadbeat response with desired settling time, this new built in function determines the coefficients (gains pole and zero) that yield the optimal deadbeat response for desired output speed or angle control, as well as performance specifications in terms of M_p , E_{ss} , T_s , final output value.

5.5.3 Inner Motor PD Position control loop with position and rate feedback

Considering the output position control, applying position and *rate* feedback (see Figure 13(b)), to have the motor follow the desired output angle, the input voltage to DC motor will be given by Eq.(23).

Rearranging, we have Eq.(24):

$$V_i = K_p [\theta_i - \theta_o] - K_D \omega \Leftrightarrow V_i = K_p [\theta_i - \theta_o] - K_D s \theta_o \tag{23}$$

$$V_i = K_p \theta_i - K_p \theta_o - K_D s \theta_o \tag{24}$$

$$V_i = K_p \theta_i - (K_p + K_D s) \theta_o$$

Finding the overall equivalent closed loop transfer function, and comparing with corresponding standard transfer function (second or third order), and by comparison, we can find the gains K_p and K_D depending on motor parameters and desired damping ratio, ζ and settling time, T_s . Standard second order system, in terms of ζ and ω_n , is given by Eq.(25):

$$T(s) = \frac{\theta_{out}}{\theta_{desired}} = \frac{\omega_n^2}{s^2 + 2\zeta\omega_n s + \omega_n^2} \tag{25}$$

Assuming the constrains for this system are to be, desired damping ratio of 0.707, or overshoot and Peak time of $T_p = 0.1$ second, we find undamped natural frequency ω_n , and correspondingly K_p , K_D

$$\zeta = \frac{-\ln(\%OS / 100)}{\sqrt{\pi^2 + \ln^2(\%OS / 100)}}, \quad T_p = \frac{\pi}{\omega_n \sqrt{1 - \zeta^2}}$$

From, the DC motor transfer function, depending on desired accuracy, and correspondingly applied mathematical model, and by substituting the value of V_i , we have:

$$V_i = s \left[\left[\frac{sJ_m R_a}{n * K_b} \right] + n * K_t \right] \theta_o(s)$$

$$V_i = K_p \theta_i - (K_p - K_D s) \theta_o \Leftrightarrow \theta_o(s) s \left[\left[\frac{sJ_m R_a}{n * K_b} \right] + n * K_t \right] = K_p \theta_i(s) - (K_p + K_D s) \theta_o(s)$$

$$\theta_o(s) s \left[\left[\frac{sJ_m R_a}{n * K_b} \right] + n * K_t \right] + (K_p + K_D s) \theta_o(s) = K_p \theta_i(s)$$

$$\theta_o(s) \left(s \left[\left[\frac{sJ_m R_a}{n * K_b} \right] + n * K_t \right] + (K_p + K_D s) \right) = K_p \theta_i(s)$$

$$\frac{\theta_o(s)}{\theta_i(s)} = \frac{1}{\left(\frac{s^2 J_m R_a}{n K_b} + (n K_t + K_D) s + K_p \right)}$$

By comparison with standard second order system, we find PD controller gains K_p , K_D

5.5.4 Inner Motor PD Position control with only position feedback

Considering the output position control, applying only position feedback with proportional and derivative terms, as shown in Fig 13(a). The input voltage to DC motor will be given by

$$V_i = K_p [\theta_i - \theta_o] - K_D \dot{\theta}_o$$

To find the gains K_p and K_D , apply the same procedure, for desired damping ratio, ζ and settling time, T_s .

5.5.5 Inner Motor PID Position control loop with only position feedback

Considering the output position control, applying only position feedback with proportional, derivative and integral terms, as shown in Fig 13(b). The input voltage to motor will be given by:

$$V_i = K_p [\theta_i - \theta_o] + s K_D \dot{\theta}_o + \frac{K_I [\theta_i - \theta_o]}{s}$$

The gains K_p , K_D and K_I , are found by applying the same procedure, for desired damping ratio, ζ and settling time, T_s .

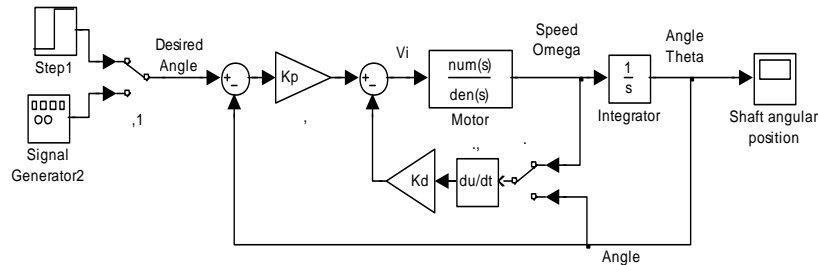


Figure 13(a) Motor PD Position control with position and/or rate feedback (to switch use manual switch)

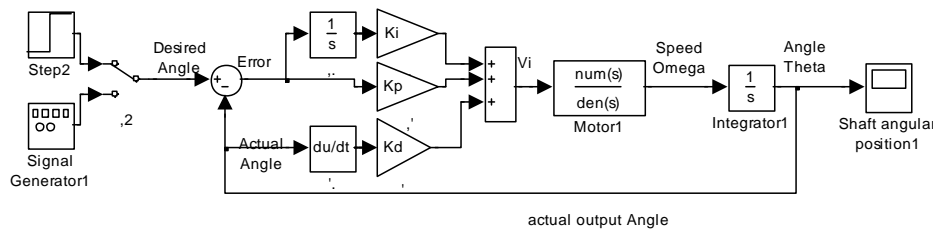


Figure 13 (b) Motor PID Position control with position feedback

5.5.6 Outer Ball and beam PD, PID Position control with only position feedback

The same procedure can be applied, to calculate controller gains, for controlling beam angle, when applying PD or PID, this is shown in Fig 13(c)

5.5.6.1 Outer ball and beam PD Position control loop with position and rate feedback

The input beam angle, α , to ball and beam system, applying PD controller, will be given by:

$$\alpha = K_p [x_i - x_o] - K_D \frac{dx_o}{dt}$$

Taking Laplace transform,

$$\alpha = K_p [X_i(s) - X_o(s)] - K_D s(s)$$

Substituting α , ball and beam transfer function, as shown below, we have

$$\frac{X(s)}{\alpha(s)} = \frac{(5/7)g}{s^2} \Leftrightarrow \alpha(s) = \frac{7s^2}{(5)(9.8)} X_o(s) \Leftrightarrow \alpha(s) = \frac{s^2}{7} X_o(s)$$

$$\frac{s^2}{7} X_o(s) = K_p [X_i(s) - X_o(s)] - K_D s(s)$$

$$\frac{X_o(s)}{X_i(s)} = \frac{7K_p}{s^2 + 7K_D s + 7K_p}$$

This is the overall equivalent closed loop transfer function of ball and beam, comparing it with standard second order transfer function, and by comparison, we can find the gains K_p and K_D depending on plant parameters and desired damping ratio, ζ and settling time, T_s . as shown next:

$$T(s) = \frac{X_o(s)}{X_i(s)} = \frac{\omega_n^2}{s^2 + 2\zeta\omega_n s + \omega_n^2} = \frac{7K_p}{s^2 + 7K_D s + 7K_p}$$

$$K_p = \frac{\omega_n^2}{7} \Leftrightarrow K_D = \frac{2\xi\omega_n}{7}$$

Assuming the constrains for this system are to be , desired damping ratio of 0.707, or overshoot and Peak time of $T_p=1$ second, we find undamped natural frequency ω_n , and correspondingly K_p, K_D

$$\xi = \frac{-\ln(\%OS / 100)}{\sqrt{\pi^2 + \ln^2(\%OS / 100)}}, T_p = \frac{\pi}{\omega_n \sqrt{1 - \xi^2}}$$

Solving we have: $\omega_n = 4.4422, K_p = 2.8190 \Leftrightarrow K_D = 0.89728$

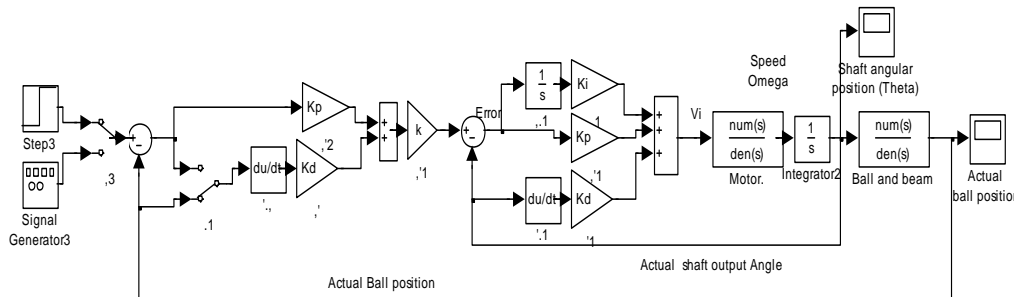


Figure 13 (c) Ball and beam position control with position feedback

5.5.7 Sensor sub-system modeling

There is a relationship between the beam angle, α , and DC motor output position angle, θ , where the distance traveled by the beam at radius equals to L , is equal to distance traveled by gear at radius, r , that is: $r\theta = L\alpha \Leftrightarrow \alpha = (r/L)\theta$, Where: The beam angle $\alpha = (r/L)\theta$, and the motor angle $\theta = (L/r)\alpha$. The transfer function between the ball position and rotor angle can be obtained based on basic transfer function given by Eq.(2) and on relation given by (11), and given as shown next:

$$\frac{Y(s)}{V_{in}(s)} = \frac{b}{s^2} = \frac{g}{s^2} \Rightarrow \frac{Y(s)}{V_{in}(s)} = \frac{r}{L} \frac{g}{s^2} = \frac{r * g}{L} \frac{1}{s^2}$$

The position of the ball on the beam can be measured using special sensors, e.g. linear Potentiometer, in [19] a linear resistive wire is used as a position sensor and the conductive ball moving along it acting as a voltage divider. Linear resistive wire has a relative large resistance of about 2.15 ohm/m. A series resistor is added to the circuit in order to divide the voltage to avoid unwanted heat. According to the position (X) of the ball, the voltage will linearly vary from 0.1 V to 0.74 V. Schematic of the resistive wire circuit is shown in Figure 14.

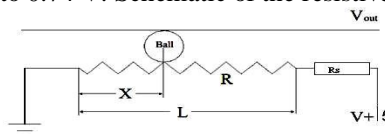


Figure 14 Schematic of the linear resistive wire circuit "position sensor" [19]

$$K_{se} = \frac{(\text{Voltage change})}{(\text{Position change})} = \frac{(0.74 - 0.1)}{(L)} = \frac{(0.64)}{(40)} = 0.016$$

For voltage range of 10 volts; $K_{se} = 10 / 40 = 0.25$

5.6 Electronics and interfaces simulation and testing; simulation in Proteus; To test and evaluate the selection and integration of circuit design, programming and interface components, simulation using ISIS-Professional Proteus is used. The control program written in C language, with the help of MikroC program is converted to Hex. File and downloaded on the simulated PIC-microcontroller and circuit, the simulation is shown in Figure 18, after testing, evaluating and optimizing various aspects, the final simulation results show the correctness of written program, interfaces, and microcontroller, all these can be used to build the physical circuit.

5.7 Ball and beam overall system simulation and analysis.

Based on the specification of requirements and design, the subsystems models and the whole system model, are to be tested and analyzed,. If the specification are not satisfied,, modifications can be made, if the specifications are satisfied the model can be Optimized.

The primary basic Simulink model, with PID control algorithm for both loops is shown in Figure 15, these two controllers will be replaced with corresponding proposed control algorithm to achieve optimal

response. Switching model, using manual switch, to nonlinear PMDC motor model, applying two Simulink built-in PD controllers for inner and outer loops, subjecting system to step input, and applying Simulink block tuning; will result in ball position,/time, speed/time, ball acceleration/time ,beam angle/time responses curves shown in Figure 16(a) , when system is subjected to random input, will result in ball and beam response curves shown in Figure 16(b). Switching model to simplified PMDC motor model, and subjecting the system to step input, will result in response curves shown in Figure 16(c)), comparing response curves, show that the overshoot using simplified motor model is less , as well as setting time, but generally system takes 10 second response to reach desired position which is large for such system.Applying Outer Ball and beam PD Position control with only position feedback, Figure 17(a) Switching model to simplified PMDC motor model, defining parameters, running the model, will result in response ball position,/time, ball speed/time, ball acceleration/time and beam angle/time response curves response curves shown in 17(b). Refining the PD Position control design, for both loops, will result in more acceptable response curves response curves shown in 17(c), the system reaches desired output at 2.3 seconds.

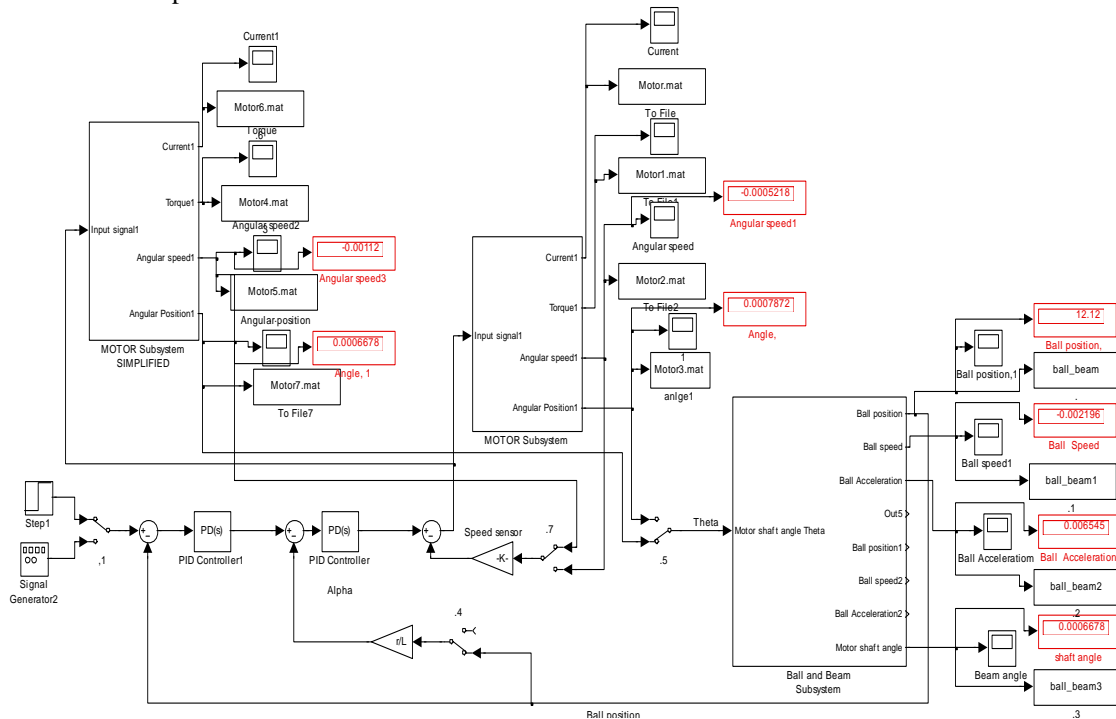


Figure 15 The primary Simulink model, with PID controller.

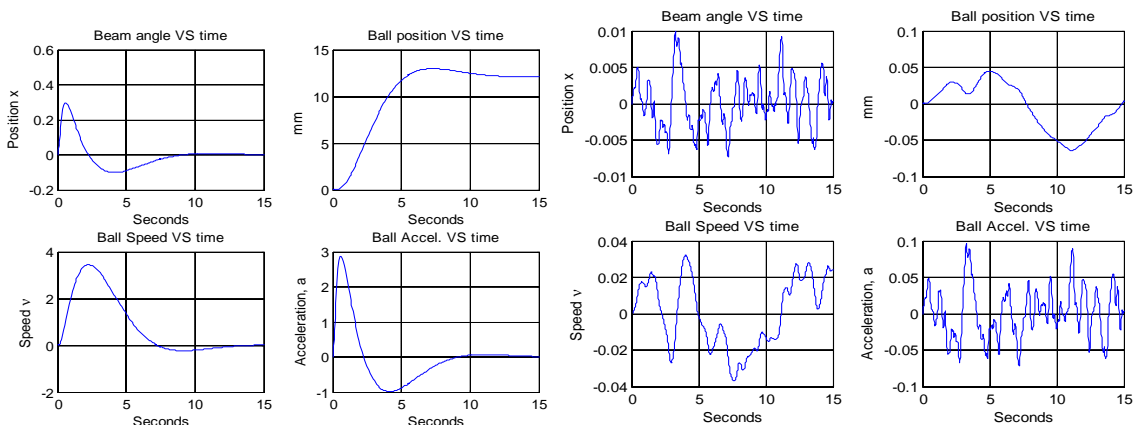


Figure 17 Ball and beam system step and random input response, using actual PMDC model.

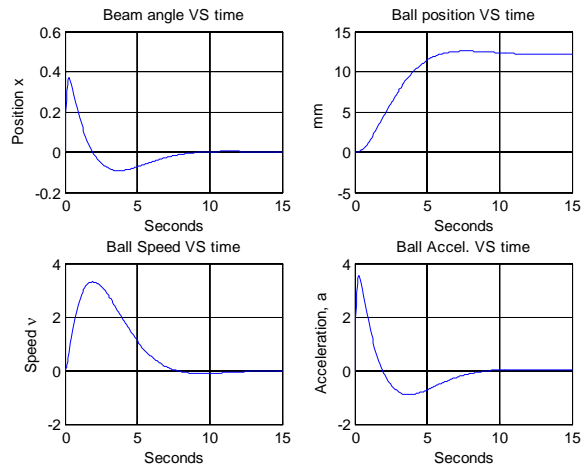


Figure 16 (c)) Ball and beam system step response, using simplified PMDC model

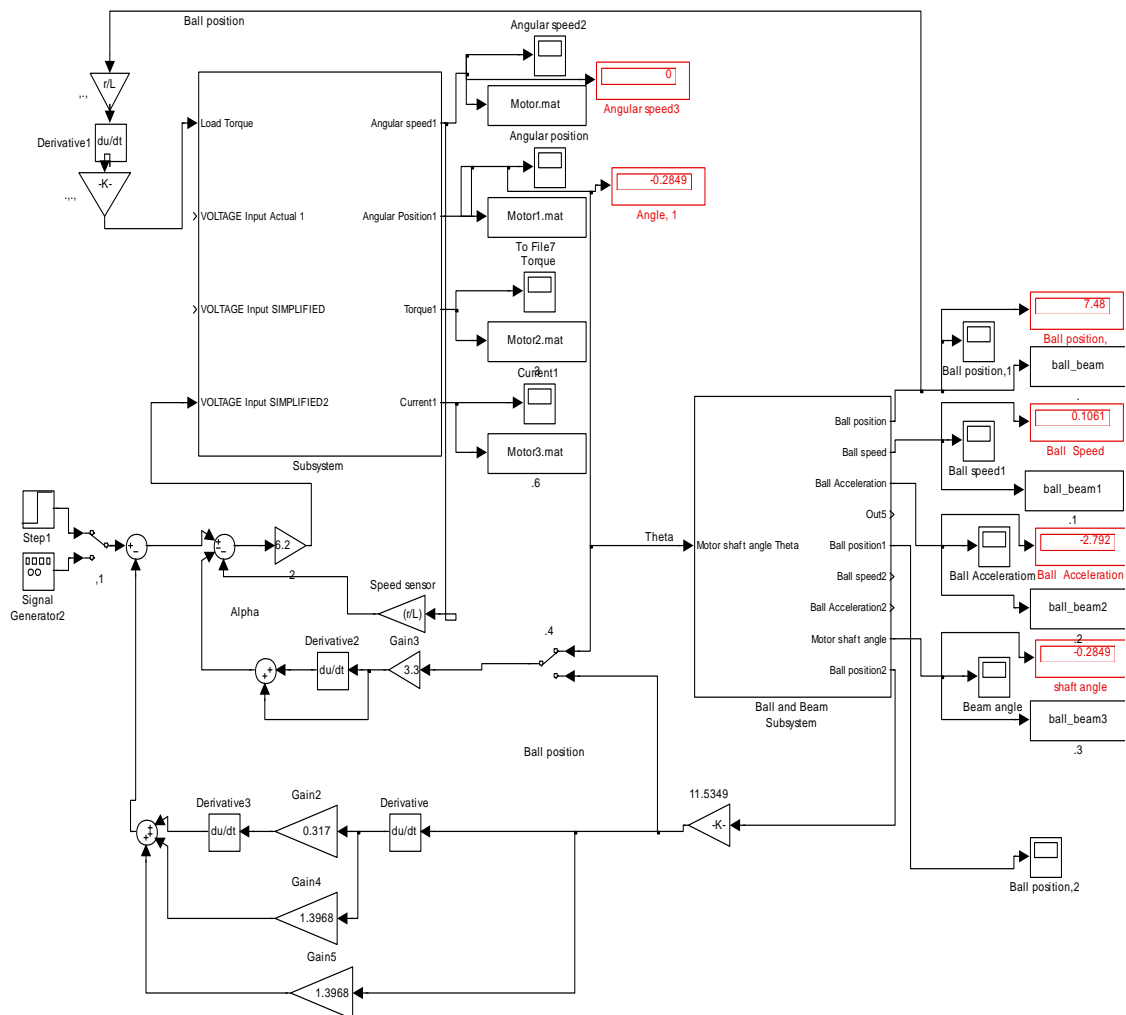


Figure 16 (a) Ball and beam PD Position control with only position feedback

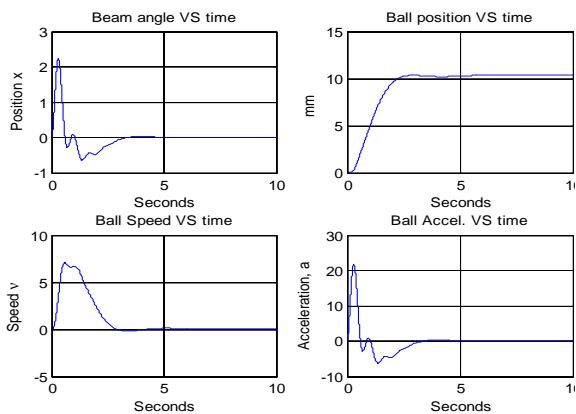


Figure 17(b) Ball and beam system step response

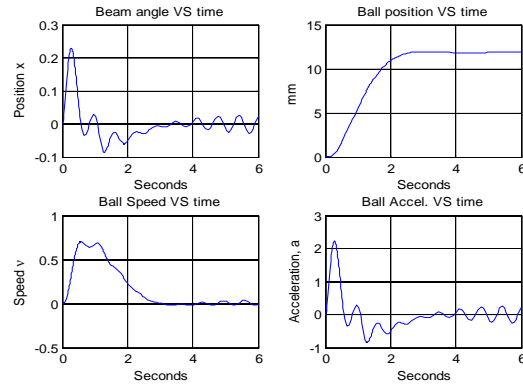


Figure 17 (c) Ball and beam system step response.

VI. PROTOTYPING, TESTING, EVALUATION AND OPTIMIZATION.

There is no single model which can ever flawlessly reproduce reality, there will always be errors called as unmodeled errors between behavior of a *product* model and the *actual* product. In order to take into account the unmodeled errors and enhance precision, performance in the design process, the Mechatronics design approach includes *prototyping* phase. Prototyping development may be carried out in the following two forms; *Virtual Prototype* and *Physical Prototype*, in this paper, only virtual prototype is built, Virtual Prototype is computer model of a product presented in a virtual environment with, *ideally*, all information and properties included, to visualize text, analyze and evaluate machine movement and logical operations. Different sources introduce different virtual prototypes for evaluating the overall system selection, integration and design, in [22], introduced model shown in Figure 18(a), the software used is MATLAB/Simulink.

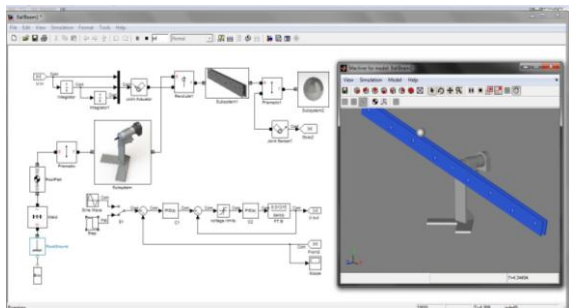


Figure 18(a) overall system virtual prototype[]

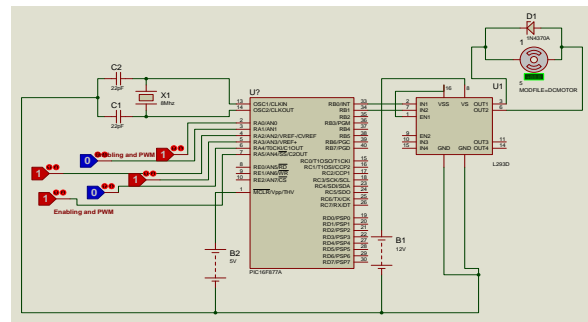


Figure 18 Electronics simulation in Proteus software

VII. CONCLUSION & FUTURE WORK

This paper proposes the conception and development of ball and beam system based on Mechatronics design approach, where realization of design is achieved applying simultaneous, parallel, design approach and consideration. A complete system's components' selection, design and integration, as well as, modeling, simulation and analysis are presented. The simulation results for PD controller design are shown. Depending on desired accuracy, different mathematical and Simulink model forms of the DC motor and plant have been developed. The proposed Mechatronics design and models are intended for research purposes, as well as, for application in educational process. The proposed models were created and verified using MATLAB Simulink, Proteus software.

This paper is part (I) of authors' research study on Mechatronics design of ball and beam system, as future work of this research, author intends to built and test physical prototype of this design, and to propose a general MATLAB/Simulink model with its function block parameters window, that can be used to control ball and beam system using different control strategies, as well as to simplify and accelerate the selection, design and verification processes

REFERENCES

- [1] Devdas Shetty, Richard A. Kolk, *Mechatronics System Design*, Second Edition, SI, Cengage Learning, 2011.
- [2] Farhan A. Salem, Ahmad A. Mahfouz, "A proposed approach to Mechatronics Design and Implementation education-oriented Methodology", *Innovative Systems Design and Engineering* Vol.4, No.10, 2013, pp12-39, 2013.
- [3] <http://www.control-systems-principles.co.uk/whitepapers/ball-and-beam1.pdf>
- [4] Eaton PH, Prokhorov DV, Wunsch DI 2nd, Neurocontroller alternatives for "fuzzy" ball-and-beam systems with nonuniform nonlinear friction, *IEEE Trans Neural Netw.* 2000;11(2):423-35. doi: 10.1109/72.839012.
- [5] Dr. Hadi Saadat; personal website; www.saadat.us.
- [6] W. Yu, F. Ortiz, "Stability Analysis of PD Regulation for Ball and Beam System", *Proceedings of IEEE Conference on Control Applications*, 2005 pp. 517 – 522.
- [7] Y. Jiang, C. McCorkell, R. B. Zmood, "Application of Neural Networks for Real Time Control of a Ball-Beam System", *Proceedings of IEEE International Conference on Neural Networks*, 1995. Vol. 5, pp. 2397 – 2402
- [8] M. A. Marra, B. E. Boling, B. L. Walcott, "Genetic Control of a Ball - Beam System", *Proceedings of the - IEEE International Conference on Control Applications*, 1996, pp. 608 – 613
- [9] Q. Wang, M. Mi, G. Ma and P. Spronck, "Evolving a Neural Controller for a Ball and Beam System", *Proceedings of the Third International Conference on Machine Learning and Cybernetics*, 2004, Vol. 2, pp. 757 -761.
- [10] K. C. Ng, M. M. Trivedi, "Fuzzy Logic Controller and Real Time Implementation of a Ball Ballancing Beam", *SPIE, Orlando, Florida* 1995, pp 261—272.
- [11] W. Yu, "Nonlinear PD Regulation for Ball and Beam System", *International Journal of Electrical Engineering Education*, Vol. 46, pp. 37–59, 2009.
- [12] Y. Guo, D. J. Hill, Z. P. Jiang, "Global Nonlinear Control of the Ball and Beam System" *Proceedings of the 35th IEEE Conference on Decision and Control*, Kobe, Japan, December, 1996, pp. 2818-2823.
- [13] K. Ogata. *Modern Control Engineering*. third Ed., New Jersey: Prentice Hall, 1997.
- [14] <http://www.library.cmu.edu/ctms/ctms/simulink/examples/ball/ballsim.htm>
- [15] Ahmad A. Mahfouz, Farhan A. Salem, *DC motor fundamentals; modeling, simulation and control*, 1st edition, Amman, 2012.
- [16] Ahmad A. Mahfouz, Mohammed M. K, Farhan A. Salem Modeling, simulation and dynamics analysis issues of electric motor, for mechatronics applications, using different approaches and verification by MATLAB/Simulink (I). Submitted and accepted, to *I.J. Intelligent Systems and Applications*, Submission ID 123, 2012.
- [17] Halila A., *Étude des machines à courant continu*, MS Thesis, University of LAVAL, (Text in French), May 2001.
- [18] Richard C. Dorf and Robert H. Bishop, "Modern Control Systems", Ninth Edition, Prentice-Hall Inc., New Jersey, 2001.
- [20] Basil Hamed Application of a LabVIEW for Real-Time Control of Ball and Beam System *International Journal of Engineering and Technology*, Vol.2, No.4, August 2010
- [21] Juan Esteban Paz, http://grabcad.com/library/ball-and-beam-control-system-simulation-with-simulink?utm_campaign=eng-similarmodels&utm_content=first-model-downloaded&utm_medium=email&utm_source=user-email, with permission.
- [22] The MathWorks (www.mathworks.com).

Improvement of Pv Systems Power Output Using Sun-Tracking Techniques

B. O. Anyaka, D. C. Ahiabuike , M. J. Mbunwe

¹Department of Electrical Engineering,

²University of Nigeria, Nsukka, Nigeria

ABSTRACT

The amount of power produced by a photovoltaic (PV) or solar panel depends on the amount of sunlight to which it is exposed. As the sun's position changes throughout the day, the PV panel must be adjusted so that it is always aimed directly at the sun and, as a result, produces the maximum possible power. A sun-tracking system tracks the motion of the sun across the sky and moves the PV panel to face directly at the sun and thereby ensuring that maximum amount of sunlight strikes the panel throughout the day. Sun-tracked PV systems are more efficient than fixed PV systems and are capable of enhancing productivity. In this paper different types of sun-tracking systems are reviewed and their energy gains are discussed.

KEYWORDS: Solar energy, PV systems, Sun-trackers, Maximum power, Environment

I. INTRODUCTION

The increasing demand for energy, the continuous reduction in existing sources of fossil fuels and the growing concern regarding environment pollution, have pushed mankind to explore new technologies for the production of electrical energy using renewable sources, such as solar energy, wind energy, etc. Among the renewable energy sources solar energy affords great potential for conversion into electric power, able to ensure an important part of the electrical energy needs of the planet [1]. The sun is regarded as a good source of energy for its consistency and cleanliness, unlike other kinds of energy such as coal, oil, and derivations of oil that pollute the atmosphere and the environment. Most scientists, because of the abundance of sunshine capable of satisfying our energy needs in the years ahead, emphasize the importance of solar energy. It is clean, renewable, and plentiful throughout the world. In addition, energy needs and costs have increased in recent years and nature continues to suffer damage during energy production [1]. Solar photovoltaic (PV) technology is a very attractive renewable energy option for clean energy generation, but has limited use due to its high cost. The cost has slightly increased in recent years to a point that is still quite high compared to the cost of other conventional power generation technologies, as well as non-conventional technology such as wind energy technology [2]. The power generated by a PV system is highly dependent on weather conditions. During cloudy periods and at night, a PV system would not generate any significant power. Concepts related to the solar energy have constantly been under heavy research and development. The amount of power produced by a solar system depends on the amount of sunlight to which it is exposed. As the sun's position changes throughout the day, the solar system must be adjusted so that it is always aimed precisely at the sun and, as a result, produces the maximum possible power. In order to ensure maximum power output from PV cells, the sunlight's angle of incidence needs to be constantly perpendicular to the solar panel [2]. This requires constant tracking of the sun's apparent daytime motion, and hence develops an automated sun tracking system which carries the solar panel and positions it in such a way that direct sunlight is always focused on the PV cells. A tracking mechanism must be reliable and able to follow the sun with a certain degree of accuracy, return the collector to its original position at the end of the day or during the night, and also track during periods of cloud cover. Regarding movement capability, two main types of sun trackers exist [2]:

- One axis trackers,
- Two axes trackers

Single-axis-tracking systems are considerably cheaper and easier to construct, but their efficiency is lower than that of two axes sun-tracking systems. Since PV power output is always non-linear in shape, there is the need to maximize the power that is being transferred to the load. High efficiency can be achieved by controlling the PV unit to operate at its maximum power extraction. In automatic sun tracker systems, the solar panels are made to track the movement of the sun. Hence, a tracking mechanism (mechanical device) that requires constant tracking of the sun's apparent daytime motion, and hence develops an automated sun tracking system which carries the solar panel and positions it in such a way that direct sunlight is always focused on the PV cells for maximum efficiency. A comparison between fixed and sun-tracked solar stills shows that sun-tracking increases productivity by over 32% [3]. For increasing sun power generation efficiency, the techniques of sun-tracking have been surveyed for maximizing solar system output.

The PV Solar Cell

Covering 0.16% of the land on earth with 10% efficient solar conversion systems would provide 20 TW of power, nearly twice the world's consumption rate of fossil energy [4]. Directly converting sunlight to electricity is accomplished via PV solar cells. The birth of the modern era of PV solar cells occurred in 1954, when D. Chapin, C. Fuller, and G. Pearson at Bell Labs demonstrated solar cells based on p-n junctions in single Silicon crystals with efficiencies of 5–6% [4]. Peak watt (Wp) rating is the power produced by a solar module illuminated under the standard conditions; 1000 W/m² solar intensity, at 25⁰C ambient temperature, and a spectrum related to sunlight passing through the atmosphere when the sun is at a 42⁰ elevation from the horizon. Because of day/night and time-of-day variations in insolation and cloud cover, the average electrical power produced by a solar cell over a year is about 20% of its Wp rating [5].

Astronomy

The earth revolves around the sun in an elliptical orbit with the sun as one of the foci. The plane of this orbit is called the ecliptic. The time taken for the earth to complete this orbit defines a year. The relative position of the sun and earth is conveniently represented by means of the celestial sphere around the earth. The equatorial plane intersects the celestial sphere in the celestial equator, and the polar axis in the celestial poles. The earth motion round the sun is then pictured by apparent motion of the sun in the elliptic which is tilted at 23.45⁰ with respect to the celestial equator. The angle between the line joining the centers of the sun and the earth and its projection on the equatorial plane is called the solar declination angle (δ). This angle is zero at the vernal (20/21 march) and autumnal (22/23 September) positions [6]. Calculating the sun's approximate path requires one to first find the declination. The declination is the angle of deviation of the sun from directly above the equator. Reference [6], evaluated a plot of declination(deg) versus day of the year for a geographical area with Latitude 10⁰ N (Precisely, the University of Nigeria, Nsukka). The declination angle is computed with the formula.

$$\delta(d) = 23.45 \text{ deg}(\sin)\left[\left(\frac{360}{365}\right)(d - 81) \text{ deg}\right] \tag{2.1}$$

The plot is shown below in fig.2.1.

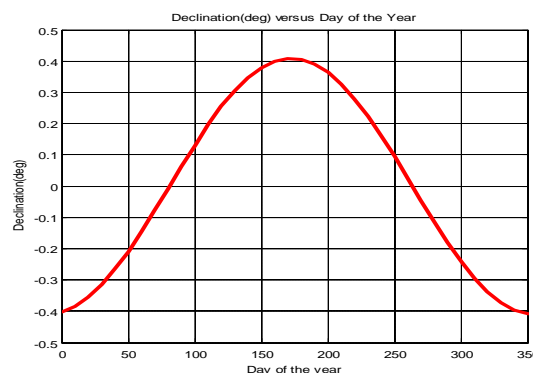


Fig:2.1 : Declination (deg) verses Day of the year[6]

Positive angles from Fig. 2.1 are considered north of the equator and negative angles are considered south of the equator. These results are only approximate, however, since the year is not exactly 365 days long.

The earth itself rotates at the rate of one revolution per day around the polar axis. The daily rotation of the earth is depicted by the rotation of the celestial sphere about the polar axis, and the instantaneous position of the sun is described by the hour angle (ω), the angle between the meridian passing through the sun and the meridian of the site. The hour angle is zero at solar noon and increases toward the east. For observers on the earth's surface at a location with geographical latitude (ϕ), a convenient coordinate system is defined by a vertical line at the site which intersects the celestial sphere in two points, the zenith and the nadir, and subtends the angle ϕ with the polar axis (Fig. 2.2). The great circle perpendicular to the vertical axis is the horizon [7].

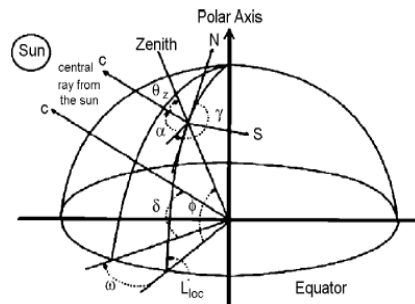


Fig 2.2. Schematic representation of the solar angles [7]

The latitude (ϕ) of a point or location is the angle made by the radial line joining the location to the center of the earth with the projection of the line on the equatorial plane. The earth's axis of rotation intersects the earth's surface at 90° latitude (North Pole) and -90° latitude (South Pole). Any location on the surface of the earth then can be defined by the intersection of a longitude angle and a latitude angle. The solar altitude angle (α) is defined as the vertical angle between the projection of sun's rays on the horizontal plane and direction of sun's rays passing through the point, as shown in Fig. 1. As an alternative, the sun's altitude may be described in terms of the solar zenith angle (θ_z) which is a vertical angle between sun's rays and a line perpendicular to the horizontal plane through the point

$$(\theta_z = 90 - \alpha) \quad (2.2)$$

Solar azimuth angle (γ) is the horizontal angle measured from south (in the northern hemisphere) to the horizontal projection of the sun's rays [7].

Radiation on Inclined and Tracking Surfaces

The solar radiation data are usually given in the form of global radiation on a horizontal surface and PV panels are usually positioned at an angle to the horizontal plane; therefore, the energy input to the PV system must be calculated accordingly. The calculation proceeds in three steps. In the first step, the data for the site are used to determine the diffuse and beam components of the global irradiation on the horizontal plane. This is carried out by using the extra-terrestrial daily irradiation, B_0 as a reference and calculating the ratio $K_T = G/B_0$, known as the clearness index where G is the daily global irradiation on a horizontal plane (usually the monthly mean), and K_T describes the average attenuation of solar radiation by the atmosphere at a given site during a given month. In the second step, the diffuse irradiation is obtained using the empirical rule that the diffuse fraction D/G of the global radiation is a universal function of the clearness index K_T (D is the monthly mean daily diffuse irradiation on a horizontal plane in W/m^2). Since $B = G - D$, this procedure determines both the diffuse and beam irradiation on the horizontal plane (B is daily beam irradiation on a horizontal plane). In the third step, the appropriate angular dependence of each component is used to determine the diffuse and beam irradiation on the inclined surface. With allowance for the reflectivity of the surrounding area, the albedo can also be determined. The total daily irradiation on the inclined surface is then obtained by adding the three components [7]. Sun is moving across the sky during the day. In the case of fixed solar collectors, the projection of the collector area on the plane, which is perpendicular to the radiation direction, is given by function cosine of the angle of incidence (Fig. 2.3).

The higher the angle of incidence θ , the lower is the power. Theoretical calculation of the extracted energy in case of using tracking collectors is carried out by assuming that the maximum radiation intensity $I = 1100\text{Wm}^{-2}$ is falling on the area which is oriented perpendicularly to the direction of radiation.

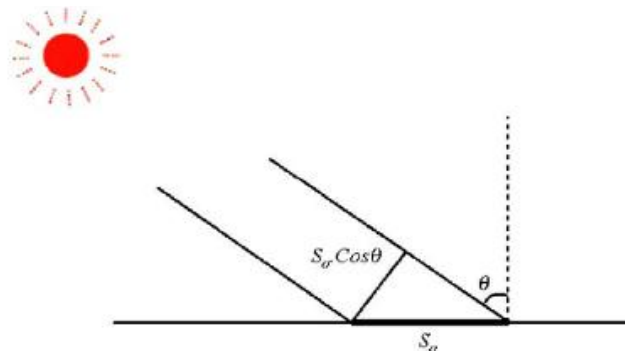


Fig. 2.3 Angle of incidence θ of the solar radiation [7].

Taking the day length $t = 12$, $h = 43,200$ s, intensity of the tracking collector which is always optimally oriented facing the sun is compared to that of a fixed collector which is oriented perpendicularly to the direction of radiation only at noon. The sun rays reaching the earth surface go through the thick layer of atmosphere. As we deviate from the noon, the solar insolation on the surface is weakened.

Fig. 2.4 shows the dependence of the energy lost on the maximum tracking angle in comparison to that of an ideal tracking.

It is clear that in tracking angles beyond $\pm 60^\circ$ no considerable energy gain is obtained.

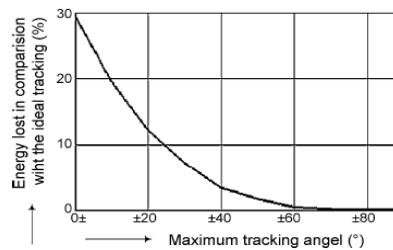


Fig.2.4 Energy lost in dependence of the maximum tracking angle in comparison with the ideal tracking [7].

Oladiran[8] assessed the mean global radiation captured by flat surfaces inclined at $f-10^\circ$, f , and $f+10^\circ$ (f as latitude), while tilting the surface from 0° to 75° at 15° intervals azimuthally for three zones in Nigeria. The mean total solar flux captured by three collector inclinations and six surface azimuth angles was calculated theoretically and a computer program was written. For graphic presentation, a data file was created for each run of the program. The total radiation per day of year, the mean monthly radiation and mean annual radiation for three zones were evaluated. Oladiran concluded that for all azimuth angles, an inclination angle equal to f produces the best all-year-round performance.

II. SUN-TRACKERS

Solar tracking can be implemented by using one-axis, and for higher accuracy, two-axis sun-tracking systems. For a two-axis sun-tracking system, two types are known as: polar (equatorial) tracking and azimuth/elevation (altitude–azimuth) tracking. The solar tracker, a device that keeps PV or photo-thermal panels in an optimum position perpendicular to the solar radiation during daylight hours, increases the collected energy. The first tracker introduced by Finster in 1962, was completely mechanical. One year later, Saavedra presented a mechanism with an automatic electronic control, which was used to orient an Epplepyrheliometer [9]. Trackers need not point directly at the sun to be effective. If the aim is off by 10° , the output is still 98.5% of that of the full-tracking maximum. In the cloudiest, haziest locations the gain in annual output from trackers can be in the low 20% range. In a generally good area, annual gains between 30 and 40% are typical. The gain in any given day may vary from almost zero to nearly 100% [10].

The presence of a solar tracker is not essential for the operation of a solar panel, but without it, performance is reduced. Although solar trackers can boost energy gain of PV arrays, in their installation some problems such as cost, reliability, energy consumption, maintenance and performance must be considered.

All tracking systems have all/some of the following characteristics

- Single column structure or of parallel console type.
- One or two moving motors.
- Light sensing device.
- Autonomous or auxiliary energy supply.
- Light following or moving according to the calendar.
- Continuous or step-wise movement.
- Tracking all year or all year except winter.
- Orientation adjustment with/without the tilt angle adjustment.

Several methods of sun following have been surveyed and evaluated to keep the solar panels, solar concentrators, telescopes or other solar systems perpendicular to the sun beam. An ideal tracker would allow the PV cell to accurately point towards the sun, compensating for both changes in the altitude angle of the sun (throughout the day), latitudinal offset of the sun (during seasonal changes) and changes in azimuth angle. Sun-tracking methods are usually classified into three categories: methods of tracker mount, methods of drives, and methods of control [11].

Methods of Tracker Mount

Single Axis Solar Trackers

Single axis solar trackers can either have a horizontal or a vertical axle. The horizontal type is used in tropical regions where the sun gets very high at noon, but the days are short. The vertical type is used in high latitudes where the sun does not get very high, but summer days can be very long. The single axis tracking system is the simplest and most commonly used.

Double Axis Solar Trackers

Double axis solar trackers have both a horizontal and a vertical axle and so can track the Sun's apparent motion exactly anywhere in the World. This type of system is used to control astronomical telescopes, and so there is plenty of software available to automatically predict and track the motion of the sun across the sky. The dual axis tracking system is also used for concentrating a solar reflector toward the concentrator on heliostat systems.

3.2 Methods Of Drive

Active Trackers

Active Trackers use motors and gear trains to direct the tracker as commanded by a controller responding to the solar direction. Light-sensing trackers typically have two photo-sensors, such as photodiodes, configured differentially so that they output a null when receiving the same light flux. Mechanically, they should be omnidirectional (i.e. flat) and are aimed 90 degrees apart. This will cause the steepest part of their cosine transfer functions to balance at the steepest part, which translates into maximum sensitivity.

Passive Trackers

Passive Trackers use a low boiling point compressed gas fluid that is driven to one side or the other (by solar heat creating gas pressure) to cause the tracker to move in response to an imbalance.

Chronological Tracker

Chronological Tracker counteracts the earth's rotation by turning at an equal rate as the earth, but in the opposite direction. Actually the rates are not quite equal, because as the earth goes around the sun, the position of the sun changes with respect to the earth by 360° every year or 365.24 days.

Methods Of Control

Closed-loop Types of Sun Tracking Systems

Closed-loop types of sun tracking systems are based on feedback control principles. In these systems, a number of inputs are transferred to a controller from sensors which detect relevant parameters induced by the sun, manipulated in the controller and then yield outputs (i.e. sensor-based).

Open-loop Types of Sun Tracking Systems

An open-loop type of controller computes its input into a system using only the current state and the algorithm of the system and without using feedback to determine if its input has achieved the desired goal (i.e. algorithm-based). The system is simpler and cheaper than the closed-loop type of sun-tracking systems. It does not observe the output of the processes that it is controlling. Consequently, an open-loop system cannot correct any errors so that it could make and may not compensate for disturbances in the system.

III. ENERGY GAIN IN TRACKING SYSTEMS

In 1986, Akhmedyarov *et al.* [12] first increased the output power of a solar photoelectric station in Kazakhstan from 357W to 500W by integrating the station with an automatic sun tracking system. Several years later, Maish [13] developed a control system called Solar Tracker to provide sun tracking, night and emergency storage, communication, and manual drive control functions for one and two axis solar trackers in a low-cost, user-friendly package. The control algorithm used a six-degree self alignment routine and a self-adjusting motor actuation time in order to improve both the pointing accuracy and the system reliability. The experimental results showed that the control system enabled a full-day pointing accuracy of better than $\pm 0.1^\circ$ to be achieved. Khalifa and Al-Mutawalli [14], developed a two-axis sun tracking system to enhance the thermal performance of a compound parabolic concentrator. The system was designed to track the sun's position every three to four minutes in the horizontal plane and every four to five minutes in the vertical plane. The tracking system was comprised of two identical sub-systems, one for each axis, with each sub-system consisting of two adjacent photo-transistors separated by a partition of a certain height. In the tracking operation, the difference in the voltage signals of the two photo-transistors was amplified and used as a command signal to drive the collector around the corresponding axis until the voltage difference reduced to zero, indicating that the sun's rays were once again normal to the collector surface. It was shown that the tracking system had a power consumption of just 0.5Whr and yielded an improvement of around 75% in the collected solar energy, compared to a fixed collector of equivalent dimensions. Mumba [15], developed a manual solar tracking system for a PV powered grain drier working in two positions. A 12 V, 0.42 A, DC suction fan powered with PV was placed in the air inlet. To improve collector module efficiency, the sun was tracked $\pm 30^\circ$ from the horizontal. Mumba investigated the performance under four cases: PV fan-off without sun-tracking, PV fan-on without sun-tracking, PV fan-off with sun-tracking and PV fan-on with sun-tracking. In the sun tracking cases the collector module angled manually eastward at 8.00 a.m. and westward at 2.00 p.m. while the collector module was tilted 15° from the horizontal to match the sun's elevation. It was concluded that from uniform air temperature point of view, the fan-on sun-tracking case was the best, giving a temperature of 60°C . From uniform energy gain point of view, the sun-tracking cases performed superior to that of non-tracking ones. It was concluded that a solar air heater with manual sun-tracking facility can improve the thermal efficiency up to 80%.

Abdallah [16] investigated the respective effects of four different electro-mechanical sun-tracking systems on the current, voltage and power characteristics of a flat-plate photovoltaic system. The results showed that tracking systems comprising two axes, one vertical axis, one east-west axis and one north-south axis, and one north-south axis, increased the electrical output powers of the photovoltaic system by around 43.87%, 37.53%, 34.43% and 15.69%, respectively, compared to that obtained from a photovoltaic system with a fixed surface inclined at 32° . Helwa [17], compared the stationary and tracking PV systems to assess the power consumption of tracking systems and the effect of tracking accuracy on the system output. The compared systems were: a fixed system tilted 40° horizontally, one vertical axis tracker (using time, date and site parameters for control), a 6° tilted axis parallel to the N-S direction (using time, date and site parameters for control) and two-axis azimuth/elevation tracker (controlled by microprocessor taking commands from a PC). Several revolution count sensor and limit switches were used. The comparison curves among different solar tracking systems showed that the increase in annual radiation gain from the two axis tracker, vertical axis tracker and tilt axis tracker over the fixed tilt system was 30%, 18% and 11%, respectively. The power consumption due to microprocessors, electric equipment, sensors, electrical switching and driving motors for tilted-axis tracker were 50Wh/day and 22Wh/day when the tracking error were $\pm 0.56^\circ$ and $\pm 10^\circ$, respectively. Chicco [18] experimentally assessed the production of the PV plants in the sun-tracking and fixed modes in three different sites. In the first site, 15 individual systems controlled by one coordinate tracking system were compared with a 0° azimuth and 36° elevation angles as fixed cases. In the second site, 90 individual systems with separate coordinate-controlled tracking were compared with 0° azimuth and 30° elevation fixed system. For the third site, the position of the sun-tracking system was being updated every 15 min and the fixed system maintained at a tilt angle of 30° with 35° elevation angle.

The results showed that the average improvement, using the sun-tracking system, was 32.9 and 35.1% from the simulated values and 37.7 and 30.4% from the actual data for the first and second sites, respectively. For the third site, an annual improvement of 31.5% for the sun-tracking system was obtained. Nann evaluated the potentials for tracking systems relative to the cost and irradiance received from a fixed (40°) system. It was mentioned although the fraction of direct normal irradiance on a surface normal to the sun was 54% greater than that of the fixed one, the surplus of irradiance received by one-axis tracking and two-axis tracking systems were 34% and 38%, respectively and at today's module costs, tracking the sun can improve the cost effectiveness of the PV plant by up to 20%. The comparison between three stationary, one-axis and two-axis tracking systems showed that irradiation received by one-axis tracker is nearly as the same as the two axis trackers; however its tracker cost is approximately half of that of the two-axis one [19]. Gay, compared daily and annual energy-delivery performance for large-scale fixed-array and two-axis tracking photovoltaic generating systems and site sensitivities were also discussed. For the studied site, it was observed that a fixed-array system would use about 40% more modules than a two-axis tracking system, for equal annual energy collection [20].

Nafeh evaluated the optimum tilt of PV arrays by using maximum global insolation technique. Theoretically, he calculated the global insolation at solar noon, incident on an inclined PV array with a predefined tilt angle and simulated the case by MATLAB-SIMULINK to calculate the optimum tilt angle for every day, month or year. Comparison curves for daily adjusted tilt angle and insolation between proposed technique and the conventional technique were given. He concluded that if the tilt angle is daily or monthly adjusted to its optimal value, then the global insolation collected at solar noon using the proposed technique will be larger than that collected at solar noon using the conventional technique over all days of the year. It was found that to obtain maximum solar insolation, using both the latitude of the site and the sun declination is necessary to orient the PV arrays [21]. Tomson [22] analyzed the performance of the two-positional control of single stand-alone flat plate concentrator. The collector was rotated around its single tilted axis twice per day with predefined deflections. The effect of different tilt angles, initial tilt angle, initial azimuth, and azimuth angle of the deflected plane were evaluated on the daily and seasonal gain. The comparison of simulation and experimental results indicated that using a simple tracking drive with low energy input for a brief daily movement, increased the seasonal energy yield by 10–20% comparing to that of a fixed south facing collector tilted at an optimal angle.

Kalogirou designed and constructed a one-axis sun-tracking system consisting of a control system with three light dependent resistor sensors and a DC motor. One sensor was responsible for direct beam detection; the second was cloud sensor and the third was daylight sensor. The control system consisted of relay, timer, many resistors and electronic parts. When any of the three sensors was shaded, the motor was switched on. The system tracked the sun in E–W direction and the final rotational speed of the collector was 0.011 rpm. Various tests of the solar collector showed that the tracking mechanism was very accurate. The accuracy for 100Wm^{-2} illumination was 0.2° while for 600 m^{-2} illumination it was reduced to 0.05° [23]. Ai et al. proposed and compared the azimuth and hour angle three-step trackers. The day length on the south facing slope was divided into three equal parts in order to adjust the tilt angle. The sum of the direct radiation received in each time interval and the sky diffusion and ground reflection radiation during a day were considered to derive the mathematical formula for the three-step tracking system to estimate the daily radiation on planes. They concluded that for the whole year, the radiation on the slope with optimized tilt angle was 30.2% and that for the two-axis azimuth three-step tracking was 72% higher than that on the horizontal surface. No significant difference was found between one-axis azimuth three-step tracking and hour angle three-step tracking power [24].

Lorenzo et al. designed a single vertical axis (azimuth axis) PV tracker and evaluated backtracking features. Each of 400 trackers installed in Spain used a 0.25 hp standard AC motor. The tilt angle of the PV surfaces remained constant. They mentioned that the energy collected by an ideal azimuth tracker was about 40% higher than that corresponding to an optimally tilted static surface and 10% higher than that of horizontal axis tracking. They calculated the E–W and N–S shadowing between two adjacent trackers occurred in the morning or afternoon. They recommended that when shadowing occurs, it can be avoided by moving the surface's azimuth angle away from its ideal value, just enough to get the shadow borderline to pass through the corner of the adjacent surface (backtracking). Their comparison showed that the azimuth tracking land was 40% greater than static surface while the corresponding energy cost can be significantly reduced [25]. Ibrahim constructed an electronically one-axis concentrating collector with an electric motor for forced circulation. The collector was hinged at two points for its tilt adjustment with a tightening screw to continuously track the sun from east to west through a range of 180° .

The collector efficiency was measured for different values of mass flow rates. It was concluded that the collector efficiency increases (reaching the maximum value of 62%) as the mass flow rate increases [26]. Brunatte et al. investigated a two-stage concentrator with one axis tracking system around a polar N–S axis. The half rim angle of the first concentrating stage was chosen to be equal to the sun's maximum declination of 23.5° . They tested the system for various conditions and theoretically calculated the concentration factor for E–W and N–S tracking. They concluded that thermodynamically, concentration factor increases by a factor of three. For the first prototype, concentration optical efficiency of 77.5% was measured at normal incidence [27]. Clifford et al. presented a novel passive solar tracker modelled with computer. They mentioned that although the expanding metals generated deflections were small, the corresponding forces were large. Their passive solar tracker design incorporates two bimetallic strips made of aluminium and steel, positioned on a wooden frame, symmetrically on either side of a central horizontal axis. The bimetallic strips are shaded so that the strip further from the sun absorbs solar radiation while the other strip remains shaded in a similar fashion to the design illustrated in Fig.4.1 [28].

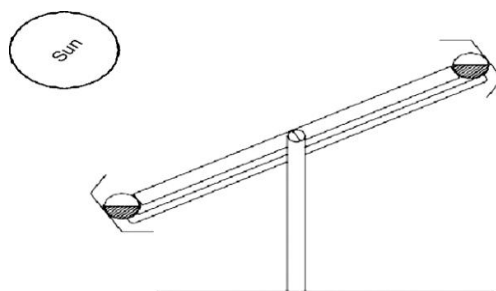


Fig.4.1 A passive solar tracker using two identical cylindrical tubes filled with a fluid under partial pressure [28]

To prevent oscillation or too sluggish respond, a damping system is linked to the sun tracker. They compared the computer model and experimental results of deflections of the bimetallic strip due to the effects of thermal radiation (in mm) and time taken for the solar tracker to reorient from W–E (in s). The computer model and experimental data showed results very similar to each other. The designed solar tracker had the potential to increase solar panel efficiency by up to 23%. Finally, they recommended night return mechanism, manually tilted axis and dual axis system for future development. Al-Mohamad designed a single-axis sun-tracking system based on a programmable logic controlling (PLC) unit to investigate the improvement in the daily output power of a photo-voltaic module. Two photo-resistive sensors were separated by a barrier to provide shadow for one of them. As solar radiation intensity increases the resistivity of the sensor decreases. Two output signals of the unit are connected directly to the analogue inputs of the PLC and compared in order to produce a proper output signal to activate an electromechanical sun-tracking system. The tracker scans through an angle of about 120° E–W. For PLC, a proper program to control, monitor and to collect data was developed using special software. A special computer program for automatic detection and PC communication with RS232 was developed using Visual Basic 5. The performance of the sun-tracker was evaluated and monitored. The output power showed a considerable increase during the early and late hours of the day. In fact, the overall improvement, in the tracking mode, exceeded 40% for the period from 6:00 to 10:00 a.m. and for the period from 15:00 to 17:00 p.m. However, the improvement was about 2–4% during mid-day. The average overall improvement during the whole day was better than 20% in comparison with that of a fixed module [29].

Abu-Khader et al. designed and constructed a PLC-controlled solar tracker system. The electromechanical system consisted of two drivers: the first for the joint rotating about the vertical axis and the second for the N–S or E–W tracking. Two bridges rectified a 220 VAC of supply network into 24 VDC to power the PLCI and into 24 VAC to supply the power for one of the electrical motors. The voltage of the second motor was 36 VDC with a worm gear while for the other motor a spur gear was used. The estimated consumed power by the electrical motor and control system was less than 3% of the collected energy by the tracking system. The PLC programming was based on the solar angles analysis divided into four intervals with corresponding motor speeds. Measurements on the PV system with and without sun-tracking showed that there was an overall increase of about 30–45% in the output power for the N–S tracking system compared to that of the fixed PV system. The optimum PV-tracking axis was the N–S that corresponded to the maximum possible power [30].

Girasolar company designed and constructed a programmable sun-tracker that can track the sun in two axes: azimuthal and zenithal. Its surface area was 58 m^2 with 2100 kg weight capable of turning with azimuthal speed of 0.5 rpm and azimuthal movement (pitch) speed of 0.06 rpm. Maximum angle of deviation was 2° from sun position. Its structure was designed to withstand wind velocity up to 105 km/h. It has been reported that its production growth is of up to 35% over fixed installations [31]. Contreras et al. in Texas University constructed a portable solar tracker using three linked robotic arm controlled microcontrollers. Its major components were PIC microcontroller, H-bridges, DC motors, PVC custom parts, IR sensor, photo-resistor and DC outlets. The first DC motor was a 10 A, 12 V, with 500:1 gear ratio, the second motor was 75 mA, 24 V, with 3000:1 gear ratio and the third motor with 220 mA (under load), 12 V and 1000:1 gear ratio. They programmed three microcontrollers using programming language PIC Basic PRO. It was concluded that the efficiency was increased by 30% [32].

Rosell et al. designed and built a PV/thermal low concentrating system and validated the developed analytical model. A two-axis sun-tracking system with two DC linear actuator and reed sensors was constructed to maximize the energy collection. In their system, mirrors reflect light onto the focal band and the solar cells are illuminated with approximately 11.1 times the solar irradiance incident beam. To obtain greater accuracy and to compute the sun position, a PLC system was designed and constructed. They quoted a 50% energy increase in comparison to that of an optimally tilted static surface [33]. Hamilton, in his thesis designed and constructed a microcontroller based sun-tracking device that used two motors to tilt the array in two planes of movement. The algorithm was designed to read and amplify sensor values and then to compare the data digitally to determine the exact position of the sun to activate the positioning uni-polar stepper motors. The sensor was a four sided pyramid in structure with solar cells mounted on each side. The microcontroller was programmed in C language. The device was tested both in the field and in the laboratory using a portable light source that was set up at 16 positions inside of a spherical area. The results showed that the sun-tracking system collected maximum energy throughout the day while stationary system collected maximum energy just when the sun was positioned overhead [34].

Huang et al. designed and evaluated a one-axis tracking mechanism for adjusting the PV position only at three fixed angles (three position tracking): morning, noon and afternoon. The mechanism includes a single pole support, a tilt adjustable platform, a PV frame driven by a motor and a solar position sensor. The sun position sensor consists of two photo-sensing elements divided by a vertical shading plate. Three touch switches were mounted on the transmission gear of the frame to signal the control circuit. The PV frame stops at the touch of the next switch once it is triggered. The designated location of the switch, thus, determines the stopping angle. Many analytical studies show that the maximum solar incident radiation can be obtained if the tilted surface angle approximately equals the latitude. For each stopping angle, they calculated the yearly total energy at various switching angles of the sensor and found the maximum yearly total energy. The results showed that the optimal stopping angle was 50° , and the optimal switching angle was 25° , which was half of the stopping angle. By repeating the calculation for different solar noon tilt angles at different latitudes, it was concluded that the optimal stopping angle was about 50° regardless of the latitude, and the optimal switching angle was half of the stopping angle. It can be shown from the results of the calculated yearly total energy that the PV power generation will increase by 24.5% as compared to that of a fixed PV module [35]. Kalogirou designed and constructed a one-axis sun-tracking system consisting of a control system with three light dependent resistor sensors and a DC motor. One sensor was responsible for direct beam detection; the second was cloud sensor and the third was daylight sensor. The control system consisted of relay, timer, many resistors and electronic parts. When any of the three sensors was shaded, the motor was switched on. The system tracked the sun in E-W direction and the final rotational speed of the collector was 0.011 rpm. Various tests of the solar collector showed that the tracking mechanism was very accurate. The accuracy for 100 Wm^{-2} illumination was 0.2° while for 600 Wm^{-2} illumination it was reduced to 0.05° [36].

Khalifa et al. investigated the performance improvement of a two-axis sun-tracking compound parabolic concentrator. The system consisted of photo-transistors separated by a partition from one another. When two sensors are unequal, the voltage difference amplifier activates a DC motor. The system tracks the sun every three to four minutes in horizontal plane and every four to five minutes in the vertical plane (depending on the height of partition). The tracking system power consumption was 0.5 Wh. To investigate the effect of two-axis tracking on the collector performance a number of tests were carried out. During these tests, the fixed collector was oriented due south at a tilt angle of 33° . It was concluded that a two-axis tracking system may increase the energy gain of a compound parabolic concentrator collector by up to 75% [37].

Canada et al. designed and constructed a sun-tracker with a maximum positional error of 28, for the measurement of global and direct spectral solar irradiance in the 330–1100 nm range. They designed a sun-tracker according to their specific needs and for a relatively low cost allowing up to 1 week work without the need for any operator supervision and returning each night to a rest position avoiding turning back over itself. The movement of the whole system is commanded by a step motor and gear speed reducer to adjust the step required. The system had 2° of freedom, one rotation in the azimuth plane over a fixed base, and the other rotation in the principal solar plane. The pass motor control is carried out by a control board that was specially designed for this type of motor, including a compatible interface that is connected to the parallel port of the PC through optical couplers. This configuration was to give the system a reference point from which to correctly position itself. Two on/off sensors indicating the initial position for each of the degrees of freedom were used. These are optical pass detectors made of an LED and a photo-detector working in the infrared zone. To cut out the sensors at the desired position, fixed aluminium reference points are used to identify the geographic north and the zero solar elevation. All codes were written in C++ Builder under Windows environment to: (a) provide movement relative to the sun, (b) control motor, (c) adjust and return to the rest position, and (d) alarm and activate/deactivate sensors. From these data, by using a subtractive method, the diffuse irradiance on a horizontal plane is calculated. Finally, using the Bouguer–Lambert–Beer law, the algorithm calculates total atmospheric thickness and aerosol optical depth in the 330–1100 nm range [38].

Gagliano et al. designed and simulated a two-axis sun-tracking system based on a photo-resistor sensor and investigated the effects of energy gain between a fixed PV panel and a tracked one. The sensing device consisted of a nine light-dependent resistor (LDRs) for rotation, and three aligned LDRs for inclination, positioned into suitable plastic supports. It was concluded that the main advantage of the proposed tracking system was the low cost of the sensing apparatus, gained from a real time elaboration procedure on sensors data [39]. Auxiliary solar cells (panels) connected directly to a permanent magnet DC motor are fixed to a rotary axle of the tracker and can both sense and provide energy for tracking. Poulek et al. described a very simple, reliable solar tracker for space and terrestrial applications. Unreliable and expensive components like batteries and driving electronics were completely eliminated (Fig. 4.2).

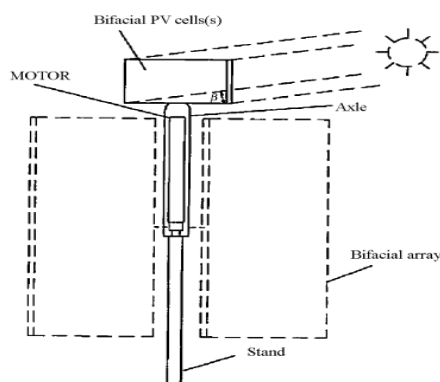


Fig. 4.2. Scheme of the terrestrial tracker [40].

It works also at low temperatures down to -40°C . The area of the auxiliary solar panel of the tracker is about 1% of the total area of moved solar arrays. Their auxiliary bifacial solar cell together with bifacial solar arrays enables backtracking from any position (360° tracking angle) while trackers based on similar technology with standard mono-facial solar cells have a tracking/backtracking angle of 120° . They concluded that the tracker follows the sun with deviation of $\pm 5^{\circ}$ without any reduction in the collected energy. The system collected more than 95% of the energy of an ideal tracker [40]. In another work they designed and constructed a solar tracking system based on an auxiliary bifacial solar cell capable of backtracking within 5 min and average tracking accuracy of $\pm 5^{\circ}$ to be installed above a V-trough concentrator with bifacial solar panel. Two anti-parallel arrangements of solar cells with 1% of the area of the moved solar collectors were connected directly to a reversible DC motor with a self-locking transmission. In a cloudy condition, once the sun starts shining, collectors will start moving. Their experimental result shows that the bifacial PV modules with reduced temperature sensitivity can boost energy gain by 15–25% in comparison with the same tracker/concentrator with mono-facial modules.

The polar axis solar tracker with C–Si bifacial PV modules will therefore deliver about 50% more energy than that of a fixed C–Si mono-facial PV array with the same rated output power. The tracking bifacial soft concentrators even double the energy gain against a fixed mono-facial PV array [41]. In the Alata et al. work, the formulation of equations that describe the sun motion in the sky and the design of three types of multi-purpose sun-tracking systems are introduced. The formulation is a replacement of the mathematical equations of altitude, azimuth, declination and hour angles by fuzzy IF–THEN rules using subtractive clustering along with ANFIS as a rule extraction method. Then, a 3D simulation of various sun-tracker types, driven by a DC motor for each axis of tracking, is demonstrated throughout a virtual reality (VR) mode. Each output of the fuzzy inference system is related directly to two inputs: the day number during the year and the time of the day in hours. The results are shown using simulation and in VR mode [42]. Rubio et al. discussed the design and implementation of a two axis PV sun-tracker using a combination of an open loop tracking strategy with a microprocessor in which the controller is based on a solar movement model, and a closed loop strategy which corresponds to the electro-optical controller. The instantaneous power generated by the arrays is measured by a sensor that emits a signal proportional to this power. Finally, they implemented a proportional and integral (PI) control strategy for each coordinate, independently. Their tracking strategy produced a close approximation of the evolution of the sun's elevation and azimuth even if the solar equations yield quite large errors. Fig. 4.3 shows a simulated example of the evolution of the three variables the sun's real movement (SMv), the progression of the values yielded by the solar equations (SEq) and the evolution obtained after the corrections (CEq).

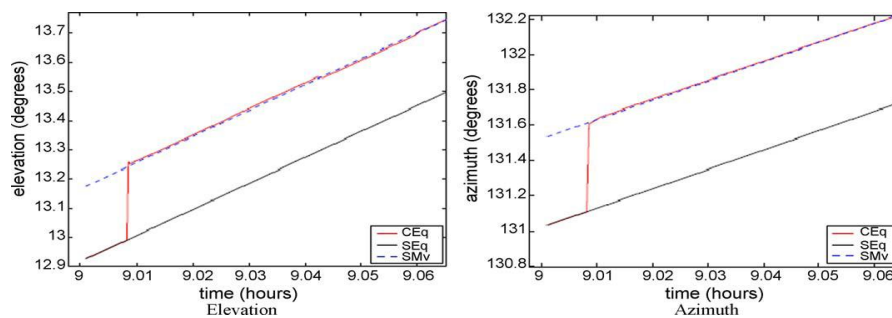


Fig. 4.3. Evaluation of the coordinates [43].

They concluded that the electric power generated using the hybrid strategy is, in mean values, 55% higher than that of the open loop one [43]. Bakos designed and constructed a two-axis sun-tracking system which is based on the combination of the conventional photo-resistors and the programming method of control. The electromechanical device consists of four relays, two electronic circuits, two photo-resistors connected in series and two AC motors. For manual operation, drawing a graphical representation and defining sunrise and sunset times, for the system connected to a computer a code is written in Visual C++ programming language. The system can track the sun in E–W and N–S direction. It was concluded that the two-axis tracking system is up to 46.46% more efficient in comparison to that of the fixed surface tilted 40° from the south [44]. Durisch et al. developed and tested a single cells and modules with sun tracker PC-based, in order to provide outdoor data under real operation conditions for optimum utilization of PV power. In their design, daily sun's declination was taken into account by a specially developed crank mechanism. A simple open-loop control provided precise tracking for both polar and declination axes, via step motors and worm gears. To measure insolation incident on the cells and modules, six pyranometers were connected in series and a reference cell was mounted on the tracker. Several measurements such as ambient and module surface temperature, direct normal irradiance, wind speed, voltage and current sensors were taken into account.

The collected data were sent to a PC and the voltage-current and power-voltage curves were drawn. Their tests revealed that the difference in the highest power obtained via two methods: one from searching highest power during voltage-current scans and second found by mathematical methods, was less than 0.02% [45]. Sangani et al. fabricated and tested a V-trough (2-sun) concentrator using different sun trackers to reduce generated electric cost with PV. Their tracking modes were seasonal tracking (A), one-axis N–S tracking (B) and diurnal tracking (C). Experimental results for I–V characteristic curves and output power from the PV module at an insolation level of 900 W/m^2 assembled at different tracking modes are shown in Fig. 4.4 [46].

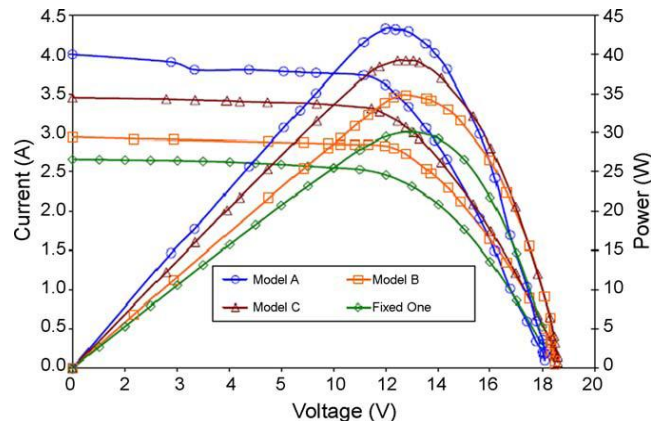


Fig. 4.4 I–V curves and power output for different V-troughs concentrator PV systems assembled according to model-A, model-B and model-C [46].

Pavel et al. analyzed experimentally and theoretically the collected energy in original tracking and non-tracking bifacial and non-bifacial PV solar systems. The calculated and measured tracking effect showed an increase of 30–40% in collected energy while for tracking case with bifacial panels and reflector collecting solar radiation for the rear face gave an increase in collected energy of 50–60% for the same panel [47]. Felske evaluated the variation of azimuth and tilt angle on effectiveness of flat plate solar collectors. It was concluded that for a given tilt angle, the yearly energy collection is almost insensitive to azimuth angle until the vertical orientation is approached at which the collected energy actually increases with increasing the azimuth angle. In this case, the optimum tilt angle is quite insensitive to azimuth angle. For a given azimuth angle, an optimum collector tilt angle is between 38 and 108 less than the latitude. Finally, it was mentioned that even for locations having symmetric irradiation about solar noon it is desirable to orient the collector west of south, since afternoon temperatures are usually higher than morning temperatures [48]. Stern et al. designed, fabricated, tested and demonstrated a modular and fully integrated 15-kW-AC, one-axis solar tracking PV power. The tracker used potentiometer and integral pendulum to provide a positive feedback signal to the tracker motor and actuator. It was concluded that single-axis solar tracking provides 20% more energy in a typical year than that of a fixed-axis PV system. Also, the net reduction in the total cost of single-axis solar tracking grid connected PV power system was found to be 23.3% [49].

Naidoo et al. developed three algorithms for parabolic trough solar collector tracking. In the first method, they used discrete number of pulses to position the trough. The rotary encoder used in this project to provide feedback on the absolute angular position of the trough had 0.144° per pulse. In the second, method the trough is positioned in the N–S axis in order to track the sun in the E–W direction. In order to position the sun, a mathematical algorithm in a PLC programmed software was used along with longitude and latitude based on the geographical location of the trough. In the third system, a fuzzy logic controller based on an intelligent control algorithm was used. Fluid temperature, wind speed and trough position were inputs where trapezoidal form and drive speed were outputs. The relation between inputs and outputs was defined with IF–THEN rule. No report was provided for any comparison or efficiency evaluation [50]. Stolfi et al. designed and constructed a working prototype two axis solar tracking and concentrating apparatus for a heliostat array. To actuate the necessary motion of the apparatus, two step motors were used. To provide a horizontal motion, the unit moves on a turntable controlled by a pair of worm gears. The reflective panel tilts up and down using a simple spring-driven hinge. In this system, a master unit is used to position the slaves. This is accomplished by both monitoring the output of the PV array and using an automatically generated database of previous known good slave positions with corresponding reflected lights, solar position, and/or time of day values. The tests showed that the tracking increases the power output by increasing the output current. These tests also showed that the reflectors created uniform, concentrated light areas suitable for focusing onto the PV cells [51].

Mwithiga et al. designed and constructed a dryer with limited sun-tracking capability that operated manually. The dryer consisted of a gauge 20 mild steel flat absorber plate formed into a topless box. The drying unit was bolted onto a shaft which in turn was mounted on to a stand so as to face E–W direction. A selector disc on the stand allowed the tilt angle that the drying unit made with the horizontal, to be easily adjusted in increments of at least 15° . This way, the collector plate could be intermittently adjusted in order to track the sun during the day. Four dryer settings for tracking the sun were created. The dryer was set at an angle of 60° to the

horizontal facing east at 8.00 a.m. They adjusted the angle of the dryer made with the horizontal either one, three, five or nine times a day when either loaded with coffee beans or under no load conditions. The results showed that the solar dryer can be used to successfully dry grains. Drying of coffee beans could be reduced to 2–3 days as opposed to sun drying without tracking system, which takes 5–7 days and the temperature inside the chamber could reach a maximum of 70.4°C [52]. Romyantsev et al. designed and constructed a close-loop sun-tracking system for 1 kWp solar installations. Their design of the sun-tracker was based on constructing the cheapest structural materials, such as roll-formed perforated channels and bendings, made of zinc-protected steel. Tracking mechanism was fully automatic managed by an analogue sun sensor. Tracker consisted of two main moving parts: a base platform moving around vertical axis and a suspended platform with PV modules moving around horizontal axis. The base platform was equipped with three wheels one of which was connected to an azimuth drive. The suspended platform was a frame where concentrator modules were installed as three steps of a stair. Position of the suspended frame can vary in the range of $\pm 45^\circ$ symmetrically about a horizontal plane ensuring alignment of the modules in elevation. The base platform was driven by one of the wheels moving along a circle of a large radius. If motors (DC 12 V) were switched in use continuously, rotation velocity of the platforms was near to 1 rotation per hour, i.e. much faster, than it was necessary for a normal tracking. Continuous rotation of the motors was carried out for returning the trackers from “sunset” to “sunrise” position and for fast “searching” the sun, after cloudy periods. At normal tracking, the motors were switched on periodically, after each 8–10 s [53].

Bingol et al. proposed, implemented and tested a microcontroller based two-axis solar tracking system. They used light dependent resistors as sensors, stepper motors as actuators and a microcontroller. In addition, the system was connected to a PC via RS232 for sun position monitoring. A crystal with a frequency of 4 MHz was used as a clock signal generator for the microcontroller. The panel degree from vertical axis was fixed at 50° . The experimental study for two solar collector panels, one stationary and the other rotary were employed in the test. Temperature of the panels versus time was measured with a minute interval and 50 data were captured. The angle of intervals was almost 5.2° . A distinction of 9 8C between rotary and stationary panel was observed. This result verified that the rotary panel containing solar tracking system took more light density than the stationary panel [54]. Lakeou et al. designed and constructed a two-axis sun-tracking system to follow the sun in azimuth and solar direction based on a programmable logic device (an 84-pin, Xilinx XC95108). Through an H-bridge structure, a controller is connected to DC motors. Initially, once the location is selected, the azimuth elevation range is determined and the angular steps are calculated. The total number of tilt steps was 12. For monitoring the power generation, they also connected this tracking device to a PC by a code written in Assembly or C++ languages. They concluded that the proposed sun-tracker was cost effective and flexible [55].

An MPPT system consists of two basic components: a switch-mode converter and a control/tracking section. The switch mode converter is the core of the entire system and allows energy at one potential to be drawn, stored as magnetic energy in an inductor, and then released at a different potential. By setting up the switch mode section in various different topologies, either high-to-low or low-to-high voltage converters can be constructed. The goal of an MPPT system is to provide a fixed input voltage and/or current, such that the solar panel is held at the maximum power point, while allowing the output to match the battery voltage. In [56], the converter was controlled to track the maximum power point of the input source under varying input and output parameters and was shown to provide a minimum input source saving of 15% for 3-5 kWh/day systems. Brown and Stone [57] developed a tracking system for solar concentrators in which a neural network was applied to an error model in order to compensate for tracking errors. The test data showed that the resulting system was capable of reducing the tracking error to a value of less than 0.01° (0.2 mrad).

In 1997, Stone and Sutherland [58] presented a multiple tracking measurement system comprising more than 100 heliostats for tracking the sun’s position on an hourly basis from early morning to late evening. Hua and Shen [59] compared the solar tracking efficiencies of various MPPT algorithms and implemented a simple control method which combined a discrete time control scheme and a proportional-integral (PI) controller to track the maximum power points (MPPs) of a solar array. Kalogirou [60] presented a one-axis sun-tracking system utilizing three light-dependent resistors (LDRs). The first LDR detected the focus state of the collector, while the second and third LDRs were designed to establish the presence (or absence) of cloud cover and to discriminate between day and night, respectively. The output signals from the three LDRs were fed to an electronic control system which actuated a low-speed 12 - V DC motor in such a way as to rotate the collector such that it remained pointed toward the sun (Fig 4.5)

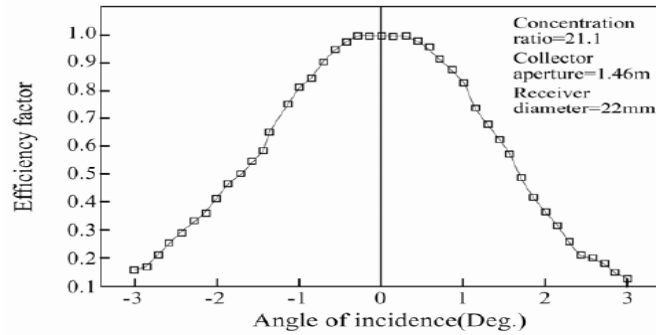


Fig 4.5 Collector acceptance angle [60].

Khalifa and Al-Mutawalli [61] developed a two-axis sun tracking system to enhance the thermal performance of a compound parabolic concentrator. The system was designed to track the sun's position every three to four minutes in the horizontal plane and every four to five minutes in the vertical plane. As shown in Fig 4.6.

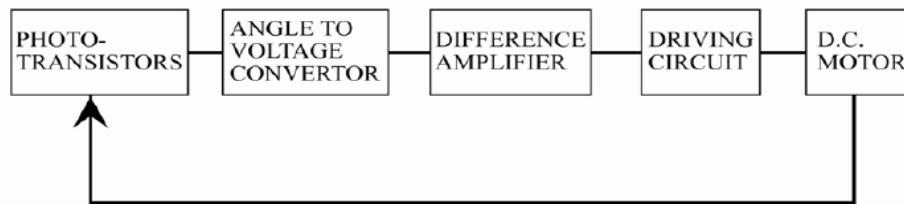


Fig 4.6 Block diagram of sun-tracking system [61]

The tracking system was comprised of two identical sub-systems, one for each axis, with each sub-system consisting of two adjacent photo-transistors separated by a partition of a certain height. In the tracking operation, the difference in the voltage signals of the two photo-transistors was amplified and used as a command signal to drive the collector around the corresponding axis until the voltage difference reduced to zero, indicating that the sun's rays were once again normal to the collector surface. It was shown that the tracking system had a power consumption of just 0.5 Whr and yielded an improvement of around 75% in the collected solar energy, compared to a fixed collector of equivalent dimensions.

Aiuchiet *al.* [62] presented a simple sun tracking photo-sensor designed to ensure a constant direction of the reflected solar radiation. In the proposed device, two photo-cells were placed side by side at the bottom of a box with an aperture. When the reflected solar radiation passed through the aperture, the photo-cells were fractionally illuminated and produced an electric current proportional to the size of the illuminated area. A constant direction of the reflected solar radiation was maintained simply by monitoring the output signals of the two photo-cells and adjusting the angle of the reflection mirror as required to ensure that the two signals remained equal at all times. It was shown that the resulting system achieved a tracking error of less than 0.6 mrad on a sunny day.

In 1983, Al-Naima and Yaghobian [63] developed a solar tracking system featuring a two-axis equatorial mount and a microprocessor, in which the tracking operation was performed on the basis of the astronomical coordinates of the sun. The experimental results demonstrated that the proposed system yielded a significantly better tracking performance than that obtained by a conventional sensor controlled system. Several years later, Lorenz [64] proposed a set of design guidelines for a window glazing which rejected solar radiation during the summer, but accepted it during the winter. The design featured a purely passive control algorithm based on seasonal changes in the incident angle of the solar rays.

Jinayim et al. designed a highly efficient low power consumption tracking solar cells of a white LED-based lighting system. Their evaluated one-axis tracker used a stepping motor commanded by a PIC microcontroller. A photo-resistor was put in a dark box with small hole on the top. With maximum illumination detection it worked by the PIC command. If no sun light is detected by the photo resistor, the zero state actuates the system until the real state is detected.

The sun energy curves and fixed and tracking panel energy curves were drawn and it was concluded that although the tracking mode was 100% efficient, the actual charge current was somewhat lower, as some power was lost due to the solar cell temperature. Finally, they recommended not using tracking system for small solar panels because of high energy losses in the stepping motor [65]. Hatfield designed, constructed and tested a microcontroller based two-axis sun-tracking device. Movement of the PV module was achieved with a 12 V linear actuator where its full course was 20 cm. A potentiometer with a voltage range of 0–5 V was used for angle measurement for a full revolution (360°) of the pot. Control of the tracker was via the light sensor and a micro controller. A DC relay was used to disconnect the load from the solar module during the open circuit voltage read by the A/D converter on the micro controller. The final results showed an efficiency increase of 27% when compared to that of a fixed panel [66].

Aiuchi et al. developed a closed loop photo-sensor controlled heliostat using an equatorial mount. Also, two sensors were used a fixed one with 32° inclination to the south. The required position was calculated in advance and was programmed into PLC. The PLC controls the actuator to adjust the panel to maintain position perpendicular to the sun. They claimed that consumed power by the control system was less than 2% of the collected energy by the tracking system. After drawing several voltage-current and power generation characteristic curves for different sun trackers, they concluded that there were increases up to 43.87, 37.53, 34.43 and 15.69% of electrical power gain, respectively for the two-axis, E–W, vertical and N–S tracking, as compared to that of the fixed one [67]. Zeroual et al. designed and constructed a closed loop sun tracking microprocessor with electro-optical sensors to control a water heating solar system. Many parameters such as wind velocity, pressure and ambient temperature were also controlled. The long period tests in variable conditions, confirmed the accuracy of the system [68].

Ioffe Institute PV Lab., designed a 1 kW closed loop tracker in which the turn angle can vary in the range of $\pm 70^\circ$ about horizontal and vertical planes. Continuous rotation of motors, turn the structure from sunrise to sunset. At normal operation, motors are switched on automatically every 5–8 s. Two multi-junction III–V cells are used as the light sensitive elements in the side walls and back walls of a special element namely main sensor and additional sensor. Photocurrent from these cells goes to a transistor and a relay to activate motor in the desired direction [69]. Gagliano et al. designed and simulated a two-axis sun-tracking system based on a photo-resistor sensor and investigated the effects of energy gain between a fixed PV panel and a tracked one. The sensing device consisted of a nine light-dependent resistor (LDRs) for rotation, and three aligned LDRs for inclination, positioned into suitable plastic supports. It was concluded that the main advantage of the proposed tracking system was the low cost of the sensing apparatus, gained from a real time elaboration procedure on sensors data [70].

Zogbi et al. designed and constructed a low cost two-axis (elevation and azimuthally) sun-tracking system by classical electronic units. Four electro-optical sensors were placed in each quadrant formed by two rectangular planes intersecting each other in a line. The tracking control unit consists of an amplifier and other electronic parts to compare the received signals from each pair of sensors and to command two motors for device rotation. The system had an east return-and-stand by circuit to system stand at night and return eastward in the following morning. If the output from one of the sensors becomes greater than the threshold, the corresponding motor is activated by an amplifier until the error signals reduce to be less than the threshold. The corresponding time duration was 15 s. It was concluded that the constructed prototype operates successfully under variable light intensity [71]. Rumala designed and constructed a closed loop automatic sun-tracking system based on the shadow method. Photo-resistive sensors were placed on a platform under a pair of back to back mounted semi-cylinder in an E–W and N–S facing. The rigid platform had two ball jointed track arms for elevation and lateral tracking that were actuated by cam driven motors. A signal conditioning circuit of a pre-amplifier along with a low pass filter feed an amplifier to move the servomotor and to correct the differential in detected solar irradiation. The shade remains in the sunset position until the auto start up of the morning of the following day [72]. Urbano et al. assessed 5-W-peak PV module for tracking solar oven concentrator system with 2.6 kW/sub-th/capacity with 200 kg weight. The tracking system was driven by means of two 36 W, 12 V DC motors to follow the sun independently in altitude and azimuth directions. The electronic circuit commands DC motor to rotate as a function of the optical sensors for altitude and azimuth positions [73]. Karimov et al. constructed a one-axis PV tracker system with four solar modules installed on a rotor; its other axis was manually adjustable in order to fix the inclination angle of modules at 23° , 34° and 45° . Solar modules were divided into two pairs and the angle between the modules of a pair was 170° . Main modules was used both for the sensing and energy conversion purposes.

The modules were connected to bridge circuit very similar to the Wheatstone bridge. If the output voltage from modules is not equal, the voltage applied to the DC motor is not zero and as a result, the motor starts turning. Their research shows for tracking system, unlike the fixed modules, the voltage output in the evening and morning are not very different and the tracking mode collects 30% more energy [74]. Aliman et al. developed a new sun-tracker to gain high concentration solar energy. Their system consists of a master mirror surrounded by several slave mirrors. The master mirror reflects sun beams to a stationary target. Sun image in this target acts as a reference for all slave mirrors. The sun-tracker had two tracking axes perpendicular to each other. One is the rotational axis pointing toward the target; the other is the elevation axis parallel to the reflector. As the sun moves through the sky from the morning to solar noon, the mirror plane will rotate starting from horizontal and turning to vertical. The angular movement about this rotation axis is denoted as ρ . They derived a formula based on time and date for ρ to represent an elevation/rotation tracking mode which was proved to be successful [75]. Saxena et al. designed and fabricated a two-axis microprocessor based controller for sun-tracking that follows the sun in azimuth and altitude directions by two step motors. The system acts in both closed-loop and open-loop modes. Their system consisted of data acquisition and storage facility, battery control facility, system monitoring, RAM, converter card, microprocessor card, and sensor card for wind, cloud, altitude reverse, altitude forward, azimuth reverse, azimuth forward detection. In the closed-loop mode, the tracker starts at about 5 a.m. and moves under CLOUD mode till the sun is out. In the evening, further forward motion stops. The tracker is brought back to HOME position in the night. The data for the PV parameters and meteorological parameters are acquired every 10 min [76].

Nuwayhid et al. presented a simple exercise in designing, building and testing a PC connected two-axis solar tracker concentrator. They predicted the solar position by using solar altitude and the solar azimuth angles which in turn vary in sinusoidal form and both functions of time. Each axis was connected to a DC motor and each motor had a relay to count certain number per revolution. The angle-per-counts relation was determined from experimental data. When the speed of the hour angle motor is reduced to 0.23 rpm, an installed gear box increases the speed to 23 rpm. The motors and their position sensors were connected to a PC. The PC computes solar time and solar angle at a given site. The system uses a temperature sensor and also nine LDR sensors in a tube to define sun image. It was concluded that tracking increases the working fluid's temperature in the range of 200–600° C in comparison to that of un-tracking that operates in the range of 80–200° C. But simple design and low cost of the un-tracking systems are attractive options to be overlooked easily [77]. Al-Jumaily et al. studied the performance of a flat linear Fresnel lens concentrating solar radiation on two absorbers connected in series. It was manufactured in such a way to track the sun in two dimensions (the altitude and azimuth angles). More than 200 tests were carried out to evaluate the thermal and optical efficiencies versus hour angle and fluid inlet and outlet temperatures. They found that due to use of two dimensional sun-trackers that keep the incident flux always perpendicular to the collector, the optical efficiency maintained constant thorough the day (about 64%) [78].

Koyuncu et al. evaluated a microprocessor based sun-tracking system to control the movement of a solar panel. To limit panel movement, the maximum positions at east and west were limited using two limit switches. The status of the limit switches is read by the microprocessor. They concluded that using tracking device to keep panels perpendicular to solar direction maximizes the thermal energy obtained from the solar panels [79]. Shaltout et al. designed and constructed a V-trough concentrator on a PV full tracking system. The system gave relatively high gain in the amorphous Si solar cell's power which was about 40% more than that without a concentrator. Their graphical comparison between concentrated horizontal and tracking radiation showed an increase in gain of about 23% for the latter one [80]. Baltas et al. evaluated the power output for fixed, step tracking and continuous tracking systems in several locations. They used direct radiation, total radiation on horizontal surface and dry bulb temperature data for computer simulation. They stated that Freon driven trackers are good for a flat plate array unlike for concentrating PV systems, due to their independence of good tracking accuracy. By comparing the energy output from various tracking systems for a typical year, they concluded that the two step tracking arrays (E–W direction varying twice per day, south facing tilt varying monthly) provides about 95% of the energy obtained from continuous tracking arrays. Also, the continuous tracking mode provided 33, 25.5 and 22.5% more energy in different locations over fixed arrays, respectively. Continuous tracking increased the energy production 29.2 and 33% over south facing fixed arrays, respectively, for reflection non-accounting and reflection accounting systems [81]. Abdallah [82], designed and constructed a two-axes, open loop, PLC controlled sun-tracking system. Two tracking motors, one for the joint rotating about the horizontal N–S axis and the other for the joint rotating about the vertical axis were used. The daylight divided into four intervals and during each of them the solar and motors speed was defined and programmed into PLC. He predicted

that the power consumption to drive motors and control systems hardly exceeds 3% of power saved by the tracking system. Fig. 4.7 shows energy comparison between the tracker and the fixed surface inclined at 32°. He concluded that the use of two-axes tracking surfaces results in an increase in total daily collection of about 41.34% as compared to that of a fixed one.

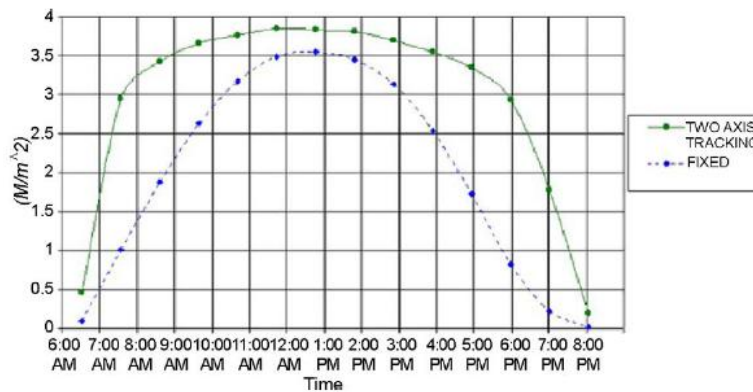


Fig.4.7. Energy comparison between tracking and fixed solar system [82]

4.1 Conclusion

Advances in the improvement of sun tracking systems have enabled the development of many solar thermal and photovoltaic systems for a diverse variety of applications in recent years. Compared to their traditional fixed-position counterparts, solar systems which track the changes in the sun's trajectory over the course of the day collect a far greater amount of solar energy, and therefore generate a significantly higher output power. This paper has presented a review of sun tracking systems developed over the past years. Overall, the results presented in this review confirm the applicability of sun tracking system for a diverse range of high performance solar-based applications.

REFERENCES

- [1] A. Zahnd, H. McKay, and H. M. Kimber, "Benefits from a Renewable Energy Village Electrification System", *Renewable Energy*, **34**(2009), pp. 362–368
- [2] A. Al-Mohamad, "Efficiency Improvements of Photo-Voltaic Panels Using a Sun-Tracking System", *Appl. Energy*, **79**(2004), pp. 345–354.
- [3] Onyegegbu S. O. "Renewable Energy Potentials and Rural Energy Scenario in Nigeria." *Renewable Energy for Rural Industrialization and Development in Nigeria*. UNIDO (2008).
- [4] California Institute of Technology. Basic research needs for solar energy utilization. Report of the basic energy sciences workshop on solar energy utilization; April 18–21, 2005.
- [5] S. Abdallaha and O. O Badranb, "Sun Tracking System for Productivity Enhancement of Solar Still", *Desalination*, **220**(2008), pp. 669–676.
- [6] D.B.N. Nnadi, "Environmental/Climatic Effect on Stand-Alone solar Energy Supply Performance For Sustainable Energy", *Nigerian Journal of Technology (NIJOTECH)* Vol. 31, No. 1, March, 2012, pp. 79-88.
- [7] Walraven R. calculating the position of the sun. *Solar Energy* 1977;20:393–7.
- [8] Oladiran M.T. Mean global radiation captured by inclined collectors at various surface azimuth angles in Nigeria. *Applied Energy* 1995;52:317–30.
- [9] Roth P, Georgiev A, Boudinov H. Cheap two-axis sun following device. *Energy Conversion and Management* 2005;46:1179–92.
- [10] Tracstar. Should you install a solar tracker?; 2007. <http://www.helmholz.us/smallpowersystems/>.
- [11] Kvasznicza Z, Elmer G. Optimizing solar tracking systems for solar cells. In: *The 4th Serbian–Hungarian joint symposium on intelligent systems*; 2006.
- [12] Akhmedyarov, K.A.; Bazarov, B.A.; Ishankuliev. B.; Karshenas, K.E.; Schaimerdangulyev, G. Economic efficiency of the FV-500 solar photoelectric station with automatic tracking of the sun. *Appl. Solar Energy* **1986**, *22*, 44-47.
- [13] Maish, A. B. Performance of a self-aligning solar array tracking controller. In *Proceedings of the IEEE Photovoltaic Specialists Conference*, Kissimmee, FL, USA, May 21-25, 1990.
- [14] Khalifa A.N.; Al-Mutawalli S.S. Effect of two-axis sun tracking on the performance of compound parabolic concentrators. *Energ. Convers. Manage.* **1998**, *39*, 1073-1079.
- [15] Mumba J. Development of a photovoltaic powered forced circulation grain dryer for use in the tropics. *Renewable Energy* 1995;6(7):855–62.
- [16] Abdallah, S. The effect of using sun tracking systems on the voltage-current characteristics and power generation of flat plate photovoltaics. *Energ. Convers. Manage.* **2004**, *45*, 1671-1679
- [17] Helwa NH, Bahgat ABG, Shafee AMRE, Shenawy ETE. Maximum collectable solar energy by different solar tracking systems. *Energy Sources* 2000;22:23–4.
- [18] Chicco G, Schlabach J, Spertino F. Performance of grid-connected photovoltaic systems in fixed and sun-tracking configurations; 2007. <http://www.labplan.ufsc.br/congressos/PowerTech07/>.
- [19] Nann S. Potential for tracking PV systems and V-troughs in moderate climates. *Solar Energy* 1990;45(6):385–93.

- [20] Gay CF, Yerkes JW, Wilson JH. Performance advantages of two-axis tracking for large flat-plate photovoltaic energy systems. In: Proceedings of the 16th photovoltaic specialists conference, San Diego, September 27–30, 1982; p. 1368–71.
- [21] Nafeh AESA. Evaluation of the optimum tilts of a PV array using maximum global insolation technique. *International Journal of Numerical Modeling Electronic Networks Devices and Fields* 2004;17:385–95.
- [22] Tomson T. Discrete two-positional tracking of solar collectors. *Renewable Energy* 2008;33:400–5.
- [23] Kalogirou SA. Design and construction of a one-axis sun-tracking. *Solar Energy* 1996;57(6):465–9.
- [24] Ai B, Shen H, Ban Q, Ji B, Liao X. Calculation of the hourly and daily radiation incident on three step tracking planes. *Energy Conversion and Management* 2003;44:1999–2011.
- [25] Lorenzo E, Perez M, Ezpeleta A, Acedo J. Design of tracking photovoltaic systems with a single vertical axis. *Progress in PV Research and Applications* 2002;10:533–43.
- [26] Ibrahim SMA. The forced circulation performance of a sun tracking parabolic concentrator collector. WFEC; 1996. <http://cat.inist.fr/>.
- [27] Brunotte M, Goetzberger A, Blieske U. Two-stage concentrator permitting concentration factors up to 300_ with one-axis tracking. *Solar Energy* 1996;56(3):285–300.
- [28] Clifford MJ, Eastwood D. Design of a novel passive solar tracker. *Solar Energy* 2004;77:269–80.
- [29] Al-Mohamad A. Efficiency improvements of photo-voltaic panels using a sun-tracking system. *Applied Energy* 2004;79:345–54.
- [30] Abu-Khader MM, Badran OO, Abdallah S. Evaluating multi-axes sun-tracking system at different modes of operation in Jordan. *Renewable and Sustainable Energy Reviews* 2008;12:864–73.
- [31] Debasol, solar power. Solar tracker; 2007. www.girasolar.com.
- [32] Contreras A, Garcia J, Gonzalez C, Martinez E. Portable solar tracker; May 08, 2006. http://engineering.utsa.edu/ee/sd/projects/spring2006/13/Team_13_Final_Presentation.
- [33] Rosell JI, Vallverdu X, Lecho MA, Ibanez M. Design and simulation of a low concentrating PV/thermal system. *Energy Conversion and Management* 2005;46:3034–46.
- [34] Hamilton SJ. Sun-tracking solar cell array system. Bachelor of Engineering Thesis Division of Electrical Engineering. Department of Computer Science & Electrical Engineering, University of Queensland; October, 1999.
- [35] Huang BJ, Sun FS. Feasibility study of one-axis three positions tracking solar PV with low concentration ratio reflector. *Energy Conversion and Management* 2007;48:1273–80.
- [36] Kalogirou SA. Design and construction of a one-axis sun-tracking. *Solar Energy* 1996;57(6):465–9.
- [37] Khalifa A-JN, Al-Mutawalli SS. Effect of two-axis sun tracking on the performance of compound parabolic concentrators. *Energy Conversion and Management* 1998;39(10):1073–9.
- [38] Canada J, Utrillas MP, Lozano JAM, Pedros R, Amo JLG, Maj A. Design of a sun tracker for the automatic measurement of spectral irradiance and construction of an irradiance database in the 330–1100 nm range. *Renewable Energy* 2007;32:2053–68.
- [39] Gagliano S, Savalli N, Tina G, Pitrone N. Two-axis sun tracking system: design and simulation. In: Eurosun 2006; 2006.
- [40] Poulek V, Libra M. A very simple solar tracker for space and terrestrial applications. *Solar Energy Materials & Solar Cells* 2000;60:99–103.
- [41] Poulek V, Libra M. New bifacial solar trackers and tracking concentrators; 2007. <http://www.solar-trackers.com>.
- [42] Alata M, Al-Nimr MA, Qaroush Y. Developing a multipurpose sun tracking system using fuzzy control. *Energy Conversion and Management* 2005;46: 1229–45.
- [43] Rubio FR, Ortega MG, Gordillo F, Lopez-Martinez M. Application of new control strategy for sun tracking. *Energy Conversion and Management* 2007;48:2174–84.
- [44] Bakos GC. Design and construction of a two-axis sun tracking system for parabolic trough collector (PTC) efficiency improvement. *Renewable Energy* 2006;31:2411–21.
- [45] Durisch W, Urban J, Smestad G. Characterization of solar cells and modules under actual operating conditions, WREC. In: Proceedings of the WREC-IV world renewable energy congress; 1996. p. 359–66.
- [46] Sangani CS, Solanki CS. Experimental evaluation of V-trough (2 suns) PV concentrator system using commercial PV modules. *Solar Energy Materials & Solar Cells* 2007;91:453–9.
- [47] Pavel YV, Gonzalez HJ, Vorobiev YV. Optimization of the solar energy collection in tracking and non-tracking PV solar system. In: Proceedings of the 1st international conference on electrical and electronics engineering, ICEEE; 2004. p. 310–4.
- [48] Felske JD. The effect of off-south orientation on the performance of flat-plate solar collectors. *Solar Energy* 1978;20:29–36.
- [49] Stern M, Duran G, Fourer G, Mackamul K, Whalen W, Loo MV, et al. Development of a low-cost integrated 20-kW-AC solar tracking sub-array for grid connected PV power system applications. Final technical report. NREL/STR-520-2475 9. National Renewable Energy Laboratory, A National Laboratory of the U.S. Department of Energy Managed by Midwest Research Institute for the U.S. Department of Energy; June 1998.
- [50] Naidoo P, Niekerk TIV, Brooks M. Intelligent control and tracking of a parabolic trough solar collector. First African Control Congress, University of Cape Town, Cape Town; 2003.
- [51] [51] Stolfi F, Bersohn D, McIver B, Shaw S, Vance N, Wang X. Solar concentrating and tracking apparatus. Final report. Columbia University, Department of Mechanical Engineering; May 2, 2007.
- [52] [52] Mwithiga G, Kigo SN. Performance of a solar dryer with limited sun tracking capability. *Journal of Food Engineering* 2006;74:247–52.
- [53] [53] Rummyantsev V, Chalov A, Ionova E, Larionov V, Andreev V. Concentrator PV modules with multi-junction cells and primary/secondary refractive optical elements. In: The 19th European photovoltaic solar energy conference; 2004.
- [54] [54] Bingol O, ALTINTAS, A, O'NER Y. Microcontroller based solar-tracking system and its implementation. *Journal of Engineering Sciences* 2006;12(2):243–8.
- [55] [55] Lakeou S, Ososanya E, Latigo BO, Mahmoud W, Karanga G, Oshumare W. Design of a low-cost digital controller for a solar tracking photo-voltaic (PV) module and wind turbine combination system. In: 21st European PV solar energy conference; 2006.
- [56] [56] Enslin, J.H.R. Maximum power point tracking: a cost saving necessity in solar systems. *Renew. Energ.* 1992, 2, 543-549.
- [57] [57] Brown, D.G.; Stone, K.W. High accuracy/low cost tracking system for solar concentrators using a neural network. In *Proceedings of the 28th Intersociety Energy Conversion Engineering Conference*, Atlanta, GA, USA, Aug. 8-13, 1993.
- [58] [58] Stone, K.W.; Sutherland J.P. Solar two heliostat tracking performance. In *Proceedings of International Solar Energy Conference*, Washington DC, USA, Apr. 27-30, 1997.
- [59] [59] Hua, C; Shen, C. Comparative study of peak power tracking techniques for solar storage system. In *Proceedings of IEEE Applied Power Electronics Conference and Exposition*, Anaheim, CA, USA, Feb. 15-19, 1998.

- [60] [60] Kalogirou, S.A. Design and construction of a one-axis sun-tracking system. *Sol. Energ.* **1996**, *57*, 465-469.
- [61] [61] Khalifa A.N.; Al-Mutawalli S.S. Effect of two-axis sun tracking on the performance of compound parabolic concentrators. *Energ.Convers. Manage.* **1998**, *39*, 1073-1079.
- [62] [62] Aiuchi, K.; Nakamura, M.; Yoshida, K.; Katayama, Y.; Nakamura, K. Sun tracking photo-sensor for solar thermal concentrating system. In *Proceedings of International Solar Energy Conference*, Portland, OR, USA, Jul. 11-14, 2004.
- [63] [63] Al-Naima, F.M.; Yaghoobian, N.A. Design and construction of a solar tracking system. *Solar Wind Technol.* **1990**, *7*, 611-617.
- [64] [64] Lorenz, W. Design guidelines for a glazing with a seasonally dependent solar transmittance. *Sol. Energ.* **1998**, *63*, 79-96.
- [65] [65] Jinayim T, Arunrungrasmi S, Tanitteerapan T, Mungkung N. Highly efficient low power consumption tracking solar cells for white LED-based lighting system.. *International Journal of Electrical Computer and Systems Engineering* 2007;1(2):1307-5179.
- [66] [66] Hatfield P. Low cost solar tracker. Bachelor of Electrical Engineering Thesis, Department of Electrical and Computer Engineering, Curtin University of Technology; October 2006.
- [67] [67] Aiuchi K, Yoshida K, Onozaki M, Katayama Y, Nakamura M, Nakamura K. Sensor-controlled heliostat with an equatorial mount. *Solar Energy* 2006;80:1089-97.
- [68] [68] Zeroual A, Raoufi M, Ankrim M, Wilkinson AJ. Design and construction of a closed loop sun-tracker with microprocessor management. *Solar Energy* 1998;19(4):263-74.
- [69] [69] Romyantsev VD. Terrestrial concentrator PV systems (book chapter); 2007. p. 151-74. <http://www.springerlink.com/content/r7244751j441832v/>.
- [70] [70] Gagliano S, Savalli N, Tina G, Pitrone N. Two-axis sun tracking system: design and simulation. In: *Eurosun 2006*; 2006.
- [71] [71] Zogbi R, Laplaze D. Design and construction of a sun tracker. *Solar Energy* 1984;33(3/4):369-72
- [72] [72] Rumala S-SN. A shadow method for automatic tracking. *Solar Energy* 1986;37(3):245-7.
- [73] [73] Urbano JA, Matsumoto Y, Asomoza R, Aceves FJ, Sotelo A, Jacome A. 5 Wp PV module-based stand-alone solar tracking system. In: *Proceedings of the 3rd world conference of photovoltaic energy conversion*, vol. 3, nos. 12-16; May 2003. p. 2463-5.
- [74] [74] KarimovKhS, Saqib MA, Akhter P, Ahmed MM, Chatthad JA, Yousafzai SA. A simple photo-voltaic tracking system. *Solar Energy Materials & Solar Cells* 2005;87:49-59.
- [75] [75] Aliman O, Daut I, Isa M, Adzman MR. Simplification of sun tracking mode to gain high concentration solar energy. *American Journal of Applied Sciences* 2007;4(3):171-5.
- [76] [76] Saxena AK, Dutta V. A versatile microprocessor based controller for solar tracking. New Delhi, India: Photovoltaic Laboratory, Centre for Energy Studies, Indian Institute of Technology; 1990. p. 1105-9.
- [77] [77] Nuwayhid RY, Mrad F, Abu-Said R. The realization of a simple solar tracking concentrator for university research applications. *Renewable Energy* 2001;24:207-22.
- [78] [78] AL-Jumaily KEJ, AL-Kaysi MKA. The study of the performance and efficiency of flat linear Fresnel lens collector with sun tracking system in Iraq. *Renewable Energy* 1998;14(14):41-8.
- [79] [79] Koyuncu B, Balasubramanian K. A microprocessor controlled automatic sun tracker. *IEEE Transactions* 1991;37(4):913-7.
- [80] [80] Shaltout MAM, Ghttas A, Sabry M. V-trough concentrator on a PV full tracking system in a hot desert climate. *Renewable Energy* 1995;6(5-6):527-32.
- [81] [81] Baltas P, Tortoreli M, Russell PE. Evaluation of power output for fixed and step tracking PV arrays. *Solar Energy* 1986;37(20):147-63.
- [82] [82] Abdallah S, Nijmeh S. Two axes sun tracking system with PLC control. *Energy Conversion and Management* 2004;45:1931-9.

Prediction of Voltage Instability in Nigeria Interconnected Electric Power System Using V-Q Sensitivity Method

Enemuoh F. O.¹, Madueme T. C.², Onuegbu J. C.¹ and Anazia A. E.¹

¹. Department of Electrical Engineering, Nnamdi Azikiwe University, Awka, Nigeria

². Department of Electrical Engineering, University of Nigeria, Nsukka Nigeria

ABSTRACT

The need to predict power system stability as it concerns voltage status is very important for the system planning, operation and control. This paper presents the prediction of voltage instability in Nigerian interconnected electric power system using V-Q sensitivity method. The method makes use of the least eigenvalue of the Jacobian matrix of the power system to calculate the V-Q sensitivity of the system. The highest sensitivity is an indication of the bus prone to voltage instability. The result from our calculations showed that Nigerian power system has the highest V-Q sensitivity of 0.1474 at the Maiduguri bus followed by Gombe, Kano and Jos with 0.1312, 0.0823 and 0.0370 respectively. It is very clear that the first bus that will collapse on the same percentage of loading will be Maiduguri followed by Gombe then Kano and Jos.

KEYWORDS: Eigenvalue analysis, prediction, voltage instability/collapse, voltage stability, V-Q sensitivity

I. INTRODUCTION

For many years, the demand for and consumption of energy in many countries of the world has been on the increase. The major portion of the energy needs of these nations is electric energy. In Nigeria and other industrial developing nations, the demand for supply of electrical power has been on the increase, which may be as a result of improved economic activities of the people. To satisfy the increasing demand for electricity, complex power system networks have been built. The most usual practice in electric power transmission and distribution is an interconnected network of transmission lines usually referred to as a grid system that links generators and loads to form a large integrated system that spans the entire country. In many countries of the world including Nigeria, generating stations are located thousands of kilometers apart and operate in parallel. The generating stations' output is connected and transmitted through the grid system to load centers nationwide. One of the several problems confronting the efficient performance of an interconnected system is voltage stability. Voltage stability issues are of major concern worldwide because of the significant number of black-outs that have occurred in recent times in which it was involved. For many power systems, assessment of voltage stability and prediction of voltage instability or collapse have become the most important types of analysis performed as part of system planning, operational planning and real-time operation. Voltage stability is defined as the ability of a power system to maintain steady acceptable voltages at all buses in the system under normal operating conditions, and after being subjected to a disturbance [1].

The ability to transfer reactive power from production sources to consumption sinks during steady operating conditions is a major aspect of voltage stability. The consumers of electric energy are used to rather small variations in the voltage level and the system behaviour from the operators' point of view is fairly well known in this normal operating state. Equipment control and operation are tuned towards specified set points giving small losses and avoiding power variation due to voltage sensitive loads. Once outside the normal operating voltage band many things may happen of which some are not well understood or properly taken into account today. A combination of actions and interactions in the power system can start a process which may cause a completely loss of voltage control. It is known that to maintain an acceptable system voltage profile, a sufficient reactive support at appropriate locations must be found. Nevertheless, maintaining a good voltage profile does not automatically guarantee voltage stability. On the other hand, low voltage although frequently associated with voltage instability is not necessarily its cause [2] and [3]. Voltage stability studies of a power system is now essential and is intended to help in the classification and the understanding of different aspects of power system stability [4].

Voltage stability evaluation requires the determination of:

- (i) The parameters and a stress test that establish the structural causes of voltage collapse and instability in each load area (exhaustion of reactive reserves in a reactive reserve basin).
- (ii) A method of identifying each load area (voltage collapse and instability area) that has a unique voltage collapse and instability problem, and
- (iii) A measure of proximity to voltage collapse for each load area (a measure of reactive reserve or voltage control areas with zero reserves in the reactive reserve basin)

One of the operating goals of an electric power system is to attend the power demand keeping the system's voltages as well as the frequency close to rated values. Deviation from these nominal conditions may result in abnormal performance of or even damage to the supplied equipment. An unacceptable voltage level means voltage instability. The voltage instability, also known as voltage collapse of power systems appears when the attempt of load dynamics to restore power consumption is just beyond the capability of the combined transmission and generator system [5]. The problem is also a main concern in power system operation and planning. It is characterized by a sudden reduction of voltage on a set of buses of the system. In the initial stage the decrease of the system voltage starts gradually and then decreases rapidly.

The following can be considered the main contributing factors to the problem [6]:

1. Stressed power system; i.e., high active power loading in the system.
2. Inadequate reactive power resources.
3. Load characteristics at low voltage magnitude and their difference from those traditionally used in stability studies.
4. Transformers tap changer response to decreasing voltage magnitudes at the load buses.
5. Unexpected and or unwanted relay operation may occur during conditions with decreased voltage magnitudes.

So, there is a requirement to have an analytical method, which can predict the voltage collapse problem in a power system. As a result, considerable attention has been given to this problem by many power system researchers. A number of techniques have been proposed in the literature for the analysis of this problem [7]. In this paper, a V-Q sensitivity method has been used to predict voltage instability of Nigerian 330kV, 30bus interconnected electric power system.

II. POWER FLOW PROBLEM

The power flow or load flow is widely used in power system analysis. It plays a major role in planning the future expansion of the power system as well as helping to run existing systems to run in the best possible way. The network load flow solution techniques are used for steady state and dynamic analysis programme [3] and [4]. The solution of power flow predicts what the electrical state of the network will be when it is subject to a specified loading condition. The result of the power flow is the voltage magnitude and the angle of each of the system nodes. These bus voltage magnitudes and angles are defined as the system state variables. That is because they allow all other system quantities to be computed such as real and reactive power flows, current flows, voltage drops, power losses, etc ... power flow solution is closely associated with voltage stability analysis. It is an essential tool for voltage stability evaluation. Much of the research on voltage stability deals with the power-flow computation methods. The power flow problem solves the complex matrix equation:

$$I = YV = \frac{S^*}{V^*} \quad (1)$$

The Newton-Raphson method is the most general and reliable algorithm to solve the power-flow problem. It involves interactions based on successive linearization using the first term of Taylor expansion of the equation to be solved. From equation (1), we can write the equation for node k (bus k) as derived in [8].

$$P_k = |V_k| \sum_{m=1}^n |V_m| [G_{km} \cos(\delta_k - \delta_m) + B_{km} \sin(\delta_k - \delta_m)] \quad (2)$$

$$Q_k = |V_k| \sum_{m=1}^n |V_m| [G_{km} \sin(\delta_k - \delta_m) - B_{km} \cos(\delta_k - \delta_m)] \quad (3)$$

This mismatch power at bus k is given by:

$$\Delta P_k = P_k^{sch} - P_k \quad (4)$$

$$\Delta Q_k = Q_k^{sch} - Q_k \quad (5)$$

The P_k and Q_k are calculated from Equation (2) and (3)

The Newton – Raphson method solves the partitioned matrix equation:

$$\begin{bmatrix} \Delta P \\ \Delta Q \end{bmatrix} = J \begin{bmatrix} \Delta \theta \\ \Delta V \end{bmatrix} \quad (6)$$

Where,

ΔP and ΔQ = mismatch active and reactive power vectors.

ΔV and $\Delta \theta$ = unknown voltage magnitude and angle correction vectors.

J = Jacobian matrix of partial derivative terms

III. EIGENVALUE ANALYSIS

The Eigenvalue analysis mainly depends on the power-flow Jacobian matrix of equation (6). Gao, Morison and Kundur [9] proposed this method in 1992. It can predict voltage collapse in complex power system networks. It involves mainly the computing of the smallest eigenvalues and associated eigenvectors of the reduced Jacobian matrix obtained from the load flow solution. The eigenvalues are associated with a mode of voltage and reactive power variation which can provide a relative measure of proximity to voltage instability.

The analysis is expressed as follows:

Equation (6) can be rewritten as:

$$\begin{bmatrix} \Delta P \\ \Delta Q \end{bmatrix} = \begin{bmatrix} J_{11} & J_{12} \\ J_{21} & J_{22} \end{bmatrix} \begin{bmatrix} \Delta \theta \\ \Delta V \end{bmatrix} \quad (7)$$

By letting $\Delta P = 0$ in Equation (7)

$$\Delta P = 0 = J_{11} \Delta \theta + J_{12} \Delta V, \quad \Delta \theta = -J_{11}^{-1} J_{12} \Delta V \quad (8)$$

and

$$\Delta Q = J_{21} \Delta \theta + J_{22} \Delta V \quad (9)$$

Substituting Equation (8) in Equation (9):

$$\Delta Q = J_R \Delta V \quad (10)$$

Where

$$J_R = \left[J_{22} - J_{21} J_{11}^{-1} J_{12} \right] \quad (11)$$

J_R is the reduced Jacobian matrix of the system.

Equation (10) can be written as

$$\Delta V = J_R^{-1} \Delta Q \quad (12)$$

IV. V – Q SENSITIVITY ANALYSIS

The relationship between system voltage stability and eigenvalues of the J_R matrix is best understood by relating the eigenvalues with the V-Q sensitivities of each bus (which must be positive for stability). J_R can be taken as a symmetric matrix and therefore the eigenvalues of J_R are close to being purely real. If all the eigenvalues are positive, J_R is positive definite and the V-Q sensitivities are also positive, indicating that the system is voltage stable.

V – Q sensitivity analysis calculates the relation between voltage change and reactive power change from equation (12).

$$\Delta V = J_R^{-1} \Delta Q$$

ΔV incremental change in bus voltage magnitude (vector)

ΔQ incremental change in bus reactive power injection (vector)

J_R reduced Jacobian matrix

The elements of the inverse of the reduced Jacobian matrix J_R are the V – Q sensitivities. The diagonal

components are the self sensitivities $\frac{\partial V_i}{\partial Q_i}$ and the nondiagonal elements are the mutual sensitivities $\frac{\partial V_k}{\partial Q_i}$

The sensitivities of voltage controlled buses are equal zero. Positive sensitivities: stable operation, the smaller the sensitivity the more stable the system. As stability decreases, the magnitude of the sensitivity increases, becoming infinite at the stability limit (maximum loadability).

Negative sensitivities: unstable operation. The system is not controllable, because all reactive power control devices are designed to operate satisfactorily when an increase in Q is accompanied by an increase in V.

V. SYSTEM DESCRIPTION OF NIGERIAN 330KV, 30-BUS INTERCONNECTED ELECTRIC POWER SYSTEM

The electrical utility is probably the largest and most complex industry in the world. The electrical engineer, who researches in this industry, will encounter challenging problems in designing future power systems to deliver increasing amounts of electrical energy in a safe, clean and economical manner [10].

The transmission network in Nigeria is characterised by several outages leading to disruption in the lives of the citizenry. According to Anil et al [11], the level of disruption is a function of the dependency of people on electricity, which can be very high for a developed country and not as much as developing countries. In Nigeria, the available energy generated is not enough to meet the demands of the users leading to constant load shedding and blackouts. The Nigerian power stations are mainly hydro and thermal plants. Power Holding Company of Nigeria.(PHCN) generating plants sum up to 6200MW out of which 1920MW is hydro and 4280MW is thermal-mainly gas fired[12].The transmission grid system in Nigeria is predominantly characterised by radial, fragile and very long transmission lines, some of which risk total or partial system collapse in the event of major fault occurrence and make voltage control difficult. These lines include Benin-Ikeja West (280Km) Oshogbo-Benin (251km), Oshogbo-Jebba (249km) Jebba-Shiroro (244km), Birnin-Kebbi-Kainji (310km), Jos-Gombe (265Km) and Kaduna-Kano (230km) [13].These lines experience high voltages under light load conditions and very low voltages under high loading conditions [12]. The Nigerian Electricity Network comprises 11,000km Transmission lines (330kV and 132kV), the sub-transmission line (33kV) is 24,000km, the distribution line (11kV) is 19000km, while the substations are 22,500 [14].

VI. SYSTEM DISTURBANCES/COLLAPSES IN NIGERIAN INTERCONNECTED POWER System

Electricity supply situation in Nigeria is inadequate and unstable; the problems cut across generation, transmission and distribution/commercial operation. Voltage instability and collapse are the major issues in today’s electric power operations. Table 1 shows the system disturbances/collapse in Nigerian Power System from 2000 to 2011. Transmission and generation faults and their effects caused most of the voltage collapse.

Table 1 Summary of System Disturbances from January to December (2000 to 2011)

S/N	Years (Jan-Dec)	No. of Disturbances	Cause of Collapse
1.	2011	19	Transmission
2.	2010	42	Generation/Transmission
3.	2009	39	Generation/Transmission
4.	2008	42	Generation/Transmission
5.	2007	27	Generation/Transmission
6.	2006	30	Generation/Transmission
7.	2005	36	Generation/Transmission
8.	2004	52	Generation/Transmission
9.	2003	53	Generation/Transmission
10.	2002	41	Generation/Transmission
11.	2001	19	Generation/Transmission
12.	2000	11	Generation/Transmission

Source [15]

VII. SAMPLE SYSTEM SIMULATION, RESULTS AND ANALYSIS

The V-Q sensitivities analysis method has been successfully applied to Nigerian power systems. A power flow program based on Matlab is developed to:

1. Calculate the power flow solution
2. Analyze the voltage stability based on eigenvalue analysis
3. Generate the V-Q sensitivities to predict voltage instability or collapse

The Nigerian 330kV, 30Bus Interconnected Power System (NIPS) is shown in the appendix, the model is achieved using elements arrangement. The data required for the simulation are as follows: Line data represented in Table 2; while Table 3 represents load distribution.

The calculated voltage profile of the Power Holding Company of Nigeria (PHCN) 330kV, 30bus interconnected network system is shown in figure 1.

**Table 2 Line Data for Nigeria Integrated Power System (NIPS)
Length 1KM**

S/N	ID	Name	From	To	R(1), Ohm	X(1), Ohm	C(1), uF	B(0), Us
1.	373	L373	B11	B6	13.26402	21.75822	0.000245	0.077
2.	389	L389	B6	B8	0.835	6.52	0.0012	0.377
3.	405	L405	B12	B8	0.7623	5.5466	0.0034	1.068
4.	413	L413	B20	B28	2.2869	16.63992	0.001685	0.529
5.	421	L421	B9	B8	5.21631	39.26934	0.001751	0.55
6.	429	L429	B19	B29	5.21631	39.2693	0.00175	0.55
7.	437	L437	B3	B9	0.20691	1.60083	1.8e-005	0.006
8.	445	L445	B17	B9	1.0291	7.7265	0.0014	0.44
9.	453	L453	B24	B26	2.05821	15.45291	0.000693	0.218
10.	461	L461	B17	B18	10.08414	76.79628	0.000864	0.271
11.	469	L469	B17	B19	7.81001	66.30921	0.000743	0.233
12.	477	L477	B19	B20	12.82842	96.57252	0.001082	0.34
13.	485	L485	B2	B8	0.20691	1.60083	1.8e-005	0.006
14.	493	L493	B12	B13	4.61736	35.19648	0.000396	0.124
15.	501	L501	B12	B14	9.62676	80.3682	0.000904	0.284
16.	509	L509	B13	B14	5.0094	38.3328	0.000496	0.156
17.	517	L517	B14	B21	2.9948	22.5423	0.004	1.257
18.	541	L541	B22	B21	2.0854	15.6925	0.0028	0.88
19.	549	L549	B29	B26	2.0854	15.6925	0.0028	0.88
20.	557	L557	B21	B1	0.5391	4.0239	0.00072	0.226
21.	573	L573	B21	B23	2.9294	22.0523	0.00098	0.308
22.	589	L589	B23	B24	5.79348	44.15895	0.000497	0.156
23.	597	L597	B24	B5	1.06722	8.03682	9.02e-005	0.028
24.	605	L605	B10	B14	0.6534	5.31432	0.000211	0.066
25.	613	L613	B10	B14	0.6534	5.31432	0.000211	0.066
26.	621	L621	B10	B16	0.3267	2.40669	0.000108	0.034
27.	629	L629	B10	B15	3.29967	24.78564	0.000278	0.087
28.	637	L637	B14	B15	0.35937	145.0548	0.000122	0.038
29.	645	L645	B14	B15	0.35937	145.0548	0.000122	0.038
30.	661	L661	B1	B25	2.70072	20.26629	0.000227	0.071
31.	669	L669	B1	B7	2.85318	21.75822	0.000245	0.077
32.	677	L677	B7	B25	1.11078	8.37441	9.38e-005	0.029
33.	685	L685	B4	B10	0.60984	4.82427	0.000884	0.278
34.	732	L732	B23	B26	3	20	0.000332	0.104
35.	829	L829	B30	B9	0.5391	4.0239	0.00072	0.226
36.	175409	L175409	B11	B27	1.4265	10.879	0.00049	0.154

Source [11]

Table 3 Load Distribution for Nigeria Integrated Power System (NIPS)

S/N	ID	Name	LF Type	P, MW	Q, MVAR
1.	182	Load 11	PQ	56.4	42.3
2.	207	Load 14	PQ	332	249
3.	201	Load 13	PQ	133	97.5
4.	213	Load 10	PQ	80	60
5.	286	Load 16	PQ	95	71.25
6.	298	Load 25	PQ	20	15
7.	292	Load 15	PQ	228	171
8.	316	Load 23	PQ	86	64.5
9.	310	Load 24	PQ	264.8	198
10.	304	Load 26	PQ	90	67.5
11.	334	Load 9	PQ	109.6	82.2
12.	322	Load 21	PQ	124.2	93.3

13.	340	Load 17	PQ	390	0
14.	364	Load 19	PQ	65	48.75
15.	370	Load 20	PQ	132.8	99.6
16.	764	Load 18	PQ	130	60
17.	779	Load 12	PQ	144.9	108.68
18.	773	Load 8	PQ	7.9	5.93
19.	175351	Load 22	PQ	20	15
20.	175420	Load 27	PQ	56.4	42.3
21.	175457	Load 30	PQ	130	60
22.	175482	Load 29	PQ	83.45	61.22
23.	175506	Load 28	PQ	80	60

Source [11]

The voltage profile of all buses of the PHCN 30 Bus system as obtained from the load flow result. To have clear indication of voltage collapse on the system loading the V-Q sensitivities calculation was carried out using the system eigenvalues. For a 30bus network with 7generator buses the expected eigenvalues will be 23 since voltage stability is load dependent we expect the eigenvalues at the 23 load buses. Table 4 is the calculated eigenvalues while Figure 2 is the plot of the eigenvalues. From Table 4, all the eigenvalues are positive and this is an indication that the system is stable. For the determination of the buses in the system that will collapse with system loading, the least eigenvalue of 3.4951 will be used.

Table 4 PHCN 30 Bus system eigenvalues

S/N	Eigenvalue	S/N	Eigenvalue
1.	3.4951	13.	183.4425
2.	12.0129	14.	194.8132
3.	21.1896	15.	198.2067
4.	23.1243	16.	214.9579
5.	34.6424	17.	223.3135
6.	49.2926	18.	289.0459
7.	51.1237	19.	420.3368
8.	58.8551	20.	495.4999
9.	107.3404	21.	1104.0739
10.	120.5424	22.	1215.5813
11.	128.6551	23.	1449.9396
12.	131.8992	--	-----

Table 5 The V-Q Sensitivities for the Network System

S/N	ID	Name	Sensitivity, Mvar
1.	175463	N175463- maiduguri- B28	0.1474
2.	53	B-53- Gombe- B20	0.1312
3.	148	N148- Kano-B18	0.0823
4.	45	N45-Jos- B19	0.0370

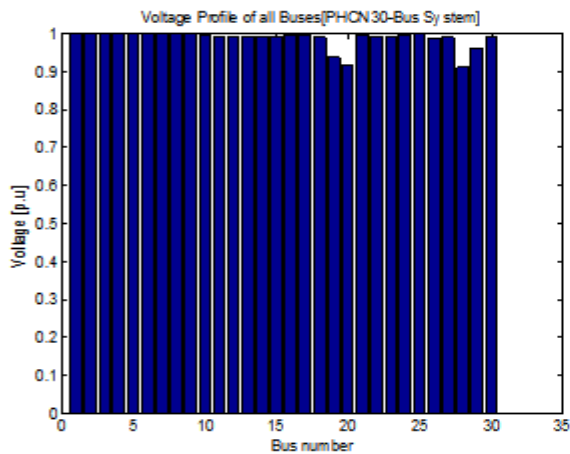


Figure 1 Voltage Profile of (PHCN) 30-Bus System

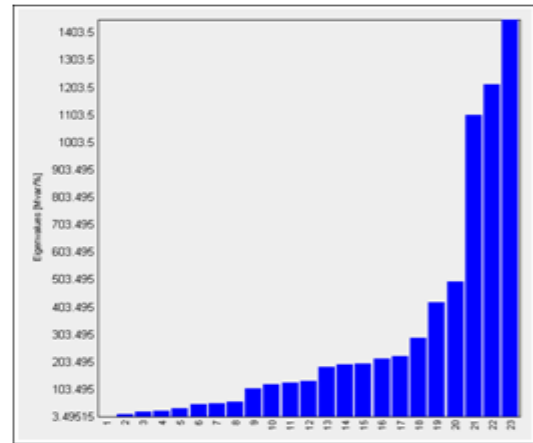


Figure 2 The eigenvalues of the 23 buses

The calculated V-Q sensitivities are represented in Table 5, while Figure 3 is V-Q sensitivities graph representation. The bus with highest sensitivity of 0.1474 is Maiduguri followed by Gombe, Kano and Jos with 0.1312, 0.0823 and 0.0370 respectively. It is now clear that the first bus that will collapse on the same percentage of loading will be Maiduguri followed by Gombe then Kano before Jos.

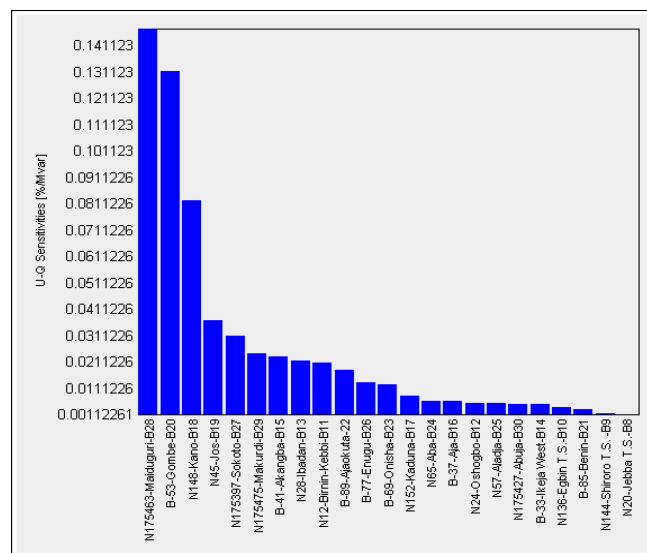


Figure 3 The V-Q sensitivities of all Buses

VIII. CONCLUSION

Voltage instability or collapse is a common feature in Nigerian interconnected electric power system. The problem cut across generation, transmission and distribution. Prediction of power system stability as it concerns voltage state is very important for the system planning, operation and control. In this work, V-Q sensitivity was carried out on the Nigerian 330kV 30Bus interconnected power system. The calculation was done using the least eigenvalue of the Jacobian matrix. The calculated values shows that Nigerian power system has the highest V-Q sensitivity of 0.1474 at the Maiduguri bus followed by Gombe, Kano and Jos with 0.1312, 0.0823 and 0.0370 respectively. It is very clear that the first bus that will collapse on the same percentage of loading will be Maiduguri followed by Gombe then Kano and Jos. V-Q sensitivity is a good method for the prediction of voltage instability of an interconnected power system, it is used in combination with eigenvalue analysis.

REFERENCES

- [1] Taylor, C.W; 'Power System Voltage Stability; MacGraw-Hill, 1994
- [2] Y. Tamura, H. Mori and S. Iwamoto, " Relationship between Voltage Stability and Multiple Load Flow Solution in Electric Systems," IEEE Trans. On Power Apparatus and Systems, Vol. PAS-102, pp.1115-1123, May 1983.
- [3] P.A Lof, T. Smed, C. Anderson and D.J.Hill, " Fast Calculation of a Voltage Stability Index," IEEE Trans. on Power Systems, Vol.7, pp59-64, Feb.1992.
- [4] CIGRE Task Force 38-01-10,; "Modelling of Voltage Collapse including dynamic phenomenon", 1993.
- [5] Abhijit Chakrabarti and Sunita Halder "Power System Analysis Operation and Control" PHI Learning Private Limited, New Delhi, 2008.
- [6] P.A. Lof, G. Anderson and D.J. Hill, "Voltage Stability Indices For Stressed Power System", IEEE Trans. on Power Systems, Vol. 8, 326-335, Feb. 1993.
- [7] V. Ajarapu, and B. Lee "Bibliograph on voltage Stability" IEEE Trans. on Power Systems, vol. 13 pp 115- 125, 1998.
- [8] F.O. Enemuoh, J.C. Onuegbu and A.E. Anazia "Modal Based Analysis and Evaluation of Voltage Stability of Bulk Power System
- [9] B. Gao, G.Morison and P. Kundur, "Voltage Stability Evaluation Using Modal Analysis", IEEE Trans. On Power Systems, Vol.7, No.4, pp. 1423-1543, Nov. 1992.
- [10] J. D. Glover and M.S. Sarma, " Power System Analysis and Design". 3rd Edition Wadsworth Group, Brooks Cole, a division of Thomson Learning Inc.
- [11] P. Anil, H. Mark and T.R. Gaunt "Estimation of Outages in Overhead Distribution Systems of South Africa and of Manhattan, Kansas, USA.7th International Conference on Power System Operation and planning, Cape Town, South Africa. 2007
- [12] O. S. Onohaebi, " Power Outages in the Nigeria Transmission Grid Research Journal of Applied Sciences 4(1): 1-9, 2009 ISSN. 1815-932X Medwell Journals, 2009.
- [13] O.S. Onohaebi and S.O. Igbinovia " Voltage Dips Reduction in the Nigeria 330kV Transmission Grid" Journal of Engineering and Applied Sciences 3(6):496-503, ISSN: 1816-949X Medwell Journals, 2008.
- [14] J. Sadoh " Ph.D. Thesis on Power System Protection : Investigation of System Protection Schemes on the 330kV of Nigeria Transmission Network" Unpublished University of Benin, pp.27.

Automated Transportation Mechanism and Obstacle Detection

Vinita Mathur¹, Dr. Rajesh Kumar², Mr. Aniruddhu Gautam²

¹M.Tech Student of AKG Engineering College, Ghaziabad

²Faculty AKG Engineering College, Ghaziabad

ABSTRACT:

The automotive sector is widely recognized as one of the industries with greatest importance and can assume in the development of a country economy this master's thesis is about the implementation and evaluation of Automated Transportation mechanism and Obstacle Detection. By using a real time visual basic concept. A concept of automated transportation by a cooperative which enable robots to process a complicated or heavy duties task and over the large abstraction in the environment a method transportation utilizing forklift mechanism for lifting process and moving process. The path is store in memory by the programmer, the motion of the vehicle is controlled by stepper motor and controlling of the machine is done by micro- controller. Autonomous robotic vehicle guidance has been developed for industrial difficult.

KEYWORDS: Automated guided vehicles; IR sensors; zigbee transmitter; zigbee receiver microcontroller.

I. INTRODUCTION

Now a day's industries are highly automated for various applications. Automated guided vehicles are now widely used in many industries due to the high level of performance and reliability. All guided vehicles feature some kind of obstacle avoidance. The functions of guided vehicles is to carrier a material and deliver products from one manufacturing point to another; where rail, conveyer and gantry systems are not a suitable option. Designing autonomous vehicle requires the integration of many sensors and actuators according to their task. Obstacle detection is primary requirement for any autonomous vehicle. The vehicle acquires the information from the outside environment and process it according to the sensor mounted over it. Various types of sensors are use for the obstacle detection which is ultrasonic sensors, laser sensor, bump sensors, infrared sensors and soon can be used. Among these entire sensor infra red sensor is most suitable because of its low cost and ranging capability. The guidance systems consist of infra red sensor for obstacle detection, range determination and avoidance the unit is highly resistant to ambient light and nearly impervious to variations in the surface reflectivity of the detected object. It can detect the obstacle within the range of 10 to 80 cm. These systems consist of infra red sensor and micro-controller the sensor is mounted on the vehicle to acquire the information from its surrounding. The infra red sensor is most suitable because of its low cost and ranging capability. The performance measurements indicated by the zigbee software using visual basic which provide the wireless communication for the long distance. Background theories and techniques of Electronic control Technology and analyzed in this paper using both hardware and software consideration.

II. SYSTEM DESCRIPTION

This vehicle is designed to detect the obstacle and avoiding collision base on the distance measurement information obtained from the infra red sensors. Hardware circuit of Automated Transportation mechanism and Obstacle Detection consist of two parts transmission of data though transmitter circuit which consist of zigbee transmitter and a receiver circuit which called as zigbee receiver which receives the data entry though the programmer. Receiver circuit also consists of an IR Sensor which is connected to the microcontroller for obstacle detection. The transmitter circuit is consist of an zigbee transmitter and power regulator LM317 for 3.3V and db 9 connector though pin no. 13 & 14 of the IC in which 5V supply is provides to data is enter though the programmer. Circuit diagram of transmitter is shown in fig 1. Here the data is received by the zigbee receiver which is controlled though the microcontroller IC AT89S52 which control the movements of the motors and up-down movements of the rack and pinion though the relay IC ULN 2003 which is connected to the six motor and the six coil the ULN2003 send the signal according to which the motor movement are decided. Here, an obstacle detection IR (Infrared sensor) sensor is also used for the detection of obstacle during the

loading and unloading of the material which is connected to the pin no. 5 of microcontroller. As shown in block Diagram of the system shown below

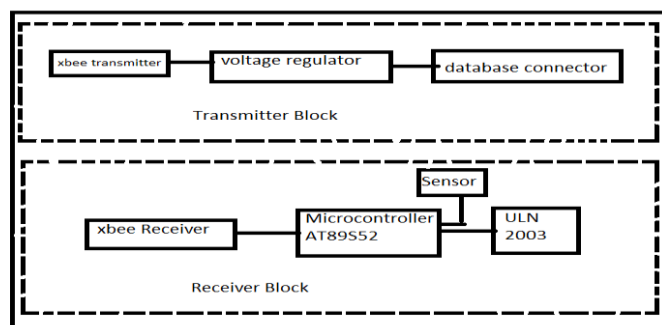


Fig 1 Block dig of Automated guided vehicle and obstacle detection

III. BASIC DESIGN AND ITS REQUIREMENTS

A) The microcontroller

The AT89C52 is a low-power, high-performance CMOS 8-bit microcomputer with 8K bytes of Flash programmable and erasable read only memory (PEROM). The device is manufactured using Atmel's high-density nonvolatile memory technology and is compatible with the industry-standard 80C51 and 80C52 instruction set and pin out. The on-chip Flash allows the program memory to be reprogrammed in-system or by a conventional nonvolatile memory programmer. By combining a versatile 8-bit CPU with Flash on a monolithic chip, the Atmel AT89C52 is a powerful microcomputer which provides a highly-flexible and cost-effective solution to many embedded control applications. The AT89C52 provides the following standard features: 8K bytes of Flash, 256 bytes of RAM, 32 I/O lines, three 16-bit timer/counters, a six-vector two-level interrupt architecture, a full-duplex serial port, on-chip oscillator, and clock circuitry.

B) IR sensor

The digital IR sensor consists of an IR transmitter, IR receiver, and an Op-Amp. Once powered, IR LED continuously keeps emitting IR light. Hence the IR LED acts as transmitter and the photodiode acts as receiver. As soon as the IR radiation is reflected back by a surface, it is absorbed by the receiver (photodiode). A standard op-amp operating in open loop configuration (without any feedback) can be used as a comparator. When the non-inverting input voltage (V_1) is higher than the inverting input voltage (V_2), the high gain of the op-amp causes it to output the most positive voltage, i.e. the output of the op-amp will be high (1). When the non-inverting input voltage (V_1) drops below the inverting input voltage (V_2), the op-amp outputs the most negative voltage, i.e. the output of the op-amp will be low (0).

C) Design and calculation of motor:

		#1	#2	#3
Voltage, V	V	1.5	3	6
No-load speed, ω	rpm	13,400	5,400	4,700
Stall torque, T_s	N-m	0.0003	0.0016	0.007
No-load current, I	A	0.02	0.016	0.01
Terminal resistance, R	Ω	5	9.5	10
Torque constant, K_t	N-m/A	0.001	0.005	0.012
Length	mm	17	21	31
Diameter	mm	8	16	23

IV. MOTOR CALCULATION

D) Voltage Regulator

Voltage regulator is used as voltage regulator in this line follower. This is applied to maintain constant output voltage. Generally it consists of 3 terminals one input one output terminals and another one is ground terminal. The output terminal is then connected to the power supply pin of the microcontroller. It looks like a transistor but it is actually an integrated circuit with 3 legs. It can take a higher, crappy DC voltage and turn it into a nice, smooth 5 volts DC.

Voltage regulator.

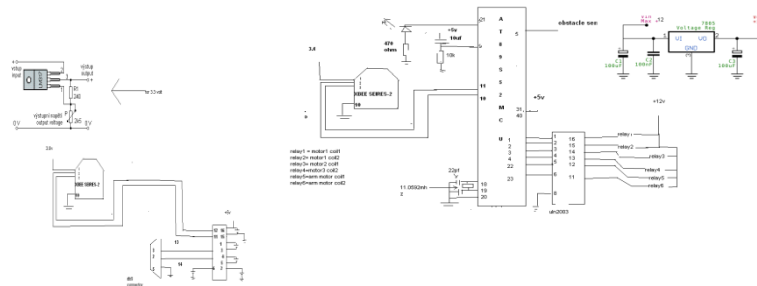


Fig 2 Transmitter and Receiver circuit

IV. CONSIDERATION OF RULES FOR OBSTACLE AVOIDING

1) Path predetermining state

The system must be pre limited for going straight distance, turning left or right and returning back straight to the starting point for no obstacles condition.

2) Obstacle is detected at the left

Stop for a while one or both sensors are detected. The system must turn to right and check if there is any obstacle or not in this turning state. It must return to left and go straight at normal position.

3) Obstacle is detected at the right

The system must be stop for a whether one or both right sensor are detected. It must turn to left and check if there is any obstacle or not in this turning state. And then it will return to right and go straight at normal position.

V. V SOFTWARE IMPLEMENTATION

The focus of network applications under the IEEE 802.15.4 / ZigBee standard include the features of low power consumption, needed for only two major modes (Tx/Rx or Sleep), high density of nodes per network, low costs and simple implementation.

These features are enabled by the following characteristics

- [1] 2.4GHz and 868/915 MHz dual PHY modes.
- [2] This represents three license-free bands: 2.4-2.4835 GHz, 868-870 MHz and 902-928 MHz The number of channels allotted to each frequency band is fixed at 16 channels in the 2.45 GHz band, 10 channels in the 915 MHz band, and 1 channel in the 868 MHz band
- [3] · Maximum data rates allowed for each of these frequency bands are fixed as 250 kbps @2.4 GHz, 40 kbps @ 915 MHz, and 20 kbps @868 MHz.
- [4] Allocated 16 bit short or 64 bit extended addresses.
- [5] Allocation of guaranteed time slots (GTSs)
- [6] Carrier sense multiple access with collision avoidance (CSMA-CA) channel
- [7] Access Yields high throughput and low latency for low duty cycle devices like sensors and controls.
- [8] Fully "hand-shake" acknowledged protocol for transfer reliability.
- [9] Low power consumption with battery life ranging from months to years.
- [10] Energy detection (ED).
- [11] Link quality indication (LQI).
- [12] Multiple topologies : star, peer-to-peer, mesh topologies

C51 COMPILER V6.03, COMPILATION OF MODULE MAIN OBJECT MODULE PLACED IN
 \MAIN.OBJCOMPILER INVOKED BY: C:\Keil\C51\BIN\C51.EXE \MAIN.C DEBUG OBJECTEXTEND

Stmt level source

```

1    #include"reg52.h"
2
3
4    #define F 1
5    #define B 2
6    #define L 3
7    #define R 4
8    #define S 5
9    #define U 6
10   #define D 7
11
12   sbit motor1_coil1=P1^0;
13   sbit motor1_coil2=P1^1;
14   sbit motor2_coil1=P1^2;
15   sbit motor2_coil2=P1^3;
16
17   sbit arm_coil1=P2^1;
18   sbit arm_coil2=P2^2;
19
20
21   sbit obstacle=P1^4;
22   sbit led=P2^0;
23   unsigned char alarm1=0;
24   unsigned char alarm2=0;
25   unsigned char alarm3=0;
26
27   void forward ();
28   void reverse ();
29   void left ();
30   void right ();
31   void stop ();

```

VI. CONCLUSION

A complete and reliable sensing system for obstacle detection can benefit a lot from the combined use of sensors. Any one particular type of technology may have difficulties to meet all necessary requirements in order to detect an obstacle in various lighting or weather condition. The path is store in memory by the programmer, the motion of the vehicle is controlled by stepper motor and controlling of the machine is done by micro- controller. Autonomous robotic vehicle guidance has been developed for industrial difficult. The guidance systems consist of infra red sensor for obstacle detection, range determination and avoidance. It can detect the obstacle within the range of 10 to 80 cm. These systems consist of infra red sensor and micro-controller the sensor is mounted on the vehicle to acquire the information from its surrounding. The infra red sensor is most suitable because of its low cost and ranging capability. The performance measurements indicated that the visual basic was fast but also had a slightly larger jitter.

REFERENCES

- [1] Aziz, A.R.A., *Designing and Constructing an Automatic Steering Vehicle (AGV)*, in *Dept of Electrical Engineering*. 2004, University Tenaga National: Malaysia. p. 50.
- [2] Wai Phyo Aung, *Software Implementation of Obstacle Detection and Avoidance System for Wheeled Mobile Robot*.2008
- [3] Ross, K. 2004. Analog and Digital Sensors
- [4] Mehran pakdaman, Design and Implementation of line follower Robot.2009,Tabari Institute of Babol.
- [5] A.Kahe "AT89S52 Architecture,"nas publication,2008.
- [6] M.Mashaghi,robotic guide,Kanone Oloum Publication,2008
- [7] Wikipedia, Mobile robots.
- [8] Cao Quoc Huy, line follower, University UPG din Ploiesti, nr 39 Bld Bucuresti, Ploiesti.

Analysis of the Hurst Exponent for M2M Applications

¹Stephen P. Emmons, ²Farhad Kamangar

The University of Texas at Arlington

ABSTRACT:

Machine-to-Machine (M2M) applications represent a class of systems that make significant demands on the global Internet infrastructure. It is important to understand and characterize the behavior of these systems so that they may be effectively engineered for scalability and reliability. This paper analyzes the “Hurst exponent” (H) for several M2M applications of varying sizes with data collected for up to six months. The Hurst exponent is a measure of the long-term dependence and self-similarity typical of Internet-based communications systems. The analysis focuses specifically on the use of the “Rescaled-Range Statistic” (R/S), and also includes several other methods for comparison, including “Absolute Moment,” “Aggregate Variance,” “Higuchi,” and “Residuals of Regression.” The results show that such applications indeed exhibit strong long-term dependence, consistent with results found for other Internet communications studies.

KEYWORDS: GSM radio communications, Hurst exponent, long-range dependence, M2M applications, R/S statistic, self similarity, vehicle tracking systems

I. INTRODUCTION

The Internet is commonly thought to be the medium for people communicating with websites, sharing files, streaming audio and video, and other uniquely human activities. However, there are other users of the Internet, making demands of its resources. Kevin Ashton, co-founder of the Auto-ID Center at MIT, is credited with first using the phrase “The Internet of Things.” He described “things” such as embedded devices using the same shared infrastructure as humans, noting that computer processors are found in home appliances, all types of vehicles, and many other places. The number of these devices is larger than the number of people using the Internet. Systems with such devices communicating on the Internet are often called “Machine-to-Machine” (M2M) applications. It is critical to study M2M applications in order to understand their behavior, and in particular, their impact on the infrastructure of the Internet. One such class of systems is vehicle-tracking applications. These applications require both “wired” Internet resources, as well as the wide-area wireless communications infrastructure operated by cellular carriers. Today, “smartphones” are common in the popular consciousness, but less visible are vehicles and other mobile assets (e.g., pallets, rail cars, etc.) that use basically the same technology for capturing local information and reporting it to aggregation points for analysis. These systems must be engineered for scalability and reliability, taking into consideration their future growth and demand on communications infrastructure. Key to understanding the communications requirements of M2M applications is an analysis of the message traffic generated by embedded devices. Typically, their behavior may be defined in probabilistic terms using one of many models describing the frequency of message arrival, potential for collisions, and duration of “bursts” of messages [1]. Such models have various parameters that map their theoretical characteristics to specific operational conditions. It is important to choose the correct model, as well as the right values for the parameters that govern it. In doing so, one attribute of the message traffic with important implications for the system’s behavior is the “Hurst exponent” [2]. This paper analyzes the long-term dependence and self-similarity characteristics of four commercial vehicle tracking applications by using the Hurst exponent. Each application has from several hundred to several thousand vehicles, and the dataset for each of them includes message arrival counts collected over up to six months. Five different methods are used and compared in this analysis. The organization of the remaining sections of this paper is as follows: Section 2 provides background on the Hurst exponent, briefly describing its development and use.

Then Section 3 reviews a cross-section of related works that elaborate on or apply the Hurst exponent in contexts similar to M2M applications. A description of the vehicle-tracking applications studied is presented in Section 4, followed by the results of the Hurst analysis of these systems in Section 5 using several estimation methods. And finally, Section 6 summarizes the conclusions of the analysis and outlines future work.

II. BACKGROUND

The Hurst exponent represents an estimated measure of “long-range dependence” (LRD) or “self-similarity” of time-series data. It is named for Harold Edwin Hurst who first introduced the concept in the field of hydrology [2]. In the 1950s, he introduced the “Rescaled Range Statistic” (R/S) as a measure of the variability of a given time-series by finding the rescaled range (R) of values and dividing it by the standard deviation (S). The rescaled range for a time-series $X = \{x_1 \dots x_n\}$ is defined as the difference between maximum and minimum of the mean-adjusted range series for a given sub-sequence of X given a length $t = 1 \dots n$ and an

$$\bar{X}_t^i = \frac{1}{t} \sum_{k=i}^{i+t} x_k \quad (1)$$

$$Y_t^i = \sum_{k=i}^{i+t} (x_k - \bar{X}_t^i) \quad (2)$$

$$R_t^i = \max(Y_t^i) - \min(Y_t^i) \quad (3)$$

offset $i = 0 \dots (n - t)$:

Thus $(R/S)_t^i$ for a sub-sequence of X is defined as follows:

$$S_t^i = \sqrt{\sum_{k=i}^{i+t} (x_k - \bar{X}_t^i)^2} \quad (4)$$

$$(R/S)_t^i = \frac{R_t^i}{S_t^i} \quad (5)$$

Note that when $t = n$, then $I = \{0\}$ and $(R/S)_t^0 = (R/S)_n$. Furthermore, it is convenient to consider only the expectation of $(R/S)_t^i$ as follows:

$$(R/S)_t = E[(R/S)_t^i] = \frac{1}{t} \sum_{k=i}^{i+t} (R/S)_t^i \quad (6)$$

Hurst found that the expectation of (R/S) as the time scale increases approaches the product of some constant C and n to the power of another constant H as follows:

$$E[(R/S)_n] = Cn^H \quad (7)$$

In this form, the exponent H can range between 0 and 1. Values of H such that $0.5 < H < 1$ result from time series values having a tendency to continue in the same direction as other recent values; thus exhibiting “long-term memory” in its behavior. Values of H such that $0 < H < 0.5$ are found for time series that are strongly “mean regressive.” In between, a value of 0.5 suggests uncorrelated, random values with no tendency to increase or decrease based on prior history. H can be estimated as the slope of the least-squares fit of the expectation of (R/S) for exponentially larger values of t up to n plotted on the log/log scale. Figure 1 illustrates the boundaries of this range with several reference examples. For each example having 2^{16} samples, the graph shows values for the $(R/S)_n$ for values of $n = 2^i$ where $i = 1 \dots 16$, plotting the results on a log/log scale:

- A simple monotonically-increasing number sequence from 1 to 2^{16} is fully self-similar at all scale levels, and as expected, shows a slope of 1.
- 2^{16} random samples shows a slope 0.5.
- A set of 2^{16} samples toggling between 1 and -1, thus always regressing toward a mean of 0, likewise shows a slope of 0.

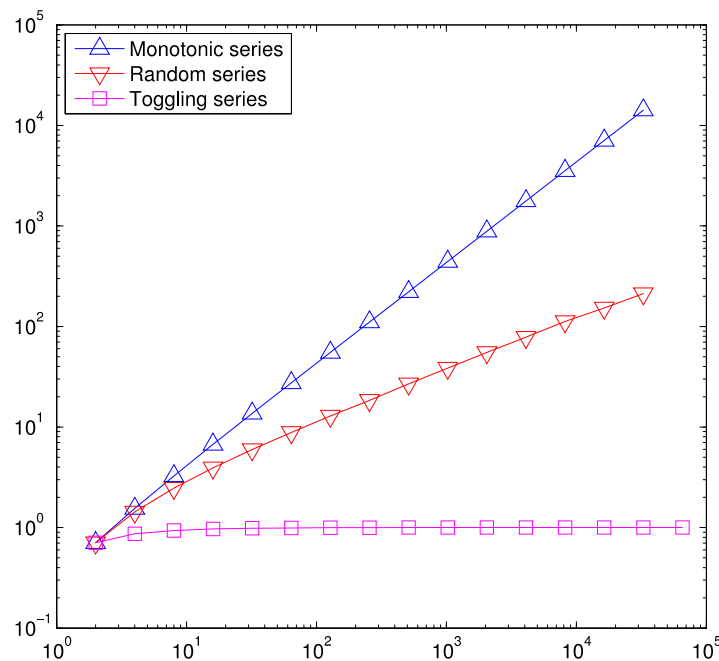


Figure 1: Three reference examples of (R/S) values on a log/log scale whose slopes correspond to H values of 1, 0.5, and 0

Note that as an estimate of H , the slope of the log/log plot of (R/S) values can be highly influenced by the choices of t used. Figure 1 provides a hint of this fact, since the first few (R/S) values in the examples for slopes 0.5 and 0 trend slightly differently than the rest. Section 5 will elaborate on this. Starting in the late 1960s, Mandelbrot related the Hurst exponent to the “roughness” of a time series [3][4]. In his work with fractals, which are known to exhibit high self-similarity at many (or all) scales, he found that higher H values occur with “smoother” shapes, whereas lower H values correspond to shapes that are more “wild” or “rough.” In the early days of the Internet, Leland et. al used an analysis of the Hurst parameter applied to Ethernet data communications [5]. They found that the “burstiness” of such data traffic appeared to occur equally at small and large time scales, similar to Mandelbrot’s fractals. This discovery was significant because the LRD indicative of such behavior is not consistent with a “memoryless” Poisson process that had been used by the telecommunications industry in the past to model the occurrence of telephone calls for capacity planning [5]. In the early 1990s, the Poisson model had been used by many in industry and government around the world when forecasting long-term Internet growth planning. In a special joint publication by both the IEEE and ACM, they successfully brought attention to the greater capacity requirements that such self-similar communications would demand [5].

III. RELATED WORK

Many methods have been studied for calculating the Hurst exponent using alternatives to (R/S).

As a contributor to the aforementioned study led by Leland, Taqqu, along with Levy, had previously investigated several Hurst estimators, including aggregated variance, periodograms, various Whittle methods, and even simple visual observation [6]. Later, Taqqu et. al analyzed additional methods [7] such as the eponymous Higuchi estimator [8] and “Residuals of Regression” by Peng [9]. More recently, Jones and Shen developed a method of estimating H by looking at level crossings for faster calculation [10]. Overall, the various available methods exhibit strengths and weaknesses based on the type of data being considered. While (R/S) is more computationally expensive than many others with a time-complexity of $O(n^2)$, it is generally recognized as the standard. Since Leland et. al, there have been many studies of the LRD qualities of data communications involving the Hurst exponent. Nash and Ragsdale used an analysis of the Hurst exponent for critical systems as part of their characterization of systems communications as a precursor to establishing criteria for an automated intrusion detection method [11]. Idris et. al used a Hurst exponent estimate as a reference against which to detect anomalies in a system [12]. Their method focused on determining an effective window size of recent traffic activity, calculating a current H and comparing it to an expected value. Park et. al explored the LRD qualities of

several TCP/IP data sets representing significantly higher data rates than those considered earlier by Leland et al [13]. They used a variety of methods to estimate the Hurst exponent and confirmed high values (i.e., between 0.8 and 0.9) for such data. Clegg used the Hurst exponent to help establish the parameters of a Markov-modulated process for simulating self-similar network traffic, overcoming the kinds of limitations found with past models as identified by Leland et al [1]. Dobrescu et al examined how the self-similarity of various networks, such as LANs and WANs, are affected by their topology, exploring multiple methods for measuring H, as well as related statistical measures [14].

IV. TARGET SYSTEMS

The datasets analyzed in this paper come from four commercial vehicle-tracking applications used by

Table 1: Dataset attributes

Dataset	Vehicles	Weeks
A	175	26
B	285	26
C	650	13
D	1000-3000	26

both business and consumer users.

Table 1 identifies each application by a letter “A” through “D,” along with the number of vehicles it had, and the total time span of the message count data collected. Each dataset contains a progressively larger number of device-attached vehicles with data collected for at least over three months, and in most cases over six months. The largest dataset, “D,” saw an increase in the number of devices by a factor of three over the six month period. For the purpose of this study, the primary focus concerns two key elements of these applications: First, there is an embedded processor and wireless GSM radio, or “device.” Messages are sent as single UDP/IP packets over GPRS to report both periodic and exception-based information about the condition of an attached vehicle. The devices in the study come from several manufacturers, including Enfora (now Novatel), Xirgo, and Calamp. The duty cycle of the devices can vary across applications, but the typical configuration involves an hourly report of location when the attached vehicle is powered off and a report of location every minute when it is on. In addition, the devices may also report their status when the vehicle is powered on or off, crosses a predefined speed threshold, enters or leaves a predefined “geofence,” or detects a state change for an attached digital and/or analog sensor. Second, there is an aggregation service known to the devices to which they send their various messages. This service receives, and in some cases acknowledges, messages from the different device types, each having its own data format, and normalizes/conditions the information contained in the message for subsequent analytical processes. Each application has a similar service configuration, but typically, is comprised of one or more virtual servers hosted in a “private cloud” in sufficient number and with sufficient allocation of resources (e.g., CPU, RAM, SAN) to handle the operational demands of the overall system.

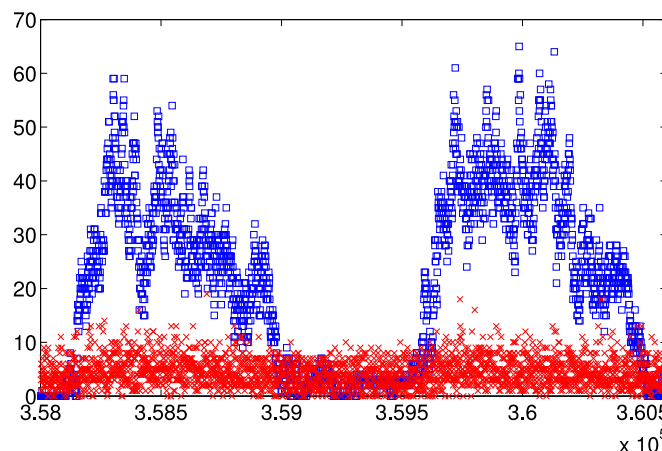


Figure 2: Message counts per minute categorized by ignition on vs. off for a 2-day period from dataset “A”

Figure 2 shows a subset of data from dataset “A” having 175 devices representing a fleet of vehicles for a construction company. The horizontal axis represents a two-day period with one-minute resolution, and the vertical axis shows the aggregated number of messages received in one minute. The red 'x's represent the counts per minute from devices with their ignition off, whereas the blue squares represent message counts from devices with their ignition on. The larger magnitude of “ignition on” counts reflects the higher reporting rate for this condition. A clear diurnal cycle is evident given that the vehicles are active with their ignition on during the course of their business day, with little or no activity during the night-time hours. For dataset “A” the ratio of messages with ignition on to those with ignition off was approximately 3 to 1. Histograms of the distribution of these types of messages in Figure 3 depict a strong half-normal frequency distribution, with the “ignition on” messages exhibiting a Gaussian mixture model. The high values on the left side of the graph for devices with ignition on indicates that a small percentage of the population of devices are on at the same time.

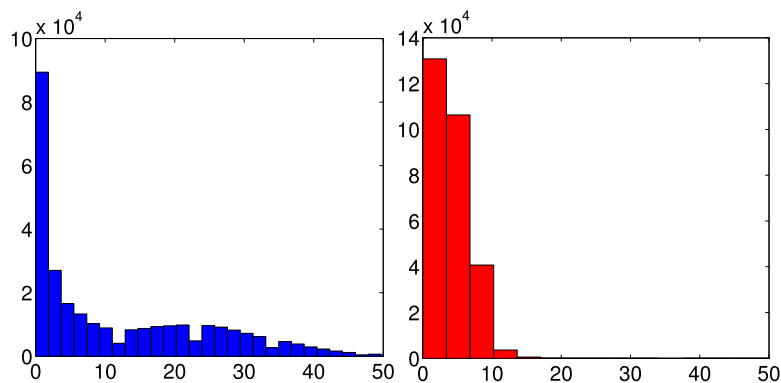


Figure 3: Distribution of message counts by minute for 175 vehicles with ignition on and off

V. RESULTS

For the purpose of this study, values of (R/S) were calculated for the per-minute message counts of each application up to six months at intervals for powers of 2 from 2^1 to 2^{18} minutes in duration. Since Figure 2 showed visually different message arrival characteristics for “ignition on” vs. “ignition off,” the possibility existed that the estimate of H might be different for each type of count history. One might imagine a possible M2M application that only reports values for vehicles with the ignition on, or another that only reports hourly, along with some exceptions representing locally-detected changes in state.

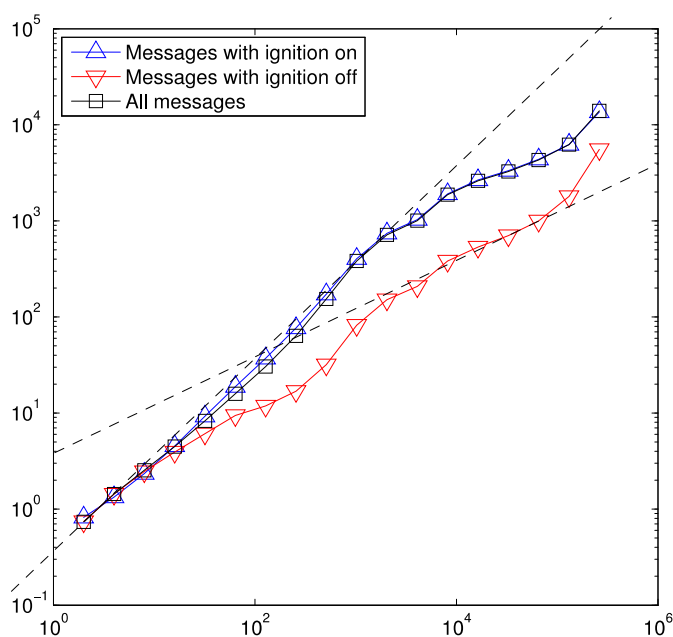


Figure 4: Changing slope for system “A” over differing scales for message counts with ignition on, off, and combined

Figure 4 shows three plots for (R/S) values representing only “ignition on,” “ignition off,” and all combined message counts for dataset “A.” Bracketing dotted reference lines with slopes 0.5 and 1 show that, at different time scales, the (R/S) values trend back and forth between these boundaries of the LRD/self-similar range for H.

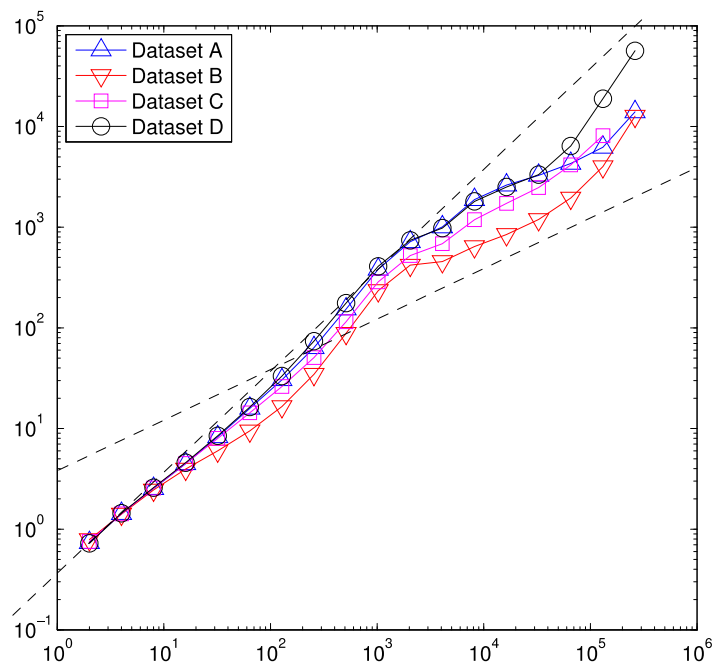


Figure 5: Log/log plot of averaged $(R/S)_n$ values at many time scales for each target system

The same characteristic change in slope is also visible for each of the other datasets “B” through “D” as shown in Figure 5. Here the data shows strong LRD with slope close to 1 for time scales 2^1 to 2^{11} , at which point the slope drops closer to 0.5. Then at time scale 2^{15} , the slope again increases back closer to 1. The time scales of lower slope correspond to the daily and weekly periodicity of the data that are necessarily “mean regressive,” and as such would be expected show a decrease in the value of H accordingly.

Table 2: Dataset Hurst estimates

Dataset	$H_{(R/S)}$	H_{AM}	H_{AV}	H_{Hig}	H_{RR}
A	0.8535	0.9098	0.9114	1.2101	1.0005
B	0.7928	0.8784	0.8717	1.0698	1.0002
C	0.8502	0.9237	0.9109	1.1131	1.0003
D	0.9180	0.9531	0.9501	1.3412	0.9994

Table 2 summarizes the values of H using (R/S) for each dataset, emphasizing that the overall LRD quality of each time series remains high, despite the fact that, at some time scales, they appear less so.

Interestingly, these periods of lower H occur at aggregation levels typically being examined by system operators for such applications. As a result, the casual observer might incorrectly assume the LRD for these applications is low. While estimating H using (R/S) is well-established as the standard, it is nevertheless computationally expensive as mentioned previously, and many other methods have been devised to estimate H more quickly [7][8][9][10]. As examples of these methods, Table 2 includes results using the “Absolute Moment” (AM), “Aggregate Variance” (AV), “Higuchi” (Hig), and Peng’s “Residuals of Regression” (RR) methods from Taqu and Levy [7] using MatLab. While these methods produced results in a few seconds or less

each versus up to 20 minutes using (R/S), all resulted in values of H higher than expected. Furthermore, all values for Higuchi and most values for Peng were found to be invalid by being greater than the maximum of 1.

VI. CONCLUSIONS AND FUTURE WORK

The systems in this study vary in number of vehicles, and while similar, are not identical in their purpose and behavior. However, all exhibit consistently high self-similar message frequency patterns at all scales measured. As a result, it should be reasonable to assume that similar system behavior would continue to persist at even larger scales as the systems grow. This, along with many other analyses of Internet-based communications systems of all types, consistently shows that they exhibit LRD characteristics. While Park et. al [13] found high Hurst exponent values between 0.8 and 0.9 for TCP/IP communications with its stream-oriented protocol overhead, the systems in this study using more simplistic UDP/IP communications, often without message acknowledgement, likewise have H values in the same range. Differences in aggregate shape of the data at time scales corresponding to days and weeks appeared to exhibit less LRD due to their “mean regressive” periodicity, but high LRD character remained true at both lower and higher scales. The well-established standard for estimating H based on (R/S) is computationally expensive, motivating the desire for alternative methods, but such methods, while confirming the high LRD of the systems in this study, appear to produce results too different from (R/S) to be equivalent. Since these systems were studied at the level of UDP packet arrival at “host”-level aggregation services, in cellular wireless communications, two additional layers of communications exist below this. For GSM networks, there is a layer of GPRS messaging and its underlying SS7 signaling protocol for which a similar Hurst analysis may be of value in the future.

REFERENCES

- [1] R. G. Clegg, “Simulating internet traffic with Markov-modulated processes,” in UK Performance Engineering Workshop, 2007.
- [2] H. E. Hurst and A. S. of Civil Engineers. Hydraulics Division, Long-term Storage Capacity of Reservoirs. American Society of Civil Engineers, 1950.
- [3] B. B. Mandelbrot, “Long-run linearity, locally gaussian processes, H-spectra and infinite variances,” 1969.
- [4] B. B. Mandelbrot and J. R. Wallis, “Computer Experiments with Fractional Gaussian Noises: Part 2, Rescaled Ranges and Spectra,” *Water Resources Research*, vol. 5, no. 1, pp. 242–259, 1969. [Online]. Available: <http://dx.doi.org/10.1029/WR005i001p00242>
- [5] W. E. Leland, M. Taqqu, W. Willinger, and D. V. Wilson, “On the Self-Similar Nature of Ethernet Traffic (Extended Version),” *IEEE/ACM Transactions on Networking*, vol. 2, no. 1, pp. 1–15, 1994.
- [6] M. Taqqu and J. Levy, “Using renewal processes to generate LRD and high variability,” in *DEPENDENCE IN PROBABILITY AND STATISTICS: A Survey of Recent Results*, E. Eberlein and M. Taqqu, Eds. Birkhaeuser, Boston, 1986, pp. 73–89.
- [7] M. Taqqu, V. Teverovsky, and W. Willinger, “Estimators for Long Range Dependence: An Empirical Study,” *Fractals*, vol. 3, pp. 785–798, 1995.
- [8] T. Higuchi, “Approach to an irregular time series on the basis of the fractal theory,” *Phys. D*, vol. 31, no. 2, pp. 277–283, Jun. 1988.
- [9] C. Peng, S. Buldyrev, S. Havlin, M. Simons, H. Stanley, and A. Goldberger, “Mosaic organization of DNA nucleotides,” *Physical review E*, vol. 49, no. 2, pp. 1685–1689, 1994.
- [10] O. Jones and Y. Shen, “Estimating the Hurst Index of a Self-Similar Process via the Crossing Tree,” *IEEE Signal Processing Letters*, vol. 11, no. 4, pp. 416–419, Apr. 2004.
- [11] D. Nash and D. Ragsdale, “Simulation of self-similarity in network utilization patterns as a precursor to automated testing of intrusion detection systems,” *IEEE Transactions on Systems, Man, and Cybernetics - Part A: Systems and Humans*, vol. 31, no. 4, pp. 327–331, Jul. 2001.
- [12] M. Y. Idris, A. H. Abdullah, and M. A. Maarof, “Iterative Window Size Estimation on Self-Similarity Measurement for Network Traffic Anomaly Detection,” *International Journal of Computing & Information Sciences*, vol. 2, no. 2, pp. 84–91, 2004.
- [13] C. Park, F. Hernandez-Campos, L. Le, J. S. Marron, J. Park, V. Pipiras, F. D. Smith, R. L. Smith, M. Trovero, and Z. Zhu, “Long Range Dependence Analysis of Internet Traffic,” *Computer Networks: The International Journal of Computer and Telecommunications Networking - Special issue: Long range dependent traffic*, vol. 48, no. 3, pp. 401–422, 2005.
- [14] R. Dobrescu, D. Hossu, and R. Ulrich, “Self-similarity Tests for Internet Traffic,” *Control Engineering and Applied Informatics*, vol. 11, no. 4, pp. 11–17, 2009.

Modelling Mutualism: A Mathematical Model Of Plant Species Interactions In A Harsh Climate

¹,E.N. Ekaka , ²E.O.Chukwuocha , Eziaku Osarolube, E.H. Amadi,

ABSTRACT.

Ecologists Have Observed That, In A Harsh Environment, Plant Species May Cease To Compete For Resources, But Display Positive Interactions Such As Mutualism. This Means That The Impact Of Climate Change, Where Harsh Envi- Ronments May Become More Benign, Could Be To Change The Nature Of Interac- Tions Between Plant Species And This May Be One Influence On Biodiversity. In This Talk, We Have Considered Whether The Observed Positive Interactions May Be Explained Through A Combination Of Existing Models Of Competition With Other Known Features Of The Environment In The Arctic (Where These Observa- Tions Have Been Made). This Provides A Prototype Model Where Sensitivity Of The Ecosystem To Different Types Of Environmental Change May Be Considered.

KEY WORDS : *And Phrases. Mathematical Models, Plant Species Interactions, Competition, Mutualism.*

I. INTRODUCTION

Following Our Previous Mathematical Modelling Of Lotka-Volterra-Like Competi- Tion Models ([22], [26]), We Have Selected The Following Parameters In The Analysis Of The Problem We Propose To Study In This Paper: The Intraspecific Coefficient Values Of 0.00165764; The Interspecific Coefficient Values Of 0.0016 For The First Variety Of Sorghum And 0.0015 For The Second Variety Of Sorghum; The Daily Intrinsic Growth Rate Of 0.15 For The Second Variety Of Sorghum And The Daily Intrinsic Growth Rate Of 0.16 For The First Variety Of Sorghum. Without A Detailed Mathematical Analysis That Leads To The Next Background Vital Ecological Information, Using This Set Of Model Parameters Provides Us With Four Possible Steady-State Solutions Namely The Trivial Steady-State (0, 0) Where The Two Varieties Of Sorghum Will Go Extinct Followed By Two Other Steady-State Solutions (0, 90.49) And (96.52, 0) When Either Of The Varieties Will Tend To Survive At Its Carrying Capacity. These Two Varieties Of Sorghum Will Coexist Together When The Biomass Of The First Variety Is 72.53 And The Biomass Of The Second Variety If 24.86. Since The Inhibiting Effect Of The Second Variety On The Growth Of Variety 1 Is 0.96 [Obtained By Dividing The Interspecific Coefficient Of 0.0016 Of The First Variety By Its Intraspecific Coefficient Of 0.00165764] ([22]) Is Less Than The Ratio Of The Carrying Capacity Of The First Variety To The Carrying Capacity Of The Second Variety [That Is Dividing 96.5228 By 90.4901], It Follows That The First Variety Of Sorghum Will Survive Under This Simplifying Tested Formula. The Second Variety Of Sorghum Will Also Survive Because The Inhibiting Effect Of The First Variety On The Growth Of The Second Variety Of Sorghum Is 0.905 Which Is Less Than 0.9375 Being The Ratio Of The Carrying Capacity Of The Second Variety Of Sorghum To The Carrying Capacity Of The First Variety Of Sorghum. The Topic Of This Research Study Will Tackle A Challenging Interdisciplinary Prob- Lem By Using The Tool Of Mathematical Modelling, Environmental And Applied Physics, Computational Science, And Numerical Simulation Of Plant Species Interactions In A Harsh Climate. As A Matter Of Fact, According To The Declarations Of The 1992 Earth Summit, Interdisciplinarity Was Cited Repeatedly As One Of The Means For In- Creasing Our Understanding Of And Developing Solutions To Pressing Environmental Issues Such As Sustainable Resource Development, Climate Change, Ecosystem Rehabi-

Tation To Mention A Few ([68]). Interesting Enough, Interdisciplinary Approaches Have Moved On To Consider Issues Other Than Broad Global Issues. In This Context, Interdisciplinarity Has Facilitated Research On Subjects Which Are More Narrow In Scope. For Example, Mutualism Has Been Suggested As An Important Factor Of Com- Munity Stability In General ([35], [44], [54], [44], [10], [63]). On The Other Hand, We Know From These Authors That Population Dynamics Of Mutualistic Interactions Are Rarely Described Except In The Case Of Positive-Density. In This Work, We Shall Attempt To Adapt Numerical Methods To Solving This Novel Ecological Problem With The Expectation Of Providing Further Insights And Contribut- Ing New Knowledge. Driving This Motivation Is Our Recognition Of The Complexity Of Inhospitable Arctic Environments And The Complex Links Between Ecological And Dynamical Systems. One Of The Well Known Ecological Interpretations Of Understanding The Interaction Between Plant Species Is Through The Process Of Competition. But In A Harsh Climate Where It Takes A Longer Time To Understand If The Process Of Competition Is Taking Place Which Is Very Rare, We Choose To Assume A Summer Growing Season Where Competition Takes Place Along With A Winter Season Where Occasional Frequency Of Storms May Affect The Biomass.

This Research Study Will Attempt To Tackle The Following Issues: First, We Would Consider Issues Relating To Global Warming, Lengthening Summer And Shortening Winter. This Would Be Followed With A Brief Introduction To The Concepts Of Mathematical Modelling And Numerical Simulation. Then, We Would Consider The Central Purpose Of This Thesis, A Few Observations Of Ecologists That Directly Relate To Our Investigation. This Will Be Followed With A List Of Objectives That This Thesis Expects To Achieve. Second, We Shall Consider The Main Methodology Which We Have Used In The Analysis Of Our Summer-Winter Model. Third, We Shall Define And Discuss The Key Ecological Hypotheses And Other Re- Search Questions On Which This Thesis Is Designed. It Is Very Important To Define And Discuss In Detail Other Important Factors And Issues That Affect The Growth Of Plant And Plant Species Interactions. For Example, We Need To Understand The Concept Of The Kinetics Of Plant Growth, Competitive Exclusion And Species Coexistence Among Other Related Ecological Concepts That Would Provide Insights To Understanding The Process Of Plant Growth And The Dynamics Of Plant Species Interactions. In This Talk, We Would Also Consider Five Types Of Plant Species Interactions On Which Our Subsequent Mathematical Analysis And Simulations Would Be Based. This Introductory Chapter Ends With A Conclusion That Points Out What We Would Expect The Next Chapters To Achieve.

1.1. Global Warming. One Of The Effects Of A Climate Change Will Take The Form Of A Significant Global Warming. This Change Is Expected To Be Most Pronounced At Polar Latitudes ([4]). As A Result Of This, Plant Species Are Predicted To Change In Response To Changing Climates ([4], [28], [46], [61], [25], [20], [62], [64], [60], [57], [40], [37]). In Particular, [62] Have Shown That A Warmer Climate Could Lead To New Competitive Relationships Between Plant Species That Will Consequently Diminish The Reproductive Capacity Of Plant Species.

1.2. Lengthening Summer And Shortening Winter. Plants Require Specific Grow- Ing Season Lengths To Complete Their Life Cycles. These Requirements Are Said To Vary Significantly With Different Species ([36]). For Example, Red Raspberries Which Are Produced In Scotland Requires A Short, Cool Growing Season While In The Tropical And Subtropical Regions, Sugarcane Requires Long, Hot, Humid Growing Seasons. On The Other Hand, Other Plant Species Can Grow And Perform Better Over A Wide Range Of Temperatures And Length Of Season. The Quantification Of Lengthening

A Summer Season And Shortening A Winter Sea- Son Has Been Reported In The Literature ([39]). According To These Researchers, The Summer Season Is Said To Be Lengthened Significantly By 11 Days Whereas The Winter Season Is Said To Be Contracted Or Shortened By 30 Days. These Climate Changes Could Alter The Complex Interactions Between Plant Species. According To A Global Warming Resource ([34]), It Was Reported That Summer Days Without Snow Cover Have Increased From Fewer Than 80 In The 1950'S To More Than 100 In The 1990'S. In The Same Context, A Group Of Other Researchers Have Reviewed The Evidence That Global Warming Has Affected The Growth Period Of Plants And Also Reported That The Lengthening Of The Growing Season Can Contribute To The Global Carbon Fixation ([55]). Hence, The Lengthening Of A Summer Growing Season Is More Likely To Enhance The Process Of Competition Than Facilitation.

1.3. Other Factors Of A Benign Environment. The Initial Biomass Is An Important Benign Factor That Can Play A Key Role In The Shift Between Positive And Negative Interactions Along Environmental Gradients ([30], [32], [41], [13]). Another Important Factor Of A Benign Environment Is The Intensity Of Species Interactions ([17], [13]).

1.4. Regional Variation Of Frequency Of Storms In The Arctic. Just As Chronic Wind Is An Important Ecological Parameter, So Is The Impact Of Fierce Storms On The Biomass ([24]). According To The Arctic Data Source, It Was Reported That The Frequency Of Storms Was Greatest During The Months Of June, July, And August With An Average Of Two Or Three Per Month ([1]). This Occurrence Of Storms Enables Us To Choose An Annual Average Of Storms To Be Between 6 And In This Thesis, We Propose To Use The Poisson Distribution To Approximate The Mean Number Of Storms Over A Period Of 10 Years Whereas We Propose To Use The Gamma Distribution To Approximate The Intensity Of Storms. These Distributions Are The Two Most Popular Models Of Studying The Occurrence Of Events In An Interval And The Increasing Intensity Of Storms In Particular.

1.5. Impact Of Temperature And Other Stresses On The Growth Of Plant Species. The Growth Of Plant Species Can Be Affected By A Range Of Abiotic Stresses Such The Temperature Stress, Soil Stress, And Ph Stress To Mention A Few ([56]). In This Thesis, We Can Investigate The Impact Of Temperature Stress On The Type Of Plant Species Interactions Indirectly By Changing Either The Daily Intrinsic Growth Rate Or The Intra-Specific Coefficient Of An Appropriate Competition Model In A Benign Climate. This Would Indirectly Provide Some Important Ecological Qualitative Insights From Our Expected Numerical Simulation In This Thesis.

1.6. Mathematical Modelling. Mathematical Modelling Is An Integral Part Of Attempting To Understand The Dynamics Of A Given Scientific Problem Which Is Familiar In The Mathematical Literatures ([51], [29], [5], [6], [9], [33]). In General, A Mathematical Description Of A System Serves To Put Our Knowledge Of That System Into A Rigorous Quantitative Form That Is Subject To Rigorous Testing. In This Sense, We Would Mention That A Mathematical Model Serves As An Embodiment Of A Hypothesis About How A System Is Constructed Or How It Functions. We Also Think That The Model Forces One To Focus Thinking And Make Inexact Ideas More Precise. In The Context Of This Thesis, We Intend To Use Only A System Of First Order Coupled Differential Equations To Study The Interaction Dynamics Between Two Competing Plant Species. Other Appropriate Models Involving Partial Differential Equations, Difference Equations, Delay Equations, And Other Types Of Functional Differential Equations Can Be Extended By Another Researcher To Model The Interaction Dynamics Between Two Competing Plant Species.

1.7. Numerical Simulation. A Numerical Simulation Is A Satisfactory Method Of Tackling A Mathematical Model Which Has Complex Characteristics And Does Not Have A Closed-Form Solution ([5], [6], [9]). It Is An Important Component Of Developing A Mathematical Model. This Viewpoint Is Consistent With The General Consensus That As Fields Of Science Develop, Dissemination Of Knowledge Seems To Evolve In Theory From Analytic To Numerical Solutions ([27]).

We Learn From This Author That, As Soon As A Theoretical Formulation Is Well Defined And Validated For Simple Test Equations, The Next Stage Of Analysis Would Involve The Application Of The Theory To Understanding More Complex Systems. When The System To Be Solved Becomes Very Complex, That Is, When The Model Equations That Describe The Phenomena Being Considered Consist Of Many Many Parameters, Familiar Analytic Mathematical Techniques Will In Most Scenarios Fail To Provide Precise Solutions. It Is At This Point That Numerical Simulation Or Computational Science Becomes An Important Mathematical Technique. For Example, To Study The Mathematical Modelling Of Plant Species Interactions In A Harsh Climate Which Is Motivated By A System Of Complex Model Equations, The Application Of A Numerical Simulation Is Inevitable In Order To Draw Useful Ecological Insights ([26]).

1.8. Purpose Of This Talk. Our Primary Goal In This Study Is To Use The Tool Of Numerical Simulation To Investigate The Effect Of Climate Change On The Extent Of Obtaining Cases Of Mutualism And Facilitation From A Combination Of Our Summer Competition Model And Our Stochastic Winter Model Which Are Consistent With Widely Accepted Ecological Theories. Our Other Secondary Goals Are To

- Find Out How Sensitive The Environment Is To Particular Model Parameters That Can Be Affected By Climate Change.
- Find Those Model Parameters, Which When Varied, Have The Biggest Effect On The Approximate Solution Of A System Of Nonlinear Deterministic Model Equations Of Competition Interaction.
- Find Those Winter And Summer Parameters Which When Varied Will Lead To Changes In The Interaction Behaviour.

1.9. Observations Of Ecologists. The Idea That Interactions Between Plant Species Are Affected By Some Environmental Conditions Such As Changes In Weather Conditions In Which The Species Grow Is Well Established ([66],[19], [21], [15]) And Several Other References Which Are Cited By These Authors. According To These Authors, The Prediction Of Ways That Changes In The Environment Will Affect Biodiversity Is Of Particular Concern.

Nevertheless, These Authors Have Reported That, In Delicate Ecosystems, The Presence Of Research Scientists May Pose A Major Influence On The Environment And On The Expected Scientific Results That Would Be Obtained.

1.10. Objectives Of Research. The Key Objectives Of This Study Are To

- Develop A Model That Will Accept As Input Data Details Of The Environmental Factors And The Distribution Of Different Plant Species.
- Develop A Model That Will Provide Predictions Of Future Distributions Of The Interacting Plants Over Time, Taking Account Of Various Hypotheses Regarding Climate Variations.
- Find Which Model Parameters When Varied Have The Biggest Effect On The Solutions.
- Decide On A Method Of Calculating The Effect Of Summer And Winter Parameters On The Biomass.
- Investigate The Possibility Of Using An Ecological Simulation To Obtain Mutualism And Facilitation From A Combination Of A Summer Competition Model And A Stochastic Winter Model Due To A Variation Of Winter Model Parameters.
- Find Out The Critical Environmental Factors That Can Cause Mutualism And Facilitation To Change To Other Patterns Of Plant Species Interactions.

II. RESEARCH METHODOLOGY

A Research Methodology Is An Important Part Of Developing A Mathematical Model ([53], [5], [6]). Our Research Methodology Consists Of Three Main Phases Namely The Modelling Phase, The Simulation Phase, And The Review/Revisit Phase.

2.1. Modelling Phase And Its Challenges: The Modelling Phase Of Our Research Methodology Considers Three Main Issues Namely

- (1) Issues About Species Interactions.
- (2) Issues About Data Availability.
- (3) Issues About Parameter Estimation Problem

2.1.1. Issues About Species Interactions. In Terms Of Species Interactions, We Would Only Consider The Competition ($-$, $-$) Interaction Between Two Competing Plant Species For Resources In Combination With A Stochastic Winter Model. Our Competition Model Is Characterised By A Set Of Defining Parameters Such As The Intrinsic Growth Rates For The Two Plant Species, The Self Or Intraspecific Interaction Coefficients For The Two Plant Species, The Interspecific Interaction Coefficients For The Two Plant Species And The Starting Biomasses Over A Long Time Interval.

2.1.2. Issues About Data Availability. In Terms Of Data Availability, We Have Only Analysed The Given Plant Growth Data Provided By ([12]) Because The Results Which We Obtain By Analysing These Data Provide Useful Ecological Insights Which Are Consistent With The Key Objective Of This Thesis. Moreover, We Could Not Find A Set Of Plant Growth Data Because Of The Constraint Of The Inhospitability Of The Arctic Climate And Lack Of Funding. In The Literature, We Are Yet To See Any Other Analysis Of These Data Using Our Method Of Analysis. Despite The Problem Of Data Paucity Which Is Characteristic Of Most Interdisciplinary Studies, Our Analysis Of These Available Data Forms A Background For Other Further Analyses.

2.1.3. Issues About Parameter Estimation Problem. The Problem Of Parameter Estimation To Be Considered In This Thesis Is Described By A System Of M Nonlinear Ordinary Differential Equations Of First Order

$$(2.1) \quad \frac{dX}{dt} = F(T, X, P)$$

Where $T \in [0, T]$ That Depend On A Set Of Parameters $P \in \mathbb{R}^p$ Where $X \in \mathbb{R}^m$ And $T \in [0, T]$. The Initial Values $X_0 = X(0)$ Are Usually Treated As Additional Unknown Parameters And These Are Included In The Parameter Set P ([9]). We Consider The Observed Quantity Y_i As A Function Of The System State X Which Are Sampled At Discrete Times T_i Such That

$$(2.2) \quad Y_i = G(X(T_i), P)$$

For $i = 1, 2, \dots, N$.

If $X(T, P)$ Is The Approximate Solution Of The Above Equation For A Given Set Of Parameters P . The Objective Function $\Phi(P)$ Is Defined As The Sum Of Squared Residues Between The Data And The Model Such That

$$(2.3) \quad \Phi(P) = \sum_{i=1}^N |Y_i - G(X(T_i), P)|^2$$

In This Talk, Our Approach Is To Choose An Error Function Which Is Also Called The Penalty Function That Measures The Agreement Between The Data And The Model. The Parameters Are Then Slightly Varied To Achieve A Minimum In The 2-Norm Penalty Function Which Will Yield The "Best-Fit" Parameters. With Nonlinear Dependencies, However, The Minimization Must Proceed Incrementally/Iteratively, That Is, Given Trial Values For The Parameters, We Develop A Procedure That Improves The Trial Solution. Our Procedure Is Then Repeated Until $\Phi(P)$ Stops Decreasing And Starts Increasing Again, Hence Indicating The Property Of A Monotone Sequence. When The Measurement Points Are Good, Our Scheme Correctly Identifies The Minimum Point And Hence The Best Fit Parameters Are Chosen Subject To A Relative Error Tolerance Of 0.1 Percent.

We Know That The Construction Of A Mathematical Model Is Not A Simple Task For Several Reasons. According To [42], It Is Impossible To Identify A Single Model Structure For A Natural System Since Such A System Is Never Closed And More Than One

Model Would Appropriately Provide Reliable Realistic Result. In Some Circumstances, The Modeller Is Compelled To Use One Single Reliable Model Which Best Describes The Phenomenon Under Investigation As Long As The Construction Of This Single Model Can Be Justified With An Appropriate Numerical Scheme. Next, Models Are Built Under Uncertainties In The Values Of The Defining Parameters, In The Parameterization Of The System And In The Choice Of Equations That Describe Dynamics ([59], [11]). Lastly, Uncertainty Can Also Be Related To An Inherent Stochasticity Of The Model Where The Dynamics Includes A Random Term. Issues Of Parsimony In Model Identification Are Discussed In Great Depth By ([71], [5]). In An Interaction Between Two Dissimilar Plant Species, A Parameter Which Is Numerically Characterised As Less Important Could Become An Important Parameter When An Interaction Between Two Similar Plant Species Is Considered. To Avoid This Type Of Contradiction And Inconsistency In The Interpretation Of Our Analysis, It Would Be A Good Idea To Simply Differentiate Those Parameters Which Have The Biggest Effect On The Solutions As Important Parameters And Those Which Have The Smallest Effect As Less Important Parameters.

2.2. Simulation Phase. Our Simulation Phase Is Characterised By Two Distinct Components Comprising Of The Numerical Simulation Of Our Summer Competition Model Using Fourth Order Runge-Kutta Methods And The Assumptions Leading To The Stochastic Winter Model.

2.2.1. Numerical Simulation Of Summer Competition Model. For Our Summer Season Prototype Model, We Consider

$$(2.4) \quad \frac{dN_1}{dt} = F(A, B, C, N_1, N_2, N_1(0), N_2(0))$$

Where $\frac{dN_2}{dt}$

$$\frac{dN_1}{dt} = G(D, E, F, N_1, N_2, N_1(0), N_2(0))$$

- (1) A Denotes The Intrinsic Growth Rate For The First Species N_1 In The Absence Of Interaction With N_2 .
- (2) B Denotes The Self Or Intraspecific Interaction Coefficient For The First Species N_1 .
- (3) C Denotes The Interspecific Interaction Coefficient Of The Second Species With The First Species Inhibiting The Growth Of The First Species.
- (4) D Denotes The Intrinsic Growth Rate For The Second Species N_2 In The Absence Of Interaction With N_1 .
- (5) E Denotes The Interspecific Interaction Coefficient Of The First Species With The Second Species Inhibiting The Growth Of The Second Species.
- (6) F Denotes The Self Or Intraspecific Interaction Coefficient For The Second Species N_2 .
- (7) N_1 And N_2 Are The Given Biomasses For The First And Second Plant Species.
- (8) $N_1(0)$ And $N_2(0)$ Are The Given Starting Biomasses For The First And Second

Plant Species. Our Summer Competition Model Is Characterised By Two Continuous And Differentiable Interaction Functions In Terms Of The Defining Model Parameters Which We Have Talked About In The Early Section Of Our Research Methodology. These Two Interaction Functions Are Solved Numerically By The Following Explicit Fourth Order Runge-Kutta Method ([38], [43]). This Numerical Method Which Is Well Established For Solving An Initial Value Problem And Also For Solving A System Of Equations Is A Procedure That Produces Approximate Solutions At Particular Points.

For A Standard System Of Two Equations, We Consider (2.6)

$$\frac{dX}{dt} = F(X, Y)$$

(2.7) With Initial Conditions

$$\frac{dY}{dt} = G(X, Y)$$

Dt

$$(2.8) X(0) = X_0$$

$$(2.9) Y(0) = Y_0$$

We Know That To Achieve A Higher Order Of Accuracy When Applying The Taylor Series, One Is Expected To Find Various Higher Order Derivatives. This Approach Involves Tedious Algebraic Manipulations. However, If The Derivatives Are Replaced By Evaluating $F(X, Y)$ And $G(X, Y)$ At Intermediate Points, It Becomes Possible To Achieve The Same Desired Accuracy. The Methods That Are Derived In This Way Are Called Runge-Kutta Methods But There Are Numerous Variations Of These Method. The Version Which We Have Used In This Study Is The One Proposed By ([43]). Our System Of Model Competition Equations Are Analysed Using A Fourth Order Runge-Kutta Scheme With Which The Starting Biomasses Before The Start Of Our Winter Season Can Be Calculated Under Our Assumption That In The Summer Season The Growing Conditions Are Reasonably Favourable And Species Will Compete For Resources.

2.2.2. Numerical Simulation Of Stochastic Winter Model. The Arctic Climate Is Also Characterised By A Dormant Season Called Winter. We Assume That In The Winter Season There Will Be No Further Growth And The Plant Populations Will Instead Be Subjected To Various Weather Events Such As Storms Which Lead To Destruction Of Some Or All Of The Biomass. The Simplifying Assumptions That Lead Us To Set Up Our Winter Model Will Be Considered In Detail In Chapter Five Of This Thesis. Some Ecological Questions Such As How Do We Approximate The Number And Intensity Of Storms Can Be Answered By Simulating The Poisson Probability Distribution And The Gamma Distribution In Order To Obtain Estimates For The Number And Intensity Of Storms. Detailed Definition And Analysis Can Be Found In Chapter Five Of This Thesis.

2.3. Review And Revisit Phase Of Our Summer-Winter Model. In This Section Of Our Research Methodology, We Used Our Summer Simulation Program To Obtain Solution Trajectories Over A Longer Time Interval For Other Variations Of The Length Of Summer Growing Season. This Confirms That Our Program Is Working Correctly.

2.3.1. Summer Season Prototype Model. For Our Summer Season Prototype Model, We Use Our Matlab Coded Runge-Kutta Program To Calculate Maximum Biomass For Each Plant Species. These Maximum Biomasses For The First And Second Species Form The Values At The Start Of Winter Dormant Season. Then, We Would Stop Our Simulation Of This Summer Growing Season.

2.3.2. Illustrating Our Winter Dormant Season. For Our Winter Season, We Follow The Following Steps In Our Research Methodology.

- (1) Use Gamma Distribution To Model Storm Intensity.
 - (2) Calculate The Proportion Of The Biomass That Remains After Storm 1, After Storm 2, After Storm 3, Etc As Generated By The Poisson Probability Distribution For The First Year Winter 1 For The First And Second Species.
 - (3) At The End Of The First Year Winter 1, Use The Biomass That Remains For Each Species To Form The Starting Biomass At The Start Of The Second Year Summer Season And Winter Season.
 - (4) Continue The Process For The Second Year Winter 2 For The First And Second Species.
 - (5) At The End Of The Second Year Winter 2, Use The Biomass That Remains For Each Species To Form The Starting Biomass At The Start Of The Third Year Summer Season And Winter Season.
 - (6) The Above Steps Are Repeated For Winter 3, Then Summer 4, Winter 4, Etc For 10 Summer Growing Seasons And 10 Dormant Winter Seasons.
- In This Talk, We Have Used A Matlab Program To Simulate Our Summer-Winter Model.

2.4. Application Of Our Research Methodology. We Have Successfully Updated Our Summer-Winter Program And Decided On A Method

- (1) For Calculating The Minimum Biomass For Each Plant Species Over A 10 Year Period Of One Example Trajectory Instead Of Exact Solutions.
 - (2) To Simulate 1000 Ten Year Periods With The Same Starting Values With Which We Can Calculate Our Experimental Probability Of Extinction Of Each Plant Species.
 - (3) To Allow Our Program To Reflect Shortened Winter And Lengthening Summer Based On Ecological Literature Idea.
 - (4) To Obtain Cases Of Mutualism, Commensalism, Parasitism, Competition, And Facilitation If Possible From A Combination Of Our Summer Model And Stochastic Winter Model Which Are Consistent With Dominant/Mainstream Ecological Theory.
- Our Next Task Is To Discuss A Few Types Of Species Interactions Which Would Form The Background To This Study.

III. TYPES OF PLANT SPECIES INTERACTIONS

From Our Discussions So Far, We Know That When Two Species In An Ecosystem Have Some Common Activities Or Requirements, They May Interact To Some Degree. The Principal Types Of Species Interactions Are Interspecific Competition, Mutualism, Commensalism, Parasitism And Predation ([26]).

IV. OTHER RESEARCH QUESTIONS

The Hypotheses Being Considered Above Have Both Ecological And Mathematical Components. Hence, We Will Need To Rely On Some Reliable Mathematical Techniques To Answer The Related Ecological Questions.

4.1. Ecological Questions. In This Study, We Shall Attempt To Focus On A Few Important Ecological Questions. These Questions Are Not Exhaustive. As Far As We Know, These Are The Ones That Relate To Our Present Analysis.

- (1) Ecologists Know How To Measure Plant Interactions Experimentally ([2]) But They Want To Know How To Measure Some Performance Variables Usually

- Biomass Between Individual Plants Interacting Together And In Isolation By A Simulation Technique In The Absence Of Actual Experimentation.
- (2) Ecologists Want To Find Out The Effect Of Varying The Length Of Summer Growing Season And Its Sensitivity On The Probability Of Extinction Of Plant Species Over A Longer Time Interval.
 - (3) In The Winter Season Characterised By Occasional Fierce Storms, Ecologists Will Like To Know If Shortening The Length Of Winter Leads To Some Degree Of Extinction Of Plant Species Over A Longer Time Interval.
 - (4) Ecologists Also Want To Know If Global Warming Could Trigger Either The Persistence Or Extinction Of Two Interacting Plant Species.
 - (5) Ecologists Want To Know If They Can Use An Alternative Mathematical Method Different From Their Classical Experimental Approach To Determine Mutualism From Competition From A Combination Of A Summer Competition Model And A Stochastic Winter Model.

4.2. Mathematical Questions. In This Talk, We Would Specify The Main Questions That Mathematicians Are Interested To Tackle:

- How Do We Set Up The Summer And Winter Models?
- How Do We Approximate The Number Of Storms That Occur In The Winter Season?
- For Each Storm, How Do We Approximate The Intensity Of Storm In The Winter Season?
- How Do We Approximate The Quantity Of Biomass That Remains At The End Of Each Storm?
- To Find Out How To Select Model Parameters Of Summer Model Only.

4.3. Modelling Assumptions. This Thesis Will Consider The Following Assumptions Which Are Based On A Few Insights About The Arctic Climate ([58], [26])

- (1) The Arctic Climate Can Be Characterised By A Growing Season Called Summer And A Dormant Season Called Winter.
- (2) In The Summer Season Growing Conditions Are Reasonably Favourable And Species Are More Likely To Compete For Plentiful Resources.
- (3) In The Winter Season There Would Be No Further Growth And The Plant Populations Would Instead Be Subjected To Fierce Weather Events Such As Storms Which Is More Likely To Lead To The Destruction Of Some Or All Of The Biomass.

Question: Under These Assumptions, Is It Possible To Find Those Changes In The Environment That Might Cause Mutualism From Competition (See Section 1.9.1) To Change?

4.4. Review Of Related Literatures. Related Literatures To This Study Can Be Found In

- (1) Facilitation In Plant Communities: The Past, The Present, And The Future ([15]).
- (2) Inclusion Of Facilitation Into Ecological Theory ([18]).
- (3) The Importance Of Complexity In Model Selection ([50]).
- (4) Computational And Mathematical Modelling Of Plant Species Interactions In A Harsh Climate
- (5) Mathematical Modelling Of Plant Species Interactions In A Harsh Climate
- (6) Modeling Mutualism Of Sorghum Species Interactions In A Context Of Climate Change: A South African Case Study ([23]).

V. NUMERICAL METHODOLOGY

Our Task In This Important Section Is To Define, Illustrate, And Discuss The Numerical Methodology Which We Have Utilized In This Chapter.5.1. Preamble. Following The Methodology Embodied In The Work Of ([22]), We Would Start To Define The Relationship Between The Length Of A Growing Season And The Daily Intrinsic Growth Rate Hereby Denoted By The Notation R . Without Delving Into A Detailed Analysis Of This Method, On The Assumption Of The Well Established Theory Of Exponential Growth For A Plant Species, We Know That If A Plant Species Doubles Its Biomass And We Know The Length Of Its Growing Season, We Can Calculate Its Daily Intrinsic Growth Rate. For Example, If The Length Of A Growing Season Is 5 Days, Our Calculated Daily Intrinsic Growth Rate Is 0.13863 Approximately. We Remark Here That These Calculations Are Only Estimations Which Are Correct To The Given Number Of Decimal Places. Next, If The Lengths Of

The Growing Season Are 10 And 20 Days, Our Calculated Daily Intrinsic Growths Are 0.069 And 0.034 Respectively. In The Same Manner, If The Lengths Of The Growing Season Are 30 And 40 Days, Our Calculated Daily Intrinsic Growth Rates Are 0.023 And 0.017 Respectively. Similarly If The Length Of The Growing Season Is Denoted By LS And The Daily Intrinsic Growth Rate Is Denoted By IGR , Then The Data Points In Each Set For These Variables Can Be De- Fined By $LS = (50, 60, 70, 80, 100)$ And $IGR = (0.014, 0.012, 0.0099, 0.0086, 0.0069)$. In This Scenario, We Can Deduce That As The Length Of The Growing Season Is Slightly Increased, The Daily Intrinsic Growth Steadily Decreases Because Over A Given Interval The Growth Of The Plant Species Is More Likely To Be Limited By Other Factors Within The Environment. We Observed A Similar Pattern In The Decreasing Values Of The Daily Intrinsic Growth Rate When The Plant Species Either Triples Or Quadruples, This Dimension Of Calculations Is Not Presented In This Work Because Of Our Observation. In Summary, The Consequence Of These Calculations Are Also Consistent With A Similar Idea Of Mathematical Modelling ([8]; [22]). Hence, The Exponential Growth Assump- Tion Would Become Unrealistic And The Logistic Growth Assumption In This Situation Can Be Applied. An Interesting Insight Can Be Gained By A Further Analysis Of The Data Which Have Been Provided By ([70]). Our Further Numerical Simulations Of These Data Indicate The Following Observations: For A Growing Season Of Six Weeks, The Growth Data Of Pea For A Starting Value Of 4 Grams Are $P = (4, 34.474, 66.6827, 100.7238, 136.7002, 174.7202)$. In This Scenario, The Weekly Growth Rate Can Be Estimated By Dividing The Beginning Of The Second

Week Data Point Which Is 34.474 By The Beginning Of The First Week Data Point Whose Value Is 4 And Taking The Logarithm Of This New Value, That Is The Logarithm Of 8.6185 Which Would Give Us The Value Of 2.153911056 For The Weekly Growth Rate. By Dividing The Weekly Growth Rate By 7, We Obtain The Daily Intrinsic Growth Rate Of 0.30770 Grams. Despite This Calculation, It Is Important To Observe The Increase Of The Starting Biomass For A Period Of Six Weeks. From These Data, The Beginning Of The Sixth Week Biomass Is 174.7202 Grams In Comparison With The First Week Starting Biomass Which Is 4 Grams. Hence, Our Calculated Percentage Increase In Biomass Over The Growing Season Of Six Weeks Is 43.68. Following ([22]), The Daily Intrinsic Growth Rate Over A Six Week Period Of Growth Is 0.089 Which We Can Obtain By Dividing The Logarithm Of The Percentage Increase In Biomass (Or 43.68) By 42 Days Being The Equivalent Of 6 Weeks. Similarly, Our Calculated Intrinsic Growth Rate Per Week Is 0.629 Which We Can Obtain By Dividing The Logarithm Of The Percentage Increase In Biomass (Or 43.68) By 6 Weeks. In Summary, From These Weekly Growth Data Of Pea, We Can Report That The Weekly Growth Rate Is Seven Times In Value Of The Daily Growth Rate. Under A Different Changing Starting Values For The WeeklGrowth Data Of Maize And Winter Wheat Crop ([70]), We Have Made A Similar Obser- Vation Which We Would Not Present In This Work. Similar Methods For Calculating Both Weekly And Daily Growth Rates For The Growth Of Agricultural Crops In Africa Will Be Applied In Our Subsequent Analysis In This Work.

5.2. Best Fit Logistic Model Parameters. Following ([22]), We Shall Find Those Logistic Model Parameters That Minimize The 2-Norm. Our Calculations Are Presented Below. What Do We Want To Find Out? We Are Interested To Find A List Of Best Fit Model Parameters Of Our Logistic Model That Minimise The Agreement Between The Provided Model And Our Simulated Model. Our Calculations Are Presented In The Table Below:

Parameter	Calculated Values Of The 2-Norm Penalty Function			
	H	G	Gh	2 - Norm
1	0.0014215	97.50	0.1386	5.4828
2	0.001418	97.75	0.1386	5.4324
3	0.0014143	98	0.1386	5.3902
4	0.0014106	98.25	0.1386	5.3564
5	0.001407	98.50	0.1386	5.3312
6	0.0014035	98.75	0.1386	5.3145
7	0.0014	99	0.1386	5.3065
8	0.0013965	99.25	0.1386	5.3071
9	0.0013929	99.50	0.1386	5.3164
10	0.0013895	99.75	0.1386	5.3342
11	0.001386	100	0.1386	5.3604
12	0.0013825	100.25	0.1386	5.3949
13	0.001379	100.50	0.1386	5.4376
14	0.001375	100.75	0.1386	5.4880

Table 1. The Calculation Of Our 2-Norm Penalty Function From The Measured Data And Our Simulated Data

What Do We Learn From This Table Of Values For The 2-Norm Penalty Function? From The Last Column Of This Table, It Is Now Clear That The Value Of The 2-Norm Penalty Function That Minimizes This Sequence Of Values Is 5.3065 Which Corresponds To When The Value Of The Carrying Capacity Is 99 Grams Per Area Of Land Required To Grow The Sorghum Species. Our Estimated Value Of The Intraspecific Coefficient Is 0.0014. Following The Methods Of ([26]) And ([22]), We Propose To Grid Further Around The Carrying Capacity Value Of 99 Grams So As To Find If We Can Find A Further Minimum Value Of The 2-Norm Penalty Function. By Using This Same Numerical Method, We Found A Minimum Value Of The 2-Norm Penalty Function To Be 5.3057 When We Considered The Carrying Capacity Interval (CCI) Where CCI = (98.96, 99.25). In This Scenario, Our Best Fit Model Parameters Are The Daily Intrinsic Growth Rate A = 0.1386, The Intraspecific Coefficient B = 0.001398, The Carrying Capacity K = 99.09, The Starting Value Of 4 Grams, And The Growing Summer Season Of 42 Days.

VI. MATHEMATICAL FORMULATION

Hence, Our Best Candidate Nonlinear Model Among A List Of Other 13 Similar Models Which We Have Selected Using The Method Of The Penalty Function Is Formulated As.1) $\frac{dN}{dt} = N(0.1386 - 0.001398N)$

Where The Starting Biomass Is 4 Grams Per Area.

Since We Are Interested To Construct A Competition Model Between Two Interacting Species Of Sorghum, Following ([45]), ([26]), And ([22]), We Propose The Following Nonlinear Coupled System Of First Order Ordinary Differential Model Equations Of The Form 6.2)

(6.3) $\frac{dN_1}{dt} = \dots$

$\frac{dN_2}{dt} = N_1(0.1386 - 0.001398N_1 - 0.0005N_2)$

$= N_2(0.002 - 0.00002N_1 - 0.000015N_2)$

Where The Starting Biomasses Are 4 Grams And 10 Grams Respectively.

From The Concept Of Doubling Time For Each Sorghum Species, The First Species Will Double Its

Biomass In 5 Days Whereas The Second Species Will Take About 346 Days To Double Its Biomass. This Is One Of Our Reasons Why The First Species Is Growing Fastly Than A Slowly Growing Second Species. Two Other Modified Versions Of These Model Equations Are
(6.4)

$$(6.5) \quad \frac{dN_1}{dt} = \dots$$

$$\begin{aligned} \frac{dN_2}{dt} &= N_1 (0.15 - 0.0016N_1 - 0.0012N_2) \\ &= N_2 (0.12 - 0.0012N_1 - 0.0016N_2) \end{aligned} \quad (6.6)$$

$$(6.7) \quad \frac{dN_1}{dt} = \dots$$

$$\frac{dN_2}{dt} = \dots$$

$$= N_2 (0.002 - 0.00002N_1 - 0.000015N_2)$$

Where The Starting Biomasses Are 4 Grams And 10 Grams Respectively.

Remark 6.1. We Remark That We Can Use Any Of These Models To Discuss Our Later Aim Of Attempting To Find The Extent Of Obtaining Mutualism From A Combination Of Our Summer Model And Stochastic Winter Model. In This Project, We Consider The Model Parameters $A = 0.15$, $B = 0.00165764$, $C = 0.0005$, $D = 0.002$, $E = 0.00002$, $F = 0.000015$. Here With A Daily Intrinsic Growth Rate Of $A = 0.15$ Grams, The Population Of Species 1 Can Be Expected To Double In Biomass In Around 4 Days While For A Daily Intrinsic Growth Rate Of 0.002 Grams, The Population Of Species 2 Can Be Expected To Double In Biomass In A Longer Time Frame Which Qualifies The Second Species As A Slow Growing Species. The Solution Trajectories Over 100 Days, 365 Days And 1825 Days Can Be Graphically Represented For The Model Parameters $A = 0.15$, $B = 0.0106$, $C = 0.008$, $D = 0.148$, $E = 0.008$, $F = 0.0108$. These Graphs Are Not Presented In This Paper.

Remark 6.2. In This Paper, We Will Use Our Numerical Simulation Matlab Program To Analyse And Answer The Following Questions

How Do We Approximate The Number Of Storms?

For Each Storm, How Do We Approximate The Intensity Of The Storm?

For Each Storm, How Do We Approximate How Much Biomass Remains At The End Of The Storm?

Decide On A Method For Calculating The Minimum Biomass For Each Plant Species Over The 10 Year Period Of One Trajectory.

Write A Program To Simulate 1000 Ten Year Periods With The Starting Values And Calculate Experimental Probabilities Of Extinction Of Each Species.

How Do We Upgrade Our Program To Reflect The Concepts Of Shortened Winter And Lengthening Summer And Use These To Calculate Experimental Probabilities Of Extinction Of Each Species?

Can We Use Our Summer-Winter Model To Produce A Situation In Which Mutualism Can Be Observed Based On A Summer Competition Model With Winter Storms?

VII. METHODOLOGY OF THE SUMMER SEASON

In This Paper, We Shall Merge The Usual Seasons Of Spring, Autumn, And Summer Into One Growing Season Called The Summer Model. In Order To Analyse This Model Subsequently, We Shall Make The Following Realistic Assumptions:

- [1] In A Summer Season Which Is Characterised By A Mild Climate, We Assume A Continuous Growth Of Two Plant Species.
- [2] We Assume The Possibility Of Two Plant Species N1 And N2 That Live Together And Compete With Each Other For The Same Limited Resource.
- [3] We Assume That Each Population Of Plant Species Is Inhibited Not Only By Members Of Its Own Species But Also By Those Of The Other Population.
- [4] We Assume Linear Growth Rates And Intra-Specific Parameters Are The Logistic Parameters For Species N1 And N2 If They Were Living Alone.
- [5] Our Deterministic Summer Model Rests On The Assumption That The Envi-
- [6] Ronmental Parameters Involved With Our Model System Are All Constants Irrespective To Time And Environmental Fluctuations.

VIII. METHODOLOGY OF THE STOCHASTIC WINTER SEASON

In This Paper, We Will Define, Characterise, And Discuss The Features Of The Sto- Chastic Winter Season.

8.1. Stochastic Winter Model. The Winter Season Is Characterised By An Occa- Sional Frequency Of Storms Which Does Not Promote The Growth Of Plant Species. According To The Analysis Of Arctic Climatology, The Number Of Storms Varies Within The Arctic Region ([1]). The Occurrence Of 2 Or 3 Storms Every Three Months Pre- Supposes That We Would Expect To Have An Annual Mean Number Of Storms To Be Between 6 Storms And 9 Storms. Since The Enviornment Is So Uncertain, We Might Consider Figures Below This Range In Our Further Analysis.

8.2. Poisson Distribution. We Are Motivated To Use The Poisson Distribution Because It Is An Important Discrete Distribution Frequently Used In Engineering To Evaluate The Risk Of Damage. By Assuming That All Possible Number Of Storms In The Winter Model Occur Only One At A Time, That All Such Events Occur Independently, And That The Probability Of A Storm Occuring Is Constant Per Unit Time, We Can Describe Our Winter Model As A Poisson Process, Where The Mean Number Of Storms Is Distributed Exponentially ([48], [49]).

Hence, A Discrete Poisson Probability Density^x Function (Pdf) Is Defined By(8.1)

$$F(X) = \frac{e^{-\Lambda} \Lambda^X}{X!}$$

For $X = 0, 1, 2, \dots$ Where $E(X) = \Lambda, \text{Var}(X) = \Lambda$.

8.3. Gamma Distribution. Another Concern Is That Of Measuring The Intensity Of Each Storm On The Biomass At The Start Of A Winter Season. In This Chapter, We Propose To Use The Gamma Distribution To Determine The Intensity Of Storm Under Some Chosen Shape And Scale Parameters ([48], [49]). The Gamma Distribution Is An Extension Of The Exponential Distribution Which Is Characterised By A Scale Parameter Which Describes The Spread Of The Exponential Distribution.

Hence, A Gamma Distribution Is A Two-Parameter Family Of Continuous Probability Distributions Characterized By A Scale Parameter And A Shape Parameter.

There Are Several Applications Of Gamma Distribution In Several Books Of Math- Ematical Statistics. The Probability Density Function Of A Gamma Distribution Is Defined By

$$(8.2) \quad f(x) = \frac{\Lambda^R}{\Gamma(R)} e^{-\Lambda x} x^{R-1} \quad x > 0$$

Elsewhere

According To [52], The Structure Of A Plant Is Characterised By Its Shape And Size. We Know That Two Plant Species Can Take Several Shapes Such As Spherical, Square, Rectangular, Triangular And So On. For Example, If The Shape Of A Plant Is Spherical, It Has A Base And The Effect Of Any External Force On The Plant Can Be Studied As The Impact Of This Force Is Distributed In Terms Of Its Shape And Base Or Scale.

The Gamma Distribution Model Is Defined In Terms Of Several Values Of The Shape And Scale Parameters. But The Shape And Scale Parameters That Could Fairly Model The Physical Structure Of A Plant Species Do Not Have Precise Values. Since The Geometries Of Plant Species Differ

([52]), We Have Followed The Idea In Our Paper To Choose The Values Of $R = 5$ And $\Lambda = 1$ ([26]). Why Do We Propose To Use A Probability Distribution? Having Mentioned In Chapter 1 Of This Thesis That Actual Experimentation In A Harsh Climate Is More Costly, The Simple Relations Between The Mean Number Of Storms And Its Frequency Of Occurrence May Not Be Realised. In This Situation, We Would Think That The Best Description We Can Provide To Model The Occurrence Of Occasional Storms In A Harsh Climate Is In Terms Of A Probability Distribution.

XI. BUCKLING

Buckling Of A Column Occurs When The Euler Critical Load Is Exceeded ([67], [69]). The Euler Load Is Defined By The Formula

$$(9.1) \quad P_E = \frac{\pi^2 EI}{L^2}$$

Where P_E Is The Euler Buckling Load, E Is The Young's Modulus For The Material, I Is The Least Second Moment Of Area Of Cross Section, L Is The Length Of The Strut Between The Pinned Ends. The Young's Modulus Is A Measure Of The Amount Of Stress That A Plant Species Can Take Before Buckling. We Assume That One End Of A Plant Species Structure Is Fixed In The Direction Of Wind And The Above Ground Section Is Free. Let The Length Of Plant Stem Above Soil Surface Be L Units And Effective Length Be $2L$ Units. According To ([52]), The Euler Buckling Load For The Plant Stem For The Case $L = 2L$ In A Wind Direction Can Be Similarly Defined By

$$(9.2) \quad P_E = \frac{\pi^2 EI}{4L^2}$$

A Detailed Mathematical Analysis And Proof Of Euler Buckling Formula Can Be Found In The Works Of ([67], [69]). Other Researchers Have Examined The Mechanical Effect Of Wind On The Growth Of Plants ([7], [3]). We Are Interested To Tackle The Effect Of Storm On The Ecology Of Plant Species In A Severe Arctic Region Where Growth Of Plants Is Not A Common Process. Next, We Will Explain How The Euler Buckling Load Will Be Used With Wind Speed In The Model To Determine How Much Biomass Is Destroyed In A Storm. Assume That The Force At The Base Of A Plant Of Height H Caused By Wind Speed V Is Proportional To $V^2 H^3$, That Is, $F = C_v V^2 H^3$. Any Force Acting On A Material Can Be Described As Producing A Stress. The Unit For Stress Is The Pascal (P A), Which Is The Force Per Unit Area. For The Above Ground Plant Species, Assume That $P_E = F$. Then

$$(9.3) \quad \frac{\pi^2 EI}{4L^2} = C_v V^2 H^3$$

From This Equation, We Can Simply Solve For C To Obtain

$$(9.4) \quad C = \frac{\pi^2 E_{\text{plantstem}} I}{4V^2 H^3 L^2}$$

In The Theory Of Elasticity ([67]), The Young's Modulus Is Defined Mathematically As The Slope Of The Stress-Strain Relationship

$$(9.5) \quad E = \frac{\Sigma}{Q}$$

Where The Symbol Σ Represents The Stress In The Material While The Symbol Q Represents The Strain In The Material.

The Amount Of Stress E That A Plant Species Can Take Before Buckling Can Be Determined By Dividing The Stress Exacted On The Plant By Any Change In The Dimension Of The Plant Component ([72], [52]).

For Example, If The Force Exerted On The Biomass Due To Increasing Storm Intensity Is 2 Newtons In A Patch Of Plant Species Of A 10m By 10m Dimension, Then The Stress

$100N/M^2$ Which Is $0.02N/M^2$. We Know That The Strain Is A Dimensionless Quantity.

Since The Value Of The Strain Does Not Have A Precise Value In The Work Of Zebrowski (1991), Let Us Consider A Situation When The Strain $\epsilon = 0.0474$. Consider When The Length Of The Plant Species Before Winter Storm Is $\ell_1 = 2\text{m}$. What Do We Want To Find? We Want To Define And Discuss How To Calculate The Amount Of Stress That A Plant Species Can Take Before Buckling.

The Effect Of Storm On The Length Of The Stem Is Modelled By $\ell_1 - \ell_2$. Since, The Strain Is Modelled By Dividing The Change In The Length Of The Stem By The Original Length Before The Winter Storms, In This Case

$$(9.6) \quad \ell_1 - \ell_2 = 0.0474.$$

From This Equation, We Know That

$$(9.7) \quad \ell_1 - \ell_2 = 0.0948.$$

By Substituting For The Value Of ℓ_1 , $\ell_2 = 2 - 0.0948 = 1.9052$. Therefore, The Amount Of Stress E That A Plant Species Can Take Before Buckling (9.8)

$$E = \frac{0.02}{0.0474}$$

$= 0.4219 \text{N/M}^2$. What Are We Trying To Find Out? We Want To Find If A Variation Of The Young's Modulus For The Grass Species Would Have Any Impact On Our Later Calculation Of The Minimum Biomass After Each Storm And Its Implication For Approximating The Experimental Probability Of Extinction Of Each Plant Species. 12

Similarly, Since The Height Of A Plant Is Approximated By $H_2 = B^3$, $H^2 = B^3$ And $H^3 = B$. Assume That $L = H$, Then $L^2 = H^2$ And $4L^2 = 4B^3$. By Substituting For These Expressions In The Above Formula, We Would Obtain

$$(9.9) \quad C = \frac{\pi^2 EI}{5 \cdot 4V^2 B^3}$$

For A Given Calculated Wind Speed And A Calculated Value For Biomass, We Can Use The Above Formula To Measure The Effect Of Fierce Storm On The Biomass Or The Effect Of Storm Intensity On The Biomass.

In Summary, Since The Young's Modulus Is Defined In Terms Of The Stress And Strain, Strain Is Dimensionless (Extension Of Material Divided By The Original Length Of Material) And Stress Is Defined As Load Per Unit Area, We Would Expect The Sectional Area To Vary From One Grass Species To Another. Therefore The Stress Is More Likely To Vary And So One Can Expect The Young Modulus E To Vary Also.

IX. ANALYSIS OF STOCHASTIC WINTER MODEL

In This Section, Our Task Is To Attempt To Analyse A Few Important Questions About The Stochastic Winter Model.

10.1. Assumptions Leading To Stochastic Winter Model. From The Literature, Taller Plant Species Are Generally Subjected To Greater Mechanical Stress Because Wind Speed Is Said To Increase With Height Above The Ground Surface ([47]). Hence, The Relationship Between Wind Speed Or Velocity V And Height Of Plant's Biomass H Can Be Defined By

$$(10.1) \quad v = Bh^2$$

Where B Is A Positive Constant.

In Order To Construct A Meaningful Winter Model, We Shall Assume That

- (1) Force At Base Of Plant Of Height H Caused By Wind Of Velocity Is Proportional To $(v^2 H^3)$.
- (2) The Impact Of This Force On The Old Biomass (Or Biomass At The Start Of Winter) Causes Some Parts Of The Old Biomass To Be Destroyed.
- (3) In The Winter Season There Will Be No Further Growth And The Plant Pop- Ulations Will Instead Be Subjected To Various Weather Events (Storms Etc.) Which Lead To Destruction Of Some Or All Of The Biomass ([26]).

10.2. Old Biomass And New Biomass. The Relationship Between New Biomass And Old Biomass Is Defined By New Biomass = (1-Proportion Destroyed)Times Old Biomass Where The Proportion Of Plant Species Destroyed Is Directly Proportional To The Force At Base Of Plant Of Height H, That Is, The Proportion Destroyed, Denoted By P_d , Is

$$(10.2) \quad P_d = C_v^2 H^3$$

Where C Is A Positive Constant That Depends On A Range Of Wind Speeds, Range Of Plant Heights, Strength Of Stem, Buckling Effect, Etc In Such A Way That The Quantity $P_d < 1$ With $H^3 = B$ Where B Represents The Quantity Of Biomass.If The Value Of Force At Base Of Plant Per Unit Area Is 1 Pascal And A Positive Constant Q Is Assumed To Control The Error Of Computing The Values Of C, By Using

$$(10.3) \quad F = C_v^2 H^3$$

We Shall Obtain

$$1 (10.4) \quad C_1 = \sqrt[3]{\frac{F}{H^3}} \frac{1}{1 + Q}$$

For Species 1 And

$$1 (10.5) \quad C_2 = \sqrt[3]{\frac{F}{H^3}} \frac{1}{2 + Q}$$

For Species 2

Here The Parameter V Measures The Effect Of Fierce Storm On The Biomass, C_1 Measures The Individual Intensity Of Storm On Species 1, C_2 Measures The Individual Intensity Of Storm On Species 2, H^3 Measures The Maximum Biomass At The Start Of Winter For Plant Species 1 And H^3 Measures The Maximum Biomass At The Start Of Winter For Plant Species 2. The Two Values Of C Are Only Calculated Once.We Have Used A Numerical Method Of Fourth Order Runge-Kutta To Simulate The Summer Only Model From Which The Maximum Biomass At The Start Of Winter Can Be Calculated.Under The Winter Model, We Are Interested To Tackle Three Important Questions: (1) How Do We Approximate The Number Of Storms? (2) For Each Storm, How Do We Approximate The Intensity Of The Storm?(3) For Each Storm, How Do We Approximate How Much "Grass" Species Remains At The End Of The Storm?

10.3. How Do We Approximate The Number Of Storms? Ecologists Are Inter- Ested About How To Determine The Number Of Storms Experimentally. But Mathe- Maticians Approximate The Number Of Storms.Having Mentioned That The Mean Number Of Storms Can Be Determined Using The Poisson Distribution, We Shall Focus On Illustrating This Idea With A Simple Example.For A 10 Year Ecological Simulation, Each Simulation Run Will Produce A Sample Of 10 Data Points Representing A Random List Of Mean Number Of Storms In The Arctic. For Example, A Possible Matlab Random Sample If Mean Number Of Storms Is 2 Is 4, 2, 3, 3, 2, 2, 2, 0, 3, 2. What These Data Mean Is That In Year 1, We Would Expect To Have 4 Storms, Followed By 2 Storms In Year 2, Then 3 Storms In Year 3 And So On. Then We Will Have No Storm In Year 8 And 2 Storms In Year 10. The Number Of Storms Varies For A 10 Year Simulation.

10.4. For Each Storm, How Do We Approximate The Intensity Of The Storm? We Have Used The Gamma Distribution To Simulate The Intensity Of 1000 Storms On The Biomass During A Ten Year Simulation Period Of One Trajectory.Given That The Other Parameters Are Positive Constants With Varying Storm In- Tensity On The Biomass And The Size Of The Biomass Before The Start Of Winter, The Storm Intensity In Our Analysis Can Be Determined By Using The Formula

$$(10.6) \quad C = \frac{\Gamma^2 E_{plantstem} I}{5 + 4V^2 B^3 + Q}$$

Where The Parameter V Measures The Wind Speed, B Measures The Biomass, And Q Is A Small Positive Constant That Takes Account Of The Error In The Calculation. By Substituting For Parameters $E_{plantstem}$ And I As 0.4219 Pa And 1.2586, We Would Obtain

$$(10.7) \quad C_1 = \frac{1.311253146}{5}$$

$$(10.8) \quad C_2 = \frac{1.311253146}{5 \sqrt{B^3 + Q}}$$

The Square Of The Storm Speed Constitutes A Huge Set Of Data In 1000 Storm Simulations. We Have Used A Matlab Function To Order The Data Generated By This Simulation In Terms Of Their Fierceness. The Topmost Value In This Sequence Of The Square Of The Wind Speed For 1000 Storms Represents How Fierce The Storm Would Be On The Biomass At The Start Of Winter During A Period Of Ten Years. The Next Values In The List After The Worst Effect Of Storm Represent The Individual Intensity Of Each Storm On Each Plant Species.

10.5. How Do We Approximate How Much Plant Species Remains At The End Of Each Storm? Both Analytically And Computationally, We Used The Following Formula To Approximate How Much Plant Species Remains At The End Of Each Storm: (10.9) $NB = (1 - P_d)OB$ Where NB , P_d And OB Represent New Biomass, Proportion Of Old Biomass That Is Destroyed And Old Biomass. In A Combined Summer-Winter Model, The Detail Of Our Numerical Approach Is Briefly Defined: (1) Use The Most Popular Version Of Fourth Order Runge-Kutta Method To Simulate The Summer Only Model With The Chosen Starting Values (2) Next, From This Simulation, We Calculated The Maximum Biomass For Each Species At Start Of Winter For The Start Of First Year Winter, Our Summer Model Is Simulated Only Once With Which The Maximum Biomass For Each Species Before The Impact Of Storm Is Calculated. At The End Of First Year Winter Season, The Biomass That Remains Becomes The Starting Values To Run The Summer Model For The Second Year From Which We Calculated The Maximum Biomass For Each Plant Species At Start Of Winter For The Second Year. This Procedure Is Repeated For The Ten Year Period.

10.6. Example: Determining How Much Biomass Is Destroyed During The Frequency Of Storms By An Analytical Method. Under A Different Starting Value Of Our Summer Competition Model, The Species Biomass Before The Start Of Winter Are 79.7979 Grams And 0.0541 Grams For Species N_1 And N_2 . We Choose The Force At Base Of Height Of Biomass To Be 1 Pascal Whereas $V = 227.5616$ Metres Per Second Is The Worst Storm Effect In A 1000 Simulations. We Used The Poisson Distribution To Determine The Number Of Storms For A Period Of 10 Years Which Gave Us A Random Sample Of 4 Storms In The First Year, 1 Storm In The Second Year, No Storms In The Third And Fourth Years, 2 Storms In The Fifth Year, 3 Storms In The Sixth Year, 3 Storms In The Seventh Year, 2 Storms In The Eight Year, 2 Storms In The Ninth Year, And 2 Storms In The Tenth Year. We Used The Gamma Distribution To Simulate 1000 Storms Subject To Scale And Shape Parameters And Observed A Sample Of A Fierce Storm Having A Speed Of 227.5616m/S, Followed By The Next Levels Of The Velocity Of Storm With 196.0322m/S, 162.9354m/S, 156.715m/S, And 151.2619m/S. To Calculate The Effect Of Storm On Species 1 For The First Year, The Value Of C_1 Can Be Calculated Using The Formula

$$(10.10) \quad C_1 = \frac{1}{(227.5616)(79.7979) + 0.2}$$

When This Formula Is Simplified, $C_1 = 0.00005506869385 < 1$ Which Measures The Effect Of Storm Intensity On Species 1. The Old Biomass OB For Species 1 Is 79.7979 Grammes. After Storm 1, The Proportion Of Species 1 Destroyed P_d Can Be Calculated By Using The Formula

$$(10.11) \quad P_d = 196.0322c_1 OB$$

Hence, $P_d = 0.861437259 < 1$.

The New Biomass NB After Storm 1 Can Be Calculated From The Formula

(10.12) $NB = OB(1 - P_d)$

By Substituting For The Old Biomass OB And The Proportion Destroyed P_d , The Calculated New Biomass NB Is 11.057 Grams. After The End Of The First Storm, The Old Biomass For The Start Of Storm 2 Is 11.057 Grams. Similarly, After Storm 2,

(10.13) $P_d = 162.9354c_1(11.057)$ Hence, $P_d = 0.099210476 < 1$. Our New Biomass NB Is

(10.14) $NB = OB(1 - P_d)$

Where $OB = 11.057$ Grams. In This Case, The New Biomass NB Is 9.96 Grams. After Storm 2, The Old Biomass Is Now 9.96 Grams For The Start Of Storm 3. Next, After Storm 3,

(10.15) $P_d = 156.715c_1 OB$

Where $OB = 9.96$ Grams And $P_d = 0.085955699 < 1$. Our New Biomass NB Is Equal To $9.96(1 - P_d)$ Which Is Approximately 9.10388 Grams. At The End Of Storm3, The Old Biomass Before The Start Of Storm 4 Is 9.10388 Grams.Our Poisson Random Sample Of The Number Of Storms When The Mean Number Of Storms Per Year Is 2 Specifies That The Number Of Storms For The First Year Is 4. That Means, We Would Stop Our First Year Calculation After Storm 4. In This Scenario,

(10.16) $P_d = 151.2619c_1 OB$

Where $OB = 9.10388$ Grams And $P_d = 0.075833456 < 1$. Our Calculated New Biomass NB Is 8.4135 Approximately. Hence, At The End Of Storm 4, The Old Biomass Before The Start Of The Second Year Winter Season Is 8.4135 Grams.This Example Illustrates How We Have Calculated The Minimum Biomass At The End Of Storm 4 In The First Year For The First Species Which Has A Starting Biomass Of 79.7979 Grams Per M^2 Before The Start Of First Year Winter. When The Starting Values Are $N_1(0) = 0.04g/M^2$ And $N_2(0) = 0.045g/M^2$, Our Calculated Biomasses Without Winter Storms Are $N_1 = 83.1887g/M^2$ And $N_2 = 0.0533g/M^2$ When The Two Plant Species Are Interacting Together Whereas Our Calculated Biomasses Without Winter Storms Are $N_{1i} = 83.2013g/M^2$ And $N_2 = 0.0787g/M^2$ When The Two Plant Species Are Interacting Separately.

By Using The Poisson Distribution To Obtain A Sequence Of Storms For A Period Of 10 Years When The Annual Number Of Storms Is 6, We Would Obtain (4, 10, 9, 9, 4, 4, 7, 5, 7, 9). That Is, We Would Expect To Have 4 Storms In The First Year And 9 Storms In The Tenth Year. We Also Use The Gamma Distribution To Measure The Extent Of The Fierceness Of Winter Storm For A Simulation Of 1000 Storms. The First Five Cases Of Storm Intensity Are (179.6793, 174.8924, 167.9871, 153.7375, 141.5542). The Next Five Cases Of Storm Intensity Are (135.5836, 129.0163, 126.8739, 124.3238, 123.7429). In This Example, We Would Simply Present Our Final Calculations For The Minimum Biomass For The First Year Winter Season In Table 5.1.

Plant Species	Analytical Calculation				
	Start Of Winter	After St1	After St2	After St3	After St4
N1	83.1887	2.21734	2.162085	2.11400585	2.071684
N2	0.0533	0.00248	0.002374352	0.002285	0.002209

Table 2. Calculations Of The Minimum Biomass For The First Year Winter Season

Where $St(I)$ Denotes Storm I. For The Second Year Winter, The Starting Biomasses Will Be $2.072g/M^2$ For The First Plant Species And $0.0022g/M^2$ For The Second Plant Species. To Avoid Lengthy Algebraic Calculations Which May Incur Approximation Errors, We Propose To Simulate Our Summer-Winter Model In Order To Calculate The Minimum Biomass After Each Storm. In Our Numerical Simulation, We Propose To Use A Fourth Order Runge-Kutta Numerical Method To Simulate Our Combination Of A Summer Model And A Winter Model In Only One Matlab Program And Hence Calculate The Minimum Biomass.

11. Other Simplifying Assumptions

Following One Of Our Assumptions ([26]), The Destructive Events During The Winter Season Can Be Modelled Based On An Annual Number Of Storms That Can Be Modelled Using A Poisson Process With Mean 4.5. Each Storm Has An Intensity That Can Be Modelled Using A Gamma Distribution And The Destructive Effect Of The Storm Is Proportional To The Intensity. Following The Principle Of Buckling, A Storm Of Given Intensity Will Destroy A Proportion Of The Biomass In Which The Proportion Destroyed Depends Linearly On The Biomass At The Start Of The Storm. In This Project, We Have Focused On The Simulation Of Our Summer-Winter Model Of Sorghum Species Interactions Which Has Enabled Us To Decide On A Method For Calculating The Minimum Biomass For Each Species Over A Ten Year Period Of One Trajectory. We Have Also Decided On How We Should Allow Our Program To Reflect Shortened Winter And Lengthened Summer For Calculating The Minimum Biomass For Each Species Over A Ten Year Period Of One Trajectory. We Use An Example To Investigate The Extent Of Obtaining Mutualism From Our Summer Competition Model Due To A Variation Of The Length Of Summer Season In Days.

12. Interpreting The Numerical Simulation Results

Following Our Previous Idea ([26]), We Would Present A Systematic Method Of Interpreting The Key Results Which We Have Observed In This Work With The Hope Of Providing Further Ecological Insights. Here, We Have Utilized The Following Numerical Estimation Technique Which Is Consistent With Our Previous Publication ([26]): We Use The Results Of 40 Simulation Runs In Which Each Run Covers A 10-Year Period Of One Trajectory, The Probability Of Reaching A Zero Biomass For One Or The Other Slow Growing Sorghum Species. In Order To Illustrate This Technique, We Start By Considering The Minimum Biomass Of Each Species Of Sorghum Over The 10-Year With Repeated Simulated Trajectories For Three Different Climate Scenarios. In Our First Climate Scenario When The Number Of Storms Is 4 Over 40 Runs, We Observe That Species 1 Reached A Zero Biomass On Five Occasions While Species 2 Survived On 38 Occasions. Hence, When The Two Species Are Growing Together, We Can Conclude That The Simulation Predicts An Experimental Probability Of $P_1 = 0.125$ That Species 1 Does Not Survive And An Experimental Probability Of $P_2 = 0.05$ That Species

2 Does Not Survive. For This Scenario And Using The Same Model Especially When Each Of Species 1 And 2 Is Growing Separately Without The Effect Of Competition With Other Species, We Observe Over 40 Repeated Simulated Trajectories That Species 1 (Alone) Reached A Zero Biomass On 26 Runs Out Of 40, Whereas Species 2 (Alone) Reached Zero Biomass On 25 Runs Out Of 40. What Do We Learn From These Observations? We Learn That When The Species Are Growing Separately, Species 1 Has An Experimental Probability Of 0.65 Of Reaching A Zero Biomass, And Species 2 Has An Experimental Probability Of 0.625 Of Reaching A Zero Biomass Based On Our Present Numerical Simulation Results. Therefore, Our Results Indicate That Both Species Of Sorghum Are More Likely To Survive When They Grow Together Than When Growing Separately. In Summary, The Two Species Can Be Said To Be Behaving Mutualistically. Our Present Observation Is Consistent With The Current Viewpoint ([26]). For The Purpose Of Clarity In The Context Of Experimental Probability Of Species Survival, We Would Present Our Present Overview Below Which We Have Not Seen Elsewhere With The View Of Contributing To This Evolving Interdisciplinary Research:

Parameter	Calculated Values Of Experimental Probabilities				
N	Sp1	Sp2	Sp1i	Sp2i	Ns
Epzerobio	0.125	0.05	0.65	0.625	4
Epsurvival	0.875	0.95	0.35	0.375	4
Epzerobio	0.2	0.15	0.7	0.7	8
Epsurvival	0.8	0.85	0.3	0.3	8
Epzerobio	0.25	0.3	0.75	0.75	10
Epsurvival	0.75	0.7	0.25	0.25	10

Table 3. The Calculation Of Experimental Probability Of Species Survival

Here, The Meaning Of The Following Notations Is

- (1) Epzerobio Stands For The Experimental Probability Of Zero Biomass For Each Species.
- (2) Epsurvival Stands For The Experimental Probability Of Survival For Each Species.

These Calculations Of Experimental Probability Of Sorghum Species Emphasize Some Aspects Of The Negative Aspects Of This Problem. We Would Expect These Experimental Numerical Simulations To Have Beneficial Effects In Terms Of Public Awareness Of The Impact Of Global Warming On Sorghum Production In The Eastern Cape Province. Despite This Observation, Assessing The Vulnerability Of Sorghum In Eastern Cape To Climate Change Would Require A Further Dedicated Collaborative Research. What Do We Learn From These Information? In This Prototype Simulation, We Ob- Serve A Systematic Instance Of Mutualism And The Sensitivity Of Experimental Prob- Ability Of Reaching Zero Biomass For Each Of The Species. At This Point, We Can Use The Model To Manipulate The Environment And Deduce Some Simple Conclusions About Climate Change Scenarios In Easter Cape Province Of South Africa. In Our Experimental Results That Are Graphically Presented Below, We Consider The Following Feasible Simplifying Examples Of Climate Change Scenarios: (1) Extending The Length Of The Growing Season. (2) Increasing The Number Of Winter Storms. Considering The Experimental Variability Of The Stochastic Model, We Repeated A 10-Year Simulation Ten Times And In This Work Recorded Our Observations Which Are Consistent In The Main With The Current Mathematical Ecological Modelling ([26]). Taking On Board The Assumption For The Existence Of Mutualism And Competition As Two Dominant Types Of Interactions, We Have Interpreted The Outcomes Of Our Simula- Tion Analysis So As To Represent Mutualism, Commensalism, Competition, And So On. The Graphs Presented Below Show The Incidence Of Each Type Of Interaction Which We Have Observed Over The Ten Repeated Simulations For Each Set Of Parameter Values. Precisely, Increasing The Length Of The Growing Season Will Reduce The Incidence Of Mutualism And Increases The Incidence Of Competition Whereas Increasing The Num- Ber Of Storms Tends To Increase The Incidence Of Mutualism And Tends To Reduce The Incidence Of Competition. Other Changing Patterns Of Mutualism And Compe- Tition Under Slightly Changing Climate Variations Are Also Presented Next. Under Other Simplifying Assumptions On The Climate Change Scenarios Over A Wider Range Of Parameter Variation, It Is Possible To Consider More Than Ten Repeated Simula- Tions Which We Have Implemented In This Work. Having Observed In A Few Instances The Decaying Patterns Of Mutualism, It Would Require A Further Dedicated Stochastic D- Bifurcation Scheme ([53]) Before We Can Detect Where Mutualism Will Completely Disappear. In The Meantime, Our Simulation Predicts A Dominant Competition To Be A Key Mechanism Behind The Loss Of Mutualism Or Facilitation Or Biodiversity. The Main Contribution Of Our Model Parameters Supports The Dominant Ecological Theory Of Mutualism. Therefore, The Concern That Climate Change Would Lead To A Loss Of Biodiversity Is Consistent With The Application Of This Model. In This Work, We Have Achieved The Following Results Which We Have Obtained From A Combination Of Our Summer Competition Model And Our Stochastic Winter Model Over A 10 Period Of One Trajectory:

13. Key Results

In This Work, We Conducted Some Numerical Simulations On Sorghum Species Inter- Actions In A Defined Harsh Climate In Eastern Cape Province Over A 10-Year Period

Of One Trajectory. For The First Time, We Have Achieved The Following Specific Contri- Butions Which We Have Not Seen Elsewhere:

- (1) A Variation In The Number Of Storms Due To Global Warming Predicts Mu- Tualism And Sunsequently Facilitation Qualitatively From A Combination Of Our Summer Model And Our Stochastic Winter Model. By Manipulating The Length Of The Summer Growing Season In Days, Both Mutualism And Facilita- Tion Are More Likely To Change To Competition.
- (2) A Variation In The Number Of Storms Due To Global Warming Predicts Com- petition And Sunsequently Facilitation Qualitatively From A Combination Of Our Summer Model And Our Stochastic Winter Model. By Manipulating The Length Of Summer Growing Season, Competition Is Seen As A Dominant Type Of Interaction While Mutualism Is A Less Dominant Type Of Interaction.
- (3) A Variation In The Number Of Storms Due To Global Warming Predicts Mutu- Alism From A Combination Of Our Summer Model And Our Stochastic Winter Model. By Manipulating A Combination Of The Volume Of Precipitation And The Length Of The Summer Growing Season In Days, Both Mutualism And Facilitation Are More Likely To Change To Competition. It Is Interesting To Report That Our Qualitative Numerical Simulation Results Are Consistent With The Dominant/Mainstream Plant Ecological Viewpoints Which Suggest That The Loss Of Mutualism And Facilitation Can Have An Impact On The Biodiversity.

Mathematical Modelling Of Sorghum Species Interactions In A Harsh Climate Scenario Of Eastern Cape Province Of South Africa Presents Major Attractions: Conventional Research Based On Substantial Data Collection Can Be Expensive During An Inhospitable Severe Climate Changes; Changes Happen Slowly Under Severe Climate Scenario And As A Result It Is May Not Be Possible To Initiate The Process Of Collecting Large Amounts Of Data; The Environmental Impact Of Large Amounts Of African Scientists Visiting The Locations Of Farms To Collect Data On The Minimum Biomass That Remains After The Effect Of Fierce Storm Events Can Change The Competition Co-Efficients. Hence, In This Situation, There Can Be Significant Environmental And Cost Advantages Of The Technique Of Mathematical Modelling And Numerical Simulation. We Would Hope That These Novel Contributions Will Provide Useful Insights Pending Some Policies Of Handling Ecological Problems Within The Eastern Cape Province.

14. Numerical Simulation And Policy Implications

The Results Of Our Present Study Suggest That The Eastern Cape Province In South Africa Will Suffer The Impact Of Climate Change. The Scale Of This Impact On Crop Growth And Production Is Yet To Be Empirically Verified. Our Numerical Simulation Approach Indicates The Possibility Of A Declining Biodiversity Which Is Capable Of Altering The Performance Of The Ecosystems Within This Region. The Results Of Our High Capacity Building Mathematical Modelling In Terms Of Predicting The Bifurcation Of Mutualism To Competition Have Implications For Appropriate Policies With Which To Mitigate This Inevitable Climate Change Effect On The Agricultural Sector And Livelihoods Of This Impoverished Dependent Populations. These Expected Policies If Well Designed And Applied Can Go A Long Way To Alleviating Poverty Within This Region. Achievable Adaptable Technologies Aimed At Improving And Sustaining The Agricultural Base Of This Region Would Have A Future Impact On Key Development Indicators.

15. Concluding Remarks And Further Research

Our Work As Presented In This Chapter Represents The First Step In Developing A Realistic Model Which Represents Harsh Climate Sorghum Species Interactions In South Africa. However, Our Results Demonstrate That It Is Possible To Obtain Outcomes Which Can Be Consistent With Other Established Scientific Observations Using A Combination Of The Summer Model And A Stochastic Winter Model Which We Have Considered In This Unique Data Manipulation And Parameterization. In Order To Take This Interesting Project Forward, We Would Anticipate The Availability Of Data Which Would Enable Us To Refine, Calibrate, And Develop This Model For Its Application In Our Future Research. However, The Gap Between Applied Scientists And Their Understanding Of Problems In The Real World And Mathematicians Who Can Answer Questions In An Idealised And Simplified World Can Be Immense. Therefore, While The Possibility Of Knowing The Extent Of The Loss Of Biodiversity Is A Good Idea In Principle For African Agriculture, One Has To Be Realistic About How Long It Will Take Before The Outcomes Of The Research Are Ready To Make A Difference In Practice In The Fields (So To Speak). The Details Of Other Related Ecosystem Characteristics In The Niger Delta Region Of Nigeria Will Be The Subject Of A Near Future Publication.

16. Acknowledgements

The Author Is Pleased To Acknowledge The Helpful Discussions With Professor Neville J. Ford And Dr. Patricia M. Lumb Of The University Of Chester And Dr. J. Potter Of Edge Hill University All In The United Kingdom Which Led To The Work Reported In This Paper And The Helpful Observations Of Professor Dan Chimere-Dan Of South Africa Research Organization And Professor Sunday Ndowa Ekoate Lale Of The Faculty Of Agriculture, University Of Port Harcourt In Port Harcourt Nigeria That Have Resulted In A Clearer Presentation Of The Ideas Which Are Presented In This Talk. We Would Like To Acknowledge The Kind Provision Of Data From The South Africa Weather Service Organization And Research Funding Received From The Gladstone Fellowship.

REFERENCES

- [1] ARCTIC CLIMATOLOGY, Internet Downloaded Resource, The Link To This Information Is Google ARCTIC CLIMATOLOGY, It Will Come Up As A 34 Page PDF Word Document, 3 – 12. I Accessed This Material For The First Time On The 20th Of November 2006 And Again On The 23rd Of July 2009. The Author And Year Of Publication Of This Material Are Not Specified.
- [2] C. Armas, R. Ordiales, And F.I. Pugnaire, Measuring Plant Interactions: A New Comparative Index, Ecology 85(10), (2004), 2682-2686.
- [3] N.P.R. Anten, R.C. Garcia, And H. Nagashima, Effects Of Mechanical Stress And Plant Density On Mechanical

- Characteristics, Growth, And Lifetime Reproduction Of Tobacco Plants, *The American Naturalist* 166, (2005), 6-10.
- [4] Atmospheric Environment Service (AES), Past Climate Change In The Canadian Arctic, , Canadian Climate Centre Rep. 85-14, Downsview, Ontario 1985.
- [5] C.T.H. Baker And F.A. Rihan, Sensitivity Analysis Of Parameter In Modelling With Delay- Differential Equations, *MCCM Numerical Analysis Report*, No. 349, Manchester University, 1999.
- [6] C.T.H. Baker, G.A. Bocharov, J.M. Ford, P.M. Lumb, S.J. Norton, C.A.H. Paul, T. Jun, P. Krebs, And B. Ludewig, Computational Approaches To Parameter Estimation And Model Selection In Immunology, *Journal Of Computational And Applied Mathematics* 184, (2005), 50-76.
- [7] C.J. Baker, The Development Of A Theoretical Model For The Windthrow Of Plants, *Journal Of Theoretical Biology* 175, (1995), 355-372.
- [8] R.B. Banks, *Growth And Diffusion Phenomena Mathematical Frameworks And Applications*, Springer-Verlag, 1994.
- [9] Y. Bard, *Nonlinear Parameter Estimation*, Academic Press, New York, 1974, 18-25.
- [10] M.D. Bertness And G.H. Leonard, The Role Of Positive Interactions In Communities: Lessons From Intertidal Habitats, *Ecology* 78, (1997), 1979-1989.
- [11] K. Beven, G. Aronica And B. Hanking, Uncertainty And Equifinality In Calibrating Distributed Roughness Coefficients In A Flood Propagation Model With Limited Data, *Advanced Water Re- Sources* 22, 4, (1998), 349-365.
- [12] V.H.Blackman, The Compound Interest Law And Plant Growth, *Annals Of Botany* 33, 131, (1919), 353-360.
- [13] R.W. Brooker, F.T. Maestre, R.M. Callaway, C.L. Lortie, L.A. Cavieres, G. Kunstler, P. Liancourt, K. Tielborger, J.M.J. Travis, F. Anthelme, C. Armas, L. Coll, E. Corcket, S. Delzon, E. Forey, Z. Kikvidze, J. Olofsson, F. Pugnaire, C. L. Quiroz, P. Saccone, K. Schifffers, M. Seifan, B. Touzard, And R. Michalet, Facilitation In Plant Communities: The Past, The Present, And The Future, *Journal Of Ecology* 96, (2008), 18-34.
- [14] R.W. Brooker, F.T. Maestre, R.M. Callaway, C.L. Lortie Et Al., Facilitation In Plant Commu- Nities: The Past, The Present, And The Future, *Journal Of Ecology* 96, (2008), 18-34.
- [15] R.W. Brooker And T.V.Callaghan, The Balance Between Positive And Negative Plant Interac- Tions And Its Relationship To Environmental Gradients: A Model *Oikos* 81(1), (1998), 196-207.
- [16] J.F. Bruno, J.J. Stachowicz, And M.D. Bertness, Inclusion Of Facilitation Into Ecological The- Ory, *Trends In Ecology And Evolution* 18(3), (2003), 119-125.
- [17] R. Brooker, Z. Kikvidze, F.I. Pugnaire, R.M. Callaway, P. Choler, C.J. Lortie And R. Michalet, The Importance Of Importance, *Oikos* 109 (2005), 63-70.
- [18] J.F. Bruno, J.J. Stachowicz, M.D. Bertness, Inclusion Of Facilitation Into Ecological Theory, *TRENDS In Ecology And Evolution* 18, (2003), 119-125.
- [19] R.M.Callaway, R.W. Brooker, P. Choler, Z. Kikvidze, C.J. Lortie, R. Michalet, L. Paolini, F.I. Pugnaire, B. Newingham, E.T. Aschehoug, C. Armas, And B.J. Cook, Positive Interactions Among Alpine Plants Increase With Stress, *Nature* 417 (2002), 844-848.
- [20] C. Casty, C.R. Christoph, F.T. Stocker, W. Heinz And L. Jury, A European Patern Climatology 1766-2000, *Climate Dynamics* 29, (2007), 791-805.
- [21] C. Dormann And R.W.Brooker, Facilitation And Competition In The High Arctic:The Impor- Tance Of The Experimental Approach, *Acta Oecologia* 23, (2002), 297-301.
- [22] E.N. Ekaka-A, Computational And Mathematical Modelling Of Plant Species Interactions In A Harsh Climate, Phd Thesis, Department Of Mathematics, The University Of Liverpool And The University Of Chester, United Kingdom, 2009.
- [23] E. Ekaka-A, O. Chimere-Dan, Modeling Mutualism Of Sorghum Species Interactions In A Con- Text Of Climate Change: A South African Case Study, Prepared For Chapter 10 Of Makiwane, M And Chimere-Dan, O. Eds Forthcoming, The State Of Population In The Eastern Cape, South Africa, Eastern Cape Provincial Department Of Social Development. Bisho, South Africa, 2010.
- [24] A.R. Ennos, Wind As An Ecological Factor, *Trends In Ecology And Evolution*, Elsevier 12,3, (1997), 108-111.
- [25] D.A. Etkin, Greenhouse Warming: Consequences For Arctic Climate, *Journal Cold Reg. Eng.* 4, (1990a), 54-66.
- [26] N.J. Ford, P.M. Lumb, E. Ekaka-A, Mathematical Modelling Of Plant Species Interactions In A Harsh Climate, *Journal Of Computational And Applied Mathematics* 234, (2010), 2732-2744.
- [27] A.J. Freeman, Materials By Design And The Exciting Role Of Quantum Computation/Simulation, *Journal Of Computational And Applied Mathematics* 149, (2002), 27-56.
- [28] H.A. French Ed, *Impact Of Climate Change On The Canadian Arctic*, Atmospheric Enviornment Service, Canadian Climate Centre, Downsview, Ontario 1986.
- [29] D.J. Gates And M. Westcott, Stability Of Plant Mixtures In The Absence Of Infection Or Pre- Dation, *J.Theor.Biol.* 131, (1988), 15-31.
- [30] D.J. Gibson, J. Connolly, D.C. Hartnett, And J.D. Weidenhamer, Designs For Greenhouse Studies Of Interactions Between Plants, *Journal Of Ecology* 87, (1999), 1-16.
- [31] S. Giliessman, *Agroecology: Ecological Processes In Sustainable Agriculture*, Sleeping Bear Press, MI, 1998.
- [32] D.E. Goldberg, T. Rajaniemi, J. Gurevitch And A. Stewart-Oaten, Empirical Approaches To Quantifying Interaction Intensity: Competition And Facilitation Along Productivity Gradients, *Ecology* 80, (1999), 1118-1131.
- [33] K.Gopalsamy, *Stability And Oscillations In Delay Diffeential Equations Of Population Dy- Namics*, Kluwer Academic Publishers, 1992, 17.
- [34] Global Warming Resource, Arctic And Antarctic Warming-Link 69, Located At The Website [Http://www.Climatehotmap.Org/References.Html](http://www.climatehotmap.org/references.html). I Accessed This Material For The First Time On The 20th Of November 2006 And Again On The 23rd Of July 2009. The Author And Year Of Publication Of This Material Are Not Specified.
- [35] D.L. Gorlick, P.D. Atkins, G.S. Losey Cleaning Stations As Water Holes, Garbage Dumps, And Sites For The

- Evolution Of Reciprocal Altruism, *American Naturalist* 112, (1978), 341-353. [36] H.T. Hartmann, W.J. Flocker, A.M. Kofranek, *Plant-Science Growth, Development, And Utilization Of Cultivated Plants*, Englewood Cliffs, N.J; Prentice-Hall, Inc, 1981.
- [37] R.W. Hofstetter, T.D. Dempsey, K.D. Klepzig, And M.P. Ayres, Temperature-Dependent Effects On Mutualistic, Antagonistic, And Commensalistic Interactions Among Insects, Fungi And Mites, *Community Ecology* 8(1), (2007), 47-56.
- [38] A. Iserles, *A First Course In The Numerical Analysis Of Differential Equations*, (First Edition) Cambridge University Press, 1996.
- [39] J. Jaagus And R. Ahas, Space-Time Variations Of Climate Seasons And Their Correlation With The Phenological Development Of Nature In Estonia, *Climate Research* 15, (2000), 207-219.
- [40] J.A. Jentsch, J. Kreyling, C. Beierkuhnlein, A New Generation Of Climate-Change Experiments: Events, Not Trends, *Frontiers In Ecology And The Environment* 5(7), (2007), 365-374.
- [41] Z. Kikvidze, C. Armas, And F.I. Pugnaire, The Effect Of Initial Biomass In Manipulative Experiments On Plants, *Functional Ecology* 20, (2006a), 1-3.
- [42] L.F. Konikov And J.D. Bredehoeft, Groundwater Models Cannot Be Validated, *Advanced Water Resources* 15, 1, (1992), 75-83.
- [43] J.D. Lambert, *Computational Methods In Ordinary Differential Systems*, (First Edition), John Wiley And Sons, 1973.
- [44] R.M. May, Mutualistic Interactions Among Species, *Nature* 296, (1982), 803-804.
- [45] R.M. May, *Stability And Complexity In Model Ecosystems*, Princeton University Press, Princeton, New Jersey, USA, 1974.
- [46] J.B. Maxwell And L.A. Barrie, Atmospheric And Climate Change In The Arctic And Antarctic, *Ambio* 18, (1989), 42-49.
- [47] J.L. Monteith, *Principles Of Environmental Physics*, Elsevier, New York, 1973.
- [48] D.C. Montgomery And G.C. Runger, *Applied Statistics And Probability For Engineers*, Third Edition, John Wiley And Sons, Inc, 2003.
- [49] D.C. Montgomery, G.C. Runger, N.F. Hubele, *Engineering Statistics*, Second Edition, John Wiley And Sons, Inc, 2001.
- [50] I.J. Myung, The Importance Of Complexity In Model Selection, *Journal Of Mathematical Psychology* 44, (2000), 190-204.
- [51] J.D. Murray, *Mathematical Biology 1: An Introduction*, Springer-Verlag, Third Edition, New York, 2002.
- [52] K.J. Nicklas, *Plant Biomechanics: An Engineering Approach To Plant Form And Function*, The University Of Chicago Press, Chicago, 1992.
- [53] N.J. Ford, S.J. Norton, Noise-Induced Changes To The Behaviour Of Semi-Implicit Euler Methods For Stochastic Delay Differential Equations Undergoing Bifurcation, *Journal Of Computational And Applied Mathematics* 229, (2009), 462-470.
- [54] O. Pellmyr, C.J. Huth, Evolutionary Stability Of Mutualism Between Yuccas And Yucca Moths, *Nature* 372, (1994), 257-260.
- [55] J. Penuelas And I. Filella, Phenology: Responses To A Warming World, *Science* 294, No. 5543, (2001), 793-795.
- [56] M. Pessarakli, *Handbook Of Plant And Crop Stress*, Second Edition, Revised And Expanded, Edited By Mohammad Pessarakli. Marcel Dekker Inc (1999), 399.
- [57] S.L. Piao, P. Friedlingstein, P. Ciais, V. Viovy And J. Demarty, Potential Impact Of The Growing Season On The Phenology Variability, *Global Biogeochemical Cycles* 21(3), (2007), 37-45.
- [58] P.O.S.T, Arctic Changes, Parliamentary Office For Science And Technology, London, Postnote 334, 2009
- [59] N. Oreskes, K. Shrader-Frechette, And K. Belitz, Verification, Validation And Confirmation Of Numerical Models In The Earth Sciences, *Science* 263, (1994), 641-646.
- [60] L. Rogers-Bennett, Is Climate Change Contributing To Range Reductions And Localized Extinctions In Northern (*Haliotis kamschatkana*) And Flat (*Haliotis walallensis*) Abalones?, *Bulletin Of Marine Science* 81(2), (2007), 283-296.
- [61] E.F. Roots, Climate Change: High-Latitude Regions, *Climatic Change* 15, (1997), 223-253.
- [62] A.R. Sherry, X. Zhou, S. Gu, A.J. Arnone III, S.D. Schimel, S.P. Verburg, L.L. Wallace, Y. Luo, Divergence Of Reproductive Phenology Under Climate Warming, *Proceedings Of National Academy Of Sciences* 104(1), (2007), 198-202.
- [63] P. Stiling, *Ecology: Theories And Applications*, (Third Edition) Prentice Hall International, London, 1999.
- [64] D. Straile And N.C. Stenseth, The North Atlantic Oscillation And Ecology: Links Between Historical Time-Series, And Lessons Regarding Future Climatic Warming, *Climate Research* 34(3), (2007), 259-262.
- [65] P. Sullivan, *Intercropping Principles And Production Practices*, Appropriate Technology Transfer For Rural Areas (ATTRA), Fayetteville, AR, 1998.
- [66] D. Tilman, *Plant Strategies And The Dynamics And Structure Of Plant Communities*, Princetown NJ, 1988. [67] S.P. Timoshenko And J.M. Gere, *Mechanics Of Materials*, Van Nostrand Reinhold, 1972. [68] United Nations, United Nations Conference On Environment And Development, Agenda 21: Program Of Action For Sustainable Development; Rio Declaration On Environment And Development; Statement Of Forest Principles, New York: United Nations Department Of Public Information, 1993.
- [69] R. Whitlow, *Materials And Structures*, 2nd Edition, Longman Scientific And Technical, 1991.
- [70] X. Yin, J. Goudriaan, E.A. Lantinga, J. Vos, H.J. Spiertz, A Flexible Sigmoid Function Of Determinate Growth, *Annals Of Botany* 91, (2003), 361-371.
- [71] P. Young, S. Parkinson And M. Lees, Simplicity Out Of Complexity In Environmental Modelling, *Journal Of Applied Statistics* 23, 2/3, (1996), 165-210.
- [72] J. Zebrowski, The Use Of Free Vibrations To Measure Peduncle Stiffness In Triticale, *Journal Of Experimental Botany* 42(242), (1991), 1207-1212.

Pedagogical Engineering to Develop Digital Fluency Among Pre-Service Teachers and Educational Leaders Of The 21st-Century

Dr Charles Kivunja

Senior Lecturer in Pedagogy and Educational Leadership
Researcher: Embedding Social Media in Digital Pedagogy
Manager Leximancer Qualitative Software
The University of New England

ABSTRACT:

*The children in our classrooms today have advanced skills for texting their friends on their eTablets and cell phones, instant messaging chats to their peers, dialoguing on MySpace, Twitter or Facebook, surfing the web or playing Xbox or Wii games. These Y Gen, Net Gen, Millennials and Z Gen, Digital Natives, are the children of the digital generation. Unfortunately, most of the teachers in today's classrooms belong to the pre-digital generation and are immigrants without the skills required for 21st century digital fluency. Moreover, their classrooms are not engineered for a digital pedagogy. This has created a teacher-student-classroom mismatch, which at worst, is characterized by the tragedy of illiterate teachers teaching literate students and by the dilemma of teachers who find the present **tense** and the past **perfect**! Pedagogical engineering is urgently needed to develop the digital fluency of teachers so they can speak their students' language. One way to achieve this is to engineer digital technologies into curriculum as discussed in this paper which reports the results of classroom trials conducted with over 400 undergraduate and 15 doctoral students by the author, in the last three years. The paper concludes that there is an urgent need to train pre-service teachers and educational leaders in digital fluency. Failure to do so will perpetuate the mismatch between digital savvy students and teachers stuck in the orthodoxy pedagogy of the last century.*

KEYWORDS: 21st Century digital fluency, Classroom infrastructure engineering and practice restructuring for digital pedagogy, Digital generation, Digital landscape, Digital nativity, Dilemma of finding "the present **tense** and the past **perfect**", Pedagogical engineering from orthodoxy pedagogy to digital pedagogy, Teacher-student-classroom mismatch, Technophiles and technophobics, The tragedy of illiterate teachers teaching literate students.

I. INTRODUCTION: THE INVASION OF THE REAL WORLD BY DIGITAL NATIVES

As Professor Plante [1] ably points out, in today's digital landscape in which we try to facilitate children and students' learning, "the world is getting more and more technology centred, focused and driven" [p. 1]. Whereas barely two decades ago when I taught at high schools in Sydney, Australia, mobile phones were not common among our students (and had to be kept at the main office as students were not allowed to use them at school), today "children of the 21st century, the Digital Generation, .. spend most of their time texting people on their cell phones, chatting with friends using instant messaging, interacting with people on Facebook or MySpace, playing games on Xbox or Wii and surfing the Internet" [2]. What is particularly interesting is the rate and extent to which digital technologies have proliferated in the real world lives of these Digital Natives. For example, Prensky's [3] rather conservative estimates were that "by the time they are 21, the Digital Generation will have played more than 10,000 hours of video games, sent and received 250,000 emails and text/instant messages, spent 10,000 hours talking on digital cell phones, and watched more than 20,000 hours of television and over 500,000 commercials" (p. 1). As Jules, McCain & Crockett [2] put it, "our students are the Digital Generation, and our generations are primarily nondigitally oriented (Digital Immigrants) (p.31). They add that "the Digital Generation has highly advanced skills for functioning in the digital world ...(and that) Teachers ... ignore the skill level of their students ... because they don't recognise the skills this generation has developed to operate in the digital world" (p. 51).

In contrast to the avid appetite for digital technologies represented in the above figures, an alarming finding by Prensky [3] was that by the time these digital natives are 21, they at the very most, might have spent only 5,000 hours reading books.

II. LITERATURE REVIEW: DIGITAL FLUENCY, DIGITAL NATIVITY AND DIGITAL IMMIGRATION

Ever since Marc Prensky [3] made the rather bold statement in 2001 that “It is very likely that our students’ brains have physically changed – and are different from ours – as a result of how they grew up ... surrounded by and using computers, videogames, digital music players, video cams, cell phones, and all the other toys and tools of the digital age” [p. 1], the issue of digital fluency and its implications for teaching and learning; and whether our scarce resources should be utilized for clicks rather than bricks, has become one of high interest. Prensky articulated the new culture that had emerged as a result of the aggressive penetration of digital technology in the lives of young people born since the last two decades of the 20th century as Digital Natives. He justified this label with the explanation that they “are all ‘native speakers’ of the digital language of computers, video games and the Internet”. So, they have the skills for digital fluency. Comparing these natives into the digital world to those of us who only discover the digital technologies as adults, he coined the term “Digital Immigrants” [3, p.3] to ably characterize the fact that we are in the process of learning a new language, - a process that is typical of all immigrants in their new country. Howell [4] has referred to them as “Gen C, Gen I, Net Gen, Gen Y, Gen Z and Internet Generation [p. 6].

A lot of literature suggests that pedagogical engineering to embed technology into teaching, particularly in the teaching of pre-service teachers and educational leaders should be a high priority in today’s educational institutions. For example, McNierney [5] admonishes that teacher educators “must model instructional methods which help future teachers understand that technology-based instruction is no longer an option. It is a requirement”. A study of the use of social media at the University of Massachusetts Dartmouth [6] found that 100% of all colleges and Universities included in their study were using some form of social media. The same study found that in higher education Facebook was the most used social media tool and its use had grown rapidly from 61% in 2008 to 87% in 2010 and to 98% in 2011. The use of Twitter had increased from 59% in 2010 to 84% in 2011. That of LinkedIn has increased from 16% in 2010 to 47% in 2011. The social media commonly used included Facebook, Twitter, LinkedIn, Blogging and Message Boards. These findings were consistent with earlier results in the Jones and Madden [7] study which found that high numbers of college students were using emails and instant messaging tools to communicate with their peers and academics and with the Kennedy et al. [8] study of ICT permeation into the lives of 1,973 Digital Natives who commenced their first studies at the University of Melbourne in 2006 and found that 96.4% of them had unrestricted access to mobile phones and 72.9% had unrestricted access to a broadband connection and [p. 4] .

Other literature from Australia shows equally high rates of fascination with digital tools particularly among adolescents and young adults. For example, a study by Oliver and Goerke [9] found that there had been a rapid increase in the numbers of students’ use of instant messaging, blogs and podcasting between 2005 and 2007 and that over 90% of 1st year engineering and business students used online resources for their study. Increasing digital nativity of Australian children is supported by data from the Australian Bureau of Statistics (ABS) which show that ten years ago, (2003) some 99% of 12 – 14 year old adolescents in Australia used a computer at home or at school. One can only assume that access to the Internet must have been significantly increased with greater access to broadband that the ABS [10] estimated to have reached 73% of the population in 2011. The same survey also found that social networking was the most popular use of the Internet technologies.

Abundant literature shows that with imagination, teachers can easily increase the permeation of digital tools into their teaching and curriculum. Excellent illustrations of this include the many apps that are freely available on the Internet and can very easily be embedded into our curriculum. Suzanne Lustenhouwer [11], for example, posted a very helpful blog on 21 August 2012 illustrating a wide range of iPad apps that could be used in the classroom to facilitate students’ engagement with learning by simply tapping on objects embedded within the Multiple Intelligence (MI) that best serves the content being taught. Figure 1 illustrates the wide range of app icons that could be used in teaching curriculum relating to the Logical-mathematical MI, Bodily-kinesthetic MI and Interpersonal MI. The app icons for the Intrapersonal MI, the Naturalist MI and Musical MI are shown in Figure 2. Examples of apps suggested for learning and teaching with the other two MIs (Visual-Spatial and Linguistic) are also given in the same blog but left out here to economise on space.

From Lustenhouwer's blog it is clear that students and teachers can easily choose whichever app serves them the best in developing their understanding of issues and concepts, for in stance, in critical thinking using Howard Gardner's [12] Multiple Intelligences. Each MI has several active icons, which a student can click on to apply that MI's orientation to critical thinking. For example, Touch Annotate, Codea, Move the Turtle, Wolfram and Khan, can all be used to work with the Logical-mathematical MI. In the Bodily-kinesthetic MI, the icons students could choose from, depending on their topic or subject, include Google Earth, Aurasma, Comic Life or SparkVue. Examples for the Interpersonal MI include Facebook, Skype, Dropbox and Nearpod. Other possibilities are illustrated in Figure 2.

A number of other studies have demonstrated the great timesaving potential of social media technologies if they are well designed for pedagogical use. For example, working with Bloom's Revised Cognitive Taxonomy Kathy Schrock [14] outlined a wide range of icons each of which has a clickable hot spot for Web 2.0, iPad, Google and Android apps that could be used to readily support our teaching of critical thinking using Bloom's Revised Taxonomy of Remembering, Understanding, Applying, Analysing, Evaluating and Creating. She identified several apps applicable to facilitate learning at each of these different cognitive levels as illustrated in Figure 3, for Web 2.0 and in Figure 4 for the iPad. In applying Web 2.0 apps while studying at the low thinking level of Remembering, Schrock listed apps including Wordle, Drigo, Google and Fotobabble. As we move to the second higher-order thinking involving Understanding, Schrock again included Drigo but added Feedly and Google Advanced Search. As she raised the bar to the third cognitive level - Applying, - she included Pipes, Podomatic and Soundation. At the fourth cognitive order of Analysing, she assembled Wufoo, Google Docs, Creator and Mentimeter as the appropriate apps. For Evaluating, -cognitive level five, the apps that Schrock highlighted again included Google and Google +, as well as Blogger. At the highest learning level of Creating, Schrock outlined Fotobabble, Wevideo, Prezi and Screenr. The common icons for all these apps are illustrated in Figure 3. Apart from these rather generalised apps for Web 2.0, Schrock also assembled apps dedicated for use on the iPad when teaching critical thinking using Bloom as illustrated in Figure 4. Space does not allow us indulgence for detailed discussion of these. It is noteworthy however, that for each cognitive level, she designed six alternative hot links that students could choose to work with. Equally instructional are Langitch's [15] apps that could be used on the iPad by teachers and students to complete class activities using Bloom's Revised Cognitive Taxonomy. As illustrated in Figure 5, they range from the simple iBook for the simple Remembering level of cognition, through to the Creating of iMovies at the highest thinking level. The interactive nature of these apps has potential to engage students deeply in their learning, utilizing tools that interest them and which are consistent with their digital fluency.

This is not to say that students' pre-occupation with digital technologies has only benefits without negatives. As Valery [16] points out, Digital Natives "are always performing multiple digital tasks simultaneously – surfing the Internet, watching a video, chatting online with friends using messaging, and downloading music at the same time, all while doing homework"[p. 3]. There is research showing that attempts at simultaneous dexterity could lead to inefficiencies, particularly if tasks require higher-order thinking and involve new processes [17]. While being cognizant of some of the possible adverse effects associated with digital technologies, we need to acknowledge that the world as seen by Digital Natives today is very different to that we older folk grew up in. In today's 24/7/365 world, we need to teach our pre-service teachers how they can maximise the benefits available from engagement of their students with digital technologies. For the Digital Natives, digital bombardment is not a curse. It is a virtue that spices their lives. It keeps them off unsafe streets, away from unsupervised parks and at home, sometimes in un-parented homes, taking on what Jules et al. [2] characterize as substituting for babysitters.

Thus, available literature appears to provide strong arguments in support of engineering digital technologies into teaching and curriculum. Howell [4] suggests that the arguments can be categorized into social imperatives and pedagogical imperatives. Among the former, she identified the expectations of students, parents, employers and the wider community. For the latter, she identified what Sabelli [18] called "constructionism". She also laid emphasis on the central metaphors of "connectivism", "computer-supported collaborative epistemology" and "technological pedagogical content knowledge (TPACK)" to name a few [18-pp. 21-31].

Logical-mathematical



Swipe the formulas to figure out the value of x with Touch Annotate. Learn to code with Codea and Move the Turtle. Learn all about Science with Wolfram and Khan. Make spreadsheets in Numbers.

Bodily - kinesthetic



Discover the planet with Google Earth, Make textbooks interactive with Aurasma. Dissect a frog. Act out a story with Comic Life. Carry out scientific measurements with SparkVue. Swipe to write poetry.

Interpersonal



Communicate via facebook or twitter. Collaborate with a class across the world with Skype. Share articles for your essay with Scoop.it. Drop your assignment in Dropbox. Learn with Nearpod.

Figure 1: Suzanne Lustenhouwer's [11] Apps for Multiple Intelligences

Intrapersonal



Doodle in Paper or draw pictures with Brushes. Follow your own interests with iTunes U. Google the answers to your questions. Keep a journal with Moleskine. Follow favourite blogs with Reeder.

Natural



Go for a scavenger hunt with Munzee, see the inside of a human heart. Keep records of your fieldtrips with Project Noah. Identify the birds in your garden with iBird Yard. See the cells in your body.

Musical



Listen to classical music to help you study with Spotify. Read up on musical theory with Wolfram. Songify your study notes with LaDiDa. Write sheet music with Sibelius and read it with Avid Scorch.

Figure 2: Suzanne Lustenhouwer's [11] Apps for Multiple Intelligences



Figure 3. Bloom's Revised Taxonomy using Kathy Schrock's [14] Web 2.0 Apps

If you go to her website (<http://www.schrockguide.net/bloomin-apps.html>) there are hotlinks to apps for this image.



Figure 4. Teaching with Bloom's Revised Taxonomy using Kathy Schrock's [14] iPad Apps

Bloom's Taxonomy for iPads

<http://langwitches.org/blog/2012/03/31/ipad-apps-and-blooms-taxonomy/>

Along with this image Langitch has also provided a definition for each category of Bloom's as well as a listing of iPad apps that could be used to meet the category.



Figure 5. Teaching Bloom's Revised Taxonomy using Langitch's [15] iPad Apps

III. METHODOLOGY FOR PEDAGOGICAL ENGINEERING FOR DIGITAL FLUENCY IN THE DIGITAL CLASSROOM

3.1.From Moodle and Sakai Learning Management Systems to Google+.Discussion Circles

This section describes the decisions and the strategies used by the author in his attempts over three years, to engineer or embed social media technologies into the planning, design and teaching curriculum of two Units, which were initially offered using Sakai and then Moodle Learning Management Systems (LMS). This journey in learning and developing appropriate use of social media technologies began with one group of 15 students enrolled in a doctoral degree Unit EDCX782 (Leadership and Culture in the workplace) in 2011 over two semesters. Encouraged by the apparent success of the first trial, the journey continued in trimester 2 of 2012 and 2013 to involve two much larger cohorts of over 400 (258 in 2012 and 169 in 2013) undergraduate pre-service teachers enrolled in Unit EDLT217 (Planning and Assessing for Active Learning) in their second year of a Bachelor in Education degree at one University in Australia. The decision to start this learning and teaching experience with the doctoral students' Unit, was underpinned by good considerations. Firstly, the number of students enrolled in this Unit each semester (now trimester) is small; being around ten per semester. This meant that it would be relatively easy to work on a new initiative with a small number. Secondly, the Unit was offered in a completely online mode to external students. This meant that they were already used to using technologies like Wikis, and online Forums.

Thirdly, most of the doctoral students were employed in Australian schools or other institutions of learning where they occupied leadership positions in middle level management such as Head Teachers in schools, Coordinators or Assistants to Principals. This gave me reason to believe that they would command a reasonable level of integrity and responsibility and respect for each other in the virtual classroom. Moreover, the online mode suited their busy work schedules quite well because of the flexible design, which facilitated their engagement with the Unit at times that suited them rather than regimented by lecture schedules. For ease of presentation (and to reserve part of this interesting story for another day) the experiences reported here relate to semester 1 of the doctoral cohort of 2011 (EDCX782, n = 9) and trimester 2 of the undergraduate cohort of 2012 (EDLT217, n = 258). All students had access to the main LMS called Sakai in 2011 and Moodle in 2012. As was standard practice, before the introduction of GDCs all cohorts relied on posts in Moodle Forums for their discussion. They had opportunities to design Wikis and to textually chat within their groups. Their activities were monitored and facilitated by an Online Tutor. Participation was mandated for the external cohort (n = 160) but ad libitum for the on-campus students (n = 98).

The design engineered in the LMS was that students formed groups of ten. Each group of ten could communicate among themselves but interactions across group boundaries were not possible. As I monitored the posts in the Moodle Forums I noted that the ability for students to communicate with each other and to provide peer support was being undermined by the restrictive group structure (of a maximum of ten). I sensed that there was a demand among the students for greater opportunities to interact with one another. I was also aware of the increasing use of smart phones and eTablets by students in their predominantly non-academic discourses. These discourses helped them to develop skills in digital fluency which, if properly guided, could be applied in learning contexts. In an attempt to meet such demand for increased students' interaction, and to take advantage of the apparent digital fluency skills, I decided to re-design these two Units so as to embed into them, selected social media technologies, namely Google+ Discussion Circles (GDC), eFoliospaces and YouTube products. I was keen to find out whether, inter alia, digital fluency skills in social media technologies could be effectively used in formal constructivist learning, teaching and assessment. This was uncharted landscape at my University and I at times wondered whether the invitation to students to utilize social media technologies in eLearning would trigger technophobia among them and lead to a fall in enrolments in this Unit or whether it would facilitate and/or increase students' engagement with their learning, along Bruner's [19] 5E Instructional Model expectations.

3.2 From Moodle Learning Management System to Social Media Technologies

Because, as already stated above, all our students have access to Moodle LMS, the starting point for their transition from Moodle to GDC were their Forums in Moodle. However, aware that the numbers in each Forum were likely to grow much larger when transferred into the GDC environment, I named them Peer Learning Networks (PLN). The aim of this transition was to enrich peer-to-peer informal learning among the students and to encourage peer support, through a-synchronous, virtual conversations using social media technologies in which they were relatively fluent, or could develop digital fluency relatively easily. This way, the PLNs were designed to become the basic unit of conversation which served as an a-synchronous round table for the participants. Specific instructions were given to the students to facilitate their transition from Moodle to GDCs. The first eleven instructions or steps were the same for all cohorts. As shown in the following list, following these common steps, those designed for undergraduates were simpler than those for the doctoral cohort. Instructions and guidelines shown in steps (xii) to (xviii) were specified for the doctoral students:

- i. Go to the Forum in Moodle and introduce yourself to your peers in 200 words
- ii. A *Google+.Discussion Circle* has been created for you.
- iii. Create a *Gmail.com* account for yourself and post it in Moodle.
- iv. Once your Gmail account has been created you will be sent an invitation to join the unit's Peer Learning Network (PLN) built around a *Google+.Discussion Circle*.
- v. Get the topic I have posted in Moodle and discuss it in your *Google+.Discussion Circle*.
- vi. Invite other students from UNE to join in the discussions in your PLN.
- vii. Invite anyone you know, from anywhere in the world, to contribute to your discussions in the GDC.
- viii. All students and invitees must strictly keep their posts to the academic topic given for discussion.
- ix. Non-compliant invitees will be deleted from the GDC and barred from further access.
- x. Continually revisit the *Google+.Discussion Circle* so that you respond to and comment on the postings of your peers.
- xi. Your response may include *YouTube* videos, *Lucidchart* graphic organisers, simple text or supporting images.

- xii. Design a personal website using *eFoliospaces* and in it discuss your understanding of the culture and climate of a workplace you are familiar with.
 - xiii. Advise members of your PLN of the URL for your *eFoliospace* so they can access it.
 - xiv. Engage with the set readings in eReserve and post three Critical Analyses of the Literature.
 - xv. You are encouraged to apply Critical Thinking Tools (e.g. *Bloom, MI, Bruner, De Bono and GOs*) in your literature critiques, embed *YouTube* products with the assistance of any digital apps you want to work with.
 - xvi. Create a link via the *Google+.Discussion Circle* and notify your peers that you have completed your critique so they can engage in dialogue conversation about your posting.
- You are to respond to three of the critiques in a manner that provokes further sought and discussion. After the conversations with your peers in the *Google+.Discussion Circle*, revisit your *eFoliospace* and using one of the Theoretical Frameworks from the selected readings on Leadership and Culture, explore and reveal your understanding of the culture and climate of that workplace.

The instructions for the undergraduates following step (xi) above were different in several respects. For example, students were given a new topic for discussion every week. The topic related to the lecture content given in the respective week. This was not the case with the doctoral students because they don't have lectures. Secondly, because of the larger numbers of the undergraduate students, they worked in many core PLNs, each starting with 10 students whereas all the students in each doctoral cohort formed one core GDC as their PLN. Furthermore, again because of the much larger numbers involved, I gave instructions to the undergraduate students to set up *Google+.Discussion Circles* by themselves whereas I started the PLN for the doctoral students and invited each one of them (steps ii and iv above). This strategy was followed because it would have been inefficient and ineffective for me to set up such a large number of *Google+.Discussion Circles* for the large undergraduate cohort (n=258; comprising 160 off- and 98 on-campus). Apart from such structural differences, the pedagogical approaches and practices were similar. All students were encouraged to apply Critical Thinking Tools drawn from Bloom's Taxonomy [13], Gardner's MI [12], Bruner's 5E Instructional Model [19], De Bono's Six Thinking Hats [20] and Graphic Organizers. The caption of the GDC-PLN-EDCX782 comprising the first 9 students in the doctoral Unit EDCX782 in trimester 2 of 2011 is illustrated in Figure 6. That for one GDC-PLNCK1 showing 47 participants is illustrated in Figure 7.

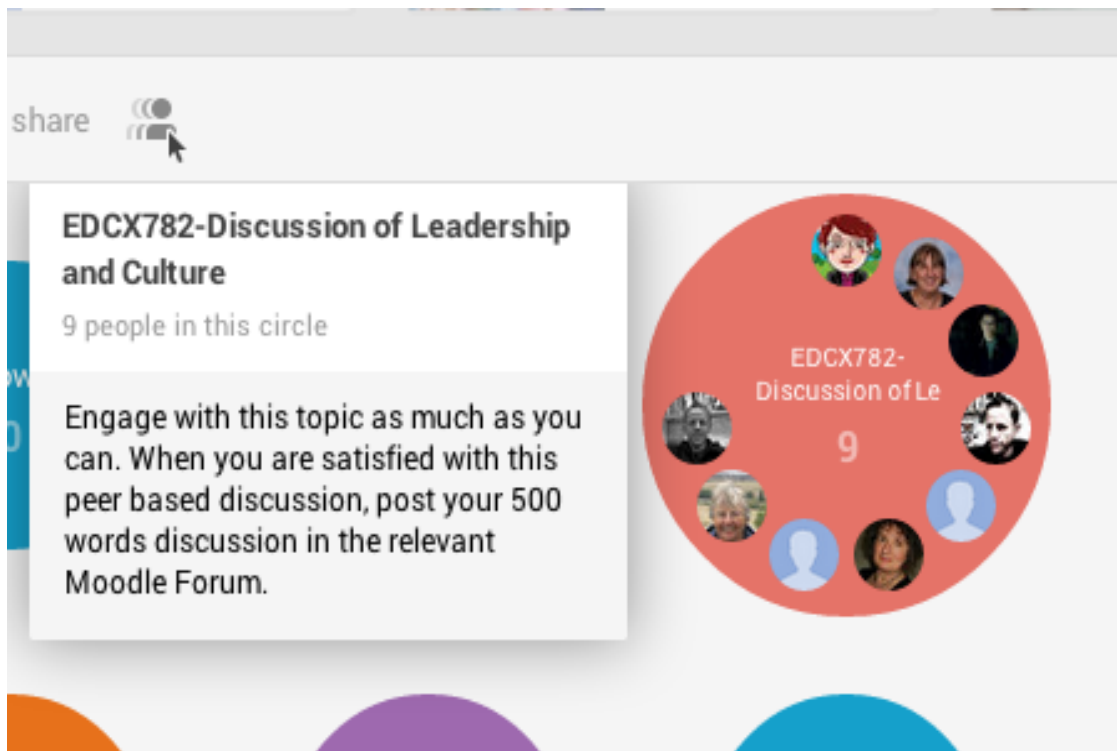


Figure 6. Google Discussion Circle for the doctoral cohort studying Leadership and Culture

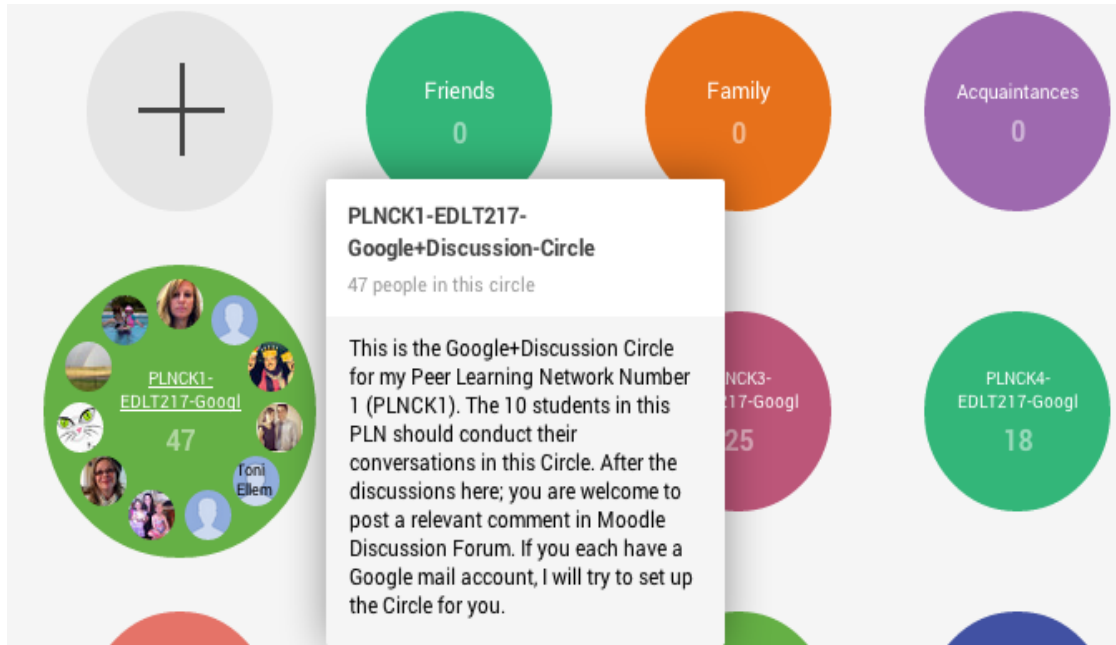


Figure 7: Examples of a Google Discussion Circle for Undergraduates PLN-CK1

IV. OBSERVATIONS AND FINDINGS

As illustrated in Figure 7, what emerged very clearly was that the introduction of GDC as social media technologies, reduced the tyranny of distance and enhanced social presence as students participated in discussions in their virtual classrooms founded on PLNs. For example, in the GDC for my first undergraduate PLNCK1, the number of participants rose by 470% from the original 10 to 47. The reason this was possible was because, whereas under the old system, every student participated and as this was a mandated requirement, there was a 100% response, under the new GDC technologies, each student was asked, not only to participate in the discussions but also given the opportunity to invite other people from outside their group of ten to participate in the GDC discussions. As a result of this design, instead of the ten members of each PLN, the PLNs increased their membership. Thus, whereas under Moodle each Group of 10 had 10 participants, under the GDCs engineering, PLNCK1 initially comprising 10 students ended up with 47 participants. Space does not allow illustration of all the GDCs but significant multiplier effects were realized across all the GDCs. For example, GDC 2 grew to 72; GDC 3 to 51 and so on. What is interesting and particularly noteworthy was the observation that group participation under the old Moodle LMS was mandated, but the invitation of others under the new GDC technologies was voluntary. So, the observed multiplier effects were the results of personal interest and desire to participate rather than a response to mandated instructions. It was evident too, that given the opportunity to apply digital technologies in their learning, students took initiative to extend their understanding of issues and concepts in a digitally connectivist mode. Looking at the streams posted in the GDCs, it was also noticeable that their engagement through PLNs was not only absolutely greater than that under the old Moodle Learning Management System, but also more frequent and with greater zest.

The results shown in Figure 7 are very encouraging for the application of GDC social media technologies in pedagogy but what is even more interesting, though not discussed here for shortage of space, and because these results are rather tentative, is that the frequencies of posts among the GDC-PLN members were much more frequent than those among the old Moodle groups. Moreover, the comments students posted in the GDC-PLNs indicated that they appeared not to see themselves as individual learners, or learning in isolation, but in PLNs that were supportive of each other. They did not appear to be competitive with each other, but collaboratively seeking to engage with the concepts and issues being discussed rather trying to outsmart each other. For students enrolled in the online, distance education mode to be expressing such feelings, lends a lot of support to and shows potential merit in learning engineering which embeds interactive, interconnecting social media technologies into pedagogical practice and curriculum development.

It was also very interesting and encouraging, to see how students sourced and shared stimulus materials with members of their PLNs. Many of the comments in the streams reflected peer mentoring and guidance for each other. The extent to which students shot videos of their own workplaces or designed Graphic Organizers using Lucidchart or used iPad apps to apply Bloom or to discuss MIs in their critiques, and freely shared these with their PLNs, indicated a move towards self-regulated learning based on interest, motivation and personal drive. The comments made on other students' posts reflected aspects of peer feedback, peer support and peer assessment.

It was clear from monitoring the streams in the GDC that students' construction of knowledge was moving from the orthodoxy cognitive constructivist thinking that emphasizes Piagetian [21] personal construction of knowledge not only towards Vygotsky's [22] social constructivism but more importantly towards digital connectivist pedagogy. By connectivist pedagogy I mean what Castells [23] characterized as learning that focuses on building and maintaining networked connections that are current and flexible. An underlying assumption of connectivism as envisaged by Castells [23] and also discussed by Anderson and Dron [24 p. 87] that I found to be very evident among my students was that "information is plentiful and that the learner's role is not to memorise or even understand everything, but to have the capacity to find and apply knowledge when and where it is needed". This is digital fluency in the 21st century of our Digital Natives. Students' apparent enthusiasm to engage in GDC (apparently more so than in Moodle Forums) appears to be very consistent with what Kanuka and Anderson [25] characterize as knowledge acquisition that needs to be subject to social discussion, validation and application in real world contexts. The fact that students took initiative to invite their friends outside of the University to participate in their academic discourses in the GDC reflected their sense of self-efficacy and personal competence in utilizing PLN-based digital technologies. These skills appeared to fall within Bloom's [13] higher-order thinking skills of Applying, Analyzing, Evaluating and even Creating. Students' critiques of readings from the eReserve, designing eFoliospaces in which they embedded technological apps and sharing their Urls with their peers demonstrated high levels of Engagement, ability to Explore, Explain, Elaborate and Evaluate that appears to be consistent with Bruner's [19] 5E Instructional Model, using tools that enhanced their digital fluency in eLearning.

V. DISCUSSION AND CONCLUSION

It has been suggested that the brains of the Digital Natives in our classrooms are wired differently. As Prensky [3] proposes, their brains are used to the "twitch-speed, multitasking, random-access, graphics-first, active, connected, fun, fantasy, quick-payoff world of their video games, MTV, and Internet". As a result these children very easily find most of what is offered in the orthodoxy, tradition engineered classroom content, boring and possibly irrelevant to their real world lives outside the classroom. If we are to engage them, keep them interested and help them to learn, we must speak their language. This means that the Digital Immigrant teachers need to rapidly acquire 21st digital fluency so they can catch up, and hopefully keep pace with their Digital Native students.

It is clear that there is a mismatch between our understanding of how to share information and construct meaning as adults and that of the children we teach, - the Digital Generation. Given this understanding, if we uphold 19th century French psychologist Jean Piaget's [21] proposition that "The principle goal of education is to create men and women who are capable of doing new things, not simply of repeating what other generations have done", then we should encourage our students (pre-service teachers, educational leaders, secondary and primary) to utilise digital tools for construction of academic knowledge in addition to their high utility as tools for sharing and construction of social knowledge. This way, we shall enable our students to learn in their own ways rather than simply replicating how we learnt in the old world. Failure to do this will perpetuate the mismatch between digital savvy students of the 21st century and teachers stuck in the orthodoxy, traditional pedagogy of the last century and fail to achieve what Fullan [26] conceptualizes as the moral purpose of education:- educating productive citizens.

This is why I argue in this paper that digital nativity should be allowed to replace digital immigration as teaching and learning in today's classrooms, at all levels, (primary, secondary and tertiary), progressively gets engineered for the digital landscape. In this new landscape, Facebook, Twitter, MySpace, Bebo, Google Circles and other social media technologies are rapidly becoming the preferred media of intellectual exchange among students rather than simply tools of recreational and conversational dialogue.

In this new landscape, institutional technophobia of social media is rapidly waning, as there is an increasing realisation of the compelling need to restructure our pedagogical approaches and to engineer our LMS so that they cater adequately to the current and future needs of our students. I believe that my experiences with the students' cohorts discussed in this paper lead to the conclusion that one of the ways technologically savvy educators can meet students' demands in this digital landscape of the 21st century is through embedding social media technologies into standard constructivist pedagogy. This paper has discussed my experiences of introducing the use of *Google+*, *Discussion Circles* in both an undergraduate and a doctoral degree program that I have taught, in the hope of encouraging other practitioners to embrace the application of social media technologies in learning, teaching and assessment. The results reveal that the application of social media technologies as instructional and learning tools has significant potential to engage students' learning in more interesting, exciting and motivating ways that enable these technologies to provide critical higher-order thinking and construction of meaning. This new approach to teaching, learning and assessment, is fully supported by leaders in the field [24] who suggest that "restructuring the curriculum to incorporate technology is no longer a trend but a requirement".

As a reflective practitioner, I often ask myself the question, 'How can I be the best teacher I can ever be?' In contemplating an answer to this question I argue that we owe it to our students, the Digital Natives, to develop a Digital Pedagogy that can make the children's learning experiences more interesting, motivational and enriching experiences of knowledge creation by the children we teach in the digital economy. I argue further that for us to be able to do this, we need to move our teaching from the orthodoxy Vygotskyian Constructivist Paradigm to a more contemporary Connectivist Paradigm that is driven by digital technologies in which our Digital Natives are fluent. I suggest that it is the expectation of our Digital Native children (and their Digital Immigrant parents), that their teachers will use the tools that they (the students) understand, are familiar with and prefer to communicate with. Failure of teachers and educational leaders to rise to this challenge will fail to enrich the learning experiences of our digital students. We should not expect that children of the present Digital Generation, (the Gen C, Gen I, Y Gen; Net Gen; Millennials; Z Gen or Internet Generation) will be taught, learn and be assessed using approaches of previous generations - technophobics. I argue that for pedagogy to be Best Practice Pedagogy, it will need to speak the language that the children understand best: – that is digital fluency of the 21st century. Traditional approaches are no longer educationally effective for our children and students in the present new world of technology and work: – the digital economy. The challenge is for all of us practising pedagogues, to shed our technophobic inclinations and become avid technophiles in the new digital economy. For as Peter Cochrane [27] succinctly puts it, can we "imagine a school with children that can read and write, but where there are many teachers who cannot"? (p.57). Hence, learning, developing and applying 21st century fluencies, are essential parts of Best Practice Pedagogy and of becoming the best teacher we want to be. They are no longer an option, but an imperative, if we are to make our instruction relevant to our pre-service teachers and educational leaders (and any other students that we are privileged to teach) and to give them a richer and memorable educational experience. Yes, as Digital Immigrants our digital fluency will inevitably have a foreign accent. However, we owe it to our students, parents, universities, educational authorities and other stakeholders, to embrace 21st century digital technologies. If we allow ourselves to get left behind by our students, our teaching and curriculum will not only suffer from our immigrant accents but will become irrelevant and an unintelligible language for the Digital Natives of today and tomorrow. Teachers in the 21st century classroom must learn the language of the present generation. It might be inconvenient, but technophobia must give way to technophilia. As ably stated in Jules et al. [2], we cannot afford to find the present **tense** and the past **perfect**. Only then shall we reap the many rewards of engineering digital, technological infrastructure into our LMSs, teaching, curriculum and assessment in the 21st century classroom.

REFERENCES

- [1] T. Plante. Digital Natives vs Digital Immigrants? Which are you? *In Do the Right Thing*. 24 July 2012. Accessed from <http://www.psychologytoday.com/blog/do-the-right-thing/2012> on 9 September 2013.
- [2] I. Jukes; T. McCain and L. Crockett. Understanding the Digital Generation: Teaching and Learning in the New Digital Landscape.
- [3] Hawker Brownlow Education, Moorabin, Australia, 2010.
- [4] M. Prensky. Digital Natives Digital Immigrants: Do They Really Think Differently? *On the Horizon*, Volume 9, No. 6, December 2001.
- [5] J. Howell. Teaching with ICT: Digital pedagogies for collaboration and creativity, Oxford University Press, Melbourne, 2012.
- [6] D. McNierney. Case Study: One Teacher's Odyssey through Resistance and Fear, *TechTrends*, Volume 48, No. 5, 2004, pp. 64 – 68.
- [7] Ed Tech Times, "*The Pros and Cons of Social Media in Education*," <http://www.edtechtimes.com/2013/02/22/the-pros-cons-of-social-media-in-education-infographic/>, Last accessed 22 February 2013.

- [8] S. Jones and M. Madden. The Internet goes to college: How students are living in the future with today's technology. Washington DC, Pew Internet & American Life Project, 2002. From http://pewinternet.org/pdfs/PIP_College_Report.pdf
Accessed 18 January 2008.
- [9] G. E. Kennedy,; T.S. Judd; A. Churward; K. Gray, and K. Krause. First year students' experiences with technology: Are they really digital natives?. Australian Journal of Educational Technology, Volume 24, No. 1, 2008, pp. 108 – 122.
- [10] B. Oliver and V. Goerke. Australian undergraduates' use and ownership of emerging technologies: Implications and opportunities
for creating engaging learning experiences for the Net Generation. Australasian Journal of Educational technology, Volume 23,
No. 2, pp. 171 – 186.
- [11] Australian Bureau of Statistics. Household use of Information Technology, Australia, 2010-11.
Released at 11:30 AM (CANBERRA TIME) 15/12/2011.
- [12] S. Lustenhouwer. Apps for multiple intelligences. Blog posted 21 August, 2012 at <http://www.ipadders.eu/apps-for-multiple-intelligences/>. Accessed 3 August 2013.
- [13] H. Gardner. Intelligence reframed: Multiple intelligences for the 21st century. Basic Books, New York, 1999.
- [14] B.H. Bloom. Taxonomy of Educational Objectives, Handbook 1: Cognitive Domain, New York, David Mackay Co, 1956.
- [15] K. Schrock. Bloomin' Apps, "*Kathy Schrock's Guide to Everything*", <http://www.schrockguide.net/bloomin-apps.html>
Accessed 9 September, 2013.
- [16] Langitch. Bloom's Taxonomy for iPads. Originally from Dave Mileham and Silvia Rosenthal. Available in blog at
<http://www.langwitches.org/blog/2012/03/31/ipad-apps-and-blooms-taxonomy/>
Accessed 24 August 2013.
- [17] P. Valery. The need for Balance. In Jules, McCain and Crockett. Understanding the Digital Generation: Teaching and
Learning in the New Digital Landscape, Hawker Brownlow Education, Moorabin, Australia, 2010.
- [18] G. Small and G. Vorgon. iBrain: Surviving the technological alteration of the modern mind. New York, Harper Collins, p. 68.
- [19] N. Sabelli. Constructionism: A new opportunity foe Elementary Science Education. DRL Division of Research on Learning in
Formal and Informal Settings, 2008, p. 196. Available online at <http://nsf.gov/awardsearch/showAwards.do?AwardNumber=8751190>.
- [20] J. S. Bruner, Toward a Theory of Instruction, Harvard University Press, Cambridge, 1966.
- [21] E. de Bono. Six Thinking Hats. Little, Brown and Company, Cambridge, 1985.
- [22] J. Piaget. The Language and Thought of the Child, (Translated M. Gabain). London, Routledge & Kegan Paul, 1923.
- [23] L. S. Vygotsky, "*Mind in Society: The Development of Higher Psychological Processes*", Cambridge, MA, Harvard University
Press, 1978.
- [24] M. Castells, "*The Information Age: Economy, Society and Culture: The Rise of the Networked Society*", Oxford, UK,
Blackwell,1996.
- [25] T. Anderson and J. Dron, "Three Generations of Distance Education Pedagogy", International Review of Research in Open and
Distance Learning, Vol. 12, No. 3, pp. 80 – 97, March 2011.
- [26] H. Kanuka and T. Anderson, "Using constructivism in technology-mediated learning: Constructing order out of chaos in the
literature", Radical Pedagogy, Vol. 2, No. 1. Retrieved from http://radicalpedagogy.icaap.org/content/issue1_2/02kanuka1.html
- [27] M. Fullan. The new meaning of educational change. New York, Teachers College Press, 2001.
- [28] P. Cochrane. A Shift to Whole-Mind Instruction. In I. Jukes; T. McCain and L. Crockett. Understanding the Digital Generation:
Teaching and Learning in the New Digital Landscape, Hawker Brownlow Education, Moorabin, Australia., Ch.7. pp.57 – 78.

Architectural Design of an Efficient Data Center

¹Sree Bishwjit Chandra Das , ²Md Kabirul Islam , ³Syed Akhter Hossain
^{2,3}Department of Computer Science and Engineering, Daffodil International University

ABSTRACT

The purpose of this study was to analyze different data centers from design and function perspectives and develop a prototype of a data center for maximum efficiency. Relevant data on the designs and functions of several data centers as well as their advantages were gathered from various sources and analyzed. This is compared and summarized in this work. Finally, an architectural model of an efficient data center is developed. The proposed data center adopts several functions such as Virtualization, monitoring systems, Green IT, and dark strategy. These functions are expected to maximize efficiency, availability and agility, and reduce power consumption, space requirement, and cost of operations and staff salary.

KEYWORDS : Data Center, Virtualization, Cloud Computing

I. INTRODUCTION

A Data center is a facility used to house computer systems and associate components such as telecommunication and storage systems. It generally includes a server, storage, redundant power supplies, data communications and security [1]. Conventional data center required huge computer rooms and special environment in which it was operated in the early stage of computer industry. A single mainframe required a great deal of power, and had to be cooled to avoid overheating. Large data centers are industrial scale operations using as much electricity as a small town [2] and sometimes are a significant source of air pollution in the form of diesel exhaust [3].

In the present world, organizations depend on their information systems to run their activities and services. If a system becomes impair the services will be stopped completely. So, it is necessary to provide a reliable and secure infrastructure for IT operations to minimize any chance of disruption. A data center must therefore keep at high standards for assuring the integrity and functionality of its hosted computer environment. There has been good number researches into data center design and functions in the past few years and the findings show that there are several designs of data centers such as traditional server centric, modular, and cloud computing [4], [5], [6], [7], & [8]. Each design of data center adopted various functions to minimize disruption, space required, power consumption, and make the data center environment friendly. Nevertheless, it is very had to find a complete data centre integrated with all modern functions to make it more sustainable. This study is conducted through investigation of the design and functions of several data centers and finally developed an architectural model of a modern and sustainable data centre. The paper is organized as follows. Section 2 discusses the plan of the study, section 3 discusses the design of data center, section 4 describes various functions, section 5 proposed the design based on the analysis of the findings, section 6 includes the validity of the model, and section 6 presents conclusion of this paper.

II. PLAN OF THE STUDY

The objectives of this study were to:

- a. Analyze design, and function with advantages of different data centers
- b. Summarize and compared findings
- c. Develop a technical design of a data centre with innovative functions

Relevant literature on data centre was collected from different sources such as online journals and conference proceedings, books, and internet websites. The data were analyzed on the basis of the design of data center, functions and their advantages. The data were then summarized to develop an architectural model of a data center. Experts' opinions were sought on applicability and sustainability of the new model. Three data center experts provided positive comments on the new model (Appendix A).

III. DESIGN OF DATA CENTER

Derived from the business objectives and requirements of the applications hosted in the data center, the common design goals are found to increase performance, scalability, flexibility to support various services, and long time viability, and ensure security, high availability and manageability [5], [6] & [9]. Literature on the design of several data centers are given below.

IV. WIRE HOUSE SCALE COMPUTER DESIGN

The typical elements in warehouse-scale systems [10] included 1U server, 7' rack with Ethernet switch, and a small cluster with a cluster-level Ethernet Switch /router (figure 1).

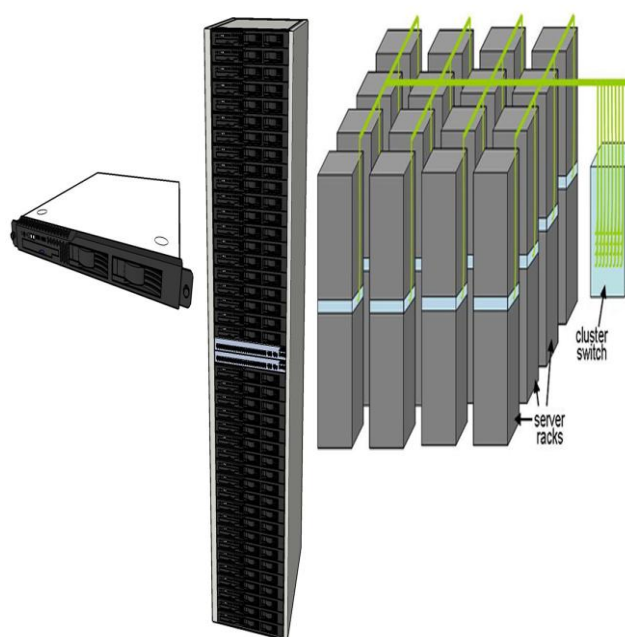


Figure 1. Warehouse-Scale System

Figure 1 depicts some of the more popular building blocks for WSCs. A set of low-end servers, typically in a 1U blade enclosure format, are mounted within a rack and interconnected using a local Ethernet switch. A key challenge for architects of WSCs is to smooth out these discrepancies in a cost-efficient manner. Conversely, a key challenge for software architects is to build cluster infrastructure and services that hide most of this complexity from application developers.

V. SUPERCOMPUTER ARCHITECTURE

Supercomputer Architecture of data centre used custom CPUs, traditionally gained their speed over conventional computers through the use of innovative designs that allow them to perform many tasks in parallel, as well as complex detail engineering. Supercomputers today most often use variants of the Linux operating system [12]. A typical supercomputer consumes large amounts of electrical power, almost all of which is converted into heat, requiring strong cooling system. The memory hierarchy of the supercomputer architecture was designed to support high bandwidth, with latency less of an issue, because supercomputers are not used for transaction processing [12].

VI. MULTI-TIER DESIGN

Multi-tier design is the most common model used in the enterprise today. This design consists primarily of web, application, and database server tiers running on various platforms including blade servers, one rack unit (1RU) servers, and mainframes. The multi-tier model relies on a multi-layer network architecture consisting of core, aggregation, and access layers, as shown in figure 2 [13].

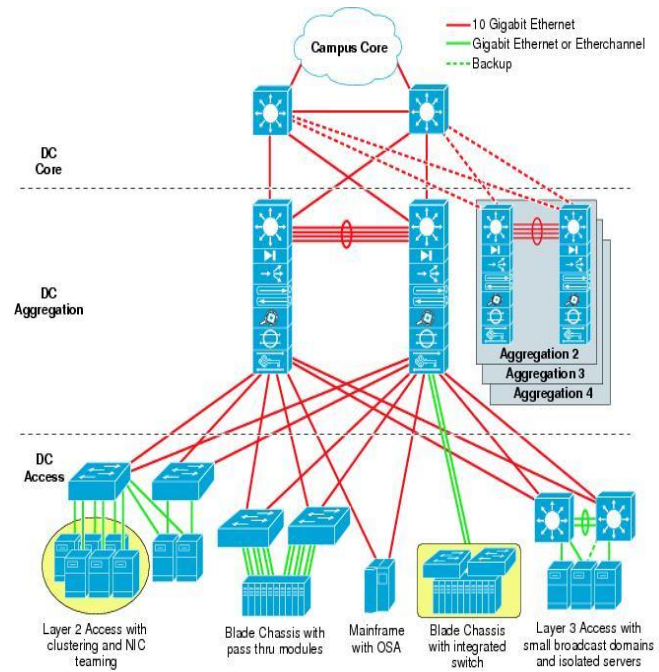


Figure 2. Multi-tier design of data center

Multi-tier design model supports many web service architectures, including those based on Microsoft.Net and Java Enterprise Edition. Today, most web-based applications are built as multi-tier applications. The multi-tier model uses software that runs as separate processes on the same machine using interprocess communication (IPC), or on different machines with communications over the network [10].

VII. CLOUD COMPUTING DESIGN

Cloud computing is an emerging field of computer science and recent trend in Information Technology. It is a computing environment where computing needs by one party can be outsourced to another party and when need be arise to use the computing power or resources like database or emails, they can access them via internet [13]. More specifically, Cloud computing moves computing and data away from desktop and portable PCs into large data centers. A simple view of cloud computing architecture of data center [6] is given in figure 3.

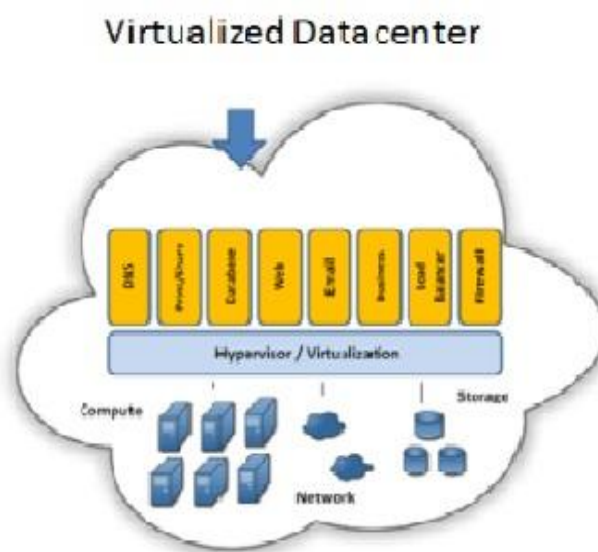


Figure 3. A simple view of cloud computing design of data center.

In the cloud computing design, the computer can no longer be thought of in terms of the physical enclosure that is, the server or box, which houses the processor, memory, storage and associated components that constitute the computer. Instead the computer in the cloud ideally comprises a pool of physical compute resources – i.e. processors, memory, network bandwidth and storage, potentially distributed physically across server and geographical boundaries which can be organized on demand into a dynamic logical entity i.e. a cloud computer [6]. It has multi-level virtualization and abstraction [14], and energy saving functions like green IT applications [15], [16]. The Design of different data centers discussed above may be categorized as traditional and virtualized data center. The data shows that the traditional data center is server centric while the virtualized data center is network centric. Further, each design of data center has different advantages. The following section has summarized the functions and their advantages.

COMPARATIVE FUNCTIONS OF DATA CENTRE

Different functions of data center and their advantages are summarized and compared. These are explained below

VIII. VIRTUALIZATION

Virtualization of data center refers to the abstraction of resources to allow multiple operating systems to run on one system at the same time [10] and clouds are attractive computing platforms for data- and compute-intensive applications [17]. These platforms provide an abstraction of nearly-unlimited computing resources through the elastic use of pools of consolidated resources, and provide opportunities for higher utilization and energy savings [17]. Virtualization results in reducing total costs, maximizing energy efficiency, reducing power and space requirement, enhancing security, and increasing availability and agility [18], [17].

MONITORING

Monitoring of operations is an important function of a modern data center. A system monitor is hardware- or software- based system used to monitor resources and performance in a computer system [19]. A central monitoring unit may be operated by integrating central grid control as well as site scan monitoring system. They are used to display items such as free space on one or more hard drives, the temperature of the Data Center, UPS room, CRAC and other important components, and networking information. Other possible displays may include the system uptime with date and time. The monitoring system can identify the temperature and Humidity of Datacenter, CRAC, UPS room, Server Performance or Status, and the Server file system usages

GREEN IT

Green IT technology is a hot topic worldwide. A Green Data Center is a repository for the storage, management, and distribution of data in which the lighting, electrical and computer systems are designed for maximum energy efficiency and minimum environmental impact [20], [21]. Building and certifying a green data center or other facility can be expensive up front, but long-term cost savings can be realized on operations and maintenance. Another advantage is the fact that green facilities offer employees a healthy, comfortable work environment [7], [10]. In addition, green facilities enhance relations with local communities. Advantages of Green IT are reduction in staffing costs, reduce the threat of attacks upon the infrastructure energy saving.

LIGHTS OUT

The ‘lights-out’ or function of a data center ideally has all but eliminated the need for direct access by personnel, except under extraordinary circumstances (23). It can be operated without lighting because of the lack of need for staff to enter the data center. All of the devices are accessed and managed by remote systems, with automation programs used to perform unattended operations. Lights out function is also called dark data centre.

IX. PLATFORM, INFRASTRUCTURE, AND SOFTWARE AS SERVICES

Within each modern computing system architecture, innovative services such as Platform as a Service (PaaS), Infrastructure as a Service (IaaS), and Software as a Service (SaaS) may be offered. PaaS is a full or partial development and deployment environment that supports online access and collaboration between users via the internet. This type of environment saves investment in hardware and additional management personnel [23]. The Customer Relationship Management (CRM) and Enterprise Resource Management (CRM) programs may be made available through the data center of a SaaS provider [14]. However, PaaS and IaaS can be used in place of a brick-and-mortar facility.

PROPOSED DESIGN OF DATA CENTER

Cloud computing design is proposed for new model as it views hardware and software as commodities, possesses mass data computing and store, holds huge scalability and novel services such as SaaS, PaaS, IaaS [23] and good availability. Hence, it offers enterprises the opportunity to reduce hardware and software cost and the potential reduction of maintenance and support staff [15], & [24]. The architectural design (figure 4) incorporates several functions such as virtualization (computer, network and storage), monitoring system, green IT, lights out and other functions like SaaS, PaaS, and IaaS.

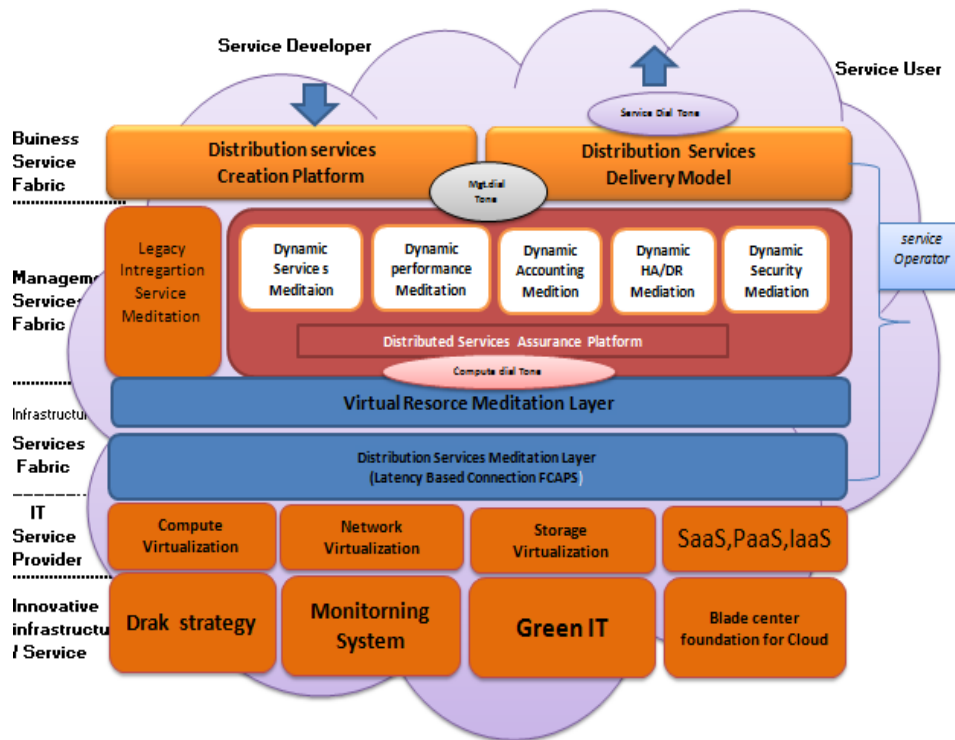


Figure 4. Architectural Design of proposed data center

The model will fulfill the needs of four categories of stake holders for deployment such as infrastructure providers, service providers, service developers, and end users [6]. Infrastructure providers are vendors who provide the underlying computing, network and storage resources that can be shaped up into logical cloud computers which will be dynamically controlled to deliver massively scalable and globally interoperable service network infrastructure. The service provider (SP) will provide organizations with consulting, legal, real estate, education, communications, storage, processing, and many other services as required and manage the application’s connection to computing, network and storage resource. The end users can dynamically provision in real-time to respond to changing demands, and provide service providers the capability to charge the end-user by metering exact resource. The proposed data center is unique and efficient because it has been developed integrating several modern applications such as dark strategy, monitoring system, green IT. These strategies will reduce consumption of electricity and cost of extra staff. Additionally, services like SaaS, PaaS, and IaaS will increase novelty of the model.

VALIDITY OF THE PROPOSED MODEL

Since simulation of the proposed design was not feasible so the proposed model was sent to three data center experts who are working in different financial organizations for their comments. The experts offered their positive opinions regarding, regarding implementation and innovation of the model. Comments from one of the three experts are presented below. “The hypothetical model of a data center is an innovative approach and may be implemented in any organization.” Another expert commented on the functions adopted in the design of the data center which is given below. “The infrastructure shown in the data center such as virtualization, central monitoring system, dark strategy and green IT are innovations in data center infrastructure. The data center is

found modern and may be implemented in any relevant organization.” Experts’ comments can be found in Appendix A.

X. CONCLUSIONS

The Proposed architectural design of data center enables dynamism, scalability, Reliability and security because of its noble functions -Virtualization, Monitoring system, Green IT, Dark Strategy and Blade Center Foundation. The functions integrated to this new model will address the main drawbacks of the traditional data center such as large infrastructure, and huge consumption of electric power. In addition, the above functions will boost efficiency of the data center. It may be mentioned that simulation of proposed data center was not possible as it is a theoretical model. However, positive comments made by three experts have increased validity and reliability of the model. Further investigation is needed to explore the limitations and challenges of the proposed architectural design.

REFERENCES

- [1] Arregoces, M. & Portolani, M. (2013). Data Center Fundamentals, CISCO Press, Indiana.
- [2] Glanz, J. (2012). Power Pollution and the Internet The New York Times, September 25, 2012.
- [3] Glanz, J. (2012). Data Barns in a Farm Town, Gobbling Power and Flexing Muscle, The New York Times, September 25, 2012.
- [4] Wu, K. (2008). A Comparative Study of Various High Density Data Center Cooling Technologies, Masters Thesis, Stony Brook University, New York.
- [5] Intel IT Center, (2011). Technology for Tomorrow’s Cloud, Intel, Retrieved on from 05.01.2013 from <http://>
- [6] Sarathy, V., Narayan, P., & Mikkilineni, (n.d). Next Generation Cloud Computing Architecture, Retrieved on 05.01.2012 from <http://>
- [7] gtsi, (n.d). Reducing Data Center Power and Energy Consumption: Saving Money and “Going Green”, Retrieved on 05.01.2012 from <http://>
- [8] CISCO, (2009). CISCO Cloud Computing Data Center Strategy, Architecture, and Solutions, CISCO Systems Inc, Uk.
- [9] Enterasy, (n.d). Data Center Networking- Connectivity and Topology Design Guide, Retrieved on 6.01.2013 from <http://>
- [10] Hossain, M. J. (2011). Data Center Design and virtualization, MyNOG, Malaysia.
- [11] Barroso, L.A. & Holze, U. (2009). The Data Center as a Computer- An Introduction to the Design of Warehouse-Scale Machines, Morgan Claypool publishers, Germany.
- [12] Wikipedia. (2013). Supercomputer, Retrieved on 07.04.2013 from <http://www.wikipedia.org/wiki/Supercomputer>
- [13] CISCO, (n.d). Data Center Multi-Tier Model Design, Retrieved on 12.01.2013, from http://www.cisco.com/en/US/docs/solutions/Enterprise/Data_Center
- [14] Jadeja, Y. & Modi, K. (2012). Cloud Computing- Concept, Architecture and Challenges, International Conference on Computing, Electronics and Electrical Technologies (ICCEET), 21-22 March, 2012, 877-880.
- [15] Islam, S. S., Molla, M. B., Huq, M. I. & Ullah, M. A. (2012). Cloud Computing for Future Generation of Computing Technology, IEEE International Conference on Cyber Technology in Automation, Control, and Intelligent Systems (CYBER), 27-31 May 2012, 129-134.
- [16] Liu, L., Masfary, O., & Li, J. (2011). Evaluation of Server Virtualization Technology for Green IT, IEE 6th International Symposium on Service Oriented System Engineering (SOSE), December 12-14, 2011, 79-84.
- [17] Xu, J., Tang, J., Kwiat, K., Zhang, W. & Xue, G. (2012). Survival Virtual Infrastructure Mapping in Virtualized Data Centers, IEEE 5th international Conference on Cloud Computing (CLOUD), 24-29 June 2012, 196-203.
- [18] Rodero, I., Jaramillo, J., Quiroz, A., Parashar, M., Guim, F. & Poole, S. (2010). Energy-efficient application-aware online provisioning for virtualized clouds and data centers, international Conference on Green Computing.
- [19] Wikipedia. (2013). Supercomputer, Retrieved on 07.04.2013 from http://www.wikipedia.org/wiki/Data_center_infrastructure_management
- [20] Lamb, J. (2011). Green It and use of Cloud Computing in South Africa, 8th International Conference & Expo on Emerging Technologies for a Smarter World (CEWIT), 2-3 November 2011, 1-6.
- [21] Mata-Toledo, M. & Gupta, P. (2010). Green Data Center: how Green can we perform? Journal of Technology Research, 2 (Sept), 1-8.
- [22] Kliazovich, D., Brevry, P., Audzevich, Y. & Khan, S. U. (2010). Green Cloud: A Packet-level Simulator of Energy-Aware Cloud Computing Data Centers, IEEE Conference on Global Telecommunication, December 6-10, 1-5.
- [23] Emersion, (n.d). Taking the Enterprise Data Center into the Cloud, Retrieved on 05.12.2013 from <http://>
- [24] Owusu, F., & Pattinson, C. (2012). The Current State of Understanding of the energy efficiency of cloud computing, 11th IEEE International Conference on Trust, Security and Privacy in Computing and Communications (TrustCom), 25-27 June 2012, 1948-1953.

APPENDIX A

Expert Opinion

For validity and reliability of the proposed model opinions were sought from three data center experts. Scanned copies of their opinions are given below.

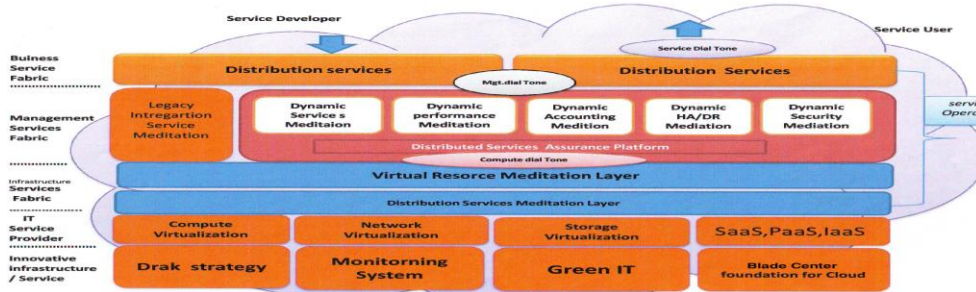


Figure. Architectural Design for Next Generation Data Center - Cloud Computing Infrastructure

The theoretical model of the data center developed by Sree Bishwjit Chandra Das, a M.Sc. Student of DIB is modern and latest and may be implemented in practical context.

Signature
15/11/2013
Manager Data Center
SBI Bank Ltd.

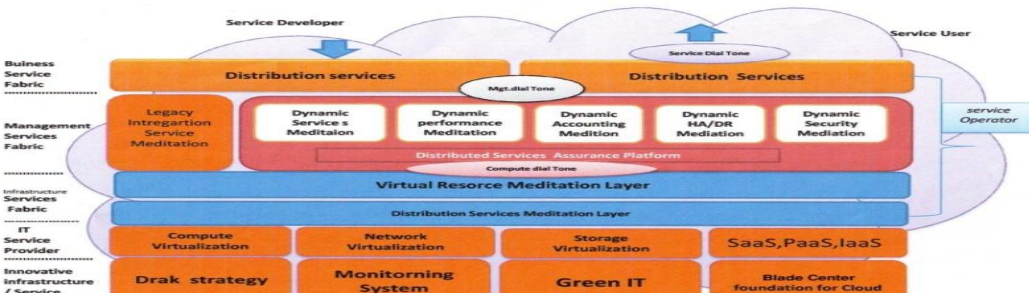


Figure. Architectural Design for Next Generation Data Center - Cloud Computing Infrastructure

The infrastructure shown in the data center such as virtualization, central monitoring system, dark strategy, and green IT are innovations in data center infrastructure. The data center is found modern and may be implemented in any relevant organization.

Signature 17-01-2013
SRED ANKAN KHOBIB (SPO)
IT INFRASTRUCTURE AND
SYSTEM MANAGER,
IT DIVISION,
EAM BANK LTD.

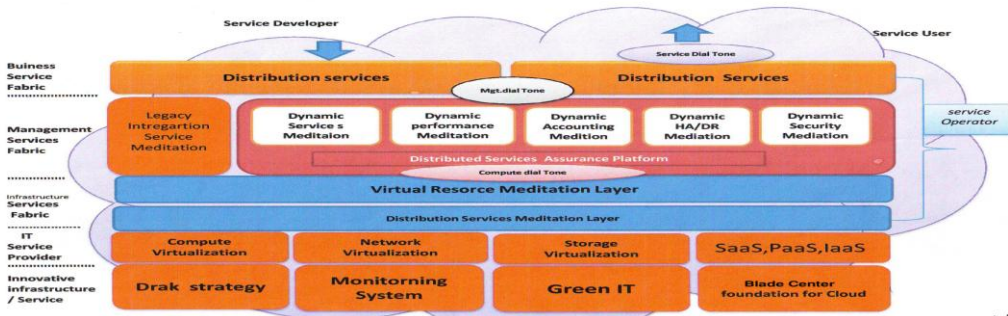


Figure. Architectural Design for Next Generation Data Center - Cloud Computing Infrastructure

The hypothetical model of a data center is an innovative approach and may be successfully implemented in any organization.

Signature 25-01-2013
Abdullah Al. Momen
Assistant Manager
ICT Division
Bangla Bank Ltd.